THE JOURNAL
OF
CHEMICAL PHYSICS

VOLUME 19, NUMBER 12 DECEMBER, 1951

Statistical Thermodynamics of Rubber Elasticity

FREDERICK T. WALL, *Noyes Chemical Laboratory, University of Illinois, Urbana, Illinois*

AND

PAUL J. FLORY, *Department of Chemistry, Cornell University, Ithaca, New York*

(Received March 17, 1950)

Two principal differences between the theories of rubber elasticity advanced by James and Guth and by other authors are examined in the light of certain fundamental concepts. First the distribution functions for molecular chain lengths in vulcanized rubber networks are considered from the point of view of symmetry. Assuming a relaxed network to be isotropic and a network subject to uniform stress in one direction to be transversely isotropic, it is possible to formulate very general mathematical forms with respect to which the actual distribution functions must be compatible. It is shown that the functions employed by Wall and by Flory and Rehner are consistent with the required general forms; those of James and Guth are incompatible with any degree of isotropy and suggest an aeolotropic structure for vulcanized rubber.

It is also shown that the configurational entropy of vulcanization must be zero and quite independent of the statistical nature of the chains comprising the network, providing the network is not deformed macroscopically. The negative entropy of vulcanization derived by James and Guth arises from their erroneous identification of the configurational probability with the number of configurations which a microscopically specified network structure could assume, rather than with the total number of configurations for all network structures which are consistent with the requirements of the vulcanization process. The assertion of James and Guth that the configurations of the polymer chains are altered in some systematic manner by the introduction of cross-linkages and their concept of "internal pressure" originate in this error. The present article attempts to clarify the currently prevalent confusion with respect to rubber elasticity theory.

DURING recent years, a number of theories of rubber-like elasticity have been published by various authors. Although all of the theories have much in common, and most of the theories are in essential agreement, James and Guth[1-3] have expressed dissatisfaction on various grounds with the contributions of Kuhn,[4,5] Wall,[6] Flory and Rehner,[7] and others.[8,9] The latter group of investigators are in close agreement, both with respect to methods employed and the final results obtained. James and Guth likewise obtain a substantially equivalent stress-strain relationship, except that their expression is less explicit in regard to the modulus of elasticity in relation to structure. They contend, however, that the methods used by the other workers are "unrealistic," "not consistent with the network structure of rubber," etc. We cannot agree that their criticisms of the other theories are valid or that their alternative hypotheses are justified. We shall accordingly restate some of the principles which form the basis of the theories so vigorously criticized by James and Guth, and will also point out the untenable implications of their alternative hypotheses.

The theories advanced earlier by the present authors[6,7] are fully compatible with each other, for they differ only in points of emphasis and in minor details. Wall[6] was particularly concerned with the relationship between macroscopic dimensions of a piece of rubber and the distribution of molecular chain lengths in the rubber. He implied, but did not emphasize, the network aspect of the problem. Flory and Rehner,[7] on the other hand, took full cognizance of the network model and showed clearly

[1] H. M. James and E. Guth, J. Chem. Phys. **11**, 455 (1943); J. Appl. Phys. **15**, 294 (1944); *Advances in Colloid Science, Vol. II*, edited by H. Mark and G. S. Whitby (Interscience Publishers, Inc., New York, 1946), chapter by E. Guth, H. M. James and H. Mark, p. 253.
[2] H. M. James and E. Guth, J. Chem. Phys. **15**, 669 (1947).
[3] H. M. James and E. Guth, J. Polymer Sci. **4**, 153 (1949).
[4] W. Kuhn, Kolloid-Z. **76**, 258 (1936); **87**, 3 (1939).
[5] W. Kuhn and F. Grün, Kolloid-Z. **101**, 248 (1942); J. Polymer Sci. **1**, 183 (1946).
[6] F. T. Wall, J. Chem. Phys. **10**, 132, 485 (1942); **11**, 527 (1943).
[7] P. J. Flory and J. Rehner, Jr., J. Chem. Phys. **11**, 512 (1943).
[8] L. R. G. Treloar, Trans. Faraday Soc. **39**, 36, 241 (1943).
[9] J. J. Hermans, Trans. Faraday Soc. **43**, 591 (1947).

how the modulus should depend on structure.[10] Accordingly, these theories can be considered to some extent complementary, and a combination of them provides a coherent theory which we shall compare with that of James and Guth.

There are two principal points with which we shall be concerned in this discussion. First we will show that the theory of James and Guth is incompatible with fundamental physical principles relating to symmetry. Next we shall point out their error in connection with the entropy of network formation.

Let us consider a piece of vulcanized rubber in a relaxed state free of stresses and strains. Such a piece of rubber can properly be assumed to be isotropic, that is to say, it will have the same macroscopic properties and statistically the same microscopic properties in all directions. Let us now cut out of such a piece of rubber a right circular cylinder of length L and radius R and let us place this cylinder in a Cartesian coordinate system (x, y, z) with the axis of the cylinder in coincidence with the x coordinate axis. Notwithstanding its physical shape and its orientation in the coordinate system, the cylindrical piece of rubber will still be isotropic when free of stresses and strains.

We shall now suppose that the vulcanized rubber consists of a three-dimensional network of "chains"[10,11] of such a nature that the ends of each chain are joined to the ends of at least two other chains at points known as junction points. Inactive elements of the structure, i.e., chains attached to the network at one end only, are excluded from consideration in the discussion immediately following.

The lengths and directions of the several chains emanating from a given junction point can be characterized by vectors drawn from that junction point to the ends of the chains, which will of course lie at other junction points. The distribution of chain lengths, and hence the probability that a chain have a certain length, can be ascertained by using as samples the vectors originating from a sufficiently large number of junction points. If all of the junction points are used for determining the distribution function, then each chain will be counted twice, with opposite vector senses for each count. If less than all of the junction points are used in providing samples, then some of the chains may be counted twice, others counted once and still others may not be counted at all. It is, however, possible to pick a truly representative sample with the restriction that no chain be counted twice. In any event, the subsequent arguments will not be altered, for the vector length distribution will not depend upon the presence or absence of the restriction suggested above.

We are now in a position to make some very general statements regarding the nature of the function describing the distribution of chain lengths. Let x, y, and z be the components of a chain vector defined above and let $p(x, y, z)dxdydz$ be the probability that a chain will have components in the ranges x to $x+dx$, y to $y+dy$, and z to $z+dz$. Then in the relaxed isotropic state, we can say that $p(x, y, z)=p(r)$ where $r=(x^2+y^2+z^2)^{\frac{1}{2}}$. This assertion is a necessary consequence of isotropy and does not depend in any way upon the particular functional form of $p(r)$.

Let us now subject the previously mentioned cylinder of rubber to equal and opposite forces in the x direction operating uniformly on, and perpendicular to, the two circular ends of the cylinder. As a result of these forces, the cylinder will be elongated or compressed; simultaneously, the cross-sectional area (but not its shape) will change, more or less, by amounts determined by the poisson ratio. In the resulting strained condition, the rubber will no longer be isotropic in three dimensions, although it will not be entirely devoid of internal symmetry. The x direction will have become a unique direction, but the material will still possess two-dimensional, or transverse, isotropy in the y, z planes. The strain ellipsoid for the rubber will be an ellipsoid of revolution with the unique axis lying along the x axis and with the other two axes of equal lengths and unspecified directions, save that they are mutually perpendicular and lie in the y, z plane. From symmetry considerations it is clear that the distribution of molecular lengths in the previously described strained condition must be of such a character that it can be expressed in the form $p(x, \rho)$ where $\rho=(y^2+z^2)^{\frac{1}{2}}$.

The distribution functions $p(r)$ and $p(x, \rho)$ have further properties which should be noted at this time. Both of the functions must be even functions of x, y, and z; i.e., they are both invariant to each or any combination of the following transformations:

$$x\rightarrow -x, \quad y\rightarrow -y, \quad \text{and} \quad z\rightarrow -z.$$

Moreover, the function $p(r)$ is invariant to rotation about any axis, although $p(x, \rho)$, applied to the strained state, is invariant to rotation about the x axis only. The transformation properties require that the average vector length of the molecular chains be zero, whether the rubber be relaxed or strained. However, the root-mean-square lengths, or components thereof, will be different from zero and will generally change with changes in the state of strain. This is in good analogy to the velocities of gaseous molecules in a stationary container; the average velocity will be zero, but the root-mean-square velocity will be variable and different from zero.

The foregoing arguments with respect to molecular length distributions are logically compelling; however, they are so general that no theory of rubber-like elasticity can be formulated on them alone. Nevertheless they do suggest a powerful means for testing the possible validity of theories involving the use of molecular length distributions. In brief, any theory which is incompatible

[10] P. J. Flory, Chem. Revs. **35**, 51 (1944); Ind. Eng. Chem. **38**, 417 (1946).

[11] James and Guth call them "segments," a term currently used in another connection in the polymer field.

with them must of necessity be in error; however, compliance with the symmetry requirements does not, of course, assure that a given theory is correct. We shall now show that the theories of Wall[6] and of Flory and Rehner[7] pass this test, whereas that of James and Guth[3] does not.

According to the theories of the former authors,[6,7] the distribution function for molecular lengths in the unstrained state is given by

$$p(x, y, z)=(\beta^3/\pi^{\frac{1}{2}}) \exp(-\beta^2[x^2+y^2+z^2]) \quad (1)$$

$$=(\beta^3/\pi^{\frac{1}{2}}) \exp(-\beta^2 r^2), \quad (1a)$$

where β is a constant depending upon chain lengths, bond angles, etc. When a cylindrical piece of rubber is stretched in the x direction from a length L_0 to a length L, then the distribution function is presumed to become

$$p'(x, y, z)=(\beta^3/\pi^{\frac{1}{2}}) \exp(-\beta^2[x^2/\alpha^2+\alpha y^2+\alpha z^2]) \\ =(\beta^3/\pi^{\frac{1}{2}}) \exp(-\beta^2[x^2/\alpha^2+\alpha\rho^2]), \quad (2)$$

where $\alpha=L/L_0$.

The detailed arguments regarding the validity of Eqs. (1) and (2) need not be repeated here. We wish to point out, however, that these equations are fully compatible with the forms required by the very powerful symmetry arguments.

According to the theory of James and Guth,[3] the chain length distribution function in one dimension is

$$p(x)=(\beta/\pi^{\frac{1}{2}}) \exp(-\beta^2[x-L/N]^2), \quad (3)$$

where L is the length of the piece of rubber and N the number of molecular chains. It is readily seen that Eq. (3) is incompatible with the general symmetry arguments previously advanced. In particular, it is not invariant to the transformation $x\rightarrow -x$, thus implying a polar character to the x axis, in violation of one of the basic symmetry conditions.[12] Only if L were equal to zero would the distribution be symmetrical. Such a condition for the macroscopic lengths could never be realized.

As a consequence of their use of Eq. (3), James and Guth are led to assert that an actual piece of rubber exhibits, upon vulcanization, a tendency to shrink to zero volume. To account for the fact that rubber does not actually so shrink, they postulate the presence within the rubber of a fluid whose pressure serves to keep the volume different from zero. The required hypothetical fluid does not obey any ordinary equation of state, but is endowed with certain bizarre characteristics.

At this point we recall that, in the theories of Wall and of Flory and Rehner, the average vector length of the chains is always zero and that the root-mean-square dimensions are different from zero and dependent upon strain. According to James and Guth the average length is not zero. Moreover, the exact profile of their distribution function for chain lengths is independent of strain and only the center of that distribution appears to move about. This is as physically unrealistic as would be shifting the origin of the maxwellian distribution of molecular velocities to accompany changes in temperature.

We shall now turn to the second principal point about which the two theories are in disagreement. This has to do with the configurational entropy of the network composed of chains joined at cross-linkage points. James and Guth express the number of configurations which a representative chain may assume as a gaussian function $c(\mathbf{r}_i)$ of the length of the vector $\mathbf{r}_i$ from one end of the chain to the other.[13] For each specification of the coordinates of every junction point, the number of configurations available to the entire network structure is taken as the product of gaussian functions, one for each chain, thus

$$C(\mathbf{r}_1, \mathbf{r}_2, \cdots)=\prod_i c(\mathbf{r}_i).$$

The total number of configurations which the given network structure may assume is obtained by integrating $C(\mathbf{r}_1, \mathbf{r}_2, \cdots)$ over the space coordinates of all the junctions. James and Guth show that the result is of the form,

$$C=\int d\mathbf{r}_1 \int d\mathbf{r}_2 \cdots C(\mathbf{r}_1, \mathbf{r}_2 \cdots) \\ =\text{const} \exp[-(K/2)(\alpha_x^2+\alpha_y^2+\alpha_z^2)], \quad (4)$$

where α_x, α_y, and α_z are the ratios of the macroscopic dimensions to those for the undeformed specimen, and K is a constant which depends upon the number of active chains and, according to James and Guth, upon the manner in which the network is formed. They proceed to express the configurational entropy of the network as

$$S=k \ln C=\text{const}-(kK/2)(\alpha_x^2+\alpha_y^2+\alpha_z^2). \quad (5)$$

Two major errors are committed in computing the "entropy" in this manner. In the first place, account is taken of only *one particular network structure* out of the many which might be formed by the cross-linking process. This single structure requires unique specification of the pairs of units which are joined with one another by cross-linkages. Although the network which is formed in any given case is, to be sure, a unique structure, there are no constraints on the cross-linking process which favor this particular array of cross-linked pairs of units over the many others which are possible. Actual cross-linking processes proceed in a random manner, as do all other chemical processes unassisted by a Maxwell Demon. For the calculation of the entropy of

[12] A three-dimensional equivalent of Eq. (3) would evidently violate all the symmetry conditions set forth earlier. Extended to three dimensions, Eq. (3) would suggest an aeolotropic (instead of isotropic) system with three mutually perpendicular polar axes.

[13] $c(\mathbf{r}_i)$ equals $p(x, y, z)$ of Eq. (1) multiplied by the total number of configurations for all values of $\mathbf{r}_i$.

the system, all states consistent with the macroscopic restraints must be considered.

This situation finds close analogy to the "frozen in" entropy of a glass. As the liquid is cooled below the glass transition temperature its molecules no longer are able to rearrange to new configurations. Hence, it may be said that the molecules of the glass are restricted to a single configuration. However, the glass is just as disordered as the liquid (although the latter is subject to rapid changes of configuration), and their configurational entropies are the same (at the glass-type second-order transition). Correct computation of the configurational entropy of the glass requires counting of *all* configurations which might have been frozen in, not merely the one which actually happened to exist. Application of the James and Guth interpretation to a glass would lead one to conclude that its entropy, like that of a crystal, should become zero at absolute zero.

The second major error committed by James and Guth in deriving the configurational entropy arises from their failure to take account of the dependence of the probability of the cross-linked state on the volume.[14] The distribution of ν units designated for cross-linking over the volume V leads to an entropy term $k\nu \ln V$, while the necessity that they meet in pairs diminishes this by $-(k\nu/2) \ln V$. We shall discuss the incorporation of the resulting term $(k\nu/2) \ln V$ in their theory later on.

An unequivocal derivation of the configurational entropy of network formation can be carried out by considering the probability that the non-cross-linked system will occur spontaneously in a configuration equivalent to that of a cross-linked network subject to such macroscopic constraints as may apply. These latter may include conditions of deformation. To this end it is appropriate to consider first the number of ways of selecting ν units for cross-linking out of a total of n units in the system. The resulting combinatory factor, $n!/\nu!(n-\nu)!$, enters as a constant which is of no particular interest in the network problem. Next, account must be taken of the probability that the chain displacement vectors (the $\mathbf{r}_i$'s) possess a suitable distribution of values. Finally, we consider the probability that $\nu/2$ pairs of the units designated for cross-linking occur in suitable juxtaposition. If no restraints are imposed on the system, i.e., if the network is to remain undeformed, the chains are unrestricted and hence will assume their most probable length distribution (gaussian). The second probability factor above may then be disregarded. The first and third would occur in precisely the same manner in the computation of the entropy for a corresponding chemical combination of analogous monomeric species; the statistical nature of the polymer chains is of no consequence whatever insofar as the entropy change on cross-linking without deformation is concerned. From a statistical point of view, all that is involved is the random scattering of cross-linkages among various acceptable sites in the system.

The theory of James and Guth is incompatible with the inescapable conclusion already drawn. According to them, the introduction of cross-linkages, even without subsequent macroscopic deformation, decreases the entropy associated with the configurational arrangement of the chains by an amount which will depend on their structural character. This fallacy is a further consequence of their identification of the configurational probability with the number of configurations which the specific network structure may assume. The same reasoning applied to a gas would lead to the conclusion that the mere insertion of a partition dividing the volume occupied by the gas would lower its entropy since fewer configurations remain possible. They further contend that the successive insertion of cross-linkages immediately inspires the chains to retract toward their most probable states, for which $\mathbf{r}=0$. They consequently conclude that the introduction of random cross-linkages will displace the system from its initially random arrangement! It would make equal sense to assert that introduction of isotopic atoms into occasional units of polymer molecules would cause each molecule to coil up tightly to satisfy the postulated retractive force in each "chain" between the isotopically tagged units. Due regard for statistical fluctuations in the $\mathbf{r}_i$ would avoid such absurdities.

When the network is deformed, the cross-linkages (or their most probable positions) must necessarily be displaced relative to one another in direct proportion, on the average, to the relative changes (α_x, α_y, and α_z) in the macrodimensions. The distribution of the $\mathbf{r}_i$'s will be correspondingly transformed. Since the structural units are selected for cross-linking at random, the sizes of the chains will vary widely. However, if it is assumed that the end-to-end vectors for chains of each size are transformed in accordance with the α's, no error is introduced if all chains are taken to be of the same size. We require the probability that these chains occur spontaneously with the required end-to-end vector distribution. Following a method employed earlier,[6] let the probability of an end-to-end vector $\mathbf{r}_j$ be expressed as a gaussian function of the magnitude of $\mathbf{r}_j$, as in equation (1a). Moreover, let the number of chains for which $\mathbf{r}=\mathbf{r}_j$ in the deformed network be represented by ν_j. The probability that the non-cross-linked chains occur spontaneously with the distribution characterized by a set of ν_j values will be given by

$$W=\nu!\prod_j[p(\mathbf{r}_j)]^{\nu_j}/\nu_j!=\nu^\nu\prod_j[p(\mathbf{r}_j)/\nu_j]^{\nu_j}. \tag{6}$$

In the undeformed state $\nu_j=\nu p(\mathbf{r}_j)$, which gives $W=1$; for the required deformed state

$$\nu_j=\nu p(x_j/\alpha_x,\ y_j/\alpha_y,\ z_j/\alpha_z), \tag{7}$$

where x_j/α_x, y_j/α_y and z_j/α_z are the components of the vector corresponding to $\mathbf{r}_j$ before deformation. Taking

[14] P. J. Flory, J. Chem. Phys. **18**, 108, 112 (1950).

the logarithm of W and replacing the sum by an integral, there is obtained

$$\ln W = -(\nu/2)(\alpha_x^2+\alpha_y^2+\alpha_z^2-3)+\nu \ln(\alpha_x\alpha_y\alpha_z).$$

The requirement that the selected units meet in pairs introduces a term $-(\nu/2)\ln V$ and an added constant, where V is the total volume.[14] Replacing V with $\alpha_x\alpha_y\alpha_z V_0$ and combining with the above, the entropy change for the cross-linking process assumes the form,

$$\Delta S_c = \text{const} - (k\nu/2)[\alpha_x^2+\alpha_y^2 + \alpha_z^2-3-\ln(\alpha_x\alpha_y\alpha_z)]. \quad (8)$$

The standard state entropy change associated with the pure chemical reaction involved is included in the constant. The same constant would apply also to the equivalent chemical combination of monomeric analogs; in fact, it represents precisely the entropy change for such a process conducted at the volume V_0. Noting further that the term in the α's (which may be regarded as the configurational entropy change) is zero when $\alpha_x=\alpha_y=\alpha_z=1$, it is apparent that the entropy change associated with vulcanization reduces, when no deformation is involved, to that for the equivalent chemical process. This is in accordance with the preceding discussion, although in contradiction with the implications of the James and Guth Eq. (5). The entropy change relative to the undeformed state $\alpha_x=\alpha_y=\alpha_z=1$ is, according to Eq. (8),

$$\Delta S = -(k\nu/2)[\alpha_x^2+\alpha_y^2+\alpha_z^2-3-\ln(\alpha_x\alpha_y\alpha_z)], \quad (9)$$

the last term being zero for a deformation at constant volume. The corresponding expression for a network of any functionality f is given in reference 14.

James and Guth have criticized the above procedure on the grounds that inclusion of the permutation factor in Eq. (7) is unrealistic because the chains are permanently fixed in the network structure. As has been discussed above, this permutation factor is included to take into account all structures consistent with network formation.[15] They have asserted also that treatments such as the foregoing rest on the assumption that the network junctions are fixed in space. No such assumption has been made for it would, in fact, be quite foreign to the treatment. Only the *distribution* of chain end-to-end vectors matters, the exact values for individual chains being of no concern. Random fluctuations of the junctions about their mean positions obviously will occur but these have no sensible influence on the entropy.

In defense of the James and Guth treatment it may be argued that a hypothetical system capable of being cross-linked in only one way may be imagined, and the unique network structure formed from it probably would be rubber-like. Suppose, for example, that among the polymer units there are two of each of $\nu/2$ *different types* of reactive groups and that two of the same type only may unite to form a cross-linkage. If the randomness associated with the distribution of the reactive units over the chains is disregarded, a network structure derived therefrom would certainly be unique (if indeed it formed at all). All that is required to render the James and Guth Eq. (5) acceptable for such a hypothetical network is the addition of a term $(k\nu/2)\ln V$ (see above) expressing the randomness of the distribution of the $\nu/2$ cross-linkages over the volume V. Taking V proportional to $\alpha_x\alpha_y\alpha_z$, and noting further that the K of James and Guth would become identical with ν, when the randomness of cross-linking is recognized, Eq. (5) with the foregoing term added to it assumes the same form as (8). Hence, appropriate correction of their theory establishes concordance with the work of others.

James and Guth[2,3] have discussed at length the status of network imperfections arising from ends of polymer chains, a subject dealt with earlier by one of us.[10] They establish the inequality (expressed in the previous notation)[10] that

$$\nu < (\nu_0 - N),$$

where ν is the effective number of chains when $\nu_0/2$ cross-linkages are introduced into N linear polymer chains. They erroneously assert that one of us has treated this as an equality. The correct relationship has been shown[10] to be

$$\nu = \nu_0 - 2N,$$

from which James and Guth's inequality follows at once. Their objections[2] to the treatment of network imperfections in butyl rubber[16] arise from their failure to transcribe this equation correctly in their notation, and hence are without foundation.

We believe that the foregoing discussion disposes of the major points of disagreement between the theoretical interpretations of James and Guth and those of other authors.

[15] The permutation entropy and its significance has been discussed in detail by Kuhn and Grün (see reference 5).

[16] P. J. Flory, Ind. Eng. Chem. **38**, 417 (1946).

Magnetic Study of Some Inorganic Compounds of Arsenic, Antimony, and Bismuth

MATA PRASAD, C. R. KANEKAR, AND L. N. MULAY
Chemical Laboratories, Institute of Science, Bombay, India

(Received April 27, 1951)

In the graphs of the molecular susceptibilities χ_m of some salts of As, Sb, and Bi, containing the same anions against Z, the total number of electrons in them are nonlinear in each case if all the salts are taken into consideration. These graphs are, however, similar in nature and bring out the family relationship of these cations. Ikenmeyer's relation is seen to hold true only in the case of the halides of As, Sb, and Bi and the salts of these cations in combination with the same anion.

The linear relation observed between χ_m of the salts of As, Sb, and Bi containing the same anion and the number of electrons N in the cations has been used to evaluate the susceptibilities of the cations and the anions in combination with them. The significance of this relation and its advantages over other methods of determining ionic susceptibilities have been discussed. The experimental susceptibilities of these cations have been compared with the theoretical values calculated by Slater's and Angus' methods and have been used to evaluate the radii of the cations.

THE literature reports widely different values deduced either theoretically or experimentally for the susceptibility of an ion or an atom. Prasad and co-workers[1a] have discussed the probable reasons for these divergences. They have systematically investigated the magnetic susceptibilities of salts of Li, Na, K, Ca, Sr, Ba, Mg, Zn, Cd, Hg(*ous*) and Hg(*ic*), Ag, NH_4, and Pb with inorganic and organic acids.[1a,1b] They have evaluated the susceptibilities of these ions by the following two methods:

1. In order to obviate errors arising out of the choice of a particular value for the susceptibility of an anion as standard, they have subtracted all the known values of several anions from the molecular susceptibilities of the several compounds containing the anions, and have taken an arithmetic mean of the values thus obtained as the standard value for the cation.

2. They have observed that almost straight line graphs are obtained on plotting the molecular susceptibilities (χ_m) of compounds having the same anions and the cations belonging to a family of elements in the periodic table, against the number of electrons (N) in the cation, and have used this linear relation for evaluating the susceptibilities of the cat- and anions in such compounds.

In view of the fact that the second method does not involve any arbitrary assumptions, Prasad and co-workers consider it more acceptable than the first one.

The present paper deals with the measurement of the susceptibilities of some inorganic compounds of arsenic, antimony, and bismuth having common anions.

A reference to the literature shows that while the susceptibility of the trivalent Bi ion has been determined by Bhatnagar and Bahl[2] (from the molar susceptibilities of some of its compounds by assuming certain values for the anions as standard), the values for the susceptibilities of trivalent As and Sb ions have not been reported so far. The values reported in International Critical Tables for trivalent As and Sb have been deduced mainly from the molar susceptibilities of the organometallic compounds using Pascal's constants. Since these compounds are covalent, the reported values would probably represent the susceptibilities of trivalent As and Sb atoms and not ions.

In this paper, attempts have been made to see whether the graphical method of Prasad and co-workers[1a,1b] is applicable to the salts of metalloids and to compare the experimentally deduced values with the theoretical ones. The value $\chi_{Bi^{+3}}$ has been theoretically calculated by Bhatnagar and Bahl[2] but the theoretical values of $\chi_{As^{+3}}$ and $\chi_{Sb^{+3}}$ do not appear to have been evaluated so far by any of the known methods.

EXPERIMENTAL

Most of the compounds used in this investigation were either of Merck's extra pure or of British Drug House Analytical Reagent quality. Those which could not be obtained in a pure state were prepared in the laboratory by the standard methods, and the irpurity was ascertained before use by analysis. Care was particularly taken to see that ferromagnetic impurities were totally absent.

The susceptibilities of these compounds were measured on a modified form of Gouy's balance specially constructed by Prasad and co-workers. The details of the apparatus and the precautions to be taken are described by Prasad, Dharmatti, and Gokhale.[1b]

RESULTS

The results obtained are given in Table I, in which column 1 gives the chemical formulas of the substances

[1a] Prasad, Dharmatti, and Ghose, J. Chem. Phys. **17**, 819 (1949); Prasad, Kanekar, Walvekar, and Khanolkar, *ibid.* **18**, 936 (1950); Prasad, Dharmatti, Kanekar, and Khanolkar, *ibid.* **18**, 941 (1950).

[1b] Prasad, Dharmatti, and Kanekar, Proc. Indian Acad. Sci. **16A**, 307 (1942); Prasad, Dharmatti, and Gokhale, *ibid.* **20A**, 224 (1944); Prasad, Dharmatti, and Amin, *ibid.* **26A**, 312 (1947); Prasad, Dharmatti, and Khanolkar, *ibid.* **26A**, 328 (1947); Prasad, Dharmatti, Kanekar, and Bhobe, *ibid.* **31A**, 289 (1950); Prasad, Dharmatti, Kanekar, and Datar, *ibid.* **31A**, 389 (1950).

[2] S. S. Bhatnagar and B. S. Bahl, Current Sci. **4**, 153, 234 (1935).

TABLE I. Susceptibilities in 10^{-6} cgs unit.

Compounds	Z	χ_a	χ_m	χ_a (other workers)
$AsOCl:H_2O$	...	0.300	43.30	
As found 59.01 percent				
As theory 59.32 percent				
AsOCl	58	...	30.34	
$AsCl_3$	84	0.400	72.50	0.408 Kido[a]
				0.440 Pascal[b]
As_2O_3	90	0.209	41.34	0.270 Meyer[c]
As_2S_3	114	0.285	70.00	0.030 Meyer[c]
$AsBr_3$	138	0.337	106.00	
AsI_3	192	0.312	142.20	0.240 Farid[d]
As found 16.43 percent				
As theory 16.47 percent				
SbOCl	76	0.212	36.71	
$SbCl_3$	102	0.364	83.03	0.364 Pascal[e]
				0.376 Kido[a]
Sb_2O_3	126	0.190	55.39	0.190 Meyer[c]
Sb_2S_3	150	0.255	85.78	
$SbBr_3$	156	0.308	111.40	0.275 Pascal[e]
				0.317 Pascal[b]
SbI_3	210	0.293	147.20	0.120 Farid[d]
Sb found 14.70 percent				
Sb theory 14.91 percent				
BiOCl	108	0.199	51.83	
Bi found 28.36 percent				
Bi theory 28.77 percent				
$BiCl_3$	134	0.322	101.55	0.316 Bhatnagar and Bahl[f]
				0.322 Gnesotto and Binghinotto[g]
$BiBr_3$	188	0.303	136.00	0.328 Bhatnagar and Bahl[f]
				0.303 Gnesotto and Binghinotto[g]
Bi_2O_3	190	0.170	80.15	0.170 Bhatnagar and Bahl[f]
				0.170 Endo[h]
Bi_2S_3	214	0.240	122.90	0.240 Bhatnagar and Bahl[f]
				0.385 Gnesotto and Binghinotto[g]
BiI_3	242	0.271	161.00	0.340 Bhatnagar and Bahl[f]
				0.440 Meyer[c]

[a] K. Kido, Sci. Repts. Tohoku, Imp. Univ. **21**, 149, 288, 867 (1932).
[b] P. Pascal, Compt. rend. **218**, 57 (1944).
[c] S. Meyer, Ann. Physik **68**, 325 (1899); **69**, 236 (1899); **1**, 664 (1900).
[d] G. Farid, Science and Culture **6**, 370 (1940).
[e] P. Pascal, Compt. rend. **152**, 862, 1010 (1911).
[f] See reference 2.
[g] Gnesotto and Binghinotto, Atti del reale Institute Venelo di Scienze, lettere ed arti **69**, 1343 (1910); **72**, 1515 (1913); **74**, 25 (1914); **75**, 333 (195).
[h] H. Endo, Sci. Repts. Tohoku. Imp. Univ. **14**, 479 (1925).

together with their analysis in the case of those which were prepared in the laboratory; column 2 gives the total number of electrons (Z) in the compounds; the observed specific (χ_a) and the molecular (χ_m) susceptibilities are given in the 3rd and 4th columns, respectively. The hydrated salt investigated was arsenic oxychloride monohydrate, and the molecular susceptibility of the anhydrous salt has been obtained by subtracting the value for the susceptibility of a molecule of water (-12.96×10^{-6} cgs unit) from the molecular susceptibility of the hydrated salt. The last column gives the values of the specific susceptibilities observed by previous workers. All the values of the susceptibilities are expressed in terms of -1×10^{-6} cgs unit.

DISCUSSION OF RESULTS

It will be seen from Table I that although the specific susceptibilities of many compounds obtained by the authors agree quite well with those found by previous workers, some of their values are much lower.

(a) Graphical Discussion of the Molar Susceptibilities

Prasad and co-workers[1a,1b] have shown that when the molecular susceptibilities (χ_m) of compounds containing (i) Li, Na, K, (ii) Mg, Zn, Cd, Hg, (iii) and Ca, Sr, Ba, which belong to a particular group or subgroup of the periodic table, are plotted against the total number of electrons (Z) in the compounds, the plots obtained form patterns which are characteristic of the cations of the group or sub-group. The graphs obtained on plotting the molecular susceptibilities (χ_m) of the compounds of As, Sb, and Bi against the corresponding values of Z, shown in Fig. 1, are strikingly similar and thus bring out a similarity in the magnetic behavior of the salts of a group of cations having similar electronic configurations, and lend support to the conclusions arrived at by Prasad and coworkers.[1a,1b]

The graphs in Fig. 1, also show that (i) the Ikenmeyer's[3] relation ($\chi_m=C_1Z+C_2$) does not hold true for all the salts of As, Sb, and Bi, and (ii) the points corre-

[3] K. Ikenmeyer, Ann. Physik **5**, 1, 190 (1929).

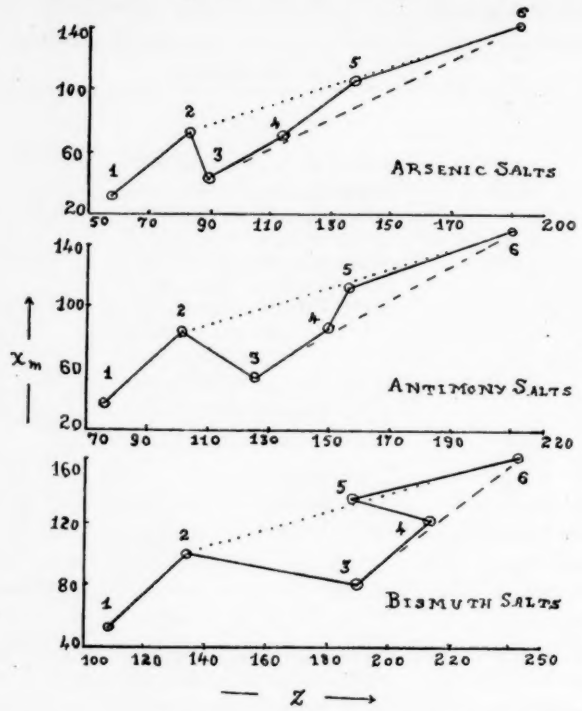

FIG. 1. χ_m plotted against Z for several salts of As, Sb, and Bi. 1—Oxychloride; 2—Chloride; 3—Oxide; 4—Sulfide; 5—Bromide; 6—Iodide.

sponding to chlorides, bromides, and iodides in each of the three curves lie on straight lines (shown by dotted lines). This indicates that Ikenmeyer's relation is probably valid for these compounds only. The constants C_1 and C_2 for each of the dotted straight lines are given in Table II, and have been used to calculate the values of χ_m with a view to establish the fact that the plotted points lie on straight lines.

It will be seen that the values of C_1 and C_2 for each straight line are nearly the same. This observation is

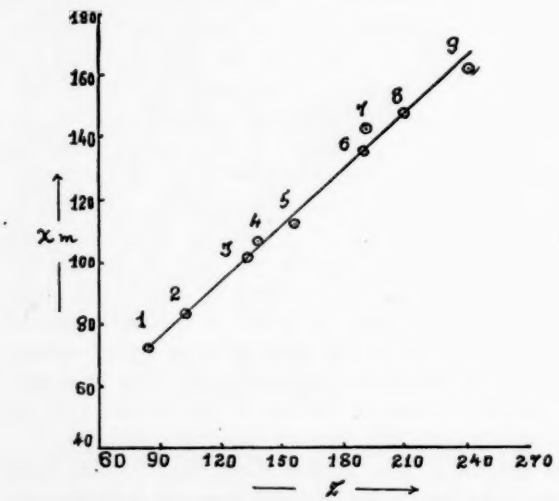

FIG. 2. χ_m plotted against Z for the halides of As, Sb, and Bi. 1, 2, 3—Chlorides; 4, 5, 6—Bromides; 7, 8, 9—Iodides; corresponding in each case to As, Sb, and Bi.

significant and shows that the plots of χ_m against Z for all halides of As, Sb, and Bi should lie on the same straight line. This is found to be so (see Fig. 2). It may be therefore concluded that the salts containing chemically related cations in combination with the chemically related anions obey Ikenmeyer's relation.[9]

It is further seen from Fig. 1 that the points 3, 4, and 6, corresponding in each case to oxide, sulfide, and iodide, are also collinear. The values of the constants C_1 and C_2 for these straight lines are given in Table III.

These values are not the same in the three cases, and hence the plots of χ_m against Z for the oxides, sulfides, and iodides of As, Sb, and Bi would not lie on the same straight line. This is seen from the zig-zag curve in Fig. 3. This shows that Ikenmeyer's relation does not hold true for salts which contain chemically related cations but not chemically related anions. However, Fig. 3 brings out the fact that Ikenmeyer's relation[3] holds true for salts of chemically related cations in combination with the same anion, since the points corresponding to the oxides, sulfides, and iodides of As, Sb, and Bi are found to lie on straight lines, shown in dashes in the figure.

TABLE II. 10^{-6} cgs unit.

Compound	C_1	C_2	X_m(cal)	X_m(obs)
$AsCl_3$			72.22	72.50
$AsBr_3$	0.642	18.30	106.89	106.00
AsI_3			141.56	142.20
$SbCl_3$			80.73	83.03
$SbBr_3$	0.615	18.00	113.94	111.40
SbI_3			147.15	147.20
$BiCl_3$			98.40	101.55
$BiBr_3$	0.600	18.00	130.80	136.00
BiI_3			163.20	161.00

(b) Ionic Susceptibilities of As^{+3}, Sb^{+3}, Bi^{+3}, and Anions in Combination with Them

The molecular susceptibilities (χ_m) of the salts of As, Sb, and Bi containing the same anion have been plotted against the number (N) of electrons in these cations and the graphs obtained are shown in Fig. 4. In each case the graphs are straight lines, that is, the relation $\chi_m = p_1 \cdot N + p_2$ is obeyed. These straight lines have been produced to meet the χ_m axis, and the values obtained for the intercepts (p_2) and the inclinations (p_1) are given in Table IV. The agreement between the values of χ_m calculated from these constants and the experimental values is fairly good.

Following the interpretation of Prasad and coworkers[1a,1b] of the above equation, the constants p_1 and p_2 have been used to calculate the susceptibilities of the cations and the anions which are recorded in Table V.

(c) Significance of $\chi_m - N$ Relation

1. The existence of a linear relation between χ_m and N for salts of As, Sb, and Bi with a common anion

shows that the susceptibility contribution per electron is the same for these cations (belonging to the same family of elements). This may be further interpreted to mean that there appears to be quantitative similarity in the linkages between these chemically related cations and the common anion.

2. The different values of the slopes (p_1) of $\chi_m - N$ straight lines indicate that the susceptibility contribution due to the cations to the molecular susceptibility of the salts depends on the nature of the combining anion.

3. The susceptibility of the anion in salts of a group of chemically related cations is a fixed quantity.

A comparison of the susceptibilities of the anions Cl′, Br′, and I′ obtained in the present investigation with the corresponding values deduced from the salts of other groups of the chemically related cations, such as (i) Li, Na, K (ii) Ca, Sr, Ba, and (iii) Mg, Zn, Cd, and Hg(*ic*) determined by Prasad and co-workers[1] by the same method indicates definitely that the susceptibility of an anion in combination with different groups of chemically related cations is different. The data reported so far by Prasad and co-workers is summarized in Table VI.

TABLE III. 10^{-6} cgs unit.

	C_1	C_2
As_2O_3, As_2S_3, AsI_3	0.970	− 44.00
Sb_2O_3, Sb_2S_3, SbI_3	1.010	− 64.00
Bi_2O_3, Bi_2S_3, BiI_3	1.500	−201.00

These results clearly bring out the advantages of the graphical method of deducing the susceptibilities over other methods.

(d) Comparison of the Experimental Values of the Susceptibilities of As^{+3}, Sb^{+3}, and Bi^{+3} with Those Obtained Theoretically

Values of the theoretical susceptibilities of As^{+3} and Sb^{+3} ions have been calculated by the authors according to Slater's[4] and Angus'[5] methods and are recorded in Table VII along with the values of Bi^{+3}. For the sake of comparison the average experimental values of the ionic susceptibilities of As^{+3}, Sb^{+3}, and Bi^{+3} have been calculated and are given in the first column of the table.

The agreement between the experimental and the theoretical values of As^{+3} and Bi^{+3} ions is quite good though it appears to be impaired to some extent in the case of Sb^{+3}.

(e) Ionic Radius

The ionic radii of As^{+3}, Sb^{+3}, and Bi^{+3} ions were calculated from their average susceptibilities by the method employed by Prasad and co-workers[1a,1b] These values expressed in A units are given in Table VIII, along with those obtained by Wyckoff.[6] The values reported by Bragg[7] for the radii of the atoms have been also given for the sake of comparison.

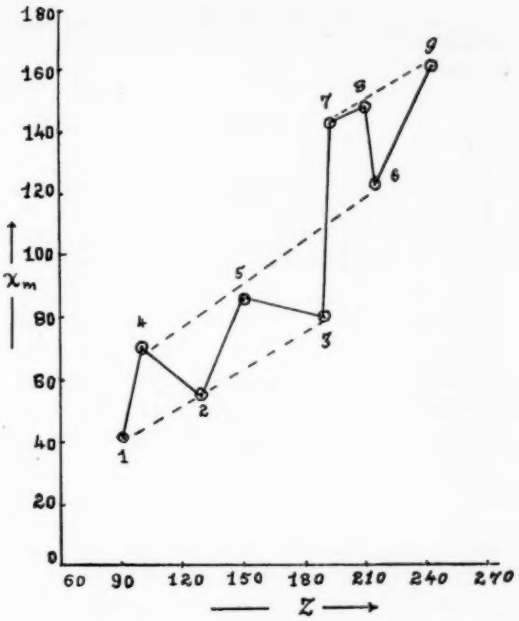

FIG. 3. χ_m plotted against Z for the oxides, sulfides, and iodides of As, Sb, and Bi. 1, 2, 3—Oxides; 4, 5, 6—Sulfides; 7, 8, 9—Iodides; corresponding in each case to As, Sb, and Bi.

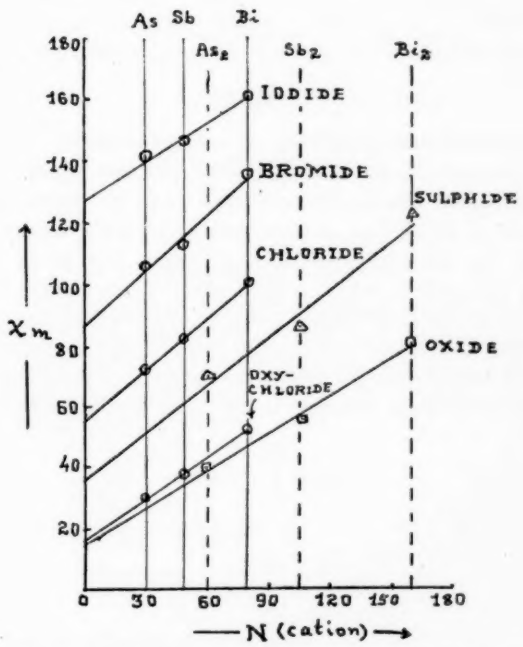

FIG. 4. χ_m plotted against N for compounds of As, Sb, and Bi containing the same anion.

[4] J. C. Slater, Proc. Leeds Phil. Soc. **1**, 484 (1929); Phys. Rev. **36**, 57 (1930).
[5] W. R. Angus, Proc. Roy. Soc. (London) **136A**, 569 (1932).
[6] Wyckoff, *The Structure of Crystals* (The Chemical Catalogue Company, Inc., New York, 1931), p. 192.
[7] W. L. Bragg, Phil. Mag. **40**, 170 (1920).

TABLE IV. 10^{-6} cgs unit.

Compounds	p_1	p_2
AsI_3, SbI_3, BiI_3	0.500	127.00
$AsBr_3$, $SbBr_3$, $BiBr_3$	0.571	87.20
$AsCl_3$, $SbCl_3$, $BiCl_3$	0.571	55.00
As_2S_3, Sb_2S_3, Bi_2S_3	0.545	36.00
AsOCl, SbOCl, BiOCl	0.500	15.00
As_2O_3, Sb_2O_3, Bi_2O_3	0.440	14.00

It will be seen that the value for the ionic radius of Bi^{+3} deduced by the authors is in good agreement with that of Wyckoff. Wyckoff has observed that the reported values 0.690 and 0.900 for As^{+3} and Sb^{+3} ions, respectively, are not very accurate.

TABLE V. 10^{-6} cgs unit.

Anions in combination	X_{anion}	$X_{As^{+3}}$	$X_{Sb^{+3}}$	$X_{Bi^{+3}}$
Bromide	29.06	17.13	27.40	45.68
Chloride	18.33	17.13	27.40	45.68
Sulfide	12.00	16.35	26.16	43.60
Iodide	42.33	15.00	24.00	40.00
Oxychloride	15.00	15.00	24.00	40.00
Oxide	4.66	13.20	21.12	35.20

SUMMARY

Magnetic susceptibilities of some inorganic salts of As, Sb, and Bi containing the same anion have been measured by the modified form of Gouy's balance. The graphs of χ_m against Z (the number of electrons in the salts) are definitely nonlinear in each case if all the salts are taken into consideration. This shows that Ikenmeyer's relation does not hold true for all the salts. The patterns obtained for the salts of As, Sb, and Bi are, however, similar and this shows the family relationship of these cations. It has been further observed that Ikenmeyer's relation holds true only for the halides of As, Sb, and Bi and the salts of these cations in combination with the same anion.

A linear relation has been shown to exist between the molecular susceptibilities (χ_m) of the salts of As, Sb, and Bi containing the same anion and the number of electrons (N) in the cations. The relation has been used to evaluate the susceptibilities of the cations and the anions in combination with them. The significance of this relation and its advantages over other methods of deducing susceptibilities of ions have been discussed.

The average values of experimental susceptibilities of As^{+3} and Bi^{+3} ions agree well with the corresponding theoretical values deduced by Slater's and Angus' methods. The agreement is impaired to some extent in the case of Sb^{+3}. These average experimental susceptibilities have been further used to calculate the ionic radii of As^{+3}, Sb^{+3}, and Bi^{+3} ions, of which the ionic radius of Bi^{+3} is in good agreement with the value reported by Wyckoff.

TABLE VI. 10^{-6} cgs unit.

Anion	X anion graphical method: Li, Na, K (Prasad and co-workers)	Mg, Ca, Sr, Ba (Prasad and co-workers)	Mg, Zn, Cd, Hg(*ic*) (Prasad and co-workers)	As, Sb, Bi authors
Iodide	49.00	49.00	44.00	42.33
Bromide	32.50	31.50	31.50	29.06
Chloride	22.50	23.00	23.00	18.33

TABLE VII. 10^{-6} cgs unit.

Cation	X_{cation} experimental (mean value)	X_{cation} Slater's method	X_{cation} Angus' method
As^{+3}	15.63	16.89	16.82
Sb^{+3}	25.01	30.50	30.44
Bi^{+3}	41.69	42.55	41.32

TABLE VIII.

Ion	Author	Wyckoff	Bragg
As^{+3}	1.901	0.690	1.260
Sb^{+3}	2.009	0.900	1.400
Bi^{+3}	1.235	1.210	1.480

A Study of Two-Center Integrals Useful in Calculations on Molecular Structure. I

C. C. J. ROOTHAAN
Department of Physics, University of Chicago, Chicago, Illinois
(Received June 22, 1951)

Convenient formulas have been obtained for the overlap integrals $\int \chi_a \chi_b dv$, kinetic energy integrals $-\frac{1}{2}\int \chi_a \Delta \chi_b dv$, nuclear attraction integrals $Z\int \chi_a(1/r_a)\chi_b dv$ and $Z\int \chi_b(1/r_a)\chi_b' dv$, and coulomb repulsion integrals $\int\int \chi_a(1)\chi_b(2)(1/r_{12})\chi_a'(1)\chi_b'(2)dv_1 dv_2$, where χ_a, χ_a', χ_b, χ_b' are Slater-type AO's on the centers a and b. Explicit formulas are given for all the integrals arising from the principal quantum numbers 1 and 2, for arbitrary values of the effective nuclear charges and the interatomic distance.

INTRODUCTION

IN calculations on molecular structure by either the VB (valence bond) or the MO (molecular orbital) method in LCAO (linear combinations of atomic orbitals) approximation, the molecular wave functions are built from AO's (atomic orbitals). The calculation of energies, transition moments, bond strengths, and other physical and chemical quantities then finally reduces to the evaluation of a great many integrals over these AO's. If we use Slater-type AO's, then all the integrals involving only two centers can be obtained in closed analytical form (except for one type, which is treated in Paper II in this series). These two-center integrals are the only ones occurring in diatomic molecules, and also the most important ones occurring in polyatomic molecules. Whereas formulas and tables for many of the two-center integrals can be found in the literature,[1] others are lacking; and it was considered worth while to undertake the systematic study of which this paper forms the first part. We shall give formulas which are convenient for numerical calculations for the overlap integrals, kinetic energy integrals, nuclear attraction integrals, and electronic repulsion integrals of the coulomb type. We shall consider all the possibilities arising from the principal quantum numbers 1 and 2, using Slater-type AO's with arbitrary values for the effective nuclear charges.

CHOICE OF UNITS AND COORDINATES

We shall use the following atomic units: lengths in units of the Bohr radius $a_H = 0.5293$A; energies in units of $e^2/a_H = 27.204$ ev. (This is twice the ionization energy of the hydrogen atom.)

In these units, the kinetic energy operator for an electron is $-\frac{1}{2}\Delta$, the potential energy of an electron at a distance r from a nucleus of charge Z is $-Z/r$, and the repulsion energy of two electrons 1 and 2 at a distance r_{12} apart is $1/r_{12}$.

The two centers we shall designate by subscripts a and b; their mutual distance by R.

To describe an electron with reference to the two centers, we shall use the following coordinate systems:

(i) Cartesian coordinates at the centers a and b. The Z axes we choose along the internuclear axis, pointing toward each other; the X axes we take parallel, and also the Y axes. Hence, on one of the two centers, say a, we have a right-handed coordinate system, and on the other center a left-handed one.

(ii) Spherical coordinates at the centers a and b; these are given in terms of the cartesian coordinates by

$$\left.\begin{aligned} r_a &= (x_a^2+y_a^2+z_a^2)^{\frac{1}{2}}, \quad \tan\theta_a = z_a/(x_a^2+y_a^2)^{\frac{1}{2}}, \quad \tan\phi_a = y_a/x_a, \\ r_b &= (x_b^2+y_b^2+z_b^2)^{\frac{1}{2}}, \quad \tan\theta_b = z_b/(x_b^2+y_b^2)^{\frac{1}{2}}, \quad \tan\phi_b = y_b/x_b. \end{aligned}\right\} \tag{1}$$

Note that if the same electron is described with reference to either atom a or atom b, then $x_a = x_b$, $y_a = y_b$, $\phi_a = \phi_b$.

(iii) Prolate spheroidal coordinates, defined by

$$\xi = (r_a+r_b)/R, \quad \eta = (r_a-r_b)/R, \quad \phi = \phi_a = \phi_b; \tag{2}$$

and conversely

$$\left.\begin{aligned} r_a &= \tfrac{1}{2}(\xi+\eta)R, \quad r_b = \tfrac{1}{2}(\xi-\eta)R, \\ \cos\theta_a &= (1+\xi\eta)/(\xi+\eta), \quad \cos\theta_b = (1-\xi\eta)/(\xi-\eta), \\ \sin\theta_a &= [(\xi^2-1)(1-\eta^2)]^{\frac{1}{2}}/(\xi+\eta), \\ \sin\theta_b &= [(\xi^2-1)(1-\eta^2)]^{\frac{1}{2}}/(\xi-\eta). \end{aligned}\right\} \tag{3}$$

For volume integration in these coordinates the volume element is $(R^3/8)(\xi^2-\eta^2)d\xi d\eta d\phi$; the integration limits are for ϕ from 0 to 2π, for η from -1 to 1, and for ξ from 1 to ∞.

TYPES OF INTEGRALS

We list below the types of integrals which we shall treat in this paper. We write for the general AO's on atom a, χ_a, χ_a', χ_a'', $\cdots$, and similarly with subscripts b for the AO's on atom b.

Overlap integrals:

$$(\chi_a|\chi_b) = \int \chi_a \chi_b dv; \tag{4}$$

Kinetic energy integrals:

$$(\chi_a|-\tfrac{1}{2}\Delta|\chi_b) = -\tfrac{1}{2}\int \chi_a \Delta \chi_b dv; \tag{5}$$

Nuclear attraction integrals:

$$(\chi_a|Z/r_a|\chi_b) = Z\int (\chi_a\chi_b/r_a)dv; \tag{6}$$

$$(\chi_b|Z/r_a|\chi_b') = Z\int (\chi_b\chi_b'/r_a)dv; \tag{7}$$

[1] See the bibliography.

TABLE I.

O_3		E	∞C_ϕ	i	∞iC_ϕ
$D_g^{(0)}$	S	1	1	1	1
$D_u^{(0)}$	S'	1	1	−1	−1
$D_g^{(1)}$	P'	3	$1+2\cos\phi$	3	$1+2\cos\phi$
$D_u^{(1)}$	P	3	$1+2\cos\phi$	−3	$-1-2\cos\phi$
$D_g^{(2)}$	D	5	$1+2\cos\phi+2\cos 2\phi$	5	$1+2\cos\phi+2\cos 2\phi$
$D_u^{(2)}$	D'	5	$1+2\cos\phi+2\cos 2\phi$	−5	$-1-2\cos\phi-2\cos 2\phi$
. . .		. . .	. . .	. . .	. . .
$D_g^{(l)}$	⋯	$2l+1$	$1+2\sum_{k=1}^{l}\cos k\phi$	$2l+1$	$1+2\sum_{k=1}^{l}\cos k\phi$
$D_u^{(l)}$	⋯	$2l+1$	$1+2\sum_{k=1}^{l}\cos k\phi$	$-2l-1$	$-1-2\sum_{k=1}^{l}\cos k\phi$

Coulomb repulsion integrals:

$$(\chi_a\chi_b|1/r|\chi_a'\chi_b') = \int\int [\chi_a(1)\chi_b(2)\chi_a'(1)\chi_b'(2)/r_{12}]dv_1dv_2. \quad (8)$$

CHOICE OF AO'S

For free atoms, the best AO's are SCF (self-consistent field) AO's obtained by solving Fock's equations for the atoms. These are available for a number of atoms in numerical tables, but are unsuitable in this form for our present purpose. A reasonable compromise is offered by Slater's AO's which are given in a simple analytical form. Moreover, it has been pointed out by Slater[2] that SCF AO's can be very closely approximated by a two- or three-term sum of Slater-type AO's.

For molecules, the best AO's are certainly not the Slater-type free-atom AO's, nor even the free-atom SCF AO's; but it should be possible to express the best AO's in this case also as a sum of Slater-type AO's. This justifies the evaluation of all our integrals with Slater-type AO's in which the effective nuclear charges are regarded as free parameters, and which contain only integral powers of r.

We shall use the Slater-type AO's in real form and normalized, namely,

$$(n, l, m) = (2\zeta)^{n+\frac{1}{2}}[(2n)!]^{-\frac{1}{2}} r^{n-1}e^{-\zeta r}S_{l,m}(\theta, \phi), \quad (9)$$

where the functions $S_{l,m}(\theta, \phi)$ are the normalized real spherical harmonics, defined by

$$S_{l,0}(\theta, \phi) = Y_{l,0}(\theta, \phi) = [(2l+1)/4\pi]^{\frac{1}{2}}P_l(\cos\theta),$$

$$S_{l,|m|}(\theta, \phi) = (1/\sqrt{2})\{Y_{l,-|m|}(\theta, \phi)+Y_{l,|m|}(\theta, \phi)\} = \left[\frac{2l+1}{2\pi}\cdot\frac{(l-|m|)!}{(l+|m|)!}\right]^{\frac{1}{2}}P_l^{|m|}(\cos\theta)\cos|m|\phi,$$

$$S_{l,-|m|}(\theta, \phi) = (1/\sqrt{2})\{Y_{l,-|m|}(\theta, \phi)-Y_{l,|m|}(\theta, \phi)\} = \left[\frac{2l+1}{2\pi}\cdot\frac{(l-|m|)!}{(l+|m|)!}\right]^{\frac{1}{2}}P_l^{|m|}(\cos\theta)\sin|m|\phi. \quad (10)$$

[2] Reference 10 in the bibliography.

The quantum number m is, of course, restricted by $-l\leqslant m\leqslant l$. The parameter ζ is connected with Slater's effective nuclear charge by $\zeta=Z/n$. The principal quantum number n is restricted by $n\geqslant l+1$, in order that (n, l, m) has no singularity at $r=0$. However, in the following we shall use for purely mathematical purposes also the AO's defined by Eq. (9) for $n=l$.

The quantum numbers l and m have a group-theoretical meaning with reference to the three-dimensional rotation-reflection group O_3, which is the symmetry group of a free atom. In Table I are given the characters of the irreducible representations of this group. The representation symbols S, P, D, ⋯, S', P', D', ⋯ are the standard spectroscopic symbols; the notation $D_{g,u}^{(l)}$ is more suitable for purely mathematical purposes.

The AO's (n, l, m) belong to $D_g^{(l)}$ or $D_u^{(l)}$ for l even or odd, respectively; m labels the $2l+1$ different AO's which transform together like $D_g^{(l)}$ or $D_u^{(l)}$ under symmetry operations. It is said that l indicates the *species*, and m the *subspecies* of the AO's *with respect to* O_3.

If two unlike atoms form a heteronuclear diatomic molecule, then the symmetry is reduced to $C_{\infty v}$. The character table of this group is given in Table II. The representation symbols Σ^+, Σ^-, Π, Δ, ⋯ are the standard spectroscopic symbols; A_1, A_2, and E_λ are more suitable for purely mathematical purposes.

The AO's (n, l, m) were defined with reference to a particular choice of the polar axis; we let this polar axis coincide with the diatomic axis. Then all AO's of the type $(n, l, 0)$ belong to the representation A_1; and every pair (n, l, λ) and $(n, l, -\lambda)$, $\lambda>0$, belongs to the representation E_λ of $C_{\infty v}$.

The customary notation for the AO's in diatomic molecules with reference to the groups O_3 and $C_{\infty v}$ is ns, $np\sigma$, $np\pi$, $nd\sigma$, $nd\pi$, $nd\delta$, ⋯; since this notation does not distinguish between $m=\pm\lambda$, we introduce a completely explicit notation by using π, δ, ⋯ for $m>0$ and $\bar{\pi}$, $\bar{\delta}$, ⋯ for $m<0$.

CHARGE DISTRIBUTIONS ON ATOMS

The integrals (7) and (8) can be interpreted as electrostatic interactions between charge distributions on the atoms a and b. Namely, Eq. (7) represents the interaction energy of a point charge Z on atom a with the charge distribution $\chi_b\chi_b'$ on atom b; and Eq. (8) represents the interaction energy of the two charge distributions $\chi_a\chi_a'$ and $\chi_b\chi_b'$. Omitting for the moment the subscript a or b, such a charge distribution $\chi\chi'$ has, apart from a numerical factor, the form

$$r^{n+n'-2}e^{-2\bar{\zeta}r}S_{l,m}(\theta,\phi)S_{l',m'}(\theta,\phi), \text{ with } \bar{\zeta}=\tfrac{1}{2}(\zeta+\zeta').$$

Now the product $S_{l,m}(\theta,\phi)S_{l',m'}(\theta,\phi)$ can always be expressed as a finite linear combination of spherical harmonics:

$$S_{l,m}(\theta,\phi)S_{l',m'}(\theta,\phi)=\sum_{L,M} a_{L,M}S_{L,M}(\theta,\phi).$$

Hence, it is obvious that the charge distribution $\chi\chi'$ can be written as a linear combination of the following *basic charge distributions*:

$$[N,L,M]=\left(\frac{2L+1}{4\pi}\right)^{\frac{1}{2}}\frac{2^L(2\bar{\zeta})^{N+2}}{(N+L+1)!}\times r^{N-1}e^{-2\bar{\zeta}r}S_{L,M}(\theta,\phi). \quad (11)$$

At a large distance $[N, L, M]$ acts like a multipole of order 2^L and magnitude $\bar{\zeta}^{-L}$. In analogy to the AO's, we shall denote these basic charge distributions by NS, $NP\Sigma, NP\Pi, NP\bar{\Pi}, ND\Sigma, ND\Pi, ND\bar{\Pi}, ND\Delta, ND\bar{\Delta}, \cdots$.

We give below the explicit expansions in terms of basic charge distributions for all the cases involving s and p electrons:

$$(ns)(n's)=(1+\tau)^{n+\frac{1}{2}}(1-\tau)^{n'+\frac{1}{2}}(n+n')![(2n)!(2n')!]^{-\frac{1}{2}}[n+n'-1,S],$$

$$\left.\begin{matrix}(ns)(n'p\sigma)\\(ns)(n'p\pi)\\(ns)(n'p\bar{\pi})\end{matrix}\right\}=\frac{1}{2\sqrt{3}}(1+\tau)^{n+\frac{1}{2}}(1-\tau)^{n'+\frac{1}{2}}\frac{(n+n'+1)!}{[(2n)!(2n')!]^{\frac{1}{2}}}\left\{\begin{matrix}[n+n'-1,P\Sigma]\\[n+n'-1,P\Pi],\\[n+n'-1,P\bar{\Pi}\end{matrix}\right.$$

$$\left.\begin{matrix}(np\sigma)(n'p\sigma)\\(np\sigma)(n'p\pi)\\(np\sigma)(n'p\bar{\pi})\\(np\pi)(n'p\pi)\\(np\pi)(n'p\bar{\pi})\\(np\bar{\pi})(n'p\bar{\pi})\end{matrix}\right\}=(1+\tau)^{n+\frac{1}{2}}(1-\tau)^{n'+\frac{1}{2}}\frac{(n+n'+2)!}{[(2n)!(2n')!]^{\frac{1}{2}}}\left\{\begin{matrix}\frac{(n+n')!}{(n+n'+2)!}[n+n'-1,S]+\frac{1}{10}[n+n'-1,D\Sigma]\\(\sqrt{3}/20)[n+n'-1,D\Pi]\\(\sqrt{3}/20)[n+n'-1,D\bar{\Pi}]\\\frac{(n+n')!}{(n+n'+2)!}[n+n'-1,S]\\\quad-(1/20)[n+n'-1,D\Sigma]+(\sqrt{3}/20)[n+n'-1,D\Delta]\\(\sqrt{3}/20)[n+n'-1,D\bar{\Delta}]\\\frac{(n+n')!}{(n+n'+2)!}[n+n'-1,S]\\\quad-(1/20)[n+n'-1,D\Sigma]-(\sqrt{3}/20)[n+n'-1,D\Delta]\end{matrix}\right. \quad (12)$$

where

$$\bar{\zeta}=\tfrac{1}{2}(\zeta+\zeta'), \quad \tau=(\zeta-\zeta')/(\zeta+\zeta'). \quad (13)$$

In Eqs. (12) the left-hand sides contain ζ and ζ' in the AO's; the right-hand sides contain $\bar{\zeta}$ in the charge distributions.

REDUCTION OF THE NUMBER OF INTEGRALS ON ACCOUNT OF THE MOLECULAR SYMMETRY

The AO's we classified according to the species and subspecies of $C_{\infty v}$, the symmetry group of our two-center problem: $\sigma, \pi, \bar{\pi}, \delta, \bar{\delta}, \cdots$.

The one-electron integrals (4), (5), and (6) all have the form $(\chi_a|M|\chi_b)$, where M is a totally symmetrical operator. Group theory provides the following useful theorem concerning such integrals:

Theorem I.—The integral $(\chi_a|M|\chi_b)$ vanishes if χ_a and χ_b belong to (i) different species, (ii) the same species, but different subspecies. Furthermore, the integral is independent of the subspecies.

TABLE II.

$C_{\infty v}$	E	$2C_\phi$	$\infty\sigma_v$
A_1 Σ^+	1	1	1
A_2 Σ^-	1	1	−1
E_1 Π	2	$2\cos\phi$	0
E_2 Δ	2	$2\cos2\phi$	0
. . . . .	. . . . .	. . . . .	. . . . .
E_λ ...	2	$2\cos\lambda\phi$	0

So, for instance, we have

$$(2p\sigma_a|M|3d\pi_b)=0,\quad (2p\pi_a|M|3d\bar{\pi}_b)=0,$$
$$(2p\pi_a|M|3d\pi_b)=(2p\bar{\pi}_a|M|3d\pi_b).$$

If we consider s and p AO's only, the integrals $(\chi_a|M|\chi_b)$ to be evaluated are

$$(ns_a|M|n's_b),\ (ns_a|M|n'p\sigma_b),$$
$$(np\sigma_a|M|n'p\sigma_b),\text{ and }(np\pi_a|M|n'p\pi_b).$$

The basic charge distributions on an atom we also classified according to the species and subspecies of $C_{\infty v}$: Σ, Π, $\bar{\Pi}$, Δ, $\bar{\Delta}$, $\cdots$. If we designate the basic charge distributions in general by Ω_a and Ω_b, then for a coulomb integral

$$[\Omega_a|\Omega_b]=\int\int[\Omega_a(1)\Omega_b(2)/r_{12}]dv_1dv_2 \qquad (14)$$

a theorem analogous to that for the one-electron integrals $(\chi_a|M|\chi_b)$ holds:

Theorem II.—The integral $[\Omega_a|\Omega_b]$ vanishes if Ω_a and Ω_b belong to (i) different species, (ii) the same species, but different subspecies. Furthermore, the integral is independent of the subspecies.

The nuclear attraction integrals (7) are similar to the coulomb integrals; instead of the charge distribution Ω_a there occurs a point charge, which we symbolize by a; so we write $Z\int\Omega_b dv/r_a=[a|\Omega_b]$. The point charge a can be considered as a limiting case of a charge distribution Ω_a of S type. Obviously then, $[a|\Omega_b]$ vanishes unless Ω_b is of species Σ.

If we consider again s and p AO's only, we obtain S, P, and D charge distributions. This leads to the following types of basic integrals: $[a|NS_b]$, $[a|NP\Sigma_b]$, $[a|ND\Sigma_b]$; $[NS_a|N'S_b]$, $[NS_a|N'P\Sigma_b]$, $[NS_a|N'D\Sigma_b]$, $[NP\Sigma_a|N'P\Sigma_b]$, $[NP\Sigma_a|N'D\Sigma_b]$, $[ND\Sigma_a|N'D\Sigma_b]$; $[NP\Pi_a|N'P\Pi_b]$, $[NP\Pi_a|N'D\Pi_b]$, $[ND\Pi_a|N'D\Pi_b]$; $[ND\Delta_a|N'D\Delta_b]$.

THE ONE-ELECTRON INTEGRALS $(\chi_a|M|\chi_b)$

The one-electron integrals $(\chi_a|M|\chi_b)$ are obviously functions of the three parameters ζ_a, ζ_b, and R. The final results are most conveniently written down in terms of the parameters ζ, τ, ρ, κ, ρ_a, and ρ_b, defined by

$$\left.\begin{aligned}&\zeta=\tfrac{1}{2}(\zeta_a+\zeta_b),\\&\tau=(\zeta_a-\zeta_b)/(\zeta_a+\zeta_b),\\&\rho=\tfrac{1}{2}(\zeta_a+\zeta_b)R;\end{aligned}\right\} \qquad (15)$$

$$\left.\begin{aligned}&\kappa=\tfrac{1}{2}(\tau+1/\tau)=(\zeta_a^2+\zeta_b^2)/(\zeta_a^2-\zeta_b^2),\\&\rho_a=(1+\tau)\rho=\zeta_aR,\\&\rho_b=(1-\tau)\rho=\zeta_bR.\end{aligned}\right\} \qquad (16)$$

We shall consider ζ, τ, ρ as the independent parameters. The original parameters ζ_a, ζ_b, and R are defined in terms of ζ, τ, and ρ by

$$\zeta_a=(1+\tau)\zeta,\quad \zeta_b=(1-\tau)\zeta,\quad R=\rho/\zeta. \qquad (17)$$

We proceed now to show how the kinetic energy integrals ($M=-\frac{1}{2}\Delta$) and the nuclear attraction integrals (6) ($M=Z/r_a$) can be expressed in terms of the overlap integrals ($M=1$). Namely, from the definition of the AO's (9) it is easily established that

$$-\tfrac{1}{2}\Delta(n,l,m)$$
$$=-\tfrac{1}{2}\zeta^2\Big\{(n,l,m)-2(2n/2n-1)^{\frac{1}{2}}(n-1,l,m)+\frac{4(n+l)(n-l-1)}{[2n(2n-1)(2n-2)(2n-3)]^{\frac{1}{2}}}(n-2,l,m)\Big\} \qquad (18)$$

and

$$(Z/r)(n,l,m)=2Z\zeta(2n)^{\frac{1}{2}}(2n-1)^{-\frac{1}{2}}(n-1,l,m). \qquad (19)$$

Applying Eqs. (18) and (19) for $(n,l,m)\rightarrow(n,l,m)_a$, $\zeta\rightarrow\zeta_a$, $r\rightarrow r_a$, and using Eqs. (17), we find

$$\{(n,l,m)_a|-\tfrac{1}{2}\Delta|(n',l',m)_b\}$$
$$=\{-\tfrac{1}{2}\Delta(n,l,m)_a|(n',l',m)_b\}$$
$$=-\tfrac{1}{2}\zeta^2(1+\tau)^2\Big[\{(n,l,m)_a|(n',l',m)_b\}-2(2n)^{\frac{1}{2}}(2n-1)^{-\frac{1}{2}}\{(n-1,l,m)_a|(n',l',m)_b\}+\frac{4(n+l)(n-l-1)}{[2n(2n-1)(2n-2)(2n-3)]^{\frac{1}{2}}}\times\{(n-2,l,m)_a|(n',l',m)_b\}\Big], \qquad (20)$$

$$\{(n,l,m)_a|Z/r_a|(n',l',m)_b\}$$
$$=2Z\zeta(1+\tau)[2n(2n-1)]^{-\frac{1}{2}}\times\{(n-1,l,m)_a|(n',l',m)_b\}. \qquad (21)$$

Applying Eqs. (20) and (21) for $1s$, $2s$, and $2p$ AO's, we obtain the explicit formulas

$$\left.\begin{aligned}&(1s_a|-\tfrac{1}{2}\Delta|1s_b)=-\tfrac{1}{2}\zeta^2(1+\tau)^2\{(1s_a|1s_b)-2\sqrt{2}(0s_a|1s_b)\},\\&(1s_a|-\tfrac{1}{2}\Delta|2s_b)=-\tfrac{1}{2}\zeta^2(1+\tau)^2\{(1s_a|2s_b)-2\sqrt{2}(0s_a|2s_b)\},\\&(2s_a|-\tfrac{1}{2}\Delta|2s_b)=-\tfrac{1}{2}\zeta^2(1+\tau)^2\{(2s_a|2s_b)-(4/\sqrt{3})(1s_a|2s_b)+(2\sqrt{2}/\sqrt{3})(0s_a|2s_b)\},\\&(1s_a|-\tfrac{1}{2}\Delta|2p\sigma_b)=-\tfrac{1}{2}\zeta^2(1+\tau)^2\{(1s_a|2p\sigma_b)-2\sqrt{2}(0s_a|2p\sigma_b)\},\\&(2s_a|-\tfrac{1}{2}\Delta|2p\sigma_b)=-\tfrac{1}{2}\zeta^2(1+\tau)^2\{(2s_a|2p\sigma_b)-(4/\sqrt{3})(1s_a|2p\sigma_b)+(2\sqrt{2}/\sqrt{3})(0s_a|2p\sigma_b)\},\\&(2p\sigma_a|-\tfrac{1}{2}\Delta|2p\sigma_b)=-\tfrac{1}{2}\zeta^2(1+\tau)^2\{(2p\sigma_a|2p\sigma_b)-(4/\sqrt{3})(1p\sigma_a|2p\sigma_b)\},\\&(2p\pi_a|-\tfrac{1}{2}\Delta|2p\pi_b)=-\tfrac{1}{2}\zeta^2(1+\tau)^2\{(2p\pi_a|2p\pi_b)-(4/\sqrt{3})(1p\pi_a|2p\pi_b)\},\end{aligned}\right\} \qquad (22)$$

and

$$\left.\begin{aligned}
(1s_a|Z/r_a|1s_b)&=\sqrt{2}Z\zeta(1+\tau)(0s_a|1s_b),\\
(1s_a|Z/r_a|2s_b)&=\sqrt{2}Z\zeta(1+\tau)(0s_a|2s_b),\\
(2s_a|Z/r_a|1s_b)&=(1/\sqrt{3})Z\zeta(1+\tau)(1s_a|1s_b),\\
(2s_a|Z/r_a|2s_b)&=(1/\sqrt{3})Z\zeta(1+\tau)(1s_a|2s_b),\\
(1s_a|Z/r_a|2p\sigma_b)&=\sqrt{2}Z\zeta(1+\tau)(0s_a|2p\sigma_b),\\
(2s_a|Z/r_a|2p\sigma_b)&=(1/\sqrt{3})Z\zeta(1+\tau)(1s_a|2p\sigma_b),\\
(2p\sigma_a|Z/r_a|1s_b)&=(1/\sqrt{3})Z\zeta(1+\tau)(1p\sigma_a|1s_b),\\
(2p\sigma_a|Z/r_a|2s_b)&=(1/\sqrt{3})Z\zeta(1+\tau)(1p\sigma_a|2s_b),\\
(2p\sigma_a|Z/r_a|2p\sigma_b)&=(1/\sqrt{3})Z\zeta(1+\tau)(1p\sigma_a|2p\sigma_b),\\
(2p\pi_a|Z/r_a|2p\pi_b)&=(1/\sqrt{3})Z\zeta(1+\tau)(1p\pi_a|2p\pi_b).
\end{aligned}\right\}\quad(23)$$

In view of Eqs. (22) and (23) we now need explicit expressions for the overlap integrals only. Our overlap integrals, except those which involve the $0s$ and $1p$ AO's, have been evaluated by Mulliken, Rieke, Orloff, and Orloff.[2] Their formulas are given in terms of the functions

$$\left.\begin{aligned}
A_n(\rho)&=\int_1^\infty \xi^n e^{-\rho\xi}d\xi=n!\rho^{-n-1}e^{-\rho}\sum_{k=0}^{n}\rho^k/k!,\\
B_n(\tau\rho)&=\int_{-1}^{1}\eta^n e^{-\tau\rho\eta}d\eta\\
&=-A_n(\tau\rho)-(-1)^nA_n(-\tau\rho).
\end{aligned}\right\}\quad(24)$$

Note that in Eqs. (24) the definition of $A_n(\rho)$ by means of the integral only applies for $\rho>0$, since otherwise the integral diverges.

The cases $\tau=0$ and $\rho=0$ had to be dealt with separately, since if one puts $\tau=0$ or $\rho=0$ in the general formulas, one obtains the difference of two infinite terms, and the limits for $\tau\to0$ and $\rho\to0$ have to be calculated.

For those overlap integrals which were given by Mulliken *et al.* we derived our final formulas in terms of the six parameters (15) and (16) by substituting for $A_n(\rho)$ and $B_n(\tau\rho)$ the explicit expressions given by Eqs. (24); the remaining integrals involving the $0s$ and $1p$ AO's we evaluated in the same manner. The results are

$$\left.\begin{aligned}
(0s_a|1s_b)&=[(1-\tau^2)^{\frac{1}{2}}/\sqrt{2}\tau\rho][-(1-\kappa)e^{-\rho_a}+\{(1-\kappa)+\rho_b\}e^{-\rho_b}],\\
(1s_a|1s_b)&=[(1-\tau^2)^{\frac{1}{2}}/\tau\rho][-(1-\kappa)\{2(1+\kappa)+\rho_a\}e^{-\rho_a}+(1+\kappa)\{2(1-\kappa)+\rho_b\}e^{-\rho_b}],\\
(0s_a|2s_b)&=[(1-\tau^2)^{\frac{1}{2}}/6^{\frac{1}{2}}\tau\rho][-(1-\kappa)(1-2\kappa)e^{-\rho_a}+\{(1-\kappa)(1-2\kappa)+2(1-\kappa)\rho_b+\rho_b^2\}e^{-\rho_b}],\\
(1s_a|2s_b)&=[(1-\tau^2)^{\frac{1}{2}}/\sqrt{3}\tau\rho][-(1-\kappa)\{2(1+\kappa)(2-3\kappa)+(1-2\kappa)\rho_a\}e^{-\rho_a}\\
&\qquad+(1+\kappa)\{2(1-\kappa)(2-3\kappa)+4(1-\kappa)\rho_b+\rho_b^2\}e^{-\rho_b}],\\
(2s_a|2s_b)&=[(1-\tau^2)^{\frac{1}{2}}/3\tau\rho][-(1-\kappa)\{2(1+\kappa)(7-12\kappa^2)+4(1+\kappa)(2-3\kappa)\rho_a+(1-2\kappa)\rho_a^2\}e^{-\rho_a}\\
&\qquad+(1+\kappa)\{2(1-\kappa)(7-12\kappa^2)+4(1-\kappa)(2+3\kappa)\rho_b+(1+2\kappa)\rho_b^2\}e^{-\rho_b}],\\
(0s_a|2p\sigma_b)&=[(1+\tau)/(1-\tau)]^{\frac{1}{2}}(1/\sqrt{2}\tau\rho^2)[-2(1-\kappa)^2(1+\rho_a)e^{-\rho_a}+\{2(1-\kappa)^2(1+\rho_b)+2(1-\kappa)\rho_b^2+\rho_b^3\}e^{-\rho_b}],\\
(1s_a|2p\sigma_b)&=[(1+\tau)/(1-\tau)]^{\frac{1}{2}}(1/\tau\rho^2)[-(1-\kappa)^2\{6(1+\kappa)(1+\rho_a)+2\rho_a^2\}e^{-\rho_a}\\
&\qquad+(1+\kappa)\{6(1-\kappa)^2(1+\rho_b)+4(1-\kappa)\rho_b^2+\rho_b^3\}e^{-\rho_b}],\\
(2s_a|2p\sigma_b)&=[(1+\tau)/(1-\tau)]^{\frac{1}{2}}(1/\sqrt{3}\tau\rho^2)[-(1-\kappa)^2\{6(1+\kappa)(3+4\kappa)(1+\rho_a)+2(5+6\kappa)\rho_a^2+2\rho_a^3\}e^{-\rho_a}\\
&\qquad+(1+\kappa)\{6(1-\kappa)^2(3+4\kappa)(1+\rho_b)+4(1-\kappa)(2+3\kappa)\rho_b^2+(1+2\kappa)\rho_b^3\}e^{-\rho_b}],\\
(1p\sigma_a|1s_b)&=[(1-\tau)/(1+\tau)]^{\frac{1}{2}}(\sqrt{3}/\tau\rho^2)[-(1-\kappa)\{2(1+\kappa)(1+\rho_a)+\rho_a^2\}e^{-\rho_a}\\
&\qquad+(1+\kappa)\{2(1-\kappa)(1+\rho_b)+\rho_b^2\}e^{-\rho_b}],\\
(1p\sigma_a|2s_b)&=[(1-\tau)/(1+\tau)]^{\frac{1}{2}}(1/\tau\rho^2)[-(1-\kappa)\{2(1+\kappa)(2-3\kappa)(1+\rho_a)+(1-2\kappa)\rho_a^2\}e^{-\rho_a}\\
&\qquad+(1+\kappa)\{2(1-\kappa)(2-3\kappa)(1+\rho_b)+(3-4\kappa)\rho_b^2+\rho_b^3\}e^{-\rho_b}],\\
(1p\sigma_a|2p\sigma_b)&=[\sqrt{3}/(1-\tau^2)^{\frac{1}{2}}\tau\rho^3][-(1-\kappa)^2\{12(1+\kappa)(1+\rho_a+\tfrac{1}{2}\rho_a^2)+2\rho_a^3\}e^{-\rho_a}\\
&\qquad+(1+\kappa)\{12(1-\kappa)^2(1+\rho_b+\tfrac{1}{2}\rho_b^2)+(3-4\kappa)\rho_b^3+\rho_b^4\}e^{-\rho_b}],\\
(2p\sigma_a|2p\sigma_b)&=[1/(1-\tau^2)^{\frac{1}{2}}\tau\rho^3][-(1-\kappa)^2\{48(1+\kappa)^2(1+\rho_a+\tfrac{1}{2}\rho_a^2)+2(5+6\kappa)\rho_a^3+2\rho_a^4\}e^{-\rho_a}\\
&\qquad+(1+\kappa)^2\{48(1-\kappa)^2(1+\rho_b+\tfrac{1}{2}\rho_b^2)+2(5-6\kappa)\rho_b^3+2\rho_b^4\}e^{-\rho_b}],\\
(1p\pi_a|2p\pi_b)&=[\sqrt{3}/(1-\tau^2)^{\frac{1}{2}}\tau\rho^3][-(1-\kappa)^2\{6(1+\kappa)(1+\rho_a)+2\rho_a^2\}e^{-\rho_a}\\
&\qquad+(1+\kappa)\{6(1-\kappa)^2(1+\rho_b)+4(1-\kappa)\rho_b^2+\rho_b^3\}e^{-\rho_b}],\\
(2p\pi_a|2p\pi_b)&=[1/(1-\tau^2)^{\frac{1}{2}}\tau\rho^3][-(1-\kappa)^2\{24(1+\kappa)^2(1+\rho_a)+12(1+\kappa)\rho_a^2+2\rho_a^3\}e^{-\rho_a}\\
&\qquad+(1+\kappa)^2\{24(1-\kappa)^2(1+\rho_b)+12(1-\kappa)\rho_b^2+2\rho_b^3\}e^{-\rho_b}];
\end{aligned}\right\}\quad(25)$$

$$
\begin{aligned}
&\tau=0,\\
&\quad(0s_a|1s_b)=(1/\sqrt{2})(1+\rho)e^{-\rho},\\
&\quad(1s_a|1s_b)=(1+\rho+\tfrac{1}{3}\rho^2)e^{-\rho},\\
&\quad(0s_a|2s_b)=6^{-\frac{1}{2}}(1+\rho+\tfrac{2}{3}\rho^2)e^{-\rho},\\
&\quad(1s_a|2s_b)=\tfrac{1}{2}\sqrt{3}[1+\rho+(4/9)\rho^2+(1/9)\rho^3]e^{-\rho},\\
&\quad(2s_a|2s_b)=[1+\rho+(4/9)\rho^2+(1/9)\rho^3\\
&\qquad\qquad+(1/45)\rho^4]e^{-\rho},\\
&\quad(0s_a|2p\sigma_b)=\tfrac{1}{3}\sqrt{2}\rho(1+\rho)e^{-\rho},\\
&\quad(1s_a|2p\sigma_b)=\tfrac{1}{2}\rho(1+\rho+\tfrac{1}{3}\rho^2)e^{-\rho},\\
&\quad(2s_a|2p\sigma_b)=(1/2\sqrt{3})\rho[1+\rho+(7/15)\rho^2\\
&\qquad\qquad+(2/15)\rho^3]e^{-\rho},\\
&\quad(1p\sigma_a|1s_b)=(1/\sqrt{3})\rho(1+\rho)e^{-\rho},\\
&\quad(1p\sigma_a|2s_b)=\tfrac{1}{6}\rho(1+\rho+\rho^2)e^{-\rho},\\
&\quad(1p\sigma_a|2p\sigma_b)=\tfrac{1}{2}\sqrt{3}(-1-\rho+\tfrac{1}{3}\rho^3)e^{-\rho},\\
&\quad(2p\sigma_a|2p\sigma_b)=[-1-\rho-\tfrac{1}{5}\rho^2+(2/15)\rho^3\\
&\qquad\qquad+(1/15)\rho^4]e^{-\rho},\\
&\quad(1p\pi_a|2p\pi_b)=\tfrac{1}{2}\sqrt{3}(1+\rho+\tfrac{1}{3}\rho^2)e^{-\rho},\\
&\quad(2p\pi_a|2p\pi_b)=[1+\rho+\tfrac{2}{5}\rho^2+(1/15)\rho^3]e^{-\rho};
\end{aligned}
\qquad (25a)
$$

$$
\begin{aligned}
&\rho=0,\\
&\quad(0s_a|1s_b)=(1/\sqrt{2})(1+\tau)^{\frac{1}{2}}(1-\tau)^{\frac{1}{2}},\\
&\quad(1s_a|1s_b)=(1+\tau)^{\frac{1}{2}}(1-\tau)^{\frac{1}{2}},\\
&\quad(0s_a|2s_b)=6^{-\frac{1}{2}}(1+\tau)^{\frac{1}{2}}(1-\tau)^{5/2},\\
&\quad(1s_a|2s_b)=\tfrac{1}{2}\sqrt{3}(1+\tau)^{\frac{1}{2}}(1-\tau)^{5/2},\\
&\quad(2s_a|2s_b)=(1+\tau)^{5/2}(1-\tau)^{5/2},\\
&\quad(0s_a|2p\sigma_b)=(1s_a|2p\sigma_b)=(2s_a|2p\sigma_b)\\
&\qquad=(1p\sigma_a|1s_b)=(1p\sigma_a|2s_b)=0,\\
&-(1p\sigma_a|2p\sigma_b)=(1p\pi_a|2p\pi_b)\\
&\qquad=\tfrac{1}{2}\sqrt{3}(1+\tau)^{\frac{1}{2}}(1-\tau)^{5/2},\\
&-(2p\sigma_a|2p\sigma_b)=(2p\pi_a|2p\pi_b)\\
&\qquad=(1+\tau)^{5/2}(1-\tau)^{5/2}.
\end{aligned}
\qquad (25b)
$$

THE NUCLEAR ATTRACTION INTEGRALS $(\chi_b|Z/r_a|\chi_b')$ AND THE COULOMB INTEGRALS $(\chi_a\chi_b|1/r|\chi_a'\chi_b')$

The nuclear attraction integrals (7) and the coulomb integrals (8) we shall evaluate making use of the charge distributions (12). We shall use the following notation which refers directly to the charge distributions:

$$
\left.
\begin{aligned}
(\chi_b|Z/r_a|\chi_b')&=[a|\chi_b\chi_b']Z,\\
(\chi_a\chi_b|1/r|\chi_a'\chi_b')&=[\chi_a\chi_a'|\chi_b\chi_b'].
\end{aligned}
\right\} \qquad (26)
$$

From Eqs. (12) we find for all the possible charge distributions arising from $1s$, $2s$, and $2p$ AO's the following expansions in terms of the basic charge distributions (11):

$$
\begin{aligned}
&(1s)(1s')=(1+\tau)^{\frac{1}{2}}(1-\tau)^{\frac{1}{2}}[1S],\\
&(1s)(2s)=\tfrac{1}{2}\sqrt{3}(1+\tau)^{\frac{1}{2}}(1-\tau)^{5/2}[2S],\\
&(2s)(2s')=(1+\tau)^{5/2}(1-\tau)^{5/2}[3S],\\
&\left.\begin{matrix}(1s)(2p\sigma)\\(1s)(2p\pi)\\(1s)(2p\bar{\pi})\end{matrix}\right\}=(1+\tau)^{\frac{1}{2}}(1-\tau)^{5/2}\left\{\begin{matrix}[2P\Sigma]\\[2P\Pi],\\[2P\overline{\Pi}]\end{matrix}\right.\\
&\left.\begin{matrix}(2s)(2p\sigma)\\(2s)(2p\pi)\\(2s)(2p\bar{\pi})\end{matrix}\right\}=(5/2\sqrt{3})(1+\tau)^{5/2}(1-\tau)^{5/2}\left\{\begin{matrix}[3P\Sigma]\\[3P\Pi],\\[3P\overline{\Pi}]\end{matrix}\right.\\
&\left.\begin{matrix}(2p\sigma)(2p\sigma')\\(2p\sigma)(2p\pi')\\(2p\sigma)(2p\bar{\pi}')\\(2p\pi)(2p\pi')\\(2p\pi)(2p\bar{\pi}')\\(2p\bar{\pi})(2p\bar{\pi}')\end{matrix}\right\}=(1+\tau)^{5/2}(1-\tau)^{5/2}\left\{\begin{matrix}[3S]+3[3D\Sigma]\\\tfrac{3}{2}\sqrt{3}[3D\Pi]\\\tfrac{3}{2}\sqrt{3}[3D\overline{\Pi}]\\[3S]-\tfrac{3}{2}[3D\Sigma]\\\quad+\tfrac{3}{2}\sqrt{3}[3D\Delta]\\\tfrac{3}{2}\sqrt{3}[3D\overline{\Delta}]\\[3S]-\tfrac{3}{2}[3D\Sigma]\\\quad-\tfrac{3}{2}\sqrt{3}[3D\Delta]\end{matrix}\right.
\end{aligned}
\qquad (27)
$$

Considering Theorem II and using Eqs. (27), we find for the nonvanishing nuclear attraction integrals the following expansions in terms of basic integrals:

$$
\begin{aligned}
&[a|1s_b1s_b']=(\tfrac{3}{2},\tfrac{3}{2})[a|1S_b],\\
&[a|1s_b2s_b]=\tfrac{1}{2}\sqrt{3}(\tfrac{3}{2},5/2)[a|2S_b],\\
&[a|2s_b2s_b']=(5/2,5/2)[a|3S_b],\\
&[a|1s_b2p\sigma_b]=(\tfrac{3}{2},5/2)[a|2P\Sigma_b],\\
&[a|2s_b2p\sigma_b]=(5/2\sqrt{3})(5/2,5/2)[a|3P\Sigma_b],\\
&[a|2p\sigma_b2p\sigma_b']=(5/2,5/2)\{[a|3S_b]\\
&\qquad\qquad+3[a|3D\Sigma_b]\};\\
&[a|2p\pi_b2p\pi_b']=[a|2p\bar{\pi}_b2p\bar{\pi}_b']\\
&\qquad=(5/2,5/2)\{[a|3S_b]\\
&\qquad\qquad-\tfrac{3}{2}[a|3D\Sigma_b]\},
\end{aligned}
\qquad (28)
$$

where (β,β') is an abbreviation for $(1+\tau)^{\beta}(1-\tau)^{\beta'}$.

In Eqs. (28) the left-hand sides contain the parameters ζ and ζ' in the AO's; the right-hand sides contain the parameter $\bar{\zeta}$ defined by Eq. (13).

In the coulomb integrals we have to deal with two charge distributions $\chi_a\chi_a'$ and $\chi_b\chi_b'$. We define accordingly

$$
\left.
\begin{aligned}
\bar{\zeta}_a&=\tfrac{1}{2}(\zeta_a+\zeta_a'),\quad \tau_a=(\zeta_a-\zeta_a')/(\zeta_a+\zeta_a'),\\
\bar{\zeta}_b&=\tfrac{1}{2}(\zeta_b+\zeta_b'),\quad \tau_b=(\zeta_b-\zeta_b')/(\zeta_b+\zeta_b').
\end{aligned}
\right\} \qquad (29)
$$

Considering Theorem II and using Eqs. (26), we find for the nonvanishing coulomb integrals the following

expansions in terms of basic integrals:

$$[1s_a1s_a'|1s_b1s_b']=(\tfrac{3}{2},\tfrac{3}{2},\tfrac{3}{2},\tfrac{3}{2})[1S_a|1S_b],$$
$$[1s_a1s_a'|1s_b2s_b]=\tfrac{1}{2}\sqrt{3}(\tfrac{3}{2},\tfrac{3}{2},\tfrac{3}{2},5/2)[1S_a|2S_b],$$
$$[1s_a1s_a'|2s_b2s_b']=(\tfrac{3}{2},\tfrac{3}{2},5/2,5/2)[1S_a|3S_b],$$
$$[1s_a2s_a|1s_b2s_b]=\tfrac{3}{4}(\tfrac{3}{2},5/2,\tfrac{3}{2},5/2)[2S_a|2S_b],$$
$$[1s_a2s_a|2s_b2s_b']=\tfrac{1}{2}\sqrt{3}(\tfrac{3}{2},5/2,5/2,5/2)[2S_a|3S_b],$$
$$[2s_a2s_a'|2s_b2s_b']=(5/2,5/2,5/2,5/2)[3S_a|3S_b],$$
$$[1s_a1s_a'|1s_b2p\sigma_b]=(\tfrac{3}{2},\tfrac{3}{2},\tfrac{3}{2},5/2)[1S_a|2P\Sigma_b],$$
$$[1s_a1s_a'|2s_b2p\sigma_b]=(5/2\sqrt{3})(\tfrac{3}{2},\tfrac{3}{2},5/2,5/2)[1S_a|3P\Sigma_b],$$
$$[1s_a2s_a|1s_b2p\sigma_b]=\tfrac{1}{2}\sqrt{3}(\tfrac{3}{2},5/2,\tfrac{3}{2},5/2)[2S_a|2P\Sigma_b],$$
$$[1s_a2s_a|2s_b2p\sigma_b]=(5/4)(\tfrac{3}{2},5/2,5/2,5/2)[2S_a|3P\Sigma_b],$$
$$[2s_a2s_a'|1s_b2p\sigma_b]=(5/2,5/2,\tfrac{3}{2},5/2)[3S_a|2P\Sigma_b],$$
$$[2s_a2s_a'|2s_b2p\sigma_b]=(5/2\sqrt{3})(5/2,5/2,5/2,5/2)[3S_a|3P\Sigma_b],$$
$$[1s_a1s_a'|2p\sigma_b2p\sigma_b']=(\tfrac{3}{2},\tfrac{3}{2},5/2,5/2)\{[1S_a|3S_b]+3[1S_a|3D\Sigma_b]\},$$
$$[1s_a1s_a'|2p\pi_b2p\pi_b']=[1s_a1s_a'|2p\bar{\pi}_b2p\bar{\pi}_b']=(\tfrac{3}{2},\tfrac{3}{2},5/2,5/2)\{[1S_a|3S_b]-\tfrac{3}{2}[1S_a|3D\Sigma_b]\},$$
$$[1s_a2s_a|2p\sigma_b2p\sigma_b']=\tfrac{1}{2}\sqrt{3}(\tfrac{3}{2},5/2,5/2,5/2)\{[2S_a|3S_b]+3[2S_a|3D\Sigma_b]\},$$
$$[1s_a2s_a|2p\pi_b2p\pi_b']=[1s_a2s_a|2p\bar{\pi}_b2p\bar{\pi}_b']=\tfrac{1}{2}\sqrt{3}(\tfrac{3}{2},5/2,5/2,5/2)\{[2S_a|3S_b]-\tfrac{3}{2}[2S_a|3D\Sigma_b]\},$$
$$[2s_a2s_a'|2p\sigma_b2p\sigma_b']=(5/2,5/2,5/2,5/2)\{[3S_a|3S_b]+3[3S_a|3D\Sigma_b]\},$$
$$[2s_a2s_a'|2p\pi_b2p\pi_b']=[2s_a2s_a|2p\bar{\pi}_b2p\bar{\pi}_b']=(5/2,5/2,5/2,5/2)\{[3S_a|3S_b]-\tfrac{3}{2}[3S_a|3D\Sigma_b]\},$$
$$[1s_a2p\sigma_a|1s_b2p\sigma_b]=(\tfrac{3}{2},5/2,\tfrac{3}{2},5/2)[2P\Sigma_a|2P\Sigma_b],$$
$$[1s_a2p\sigma_a|2s_b2p\sigma_b]=(5/2\sqrt{3})(\tfrac{3}{2},5/2,5/2,5/2)[2P\Sigma_a|3P\Sigma_b],\qquad(30)$$
$$[2s_a2p\sigma_a|2s_b2p\sigma_b]=(25/12)(5/2,5/2,5/2,5/2)[3P\Sigma_a|3P\Sigma_b],$$
$$[1s_a2p\pi_a|1s_b2p\pi_b]=[1s_a2p\bar{\pi}_a|1s_b2p\bar{\pi}_b]=(\tfrac{3}{2},5/2,\tfrac{3}{2},5/2)[2P\Pi_a|2P\Pi_b],$$
$$[1s_a2p\pi_a|2s_b2p\pi_b]=[1s_a2p\bar{\pi}_a|2s_b2p\bar{\pi}_b]=(5/2\sqrt{3})(\tfrac{3}{2},5/2,5/2,5/2)[2P\Pi_a|3P\Pi_b],$$
$$[2s_a2p\pi_a|2s_b2p\pi_b]=[2s_a2p\bar{\pi}_a|2s_b2p\bar{\pi}_b]=(25/12)(5/2,5/2,5/2,5/2)[3P\Pi_a|3P\Pi_b],$$
$$[1s_a2p\sigma_a|2p\sigma_b2p\sigma_b']=(\tfrac{3}{2},5/2,5/2,5/2)\{[2P\Sigma_a|3S_b]+3[2P\Sigma_a|3D\Sigma_b]\},$$
$$[1s_a2p\sigma_a|2p\pi_b2p\pi_b']=[1s_a2p\sigma_a|2p\bar{\pi}_b2p\bar{\pi}_b']=(\tfrac{3}{2},5/2,5/2,5/2)\{[2P\Sigma_a|3S_b]-\tfrac{3}{2}[2P\Sigma_a|3D\Sigma_b]\},$$
$$[2s_a2p\sigma_a|2p\sigma_b2p\sigma_b']=(5/2\sqrt{3})(5/2,5/2,5/2,5/2)\{[3P\Sigma_a|3S_b]+3[3P\Sigma_a|3D\Sigma_b]\},$$
$$[2s_a2p\sigma_a|2p\pi_b2p\pi_b']=[2s_a2p\sigma_a|2p\bar{\pi}_b2p\bar{\pi}_b']=(5/2\sqrt{3})(5/2,5/2,5/2,5/2)\{[3P\Sigma_a|3S_b]-\tfrac{3}{2}[3P\Sigma_a|3D\Sigma_b]\},$$
$$[1s_a2p\pi_a|2p\sigma_b2p\pi_b']=[1s_a2p\bar{\pi}_a|2p\sigma_b2p\bar{\pi}_b']=\tfrac{3}{2}\sqrt{3}(\tfrac{3}{2},5/2,5/2,5/2)[2P\Pi_a|3D\Pi_b],$$
$$[2s_a2p\pi_a|2p\sigma_b2p\pi_b']=[2s_a2p\bar{\pi}_a|2p\sigma_b2p\bar{\pi}_b']=(15/4)(5/2,5/2,5/2,5/2)[3P\Pi_a|3D\Pi_b],$$
$$[2p\sigma_a2p\sigma_a'|2p\sigma_b2p\sigma_b']=(5/2,5/2,5/2,5/2)\{[3S_a|3S_b]+3[3S_a|3D\Sigma_b]+3[3D\Sigma_a|3S_b]+9[3D\Sigma_a|3D\Sigma_b]\},$$
$$[2p\sigma_a2p\sigma_a'|2p\pi_b2p\pi_b']=[2p\sigma_a2p\sigma_a'|2p\bar{\pi}_b2p\bar{\pi}_b']$$
$$=(5/2,5/2,5/2,5/2)\{[3S_a|3S_b]-\tfrac{3}{2}[3S_a|3D\Sigma_b]+3[3D\Sigma_a|3S_b]-(9/2)[3D\Sigma_a|3D\Sigma_b]\},$$
$$[2p\pi_a2p\pi_a'|2p\pi_b2p\pi_b']=[2p\bar{\pi}_a2p\bar{\pi}_a'|2p\bar{\pi}_b2p\bar{\pi}_b']=(5/2,5/2,5/2,5/2)\{[3S_a|3S_b]-\tfrac{3}{2}[3S_a|3D\Sigma_b]$$
$$-\tfrac{3}{2}[3D\Sigma_a|3S_b]+(9/4)[3D\Sigma_a|3D\Sigma_b]+(27/4)[3D\Delta_a|3D\Delta_b]\},$$
$$[2p\pi_a2p\pi_a'|2p\bar{\pi}_b2p\bar{\pi}_b']=(5/2,5/2,5/2,5/2)\{[3S_a|3S_b]-\tfrac{3}{2}[3S_a|3D\Sigma_b]-\tfrac{3}{2}[3D\Sigma_a|3S_b]$$
$$+(9/4)[3D\Sigma_a|3D\Sigma_b]-(27/4)[3D\Delta_a|3D\Delta_b]\},$$
$$[2p\pi_a2p\bar{\pi}_a'|2p\pi_b2p\bar{\pi}_b']=(27/4)(5/2,5/2,5/2,5/2)[3D\Delta_a|3D\Delta_b],$$
$$[2p\sigma_a2p\pi_a'|2p\sigma_b2p\pi_b']=(27/4)(5/2,5/2,5/2,5/2)[3D\Pi_a|3D\Pi_b],$$

where $(\alpha, \alpha', \beta, \beta')$ is an abbreviation for $(1+\tau_a)^{\alpha}(1-\tau_a)^{\alpha'}(1+\tau_b)^{\beta}(1-\tau_b)^{\beta'}$.

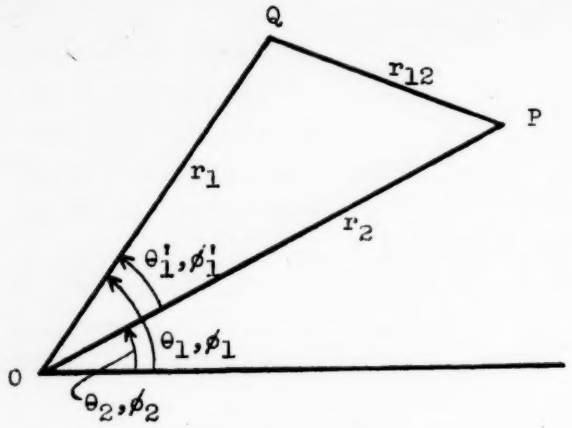

FIG. 1. Diagram of notation.

We turn now to the evaluation of the basic integrals. The integrals $[a|\Omega_b]$ are functions of $\bar{\xi}$ and R; we replace this set of parameters by $\bar{\xi}$ and $\rho=\bar{\xi}R$. The integrals are easily evaluated by introducing the spheroidal coordinates (2); they appear then in terms of $A_n(\rho)$ and $B_n(-\rho)$, the latter of which we convert to $B_n(\rho)$ by means of $B_n(-\rho)=(-1)^nB_n(\rho)$. Writing out $A_n(\rho)$ and $B_n(\rho)$, we obtain the final formulas:

$$\left.\begin{aligned}
[a|1S_b] &= (\bar{\xi}/\rho)\{1-(1+\rho)e^{-2\rho}\},\\
[a|2S_b] &= (\bar{\xi}/\rho)\{1-[1+(4/3)\rho+\tfrac{2}{3}\rho^2]e^{-2\rho}\},\\
[a|3S_b] &= (\bar{\xi}/\rho)\{1-(1+\tfrac{3}{2}\rho+\rho^2+\tfrac{1}{3}\rho^3)e^{-2\rho}\},\\
[a|2P\Sigma_b] &= (\bar{\xi}/\rho^2)\{1-(1+2\rho+2\rho^2+\rho^3)e^{-2\rho}\},\\
[a|3P\Sigma_b] &= (\bar{\xi}/\rho^2)\{1-[1+2\rho+2\rho^2+(6/5)\rho^3\\
&\qquad +\tfrac{2}{5}\rho^4]e^{-2\rho}\},\\
[a|3D\Sigma_b] &= (\bar{\xi}/\rho^3)\{1-[1+2\rho+2\rho^2+(4/3)\rho^3\\
&\qquad +\tfrac{2}{3}\rho^4+(2/9)\rho^5]e^{-2\rho}\}.
\end{aligned}\right\} \quad (31)$$

The integrals

$$[\Omega_a|\Omega_b]=\int\int[\Omega_a(1)\Omega_b(2)/r_{12}]dv_1dv_2$$

involve two volume integrations. The integration over the coordinates of one electron, say 1, amounts to calculating the potential of the corresponding charge distribution. These potentials can be found from the integrals (31) in the following manner.

Let the charge distribution of which we wish to know the potential be (see Eq. (11))

$$[N, L, M]=F(r)S_{L,M}(\theta, \phi).$$

Then the potential for electron 2 at the point P due to the charge distribution $[N, L, M]$ of electron 1 is given by (see Fig. 1)

$$U_{NLM}(r_2, \theta_2, \phi_2)=\int\int[F(r_1)S_{L,M}(\theta_1, \phi_1)/r_{12}]r_1^2dr_1d\omega_1,$$

where $d\omega_1$ is the infinitesimal solid angle. The angles θ_1, ϕ_1, and θ_2, ϕ_2 are defined with reference to the same polar axis and zero meridian. We now carry out a transformation of the integration variables $\theta_1, \phi_1 \rightarrow \theta_1', \phi_1'$, so that the new polar axis coincides with OP. Since the spherical harmonics $S_{L,M}$ are the basis of an irreducible representation of the rotation-reflection group O_3, we have

$$S_{L,M}(\theta_1, \phi_1)=\sum_{M'} c_{M'}S_{L,M'}(\theta_1', \phi_1'),$$

where the $c_{M'}$ are constants as far as the integration is concerned, but may depend on θ_2, ϕ_2, L, M. Because of the orthonormality of the spherical harmonics these $c_{M'}$ are given by

$$c_{M'}=\int S_{L,M}(\theta_1, \phi_1)S_{L,M'}(\theta_1', \phi_1')d\omega_1'.$$

It is further easily seen that

$$d\omega_1=d\omega_1'.$$

Carrying out the transformation, we find

$$U_{NLM}(r_2, \theta_2, \phi_2)$$
$$=\sum_{M'} c_{M'}\int[F(r_1)S_{L,M'}(\theta_1', \phi_1')/r_{12}]r_1^2dr_1d\omega_1'.$$

Now the integrals involving $S_{L,M'}(\theta_1', \phi_1')$ are just the nuclear attraction integrals $[a|\Omega_b]$ if we identify a with P, b with O, and R with r_2. We have seen that these integrals vanish unless Ω_b is of species Σ, that is, $M'=0$. Hence, we have

$$U_{NLM}(r_2, \theta_2, \phi_2)=c_0[a|NL0_b]_{\rho=\bar{\xi}r_2}.$$

The constant c_0 we find from

$$c_0=\int S_{L,M}(\theta_1, \phi_1)S_{L,0}(\theta_1', \phi_1')d\omega_1'.$$

This integral we evaluate by transforming θ_1', ϕ_1' back to θ_1, ϕ_1. Now

$$S_{L,0}(\theta_1', \phi_1')=[(2L+1)/4\pi]^{\frac{1}{2}}P_L(\cos\theta_1').$$

Since θ_1' is the angle POQ, we can make use of the addition theorem for the Legendre polynomials:

$$P_L(\cos\theta_1')$$
$$=[4\pi/(2L+1)]\sum_{M'} S_{L,M'}(\theta_2, \phi_2)S_{L,M'}(\theta_1, \phi_1),$$

so that

$$c_0=\sum_{M'}[4\pi/(2L+1)]^{\frac{1}{2}}S_{L,M'}(\theta_2, \phi_2)$$
$$\times\int S_{L,M}(\theta_1, \phi_1)S_{L,M'}(\theta_1, \phi_1)d\omega_1$$
$$=[4\pi/(2L+1)]^{\frac{1}{2}}S_{L,M}(\theta_2, \phi_2);$$

hence, we have

$$U_{NLM}(r, \theta, \phi)=[4\pi/(2L+1)]^{\frac{1}{2}}S_{L,M}(\theta, \phi)[a|NLO_b]_{\rho=\sigma}, \quad (32)$$

where $\sigma=\bar{\xi}r$.

Explicitly, we find for the potentials of the charge distributions arising from $1s$, $2s$, and $2p$ AO's

$$\left.\begin{aligned}
&U_{1S}=(\bar{\xi}/\sigma)\{1-(1+\sigma)e^{-2\sigma}\},\\
&U_{2S}=(\bar{\xi}/\sigma)\{1-[1+(4/3)\sigma+\tfrac{2}{3}\sigma^2]e^{-2\sigma}\},\\
&U_{3S}=(\bar{\xi}/\sigma)\{1-(1+\tfrac{3}{2}\sigma+\sigma^2+\tfrac{1}{3}\sigma^3)e^{-2\sigma}\},\\
&U_{\left\{\begin{smallmatrix}2P\Sigma\\2P\Pi\\2P\bar{\Pi}\end{smallmatrix}\right\}}=(\bar{\xi}/\sigma^2)\{1-(1+2\sigma+2\sigma^2+\sigma^3)e^{-2\sigma}\}\begin{cases}\cos\theta\\ \sin\theta\cos\phi,\\ \sin\theta\sin\phi\end{cases}\\
&U_{\left\{\begin{smallmatrix}3P\Sigma\\3P\Pi\\3P\bar{\Pi}\end{smallmatrix}\right\}}=(\bar{\xi}/\sigma^2)\{1-[(1+2\sigma+2\sigma^2+(6/5)\sigma^3+\tfrac{2}{5}\sigma^4]e^{-2\sigma}\}\begin{cases}\cos\theta\\ \sin\theta\cos\phi,\\ \sin\theta\sin\phi\end{cases}\\
&U_{\left\{\begin{smallmatrix}3D\Sigma\\3D\Pi\\3D\bar{\Pi}\\3D\Delta\\3D\bar{\Delta}\end{smallmatrix}\right\}}=(\bar{\xi}/\sigma^3)\{1-[1+2\sigma+2\sigma^2+(4/3)\sigma^3+\tfrac{2}{3}\sigma^4+(2/9)\sigma^5]e^{-2\sigma}\}\begin{cases}\tfrac{3}{2}\cos^2\theta-\tfrac{1}{2}\\ \sqrt{3}\cos\theta\sin\theta\cos\phi\\ \sqrt{3}\cos\theta\sin\theta\sin\phi\\ (\sqrt{3}/2)\sin^2\theta(\cos^2\phi-\sin^2\phi)\\ \sqrt{3}\sin^2\theta\cos\phi\sin\phi\end{cases}.
\end{aligned}\right\}\tag{33}$$

The basic coulomb integrals $[\Omega_a|\Omega_b]$ can now be calculated as one-electron integrals using the potentials (33). The integrations were carried out in the spheroidal coordinates (2). For those integrals which involve the potentials U_{NS} (pole potentials), the evaluation is easy and straightforward. However, the integrals involving the potentials U_{NP} and U_{ND} (dipole and quadrupole potentials) require elaborate partial integrations.

The integrals are obviously functions of $\bar{\xi}_a$, $\bar{\xi}_b$, and R; the final formulas are most easily written down in terms of the parameters ζ, τ, ρ, κ, ρ_a, ρ_b, which are defined in the same way as previously in Eqs. (15) and (16), except that ζ_a and ζ_b have to be replaced by $\bar{\xi}_a$ and $\bar{\xi}_b$. The results are

$$[1S_a|1S_b]=(\zeta/\rho)[1-(1-\kappa)^2\{\tfrac{1}{4}(2+\kappa)+\tfrac{1}{4}\rho_a\}e^{-2\rho_a}-(1+\kappa)^2\{\tfrac{1}{4}(2-\kappa)+\tfrac{1}{4}\rho_b\}e^{-2\rho_b}],$$

$$[1S_a|2S_b]=(\zeta/\rho)[1-(1-\kappa)^2\{\tfrac{1}{4}(1-\kappa-\kappa^2)+(1/12)(1-2\kappa)\rho_a\}e^{-2\rho_a}$$
$$-(1+\kappa)^2\{\tfrac{1}{4}(3-3\kappa+\kappa^2)+\tfrac{1}{3}(2-\kappa)\rho_b+\tfrac{1}{6}\rho_b^2\}e^{-2\rho_b}],$$

$$[1S_a|3S_b]=(\zeta/\rho)[1-(1-\kappa)^3\{\tfrac{1}{16}(1-5\kappa-4\kappa^2)-\tfrac{1}{8}\kappa\rho_a\}e^{-2\rho_a}-(1+\kappa)^2\{\tfrac{1}{16}(15-22\kappa+15\kappa^2-4\kappa^3)$$
$$+\tfrac{3}{5}(3-3\kappa+\kappa^2)\rho_b+\tfrac{1}{4}(2-\kappa)\rho_b^2+(1/12)\rho_b^3\}e^{-2\rho_b}],$$

$$[2S_a|2S_b]=(\zeta/\rho)[1-(1-\kappa)^2\{(1/12)(6-\kappa-8\kappa^2-4\kappa^3)+\tfrac{1}{3}(1-\kappa+\kappa^2)\rho_a+(1/18)(1-2\kappa)\rho_a^2\}e^{-2\rho_a}$$
$$-(1+\kappa)^2\{(1/12)(6+\kappa-8\kappa^2+4\kappa^3)+\tfrac{1}{3}(1+\kappa+\kappa^2)\rho_b+(1/18)(1+2\kappa)\rho_b^2\}e^{-2\rho_b}],$$

$$[2S_a|3S_b]=(\zeta/\rho)[1-(1-\kappa)^3\{(1/48)(11-19\kappa-44\kappa^2-20\kappa^3)+(1/12)(1-5\kappa-4\kappa^2)\rho_a-(1/12)\kappa\rho_a^2\}e^{-2\rho_a}$$
$$-(1+\kappa)^2\{(1/48)(37-22\kappa-39\kappa^2+56\kappa^3-20\kappa^4)+\tfrac{1}{8}(6+\kappa-8\kappa^2+4\kappa^3)\rho_b$$
$$+\tfrac{1}{4}(1+\kappa-\kappa^2)\rho_b^2+(1/36)(1+2\kappa)\rho_b^3\}e^{-2\rho_b}],$$

$$[3S_a|3S_b]=(\zeta/\rho)[1-(1-\kappa)^3\{\tfrac{1}{16}(8-\kappa-27\kappa^2-30\kappa^3-10\kappa^4)+\tfrac{1}{32}(11-19\kappa-44\kappa^2-20\kappa^3)\rho_a$$
$$+\tfrac{1}{16}(1-5\kappa-4\kappa^2)\rho_a^2-(1/24)\kappa\rho_a^3\}e^{-2\rho_a}-(1+\kappa)^3\{\tfrac{1}{16}(8+\kappa-27\kappa^2+30\kappa^3-10\kappa^4)$$
$$+\tfrac{1}{32}(11+19\kappa-44\kappa^2+20\kappa^3)\rho_b+\tfrac{1}{16}(1+5\kappa-4\kappa^2)\rho_b^2+(1/24)\kappa\rho_b^3\}e^{-2\rho_b}],$$

$$[1S_a|2P\Sigma_b]=[\zeta/(1-\tau)\rho^2][1-(1-\kappa)^3\{\tfrac{1}{16}(5+3\kappa)(1+2\rho_a)+\tfrac{1}{4}\rho_a^2\}e^{-2\rho_a}$$
$$-(1+\kappa)^2\{\tfrac{1}{16}(11-10\kappa+3\kappa^2)(1+2\rho_b)+\tfrac{1}{2}(2-\kappa)\rho_b^2+\tfrac{1}{4}\rho_b^3\}e^{-2\rho_b}],$$

$$[1S_a|3P\Sigma_b]=[\zeta/(1-\tau)\rho^2][1-(1-\kappa)^3\{(1/80)(13-9\kappa-12\kappa^2)(1+2\rho_a)+(1/20)(2-3\kappa)\rho_a^2\}e^{-2\rho_a}$$
$$-(1+\kappa)^2\{(1/80)(67-86\kappa+51\kappa^2-12\kappa^3)(1+2\rho_b)$$
$$+(1/20)(29-28\kappa+9\kappa^2)\rho_b^2+(3/10)(2-\kappa)\rho_b^3+(1/10)\rho_b^4\}e^{-2\rho_b}],$$

$$[2S_a|2P\Sigma_b]=[\zeta/(1-\tau)\rho^2][1-(1-\kappa)^3\{\tfrac{1}{16}(9+11\kappa+4\kappa^2)(1+2\rho_a)+\tfrac{1}{4}(3+2\kappa)\rho_a^2+\tfrac{1}{6}\rho_a^3\}e^{-2\rho_a}$$
$$-(1+\kappa)^2\{\tfrac{1}{16}(7+2\kappa-9\kappa^2+4\kappa^3)(1+2\rho_b)+\tfrac{1}{2}(1+\kappa-\kappa^2)\rho_b^2+(1/12)(1+2\kappa)\rho_b^3\}e^{-2\rho_b}],$$

$$[2S_a|3P\Sigma_b]=[\zeta/(1-\tau)\rho^2][1-(1-\kappa)^3\{(1/80)(29+3\kappa-36\kappa^2-20\kappa^3)(1+2\rho_a)+(1/20)(8-5\kappa-8\kappa^2)\rho_a^2$$
$$+(1/30)(2-3\kappa)\rho_a^3\}e^{-2\rho_a}-(1+\kappa)^2\{(1/80)(51-18\kappa-57\kappa^2+64\kappa^3-20\kappa^4)(1+2\rho_b)$$
$$+(1/20)(19+4\kappa-25\kappa^2+12\kappa^3)\rho_b^2+(3/10)(1+\kappa-\kappa^2)\rho_b^3+(1/30)(1+2\kappa)\rho_b^4\}e^{-2\rho_b}],$$

$$[3S_a|2P\Sigma_b]=[\zeta/(1-\tau)\rho^2][1-(1-\kappa)^3\{\tfrac{1}{16}(13+24\kappa+18\kappa^2+5\kappa^3)(1+2\rho_a)+\tfrac{1}{8}(11+15\kappa+6\kappa^2)\rho_a^2$$
$$+(1/24)(13+9\kappa)\rho_a^3+(1/12)\rho_a^4\}e^{-2\rho_a}-(1+\kappa)^3\{\tfrac{1}{16}(3+6\kappa-12\kappa^2+5\kappa^3)(1+2\rho_b)$$
$$+\tfrac{1}{8}(1+5\kappa-4\kappa^2)\rho_b^2+\tfrac{1}{8}\kappa\rho_b^3\}e^{-2\rho_b}],$$

$$[3S_a|3P\Sigma_b]=[\zeta/(1-\tau)\rho^2][1-(1-\kappa)^3\{\tfrac{1}{16}(10+9\kappa-9\kappa^2-16\kappa^3-6\kappa^4)(1+2\rho_a)$$
$$+(1/40)(37+9\kappa-48\kappa^2-30\kappa^3)\rho_a^2+(1/120)(35-21\kappa-36\kappa^2)\rho_a^3+(1/60)(2-3\kappa)\rho_a^4\}e^{-2\rho_a}$$
$$-(1+\kappa)^3\{\tfrac{1}{16}(6+3\kappa-21\kappa^2+20\kappa^3-6\kappa^4)(1+2\rho_b)+(1/40)(17+31\kappa-68\kappa^2+30\kappa^3)\rho_b^2$$
$$+(3/40)(1+5\kappa-4\kappa^2)\rho_b^3+(1/20)\kappa\rho_b^4\}e^{-2\rho_b}],$$

$$[1S_a|3D\Sigma_b]=[\zeta/(1-\tau)^2\rho^3][1-(1-\kappa)^4\{\tfrac{1}{16}(3+2\kappa)(1+2\rho_a)+(1/24)(7+4\kappa)\rho_a^2+(1/12)\rho_a^3\}e^{-2\rho_a}$$
$$-(1+\kappa)^2\{\tfrac{1}{16}(13-16\kappa+9\kappa^2-2\kappa^3)(1+2\rho_b)+(1/24)(37-42\kappa+21\kappa^2-4\kappa^3)\rho_b^2$$
$$+(1/12)(11-10\kappa+3\kappa^2)\rho_b^3+\tfrac{1}{6}(2-\kappa)\rho_b^4+(1/18)\rho_b^5\}e^{-2\rho_b}],$$

$$[2S_a|3D\Sigma_b]=[\zeta/(1-\tau)^2\rho^3][1-(1-\kappa)^4\{(1/48)(19+26\kappa+10\kappa^2)(1+2\rho_a)+(1/72)(49+60\kappa+20\kappa^2)\rho_a^2$$
$$+(1/36)(11+8\kappa)\rho_a^3+(1/18)\rho_a^4\}e^{-2\rho_a}-(1+\kappa)^2\{(1/48)(29-8\kappa-33\kappa^2$$
$$+34\kappa^3-10\kappa^4)(1+2\rho_b)+(1/72)(79-10\kappa-93\kappa^2+80\kappa^3-20\kappa^4)\rho_b^2+(1/12)(7$$
$$+2\kappa-9\kappa^2+4\kappa^3)\rho_b^3+\tfrac{1}{6}(1+\kappa-\kappa^2)\rho_b^4+(1/54)(1+2\kappa)\rho_b^5\}e^{-2\rho_b}],$$

$$[3S_a|3D\Sigma_b]=[\zeta/(1-\tau)^2\rho^3][1-(1-\kappa)^4\{\tfrac{1}{32}(21+44\kappa+35\kappa^2+10\kappa^3)(1+2\rho_a)$$
$$+(1/24)(29+56\kappa+40\kappa^2+10\kappa^2)\rho_a^2+(1/12)(8+12\kappa+5\kappa^2)\rho_a^3$$
$$+(1/24)(5+4\kappa)\rho_a^4+(1/36)\rho_a^5\}e^{-2\rho_a}-(1+\kappa)^3\{\tfrac{1}{32}(11+7\kappa-39\kappa^2+35\kappa^3-10\kappa^4)(1+2\rho_b)$$
$$+(1/24)(14+13\kappa-51\kappa^2+40\kappa^3-10\kappa^4)\rho_b^2+(1/12)(3+6\kappa-12\kappa^2+5\kappa^3)\rho_b^3$$
$$+(1/24)(1+5\kappa-4\kappa^2)\rho_b^4+(1/36)\kappa\rho_b^5\}e^{-2\rho_b}],$$

$$[2P\Sigma_a|2P\Sigma_b]=[2\zeta/(1+\tau)(1-\tau)\rho^3][1-(1-\kappa)^3\{\tfrac{1}{16}(8+9\kappa+3\kappa^3)(1+2\rho_a+2\rho_a^2)+\tfrac{3}{16}(3+2\kappa)\rho_a^3+\tfrac{1}{8}\rho_a^4\}e^{-2\rho_a}$$
$$-(1+\kappa)^3\{\tfrac{1}{16}(8-9\kappa+3\kappa^2)(1+2\rho_b+2\rho_b^2)+\tfrac{3}{16}(3-2\kappa)\rho_b^2+\tfrac{1}{8}\rho_b^4\}e^{-2\rho_b}],$$

$$[2P\Sigma_a|3P\Sigma_b]=[2\zeta/(1+\tau)(1-\tau)\rho^3][1-(1-\kappa)^3\{\tfrac{1}{16}(5-6\kappa^2-3\kappa^3)(1+2\rho_a+2\rho_a^2)+(3/80)(8-5\kappa-8\kappa^2)\rho_a^3$$
$$+(1/40)(2-3\kappa)\rho_a^4\}e^{-2\rho_a}-(1+\kappa)^3\{\tfrac{1}{16}(11-18\kappa+12\kappa^2-3\kappa^3)(1+2\rho_b+2\rho_b^2)$$
$$+(1/80)(71-93\kappa+36\kappa^2)\rho_b^3+(1/40)(13-9\kappa)\rho_b^4+(1/20)\rho_b^5\}e^{-2\rho_b}],$$

$$[3P\Sigma_a|3P\Sigma_b]=[2\zeta/(1+\tau)(1-\tau)\rho^3][1-(1-\kappa)^3\{(1/80)(40+27\kappa-39\kappa^2-54\kappa^3-18\kappa^4)(1+2\rho_a+2\rho_a^2)$$
$$+(1/80)(47+9\kappa-60\kappa^2-36\kappa^3)\rho_a^3+(1/200)(35-21\kappa-36\kappa^2)\rho_a^4+(1/100)(2-3\kappa)\rho_a^5\}e^{-2\rho_a}$$
$$-(1+\kappa)^3\{(1/80)(40-27\kappa-39\kappa^2+54\kappa^3-18\kappa^4)(1+2\rho_b+2\rho_b^2)$$
$$+(1/80)(47-9\kappa-60\kappa^2+36\kappa^3)\rho_b^3+(1/200)(35+21\kappa-36\kappa^2)\rho_b^4+(1/100)(2+3\kappa)\rho_b^5\}e^{-2\rho_b}],$$

$$[2P\Pi_a|2P\Pi_b]=[\zeta/(1+\tau)(1-\tau)\rho^3][1-(1-\kappa)^3\{\tfrac{1}{16}(8+9\kappa+3\kappa^2)(1+2\rho_a)+\tfrac{1}{8}(5+3\kappa)\rho_a^2+\tfrac{1}{8}\rho_a^3\}e^{-2\rho_a}$$
$$-(1+\kappa)^3\{\tfrac{1}{16}(8-9\kappa+3\kappa^2)(1+2\rho_b)+\tfrac{1}{8}(5-3\kappa)\rho_b^2+\tfrac{1}{8}\rho_b^3\}e^{-2\rho_b}],$$

$$[2P\Pi_a|3P\Pi_b]=[\zeta/(1+\tau)(1-\tau)\rho^3][1-(1-\kappa)^3\{\tfrac{1}{16}(5-6\kappa^2-3\kappa^3)(1+2\rho_a)+(1/40)(13-9\kappa-12\kappa^2)\rho_a^2$$
$$+(1/40)(2-3\kappa)\rho_a^3\}e^{-2\rho_a}-(1+\kappa)^3\{\tfrac{1}{16}(11-18\kappa+12\kappa^2-3\kappa^3)(1+2\rho_b)$$
$$+(1/40)(43-51\kappa+18\kappa^2)\rho_b^2+(3/40)(5-3\kappa)\rho_b^3+(1/20)\rho_b^4\}e^{-2\rho_b}],$$

$$[3P\Pi_a|3P\Pi_b]=[\zeta/(1+\tau)(1-\tau)\rho^3][1-(1-\kappa)^3\{(1/80)(40+27\kappa-39\kappa^2-54\kappa^3-18\kappa^4)(1+2\rho_a)$$
$$+(1/200)(137+9\kappa-168\kappa^2-90\kappa^3)\rho_a^2+(3/200)(13-9\kappa-12\kappa^2)\rho_a^3+(1/100)(2-3\kappa)\rho_a^4\}e^{-2\rho_a}$$
$$-(1+\kappa)^3\{(1/80)(40-27\kappa-39\kappa^2+54\kappa^3-18\kappa^4)(1+2\rho_b)+(1/200)(137-9\kappa-168\kappa^2+90\kappa^3)\rho_b^2$$
$$+(3/200)(13+9\kappa-12\kappa^2)\rho_b^3+(1/100)(2+3\kappa)\rho_b^4\}e^{-2\rho_b}],$$

$$[2P\Sigma_a|3D\Sigma_b]=[[3\zeta/(1+\tau)(1-\tau)^2\rho^4][1-(1-\kappa)^4\{\tfrac{1}{32}(11+14\kappa+5\kappa^2)(1+2\rho_a)+(1/72)(47+58\kappa+20\kappa^2)\rho_a^2$$
$$+(1/36)(14+16\kappa+5\kappa^2)\rho_a^3+(1/72)(11+8\kappa)\rho_a^4+(1/36)\rho_a^5\}e^{-2\rho_a}$$
$$-(1+\kappa)^3\{\tfrac{1}{32}(21-33\kappa+21\kappa^2-5\kappa^3)(1+2\rho_b)+(1/72)(92-141\kappa+87\kappa^2-20\kappa^3)\rho_b^2$$
$$+(1/36)(29-42\kappa+24\kappa^2-5\kappa^3)\rho_b^3+(1/24)(9-11\kappa+4\kappa^2)\rho_b^4$$
$$+(1/108)(13-9\kappa)\rho_b^5+(1/54)\rho_b^6\}e^{-2\rho_b}],$$

$$[3P\Sigma_a|3D\Sigma_b]=[3\zeta/(1+\tau)(1-\tau)^2\rho^4][1-(1-\kappa)^4\{\tfrac{1}{32}(17+32\kappa+23\kappa^2+6\kappa^3)(1+2\rho_a)$$
$$+(1/72)(74+136\kappa+95\kappa^2+24\kappa^3)\rho_a^2+(1/36)(23+40\kappa+26\kappa^2+6\kappa^3)\rho_a^3$$
$$+(1/360)(103+148\kappa+60\kappa^2)\rho_a^4+(1/60)(5+4\kappa)\rho_a^5+(1/90)\rho_a^6\}e^{-2\rho_a}$$
$$-(1+\kappa)^3\{\tfrac{1}{32}(15-9\kappa-15\kappa^2+19\kappa^3-6\kappa^4)(1+2\rho_b)+(1/72)(65-36\kappa-66\kappa^2+79\kappa^3-24\kappa^4)\rho_b^2$$
$$+(1/36)(20-9\kappa-21\kappa^2+22\kappa^3-6\kappa^4)\rho_b^3+(1/120)(29-3\kappa-36\kappa^2+20\kappa^3)\rho_b^4$$
$$+(1/540)(35+21\kappa-36\kappa^2)\rho_b^5+(1/270)(2+3\kappa)\rho_b^6\}e^{-2\rho_b}],$$

$$[2P\Pi_a|3D\Pi_b]=[\sqrt{3}\zeta/(1+\tau)(1-\tau)^2\rho^4][1-(1-\kappa)^4\{\tfrac{1}{32}(11+14\kappa+5\kappa^2)(1+2\rho_a)+(1/24)(14+16\kappa+5\kappa^2)\rho_a^2$$
$$+(1/12)(3+2\kappa)\rho_a^3+(1/24)\rho_a^4\}e^{-2\rho_a}-(1+\kappa)^3\{\tfrac{1}{32}(21-33\kappa+21\kappa^2-5\kappa^3)(1+2\rho_b)$$
$$+(1/24)(29-42\kappa+24\kappa^2-5\kappa^3)\rho_b^2+(1/12)(8-9\kappa+3\kappa^2)\rho_b^3$$
$$+(1/24)(5-3\kappa)\rho_b^4+(1/36)\rho_b^5\}e^{-2\rho_b}],$$

$$[3P\Pi_a|3D\Pi_b]=[\sqrt{3}\zeta/(1+\tau)(1-\tau)^2\rho^4][1-(1-\kappa)^4\{\tfrac{1}{32}(17+32\kappa+23\kappa^2+6\kappa^3)(1+2\rho_a)$$
$$+(1/24)(23+40\kappa+26\kappa^2+6\kappa^3)\rho_a^2+(1/12)(6+8\kappa+3\kappa^2)\rho_a^3+(1/120)(17+12\kappa)\rho_a^4$$
$$+(1/60)\rho_a^5\}e^{-2\rho_a}-(1+\kappa)^3\{\tfrac{1}{32}(15-9\kappa-15\kappa^2+19\kappa^3-6\kappa^4)(1+2\rho_b)$$
$$+(1/24)(20-9\kappa-21\kappa^2+22\kappa^3-6\kappa^4)\rho_b^2+(1/12)(5-6\kappa^2+3\kappa^3)\rho_b^3$$
$$+(1/120)(13+9\kappa-12\kappa^2)\rho_b^4+(1/180)(2+3\kappa)\rho_b^5\}e^{-2\rho_b}],$$

$$[3D\Sigma_a|3D\Sigma_b]=[6\zeta/(1+\tau)^2(1-\tau)^2\rho^5][1-(1-\kappa)^4\{\tfrac{1}{32}(16+29\kappa+20\kappa^2+5\kappa^3)(1+2\rho_a)$$
$$+(1/144)(139+246\kappa+165\kappa^2+40\kappa^3)\rho_a^2+(1/72)(43+72\kappa+45\kappa^2+10\kappa^3)\rho_a^3$$
$$+(1/216)(57+88\kappa+50\kappa^2+10\kappa^3)\rho_a^4+(1/432)(39+52\kappa+20\kappa^2)\rho_a^5+(1/216)(5+4\kappa)\rho_a^6$$
$$+(1/324)\rho_a^7\}e^{-2\rho_a}-(1+\kappa)^4\{\tfrac{1}{32}(16-29\kappa+20\kappa^2-5\kappa^3)(1+2\rho_b)$$
$$+(1/144)(139-246\kappa+165\kappa^2-40\kappa^3)\rho_b^2+(1/72)(43-72\kappa+45\kappa^2-10\kappa^3)\rho_b^3$$
$$+(1/216)(57-88\kappa+50\kappa^2-10\kappa^3)\rho_b^4+(1/432)(39-52\kappa+20\kappa^2)\rho_b^5$$
$$+(1/216)(5-4\kappa)\rho_b^6+(1/324)\rho_b^7\}e^{-2\rho_b}\},$$

$$[3D\Pi_a|3D\Pi_b]=[4\zeta/(1+\tau)^2(1-\tau)^2\rho^5][1-(1-\kappa)^4\{\tfrac{1}{32}(16+29\kappa+20\kappa^2+5\kappa^3)(1+2\rho_a)$$
$$+(1/96)(91+159\kappa+105\kappa^2+25\kappa^3)\rho_a^2+(1/48)(27+43\kappa+25\kappa^2+5\kappa^3)\rho_a^3$$
$$+(1/48)(11+14\kappa+5\kappa^2)\rho_a^4+(1/288)(17+12\kappa)\rho_a^5+(1/144)\rho_a^6\}e^{-2\rho_a}$$
$$-(1+\kappa)^4\{\tfrac{1}{32}(16-29\kappa+20\kappa^2-5\kappa^3)(1+2\rho_b)+(1/96)(91-159\kappa+105\kappa^2-25\kappa^3)\rho_b^2$$
$$+(1/48)(27-43\kappa+25\kappa^2-5\kappa^3)\rho_b^3+(1/48)(11-14\kappa+5\kappa^2)\rho_b^4$$
$$+(1/288)(17-12\kappa)\rho_b^5+(1/144)\rho_b^6\}e^{-2\rho_b}],$$

$$[3D\Delta_a|3D\Delta_b]=[\zeta/(1+\tau)^2(1-\tau)^2\rho^5][1-(1-\kappa)^4\{\tfrac{1}{32}(16+29\kappa+20\kappa^2+5\kappa^3)(1+2\rho_a)$$
$$+(1/48)(43+72\kappa+45\kappa^2+10\kappa^3)\rho_a^2+(1/24)(11+14\kappa+5\kappa^2)\rho_a^3+(1/24)(3+2\kappa)\rho_a^4$$
$$+(1/72)\rho_a^5\}e^{-2\rho_a}-(1+\kappa)^4\{\tfrac{1}{32}(16-29\kappa+20\kappa^2-5\kappa^3)(1+2\rho_b)$$
$$+(1/48)(43-72\kappa+45\kappa^2-10\kappa^3)\rho_b^2+(1/24)(11-14\kappa+5\kappa^2)\rho_b^3$$
$$+(1/24)(3-2\kappa)\rho_b^4+(1/72)\rho_b^5\}e^{-2\rho_b}]; \quad (34)$$

$\tau=0$,

$$[1S_a|1S_b]=\frac{\zeta}{\rho}\left\{1-\left(1+\frac{11}{8}\rho+\frac{3}{4}\rho^2+\frac{1}{6}\rho^3\right)e^{-2\rho}\right\},$$

$$[1S_a|2S_b]=\frac{\zeta}{\rho}\left\{1-\left(1+\frac{71}{48}\rho+\frac{23}{24}\rho^2+\frac{1}{3}\rho^3+\frac{1}{18}\rho^4\right)e^{-2\rho}\right\},$$

$$[2S_a|2S_b]=\frac{\zeta}{\rho}\left\{1-\left(1+\frac{37}{24}\rho+\frac{13}{12}\rho^2+\frac{4}{9}\rho^3+\frac{1}{9}\rho^4+\frac{2}{135}\rho^5\right)e^{-2\rho}\right\},$$

$$[1S_a|3S_b]=\frac{\zeta}{\rho}\left\{1-\left(1+\frac{25}{16}\rho+\frac{9}{8}\rho^2+\frac{23}{48}\rho^3+\frac{1}{8}\rho^4+\frac{1}{60}\rho^5\right)e^{-2\rho}\right\},$$

$$[2S_a|3S_b]=\frac{\zeta}{\rho}\left\{1-\left(1+\frac{307}{192}\rho+\frac{115}{96}\rho^2+\frac{79}{144}\rho^3+\frac{1}{6}\rho^4+\frac{1}{30}\rho^5+\frac{1}{270}\rho^6\right)e^{-2\rho}\right\},$$

$$[3S_a|3S_b]=\frac{\zeta}{\rho}\left\{1-\left(1+\frac{419}{256}\rho+\frac{163}{128}\rho^2+\frac{119}{192}\rho^3+\frac{5}{24}\rho^4+\frac{1}{20}\rho^5+\frac{1}{120}\rho^6+\frac{1}{1260}\rho^7\right)e^{-2\rho}\right\},$$

$$[1S_a|2P\Sigma_b]=\frac{\zeta}{\rho^2}\left\{1-\left(1+2\rho+2\rho^2+\frac{59}{48}\rho^3+\frac{11}{24}\rho^4+\frac{1}{12}\rho^5\right)e^{-2\rho}\right\},$$

$$[1S_a|3P\Sigma_b]=\frac{\zeta}{\rho^2}\left\{1-\left(1+2\rho+2\rho^2+\frac{19}{15}\rho^3+\frac{8}{15}\rho^4+\frac{43}{300}\rho^5+\frac{1}{50}\rho^6\right)e^{-2\rho}\right\},$$

$$[2S_a|2P\Sigma_b]=\frac{\zeta}{\rho^2}\left\{1-\left(1+2\rho+2\rho^2+\frac{61}{48}\rho^3+\frac{13}{24}\rho^4+\frac{3}{20}\rho^5+\frac{1}{45}\rho^6\right)e^{-2\rho}\right\},$$

$$[2S_a|3P\Sigma_b]=\frac{\zeta}{\rho^2}\left\{1-\left(1+2\rho+2\rho^2+\frac{103}{80}\rho^3+\frac{23}{40}\rho^4+\frac{9}{50}\rho^5+\frac{17}{450}\rho^6+\frac{1}{225}\rho^7\right)e^{-2\rho}\right\},$$

$$[3S_a|2P\Sigma_b]=\frac{\zeta}{\rho^2}\left\{1-\left(1+2\rho+2\rho^2+\frac{83}{64}\rho^3+\frac{19}{32}\rho^4+\frac{23}{120}\rho^5+\frac{13}{360}\rho^6+\frac{1}{180}\rho^7\right)e^{-2\rho}\right\},$$

$$[3S_a|3P\Sigma_b]=\frac{\zeta}{\rho^2}\left\{1-\left(1+2\rho+2\rho^2+\frac{417}{320}\rho^3+\frac{97}{160}\rho^4+\frac{5}{24}\rho^5+\frac{19}{360}\rho^6+\frac{59}{6300}\rho^7+\frac{1}{1050}\rho^8\right)e^{-2\rho}\right\},$$

$$[1S_a|3D\Sigma_b]=\frac{\zeta}{\rho^3}\left\{1-\left(1+2\rho+2\rho^2+\frac{4}{3}\rho^3+\frac{2}{3}\rho^4+\frac{31}{120}\rho^5+\frac{13}{180}\rho^6+\frac{1}{90}\rho^7\right)e^{-2\rho}\right\},$$

$$[2S_a|3D\Sigma_b]=\frac{\zeta}{\rho^3}\left\{1-\left(1+2\rho+2\rho^2+\frac{4}{3}\rho^3+\frac{2}{3}\rho^4+\frac{71}{270}\rho^5+\frac{11}{135}\rho^6+\frac{1}{54}\rho^7+\frac{1}{405}\rho^8\right)e^{-2\rho}\right\},$$

$$[3S_a|3D\Sigma_b]=\frac{\zeta}{\rho^3}\left\{1-\left(1+2\rho+2\rho^2+\frac{4}{3}\rho^3+\frac{2}{3}\rho^4+\frac{191}{720}\rho^5+\frac{31}{360}\rho^6+\frac{19}{840}\rho^7+\frac{17}{3780}\rho^8+\frac{1}{1890}\rho^9\right)e^{-2\rho}\right\},$$

$$[2P\Sigma_a|2P\Sigma_b]=\frac{2\zeta}{\rho^3}\left\{1-\left(1+2\rho+2\rho^2+\frac{263}{192}\rho^3+\frac{71}{96}\rho^4+\frac{77}{240}\rho^5+\frac{1}{10}\rho^6+\frac{1}{60}\rho^7\right)e^{-2\rho}\right\},$$

$$[2P\Sigma_a|3P\Sigma_b]=\frac{2\zeta}{\rho^3}\left\{1-\left(1+2\rho+2\rho^2+\frac{2609}{1920}\rho^3+\frac{689}{960}\rho^4+\frac{37}{120}\rho^5+\frac{5}{48}\rho^6+\frac{1}{40}\rho^7+\frac{1}{300}\rho^8\right)e^{-2\rho}\right\},$$

$$[3P\Sigma_a|3P\Sigma_b]=\frac{2\zeta}{\rho^3}\left\{1-\left(1+2\rho+2\rho^2+\frac{2597}{1920}\rho^3+\frac{677}{960}\rho^4+\frac{719}{2400}\rho^5+\frac{31}{300}\rho^6+\frac{29}{1050}\rho^7+\frac{11}{2100}\rho^8+\frac{1}{1750}\rho^9\right)e^{-2\rho}\right\},$$

$$[2P\Pi_a|2P\Pi_b]=\frac{\zeta}{\rho^3}\left\{1-\left(1+2\rho+2\rho^2+\frac{121}{96}\rho^3+\frac{25}{48}\rho^4+\frac{2}{15}\rho^5+\frac{1}{60}\rho^6\right)e^{-2\rho}\right\},$$

$$[2P\Pi_a|3P\Pi_b]=\frac{\zeta}{\rho^3}\left\{1-\left(1+2\rho+2\rho^2+\frac{1231}{960}\rho^3+\frac{271}{480}\rho^4+\frac{41}{240}\rho^5+\frac{1}{30}\rho^6+\frac{1}{300}\rho^7\right)e^{-2\rho}\right\},$$

$$[3P\Pi_a|3P\Pi_b]=\frac{\zeta}{\rho^3}\left\{1-\left(1+2\rho+2\rho^2+\frac{1243}{960}\rho^3+\frac{283}{480}\rho^4+\frac{29}{150}\rho^5+\frac{9}{200}\rho^6+\frac{73}{10500}\rho^7+\frac{1}{1750}\rho^8\right)e^{-2\rho}\right\},$$

$$[2P\Sigma_a|3D\Sigma_b]=\frac{3\zeta}{\rho^4}\left\{1-\left(1+2\rho+2\rho^2+\frac{4}{3}\rho^3+\frac{2}{3}\rho^4+\frac{583}{2160}\rho^5+\frac{103}{1080}\rho^6+\frac{11}{360}\rho^7+\frac{13}{1620}\rho^8+\frac{1}{810}\rho^9\right)e^{-2\rho}\right\},$$

$$[3P\Sigma_a|3D\Sigma_b]=\frac{3\zeta}{\rho^4}\left\{1-\left(1+2\rho+2\rho^2+\frac{4}{3}\rho^3+\frac{2}{3}\rho^4+\frac{29}{108}\rho^5+\frac{5}{54}\rho^6+\frac{1}{35}\rho^7+\frac{22}{2835}\rho^8+\frac{47}{28350}\rho^9+\frac{1}{4725}\rho^{10}\right)e^{-2\rho}\right\},$$

$$[2P\Pi_a|3D\Pi_b]=\frac{\sqrt{3}\zeta}{\rho^4}\left\{1-\left(1+2\rho+2\rho^2+\frac{4}{3}\rho^3+\frac{2}{3}\rho^4+\frac{377}{1440}\rho^5+\frac{19}{240}\rho^6+\frac{1}{60}\rho^7+\frac{1}{540}\rho^8\right)e^{-2\rho}\right\},$$

$$[3P\Pi_a|3D\Pi_b]=\frac{\sqrt{3}\zeta}{\rho^4}\left\{1-\left(1+2\rho+2\rho^2+\frac{4}{3}\rho^3+\frac{2}{3}\rho^4+\frac{19}{72}\rho^5+\frac{1}{12}\rho^6+\frac{17}{840}\rho^7+\frac{13}{3780}\rho^8+\frac{1}{3150}\rho^9\right)e^{-2\rho}\right\},$$

$$[3D\Sigma_a|3D\Sigma_b]=\frac{6\zeta}{\rho^5}\left\{1-\left(1+2\rho+2\rho^2+\frac{4}{3}\rho^3+\frac{2}{3}\rho^4+\frac{511}{1920}\rho^5+\frac{253}{2880}\rho^6+\frac{2237}{90720}\rho^7+\frac{71}{11340}\rho^8\right.\right.$$
$$\left.\left.+\frac{1}{630}\rho^9+\frac{13}{34020}\rho^{10}+\frac{1}{17010}\rho^{11}\right)e^{-2\rho}\right\},$$

$$[3D\Pi_a|3D\Pi_b]=\frac{4\zeta}{\rho^5}\left\{1-\left(1+2\rho+2\rho^2+\frac{4}{3}\rho^3+\frac{2}{3}\rho^4+\frac{1027}{3840}\rho^5+\frac{521}{5760}\rho^6+\frac{67}{2520}\rho^7\right.\right.$$
$$\left.\left.+\frac{67}{10080}\rho^8+\frac{19}{15120}\rho^9+\frac{1}{7560}\rho^{10}\right)e^{-2\rho}\right\},$$

$$[3D\Delta_a|3D\Delta_b]=\frac{\zeta}{\rho^5}\left\{1-\left(1+2\rho+2\rho^2+\frac{4}{3}\rho^3+\frac{2}{3}\rho^4+\frac{253}{960}\rho^5+\frac{119}{1440}\rho^6+\frac{11}{560}\rho^7+\frac{1}{315}\rho^8+\frac{1}{3780}\rho^9\right)e^{-2\rho}\right\}; \tag{34a}$$

$$\left.\begin{aligned}
&\rho=0,\\
&\quad[1S_a|1S_b]=\tfrac{1}{8}(1-\tau^2)(5-\tau^2)\zeta,\\
&\quad[1S_a|2S_b]=(1/48)(1-\tau^2)(25-7\tau-5\tau^2+3\tau^3)\zeta,\\
&\quad[2S_a|2S_b]=(1/24)(1-\tau^2)(11-4\tau^2+\tau^4)\zeta,\\
&\quad[1S_a|3S_b]=\tfrac{1}{32}(1-\tau^2)(14-7\tau-\tau^2+3\tau^3-\tau^4)\zeta,\\
&\quad[2S_a|3S_b]=(1/192)(1-\tau^2)(77-19\tau-28\tau^2+16\tau^3+7\tau^4-5\tau^5)\zeta,\\
&\quad[3S_a|3S_b]=(1/256)(1-\tau^2)(93-47\tau^2+23\tau^4-5\tau^6)\zeta,\\
&[NS_a|N'P\Sigma_b]=0,\\
&[NS_a|N'D\Sigma_b]=0,\\
-&[2P\Sigma_a|2P\Sigma_b]=[2P\Pi_a|2P\Pi_b]=(1/96)(1-\tau^2)^2(7-3\tau^2)\zeta,\\
-&[2P\Sigma_a|3P\Sigma_b]=[2P\Pi_a|3P\Pi_b]=(1/960)(1-\tau^2)^2(49-27\tau-21\tau^2+15\tau^3)\zeta,\\
-&[3P\Sigma_a|3P\Sigma_b]=[3P\Pi_a|3P\Pi_b]=(1/960)(1-\tau^2)^2(37-30\tau^2+9\tau^4)\zeta,\\
&[NP\Sigma_a|N'D\Sigma_b]=[NP\Pi_a|N'D\Pi_b]=0,\\
&\quad[3D\Sigma_a|3D\Sigma_b]=-[3D\Pi_a|3D\Pi_b]=[3D\Delta_a|3D\Delta_b]=(1/2880)(1-\tau^2)^3(9-5\tau^2)\zeta.
\end{aligned}\right\} \tag{34b}$$

The formulas (30), (34), (34a), and (34b) enable us to obtain any desired coulomb integral $[\chi_a\chi_a'|\chi_b\chi_b']$. It is to be noted that in Eqs. (30) there occur the basic integrals $[2P\Sigma_a|3S_b]$, $[3P\Sigma_a|3S_b]$, and $[3D\Sigma_a|3S_b]$, which are not listed explicitly in Eqs. (34), (34a), and (34b). However, these integrals follow directly from $[3S_a|2P\Sigma_b]$, $[3S_a|3P\Sigma_b]$, and $[3S_b|3D\Sigma_b]$, respectively, when the following change is made in the latter: $\rho_a\leftrightarrow\rho_b$, $\kappa\rightarrow-\kappa$, $\tau\rightarrow-\tau$.

BIBLIOGRAPHY*

The wave functions employed in the formulas are real Slater (nodeless) wave functions, unless explicitly stated otherwise.

(1) E. Hylleraas, Z. Physik **51**, 150 (1928);
$[1s_a1s_a|2s_b2s_b]$, $[1s_a2s_a|1s_b2s_b]$
evaluated over hydrogen wave functions in terms of R.

(2) E. C. Kemble and C. Zener, Phys. Rev. **33**, 512 (1929);
$[1s_a1s_a|2p\pi_b2p\pi_b]$
evaluated over complex Slater AO's in terms of R. Also, certain linear combinations of nuclear attraction integrals are evaluated.

(3) J. H. Bartlett, Phys. Rev. **37**, 507 (1931), using complex Slater AO's, evaluates
$(2p\sigma_a|2p\sigma_b)$, $(2p\pi_a|2p\pi_b)$,
$[2p\pi_a2p\pi_a|2p\pi_b2p\pi_b]$, $[2p\pi_a2p\pi_a|2p\sigma_b2p\sigma_b]$,
$[2p\sigma_a2p\pi_a|2p\sigma_b2p\pi_b]$, $[2p\sigma_a2p\sigma_a|2p\sigma_b2p\sigma_b]$,
in terms of A_n for $\tau=0$.

(4) N. Rosen, Phys. Rev. **38**, 255 (1931);
$(ns_a|ns_b)$, $(ns_a|1/r_a|ns_b)$,
$[a|ns_bns_b]$, $[ns_ans_a|ns_bns_b]$,
expressed in terms of A_n for $\tau=0$, A_n and B_n for $\tau\neq0$.

(5) N. Rosen, Phys. Rev. **38**, 2099 (1931);
$(1s_a|1s_b)$, $(1s_a|2p\sigma_b)$, $(2p\sigma_a|2p\sigma_b)$,
$(1s_a|1/r_a|1s_b)$, $(1s_a|1/r_a|2p\sigma_b)$,
$(2p\sigma_a|1/r_a|1s_b)$, $(2p\sigma_a|1/r_a|2p\sigma_b)$,
$[a|1s_a1s_a]$, $[a|1s_b1s_b]$, $[a|1s_b2p\sigma_b]$,

* The author hereby wishes to acknowledge the help of Mr. W. Jaunzemis in compiling this bibliography.

$[a|2p\sigma_a\ 2p\sigma_a]$, $[a|2p\sigma_b 2p\sigma_b]$,
$[1s_a 1s_a|1s_b 1s_b]$, $[1s_a 1s_a|1s_b 2p\sigma_b]$,
$[1s_a 1s_a|2p\sigma_b 2p\sigma_b]$, $[1s_a 2p\sigma_a|2p\sigma_b 2p\sigma_b]$,
$[1s_a 2p\sigma_a|1s_b 2p\sigma_b]$, $[2p\sigma_a 2p\sigma_a|2p\sigma_b 2p\sigma_b]$,
expressed in terms of ρ for $\tau=0$.

(6) W. H. Furry and J. H. Bartlett, Phys. Rev. **39**, 210 (1932); master formulas with numerical tables for auxiliary functions given for the following integrals over complex Slater AO's:
$[2s_a 2s_a|2s_b 2s_b]$, $[2s_a 2s_a|2s_b 2p\sigma_b]$,
$[2s_a 2s_a|2p\sigma_b 2p\sigma_b]$, $[2s_a 2p\sigma_a|2s_b 2p\sigma_b]$,
$[2s_a 2s_a|2p\pi_b 2p\pi_b]$, $[2s_a 2p\pi_a|2s_b 2p\pi_b]$.

(7) B. N. Dickinson, J. Chem. Phys. **1**, 317 (1933); using $Z'=\epsilon Z$ for $2p\sigma$ orbitals, evaluates
$(1s_a|2p\sigma_b)$, $(1s_a|1/r_a|2p\sigma_b)$,
$[a|1s_a 2p\sigma_a]$, $[a|1s_b 2p\sigma_b]$,
in terms of ϵ, ρ.

(8) Kotani, Amomiya, and Simose, Proc. Phys.-Math. Soc. Japan **20**, Extra No. 1 (1938); **22**, Extra No. 1 (1940), independently of the previous papers, evaluated
$(2s_a|2s_b)$, $(2s_a|2p\sigma_b)$, $(2p\sigma_a|2p\sigma_b)$, $(2p\pi_a|2p\pi_b)$,
$(2s_a|1/r_a|2s_b)$, $(2p\sigma_a|1/r_a|2p\sigma_b)$, $(2p\pi_a|1/r_a|2p\pi_b)$,
$(2s_a|1/r_a|2p\sigma_b)$, $(2p\sigma_a|1/r_a|2s_b)$
in terms of A_n for $\tau=0$;
$[a|1s_b 1s_b]$, $[a|2s_b 2s_b]$, $[a|2p\sigma_b 2p\sigma_b]$,
$[a|2p\pi_b 2p\pi_b]$, $[a|2s_b 2p\sigma_b)$ in terms of A_n;
$[2s_a 2s_a|2s_b 2s_b]$, $[2p\sigma_a 2s_a|2s_b 2s_b]$,
$[2p\sigma_a 2s_a|2p\sigma_b 2s_b]$, $[2p\sigma_a 2p\sigma_a|2p\sigma_b 2s_b]$,
$[2s_a 2s_a|2p\pi_b 2p\pi_b]$, $[2s_a 2p\pi_a|2s_b 2p\pi_b]$,
$[2p\sigma_a 2p\pi_a|2p\sigma_b 2p\pi_b]$, $[2p\sigma_a 2p\pi_a|2s_b 2p\pi_b]$,
in terms of ρ for $\tau=0$;
$(1s_a|2s_b)$, $(1s_a|2p\sigma_b)$,
$(2s_a|1/r_a|1s_b)$, $(2p\sigma_a|1/r_a|1s_b)$,
$(1s_a|1/r_a|2s_b)$, $(1s_a|1/r_a|2p\sigma_b)$,
in terms of A_n and B_n for $\tau\neq 0$.

(9) C. A. Coulson, Proc. Cambridge Phil. Soc. **38**, 210 (1941). A variety of integrals over nonorthogonalized Slater AO's is treated, including overlap and nuclear attraction integrals over ns, $np\sigma$ AO's for $n=1-3$, and a few more. Special formulas in terms of R, ζ_a, ζ_b are given for both $\tau=0$ and $\tau\neq 0$.

(10) Mulliken, Rieke, Orloff, and Orloff, J. Chem. Phys. **17**, 1278 (1949).
Overlap integrals for all combinations of ns, $np\sigma$, and $np\pi$ AO's for $n=1$, 2, 3, 5 are evaluated in terms of A_n and B_n for $\tau=0$ and $\tau\neq 0$; and special formulas in terms of ρ for $\tau=0$ and in terms of τ for $\rho=0$ are given.

(11) H. J. Kopineck, Z. Naturforsch. **5a**, 420 (1950); based on (8), with many results recalculated and compared with the American papers, therefore, a rather up-to-date survey. Besides the integrals given in (8), it lists
$(2s_a|2s_b)$, $(2s_a|1/r_a|2s_b)$, $[a|2s_b 2s_b]$
evaluated over hydrogen AO's in terms of A_n for $\tau=0$,
$[2s_a 2s_a|2s_b 2s_b]$ in terms of ρ.

(12) J. O. Hirshfelder and J. W. Linnett, J. Chem. Phys. **18**, 130 (1950);
$[1s_a 2p\pi_a|1s_b 2p\pi_b]$,
$[2p\pi_a 2p\pi_a|2p\pi_b 2p\pi_b]+[2p\pi_a 2p\bar{\pi}_a|2p\pi_b 2p\bar{\pi}_b]$
expressed in terms of ρ for $\tau=0$. Also, certain linear combinations of overlap and nuclear attraction integrals are evaluated, and a compilation of integrals evaluated by other authors is made.

(13) M. P. Barnett and C. A. Coulson, Trans. Roy. Soc. London **243**, 221 (1951). All our integrals, except for the kinetic energy integrals (5), expressed in terms of auxiliary functions.

THE JOURNAL OF CHEMICAL PHYSICS VOLUME 19, NUMBER 12 DECEMBER, 1951

A Study of Two-Center Integrals Useful in Calculations on Molecular Structure. II. The Two-Center Exchange Integrals*

KLAUS RÜDENBERG
Department of Physics, University of Chicago, Chicago, Illinois
(Received June 27, 1951)

The problem of the two-center exchange integrals is solved in the most general way for Slater-type atomic orbitals with integral effective quantum numbers. No other restrictions are placed upon effective quantum numbers and effective nuclear charges, The integrals are expressed linearly in terms of certain auxiliary functions. A rule for finding the coefficients is given. The coefficients are explicitly computed for all cases involving orbitals with the quantum numbers 1, 2, and 3. The auxiliary functions are discussed in detail. The existing literature is reviewed, and a survey of present tables is made.

IF one attacks the quantum-mechanical problems of molecular structure by an expansion of the wave functions in terms of AO's (atomic orbitals), then the differential equations are reduced to matrix equations and the difficulties concentrate to a large extent in the evaluation of the integrals in terms of which the matrix elements are defined. The hardest of these are the electron-electron interaction integrals,

$$I=\int dV_1\int dV_2(1/r_{12})\Omega(1)\bar{\Omega}(2)=[\Omega|\bar{\Omega}], \qquad \text{(A)}$$

$$\Omega(1)=\chi_a(1)\chi_b(1), \quad \bar{\Omega}(2)=\chi_c(2)\chi_d(2),$$

$$(i)=(X_iY_iZ_i), \quad dV_i=dX_idY_idZ_i,$$

$$r_{12}=[(X_1-X_2)^2+(Y_1-Y_2)^2+(Z_1-Z^2)^2]^{\frac{1}{2}},$$

where the integration extends over the position coordinates of the two electrons, and the functions χ_a, χ_b, χ_c, χ_d represent any real AO's on the atoms a, b, c, d, respectively. Atomic units are used in Eq. (A) and below: the Bohr radius $a_H=0.529$A is the unit of length, the electron charge e is the unit of charge, and twice the ionization potential of the hydrogen atom $(e^2/a_H)=27.2$ ev is the energy unit. The integral (A) may be interpreted as the mutual electrostatic energy of the charge distributions Ω and $\bar{\Omega}$.

For the AO's one has to choose between numerically calculated and analytical functions. In the latter case the radially nodeless so-called Slater AO's seem to be the most appropriate, especially since it is known that the numerical functions obtained by Hartree and others can be expressed by superposition of a few Slater AO's.[1] When these are adopted, all two-center integrals, which for diatomic molecules are the only ones required, can be evaluated analytically. Furthermore, although they depend on five parameters, they can be expressed in terms of, at worst, two-parameter functions; and this makes tabulation of these integrals possible.

Therefore, it seemed to be worth while to investigate systematically the two-center integrals and to compute tables of their numerical values. This is a program of which the work of R. S. Mulliken, C. A. Rieke, D. Orloff, and H. Orloff,[1] the work of C. C. J. Roothaan,[2] and this paper form parts. We hope to complete the theoretical side of this project by an investigation (now in progress) of the hybrid integrals, and it is intended to prepare tables which permit interpolation.

The present paper deals with the two-center exchange integrals, that is, those integrals (A) for which

$$\Omega(1)=\chi_a(1)\chi_b'(1), \quad \bar{\Omega}(2)=\bar{\chi}_a(2)\bar{\chi}_b'(2), \qquad \text{(B)}$$

where χ, χ', $\bar{\chi}$, $\bar{\chi}'$ denote four different Slater AO's. Since Y. Sugiura evaluated the first integral of this type, many special cases have been treated; but hitherto no comprehensive approach seems to have been made. Our results apply to Slater AO's with any integral effective quantum number and include the case of four different effective nuclear charges. The numerical coefficients through which the integrals are expressed in terms of certain auxiliary functions are computed for all cases involving orbitals with quantum numbers 1, 2, and 3 (see Table II). The method, while based like most of the earlier work on the Neumann expansion, still differs from previous investigations in several respects. A survey of the literature and of existing numerical tables will be given in Sec. 5.

1. THE GENERAL FORMULA FOR THE EXCHANGE INTEGRAL

I

Let us introduce the normalized Legendre functions,

$$\mathcal{P}_l^m(\cos\vartheta)=\left[\frac{(2l+1)(l-m)!}{2(l+m)!}\right]^{\frac{1}{2}}P_l^m(\cos\vartheta), \qquad (1.1)$$

where

$$P_l^m(\cos\vartheta)=\sin^m\vartheta P_l^{(m)}(\cos\vartheta),$$
$$P_l^{(m)}(t)=(d^m/dt^m)P_l(t). \qquad (1.2)$$

The $P_l(t)$ are the Legendre polynomials. We then may

* This work was assisted in part by the ONR under Task Order IX of Contract N6ori-20 with the University of Chicago.
[1] See Mulliken, Rieke, Orloff, and Orloff, J. Chem. Phys. **17**, 1248 (1949).
[2] See C. C. J. Roothaan, J. Chem. Phys. **19**, 1445 (1951).

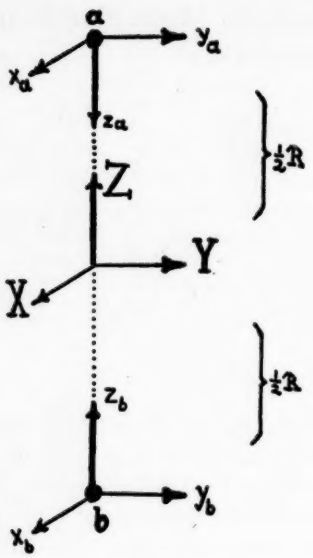

FIG. 1.

write the normalized Slater orbitals,

$$C_n r^{n-1} e^{-\zeta r} \mathcal{P}_l^m(\cos\vartheta) \cdot \begin{cases} 1/\sqrt{2}, & (m=0,\ l+1\leqslant n), \\ \cos m\varphi, \\ \sin m\varphi, \end{cases} \Big\} (1\leqslant m\leqslant l,\ l+1\leqslant n), \tag{1.3}$$

where

$$C_n = (2\zeta)^{n+\frac{1}{2}}/[\pi(2n)!]^{\frac{1}{2}}. \tag{1.3'}$$

In order to form the charge distributions (B), we define the polar coordinates on the two nuclei a and b (see Fig. 1):

$$\left.\begin{aligned} x_a = x_b = X, \quad y_a = y_b = Y, \quad d = [X^2+Y^2]^{\frac{1}{2}}, \\ \varphi_a = \varphi_b = \varphi = \arccos(X/d) = \arcsin(Y/d), \\ z_a = \tfrac{1}{2}R - Z, \qquad z_b = \tfrac{1}{2}R + Z, \\ \cos\vartheta_a = z_a/r_a, \qquad \cos\vartheta_b = z_b/r_b. \end{aligned}\right\} \tag{1.4}$$

In the charge distributions (B) which are formed as products from the orbitals (1.3, 3'), we may then substitute

$$\begin{aligned} \cos m\varphi \cos m'\varphi &= \tfrac{1}{2}\{\cos(m+m')\varphi + \cos(m-m')\varphi\}, \\ \sin m\varphi \sin m'\varphi &= \tfrac{1}{2}\{-\cos(m+m')\varphi + \cos(m-m')\varphi\}, \\ \sin m\varphi \cos m'\varphi &= \tfrac{1}{2}\{\sin(m+m')\varphi + \sin(m-m')\varphi\}. \end{aligned} \tag{1.5}$$

This permits us to consider the charge distributions

$$\Omega = C_n C_{n'} r_a^{n-1} r_b^{n'-1} \exp(-\zeta_a r_a - \zeta_b r_b) \times \mathcal{P}_l^m(\cos\vartheta_a)\mathcal{P}_{l'}^{m'}(\cos\vartheta_b) \begin{cases} \cos(m+m')\varphi \\ \sin(m+m')\varphi \\ \cos|m-m'|\varphi \\ \sin|m-m'|\varphi \end{cases} \tag{1.6}$$

as basic distributions. According to Eqs. (1.5) the original product distributions are simple linear combinations of the distributions (1.6).

On the basis of Eqs. (1.1, 2, 4) one concludes that *all these* distributions have the analytical form:

$$\Omega = C \exp(-\zeta_a r_a - \zeta_b r_b) p(z_a, r_a, z_b, r_b) \times d^{2q} d^M \begin{cases} \cos M\varphi & (1.7) \\ \sin M\varphi, & (1.7') \end{cases}$$

where $(2q)$ is an *even* number, C depends on ζ, ζ', M is zero or a positive integer, and the function p is a *polynomial*, homogeneous in (z_a, r_b, z_b, r_b).

We now introduce elliptic coordinates (ξ, η) by means of the relations[3]

$$\left.\begin{aligned} r_a = \tfrac{1}{2}R(\xi-\eta), \quad r_b = \tfrac{1}{2}R(\xi+\eta), \qquad (1\leqslant\xi\leqslant\infty), \\ d = \tfrac{1}{2}R[(\xi^2-1)(1-\eta^2)]^{\frac{1}{2}}, \ Z = \tfrac{1}{2}R\xi\eta, \quad (-1\leqslant\eta\leqslant 1). \end{aligned}\right\} \tag{1.8}$$

Thereby, the distributions (1.7, 7') become

$$\Omega = k\omega(\xi,\eta) e^{-\alpha\xi} e^{\beta\eta} (\xi^2-1)^{M/2} (1-\eta^2)^{M/2} \begin{cases} \cos M\varphi & (1.9) \\ \sin M\varphi, & (1.9') \end{cases}$$

where

$$\alpha = \tfrac{1}{2}R(\zeta_a+\zeta_b), \quad \beta = \tfrac{1}{2}R(\zeta_a-\zeta_b), \tag{1.10}$$

$$k = R^{-3}(R\zeta_a)^{n_a+\frac{1}{2}}(R\zeta_b)^{n_b+\frac{1}{2}}, \tag{1.11}$$

where n_a, n_b denote the two principal quantum numbers, which were previously called n, n'. The function $\omega(\xi, \eta)$ is a *polynomial* in (ξ, η) in which the coefficients are *pure numbers*. In the final equations (1.16, 17, 19) we shall use the numbers ω_{nj} defined by

$$\tfrac{1}{2}\pi[\tfrac{1}{2}(1+\delta_{M0})]^{\frac{1}{2}}(\xi^2-\eta^2)\omega(\xi,\eta) = \sum_{n=0}^{N}\sum_{j=0}^{J} \omega_{nj}\xi^n\eta^j. \tag{1.12}$$

Explicit relations between orbital products (B) and properly defined charge distributions (1.9, 9') are given in Table I for all cases involving the quantum numbers 1, 2, and 3. The corresponding constants ω_{nj} (see 1.12) are listed in Table II.

II

We proceed now to form the integrals (A) between all possible distributions of the type (1.9, 9'). Since for a given value of M, the two distributions (1.9, 9') form the basis of an irreducible representation of the two-dimensional rotation-reflection group $C_{\infty v}$, it follows that the integral (A) will be different from zero only if the distributions $\Omega(1)$ and $\overline{\Omega}(2)$ in (A) *both* contain the *same* factor $\cos M\varphi$, or if they *both* contain the *same*

[3] Commonly, η is defined with the opposite sign. The present choice leads to functions $B_j^{Ml}(\beta)$, (1.20), which contain the exponential with a positive exponent instead of a negative one. This is preferable from every point of view.

TABLE I. The 14 Slater AO's for quantum numbers 1, 2, 3, and the 65 corresponding charge distributions.

The real Slater AO's are defined in Eqs. (1.3, 3′, 3″). The following list gives the orbitals for $n=1, 2, 3$, and at the same time explains our notation.

$$(1s)=(\zeta^3/\pi)^{\frac{1}{2}}e^{-\zeta r}$$
$$(2s)=(\zeta^5/3\pi)^{\frac{1}{2}}re^{-\zeta r} \qquad (3s)=(2\zeta^7/5\pi)^{\frac{1}{2}}(r^2/3)e^{-\zeta r}$$
$$(2p\sigma)=(\zeta^5/\pi)^{\frac{1}{2}}ze^{-\zeta r} \qquad (3p\sigma)=(2\zeta^7/15\pi)^{\frac{1}{2}}zre^{-\zeta r}$$
$$(2p\pi)=(\zeta^5/\pi)^{\frac{1}{2}}xe^{-\zeta r} \qquad (3p\pi)=(2\zeta^7/15\pi)^{\frac{1}{2}}xre^{-\zeta r}$$
$$(2p\bar{\pi})=(\zeta^5/\pi)^{\frac{1}{2}}ye^{-\zeta r} \qquad (3p\bar{\pi})=(2\zeta^7/15\pi)^{\frac{1}{2}}yre^{-\zeta r}$$
$$(3d\sigma)=(\zeta^7/2\pi)^{\frac{1}{2}}(z^2-r^2/3)e^{-\zeta r}$$
$$(3d\pi)=(2\zeta^7/3\pi)^{\frac{1}{2}}xze^{-\zeta r} \qquad (3d\delta)=(2\zeta^7/3\pi)^{\frac{1}{2}}\tfrac{1}{2}(x^2-y^2)e^{-\zeta r}$$
$$(3d\bar{\pi})=(2\zeta^7/3\pi)^{\frac{1}{2}}yze^{-\zeta r} \qquad (3d\bar{\delta})=(2\zeta^7/3\pi)^{\frac{1}{2}}xye^{-\zeta r}$$

where $z=r\cos\vartheta$, $x=r\sin\vartheta\cos\varphi$, $y=r\sin\vartheta\sin\varphi$.

The complex orbitals are defined by

$$\left.\begin{matrix}(2p1)\\(2p\bar{1})\end{matrix}\right\}=\frac{1}{\sqrt{2}}[(2p\pi)\pm i(2p\bar{\pi})], \qquad \left.\begin{matrix}(3p1)\\(3p\bar{1})\end{matrix}\right\}=\frac{1}{\sqrt{2}}[(3p\pi)\pm i(3p\bar{\pi})],$$
$$\left.\begin{matrix}(3d1)\\(3d\bar{1})\end{matrix}\right\}=\frac{1}{\sqrt{2}}[(3d\pi)\pm i(3d\bar{\pi})], \qquad \left.\begin{matrix}(3d2)\\(3d\bar{2})\end{matrix}\right\}=\frac{1}{\sqrt{2}}[(3d\delta)\pm i(3d\bar{\delta})],$$
$$(2p0)=(2p\sigma), \quad (3p0)=(3p\sigma), \quad (3d0)=(3d\sigma).$$

Taking all products between the 14 real AO's, we obtain all possible charge distributions Ω (see formula (B) in the introduction). Our notation for these products is exemplified by

$$(2p\sigma)_a\cdot(3p\sigma)_b=(2p\sigma_a3p\sigma_b).$$

However, instead of those products in which neither of the two factors is a Σ^+ type orbital (i.e., s, $p\sigma$, $d\sigma$) we introduce the linear combinations which are defined in the following formulas, where n, n' represent one of the numbers 2, 3 and l, l' represent one of the symbols p, d (see Sec. 1, Eqs. (1.5, 6)):

$$\tfrac{1}{2}[(nl\pi_an'l'\pi_b)+(nl\bar{\pi}_an'l'\bar{\pi}_b)]=(nl\pi_an'l'\pi_b\Sigma),$$
$$\tfrac{1}{2}[(nl\pi_an'l'\pi_b)-(nl\bar{\pi}_an'l'\bar{\pi}_b)]=(nl\pi_an'l'\pi_b\Delta),$$
$$(nl\pi_an'l'\bar{\pi}_b)=(nl\bar{\pi}_an'l'\pi_b)=(nl\pi_an'l'\pi_b\bar{\Delta}),$$
$$\tfrac{1}{2}[(3d\delta_a3d\delta_b)+(3d\bar{\delta}_a3d\bar{\delta}_b)]=(3d\delta_a3d\delta_b\Sigma),$$
$$\tfrac{1}{2}[(3d\delta_a3d\delta_b)-(3d\bar{\delta}_a3d\bar{\delta}_b)]=(3d\delta_a3d\delta_b\Gamma),$$
$$(3d\delta_a3d\bar{\delta}_b)=(3d\bar{\delta}_a3d\delta_b)=(3d\delta_a3d\delta_b\bar{\Gamma}),$$
$$\tfrac{1}{2}[(nl\pi_a3d\delta_b)+(nl\bar{\pi}_a3d\bar{\delta}_b)]=(nl\pi_a3d\delta_b\Pi),$$
$$\tfrac{1}{2}[(nl\pi_a3d\delta_b)-(nl\bar{\pi}_a3d\bar{\delta}_b)]=(nl\pi_a3d\delta_b\Phi),$$
$$\tfrac{1}{2}[(nl\pi_a3d\bar{\delta}_b)+(nl\bar{\pi}_a3d\delta_b)]=(nl\pi_a3d\delta_b\bar{\Phi}),$$
$$\tfrac{1}{2}[(nl\pi_a3d\bar{\delta}_b)-(nl\bar{\pi}_a3d\delta_b)]=(nl\pi_a3d\delta_b\bar{\Pi}).$$

Thereby, all our charge distributions belong to irreducible representations of the two-dimensional rotation-reflection group $C_{\infty v}$ around the ab axis, and the following table classifies them according to representations. For the representations II, Δ, Φ, Γ, only one distribution of each pair is listed. For example, $(2p\pi_a3d\pi_b\Delta)$ is listed and $(2p\pi_a3d\pi_b\bar{\Delta})$ is omitted, since this is sufficient for the evaluation of integrals (see Sec. 1, before Eq. (1.13)). Furthermore, when two distributions differ only by the interchange of the two nuclei a and b, only one of them is listed (see Secs. 1, III and 2, VI). In this sense there exist 65 essentially different charge distributions, which are given below.

28 Σ^+ type distributions (containing the factor $\cos 0\varphi=1$)

I. $(1s_a1s_b)(2s_a2s_b)(3s_a3s_b)(1s_a2s_b)(1s_a3s_b)(2s_a3s_b)$
II. $(2p\sigma_a2p\sigma_b)(3p\sigma_a3p\sigma_b)(2p\sigma_a3p\sigma_b)$
III. $(3d\sigma_a3d\sigma_b)$
IV. $(1s_a2p\sigma_b)(2s_a2p\sigma_b)(3s_a2p\sigma_b)(1s_a3p\sigma_b)(2s_a3p\sigma_b)(3s_a3p\sigma_b)$
V. $(1s_a3d\sigma_b)(2s_a3d\sigma_b)(3s_a3d\sigma_b)$
VI. $(2p\sigma_a3d\sigma_b)(3p\sigma_a3d\sigma_b)$
VII. $(2p\pi_a2p\pi_b\Sigma)(3p\pi_a3p\pi_b\Sigma)(2p\pi_a3p\pi_b\Sigma)$
$(2p\pi_a3d\pi_b\Sigma)(3p\pi_a3d\pi_b\Sigma)(3d\pi_a3d\pi_b\Sigma)$
VIII. $(3d\delta_a3d\delta_b\Sigma)$

21 Π-type distributions (containing $\cos\varphi$)

IX. $(1s_a2p\pi_b)(2s_a2p\pi_b)(3s_a2p\pi_b)(2p\sigma_a2p\pi_b)(3p\sigma2p\pi_b)(3d\sigma_a2p\pi_b)$
X. $(1s_a3p\pi_b)(2s_a3p\pi_b)(3s_a3p\pi_b)(2p\sigma_a3p\pi_b)(3p\sigma_a3p\pi_b)(3d\sigma_a3p\pi_b)$
XI. $(1s_a3d\pi_b)(2s_a3d\pi_b)(3s_a3d\pi_b)(2p\sigma_a3d\pi_b)(3p\sigma_a3d\pi_b)(3d\sigma_a3d\pi_b)$
XII. $(2p\pi_a3d\delta_b\Pi)(3p\pi_a3d\delta_b\Pi)(3d\pi_a3d\delta_b\Pi)$

12 Δ-type distributions (containing $\cos 2\varphi$)

XIII. $(1s_a3d\delta_b)(2s_a3d\delta_b)(3s_a3d\delta_b)(2p\sigma_a3d\delta_b)(3p\sigma_a3d\delta_b)(3d\sigma_a3d\delta_b)$
XIV. $(2p\pi_a2p\pi_b\Delta)(3p\pi_a3p\pi_b\Delta)(2p\pi_a3p\pi_b\Delta)$
$(3d\pi_a3d\pi_b\Delta)(2p\pi_a3d\pi_b\Delta)(3p\pi_a3d\pi_b\Delta)$

3 Φ-type distributions (containing $\cos 3\varphi$)

XV. $(2p\pi_a3d\delta_b\Phi)(3p\pi_a3d\delta_b\Phi)(3d\pi_a3d\delta_b\Phi)$

1 Γ-type distribution (containing $\cos 4\varphi$)

XVI. $(3d\delta_a3d\delta_b\Gamma)$

factor $\sin M\varphi$. (See reference 2 in the section: "Choice of AO'S." M must be the same in Ω and $\bar{\Omega}$.) Moreover, these two types of integrals will yield the same result if M is the same. Thus, we may restrict ourselves to the cases that $\Omega(1)$ and $\bar{\Omega}(2)$ both contain the same factor $\cos M\varphi$.

Let us, therefore, assume that electron (1) occupies the distribution (1.9) and electron (2) occupies the distribution

$$\bar{\Omega}=\bar{k}\bar{\omega}(\xi,\eta)e^{-\bar{\alpha}\xi}e^{\bar{\beta}\eta}(\xi^2-1)^{M/2}(1-\eta^2)^{M/2}\cos M\varphi, \quad (1.13)$$

$$\bar{\alpha}=\tfrac{1}{2}R(\bar{\zeta}_a+\bar{\zeta}_b), \quad \bar{\beta}=\tfrac{1}{2}R(\bar{\zeta}_a-\bar{\zeta}_b), \quad (1.13')$$

$$\bar{k}=R^{-3}(R\zeta_a)^{\bar{n}_a+\frac{1}{2}}(R\bar{\zeta}_b)^{\bar{n}_a+\frac{1}{2}}. \quad (1.13'')$$

For the integration the inverse distance $1/r_{12}$ has to be expressed as a function of the elliptic coordinates of its two endpoints. This is accomplished in a convenient way by the expansion of F. E. Neumann, which we write

$$\frac{R}{r_{12}}=4\sum_{l=0}^{\infty}\sum_{m=-l}^{l}(-1)^m\frac{(l-|m|)!}{(l+|m|)!}P_l^{|m|}(\xi_1)Q_l^{|m|}(\xi_2)$$
$$\times\mathcal{P}_l^{|m|}(\eta_1)\mathcal{P}_l^{|m|}(\eta_2)e^{im\varphi_1}e^{-im\varphi_2}. \quad (1.14)$$

A short derivation of (1.14) is given in Sec. 4 (see Eq. (4.14)). The Q_l^m are the associated Legendre functions of the second kind.[4]

Formula (1.14) holds for $\xi_1<\xi_2$; one has to exchange ξ_1 and ξ_2 in it for the case $\xi_1>\xi_2$. We have therefore to split up the integral into two corresponding parts in order to be able to use Eq. (1.14).

After introducing (1.9, 13, 14) and the volume element in elliptic coordinates

$$dV=(\tfrac{1}{2}R)^3(\xi^2-\eta^2)d\xi d\eta d\varphi,$$

in the integral (A) one rearranges the terms and performs

[4] Our definitions of P_l^m, Q_l^m are those of E. Jahnke and F. Emde, *Tables of Functions* (Dover Publications, New York, 1945). Hence, we have $P_l^m(\eta)=(1-\eta^2)^{m/2}P_l^{(m)}(\eta)$, but $P_l^m(\xi)=(\xi^2-1)^{m/2}P_l^{(m)}(\xi)$, $Q_l^m(\xi)=(\xi^2-1)^{m/2}Q_l^{(m)}(\xi)$.

TABLE II. The constants ω_{nj} for the 65 distributions.

All 65 distributions of Table I are of the form,

$$k\omega(\xi,\eta)e^{-\alpha\xi}e^{\beta\eta}(\xi^2-1)^{M/2}(1-\eta^2)^{M/2}\cos M\varphi,$$

where $\omega(\xi,\eta)$ is a polynomial in ξ and η; see Eq. (1.9). Table II lists the constants ω_{nj} which characterize the related polynomials

$$\tfrac{1}{2}\pi[\tfrac{1}{2}(1+\delta_{M0})]^{\frac{1}{2}}(\xi^2-\eta^2)\omega(\xi,\eta)=\Sigma_{nj}\,\omega_{nj}\xi^n\eta^j;$$

see Eqs. (1.12), (1.19), and Sec. 1, III. The rows correspond to the index n, and the columns correspond to the index j. The last column of each table denoted by "cf" contains a common factor by which each element is to be multiplied. The order in which the 65 distributions are arranged corresponds exactly to the order employed in Table I.

Σ^+ type distributions

I

$n\downarrow$ \ $j\rightarrow$ $1s_a1s_b$	0	1	2	cf
0			−1	
1				1/2
2	1			

$n\downarrow$ \ $j\rightarrow$ $2s_a2s_b$	0	1	2	3	4	cf
0					1	
1						
2			−2			1/24
3						
4		1				

$3s_a3s_b$	0	1	2	3	4	5	6	cf
0							−1	
1								
2					3			
3								1/720
4			−3					
5								
6	1							

$1s_a2s_b$	0	1	2	3	cf
0				−1	
1			−1		
2		1			1/4(3)$^{\frac{1}{2}}$
3	1				

$1s_a3s_b$	0	1	2	3	4	cf
0					−1	
1				−2		
2						1/12(10)$^{\frac{1}{2}}$
3		2				
4	1					

$2s_a3s_b$	0	1	2	3	4	5	cf
0						1	
1					1		
2				−2			
3			−2				1/24(30)$^{\frac{1}{2}}$
4		1					
5	1						

Σ^+ type distributions—*Continued.*

II

$2p\sigma_a2p\sigma_b$	0	1	2	3	4	cf
0			−1			
1						
2	1				1	1/8
3						
4			−1			

$3p\sigma_a3p\sigma_b$	0	1	2	3	4	5	6	cf
0					1			
1								
2			−2				−1	
3								1/240
4	1				2			
5								
6			−1					

$2p\sigma_a3p\sigma_b$	0	1	2	3	4	5	cf
0				−1			
1			−1				
2		1				1	
3	1				1		1/8(30)$^{\frac{1}{2}}$
4				−1			
5			−1				

III

$3d\sigma_a3d\sigma_b$	0	1	2	3	4	5	6	cf
0			−9		6		−1	
1								
2	9				−3		6	
3								1/576
4	−6		3				−9	
5								
6	1		−6		9			

IV

$1s_a2p\sigma_b$	0	1	2	3	cf
0			−1		
1				−1	1/4
2	1				
3		1			

$2s_a2p\sigma_b$	0	1	2	3	4	cf
0				1		
1			−1		1	
2		−1		−1		1/8(3)$^{\frac{1}{2}}$
3	1		−1			
4		1				

$3s_a2p\sigma_b$	0	1	2	3	4	5	cf
0					−1		
1				2		−1	
2					2		
3		−2					1/24(10)$^{\frac{1}{2}}$
4	1		−2				
5		1					

TABLE II—*Continued.*

Σ^+ type distributions—*Continued.*

IV—*Continued.*

$1s_a3p\sigma_b$	0	1	2	3	4	cf
0				−1		
1			−1		−1	
2		1		−1		1/4(30)½
3	1		1			
4		1				

$2s_a3p\sigma_b$	0	1	2	3	4	5	cf
0					1		
1						1	
2			−2				
3				−2			1/24(10)½
4	1						
5		1					

$3s_a3p\sigma_b$	0	1	2	3	4	5	6	cf
0						−1		
1					1		−1	
2				2		1		
3			−2		2			1/240(3)½
4		−1		−2				
5	1		−1					
6		1						

V

$1s_a3d\sigma_b$	0	1	2	3	4	cf
0			−3		1	
1				−4		
2	3				−3	1/24(2)½
3		4				
4	−1		3			

$2s_a3d\sigma_b$	0	1	2	3	4	5	cf
0				3		−1	
1			−3		5		
2		−3		−4		3	
3	3		−4		−3		1/48(6)½
4		5		−3			
5	−1		3				

$3s_a3d\sigma_b$	0	1	2	3	4	5	6	cf
0					−3		1	
1				6		−6		
2					9		−3	
3		−6				6		1/288(5)½
4	3		−9					
5		6		−6				
6	−1		3					

VI

$2p\sigma_a3d\sigma_b$	0	1	2	3	4	5	cf
0			−3		1		
1				−1		−1	
2	3				1		
3		1				3	1/48(2)½
4	−1		−1				
5		1		−3			

Σ^+ type distributions—*Continued.*

VI—*Continued*

$3p\sigma_a3d\sigma_b$	0	1	2	3	4	5	6	cf
0				3		−1		
1			−3		2		1	
2		−3		−1		−2		
3	3		−1		1		−3	1/96(15)½
4		2		1		3		
5	−1		−2		3			
6		1		−3				

VII

$2p\pi_a2p\pi_b\Sigma$	0	1	2	3	4	cf
0			1		−1	
1						
2		−1			1	1/16
3						
4		1		−1		

$3p\pi_a3p\pi_b\Sigma$	0	1	2	3	4	5	6	cf
0					−1		1	
1								
2			2		−1		−1	
3								1/480
4	−1		−1		2			
5								
6	1		−1					

$2p\pi_a3p\pi_b\Sigma$	0	1	2	3	4	5	cf
0				1		−1	
1			1		−1		
2		−1				1	
3	−1				1		1/16(30)½
4		1		−1			
5	1		−1				

$2p\pi_a3d\pi_b\Sigma$	0	1	2	3	4	5	cf
0			1		−1		
1				1		−1	
2	−1				1		
3		−1				1	1/16(6)½
4			−1				
5	1	1		−1			

$3p\pi_a3d\pi_b\Sigma$	0	1	2	3	4	5	6	cf
0				−1		1		
1			1		−2		1	
2		1		1		−2		
3	−1		1		1		−1	1/96(5)½
4		−2		1		1		
5	1		−2		1			
6		1		−1				

$3d\pi_a3d\pi_b\Sigma$	0	1	2	3	4	5	6	cf
0			1		−1			
1								
2	−1						1	
3								1/96
4	1						−1	
5								
6			−1		1			

TABLE II—*Continued.*

Σ⁺ type distributions—*Continued.*

VIII

$3d\delta_a 3d\delta_b\Sigma$	0	1	2	3	4	5	6	cf
0			−1		2		−1	
1								
2	1				−3		2	
3								1/384
4	−2		3				−1	
5								
6	1		−2		1			

Π-type distributions

IX

$1s_a 2p\pi_b$	0	1	2	cf
0			−1	
1				1/4(2)½
2	1			

$2s_a 2p\pi_b$	0	1	2	3	cf
0				1	
1			−1		
2		−1			1/8(6)½
3	1				

$3s_a 2p\pi_b$	0	1	2	3	4	cf
0					−1	
1				2		
2						1/48(5)½
3		−2				
4	1					

$2p\sigma_a 2p\pi_b$	0	1	2	3	cf
0			−1		
1				1	
2		1			1/8(2)½
3			−1		

$3p\sigma_a 2p\pi_b$	0	1	2	3	4	cf
0				1		
1			−1		−1	
2		−1		1		1/16(15)½
3	1		1			
4		−1				

$3d\sigma_a 2p\pi_b$	0	1	2	3	4	cf
0			−3		1	
1				4		
2	3				−3	1/96
3		−4				
4	−1		3			

X

$1s_a 3p\pi_b$	0	1	2	3	cf
0				−1	
1			−1		
2		1			1/8(15)½
3	1				

H-type distributions—*Continued.*

X—*Continued.*

$2s_a 3p\pi_b$	0	1	2	3	4	cf
0					1	
1						
2			−2			1/48(5)½
3						
4	1					

$3s_a 3p\pi_b$	0	1	2	3	4	5	cf
0						−1	
1					1		
2				2			1/240(6)½
3			−2				
4		−1					
5	1						

$2p\sigma_a 3p\pi_b$	0	1	2	3	4	cf
0				−1		
1			−1		1	
2		1		1		1/16(15)½
3	1		−1			
4		−1				

$3p\sigma_a 3p\pi_b$	0	1	2	3	4	5	cf
0					1		
1						−1	
2			−2				1/240(2)½
3				2			
4	1						
5		−1					

$3d\sigma_a 3p\pi_b$	0	1	2	3	4	5	cf
0				−3		1	
1			−3		5		
2		3		4		−3	1/96(30)½
3	3		−4		−3		
4		−5		3			
5	−1		3				

XI

$1s_a 3d\pi_b$	0	1	2	3	cf
0			−1		
1				−1	
2		1			1/8(3)½
3			1		

$2s_a 3d\pi_b$	0	1	2	3	4	cf
0				1		
1			−1		1	
2		−1		−1		1/48
3	1		−1			
4		1				

$3s_a 3d\pi_b$	0	1	2	3	4	5	cf
0					−1		
1				2		−1	
2					2		
3		−2					1/48(30)½
4	1		−2				
5		1					

TABLE II—*Continued.*

H-type distributions—*Continued.*

XI—*Continued.*

$2p\sigma_a 3d\pi_b$	0	1	2	3	4	cf
0			−1			
1						
2		1			1	1/16(3)½
3						
4			−1			

$3p\sigma_a 3d\pi_b$	0	1	2	3	4	5	cf
0				1			
1			−1				
2		−1				−1	
3	1				1		1/48(10)½
4				1			
5			−1				

$3d\sigma_a 3d\pi_b$	0	1	2	3	4	5	cf
0			−3		1		
1				1		1	
2	3				1		
3		−1				−3	1/96(6)½
4	−1		−1				
5		−1		3			

XII

$2p\pi_a 3d\delta_b$II	0	1	2	3	4	cf
0			1		−1	
1						
2		−1			1	1/64(3)½
3						
4		1		−1		

$3p\pi_a 3d\delta_b$II	0	1	2	3	4	5	cf
0				−1		1	
1			1		−1		
2		1				−1	
3	−1				1		1/192(10)½
4		−1		1			
5	1		−1				

$3d\pi_a 3d\delta_b$II	0	1	2	3	4	5	cf
0			1		−1		
1				−1		1	
2	−1				1		
3		1				−1	1/192(2)½
4	1		−1				
5		−1		1			

Δ-type distributions

XIII

$1s_a 3d\delta_b$	0	1	2	cf
0			−1	
1				1/16(3)½
2	1			

$2s_a 3d\delta_b$	0	1	2	3	cf
0				1	
1			−1		1/96
2		−1			
3	1				

Δ-type distributions—*Continued.*

XIII—*Continued.*

$3s_a 3d\delta_b$	0	1	2	3	4	cf
0					−1	
1				2		
2						1/96(30)½
3		−2				
4	1					

$2p\sigma_a 3d\delta_b$	0	1	2	3	cf
0			−1		
1				1	
2	1				1/32(3)½
3		−1			

$3p\sigma_a 3d\delta_b$	0	1	2	3	4	cf
0				1		
1			−1		−1	
2		−1		1		1/96(10)½
3	1		1			
4		−1				

$3d\sigma_a 3d\delta_b$	0	1	2	3	4	cf
0			−3		1	
1				4		
2	3				−3	1/192(6)½
3		−4				
4	−1		3			

XIV

$2p\pi_a 2p\pi_b\Delta$	0	1	2	cf
0			−1	
1				1/16(2)½
2		1		

$3p\pi_a 3p\pi_b\Delta$	0	1	2	3	4	cf
0					1	
1						
2			−2			1/480(2)½
3						
4	1					

$2p\pi_a 3p\pi_b\Delta$	0	1	2	3	cf
0				−1	
1			−1		
2		1			1/32(15)½
3	1				

$3d\pi_a 3d\pi_b\Delta$	0	1	2	3	4	cf
0			−1			
1						
2	1				1	1/96(2)½
3						
4			−1			

TABLE II—*Continued.*

Δ-type distributions—*Continued.*

XIV—*Continued.*

$2p\pi_a 3d\pi_b\Delta$	0	1	2	3	cf
0			−1		
1				−1	$1/32(3)^{\frac{1}{2}}$
2	1				
3		1			

$3p\pi_a 3d\pi_b\Delta$	0	1	2	3	4	cf
0				1		
1			−1		1	
2		−1		−1		$1/96(10)^{\frac{1}{2}}$
3	1		−1			
4		1				

Φ-type distributions

XV

$2p\pi_a 3d\delta_b\Phi$	0	1	2	cf
0			−1	
1				$1/64(3)^{\frac{1}{2}}$
2	1			

Φ-type distributions—*Continued.*

XV—*Continued.*

$3p\pi_a 3d\delta_b\Phi$	0	1	2	3	cf
0				1	
1			−1		$1/192(10)^{\frac{1}{2}}$
2		−1			
3	1				

$3d\pi_a 3d\delta_b\Phi$	0	1	2	3	cf
0			−1		
1				1	$1/192(2)^{\frac{1}{2}}$
2	1				
3		−1			

Γ-type distributions

XVI

$3d\delta_a 3d\delta_b\Gamma$	0	1	2	cf
0			−1	
1				$1/384(2)^{\frac{1}{2}}$
2	1			

a partial integration of the type,

$$\int_1^\infty d\xi(\xi^2-1)^{M/2}P_l^M(\xi)e^{-\alpha\xi}\xi^n \times\int_\xi^\infty dx(x^2-1)^{M/2}Q_l^M(x)e^{-\bar\alpha x}x^{\bar n} =\int_1^\infty d\xi(\xi^2-1)^{M/2}Q_l^M(\xi)e^{-\bar\alpha\xi}\xi^{\bar n} \times\int_1^\xi dx(x^2-1)^{M/2}P_l^M(x)e^{-\alpha x}x^n. \quad (1.15)$$

Thereby, the integral (A) assumes the form,

$$I=R^{-1}(R\zeta_a)^{n_a+\frac{1}{2}}(R\zeta_b)^{n_b+\frac{1}{2}}(R\bar\zeta_a)^{\bar n_a+\frac{1}{2}}(R\bar\zeta_b)^{\bar n_b+\frac{1}{2}}\sum_{l=M}^\infty I_l, \quad (1.16)$$

$$I_l=I_l(\alpha,\bar\alpha,\beta,\bar\beta)=\sum_{n=0}^N\sum_{\bar n=0}^{\bar N}\omega_n{}^l(\beta)\bar\omega_{\bar n}{}^l(\bar\beta)\phi_{n\bar n}{}^{Ml}(\alpha,\bar\alpha), \quad (1.17)$$

where

$$\phi_{n\bar n}{}^{Ml}(\alpha,\bar\alpha)=\phi_{\bar n n}{}^{Ml}(\bar\alpha,\alpha) =(-1)^M\frac{(l-M)!}{(l+M)!}\int_1^\infty d\xi Q_l^M(\xi)(\xi^2-1)^{M/2} \times\left\{e^{-\alpha\xi}\xi^n\int_1^\xi dxP_l^M(x)(x^2-1)^{M/2}e^{-\bar\alpha x}x^{\bar n} +e^{-\bar\alpha\xi}\xi^{\bar n}\int_1^\xi dxP_l^M(x)(x^2-1)^{M/2}e^{-\alpha x}x^n\right\}, \quad (1.18)$$

and (see Eq. (1.12))

$$\omega_n{}^l(\beta)=\sum_{j=0}^J\omega_{nj}B_j{}^{Ml}(\beta),\quad \bar\omega_{\bar n}{}^l(\bar\beta)=\sum_{\bar j=0}^{\bar J}\bar\omega_{\bar n\bar j}B_{\bar j}{}^{Ml}(\bar\beta), \quad (1.19)$$

$$B_j{}^{Ml}(\beta)=\int_{-1}^1 d\eta\mathcal{P}_l^M(\eta)(1-\eta^2)^{M/2}e^{\beta\eta}\eta^j =\left[\frac{2l+1}{2}\frac{(l-m)!}{(l+m)!}\right]^{\frac{1}{2}}\int_{-1}^1 d\eta P_l^M(\eta)(1-\eta^2)^{M/2}e^{\beta\eta}\eta^j. \quad (1.20)$$

III

The general result (1.16, 17) is built up from two kinds of functions: (1) the two-parameter functions $\phi_{n\bar n}{}^{Ml}(\alpha,\bar\alpha)$ which are independent of the particular charge distributions Ω, $\bar\Omega$, except for the symmetry characteristic M; (2) the one-parameter functions $\omega_n{}^l(\beta)$ and $\bar\omega_{\bar n}{}^l(\bar\beta)$, which do depend on the particular distributions Ω and $\bar\Omega$, respectively. This situation suggests that the $\phi_{n\bar n}{}^{Ml}(\alpha,\bar\alpha)$ should be tabulated as functions of α and $\bar\alpha$; these tables may then be used for all integrals involving functions of the symmetry species M. Secondly, one would tabulate the $\omega_n{}^l(\beta)$ as functions of β for every charge distribution Ω. There are 11 such distributions for the quantum numbers 1 and 2, and altogether 65 distributions for the quantum numbers 1, 2, and 3 (see Table I). It may be mentioned that the same functions $\omega_n{}^l(\beta)$ appear in the three-center nuclear attraction integrals.

In order to obtain the value of a particular integral I (There are 47 for quantum numbers 1 and 2; see Table III.) for certain parameter values α, $\bar\alpha$, β, $\bar\beta$, one has then to perform the summations in Eqs. (1.16, 17) by

a desk computing machine according to the following pattern. One calculates the quadratic form (1.17) successively for $l=0, 1, 2, \cdots$. If the tables are arranged in an appropriate manner, this is not difficult, since the summation over n comprises only a few terms: for the quantum numbers 1 and 2 we have $N, \bar{N} \leqslant 4$; for the quantum numbers 1, 2, and 3 we have $N, \bar{N} \leqslant 6$. One then obtains for I the series (1.16).

This series breaks off after a few terms, if $\beta=0$ *or* $\bar{\beta}=0$ (see Sec. 2), i.e., if $\zeta_a=\zeta_b$ or $\bar{\zeta}_a=\bar{\zeta}_b$. If β and $\bar{\beta}$ are *both* different from zero but have their absolute value <1, then the convergence is rapid. For larger values of β, $\bar{\beta}$ the integral is small as a whole.

According to Eq. (1.19) the functions $\omega_n{}^l(\beta)$ in turn are linear combinations of functions $B_j{}^{Ml}(\beta)$, which again are independent of the particular charge distributions. In Table II the coefficients ω_{nj} of formula (1.19) are listed for all the 65 distributions with the quantum numbers 1, 2, and 3. To be exact, there are more such charge distributions, since to some of our 65 distributions there correspond others which are obtained by interchanging the nuclei a and b. They are not listed, since we shall see in Sec. 2 (see Eq. (2.33)) that this interchange amounts at most to a change in sign of the functions $\omega_n{}^l(\beta)$.

We are then left with the problem of evaluating the general functions $B_j{}^{Ml}(\beta)$, Eq. (1.20), and $\phi_{n\bar{n}}{}^{Ml}(\alpha, \bar{\alpha})$, (1.18). The following sections 2, 3 will deal with this question.

When the exponents ξ are the same for the two electrons: $\zeta_a=\bar{\zeta}_a$, $\zeta_b=\bar{\zeta}_b$, then the product $(I\cdot R)$ depends, according to Eq. (1.16), on the two parameters $\alpha=\bar{\alpha}$ and $\beta=\bar{\beta}$ only; if in addition, $\zeta_a=\zeta_b$, then $(I\cdot R)$ is a function of the one parameter α. In both cases $(I\cdot R)$ can therefore be tabulated as a whole. All tables of exchange integrals that have hitherto been made are of this kind (see Sec. 5, II). For tabulation it may be useful to replace the parameters, α, $\bar{\alpha}$ by the new parameters

$$\rho=\tfrac{1}{2}(\alpha+\bar{\alpha}), \quad \sigma=(\alpha-\bar{\alpha})/(\alpha+\bar{\alpha}). \qquad (1.21)$$

2. THE FUNCTIONS $B_j{}^{Ml}(\beta)$

I

From Eq. (1.20) it follows that the functions $B_j{}^{Ml}(\beta)$ may be defined by the expansion,

$$(1-t^2)^{M/2}e^{\beta t}t^j=\sum_{l=M}^{\infty} B_j{}^{Ml}(\beta)\mathcal{P}_l{}^M(t), \qquad (2.1)$$

which by virtue of Eqs. (1.1, 2) is equivalent to the expansion

$$e^{\beta t}t^j=\sum_{l=M}^{\infty}\left[\frac{(l-M)!}{(l+M)!}\right]^{\frac{1}{2}} B_j{}^{Ml}(\beta)\mathcal{P}_l{}^{(M)}(t). \qquad (2.2)$$

TABLE III. The 47 two center exchange integrals between Slater orbitals with quantum numbers 1 and 2.

Among the 65 distributions of Table I one finds 11 distributions which involve only orbitals with quantum numbers 1 and 2. Between these 11 distributions there exist altogether 47 exchange integrals which do not vanish. They are listed below.

The following notation is adopted:

$$\int dV_1 \int dV_2 (1/r_{12})\Omega(1)\bar{\Omega}(2)=[\Omega|\bar{\Omega}].$$

It is applicable to any integral of the type defined in formula (A) in the introduction. For the exchange integral (see Eq. (B) of the introduction) we have therefore

$$[\Omega|\bar{\Omega}]=[\chi_a\chi_b'|\bar{\chi}_a\bar{\chi}_b']=(\chi_a(1)\bar{\chi}_a(2)\,|\,1/r_{12}\,|\,\bar{\chi}_b'(1)\chi_b'(2)),$$

where the well-known Dirac notation has been employed on the right-hand side.

34 integrals involving Σ^+ type distributions.

I.
$[1s_a1s_b|1s_a1s_b]$, $[2s_a2s_b|2s_a2s_b]$, $[1s_a1s_b|2s_a2s_b]$
$[1s_a1s_b|1s_a2s_b]$, $[2s_a2s_b|1s_a2s_b]$, $[1s_a2s_b|1s_a2s_b]$, $[1s_a2s_b|2s_a1s_b]$

II.
$[1s_a2p\sigma_b|1s_a2p\sigma_b]$, $[1s_a2p\sigma_b|2p\sigma_a1s_b]$, $[2s_a2p\sigma_b|2s_a2p\sigma_b]$
$[2s_a2p\sigma_b|2p\sigma_a2s_b]$, $[1s_a2p\sigma_b|2s_a2p\sigma_b]$, $[1s_a2p\sigma_b|2p\sigma_a1s_b]$

III.
$[1s_a1s_b|1s_a2p\sigma_b]$, $[1s_a1s_b|2s_a2p\sigma_b]$, $[2s_a2s_b|1s_a2p\sigma_b]$
$[2s_a2s_b|2s_a2p\sigma_b]$, $[1s_a2s_b|1s_a2p\sigma_b]$, $[1s_a2s_b|2p\sigma_a1s_b]$
$[1s_a2s_b|2s_a2p\sigma_b]$, $[1s_a2s_b|2p\sigma_a2s_b]$

IV.
$[2p\sigma_a2p\sigma_b|2p\sigma_a2p\sigma_b]$
$[1s_a1s_b|2p\sigma_a2p\sigma_b]$, $[2s_a2s_b|2p\sigma_a2p\sigma_b]$, $[1s_a2s_b|2p\sigma_a2p\sigma_b]$
$[1s_a2p\sigma_b|2p\sigma_a2p\sigma_b]$, $[2s_a2p\sigma_b|2p\sigma_a2p\sigma_b]$

V.
$[2p\pi_a2p\pi_b\Sigma|2p\pi_a2\pi_b\Sigma]$
$[1s_a1s_b|2p\pi_a2p\pi_b\Sigma]$, $[2s_a2s_b|2p\pi_a2p\pi_b\Sigma]$, $[1s_a2s_b|2p\pi_a2p\pi_b\Sigma]$
$[1s_a2p\sigma_b|2p\pi_a2p\pi_b\Sigma]$, $[2s_a2p\sigma_b|2p\pi_a2p\pi_b\Sigma]$
$[2p\sigma_a2p\sigma_b|2p\pi_a2p\pi_b\Sigma]$

12 integrals involving Π-type distributions.

VI.
$[1s_a2p\pi_b|1s_a2p\pi_b]$, $[1s_a2p\pi_b|2p\pi_a1s_b]$, $[2s_a2p\pi_b|2s_a2p\pi_b]$
$[2s_a2p\pi_b|2p\pi_a2s_b]$, $[1s_a2p\pi_b|2s_a2p\pi_b]$, $[1s_a2p\pi_b|2p\pi_a2s_b]$

VII.
$[2p\sigma_a2p\pi_b|2p\sigma_a2p\pi_b]$, $[2p\sigma_a2p\pi_b|2p\pi_a2p\sigma_b]$
$[1s_a2p\pi_b|2p\sigma_a2p\pi_b]$, $[1s_a2p\pi_b|2p\pi_a2p\sigma_b]$
$[2s_a2p\pi_b|2p\sigma_a2p\pi_b]$, $[2s_a2p\pi_b|2p\pi_a2p\sigma_b]$

1 integral involving Δ-distributions

VIII.
$[2p\pi_a2p\pi_b\Delta|2p\pi_a2p\pi_b\Delta]$

II

Let us start by showing how to compute the $B_j{}^{Ml}$ for the value $\beta=0$. We differentiate (see Eq. (2.1))

$$t^j=\sum_{l=0}^{\infty} B_j{}^{0l}(0)\mathcal{P}_l(t) \qquad (2.3)$$

M times and compare with Eq. (2.2), where we put $\beta=0$. Thereby, we obtain

$$B_j{}^{Ml}(0)=\left[\frac{(l+M)!}{(l-M)!}\right]^{\frac{1}{2}}\frac{j!}{(j+M)!}B_{j+M}{}^{0l}(0), \qquad (2.4)$$

which enables us to compute the $B_j^{Ml}(0)$ from the $B_j^{0l}(0)$. In order to compute the latter let us write (see Eq. (1.20))

$$B_j^{0l}(\beta)=[2(2l+1)]^{\frac{1}{2}}b_j^l(\beta),$$
$$b_j^l(\beta)=\tfrac{1}{2}\int_{-1}^{1}dtP_l(t)e^{\beta t}t^j. \tag{2.5}$$

Then we have the well-known result[5]

$$\left.\begin{aligned} b_j^l(0)&=2^l\frac{j!}{(j+l+1)!}\frac{(\frac{1}{2}\langle j+l\rangle)!}{(\frac{1}{2}\langle j-l\rangle)!}\Big\}\text{for } (j-l)\geqslant 0 \\ &\quad\text{and even,} \\ b_j^l(0)&=0 \text{ for all other } j\text{-values.}\end{aligned}\right\} \tag{2.6}$$

III

Now we note that according to Eq. (1.20)

$$(d/d\beta)B_j^{Ml}(\beta)=B_{j+1}^{Ml}(\beta), \tag{2.7}$$

whence the Taylor expansion,

$$B_j^{Ml}(\beta)=B_j^{Ml}(\beta_0+h)=\sum_{k=0}^{\infty}\frac{h^k}{k!}B_{j+k}^{Ml}(\beta_0), \tag{2.8}$$

which converges for any value of h, since it can be obtained by expanding the exponential in Eq. (1.20).

In the case of small β-values we can therefore compute the B_l^{Ml} through the series

$$B_j^{Ml}(\beta)=\sum_{k=0}^{\infty}\frac{\beta^k}{k!}B_{j+k}^{Ml}(0), \tag{2.9}$$

which employs the values $B_j^{Ml}(0)$, which we have just discussed.[6]

Having found the B_j^{Ml} for a certain range of β-values, one can then proceed step by step to larger β-values by means of Eq. (28). This method of successive Taylor expansions is known as "derivative method," it is self-checking.[7]

IV

The computations can be simplified or checked by means of the following two recurrence formulas:

$$B_{j+1}^{Ml}=a_M(l)B_j^{M(l-1)}+a_M(l+1)B_j^{M(l+1)}, \tag{2.10}$$

where

$$a_M(l)=a_0(l)[1-(M/l)^2]^{\frac{1}{2}}, \qquad a_0(l)=(4-1/l^2)^{-\frac{1}{2}}; \tag{2.11}$$

and

$$B_0^{Ml}(\beta)=\frac{1}{\beta^M}\left[\frac{(l+M)!}{(l-M)!}\right]^{\frac{1}{2}}B_0^{0l}(\beta). \tag{2.12}$$

Equation (2.10), which permits the computation of the B_j^{Ml} from the B_0^{Ml}, is verified in the following way. One multiplies Eq. (2.1) by t and then applies the relation,

$$t\mathcal{P}_l^M=a_M(l)\mathcal{P}_{l-1}^M+a_M(l+1)\mathcal{P}_{l+1}^M, \tag{2.13}$$

which is equivalent to the well-known recurrence formula for the Legendre functions. Equation (2.12), which permits the computation of the $B_0^{Ml}(\beta)$ from the $B_0^{0l}(\beta)$, is obtained when one compares the Mth derivative of (see Eq. (2.1))

$$e^{\beta t}=\sum_{l=0}^{\infty}B_0^{0l}(\beta)\mathcal{P}_l(t) \tag{2.14}$$

with Eq. (2.2) for $j=0$.

Through Eqs. (2.5, 10, 12) all functions B_j^{Ml} are reduced to the functions:

$$b_0^l(\beta)=\tfrac{1}{2}\int_{-1}^{1}dtP_l(t)e^{\beta t}. \tag{2.15}$$

These are related to the Bessel functions whose order is half an odd integer. In fact the b_0^l are the so-called spherical Bessel functions of purely imaginary argument,

$$b_0^l(\beta)=[\pi/2\beta]^{\frac{1}{2}}I_{l+\frac{1}{2}}(\beta). \tag{2.16}$$

Here $I_\nu(x)$ is the modified Bessel function of purely imaginary argument of order ν, defined by

$$I_\nu(x)=i^{-\nu}J_\nu(ix) \quad (x \text{ real}), \tag{2.17}$$

where $J_\nu(z)$ denotes the ordinary Bessel functions of the first kind.[8] The recurrence formula for the Bessel functions is equivalent to

$$(2l+1)b_0^l=\beta(b_0^{l-1}-b_0^{l+1}), \tag{2.18}$$

which follows from Eq. (2.15) through partial integration by virtue of the relation:[9]

$$(2l+1)P_l(t)=(d/dt)\{P_{l+1}(t)-P_{l-1}(t)\}. \tag{2.19}$$

The explicit form of b_0^l is

$$b_0^l=\sum_{m=0}^{l}P_l^{(m)}(1)\frac{1}{\beta^{m+1}}\{(-1)^me^{\beta}-(-1)^le^{-\beta}\}\tfrac{1}{2}. \tag{2.20}$$

It is derived from Eq. (2.15) by successive partial integrations. We have[10]

$$P_l^{(m)}(1)=\frac{1}{2^m m!}\frac{(l+m)!}{(l-m)!}, \tag{2.21}$$

$$P_l^{(m)}(1)=[(l+m)(l+1-m)/2m]P_l^{(m-1)}(1),$$
$$P_l^{(0)}(1)=1, \tag{2.22}$$

$$b_0^0=(1/\beta)\sinh\beta, \quad b_0^1=(1/\beta)(\cosh\beta-b_0^0). \tag{2.23}$$

[5] See E. T. Whittaker and G. N. Watson, *Modern Analysis* (Cambridge University Press, London, 1946), p. 310.

[6] The computation of the functions $U_k=x^k/k!$ is discussed in *Tables of Sine, Cosine and Exponential Integral*, prepared by the Federal Works Agency under the Sponsorship of the National Bureau of Standars (N.Y.M.T.P., 1940), p. xii of the Introduction to Vol. I. See also Sec. 5, II(4) of the present article.

[7] For a detailed description see the "derivative method" on page xiii ff. of the introduction of Vol. II of reference 6.

[8] See G. N. Watson, *Bessel Functions* (Cambridge University Press, London, 1944), p. 50, formula (2), and p. 77, formula (2). See also reference 12, pp. 231–232.

[9] See reference 5, p. 309.

[10] See, reference 4, page 111.

The spherical Bessel functions have recently been very accurately tabulated for real values of the argument,[11] but for purely imaginary argument values no extensive tables seem to exist yet.[12,13] According to a recent personal communication of Dr. M. P. Barnett,[13,13a] the Department of Applied Mathematics in the University of Liverpool (Director Dr. C. W. Jones) *has* computed such tables; they are not yet published.

V

In order to calculate the functions $b_0{}^l$, the method of successive Taylor expansions, as described by Eq. (2.8) for $M=0$, is the most systematic one. However, other ways of evaluation are possible.

The recurrence formula (2.18) reduces the number of significant figures rapidly if one tries to proceed from lower to higher l-values, but it is possible to employ it in the inverse direction, descending from higher to lower l-values:

$$b_0{}^l=[(2l+3)/\beta]b_0{}^{l+1}+b_0{}^{l+2}. \tag{2.24}$$

This procedure involves a loss of decimal places but not of significant figures.

For sufficiently large values of β the explicit result (2.20) may be used for computation.

Another method consists in decomposing the $P_l(t)$ into powers of t:

$$P_l(t)=p_{ll}t^l+p_{l(l-2)}t^{l-2}+\cdots+\{p_{l1}t \text{ or } p_{l0}\}, \tag{2.25}$$

$$p_{l\nu}=-[(\nu+1)(\nu+2)/(l+\nu+1)(l-\nu)]p_{l(\nu+2)},$$

$$p_{ll}=(2l)!/2^l(l!)^2. \tag{2.26}$$

Then the functions (2.15) can be expressed in terms of the functions[14] (see Eq. (2.5))

$$\tfrac{1}{2}\int_{-1}^{1}dt e^{\beta t}t^n=b_n{}^0(\beta), \tag{2.27}$$

which have to be evaluated separately by means of the recurrence formulas:

$$\left.\begin{aligned} xb_n{}^0(x)&=\sinh x-nb_{n-1}{}^0(x), \quad n=\text{even},\\ xb_n{}^0(x)&=\cosh x-nb_{n-1}{}^0(x), \quad n=\text{odd},\\ xb_0{}^0(x)&=\sinh x. \end{aligned}\right\} \tag{2.28}$$

This method and the computation from Eq. (2.20) both contain the difficulty that for small β-values large terms with opposite signs add up to a small result. One can avoid this partially by grouping together consecutive terms and using the recurrence formulas (2.22) and (2.26), respectively.

VI

Let us add that the functions $B_j{}^{Ml}(\beta)$ have to be computed only for $\beta\geqslant 0$, since from Eq. (1.20) we find

$$B_j{}^{Ml}(-\beta)=(-1)^{j+l+M}B_j{}^{Ml}(\beta). \tag{2.29}$$

This permits a further simplification: Let us consider the two charge distributions (see Eq. (B) in the introduction)

$$\Omega(1)=\chi_a(1)\chi_b'(1) \quad \text{and} \quad \Omega'(1)=\chi_a'(1)\chi_b(1). \tag{2.30}$$

These will lead to two different polynomials $\omega(\xi,\eta)$ and $\omega'(\xi,\eta)$ (see Eq. 1.9)), which according to Eqs. (1.4, 8) will satisfy the relation,

$$\omega'(\xi,\eta)=\omega(\xi,-\eta), \tag{2.31}$$

whence by virtue of Eq. (1.12),

$$\omega_{nj}{}'=(-1)^j\omega_{nj}. \tag{2.32}$$

Introducing this and Eq. (2.29) in the definition (1.19), we finally obtain

$$\omega_n{}'{}^l(\beta)=(-1)^{l+m}\omega_n{}^l(-\beta). \tag{2.33}$$

Therefore, only one of these two sets of functions has to be computed. The generalization for the case that the distribution Ω (1.9) is a sum of two orbital products is obvious.

3. THE FUNCTIONS $\phi_{n\bar{n}}{}^{Ml}(\alpha,\bar{\alpha})$

I

If one intends to evaluate the functions $\phi_{n\bar{n}}{}^{Ml}$ (1.18) by a numerical integration, the following transformation seems to be useful. From Eq. (1.18) it follows that

$$\phi_{n\bar{n}}{}^{Ml}=(-1)^M\frac{(l-M)!}{(l+M)!}\int_1^\infty d\xi\frac{Q_l{}^M(\xi)}{P_l{}^M(\xi)}(d/d\xi)$$

$$\times\left\{\int_1^\xi dx P_l{}^M(x)(x^2-1)^{M/2}\exp(-\alpha x)x^n\right.$$

$$\left.\times\int_1^\xi d\bar{x}P_l{}^M(\bar{x})(\bar{x}^2-1)^{M/2}\exp(-\bar{\alpha}\bar{x})\bar{x}^{\bar{n}}\right\}.$$

Partial integration yields

$$\phi_{n\bar{n}}{}^{Ml}=-(-1)^M\frac{(l-M)!}{(l+M)!}\int_1^\infty d\xi\left[\frac{d}{d\xi}\frac{Q_l{}^M(\xi)}{P_l{}^M(\xi)}\right]\{\cdots\}.$$

In differentiating the quotient $(Q_l{}^M/P_l{}^M)$, we make use of the relation (4.19) in the Appendix of Sec. 4. This

[11] Mathematical Tables Project, National Bureau of Standards, *Tables of Spherical Bessel Functions* (Columbia University Press, New York, 1947), 2 volumes.

[12] A comprehensive bibliography of tables of Bessel functions has been published by H. Bateman and R. C. Archibald, in *Mathematical Tables and Other Aids to Computation* (July, 1944), Vol. I, p. 205. Spherical bessel functions on p. 231.

[13] Kotani, Amemiya, and Simose (see reference 40) have prepared a limited table of the functions $(-1)^l 2b_0{}^l$, which is not mentioned in reference 12. Recently, Barnett and Coulson (see reference 43) have given a short table of the functions $I_{l+\frac{1}{2}}(x)$.

[13a] M. P. Barnett and C. A. Coulson, Trans. Roy. Soc. (London) **243**, 221 (1951).

[14] The functions (2.27), all of which are positive for positive β-values, are related to the functions $B_n(x)$ of reference 1, reference 40, by $B_n(x)=(-1)^n 2b_n{}^0(x)$.

leads to the result,

$$\phi_{n\bar{n}}^{Ml}(\alpha, \bar{\alpha}) = \int_1^\infty d\xi(\xi^2-1)^{-1} f_n^{Ml}(\xi, \alpha) f_{\bar{n}}^{Ml}(\xi, \bar{\alpha}), \quad (3.1)$$

where

$$f_n^{Ml}(\xi, \alpha) = [1/P_l^M(\xi)] \int_1^\xi dx P_l^M(x)(x^2-1)^{M/2} e^{-\alpha x} x^n. \quad (3.2)$$

From Eqs. (3.1, 2) it is seen that the functions $\phi_{n\bar{n}}^{Ml}$ are always positive.

It would be tedious to compile a table by numerical integration, but this method could be employed for one set of values $(\alpha, \bar{\alpha})$, let us say, for $\alpha = \bar{\alpha} = 1$. (For $\alpha = \bar{\alpha} = 0$ the elliptic coordinates are inappropriate.) One could then continue by the method of successive Taylor expansions based on the formulas,

$$\phi_{n\bar{n}}^{Ml}(\alpha+h, \bar{\alpha}) = \sum_{k=0}^\infty \frac{h^k}{k!}(-1)^k \phi_{(n+k)\bar{n}}^{Ml}(\alpha, \bar{\alpha}), \quad (3.3)$$

$$\phi_{n\bar{n}}^{Ml}(\alpha, \bar{\alpha}+h) = \sum_{k=0}^\infty \frac{h^k}{k!}(-1)^k \phi_{n(\bar{n}+k)}^{Ml}(\alpha, \bar{\alpha}), \quad (3.3')$$

which are analagous to Eq. (2.8).

Another way of evaluating the $\phi_{n\bar{n}}^{Ml}$ is furnished by the recurrence procedure which will be discussed subsequently.

II

Proceeding from the simple to the complex, let us start by computing (see Eq. (1.18))

$$\phi_{00}^{00}(\alpha, \bar{\alpha}) = \phi(\alpha, \bar{\alpha}). \quad (3.4)$$

From Eqs. (3.1, 2) it follows that

$$\phi = (1/\alpha\bar{\alpha}) \int_1^\infty d\xi(\xi^2-1)^{-1} \times \{\exp[-(\alpha+\bar{\alpha})] + \exp[-(\alpha+\bar{\alpha})\xi] - \exp(-\alpha)\exp(-\bar{\alpha}\xi) - \exp(-\bar{\alpha})\exp(-\alpha\xi)\}. \quad (3.5)$$

The first term yields $\coth^{-1}\xi$ again. The remaining three terms are integrated by decomposing $(\xi^2-1)^{-1}$ into partial fractions and introducing the exponential integral[15]

$$\mathrm{Ei}(x) = \int_{-\infty}^x dt(e^t/t) \text{ for } x \text{ real and } <0. \quad (3.6)$$

Before inserting the lower limit $\xi = 1$, one expands[15]

$$\mathrm{Ei}(x) = C + \log|x| + \sum_{n=1}^\infty \frac{x^n}{n \cdot n!}, \quad (3.7)$$

where $C = 0.577215\cdots$ is the constant of Euler. Thereby, all infinities at the point $\xi = 1$ cancel, and one obtains the result,

$$\phi = (1/\alpha\bar{\alpha}) \exp[-(\alpha+\bar{\alpha})]\{\mathcal{E}(\alpha) + \mathcal{E}(\bar{\alpha}) - \mathcal{E}(\alpha+\bar{\alpha})\}, \quad (3.8)$$

where

$$\mathcal{E}(x) = \tfrac{1}{2}\{C + \log 2x - e^{2x}\,\mathrm{Ei}(-2x)\}. \quad (3.9)$$

Let us define

$$G_0(x) = e^{-x}\mathcal{E}(x), \quad (3.10)$$

$$F_0(x) = (1/x)G_0(x), \quad (3.11)$$

$$A_0(x) = (1/x)e^{-x}. \quad (3.12)$$

Then the function ϕ (3.8) may also be written

$$\phi = (1/\alpha\bar{\alpha})\{\exp(-\alpha)G_0(\bar{\alpha}) + \exp(-\bar{\alpha})G_0(\alpha) - G_0(\alpha+\bar{\alpha})\}, \quad (3.13)$$

$$\phi = A_0(\alpha)F_0(\bar{\alpha}) + A_0(\bar{\alpha})F_0(\alpha) - [(1/\alpha) + 1/\bar{\alpha}]F_0(\alpha+\bar{\alpha}). \quad (3.14)$$

III

Our next step is to evaluate the functions $\phi_{n\bar{n}}^{00}(\alpha, \bar{\alpha})$. It is however convenient first to consider three sets of auxiliary function which are derived from the functions A_0, F_0, G_0 (3.10–12):

$$A_n(x) = \int_1^\infty dt e^{-xt} t^n = (-1)^n (d^n/dx^n) A_0(x), \quad (3.15)$$

$$F_n(x) = \int_1^\infty dt Q_0(t) e^{-xt} t^n = (-1)^n (d^n/dx^n) F_0(x), \quad (3.16)$$

$$G_n(x) = (-1)^n (d^n/dx^n) G_0(x). \quad (3.17)$$

From Eqs. (3.15, 16) one obtains, by the method illustrated below in Eq. (3.24), the recurrence formulas,

$$xA_n(x) = nA_{n-1}(x) + e^{-x}, \quad (3.18)$$

$$xF_n(x) = nF_{n-1}(x) + G_n(x), \quad (3.19)$$

which together with Eqs. (3.11, 12) permit the computation of the A_n and the F_n when the G_n are known. For the latter we find the recurrence procedure:

$$G_0(x) = \tfrac{1}{2}e^{-x}\{C + \log 2x - e^{2x}\,\mathrm{Ei}(-2x)\}, \quad (3.20)$$

$$G_1(x) = \tfrac{1}{2}e^{-x}\{C + \log 2x + e^{2x}\,\mathrm{Ei}(-2x)\}, \quad (3.20')$$

$$G_n(x) = G_{n-2}(x) - A_{n-2}(x), \quad (3.20'')$$

which follows from Eqs. (3.9, 10, 17).

Let us proceed to the functions $\phi_{n\bar{n}}^{00}$. Several methods of computation are possible. By inserting Eq. (3.13) in

$$\phi_{n\bar{n}}^{00}(\alpha, \bar{\alpha}) = \phi_{n\bar{n}}(\alpha, \bar{\alpha}) = (-1)^{n+\bar{n}}(\partial^{n+\bar{n}}/\partial\alpha^n \partial\bar{\alpha}^{\bar{n}})\phi(\alpha, \bar{\alpha}), \quad (3.21)$$

[15] See reference 4, p. 1. Sometimes the exponential integral is defined with a different sign. We employ the definition of Jahnke and Emde, which is also adopted in reference 6.

we obtain the recurrence formula,

$$\phi_{n\bar{n}}=(n/\alpha)\phi_{(n-1)\bar{n}}+(\bar{n}/\bar{\alpha})\phi_{n(\bar{n}-1)} -(n\bar{n}/\alpha\bar{\alpha})\phi_{(n-1)(\bar{n}-1)}+(1/\alpha\bar{\alpha})R_{n\bar{n}}(\alpha,\bar{\alpha}), \quad (3.22)$$

where

$$R_{n\bar{n}}(\alpha,\bar{\alpha})=G_n(\alpha)\exp(-\bar{\alpha}) +\exp(-\alpha)G_{\bar{n}}(\bar{\alpha})-G_{n+\bar{n}}(\alpha+\bar{\alpha}), \quad (3.23)$$

that is:

$$\phi_{n\bar{n}}=(1/\alpha\bar{\alpha})\{\bar{\alpha}n\phi_{(n-1)\bar{n}}+\alpha^{\bar{n}}\phi_{n(\bar{n}-1)}-n\bar{n}\phi_{(n-1)(\bar{n}-1)} +e^{-\alpha}G_{\bar{n}}(\bar{\alpha})+e^{-\bar{\alpha}}G_n(\alpha)-G_{n+\bar{n}}(\alpha+\bar{\alpha})\}. \quad (3.23')$$

This method requires only the auxiliary functions $A_n(x)$ and the $G_n(x)$, which are easily obtained from the $A_n(x)$. The relation (3.23′) follows from the identity (see 3.13)

$$\left.\begin{aligned}&(-1)^{n+\bar{n}}(\partial^{n+\bar{n}}/\partial\alpha^n\partial\bar{\alpha}^{\bar{n}})(\alpha\bar{\alpha}\phi)\\&\quad=(-1)^{n+\bar{n}}(\partial^{n+\bar{n}}/\partial\alpha^n\partial\bar{\alpha}^{\bar{n}})\\&\quad\times\{e^{-\alpha}G_0(\bar{\alpha})+e^{-\bar{\alpha}}G_0(\alpha)-G_0(\alpha+\bar{\alpha})\}\\&\sum_{j=0}^{n}\sum_{k=0}^{\bar{n}}\binom{n}{j}\binom{\bar{n}}{k}\phi_{(n-j)(\bar{n}-k)}\frac{\partial^{j+k}(\alpha\bar{\alpha})}{\partial(-\alpha)^j\partial(-\bar{\alpha})^k}\\&\quad=e^{-\alpha}G_{\bar{n}}(\bar{\alpha})+e^{-\bar{\alpha}}G_n(\alpha)-G_{n+\bar{n}}(\alpha+\bar{\alpha}).\end{aligned}\right\}(3.24)$$

In the same way one finds the less simple recurrence formulas,

$$\alpha\phi_{n\bar{n}}(\alpha,\bar{\alpha})=n\phi_{(n-1)\bar{n}}(\alpha,\bar{\alpha}) +\sum_{\bar{\nu}=0}^{\bar{n}}\frac{\bar{n}!}{\bar{\nu}!}\frac{1}{(\bar{\alpha}^{\bar{n}-\bar{\nu}+1})}R_{n\bar{\nu}}(\alpha,\bar{\alpha}), \quad (3.25)$$

$$\bar{\alpha}\phi_{n\bar{n}}(\alpha,\bar{\alpha})=\bar{n}\phi_{r(\bar{n}-1)}(\alpha,\bar{\alpha}) +\sum_{\nu=0}^{n}\frac{n!}{\nu!}\frac{1}{(\alpha^{n-\nu+1})}R_{\nu\bar{n}}(\alpha,\bar{\alpha}). \quad (3.25')$$

A second method is obtained if one inserts Eqs. (3.12, 14) in (3.21). Then we may write (Kotani)

$$\phi_{n\bar{n}}(\alpha,\bar{\alpha})=S_{n\bar{n}}(\alpha,\bar{\alpha})+S_{\bar{n}n}(\bar{\alpha},\alpha), \quad (3.26)$$

where (see Eq. (3.16))

$$S_{n\bar{n}}(\alpha,\bar{\alpha})=(-1)^n(\partial^n/\partial\alpha^n)(1/\alpha) \times\{e^{-\alpha}F_{\bar{n}}(\bar{\alpha})-F_{\bar{n}}(\alpha+\bar{\alpha})\}, \quad (3.27)$$

whence, by the method illustrated in Eq. (3.24), the recurrence formula,

$$S_{n\bar{n}}(\alpha,\bar{\alpha})=(1/\alpha)\{nS_{(n-1)\bar{n}}(\alpha,\bar{\alpha}) +e^{-\alpha}F_{\bar{n}}(\bar{\alpha})-F_{n+\bar{n}}(\alpha+\bar{\alpha})\}. \quad (3.28)$$

This method excludes the possibility of exploiting the relation,

$$\phi_{n\bar{n}}(\alpha,\bar{\alpha})=\phi_{\bar{n}n}(\bar{\alpha},\alpha). \quad (3.29)$$

Third method: By inserting Eq. (3.14) in Eq. (3.21), one may also write (see Eqs. (3.15, 16)) (Rosen-James)

$$\phi_{n\bar{n}}(\alpha,\bar{\alpha})=A_n(\alpha)F_{\bar{n}}(\bar{\alpha}) +F_n(\alpha)A_{\bar{n}}(\bar{\alpha})-T_{n\bar{n}}(\alpha,\bar{\alpha}), \quad (3.30)$$

where

$$T_{n\bar{n}}(\alpha,\bar{\alpha})=T'_{n\bar{n}}(\alpha,\bar{\alpha})+T'_{\bar{n}n}(\bar{\alpha},\alpha), \quad (3.31)$$

$$T'_{n\bar{n}}(\alpha,\bar{\alpha})=(-1)^n(\partial^n/\partial\alpha^n)(1/\alpha)F_{\bar{n}}(\alpha+\bar{\alpha}), \quad (3.32)$$

or (see Eq. (3.13))

$$T_{n\bar{n}}=(-1)^{n+\bar{n}}(\partial^{n+\bar{n}}/\partial\alpha^n\partial\bar{\alpha}^{\bar{n}})(1/\alpha\bar{\alpha})G_0(\alpha+\bar{\alpha}). \quad (3.33)$$

From Eq. (3.32) there follows the recurrence formula,

$$T'_{n\bar{n}}(\alpha,\bar{\alpha})=(1/\alpha)\{nT'_{(n-1)\bar{n}}(\alpha,\bar{\alpha}) +F_{n+\bar{n}}(\alpha+\bar{\alpha})\} \quad (3.34)$$

for $T'_{n\bar{n}}$. For $T_{n\bar{n}}$ one finds from Eq. (3.33)

$$T_{n\bar{n}}=(n/\alpha)T_{(n-1)\bar{n}}+(\bar{n}/\bar{\alpha})T_{n(\bar{n}-1)} -(n\bar{n}/\alpha\bar{\alpha})T_{(n-1)(\bar{n}-1)}+(1/\alpha\bar{\alpha})G_{n+\bar{n}}(\alpha+\bar{\alpha}) \quad (3.35)$$

and

$$\alpha T_{n\bar{n}}(\alpha,\bar{\alpha})=nT_{(n-1)\bar{n}}(\alpha,\bar{\alpha}) +\sum_{\bar{\nu}=0}^{\bar{n}}\frac{\bar{n}!}{\bar{\nu}!}\frac{1}{(\bar{\alpha}^{\bar{n}-\bar{\nu}+1})}G_{n+\bar{\nu}}(\alpha+\bar{\alpha}), \quad (3.36)$$

$$\bar{\alpha}T_{n\bar{n}}(\alpha,\bar{\alpha})=\bar{n}T_{n(\bar{n}-1)}(\alpha,\bar{\alpha}) +\sum_{\nu=0}^{n}\frac{n!}{\nu!}\frac{1}{(\alpha^{n-\nu+1})}G_{\nu+\bar{n}}(\alpha+\bar{\alpha}). \quad (3.37)$$

The derivation of Eqs. (3.34–37) follows the pattern of Eq. (3.24).

IV

We come now to the third step, which consists of finding the function $\phi_{n\bar{n}}{}^{0l}(\alpha,\bar{\alpha})$. Let us write

$$\phi_{n\bar{n}}{}^{00}=\varphi_{n\bar{n}}{}^0, \quad \phi_{n\bar{n}}{}^{0l}=[(2l-1)/l^2]\varphi_{n\bar{n}}{}^l \quad (l\geqslant 1). \quad (3.38)$$

We will prove that the $\varphi_{n\bar{n}}{}^l$ can be obtained by the following recurrence procedure:

$$\varphi_{n\bar{n}}{}^l=(b_{l-2}/b_{l-1})\varphi_{n\bar{n}}{}^{l-2}+\psi_{n\bar{n}}{}^{l-1}, \quad (l\geqslant 2), \quad (3.39)$$

$$\overset{l}{\psi}_{n\bar{n}}=\overset{l-2}{\psi}_{n\bar{n}}+b_l\overset{l}{\varphi}_{(n+1)(\bar{n}+1)}+b_{l-2}\overset{l-2}{\varphi}_{(n+1)(\bar{n}+1)} -b_{l-1}\{\overset{l-1}{\varphi}_{(n+2)\bar{n}}+\overset{l-1}{\varphi}_{n(\bar{n}+2)}\}, \quad (l\geqslant 2), \quad (3.40)$$

where

$$b_0=1, \quad b_l=4-(1/l^2) \text{ for } l\geqslant 1. \quad (3.41)$$

The reciprocal of b_l is equal to the square of $a_0(l)$ defined in Eq. (2.11). The procedure (3.39, 40) consists of two steps: From the $\varphi_{n\bar{n}}{}^l$ one computes the $\psi_{n\bar{n}}{}^l$, and one then passes from the $\psi_{n\bar{n}}{}^l$ to the $\varphi_{n\bar{n}}{}^{l+1}$. For

$l=0, 1$ the following relations have to be added

$$\overset{1}{\varphi}_{n\bar{n}}=\overset{0}{\psi}_{n\bar{n}}, \tag{3.42}$$

$$\overset{1}{\psi}_{n\bar{n}}=3\overset{1}{\varphi}_{(n+1)(\bar{n}+1)}+\overset{1}{\varphi}_{n\bar{n}}-\overset{0}{\varphi}_{(n+1)(\bar{n}+1)}-\overset{0}{\varphi}_{(n+2)\bar{n}}$$
$$-\overset{0}{\varphi}_{n(\bar{n}+2)}+A_n(\alpha)A_{\bar{n}+1}(\bar{\alpha})+A_{n+1}(\alpha)A_{\bar{n}}(\bar{\alpha}), \tag{3.43}$$

$$\overset{0}{\psi}_{n\bar{n}}=\overset{0}{\varphi}_{(n+1)(\bar{n}+1)}-A_n(\alpha)A_{\bar{n}}(\bar{\alpha})-A_{n\bar{n}}(\alpha, \bar{\alpha}), \tag{3.44}$$

where

$$A_{n\bar{n}}(\alpha, \bar{\alpha})=(-1)^{n+\bar{n}}(\partial^{n+\bar{n}}/\partial\alpha^n\partial\bar{\alpha}^{\bar{n}})$$
$$\times[1/\alpha\bar{\alpha}(\alpha+\bar{\alpha})]\exp[-(\alpha+\bar{\alpha})]. \tag{3.45}$$

These functions are computed by means of the recurrence relations:

$$A_{n\bar{n}}=(1/\alpha+\bar{\alpha})\{nA_{(n-1)\bar{n}}+\bar{n}A_{n(\bar{n}-1)}+A_n(\alpha)A_{\bar{n}}(\bar{\alpha})\}, \tag{3.46}$$

$$A_{00}(\alpha, \bar{\alpha})=(1/\alpha+\bar{\alpha})A_0(\alpha)A_0(\bar{\alpha}), \tag{3.47}$$

which are found by the method illustrated in Eq. (3.24).

Proof of Eqs. (3.39–45)

Multiplying the two recurrence formulas[16]

$$\left.\begin{aligned} lP_l(x)&=(2l-1)xP_{l-1}(x)-(l-1)P_{l-2}(x), \\ lQ_l(\xi)&=(2l-1)\xi Q_{l-1}(\xi)-(l-1)Q_{l-2}(\xi), \end{aligned}\right\}(l\geqslant 2) \tag{3.48, 3.49}$$

we find for $l\geqslant 2$

$$R_l(x, \xi)=(b_{l-2}/b_{l-1})R_{l-2}(x, \xi)$$
$$+b_{l-1}x\xi R_{l-1}(x, \xi)-S_{l-1}(x, \xi), \tag{3.50}$$

where

$$R_0(x, \xi)=P_0(x)Q_0(\xi);$$

$$R_l(x, \xi)=(l^2/2l-1)P_l(x)Q_l(\xi), \quad (l\geqslant 1); \tag{3.51}$$

and

$$S_l(x, \xi)=l\{xP_l(x)Q_{l-1}(\xi)+\xi P_{l-1}(x)Q_l(\xi)\},$$
$$(l\geqslant 1); \tag{3.52}$$

b_l is given by Eq. (3.41). Applying the two relations (3.48, 49) to (3.52), we furthermore find for $l\geqslant 3$, that

$$S_l(x, \xi)=S_{l-2}(x, \xi)-2b_{l-2}x\xi R_{l-2}(x, \xi)$$
$$+b_{l-1}(x^2+\xi^2)R_{l-1}(x, \xi), \tag{3.53}$$

and for $l=2$

$$S_2(x, \xi)=-R_1(x, \xi)-x\xi R_0(x, \xi)$$
$$+b_1(x^2+\xi^2)R_1(x, \xi). \tag{3.54}$$

Now we have from Eqs. (1.18), (3.38, 51)

$$\varphi_{n\bar{n}}{}^l=\int_1^\infty d\xi\Big\{\exp(-\alpha\xi)\xi^n\int_1^\xi dx\exp(-\bar{\alpha}x)x^{\bar{n}}R_l(x, \xi)$$
$$+\exp(-\bar{\alpha}\xi)\xi^{\bar{n}}\int_1^\xi dx\exp(-\alpha x)x^nR_l(x, \xi)\Big\}. \tag{3.55}$$

[16] See reference 4, p. 114.

In addition, we define for $l\geqslant 1$

$$\psi_{n\bar{n}}{}^l(\alpha, \bar{\alpha})=b_l\overset{l}{\varphi}_{(n+1)(\bar{n}+1)}(\alpha, \bar{\alpha})-\int_1^\infty d\xi\Big\{\exp(-\alpha\xi)\xi^n$$
$$\times\int_1^\xi dx\exp(-\bar{\alpha}x)x^{\bar{n}}S_l(x, \xi)$$
$$+\exp(-\bar{\alpha}\xi)\xi^{\bar{n}}\int_1^\xi dx\exp(-\alpha x)x^nS_l(x, \xi)\Big\}, \tag{3.56}$$

and

$$\psi_{n\bar{n}}{}^0(\alpha, \bar{\alpha})=\varphi_{n\bar{n}}{}^1(\alpha, \bar{\alpha}). \tag{3.57}$$

Then Eq. (3.50) combined with Eqs. (3.55, 56) yields Eq. (3.39). Equation (3.53) combined with Eqs. (3.55, 56) yields Eq. (3.40) for $l\geqslant 3$. Equation (3.54) combined with Eqs. (3.55, 56, 57) yields Eq. (3.40) for $l=2$. Furthermore, Eq. (3.57) is identical with Eq. (3.42).

Therefore Eqs. (3.43, 44) remain to be proved. From the equation,

$$P_1(x)Q_1(\xi)=x\{\xi Q_0(\xi)-1\}=x\xi P_0(x)Q_0(\xi)-x \tag{3.58}$$

follows [see Eqs. (3.55, 57)]

$$\overset{0}{\psi}_{n\bar{n}}=\overset{0}{\varphi}_{(n+1)(\bar{n}+1)}$$
$$-\int_1^\infty d\xi\Big\{\xi^n\exp(-\alpha\xi)\int_1^\xi dx\exp(-\bar{\alpha}x)x^{\bar{n}+1}$$
$$+\xi^{\bar{n}}\exp(-\bar{\alpha}\xi)\int_1^\xi dx\exp(-\alpha x)x^{n+1}\Big\}, \tag{3.59}$$

$$\overset{0}{\psi}_{n\bar{n}}=\overset{0}{\varphi}_{(n+1)(\bar{n}+1)}-(-1)^{n+\bar{n}}\frac{\partial^{n+\bar{n}}}{\partial\alpha^n\partial\bar{\alpha}^{\bar{n}}}$$
$$\times\left\{\frac{\exp(-\alpha)}{\alpha}\frac{\exp(-\bar{\alpha})}{\bar{\alpha}}+\frac{\exp[-(\alpha+\bar{\alpha})]}{\alpha\bar{\alpha}(\alpha+\bar{\alpha})}\right\}.$$

This formula becomes identical with Eq. (3.44) when we insert the definitions (3.12, 15) and (3.45).

Finally, from Eq. (3.51, 52) we have

$$S_1(x, \xi)=x^2Q_0(\xi)+\xi\{\xi Q_0(\xi)-1\}$$
$$=(x^2+\xi^2)R_0(x, \xi)-\xi. \tag{3.60}$$

To this we add Eq. (3.58), whence

$$S_1(x, \xi)=(x^2+\xi^2+x\xi)R_0(x, \xi)-R_1(x, \xi)-(x+\xi), \tag{3.61}$$

which by virtue of Eqs. (3.55, 56) yields

$$\overset{1}{\psi}_{n\bar{n}}=b_1\overset{1}{\varphi}_{(n+1)(\bar{n}+1)}+\overset{1}{\varphi}_{n\bar{n}}-\overset{0}{\varphi}_{(n+1)(\bar{n}+1)}$$
$$-\overset{0}{\varphi}_{(n+2)\bar{n}}-\overset{0}{\varphi}_{n(\bar{n}+2)}+J_{n\bar{n}}, \tag{3.62}$$

where (see Eqs. (3.12, 15))

$$J_{n\bar{n}}=(-1)^{n+\bar{n}}(\partial^{n+\bar{n}}/\partial\alpha^n\partial\bar{\alpha}^{\bar{n}})\int_1^\infty d\xi(d/d\xi)\times\left\{\int_1^\xi dx\exp(-\alpha x)\int_1^\xi d\bar{x}\exp(\bar{\alpha}\bar{x})\bar{x}+\int_1^\xi dx\exp(-\alpha x)x\int_1^\xi d\bar{x}\exp(-\bar{\alpha}\bar{x})\right\},\quad(3.63)$$

$$J_{n\bar{n}}=A_n(\alpha)A_{\bar{n}+1}(\bar{\alpha})+A_{n+1}(\alpha)A_{\bar{n}}(\bar{\alpha}).$$

Thereby, we have verified all of the Eqs. (3.39–45).

V

The final step of our evaluation leads from the functions $\phi_{n\bar{n}}{}^{0l}$ to the functions $\phi_{n\bar{n}}{}^{Ml}$. It is performed by the simple recurrence formula,

$$\phi_{n\bar{n}}{}^{(M+1)l}=\phi_{(n+1)(\bar{n}+1)}{}^{Ml}-[(l+M)/(2l+1)]\phi_{n\bar{n}}{}^{M(l-1)}-[(l+1-M)/(2l+1)]\phi_{n\bar{n}}{}^{M(l+1)},\quad(3.64)$$

which we shall now derive.

Let us call

$$f_l{}^M(x)=(x^2-1)^{M/2}P_l{}^M(x)=(x^2-1)^M(d^M/dx^M)P_l(x).\quad(3.65)$$

By performing the product differentiation on both sides of the identity

$$(x^2-1)(d/dx)(x^2-1)^{M/2}P_l{}^M(x)=(x^2-1)(d/dx)(x^2-1)^MP_l{}^{(M)}(x),$$

we get

$$f_l{}^{M+1}(x)=-Mxf_l{}^M(x)+(x^2-1)^{M/2}(x^2-1)(d/dx)P_l{}^M(x).\quad(3.66)$$

This equation we combine with either one of the following two recurrence formulas.[17]

$$(x^2-1)(d/dx)P_l{}^M(x)=(l+1-M)P_{l+1}{}^M(x)-(l+1)xP_l{}^M(x),\quad(3.67)$$

$$(x^2-1)(d/dx)P_l{}^M(x)=-(l+M)P_{l-1}{}^M(x)+lxP_l{}^M(x),\quad(3.68)$$

whence

$$f_l{}^{M+1}(x)=(l+1-M)f_{l+1}{}^M(x)-(l+1+M)xf_l{}^M(x),\quad(3.69)$$

$$f_l{}^{M+1}(x)=-(l+M)f_{l-1}{}^M(x)+(l-M)xf_l{}^M(x).\quad(3.70)$$

The same relations must hold for

$$g_l{}^M(\xi)=(\xi^2-1)^{M/2}Q_l{}^M(\xi),\quad(3.71)$$

hence

$$g_l{}^{M+1}(\xi)=(l+1-M)g_{l+1}{}^M(\xi)-(l+1+M)\xi g_l{}^M(\xi),\quad(3.72)$$

$$g_l{}^{M+1}(\xi)=-(l+M)g_{l-1}{}^M(\xi)+(l-M)\xi g_l{}^M(\xi).\quad(3.73)$$

[17] See reference 4, pp. 114, 155.

Now we perform the following operation

$$\frac{[l-(M+1)]!}{[l+(M+1)]!}\{(l-M)\cdot(\text{Eq. }3.69)\cdot(\text{Eq. }3.72)+(l+1+M)\cdot(\text{Eq. }3.70)\cdot(\text{Eq. }3.73)\},\quad(3.74)$$

and use the relations[18]

$$(2l+1)xf_l{}^M(x)=(l+M)f_{l-1}{}^M(x)+(l+1-M)f_{l+1}{}^M(x),\quad(3.75)$$

$$(2l+1)\xi g_l{}^M(\xi)=(l+M)g_{l-1}{}^M(\xi)+(l+1-M)g_{l+1}{}^M(\xi),\quad(3.76)$$

in order to simplify the expression on the right-hand side of Eq. (3.74). The result is

$$\frac{[l-(M+1)]!}{[l+(M+1)]!}f_l{}^{M+1}(x)g_l{}^{M+1}(\xi)=-\frac{(l-M)!}{(l+M)!}x\xi f_l{}^M(x)g_l{}^M(\xi)+\frac{l+1-M}{2l+1}\frac{(l+1-M)!}{(l+1+M)!}f_{l+1}{}^M(x)g_{l+1}{}^M(\xi)+\frac{l+M}{2l+1}\frac{(l-1-M)!}{(l-1+M)!}f_{l-1}{}^M(x)g_{l-1}{}^M(\xi).\quad(3.77)$$

Upon substituting Eqs. (3.77) and (3.65) in Eq. (1.18), we obtain Eq. (3.64).

VI

There exist other formulas which are satisfied by the functions $\phi_{n\bar{n}}{}^{Ml}$.

A relation connecting the $\phi_{n\bar{n}}{}^{Ml}$ with the $\phi_{n\bar{n}}{}^{(M+1)l}$ can be derived from (1.18) by partial integration and application of Eq. (4.19), but this relation is more complicated than Eq. (3.64).

A relation connecting the $\phi_{n\bar{n}}{}^{Ml}$ with the $\phi_{n\bar{n}}{}^{M(l+1)}$ can be derived by first introducing Eqs. (3.67, 68) into (1.18), then integrating by parts and finally simplifying by virtue of Eq. (4.19). The recurrence relation obtained in this way is again more complicated than the scheme (3.39–45).

Finally, it should be mentioned that the functions $\phi_{n\bar{n}}{}^{Ml}$ are related to the generalized exponential integrals[19] $E_n(x)$ defined by

$$E_n(x)=\int_{-\infty}^x dx_n\int_{-\infty}^{x_n}dx_{n-1}\int_{-\infty}^{x_{n-1}}dx_{n-2}\cdots\times\int_{-\infty}^{x_3}dx_2\int_{-\infty}^{x_2}dx_1e^{x_1}/x_1.\quad(3.78)$$

[18] See Eq. (3.65) and reference 4, p. 114.

[19] See A. Unsöld, *Physik der Sternatmosphären* (Verlag. Julius Springer, Berlin, 1938), p. 467. V. Kourganoff, Ann. astrophys. **10**, 282, 329 (1947). G. Placzek, "The functions $E_n(x)$," and J. Lecaine, "Integrals involving the functions $E_n(x)$," both edited by the National Research Council of Canada, Atomic Energy Project, N.R.C. No. 1547 and No. 1553. Kourganoff uses the

Considering, for example, the functions $\phi_{nn}{}^{0l}$, one may introduce the Neumann formula,[20]

$$Q_l(x)=\tfrac{1}{2}\int_{-1}^{1} dtP_l(t)/(x-t) \tag{3.79}$$

in Eq. (1.18). Then partial integration yields

$$\begin{aligned}\phi_{00}{}^{0l}=-\tfrac{1}{2}\int_{-1}^{1} dtP_l(t)\exp[-(\alpha+\bar{\alpha})t]\int_{1}^{\infty} dxP_l(x)\\ \times\{\exp[-\alpha(x-t)]\mathrm{Ei}(-\bar{\alpha}(x-t))\\ +\exp[-\bar{\alpha}(x-t)]\mathrm{Ei}(-\alpha(x-t))\},\end{aligned} \tag{3.80}$$

and by further partial integrations, the $\phi_{00}{}^{0l}$ can be expressed in terms of the functions,

$$(1/x^n)\int_{-1}^{1} dtP_l(t)e^{x(1-t)}E_{n+1}(-x(1-t)). \tag{3.81}$$

4. THE NEUMANN EXPANSION

Since Neumann's deduction[21] is rather cumbersome, the following short derivation which proceeds along different lines, will perhaps be appreciated.

Let the elliptic coordinates (ξ, η) again be defined by Eq. (1.8). We note that the directional derivative in the outward direction perpendicular to the ellipsoid $\xi=\text{const}$ is given by[22]

$$\begin{aligned}(\partial/\partial n)&=(1/N)(\partial/\partial\xi),\\ N=N(\xi,\eta)&=\tfrac{1}{2}R[(\xi^2-\eta^2)/(\xi^2-1)]^{\frac{1}{2}}.\end{aligned} \tag{4.1}$$

Furthermore, we denote by (see Eqs. (1.1, 2))

$$\left.\begin{aligned}Y_l{}^m(\eta,\varphi)&=\left[\frac{2l+1}{4\pi}\frac{(l-|m|)!}{(l+|m|)!}\right]^{\frac{1}{2}}P_l{}^{|m|}(\eta)e^{im\varphi}\\ &=[1/2\pi]^{\frac{1}{2}}\mathcal{P}_l{}^{|m|}(\eta)e^{im\varphi},\end{aligned}\right\} \tag{4.2}$$

the normalized spherical harmonics.

As a preliminary problem, we calculate the potential of a surface charge distribution $\sigma(\eta, \varphi; \xi')$ on the prolate spheroid $\xi=\text{const}=\xi'$ (ξ' plays the role of a parameter).

The result is, that if the coefficients $A_l{}^m$ are defined by the expansion

$$N(\xi',\eta)\cdot(\xi'^2-1)\cdot\sigma(\eta,\varphi;\xi')=\sum_{l=0}^{\infty}\sum_{m=-l}^{l}A_l{}^m(\xi')Y_l{}^m(\eta,\varphi), \tag{4.3}$$

then the potential is given by [23]

$$\begin{aligned}U_e(\xi,\eta,\varphi;\xi')&=4\pi\sum_{l=0}^{\infty}\sum_{m=-l}^{l}(-1)^m\frac{(l-|m|)!}{(l+|m|)!}\\ &\quad\times A_l{}^m(\xi')P_l{}^{|m|}(\xi')Q_l{}^{|m|}(\xi)Y_l{}^m(\eta,\varphi),\\ U_i(\xi,\eta,\varphi;\xi')&=4\pi\sum_{l=0}^{\infty}\sum_{m=-l}^{l}(-1)^m\frac{(l-|m|)!}{(l+|m|)!}\\ &\quad\times A_l{}^m(\xi')Q_l{}^{|m|}(\xi')P_l{}^{|m|}(\xi)Y_l{}^m(\eta,\varphi),\end{aligned} \tag{4.4}$$

where U_e holds for $\xi>\xi'$, and U_i for $\xi<\xi'$.

Proof of (4.4)

Firstly, it is seen that the potential is continuous for $\xi=\xi'$. Secondly, it is well known that all functions $[Q_l{}^{|m|}(\xi)Y_l{}^m(\eta,\varphi)]$ and $[P_l{}^{|m|}(\xi)Y_l{}^m(\eta,\varphi)]$ are solutions of the Laplace equation in elliptic coordinates, so that we have

$$\nabla^2U_e=0 \text{ for } \xi>\xi', \quad \nabla^2U_i=0 \text{ for } \xi<\xi'.$$

In the third place, we find that on the spheroid $\xi=\xi'$ the normal derivative has the discontinuity

$$\begin{aligned}&\{(\partial U_e/\partial n)-(\partial U_i/\partial n)\}_{\xi=\xi'}\\ &=\{1/N(\xi',\eta)\}\{(\partial U_e/\partial\xi)-(\partial U_i/\partial\xi)\}_{\xi=\xi'}\\ &=\frac{4\pi}{N(\xi',\eta)}\sum_{l,m}(-1)^m\frac{(l-|m|)!}{(l+|m|)!}A_l{}^m(\xi')\\ &\quad\times\left\{P_l{}^{|m|}(\xi')\frac{dQ_l{}^{|m|}(\xi)}{d\xi}-Q_l{}^{|m|}(\xi')\frac{dP_l{}^{|m|}(\xi)}{d\xi}\right\}_{\xi=\xi'}Y_l{}^m(\eta,\varphi),\end{aligned}$$

which by virtue of the formula (4.19) in the Appendix of this section becomes

$$\begin{aligned}&\{(\partial U_e/\partial n)-(\partial U_i/\partial n)\}_{\xi=\xi'}\\ &\quad=[4\pi/(1-\xi'^2)N(\xi',\eta)]\textstyle\sum_{l,m}A_l{}^m(\xi')Y_l{}^m(\eta,\varphi)\\ &\quad=-4\pi\sigma(\eta,\varphi;\xi'). \qquad \text{q.e.d.}\end{aligned}$$

Let us now pass to the potential of a 3-dimensional charge distribution $\rho(\xi, \eta, \varphi)$:

$$\begin{aligned}\mathfrak{U}(\xi,\eta,\varphi)&=\int dV'\rho(\xi',\eta',\varphi')/r\\ &=\int_1^{\infty}d\xi'\int_{S(\xi')}dS'N(\xi',\eta')\rho(\xi',\eta',\varphi')/r.\end{aligned} \tag{4.5}$$

Here $S(\xi')$ is the spheroid surface $\xi=\xi'$ and dS' the surface element on it. N is defined in Eq. (4.1). When

functions $K_n(x)=-E_n(-x)$, and Placzek-Lecaine denote $K_n(x)$ by the symbol $E_n(x)$.

[20] See reference 5, p. 320.

[21] F. E. Neumann, *Vorlesungen über die Theorie des Potentials und der Kugelfunktionen* (B. G. Teubner, Leipzig, 1878), Chapter 13. Original publication: Crelles Journal für reine und angew. Mathematik **37**, 21 (1848).

[22] See, e.g., L. Pauling and E. B. Wilson, *Quantum Mechanics* (McGraw-Hill Book Company, Inc., New York, 1935), p. 444.

[23] Concerning the definitions of $P_l{}^m$, $Q_l{}^m$ see footnote 4. Neumann used different $Q_l{}^m$.

we rewrite (4.5) in the form,

$$\mathfrak{U}(\xi,\eta,\varphi)=\int_1^\infty d\xi' U(\xi,\eta,\varphi;\xi'), \tag{4.6}$$

$$U(\xi,\eta,\varphi;\xi')=\int_{S(\xi')} dS'\sigma(\eta',\varphi';\xi')/r,$$

$$\sigma(\eta',\varphi';\xi')=N(\xi',\eta')\cdot\rho(\xi',\eta',\varphi'), \tag{4.7}$$

then we may interpret U (4.7) as the potential of the surface charge distribution σ on the spheroid $\xi=\xi'$. We therefore apply Eq. (4.4) and obtain for $\mathfrak{U}$ (4.6)

$$\mathfrak{U}(\xi,\eta,\varphi)=\int_1^\xi d\xi' U_e(\xi,\eta,\varphi;\xi')+\int_\xi^\infty d\xi' U_i(\xi,\eta,\varphi;\xi'). \tag{4.8}$$

By virtue of Eqs. (4.1, 3, 7), the coefficients $A_l{}^m$ in Eq. (4.4) are now defined by the expansion,

$$(\tfrac{1}{2}R)^2(\xi'^2-\eta'^2)\rho(\xi',\eta',\varphi')=\sum_{l,m} A_l{}^m(\xi')Y_l{}^m(\eta',\varphi'), \tag{4.9}$$

hence

$$A_l{}^m(\xi')=(\tfrac{1}{2}R)^2\int_{-1}^1 d\eta'\int_0^{2\pi} d\varphi'[Y_l{}^m(\eta',\varphi')]^*$$
$$\times(\xi'^2-\eta'^2)\rho(\xi',\eta',\varphi'). \tag{4.10}$$

We introduce Eq. (4.10) in Eq. (4.4) and subsequently Eq. (4.4) in Eq. (4.8). Furthermore we substitute

$$d\xi'd\eta'd\varphi'(\xi'^2-\eta'^2)(\tfrac{1}{2}R)^2=(\tfrac{1}{2}R)^{-1}dV',$$

and obtain for Eq. (4.8)

$$\mathfrak{U}(\xi,\eta,\varphi)=(\tfrac{1}{2}R)^{-1}\int dV'\Psi(\xi,\eta,\varphi;\xi',\eta',\varphi')\rho(\xi',\eta',\varphi'), \tag{4.11}$$

where the function Ψ is defined by

$$\Psi(\xi,\eta,\varphi;\xi',\eta',\varphi')$$
$$=4\pi\sum_{lm}(-1)^m\frac{(l-|m|)!}{(l+|m|)!}P_l{}^{|m|}\begin{pmatrix}\xi\\ \xi'\end{pmatrix}Q_l{}^{|m|}\begin{pmatrix}\xi'\\ \xi\end{pmatrix}$$
$$\times Y_l{}^m(\eta,\varphi)[Y_l{}^m(\eta',\varphi')]^*. \tag{4.12}$$

Here the upper choice of (ξ,ξ') holds for $\xi<\xi'$ and the lower choice for $\xi>\xi'$. Now it follows from Eqs. (4.5) and (4.11) that

$$\int dV'\{(1/r)-(2/R)\Psi\}\rho=0$$

for any arbitrary space functions ρ of suitable regularity, which implies that $(1/r)\equiv(2/R)\Psi$ identically in all arguments. This furnishes the expansion of Neumann:

$$\frac{R}{r}=8\pi\sum_{l=0}^\infty\sum_{m=-l}^{l}(-1)^m\frac{(l-|m|)!}{(l+|m|)!}P_l{}^{|m|}(\xi)$$
$$\times Q_l{}^{|m|}(\xi')Y_l{}^m(\eta,\varphi)[Y_l{}^m(\eta',\varphi')]^*. \tag{4.13}$$

Equation (4.13) is valid for $\xi<\xi'$; one must interchange ξ and ξ' for $\xi>\xi'$. By virtue of Eq. (4.2), the expansion (4.13) can be written

$$\frac{R}{r}=4\sum_{l=0}^\infty\sum_{m=-l}^{l}(-1)^m\frac{(l-|m|)!}{(l+|m|)!}P_l{}^{|m|}(\xi)Q_l{}^{|m|}(\xi')$$
$$\times\mathcal{P}_l{}^{|m|}(\eta)\mathcal{P}_l{}^{|m|}(\eta')e^{im\varphi}e^{-im\varphi}, \tag{4.14}$$

and this is obviously equivalent (see Eq. (1.1)) to the form originally given by Neumann:

$$\frac{R}{r}=\sum_{l=0}^\infty\sum_{m=0}^{l}C_l{}^mP_l{}^m(\xi)Q_l{}^m(\xi')P_l{}^m(\eta)$$
$$\times P_l{}^m(\eta')\cos m(\varphi-\varphi'), \tag{4.15}$$

where

$$\left.\begin{aligned}&C_l{}^m=\epsilon_m(-1)^m(2l+1)[(l-m)!/(l+m)!]^2,\\ &\epsilon_0=2,\quad \epsilon_m=4 \text{ for } m>0.\end{aligned}\right\} \tag{4.15'}$$

The constants can be checked by passing, to the limit $R\to 0$, i.e., to spherical coordinates (ρ,ϑ,φ):

$$\left.\begin{aligned}&\rho=\lim(\tfrac{1}{2}R\xi),\quad \rho'=\lim(\tfrac{1}{2}R\xi'),\\ &\cos\vartheta=\lim\eta,\quad \cos\vartheta'=\lim\eta'.\end{aligned}\right\} \tag{4.16}$$

Then we obtain from Eq. (4.13)

$$\frac{1}{r}=\frac{4\pi}{\rho'}\sum_{l,m}(-1)^m\frac{(l-m)!}{(l+m)!}\{\lim\xi'Q_l{}^{|m|}(\xi')P_l{}^{|m|}(\xi)\}$$
$$\times Y_l{}^m(\vartheta,\varphi)[Y_l{}^m(\vartheta',\varphi')]^*, \tag{4.17}$$

hence

$$\frac{1}{r}=\frac{4\pi}{\rho'}\sum_{l=0}^\infty\sum_{m=-l}^{l}\left(\frac{\rho}{\rho'}\right)^l\frac{1}{(2l+1)}Y_l{}^m(\vartheta,\varphi)[Y_l{}^m(\vartheta',\varphi')]^* \tag{4.18}$$

for $\rho'>\rho$, which indeed is the expansion of $(1/r)$ in spherical coordinates of the two end points.[24]

APPENDIX TO SECTION 4

We wish to prove the following relation $(m\geqslant 0)$:

$$P_l{}^m(x)\frac{d}{dx}Q_l{}^m(x)-Q_l{}^m(x)\frac{d}{dx}P_l{}^m(x)=\frac{(-1)^m}{1-x^2}\frac{(l+m)!}{(l-m)!}. \tag{4.19}$$

If Eq. (4.19) is assumed to be valid, then the analogous formula for $(m+1)$ is derived by differentiating Eq. (4.19) and applying the differential equation of the Legendre functions. Now Eq. (4.19) is true[25] for $m=0$; hence, Eq. (4.19) is valid for any value of m.

5. LITERATURE AND TABLES

I. Literature

The first exchange integral namely $[1s_a1s_b|1s_a1s_b]$, with $\zeta_a=\zeta_b=\bar{\zeta}_a=\bar{\zeta}_b=1$, was evaluated by Y. Sugiura,[26] whose evalu-

[24] See, e.g., Eyring, Walter, and Kimball, *Quantum Chemistry* (John Wiley and Sons, Inc., New York, 1947), p. 371.

[25] See, e.g., reference 4, p. 114, or E. W. Hobson, *Spherical and Ellipsoidal Harmonics* (Cambridge University Press, London, 1931), p. 72.

[26] Y. Sugiura, Z. Physik **45**, 484 (1927).

ation supplemented the treatment of the H_2 molecule by W. Heitler and F. London.[27] An approximation to the integral $[2s_a2s_b|2s_a2s_b]$ was given by M. Delbrück.[28] I. Podolansky[29] showed that all exchange integrals can be expressed in terms of powers, exponentials, the logarithm, and the exponential integral. E. C. Kemble and C. Zener[30] employed graphical integration for two exchange integrals.

Substantial progress for computation was made by the systematic use of auxiliary functions, introduced by C. Zener and V. Guillemin,[31] who discussed integrals involving Σ-type charge distributions. J. H. Bartlett and W. H. Furry[32] treated exchange integrals between $2s$ and $2p$ orbitals. N. Rosen[33] discussed integrals between s-orbitals, and later[34] between $(1s)$ and $(2p\sigma)$ orbitals. He improved the method of Zener and Guillemin, and his procedure has recently been used by P. J. Wheatley and J. W. Linnett[35] and by J. O. Hirschfelder and J. W. Linnett[36] to compute integrals between $2p$ and $2s$ orbitals. Independent evaluations of similar integral had been made by W. E. Bleick and J. E. Mayer.[37]

In all these treatments the functions $P_l^m(x)$ and $Q_l^m(x)$ are broken down into their components, i.e., powers x^k and $\log x$. Thus in the Rosen method the integrals are expressed in terms of the functions $\phi_{n\bar{n}}^{00}$ (see Sec. 3, III). H. M. James and A. S. Coolidge[38] investigated recurrence formulas between integrals which contained the undecomposed $P_l^m(x)$, $Q_l^m(x)$ (see Sec. 3, IV, V), thus suggesting a considerable improvement. Furthermore, H. M. James[39] was the first to make computations for different effective nuclear charges.

The most extensive computations of molecular integrals yet made are those of M. Kotani, A. Amemiya, and T. Simose,[40] who adopted the method of James and Coolidge. Their extensive tables contain all exchange integrals between $2s$ and $2p$ orbitals for equal effective nuclear charges and four integrals for different nuclear charges (case $\alpha=\bar{\alpha}$, $\beta=\bar{\beta}$, see Sec. 1, III). Recently, H. J. Kopineck[41] has reviewed and checked the Japanese tables. His paper presents the results for equal effective nuclear charges in a condensed form.

In all the quoted papers, the Neumann expansion is used. A. S. Coolidge[42] first suggested a different approach, namely to expand the orbitals on one center in terms of spherical harmonics around the second center. Recently, this method has been rather thoroughly investigated by M. P. Barnett and C. A. Coulson,[13a] and by S. O. Lundquist and P. O. Löwdin[43] where further references can be found. It is valuable in the case of three- and four-center integrals and for orbitals with a numerically given radial part, but it seems to be less advantageous for exchange integrals between Slater AO's.

[27] W. Heitler and F. London, Z. Physik **44**, 455 (1927).
[28] M. Delbrück, Ann. Physik **5**, 36 (1930).
[29] I. Podolansky, Ann. Physik **10**, 868 (1931).
[30] E. C. Kemble and C. Zener, Phys. Rev. **33**, 512 (1929).
[31] C. Zener and V. Guillemin, Phys. Rev. **34**, 999 (1929).
[32] J. H. Bartlett and W. H. Furry, Phys. Rev. **37**, 507 (1931); **38**, 1615 (1931); **39**, 209 (1932).
[33] N. Rosen, Phys. Rev. **38**, 255 (1931).
[34] N. Rosen, Phys. Rev. **38**, 2099 (1931).
[35] P. J. Wheatley and J. W. Linnett, Trans. Faraday Soc. **45**, 897 (1949).
[36] J. O. Hirschfelder and J. W. Linnett, J. Chem. Phys. **18**, 130 (1950).
[37] W. E. Bleick and J. E. Mayer, J. Chem. Phys. **2**, 252 (1934).
[38] H. M. James and A. S. Coolidge, J. Chem. Phys. **1**, 825 (1933).
[39] H. M. James, J. Chem. Phys. **2**, 794 (1934).
[40] Kotani, Amemiya, and Simose, Proc. Phys.-Math. Soc. Japan **20**, Extra No. 1 (1938); **22**, Extra No. 1 (1940).
[41] H. J. Kopineck, Z. Naturforsch. **5a**, 420 (1950).
[42] A. S. Coolidge, Phys. Rev. **42**, 189 (1932).
[43] S. O. Lundquist and P. O. Löwdin, Arkiv Fysik (Stockholm) **3**, 147 (1951).

II. Tables

(1) *Auxiliary Functions*

The paper of N. Rosen[34] contains tables of the functions $A_n(\alpha)$ and $F_n(\alpha)$ [see Eqs. (3.15, 16)], for $n=0(1)20$ and $\alpha=0.5(0.5)5(1)14$.

The paper of J. O. Hirschfelder and J. W. Linnett[36] contains a table, computed by N. Rosen, of the functions

$$H(n,\bar{n},\alpha)=\phi_{n\bar{n}}^{00}(\alpha,\alpha)=\phi_{n\bar{n}}(\alpha,\alpha)\ \text{[see Eqs. (1.18), (3.21)]},$$

for $n,\bar{n}=0(2)6$; $\alpha=0.5,\ 1,\ 1.5,\ 1.75,\ 2(0.5)5(1)14$.

The tables of Kotani, Amemiya, and Simose[40] contain the following functions:

$A_n(\alpha)$ [see Eq. (3.15)], for $n=0(1)15$;
$B_n(\beta)$ [see reference 14], for $n=0(1)8$; and

$$\alpha=\left\{\begin{matrix}0.25(0.25)8(0.5)13\\13(1)16,\ 18,\ 20,\ 21,\ 22,\ 24.\end{matrix}\right.$$

$f_0(n,\alpha)=F_n(\alpha)$, [see Eq. (3.16)], for $n=0(1)15$, and $\alpha=0.5$, $1(0.25)6.5(0.5)11,\ 12,\ 12.5,\ 13(1)16,\ 18,\ 20,\ 21,\ 24$. From this table one obtains immediately the functions G_n (3.17) by means of Eq. (3.19).

$$G_l^M(j;\beta)=(-1)^{j+l+M}\left[\frac{2}{2l+1}\frac{(l+M)!}{(l-M)!}\right]^{\frac{1}{2}}B_j^{Ml}(\beta),$$

[see Eqs. (1.20), (2.29), and Sec. 2], for $\beta=0.25(0.25)5.5(0.5)7$ and the following index values:

$$M=0:\ \begin{array}{c|ccccccc} l & 0(1)4 & 5 & 6 & 7 & 8\\ \hline j & 0(1)4 & 0(1)3 & 0,1,2 & 0,1 & 0\end{array},$$

$$M=1:\ \begin{array}{c|cc} l & 1(1)4 & 5\\ \hline j & 0(1)3 & 0,2\end{array},$$

$$M=2:\ l=2,3,4,\quad j=0,2.$$

$W_l^M(n,\bar{n};\alpha)=(-1)^M\dfrac{(l+M)!}{(l-M)!}\phi_{n\bar{n}}^{Ml}(\alpha,\alpha)$ [see Eq. (1.18) and Sec. 3], for $\alpha=1(0.25)5.5(0.5)7$, and for the following index values:

$$M=0:\ \begin{array}{c|cccccccc} l & 0 & 1 & 2 & 3 & 4 & 5 & 6\\ \hline n,\bar{n} & 0(1)8 & 0(1)7 & 0(1)6 & 0(1)5 & 0(1)4 & 0(1)3 & 0,2\end{array},$$

$$M=1:\ \begin{array}{c|ccccccc} l & 1 & 2 & 3 & 4 & 5\\ \hline n,\bar{n} & 0(1)6 & 0(1)5 & 0(1)4 & 0(1)3 & 0,2\end{array},$$

$$M=2:\ l=2,4,\quad n,\bar{n}=0,2.$$

It should be noted that Part II of the Japanese tables contains 12 pages of errata concerning Part I.

(2) *Integrals Involving Orbitals with Equal ζ-Values*

In this case one has $\beta=\bar{\beta}=0$, $\alpha=\bar{\alpha}$, so that the integrals are linear combinations of a finite number of functions $\phi_{n\bar{n}}^{Ml}(\alpha,\alpha)$. Furthermore, they depend only on the one parameter α.

For the 18 exchange integrals between $2s$ and $2p$ orbitals, H. J. Kopineck[41] has therefore given the following tables: (a) each exchange integral in terms of $\phi_{n\bar{n}}^{Ml}$, (b) each exchange integral as a function of α for $\alpha=1(0.5)7$. These are based on the Japanese tables, but the errata are eliminated and the values reported in the English and American literature are taken into account. Table (a) is in agreement with our Table II.

J. O. Hirschfelder and J. W. Linnett[36] have given a table of the exchange integrals

$$L_{00,\ 00}=[1s_a1s_b|1s_a1s_b],\quad L_{cc,\ cc}=[2p\sigma_a2p\sigma_b|2p\sigma_a2p\sigma_b],$$
$$L_{ss,\ ss}=\tfrac{1}{2}[2p\pi_a2p\pi_b\Sigma|2p\pi_a2p\pi_b\Sigma]+[2p\pi_a2p\pi_b\Delta|2p\pi_a2p\pi_b\Delta].$$
$$L_{0s,\ 0s}=2[1s_a2p\pi_b|1s_a2p\pi_b],\quad L_{0c,\ 0c}=-[1s_a2p\sigma_b|2p\sigma_a1s_b],$$
$$L_{cs,\ cs}=-2[2p\sigma_a2p\pi_b|2p\pi_a2p\sigma_b]\ \text{for}\ \alpha=0,\ 1,\ 1.5,\ 1.75,\ 2(0.5)5(1)8,\ 10,\ 12.$$

(3) *Integrals Involving Orbitals with Different ζ-Values*

Part II of the paper of Kotani, Amemiya, Simose contains tables for the four exchange integrals

$$N_{ss}=[1s_a2s_b|1s_a2s_b],\quad N_{00}=[1s_a2p\sigma_b|1s_a2p\sigma_b],$$
$$N_{s0}=[1s_a2s_b|1s_a2p\sigma_b],\quad N_{\pi\pi}=[1s_a2p\pi_b|1s_a2p\pi_b],$$

assuming $\zeta_a=\bar{\zeta}_a$, $\zeta_b=\bar{\zeta}_b$, so that $\alpha=\bar{\alpha}$, $\beta=\bar{\beta}$. Values of the integrals are given for $\alpha=2(0.25)3.25$, $\beta=-0.5(0.25)1$.

(4) The Functions $U_n(x)=x^n/n!$

Tables of these functions can be obtained from the National Bureau of Standards, Computation Laboratory, Washington 25. A table exact to 10 significant figures exists for $n=0(1)40$, $x=1(1)10$; and a table exact to 15 decimal places exists for $n=0(1)18$, $x=0(0.01)2$. The table is necessary for the method of successive Taylor expansions; see Secs. 2, III and 3, I. It should be noted that this method can be employed to interpolate the Japanese tables.

ACKNOWLEDGMENTS

I wish to acknowledge the help of Walter Jaunzemis in carrying out the numerical computations and to express my thanks to Professors R. S. Mulliken and R. G. Parr and to Dr. C. C. J. Roothaan for helpful discussions.

THE JOURNAL OF CHEMICAL PHYSICS VOLUME 19, NUMBER 12 DECEMBER, 1951

Internal Rotation in Ethylene Chlorhydrin

SAN-ICHIRO MIZUSHIMA, TAKEHIKO SHIMANOUCHI, TATSUO MIYAZAWA, KOO ABE, AND MASASHI YASUMI
Chemical Laboratory, Faculty of Science, Tokyo University, Hongo, Tokyo, Japan

(Received August 22, 1951)

The Raman and the infrared spectra of ethylene chlorhydrin have been remeasured with the result that the molecules take both the *trans* and the *gauche* forms in the gaseous and the liquid states, while they take only the *gauche* form in the solid state. By the measurement of the temperature dependence of the infrared absorption the energy difference between these two forms has been found as 0.95 kcal/mol.

PREVIOUS researches in our laboratory[1,2] have shown that the molecules of ethylene chlorhydrin ClH_2C-CH_2OH take two forms in the liquid and the gaseous states and in carbon tetrachloride solutions, while they take only one of these forms in the solid state. These two forms are the *trans* and the *gauche* forms as shown in Fig. 1. The *cis* form which was once considered in place of the *gauche* form has been ruled out just as in the case of 1,2-dihalogenoethanes.[3,4] As there are, however, some points to be clarified with regard to the internal rotation of this molecule, we have made more detailed measurements of the Raman and the infrared spectra of this substance and have also calculated the normal vibrations. The result will be reported in the present paper.

Trans form *Gauche* form

FIG. 1. ClH_2C-CH_2OH as viewed along the C–C bond.

TABLE I. The Raman and the infrared spectra of ethylene chlorhydrin in the liquid state.

Raman spectrum	Infrared spectrum
164(2) *e*	
259(1) *e*	
2?4(4)* *e*	
394(5) *e, k*	
477(4)* *e, k*	
662(10)* *e, k, (i), f, g*	664(*m*)
751(7) *e, k*	749(*m*)
851(7)* *e, k*	850(*m*)
942(6)* *e, k*	939(*m*)
1035(6)* *e, k*	1030(*st*)
1055(2) *e*	
1078(4)* *e, k*	1073(*st*)
1180(4)* *e, k*	1161(*w*)
1243(5)* *e, k*	1247(*w*)
1283(2) *e, k*	
1298(4) *e, k*	1300(*m*)
1379(2)* *e, k*	1381(*w*)
1434(5)* *e, k*	1431(*m*)
1459(5)* *e, k*	1458(*w*)
2724(3) *e, k*	
2874(7) (*e*), *k*	2880(*m*)
2925(6)* *e, k, i*	
2964(10)* *e, k, i*	2960(*m*)
3011(7)* *e, k, (i)*	
	3230(*st*)

The Raman frequencies marked with asterisks are also observed in the solid state.

TABLE II. Force constants (in 10^5 dyne/cm).*

$K(CH_2-CH_2)=4.0$	$H(C-CH_2-OH)=0.13$		
$K(CH_2-CH_2)=3.7$	$H(C-CH_2-Cl)=0.075$		
$K(CH_2-Cl)=2.53$	$F(C\cdots Cl)=0.76$	$F'=-F/12$	
$K(CH_2-OH)=3.55$	$F(C\cdots OH)=0.90$		

* As to the meaning of K, H, F and F' see reference 5.

TABLE III. Calculated and observed skeletal frequencies of $Cl-CH_2-CH_2-OH$.

Vibrational type	*Trans* form calc	*Trans* form obs	*Gauche* form calc	*Gauche* form obs
Stretching vibration	1063	1055	1055	1035
	914	942	898	851
	704	751	662	662
Deformation vibration	368	394	482	477
	256	259	271	294

[1] Mizushima, Morino, and Nakamura, Sci. Pap. Inst. Phys. Chem. Research (Tokyo) **37**, 205 (1940).
[2] Mizushima, Morino and Kubota, Bull. Chem. Soc. Japan **14**, 15 (1939).
[3] Yamaha, Annual meeting, Chem. Soc. Japan (1949).
[4] Mizushima, Morino, Watanabe, Shimanouchi, and Yamaguchi, J. Chem. Phys. **17**, 591 (1949).

TABLE IV. Ratio of the optical density D_t/D_g observed for the two bands at 760 cm^{-1} and at 669 cm^{-1} at different temperatures.

t°C	D_t/D_g
82	0.551
105	0.595
155	0.685
204	0.781
250	0.848

The sample used in the measurement was purified by redistillation (bp 127.5–128.0°C). The Raman spectrum observed in the liquid state is shown in Table I and is almost the same as that reported in our previous paper[1] except the new line at 259 cm^{-1}. The frequencies marked with asterisks were also observed in the solid state, but others disappeared on solidification.

The same table also contains the result of the infrared absorption in the rocksalt region observed in the liquid state by use of Baird's automatic recording spectrometer. The skeletal frequencies calculated for the *trans* and the *gauche* molecules by use of the Urey-Bradley field are shown in Table III.[5] The force constants used in this calculation were chosen as to fit the spectral frequencies of CH_3-CH_2-Cl, CH_3-CH_2-OH, $Cl-CH_2-CH_2-Cl$ and $HO-CH_2-CH_2-OH$ (see Table II).

Of the two absorption bands at 669 cm^{-1} and 760 cm^{-1} observed in the gaseous state, the latter increased its intensity as compared with the former, as the temperature is raised. This means that the former arises from the lower energy form and the latter from the higher energy one. Corresponding to these two absorption bands in the gaseous state we found the two Raman lines at 662 cm^{-1} and at 751 cm^{-1} in the liquid state, of which the latter disappeared on solidification. This experimental result of the Raman effect is quite compatible with that of the infrared measurement, since the lower energy form remained to exist in the solid state.

It is easily seen from Table III that the result of the normal vibration calculation favors the assignment of the lower energy form to the *gauche* form and the higher energy form to the *trans* form. This is quite consistent with the experimental result of the entropy difference between these two forms.[6] All the Raman frequencies marked with asterisks in Table I can, therefore, be assigned to the *gauche* form and the other lines to the *trans* form. As to the equilibrium ratio of these two forms we have found no appreciable difference from spectroscopic data, because the intensity ratio of the two absorption bands at 669 cm^{-1} and at 760 cm^{-1} in the gaseous state was found practicallly the same as that of the two corresponding bands at 664 cm^{-1} and 749 cm^{-1} in the liquid state at the same temperature.

In order to obtain the energy difference between these two kinds of molecules in the gaseous state, we have measured the temperature dependence of the intensity ratio of the two bands stated above according to the method described in our previous paper.[7] (The absorption cell with silvine windows was 8 cm in length.) Let $\Delta E=E_t-E_g$ and $\Delta S=S_t-S_g$ be the difference in energy and entropy between the *trans* and the *gauche* molecules, then the equilibrium ratio will be expressed as

$$N_t/N_g=\tfrac{1}{2}\exp(\Delta S/R)\exp(-\Delta E/RT), \qquad (1)$$

where N_t and N_g denote the number of the *trans* and the *gauche* molecules, respectively. Further let κ be the molecular absorption coefficient and D the optical density. We have then

$$D_t/D_g=\frac{\kappa_t N_t}{\kappa_g N_g}=\frac{1}{2}\frac{\kappa_t}{\kappa_g}\exp(\Delta S/R)\exp(-\Delta E/RT). \qquad (2)$$

If, therefore, we observe the ratio of optical density D_t/D_g at several temperatures, we can calculate the value of ΔE through Eq. (2), assuming ΔE and ΔS constant in the small temperature range in which we have made our measurements. From the experimental data shown in Table IV we obtain

$$\Delta E=0.95\pm0.02 \text{ kcal/mol.}$$

This value of ΔE is much smaller than that obtained by Zumwalt and Badger[8] from the intensity measurement of OH absorption bands (2.0 ± 0.5 kcal/mol), but we have good reason to believe that there may be some difference between our value and theirs. With regard to the position of the hydrogen atom of the hydroxyl group the *trans* molecule has three stable positions of almost the same energy. Similarly the *gauche* molecule has three stable positions with regard to the internal rotation about the C–O bond as axis, but one of them is much more stable than the other two owing to the internal hydrogen bond, without which the *gauche* form would be less stable than the *trans* form as in the case of 1,2-dihalogenoethanes.[4] Since the skeletal frequencies are almost independent of the position of hydrogen atom, the energy difference observed by us is that between the weighted mean energy of the *trans* molecule and that of the *gauche* molecule. However, the energy difference obtained by Zumwalt and Badger is that between the weighted mean energy of the *trans* and the *gauche* molecules without hydrogen bond and that of the *gauche* molecule with internal hydrogen bond, since they measured the absorption intensity of the OH bands as stated above. Therefore, as the energy difference between the *trans* and the *gauche* molecules we have to use the value of 0.95 kcal/mol obtained in the present experiment.

[5] For the details of the calculation see, e.g., Shimanouchi, J. Chem. Phys. **17**, 245 (1949).

[6] Mizushima, Shimanouchi, Kuratani, and Miyazawa, 12th Internat. Cong. Pure and Appl. Chem. (New York, 1951).

[7] Shimanouchi, Tsuruta, and Mizushima, Sci. Pap. Inst. Phys. Chem. Research (Tokyo) **42**, 51 (1944).

[8] L. R. Zumwalt and R. M. Badger, J. Am. Chem. Soc. **62**, 305 (1940).

The Infrared Dichroism of Diketopiperazine

TAKEHIKO SHIMANOUCHI, KENJI KURATANI, AND SAN-ICHIRO MIZUSHIMA
Chemical Laboratory, Faculty of Science, Tokyo University, Hongo, Tokyo, Japan
(Received August 22, 1951)

The absorption of polarized infrared radiations by diketopiperazine crystal has been measured in the wavelength region from 2.8 to 15μ. From the observed infrared dichroism the assignment of the absorption bands has been made.

ACCORDING to Corey[1] diketopiperazine $(CH_2NHCO)_2$ forms a monoclinic crystal with planes of the flat ring molecules lying parallel to one another and perpendicular to the (010) cleavage plane. This arrangement of molecules in the crystal suggests that the polarized infrared radiation may be very useful for the structural study of this molecule. In the present note we shall report our experimental results obtained for this substance in the wavelength region from 2.8 to 3.6μ (using quartz prism) and in that from 5 to 15μ (using rock-salt prism).[2]

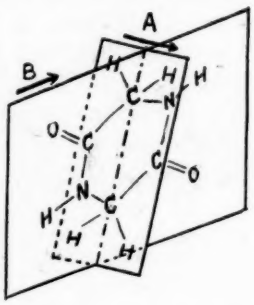

FIG. 1. The two directions of the electric vectors of the incident infrared radiation.

The apparatus and the method of the absorption measurement are the same as reported in our previous paper[3] except that a selenium reflection polarizer (incident angle 68°) was used to obtain plane polarized infrared radiation. A (010) cleavage piece, 1 mm×2 mm in area and about 0.03 mm in thickness, was used as the sample and the two directions of the polarization were chosen in such a way that the incident beam was perpendicular to the (010) plane and the electric vector was either perpendicular or parallel to the plane of the flat ring molecules (Fig. 1, A and B).

The difference between the two absorption curves, A and B, is very striking as shown in Fig. 2, when the direction of the electric vector of the incident radiation was parallel to the plane of the molecule and almost perpendicular to the peptide C—N bonds (curve B), we observed seven strong absorption bands at 805, 920, 1075, 1480, 1700, 2950, and 3050~3400 cm^{-1}, all of which should be assigned to in-plane vibrations. When, however, the direction of the electric vector was perpendicular to the plane of the molecule (curve A), we observed two strong absorption bands at 720~950 cm^{-1} and at 1015 cm^{-1} which should correspond to out-of-plane vibrations. In curve A of Fig. 2 there are other weaker absorptions which arise also from out-of-plane vibrations except the two at ~1480 cm^{-1} and at ~1700 cm^{-1} which can be considered to arise from in-plane vibrations owing to the fact that the molecule ring of diketopiperazine is not completely coplanar

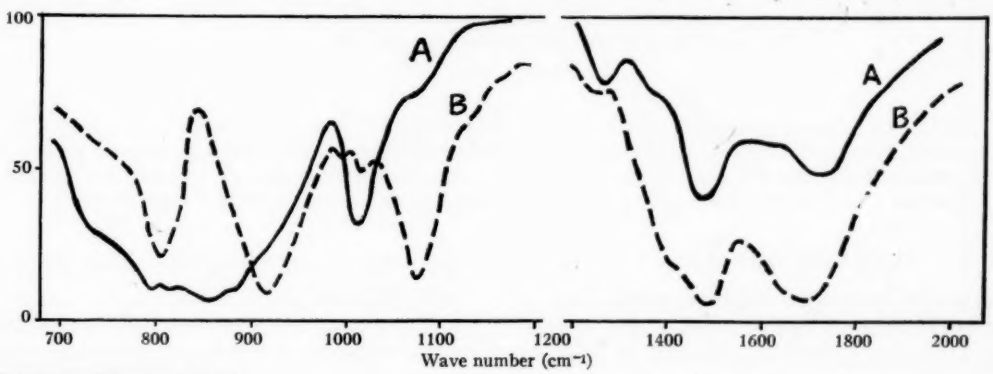

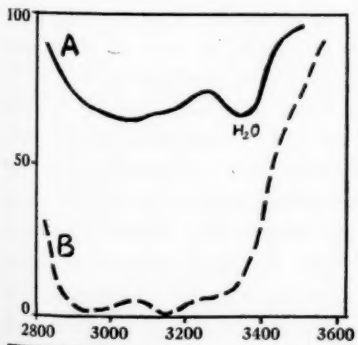

FIG. 2. The transmission of the polarized infrared radiations in two directions, A and B.

[1] R. B. Corey, J. Am. Chem. Soc. **60**, 1598 (1938).
[2] As to the measurement in the near infrared region (1~2.5μ), see J. W. Ellis and J. Bath, J. Chem. Phys. **7**, 862 (1939).
[3] Shimanouchi, Tsuruta, and Mizushima, Sci. Pap. Inst. Phys. Chem. Research (Tokyo) **42**, 51 (1944).

TABLE I. Assignment of the observed absorption frequencies (cm^{-1}).

Direction of electric vectors	Modes of vibration	Frequencies in other molecules containing the same groups	Frequencies in diketopiperazine molecule
A	CH_2 stretching, anti-sym.	3045[a], 2926[b]	3050
	CH_2 rocking, out-of-plane	899[a], 728[b]	1015
	NH perpend., out-of-plane		720∼950
	NH stretching	∼3300[c]	the main part of the band at 3050 ∼3400
B	CH_2 stretching, symmetric	2984,[a] 2853[b]	2950
	C=O stretching	∼1700[c]	1700
	HCH deformation	1429,[a] 1475[b]	1480
	CH_2 rocking, in-plane	1266,[a] 1375[b]	1075
	$C_\alpha N$ stretching[d]	∼1000	920
	$C_\alpha C$ stretching		805

[a] Methylene chloride.
[b] Polyethylene.
[c] Many substances with these groups in their molecules.
[d] C_α denotes the carbon atom of the CH_2-group. The CN stretching vibration of the peptide $-CO-NH-$ group takes place almost perpendicularly to (010) plane and the absorption band due to this vibration would not be observed for both of the incident polarized radiations.

and that the incident radiation is not completely polarized.

The molecule of diketopiperazine has a center of symmetry to which all the infrared active vibrations must be antisymmetric. There are fifteen such vibrations, of which about ten are expected to appear in the wavelength region stated above, which was actually the case as shown in Table I. In the second column of this table we showed the observed frequencies of methylene chloride, polyethylene, etc., which contain the same groups in their molecules as diketopiperazine. The assignment of these frequencies can be made as shown in the first column according to the normal vibration calculations reported in our previous papers.[4] If we compare these frequencies with those observed for diketopiperazine and take into account the probable shift of frequencies due to the structural difference in the other parts of molecules, we can reasonably assign the diketopiperazine frequencies as shown in the last column of Table I.

So far as we know, the frequency of perpendicular vibration of the hydrogen-bonded N−H group in the peptide bond has not been reported. We believe our assignment of the absorption band at 720∼950 cm^{-1} to this vibration is correct, because on one hand this absorption is observed only in curve A and not in curve B, and on the other hand this band is extremely broad.

[4] For methylene chloride see T. Shimanouchi, J. Chem. Phys. **17**, 245, 734 (1949), and for polyethylene see T. Shimanouchi and S. Mizushima, J. Chem. Phys. **17**, 1102 (1949).

THE JOURNAL OF CHEMICAL PHYSICS VOLUME 19, NUMBER 12 DECEMBER, 1951

Variation of Lattice Frequencies with Concentration in Molecular Mix-Crystals

RAM RATAN AGGARWAL* AND B. D. SAKSENA
Division of Physics, National Research Council, Ottawa, Canada

(Received July 12, 1951)

Assuming a unique linear periodic lattice for a non-ionic molecular mix-crystal, the lattice frequencies of the translational and rotational modes have been calculated for several concentration ratios of the two components. The observed variation in frequency in such crystals has been explained. The calculations also require that additional frequencies, not yet observed, should appear in Raman and infrared spectra.

INTRODUCTION

IN the spectra of mix-crystals so far reported, there is a gradual shift in the lattice frequencies with concentration of the constituents. The earlier work on infrared spectra[1] of mix-crystals of alkali-halides showed a single frequency for any known ratio of the constituents. The wave number increased gradually from 165 cm^{-1} in pure KCl to 195 cm^{-1} in pure NaCl. With the same object in view, Vuks[2] obtained the Raman spectra in the low frequency region, to investigate the rotational frequencies for the mix-crystals of *p*-dichlorobenzene and *p*-dibromobenzene. He found a gradual shift in wave number from 20.1 and 37.8 cm^{-1} (100 percent *p*-dibromobenzene) to 27.5 and $\frac{46.5}{54.0}$ cm^{-1} (100 percent *p*-dichlorobenzene). Sircar and Bishui,[3] however, did not completely agree with Vuks.

Saksena[4] tried to interpret this change in rotational lattice frequencies by using a statistical average of the moments of inertia of the molecules forming the mix-crystal. Matossi,[5] working with the idea of a unique linear lattice for mix-crystals discussed the case of ionic crystals by taking a 50:50 ratio of NaCl and KCl. This idea of linear lattices for the mix-crystals can be extended to molecular crystals, if one is interested in the lattice vibrations due to intermolecular forces. Since the intermolecular forces are very weak, these vibrations will have a low frequency. For such a case we have calculated the lattice frequencies of the mix-crystals for the translational and rotational modes of vibration for

* National Research Council of Canada Postdoctorate Fellow.
[1] Krueger, Reinkober, and Koch-Holm, Ann. Physik **85**, 110 (1928).
[2] M. Vuks, Acta Physicochim. U.R.S.S. **6**, 11 (1937).
[3] S. C. Sircar and I. Bishui, Indian J. Phys. **11**, 417 (1937).
[4] B. D. Saksena, J. Chem. Phys. **18**, 1653 (1950).
[5] F. Matossi, J. Chem. Phys. **19**, 161 (1951).

TABLE I.

Concentration A	Concentration B	Expressions for the different frequencies	Relative amplitudes	Modes of vibration[a]	ω^2[b]
0	100	$\omega^2=4f/m'$	Consecutive molecules have equal and opposite amplitudes	↑ . ↓ · ↑ .	$4.00f$
16.7	83.3	$mm'^3\omega^6-m'^2\omega^4f(6m+2m')+m'\omega^2f^2(9m+10m')-f^3(2m+10m')=0$			$3.80f$
20	80	$mm'^2\omega^6-m'\omega^4f(5m+2m')+\omega^2f^2(5m+8m')-4f^3=0$			$3.73f$
25	75	$\omega^2=0$	Translation		
		$\omega^2=2f/m'$	$A_1=B_3=0;\ B_2=-B_4$	* ↑ . . ↓ · *	
		$\omega^2=f\left[\frac{m'+2m-(m'^2+2m^2-2mm')^{\frac{1}{2}}}{mm'}\right]$	$B_2=B_4;\ \frac{A_1}{B_3}=-\frac{m'}{m^2}\{(m-m')+[(m-m')^2+m^2]^{\frac{1}{2}}\}$ $m>m'$ $\frac{B_4}{B_3}=-\frac{1}{2m}\{m'-[(m-m')^2+m^2]^{\frac{1}{2}}\}$ $m<m'$	↓ * ↑ . ↑ . ↑ . ↓ * ↓ * ↓ · ↑ . ↓ · ↓ *	
		$\omega^2=f\left[\frac{m'+2m+(m'^2+2m^2-2mm')^{\frac{1}{2}}}{mm'}\right]$	$B_2=B_4;\ \frac{A_1}{B_3}=\frac{m'}{m^2}\{[(m-m')^2+m^2]^{\frac{1}{2}}-(m-m')\}$ $\frac{B_4}{B_3}=-\frac{1}{2m}\{m'+[(m-m')^2+m^2]^{\frac{1}{2}}\}$	↑ * ↓ · ↑ . ↓ · ↑ *	$3.62f$
33.3	66.7	$\omega^2=0$	Translation		
		$\omega^2=f/m'$	$A_1=B_3=A_4=B_5=0;\ B_2=-B_6$	* ↑ . . * . ↓ · *	
		$\omega^2=3f/m'$	$A_1=A_4=0;\ B_2=B_5=-B_3=-B_6$	* ↑ . ↓ · * ↑ . ↓ · *	
		$\omega^2=f\left(\frac{2}{m}+\frac{1}{m'}\right)$	$A_1=A_4;\ B_2=B_3=B_5=B_6=-(m/2m')A_1$	↑ * ↓ · ↓ · ↑ * ↓ · ↓ · ↑ *	
		$\omega^2=f\left[\frac{2m'+3m-(4m'^2+9m^2-4mm')^{\frac{1}{2}}}{2mm'}\right]$	$B_2=B_6=-B_3=-B_5;\ A_1=-A_4$ $\frac{B_2}{A_1}=\frac{(2m'-3m)+[(2m'-3m)^2+8mm']^{\frac{1}{2}}}{4m'}$	↑ * ↑ . ↓ · ↓ * ↓ · ↑ . ↑ *	
		$\omega^2=f\left[\frac{2m'+3m+(4m'^2+9m^2-4mm')^{\frac{1}{2}}}{2mm'}\right]$	$B_2=B_6=-B_3=-B_5;\ A_1=-A_4$ $\frac{B_2}{A_1}=\frac{(2m'-3m)-[(2m'-3m)^2+8mm']^{\frac{1}{2}}}{4m'}$	↑ * ↓ · ↑ . ↓ * ↑ . ↓ · ↑ *	$3.14f$
50	50	$\omega^2=0$	Translation		
		$\omega^2=2f\left(\frac{1}{m}+\frac{1}{m'}\right)$	$B_2=-\frac{m}{m'}A_1$	↑ * ↓ · ↑ *	$3.00f$
66.7	33.3		Similar results as for the concentration ratio 33.3:66.7 with the masses m and m' interchanged		$2.78f$
75	25		Similar results as for the concentration ratio 25:75 with the masses m and m' interchanged		$2.70f$
80	20		Similar results as for the concentration ratio 20:80 with the masses m and m' interchanged		$2.68f$
83.3	16.7		Similar results as for the concentration ratio 16.7:83.3 with the masses m and m' interchanged		$2.67f$
100	0		Similar results as for the concentration ratio 0:100 with the masses m and m' interchanged		$2.00f$

[a] Represents molecules of type A and (·) represents molecules of type B.
[b] This column represents the value of ω^2 for the fundamental mode of vibration when the consecutive molecules have opposite phases for a hypothetical case when $m=2$ and $m'=1$.

various concentration ratios of the two components. As pointed out by Matossi, the approach to the problem is highly idealized.

UNIQUE LATTICE FOR A MOLECULAR MIX-CRYSTAL

In molecular crystals where the intramolecular force is very high compared to the intermolecular force of the van der waals type, each molecule may be regarded as a rigid body having three degrees of freedom of translation and three of rotation. A lattice formed of such molecules will show vibrations of low frequencies. For simplicity, let us consider a uni-dimensional model, which repeats itself periodically. For the pure crystal, consisting of molecules A only, all the molecules will be alike. When another substance with molecules of type B is mixed with it, some of the positions occupied by molecules A will be occupied by molecules B, thus giving a new lattice for the mix-crystal. Though this replacement is random, yet for the sake of argument we can assign a definite order to the positions of molecules A and B which repeats itself periodically. For a concentration ratio $1:n$ let us assume that n molecules of type B always occur between 2 successive molecules of type A. The different values of n will then correspond to different concentration ratios. The lattice vibrations of these linear periodic lattices may now be studied with the help of Born's idea of cyclic lattice, by assigning proper boundary conditions. Apparently the boundary conditions, for the fundamental modes of vibration, are different according to whether n is odd or even. For n odd each consecutive molecule A may be regarded as having identical displacement, whereas for n even every alternate molecule A will be considered as equivalent, thus increasing the size of our lattice. This difference does not present any fundamental difficulty as far as the discussion of the variation of lattice frequency with concentration is concerned, since one must always compare similar modes of vibration for such a comparison. The increase in the size of the unit cell only introduces some additional frequencies when n is even.

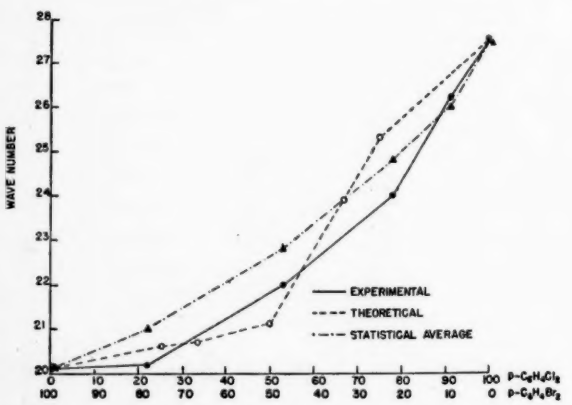

FIG. 1. Variation of the rotational frequency in the mix-crystals of p-$C_6H_4Cl_2$ and p-$C_6H_4Br_2$ about the axis of greatest moment of inertia.

With these considerations we can proceed to calculate the translational and rotational modes of vibration.

TRANSLATIONAL MODES

Confining ourselves to a longitudinal mode of vibration, let us consider the following linear model for the molecules A and B.

$$A_1B_2\cdots B_{n+1}A_{n+2}B_{n+3}\cdots B_{2n+2}A_{2n+3}.$$

For the sake of simplicity let us consider only the effect of neighboring molecules and further assume that the force between the various molecules is the same, having magnitude f per unit displacement. If $x_1, x_2, x_3\cdots$etc. represent the displacements about the equilibrium positions of the molecules $A_1, B_2, B_3\cdots$etc., m and m' the masses of the molecules of type A and B, the equations of motion may be written when n is odd:

$$\begin{aligned} m\ddot{x}_1 &= f(x_{n+1}+x_2-2x_1) \\ m'\ddot{x}_r &= f(x_{r+1}+x_{r-1}-2x_r) \quad r=2, 3, \cdots n \\ m'\ddot{x}_{n+1} &= f(x_1+x_n-2x_{n+1}), \end{aligned}$$

when n is even:

$$\begin{aligned} m\ddot{x}_1 &= f(x_{2n+2}+x_2-2x_1) \\ m'\ddot{x}_r &= f(x_{r+1}+x_{r-1}-2x_r) \qquad r=2, 3, \cdots (n+1) \\ m\ddot{x}_{n+2} &= f(x_{n+3}+x_{n+1}-2x_{n+2}) \\ m'\ddot{x}_r &= f(x_{r+1}+x_{r-1}-2x_r) \qquad r=(n+3)\cdots(2n+1) \\ m'\ddot{x}_{2n+2} &= f(x_1+x_{2n+1}-2x_{2n+2}). \end{aligned}$$

These equations have been solved in the usual manner for $n=0$, 1, 2, 3, 4, and 5, which correspond to concentration ratios of 100 percent (A); $50(A):50(B)$; $33.3(A):66.7(B)$; $25(A):75(B)$; $20(A):80(B)$; and $16.7(A):83.3(B)$, respectively. The results are shown in Table I, where $A_1, B_2\cdots$etc. represent the displacement amplitudes of molecules $A_1, B_2\cdots$etc., and ω is the angular frequency. It may be remarked here that the modes of vibrations have been represented by arrows perpendicular to the lattice axis only for a better graphical picture. Actually the motion corresponds to displacements along the lattice axis. In addition, in cases when $n=4$ and 5, only the cubic equation, the maximum root of which gives the limiting optical mode (where the consecutive molecules move in opposite phases), has been given.

Two important conclusions can be drawn from Table I. Firstly, the frequency corresponding to the limiting optical mode shows a gradual change with concentration, as seen from the last column, which confirms the experimental results. As shown by Matossi, this frequency corresponds to the most intense line in the infrared spectra. Secondly, in addition to the limiting optical mode, there are other optical modes which will be active in Raman and infrared spectra, e.g., the mode where all the molecules of type B move against molecules of type A. Such optical modes should bring out additional frequencies in Raman and infrared

spectra, unless they are rigorously inactive because of other reasons.

For a comparison of our results with those of Matossi, it may be remarked that his frequency ω_0 or ω_0' corresponds to our frequency $\omega^2=2f[(1/m)+(1/m')]$ appearing in the 50:50 concentration case. The treatment of 50:50 by Matossi will correspond to our concentration ratio 25:75, if Y and Z (Matossi) are regarded as identical. The four frequencies ω_1, ω_2, ω_3 and ω_4 discussed by him follow the reverse order in our table, i.e., ω_4, ω_3, ω_2, and ω_1.

ROTATIONAL MODES

The case of rotational motion can be treated in the same way as the translational one by replacing the force per unit displacement by torque per unit radian, and the masses m and m' by moments of inertia I and I', about an axis perpendicular to the plane in which the motion is considered. The results of Table I will also hold true in this case, and selection rules can be applied to decide whether a particular mode of vibration is active or inactive in Raman or infrared spectrum. For a more precise calculation let us now take c_1, c_2, and c' as the torques per unit radian between A–A, B–B, and A–B, respectively. The frequency for the limiting optical mode will then be

for $n=0$ $$\omega^2=4c_1/I,$$

for $n=1$ $$\omega^2=2c'\left(\frac{1}{I}+\frac{1}{I'}\right),$$

for $n=2$ $$\omega^2=\frac{(c'+2c_2)I+2c'I'+\{[(c'+2c_2)I+2c'I']^2-16II'c'c_2\}^{\frac{1}{2}}}{2II'},$$

for $n=3$ $$\omega^2=\frac{(c'+3c_2)I+2c'I'+\{[(c'+3c_2)I+2c'I']^2-8Ic'c_2(I+3I')\}^{\frac{1}{2}}}{2II'}.$$

These cases correspond to the concentration ratios 100 percent (A); $50(A):50(B)$; $33.3(A):66.7(B)$ and $25(A):75(B)$. The frequency for the inverse ratio may be obtained by interchanging I, I' and c_1, c_2.

The values of the torques c_1, c_2 can be evaluated so as to fit the observed rotational frequencies for the pure crystals and that of c' to fit the observed rotational frequency for a 50:50 mix-crystal. The necessary values of c_1, c_2, and c' for the two variable rotational frequencies observed by Vuks[3] are

(a) for rotational vibration about the axis with greatest moment of inertia $I=3155\times10^{-40}$ g×cm²; $I'=1384\times10^{-40}$ g×cm²; $c_1=32k$; $c_2=26k$; $c'=21k$.

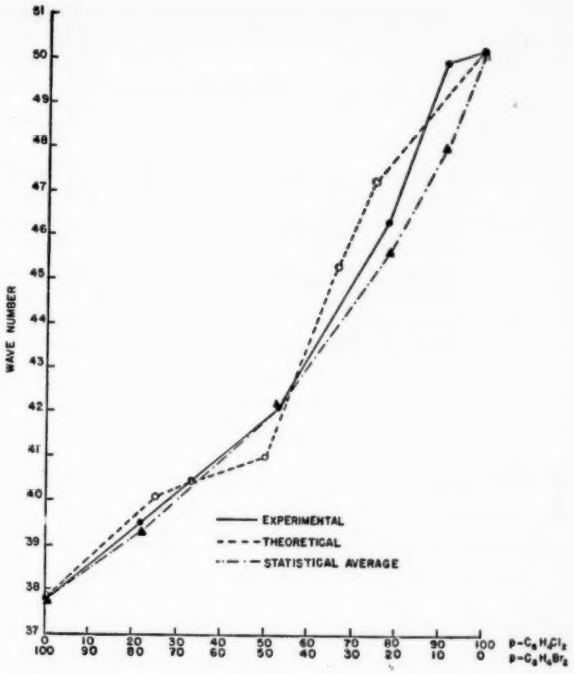

FIG. 2. Variation of the rotational frequency in the mix-crystals of p-$C_6H_4Cl_2$ and p-$C_6H_4Br_2$ about the axis of intermediate moment of inertia.

(b) for rotational vibration about the axis with intermediate moment of inertia $I=3004\times10^{-40}$ g×cm²; $I'=1234\times10^{-40}$ g×cm²; $c_1=107k$; $c_2=78k$; $c'=74k$. where k is a constant.

With the above values of c_1, c_2 and c' we have calculated the rotational frequencies for the other concentrations and plotted them in Figs. 1 and 2. The figures also show the frequencies obtained experimentally and those obtained by Saksena[4] on the basis of statistical average. The diagrams only suggest a *possible* explanation for the variation of frequency with concentration in binary mix-crystals, on the basis of assuming a unique linear lattice for the mix-crystal.

Dielectric Relaxation in Glycerol, Propylene Glycol, and *n*-Propanol*

D. W. DAVIDSON† AND R. H. COLE
Metcalf Research Laboratory, Brown University, Providence, Rhode Island

(Received July 16, 1951)

Complex dielectric constants have been measured at frequencies from below 20 c/s to 5 mc/s over the temperature range −40° to −75°C in glycerol, −45° to −90° in propylene glycol, and −80° to −140° in *n*-propanol. The results for *n*-propanol are described by the Debye equation, but the values for the other two require a modified equation corresponding to a broader range of dispersion at higher frequencies. In all three liquids, evidence is found for a second dispersion region at still higher frequencies, which accounts for much of the difference between the radio frequency and optical dielectric constant. The relaxation times are quantitatively described over wide ranges by an empirical rate equation of a form which also fits viscosity data. The significance of the various results is discussed.

I. INTRODUCTION

THE work reported here resulted from incidental measurements on glycerol in the supercooled liquid state at *ca* −50°C. These results showed that the dielectric relaxation process has simple and characteristic, but unexpected, properties not readily explained in terms of any simple picture of molecular association or bonding of hydroxyl groups. This behavior, reported in a previous note,[1] has been followed over the range of temperature for which the frequencies of measurement adequately defined the strongly temperature dependent dispersion. Similar measurements have been made on propylene glycol and *n*-propanol in order to determine the effect of number and position of hydroxyl groups on the observed properties.

The available frequency range was such that dispersion regions were observed in the supercooled liquids for the most part, but there is no evidence to indicate that the behavior is qualitatively different at higher temperatures in any of the liquids. The present results are in reasonably good agreement with earlier, less extensive ones[2] where comparison is possible, but the wider frequency range available for this work has permitted a more nearly complete determination of the dielectric properties and a more quantitative description of them.

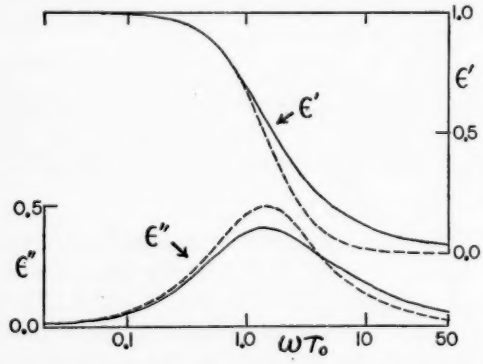

FIG. 1. Real and imaginary dielectric constants ϵ' and ϵ'' in reduced units *versus* $\omega\tau_0$ (log scale) for empirical dispersion function (1) ($\beta=0.67$, solid curve), and for the Debye equations ($\beta=1.0$, dashed curves). The frequency scale for the latter is shifted to the right by a factor 1.4 to show the differences at high frequencies more clearly.

II. EXPERIMENTAL

A. Purification and Handling of Materials

Glycerol (synthetic—Shell Chemical Corporation) and propylene glycol (Eastman CP) were distilled in a stream of dry nitrogen at low pressure—B.p. (glycerol) 143–144°C at 2.3 mm, b.p. (propylene glycol) 86.5–87°C at 5.3 mm. Specific conductances were in the range 10^{-9}–10^{-8} mho/cm at room temperature, and were not appreciably reduced by additional distillations. *n*-Propanol (Eimer and Amend, reagent grade) was dried by rolling with activated alumina and distilled, the fraction boiling in the range 96.2–96.7°C (760 mm) being used. Specific conductance 1.8×10^{-8} mho/cm at 25°C. In none of the runs reported here was there any indication of solid formation in the supercooled glycerol. After completion of these runs the cell was opened and no trace of solid found. In the runs where opaque solid globules were later found, the capacitances and conductance values had been found to drop rapidly with time, especially at low frequencies.

B. Measuring Cell

The test condenser used in this work is of stainless steel with coaxial cylindrical electrodes and Teflon insulation, as described by Gross and Taylor,[3] interchangeable central electrodes giving air capacitances of 4.8 and 9.1 $\mu\mu$f. The cell was not completely airtight, and over a period of a day or two the liquids showed a gradual slow rise in direct current conductance, which, however, had no measurable effect on the observed

* This paper is based on a thesis presented by D. W. Davidson in partial fulfillment of the requirements for the degree of Doctor of Philosophy in the Graduate School of Brown University.

† Present address: National Research Council of Canada, Ottawa.

[1] D. W. Davidson and R. H. Cole, J. Chem. Phys. **18**, 1417 (1950).

[2] For glycerol, S. O. Morgan, Trans. Am. Electrochem. Soc. **65**, 109 (1934); for propylene glycol, A. H. White and S. O. Morgan, Physics **2**, 313 (1932); for *n*-propanol, references 13 and 23.

[3] P. M. Gross, Jr., and R. C. Taylor, J. Am. Chem. Soc. **72**, 2075 (1950).

dielectric behavior (after subtraction of dc conductance from total observed conductance).

C. Temperature Control

For temperatures down to $-75°C$, the cell was placed in an acetone bath in a large Dewar flask and the temperature regulated by adding small amounts of solid carbon dioxide. Control of temperature to $\pm 0.05°C$ was possible over the period of thirty to forty minutes for a complete frequency run.

At temperatures below $-75°C$, a noninflammable five component bath liquid described by Kanolt[4] was used which remains fluid to temperatures below $-140°$. The temperature was regulated to $\pm 0.1°C$ by adding small amounts of liquid nitrogen to a shallow metal tray in the Dewar above the cell and bath liquid surface.

Temperatures were measured by a copper-constantan couple immersed in the liquid volume of the cell and a Leeds and Northrup Type K potentiometer. The couple was calibrated at the freezing point of mercury, sublimation point of carbon dioxide, and by comparison with a standard thermocouple.

D. Electrical Measurements

A capacitance-conductance bridge described elsewhere[5] was used over the frequency range 20 c/s to 5 mc/s. At frequencies for which absorption conductances were very large (greater than 10^{-4} mho), corrections of the capacitance data for effects of residual inductance in the conductance network were made, these being determined by an iteration process.

For measurements of the very slow relaxation at the lowest temperatures a transient method was employed in which the charging current following application of a linearly rising potential across the dielectric was recorded. This method[6] gives the equivalent of charge resulting from a constant voltage as a function of time after its application, and made possible measurements at times too long to be practical for study by steady state bridge methods. With the combination of both procedures, a range of eight decades in time could be used to study the relaxation process.

III. ANALYSIS OF THE DATA

The major portion of the dielectric dispersion in *n*-propanol from $-80°C$ to $-145°C$ is described quantitatively by the familiar Debye formulas. The data for propylene glycol and glycerol can be fitted except at high frequencies by an empirical dispersion formula previously reported[1] which reduces to the Debye result as a limiting case. Because the parameters of this expression provide a compact summary of a quantity of data too great to be reported in full, the results will be presented in this way after a discussion of the methods used to determine the parameters.

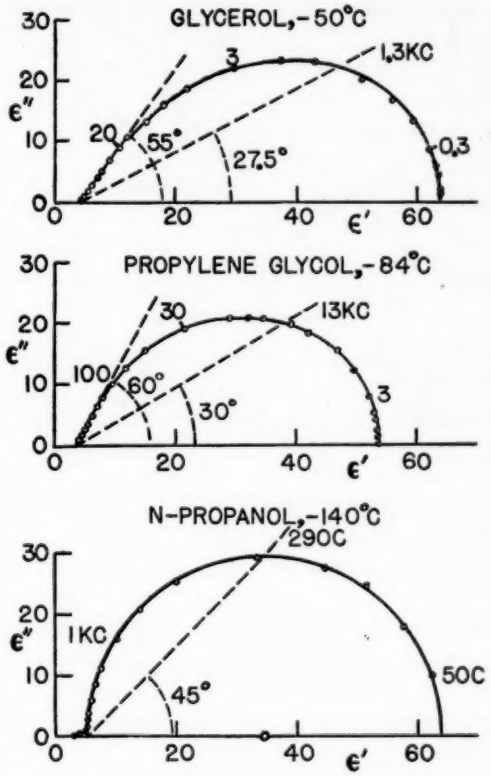

FIG. 2. Complex dielectric constant loci for glycerol at $-50°C$, propylene glycol at $-84°C$, and *n*-propanol at $-140°C$.

A. Steady State Measurements

The empirical expression for the complex dielectric constant ϵ^* as a function of radian frequency ω ($=2\pi \times$cyclic frequency) is

$$\epsilon^* = \epsilon' - i\epsilon'' = \epsilon_\infty + (\epsilon_0 - \epsilon_\infty)/(1+i\omega\tau_0)^\beta, \qquad (1)$$

where ϵ_0 and ϵ_∞ are the limiting low and high frequency dielectric constants and τ_0 is a relaxation time. The parameter β may assume values between zero and one, and reduces to the Debye result in the latter case. The real and imaginary parts of Eq. (1) are given by

$$\begin{aligned} \epsilon' - \epsilon_\infty &= (\epsilon_0 - \epsilon_\infty)(\cos\varphi)^\beta \cos\beta\varphi, \\ \epsilon'' &= (\epsilon_0 - \epsilon_\infty)(\cos\varphi)^\beta \sin\beta\varphi, \end{aligned} \qquad (2)$$

where $\tan\varphi = \omega\tau_0$.

These equations are plotted in Fig. 1 as a function of ω for the case $\beta = 0.67$, and the Debye curves ($\beta = 1$) are shown as dashed lines for comparison.

It is apparent that the chief difference is the more gradual falling off of the curves at higher frequencies. Analysis of the data is facilitated by using two derived expressions: one for the complex plane locus of ϵ'' *versus* ϵ', and the other for the quantity $\omega\tau_0$ as a function of ϵ'' and ϵ'.

[4] C. W. Kanolt, U. S. Bur. Standards Paper No. 520 (March, 1926); described as Mixture No. 39 in this paper.

[5] R. H. Cole and P. M. Gross, Jr., Rev. Sci. Instr. **20**, 252 (1949).

[6] Davidson, Auty, and Cole, Rev. Sci. Instr. **22**, 678 (1951).

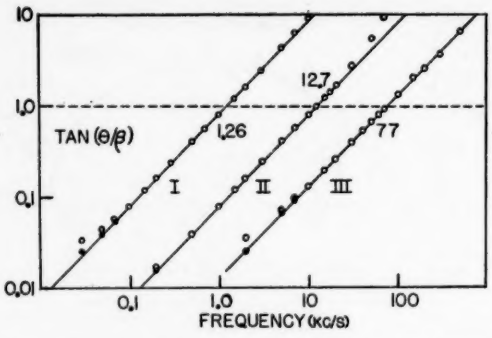

FIG. 3. Frequency plots to verify Eq. (4) and determine relaxation time τ_0. Curve I, glycerol at $-50°C$ ($\beta=0.60$); curve II, propylene glycol at $-64°C$ ($\beta=0.66$); curve III, *n*-propanol at $-113°C$ ($\beta=1.0$). The solid points represent data after correction for dc conductance.

The equations are most conveniently written in polar coordinates

$$r=[(\epsilon'-\epsilon_\infty)^2+\epsilon''^2]^{\frac{1}{2}} \quad \text{and} \quad \theta=\tan^{-1}\epsilon''/(\epsilon'-\epsilon_\infty),$$

and one readily finds from Eqs. (2) that

$$r=(\epsilon_0-\epsilon_\infty)[\cos(\theta/\beta)]^\beta, \tag{3}$$

and

$$\tan\theta=\tan\beta\varphi, \quad \text{or} \quad \omega\tau_0=\tan(\theta/\beta). \tag{4}$$

The locus of Eq. (3) in the complex plane is, as shown in the upper two examples of Fig. 2, an arc with intercepts on the ϵ' axis at ϵ_0 and ϵ_∞, the limiting curve as $\omega\rightarrow 0$ being a semicircle with center on the real axis, and as $\omega\rightarrow\infty$ a straight line making an angle $\beta\pi/2$ with the ϵ' axis. If Eq. (1) is valid, this plot then determines the values of ϵ_0, ϵ_∞, and β directly. The frequency dependence predicted by Eq. (4) is readily verified, and the value of τ_0 determined, by plotting $\tan(\theta/\beta)=\tan\epsilon''/(\epsilon'-\epsilon_\infty)\beta$ against frequency. This should give a straight line, as shown in the log-log plots of Fig. 3, and the frequency f_c for which $\tan(\theta/\beta)=1$ gives $\tau_0=1/2\pi f_c$. We note that this frequency is lower than the one for which ϵ'' is a maximum, and corresponds to the point on the complex plane locus for which $\theta=\beta\pi/4$, as indicated in the plots of Fig. 2.

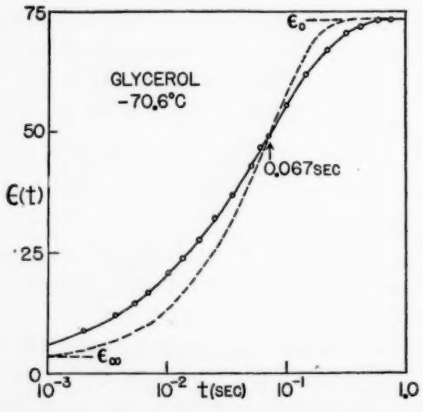

FIG. 4. Plot of transient dielectric constant values *versus* time (log scale) for glycerol at $-71°C$. Solid curve computed from Eq. (5) with $\beta=0.56$, $\tau_0=0.141$ sec; dashed curve, exponential with time constant $\tau_0=0.067$ sec.

B. Transient Measurements

The transient response data obtained give the equivalent of the charge following application of a unit step voltage across the dielectric sample which we may conveniently, if loosely, call the "transient" dielectric constant $\epsilon(t)$ for a condenser of unit capacitance. By the Fourier integral theorem, this transient value is given by

$$\epsilon(t)=\frac{1}{\pi}\int_0^\infty \frac{\epsilon^*(i\omega)}{i\omega}e^{i\omega t}d\omega.$$

For the expression (1) for $\epsilon^*(i\omega)$, this becomes[7]

$$\epsilon(t)=\epsilon_\infty+(\epsilon_0-\epsilon_\infty)T_{t/\tau_0}(\beta)/T(\beta). \tag{5}$$

The ratio of the incomplete gamma function $T_{t/\tau_0}(\beta)$ to the complete function $T(\beta)$ is given in tables by Pearson.[8]

The choice of best values for both β and τ_0 to fit the observed points would be a tedious process in the absence of other information, but in our case the values of β and ϵ_∞ were known from bridge measurements of the high frequency part of the dispersion and determination of the best values for ϵ_0 and τ_0 was then a relatively simple matter. The agreement between observed and calculated values of $\epsilon(t)$ in the representative case of glycerol at $-70°C$ is shown in Fig. 4, a logarithmic time scale being used for clarity. An exponential approach to the final values, as the Debye type equation predicts, is shown as a dashed line for comparison.

C. High Frequency Data

In analyzing the data, it soon became apparent that, while most of the dispersion was described quite accurately by Eq. (1), a second dispersion process occurs for all three liquids at frequencies high compared with $1/\tau_0$. Except at the lowest temperatures, this was evident only as a slight decrease of the values of ϵ' below the straight line locus obtained by extrapolation of lower frequency data, and corresponding values of ϵ'' in excess of those to be expected.

The nature of these departures is shown in typical cases in Fig. 5, where only a small high frequency part of the complete locus is plotted. The present results unfortunately do not define this second dispersion adequately for two reasons: the available bridge method did not extend to sufficiently high frequencies except at the lowest temperatures, and the values are not as accurate as one would like because of the small capacitance values and the presence of residual bridge errors at the highest frequencies. When possible, extrapolations

[7] G. A. Campbell and R. M. Foster, Bell Telephone Monograph B-584 (1931), Pair 524.2.

[8] K. Pearson, *Tables of the Incomplete Gamma Function* (H. M. Stationery Office, London, 1922). (The arguments u and p employed in the tables are related to ours by the equation $u=\beta^{-\frac{1}{2}}(t/\tau_0)$, $p=\beta-1$.)

of this second dispersion locus to the ϵ' axis were made, and these intercepts ϵ_d are listed in Table IV as a matter of interest for the discussion. They should, however, be considered as only approximate values which we hope to improve by further measurements under better conditions.

IV. RESULTS

As the typical complex plane loci in Fig. 2, frequency plots of Fig. 3, and transient curve of Fig. 4 illustrate, the observed dielectric behavior of all three liquids is quantitatively described, except at the highest frequencies, by the empirical dispersion Eq. (1) or its transient equivalent (5). Representative values of ϵ_0, ϵ_∞, τ_0, and β necessary to fit the measurements are listed in Table I. In the case of *n*-propanol, the value of β is unity within experimental error at all temperatures (complex plane locus a semicircle).

Values obtained from repeat runs on different samples are given in parentheses in a few cases to indicate the reproducibility. To save space this is done for glycerol only as similar agreement was found for the other two liquids. The starred values were obtained from the transient analysis.

V. DISCUSSION

A. Equilibrium Dielectric Constants

The limiting dielectric constants ϵ_0 at low frequencies all show the gradual increase with decreasing temperature characteristic of polar liquids. As expected for hydrogen-bonding substances, the numbers are larger than predicted for Onsager's equation[9] and their significance can be examined in terms of Kirkwood's generalization of Onsager's results which takes explicit account of short range molecular interaction in a way which can be calculated for a suitable model. Kirkwood's equation[10] can be written

$$\epsilon_0-\epsilon_\infty=\frac{2}{9}(n_0^2+2)^2\left(\frac{2\epsilon_0}{2\epsilon_0+n_0^2}\right)\left(\frac{\pi N\mu_0^2}{kTV}\right)g, \qquad (6)$$

where μ_0 and n_0 are the dipole moment and dielectric constant for induced polarization of the molecule in question, N is Avogadro's number, V, the molar volume, and kT has the usual meaning. The value of the correlation parameter g, for which Oster and Kirkwood[11] have given approximate expressions in the case of water and normal alcohols, is unity if hydrogen bonding or other short range forces are not important, and Eq. (6) then reduces essentially to Onsager's result.

If, as for glycerol and propylene glycol, insufficient data exist for a reasonable model of the hydrogen bonding, the necessary values of g for Eq. (6) to give agreement with experiment can be taken as a semi-

[9] L. Onsager, J. Am. Chem. Soc. **58**, 1486 (1936).
[10] J. G. Kirkwood, J. Chem. Phys. **7**, 911 (1939).
[11] G. Oster and J. G. Kirkwood, J. Chem. Phys. **11**, 175 (1943); G. Oster, Bull. Soc. Chim. France **16**, D 353 (1949).

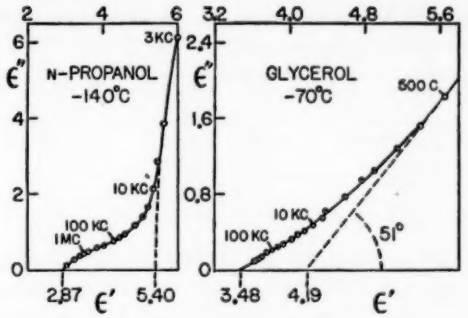

FIG. 5. High frequency dielectric constant loci for *n*-propanol at −140°C and glycerol at −70°C.

empirical measure of the short range molecular coordination. Table II gives values of g found in this way from data of Table I, the molecular dipole moment μ_0 (Debye units), and n_0^2. From this table, it is seen that the values of g are smaller for glycols than for *n*-propanol, and that they all increase appreciably at lower temperatures.

Oster and Kirkwood give the value $g=2.57$ for a

TABLE I. Parameters of the dispersion equation for glycerol, propylene glycol, and *n*-propanol.

A. Glycerol

t°C	ϵ_0	ϵ_∞	τ_0(sec)	β
28	42.1	...	...	...
0	48.2	...	...	...
− 10	50.9(51.0)	...	...	...
− 20	53.7	...	...	...
− 30	56.8(57.2)	...	...	...
− 40	60.5	4.20	1.15×10^{-5}	0.608
	(60.2)	(4.13)	(1.12×10^{-5})	(0.607)
− 50	63.9	4.10	1.25×10^{-4}	0.603
− 60	67.4*	4.16	2.5×10^{-3}*	0.593
			2.23×10^{-3}*	
− 65.5	70.5*	4.3	1.86×10^{-2}*	0.595
− 70	74.2*	4.19	0.118*	0.566
	(73.9*)	(4.1)	(0.141*)	(0.562)
− 74.6	76.2*	4.18	0.96	0.550

B. Propylene glycol

t°C	ϵ_0	ϵ_∞	τ_0(sec)	β
− 35.5	43.1			
− 45.4	45.7	3.53	3.85×10^{-7}	0.663
− 55.4	49.5	3.59	2.11×10^{-6}	0.664
− 65.5	53.8	3.52	1.68×10^{-5}	0.666
− 75.0	57.7	3.51	1.89×10^{-4}	0.662
− 80.0	60.1	3.58	9.0×10^{-4}	0.663
− 84.1	63.7*	3.56	4.1×10^{-3}*	0.664
− 89.1	65.3*	3.57	2.5×10^{-2}*	0.650

C. *n*-Propanol

t°C	ϵ_0	ϵ_∞	τ_0(sec)
24.5	20.47	...	...
18.6	21.15	...	...
− 0.7	24.34	...	...
− 24.7	28.4	...	...
− 46.3	32.6	...	$\sim9\times10^{-9}$
− 64.4	36.8	...	2.39×10^{-8}
− 78.2	40.5	...	6.2×10^{-8}
− 89.0	43.7	...	1.49×10^{-7}
−100.4	47.6	4.90	4.71×10^{-7}
−113.0	52.2	5.22	2.07×10^{-6}
−126.6	54.6	5.32	2.12×10^{-5}
−140.4	64.0	5.40	5.6×10^{-4}
−144.7	67.4	5.56	1.89×10^{-3}

TABLE II. Values of Kirkwood's correlation parameter g.

n-Propanol $\mu_0=1.69$ $n_0^2=2.11$		Propylene glycol $\mu_0=2.0$ $n_0^2=2.17$		Glycerol $\mu_0=2.67$ $n_0^2=2.22$	
t°C	g	t°C	g	t°C	g
20	3.19	−35	3.34	28	2.35
−40	3.56	−84	3.76	−70	2.66
−80	3.67				

model of n-propanol in which linear OHO-bonded molecules with free rotation about the bonds are assumed. The higher experimental values may arise from inadequacies of the model, approximations made in deriving Eq. (6) from the theory, or uncertainty as to the proper value of n_0^2 (see discussion in D). However, the fact that the "experimental" values increase only slightly for propylene glycol and are appreciably less for glycerol suggests that a less regular and effective coordination exists when hydrogen bonding may take place on two or three hydroxyl groups of the molecule.

B. Relaxation Times

The relaxation times τ_0 vary strongly with temperature for all three liquids in the fashion to be expected of a chemical rate process. If, however, one attempts to fit the data to a simple rate law of the form $\tau_0=A\exp(B/T)$, large systematic deviations are found. Curiously enough, most of the data are fitted within their experimental error by the expression,

$$\tau_0=A\exp B/(T-T_\infty), \qquad (7)$$

some deviation being found for n-propanol at the lowest temperatures. This relation is identical in form with an empirical equation proposed by Tammann and Hesse[12] for the temperature dependence of viscosity of a number of polar liquids.

The nature of the agreement over several decades in τ_0 is shown in Fig. 6, where values of $\log\tau_0$ are plotted against $1000/(T-T_\infty)$, the same values of T_∞ as found by Tammann and Hesse being used for glycerol and n-propanol. A significant further result is that the values of B required to fit the dielectric data also are the same, within combined experimental error, as the values from the viscosity data for glycerol and n-propanol as shown in Table III.

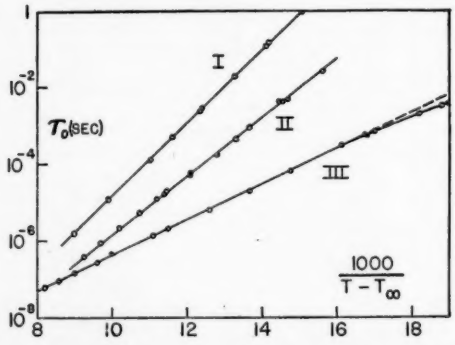

FIG. 6. Relaxation times τ_0 (log scale) as a function of the reciprocal of $(T-T_\infty)$. Curve I, glycerol ($T_\infty=132$°K); curve II, propylene glycol ($T_\infty=120$°K); curve III, n-propanol ($T_\infty=73.5$°K).

[12] G. Tammann and W. Hesse, Z. anorg. allgem. Chem. **156**, 245 (1926).

The agreement is too good to be fortuitous and gives strong support to the conclusion that in these liquids the processes by which dipole reorientation and molecular flow in shear are realized must be intimately related. A further interesting line of evidence is the fact that the measured low frequency conductances of these liquids also follow a similar rate expression. The slow drift of these values with time in our experimental arrangement makes this result less well established, but the inference is plain that the translational mobility of conducting ions in these liquids is governed by the same sort of process. This general similarity of dielectric rate process to viscosity and conductance in these liquids has been noted by Kobeko *et al.*[13] and our results amplify and confirm theirs.

The question of the significance of the characteristic temperature T_∞ in Eq. (7) is an interesting one. Taken literally, Eq. (7) would require an infinitely slow relaxation process in the limit $T=T_\infty$. Our data extend only to temperatures some tens of degrees higher than T_∞, and show very rapid increases in τ_0 at the lowest temperatures. The values of T_∞ are 20° to 40° below the so-called "glass" temperatures at which viscosities of the order 10^{13} poise are realized.[14]

TABLE III. Parameters of dielectric and viscosity data equations.

	Measurement	Temperature range (°C)	log$A$	B(°K)	T_∞(°K)
n-Propanol	Dielectric	−75 to −160	−10.99	461	73.5
	Viscosity	−97 to −136	− 4.06	459	73.5
Propylene glycol	Dielectric	−45 to − 90	−13.56	770	120
Glycerol	Dielectric	−40 to − 75	−14.41	957	132
	Viscosity	0 to − 40	− 4.76	950	132

In the case of n-propanol, the lowest temperature values do show the slower rate of increase one would expect.

The observed correspondence of dielectric relaxation time with viscosity η is predicted by Debye's hydrodynamic model[15] according to which the molecular relaxation time τ_D is given by $\tau_D=3\eta\nu/kT$, ν being the volume of the molecule (assumed spherical). Calculations of the volumes ν necessary for numerical agreement give values which are much too small for glycerol and propylene glycol (*ca.* 0.1×10^{-24} cc), and of reasonable size for n-propanol (60–900×10^{-24} cc).‡ The in-

[13] Kobeko, Kuvshinski, and Shishkin, J. Tech. Phys. U.S.S.R. **5**, 413 (1938).

[14] W. Kauzmann, Chem. Revs. **43**, 219 (1948).

[15] P. Debye, *Polar Molecules* (Dover Publications, New York, 1929), p. 84.

‡ The spread in these values arises from uncertainty as to the relation between τ_D and the value τ_0 derived directly from the dispersion measurements, the difference between the two depending on one's assumptions as to the average field acting to cause dipole reorientations. For the Lorentz field $\tau_D=[(\epsilon_\infty+2)/$

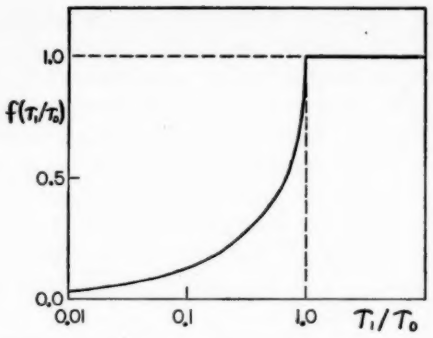

FIG. 7. The fraction $f(\tau_1/\tau_0)$ of processes with relaxation times less than τ_1 computed for $\beta=0.60$.

ference is natural that for the glycols much smaller units than the molecule are involved, while for *n*-propanol the individual molecule may well be the significant structural unit to consider. These ideas are consistent with the nature of the dispersion functions which we now consider.

C. The Dispersion Functions

The characteristic differences in frequency dependence for the alcohol on the one hand and the glycols on the other show that, while most of the dispersion in *n*-propanol is represented by a simple relaxation process, the two glycols exhibit dispersion both at relatively much higher frequencies and over a broader frequency range.

One can describe the broader dispersion formally in terms of a distribution of simple relaxation processes characterized by a distribution function $F(\tau/\tau_0)$ for relaxation times τ in the interval $d\ln(\tau/\tau_0)$, the expression being

$$\epsilon^*(i\omega\tau_0)-\epsilon_\infty=(\epsilon_0-\epsilon_\infty)\int_{-\infty}^{\infty}\frac{F(\tau/\tau_0)}{1+i\omega\tau}d\ln(\tau/\tau_0). \quad (8)$$

The solution of this integral equation for $F(\tau/\tau_0)$ using the imaginary part only has been given by Fuoss and Kirkwood.[16] An alternative and here more convenient procedure is to solve Eq. (8) in the complex form as a Stieltje integral for which the solution by Fourier transforms is known.[17] The result is

$$F(\tau/\tau_0)=\frac{1}{\epsilon_0-\epsilon_\infty}\cdot\frac{1}{2\pi i}[\epsilon^*(\tau_0/\tau e^{i\pi})-\epsilon^*(\tau_0/\tau e^{-i\pi})],$$

and for the ϵ^* of Eq. (1) this gives

$$F(\tau/\tau_0)=\frac{\sin\beta\pi}{\pi}\left(\frac{\tau}{\tau_0-\tau}\right)^\beta, \quad \tau<\tau_0,$$
$$=0, \quad \tau>\tau_0. \quad (9)$$

$(\epsilon_0+2)]\tau_0$, while for the Onsager field $\tau_D\cong\tau_0$. The true relation, to the extent that a valid one is simply expressed by a local field model, presumably lies between these extremes.

[16] R. M. Fuoss and J. G. Kirkwood, J. Am. Chem. Soc. **63**, 385 (1941).

[17] E. C. Titchmarsh, *Theory of Fourier Integrals* (Clarendon Press, Oxford, 1949), p. 92.

TABLE IV. High frequency dielectric constants.

	t°C	n_0^2	$n^2(150\mu)$	ϵ_d	ϵ_∞
Glycerol	− 70	2.22	3.5	3.4	4.18
Propylene glycol	− 84	2.17	—	2.9	3.56
n-Propanol	−140	2.11	2.2*	2.9	5.40

* Estimated by comparison of data for several normal alcohols.

There is thus a maximum, or cutoff, time τ_0 of a continuous distribution for times τ less than τ_0. The result is not what one would expect from a picture of associated molecules of varying size, in view of the fact that the maximum values of τ are already small for a single molecule and the necessary distribution extends in the direction of smaller times. The function (9) implies a broad distribution for β of the order 0.6, as can be seen by considering how the fraction f of processes with relaxation time less than a given τ_1 varies with τ_1. This is given by

$$f(\tau_1/\tau_0)=\int_{-\infty}^{\tau_1/\tau_0}\left(\frac{\sin\beta\pi}{\pi}\right)\left(\frac{\tau}{\tau_0-\tau}\right)^\beta d\ln(\tau/\tau_0)$$
$$=\left(\frac{\sin\beta\pi}{\pi}\right)B_{\tau_1/\tau_0}(\beta,1-\beta), \quad \tau_1<\tau_0,$$
$$=1, \quad \tau_1>\tau_0,$$

where B is the incomplete beta function for which tables exist.[18] A plot of $f(\tau_1/\tau_0)$ *versus* τ_1/τ_0 for $\beta=0.6$ is shown in Fig. 7, and one sees, for example, that ten percent of the assumed processes must have τ_1 less than $\tau_0/20$.

The breadth of the distribution in the wrong direction for a simple picture of molecular association suggests that we have rather a situation in which reorientation of hydroxyl dipole groups is made possible by breaking of hydrogen bonds to neighboring ones. The existence of a single relaxation process for the low frequency dispersion in *n*-propanol implies that a single unit rather than a linear polymer with a variety of modes of reorientation is involved. This hypothesis is not incompatible with the coordination number of two inferred from x-ray studies[19] or with the large *g*-factor (see A) for the equilibrium dielectric constant, as we have only to suppose that breaking and reforming of intermolecular bonds occurs in such a way that each molecule spends most of its time having two neighbors in positions consistent with bond angles.

Attempts to relate such a picture to rate theory considerations of activation energies[20] meet the difficulty that a strongly temperature dependent free energy ΔF^*

[18] K. Pearson, Tables of the Incomplete Beta Function (University Press, Cambridge, 1934).

[19] W. C. Pierce and D. P. MacMillan, J. Am. Chem. Soc. **60**, 779 (1938).

[20] W. Kauzmann, Revs. Modern Phys. **14**, 12 (1942).

must be assumed if a rate law of the form,

$$\tau_0=(h/kT)\exp(\Delta F^*/RT),$$

is to agree with the empirical expression (7) that

$$\tau_0=A\exp B/(T-T_\infty).$$

In this situation, ΔF^* has no simple interpretation nor can activation energies and entropies be deduced. Frenkel[21] has discussed such temperature dependent activation energies in terms of changes in local order of the liquids, a plausible conclusion which can neither be confirmed nor refuted in the absence of a more quantitative model.

A further complication for glycerol and propylene glycol is the fact that on the basis of the rate theory a distribution of free energies of activation below a maximum cutoff value is required, the width being such that 90 percent of the free energies lie in a range $3RT$ for $\beta=0.6$. The experimental values of β change only slightly with temperature over the range investigated, even though the times τ_0 change by a factor of 10^6, hence the form of the distribution is essentially independent of temperature despite the changes in magnitude of ΔF^* one would have to assume.

A possible approach to the explanation of these observations may be in terms of the activation energy for formation of "holes" by use of free volume of the liquid. It is of interest to note in this connection that Danforth[22] was able to lower the dispersion range in glycerol to radio frequencies at 0°C by pressures of several thousand atmospheres which increased the density by 12 percent.

D. High Frequency Dispersion

The observation at low temperatures of a second high frequency dispersion region is of interest as it indicates that a large part of the difference between the square of the refractive index n and the limiting value ϵ_∞ of the low frequency dispersion may be attributed to this second temperature dependent dipole polarization. Measurements by Cartwright and Errera[23] in the far infrared (50–150μ) at room temperature permit rough estimate by use of the Lorenz-Lorentz formula of $n^2(150\mu)$ at the temperatures for which we have been able to estimate the high frequency limit ϵ_d of our second dispersion, as indicated in Fig. 5. These values are listed in Table IV together with the extrapolated optical value n_0^2 and the limiting value ϵ_∞ of the low frequency dispersion.

The values of $n^2(150\mu)$ are only approximate but do suggest by comparison with ϵ_d that most of the difference between $n^2(150\mu)$ and ϵ_∞ is accounted for by the observed radio-frequency dispersion. Our data are too limited to permit very detailed discussion of this dispersion, but the center frequency is approximately 500 kc/s for n-propanol at −140°C as compared to the cutoff frequency $f_c=1/2\pi\tau_0=290$ c/s of the low frequency dispersion, and the frequency range is apparently wider than for a Debye type curve. The data so far obtained indicate that the frequency range varies with temperature in the fashion to be expected of a dipole relaxation process, and in fact the central frequencies appear to follow a rate law of the same form found for the low frequency dispersion. These results will be presented in detail later, when more comprehensive data are available. Indications of a second dispersion region at room temperature have been found by Girard and Abadie[24] in microwave measurements, and the same process may well be involved.

ACKNOWLEDGMENT

We wish to thank the Research Corporation for a grant which made possible development of the transient equipment used in this work and a fellowship for one of us (D.W.D.).

[21] J. Frenkel, *Kinetic Theory of Liquids* (Oxford University Press, London, 1946), Chapter IV.
[22] W. E. Danforth, Phys. Rev. **38**, 1224 (1931).
[23] C. H. Cartwright and J. Errera, Proc. Roy. Soc. (London) **A154**, 138 (1936).
[24] P. Girard and P. Abadie, Trans. Faraday Soc. **42A**, 40 (1946); Bull. Soc. Chim. France **12**, 207 (1945); J. Chem. Phys. **44**, 313 (1947).

The Dielectric Constant of Ethylene at High Pressures

H. G. DAVID, S. D. HAMANN, AND J. F. PEARSE
High Pressure Laboratory, Division of Industrial Chemistry, Commonwealth Scientific and Industrial Research Organization, University of Sydney, Australia

(Received August 13, 1951)

The dielectric constant of ethylene has been measured at pressures up to 500 atmospheres and at temperatures of 25°C and 50°C. At both temperatures the Clausius-Mosotti function has been found to pass through a maximum with increasing density. The results have been discussed with reference to Kirkwood's theory of dielectric polarization.

INTRODUCTION

THE study of the dielectric constant of gases over a wide range of densities is of interest in the development of theories of dielectric behavior. A review of work done in this field has been recently given by Miller.[1]

The Clausius-Mosotti (C-M) treatment requires that $(\epsilon-1)/(\epsilon+2)d$, where ϵ and d are the dielectric constant and density of the gas respectively, should be independent of density. Also for gases with non-polar molecules, the C-M ratio should be independent of temperature. However, variations in the value of the C-M ratio with density have been found for carbon dioxide,[2,3] ammonia,[4] and propane.[2] Several authors have advanced explanations for these variations,[4–8] but the agreement between theory and experiment leaves much to be desired.

It was decided in this work to extend the range of experimental data by measuring the dielectric constant of ethylene at various densities and at temperatures of 25°C and 50°C, and to consider the implications of the results.

APPARATUS

The procedure adopted for this study was to confine ethylene at a known temperature and various pressures between the plates of a gas condenser contained in a pressure vessel and to measure the capacity of the condenser and the pressure of the gas. To achieve this, it was necessary to have a supply of pure ethylene, a means of compressing it in the gas condenser, and equipment for accurately measuring temperature, pressure, and capacity.

Gas Condenser

The condenser and containing vessel were similar to those used by Michels.[9] The former consisted of two concentric brass cylinders with the outer supported from the inner cylinder by silica disks. The outer cylinder was in electrical contact with the pressure vessel and connection with the inner cylinder was made through a low capacity insulated plug of the type described by Michels.[9] The design of the condenser was such as to ensure minimum distortion of the cylinders at high gas pressures.

The containing pressure vessel was made of high tensile steel. It was rigidly and independently supported in an oil thermostat. The capacity measuring equipment was mounted on the same support and a rigid coaxial lead connected the gas condenser to this equipment.

The temperature of the oil thermostat was maintained constant to ±0.005°C by an electronic temperature controller (see Wylie).[10] It was measured by a Leeds and Northrup Platinum Resistance Thermometer and G-2 Mueller Bridge. The thermometer and bridge were calibrated by the U. S. National Bureau of Standards and the Ice Point resistance of the thermometer was determined in this laboratory.

Pressure Balance

The pressures were measured by a modified Budenberg-type Pressure Balance which has been described by one of the authors.[11] The balance was used in conjunction with a *U*-tube containing mercury and an oil injector as described by Keyes.[12] The pressures were measured over the whole range (20–530 atmospheres) with a piston-cylinder unit of nominal piston area of 0.02 sq. in. It was calibrated against the vapor pressure of carbon dioxide at 0°C (see Bridgman).[13] In this calibration it was found that a change in the weight on the piston of one part in 95,000 was sufficient to make or break contacts in the *U*-tube and readings were reproducible to one part in 25,000. The calibrated value of the gauge constant was assumed to be correct up to 530 atmospheres. Keyes[12] has shown this assumption to be justifiable.

[1] J. G. Miller, Trans. Am. Soc. Mech. Engrs. **70**, 621 (1948).
[2] F. G. Keyes and J. L. Oncley, Chem. Revs. **19**, 195 (1936).
[3] A. Michels and L. Kleerekoper, Physica **6**, 586 (1939).
[4] F. G. Keyes and J. G. Kirkwood, Phys. Rev. **36**, 1570 (1930); **37**, 202 (1931); J. G. Kirkwood, J. Chem. Phys. **4**, 592 (1936).
[5] J. H. Van Vleck, J. Chem. Phys. **5**, 556, 991 (1937).
[6] Michels, de Boer, and Bijl, Physica **4**, 981 (1937).
[7] C. J. F. Böttcher, Physica **9**, 937, 945 (1942).
[8] W. F. Brown, J. Chem. Phys. **18**, 1193, 1200 (1950).
[9] A. Michels and Mrs. C. Michels, Trans. Roy. Soc. (London) (A) **231**, 409 (1933).
[10] R. G. Wylie, Natl. Standards Lab. C.S.I.R.O. Report No. *PA*-2 (1948).
[11] J. F. Pearse, submitted for publication in J. Sci. Instr.
[12] F. G. Keyes, Proc. Am. Acad. Arts Sci. **68**, 505 (1933).
[13] O. C. Bridgman, J. Am. Chem. Soc. **49**, 1174 (1927).

Mercury Gas-Compressor

This unit was based on a design developed by Michels and described by Tongue.[14] It was used in conjunction with a "Cook" 3000 atmospheres two-stage pump.[15]

Ethylene Storage Cylinder and Transfer Vessel

The gas was stored in a high tensile steel pressure vessel of one liter capacity. The transfer vessel, the use of which will be described later, was made of stainless steel and had a capacity of 150 ml.

Electrical Equipment

The method used for capacity measurements was that described by P. Cohen Henriquez.[16] The circuit consisted of a pentode valve, type *6F6G*, with a 1000 Kc quartz crystal controlling the grid circuit. The anode circuit was tuned by means of an inductance in parallel with the gas condenser and a standard variable condenser. The anode voltage was supplied by a stabilized power pack and the heater current was taken from a 6-volt battery. Such a circuit exhibits the usual minimum of anode current at the capacity corresponding to the natural frequency of the crystal with the important feature that the slope of the curve on the high capacitance side is very steep. A suitable operating point is chosen on the steepest portion of the curve and capacitance adjusted until the anode current is at the chosen value. To obviate errors in the capacity measurements caused by drifts in the oscillator circuit, a reference condenser was included, as suggested by P. Cohen Henriquez.[16]

The standard condenser was constructed from a transmitting condenser. The spindle, supported in a lapped conical bearing, was rotated by a worm and wheel drive fitted with an anti-backlash device. The worm spindle carried a graduated drum on which one division was equivalent to 1/100 $\mu\mu$F. The instrument was calibrated by the Division of Electrotechnology of the C.S.I.R.O. and found to be consistent to ± 0.02 $\mu\mu$F over a long period. The whole of the capacity measuring equipment was screened.

EXPERIMENTAL PROCEDURE

Preparation of Ethylene

The gas was prepared by the dehydration of ethyl alcohol by Pyro-phosphoric acid at 220–240°C. An apparatus was set up in which to carry out this preparation in a continuous manner. The alcohol was led into a flask containing 100 cc of Pyro-phosphoric acid (prepared *in situ* by dehydration of ortho-phosphoric acid) at the required temperature. The ethylene was passed successively at atmospheric pressure through a dry ice and alcohol trap, a wash bottle containing concentrated sulfuric acid, another containing 50 percent caustic soda, a further dry ice and alcohol trap, and a liquid air trap in which it was finally condensed.

When sufficient gas had been collected in the last trap, production was ceased and the permanent gases were pumped off. The ethylene was then fractionally distilled in batches in a low temperature fractionating column similar to that described by Lu, Newitt, and Ruhemann.[17] The middle fractions of ethylene were condensed in the gas transfer vessel immersed in liquid air. The vessel was then warmed and the ethylene passed into the mercury gas-compressor and pumped into the gas storage cylinder. One hundred liters of ethylene were prepared. Before preparation and storage of the gas, the glass apparatus was pumped out at a pressure of less than 1/10th micron and flamed and the gas compressor and vessels were pumped out for several days. A sample of the ethylene was analyzed and 99.7 percent by volume was adsorbed by bromine water. The residual gas was shown to be non-condensable at liquid air temperature.

Calibration of Gas Condenser

The vacuum capacity of the gas condenser was determined in the usual way by calibration with benzene.[18] Carefully fractionated benzene, dried for several weeks over sodium, was refluxed and stored over sodium in a glass vessel. It was degassed and distilled in vacuum into the previously evacuated gas condenser. Mercury *U*-tube valves were used in the system to prevent contamination of the benzene by tap-grease.

The vacuum capacity at 25°C was found to be 148.96 ± 0.05 $\mu\mu$f (taking $\epsilon_{25} = 2.2725$ for benzene),[19] compared with the value 149.4 $\mu\mu$f calculated from the condenser dimensions. The change in capacity of the evacuated condenser between 25°C and 50°C was found to be $+0.04$ $\mu\mu$f (calculated value, $+0.07$ $\mu\mu$f). Since this variation is smaller than the probable error in the calibration, the same value of the vacuum capacity was used at both temperatures.

Capacity Measurements

The condenser was filled from the storage vessel (via the gas compressor) with ethylene at the desired pressure and temperature (25°C or 50°C). Readings of the standard condenser and pressure balance were taken when the values appeared constant. These were checked after an interval of five minutes to confirm that the system was in equilibrium. Measurements were made over a range of pressures, the points being chosen so that the capacity of the gas condenser changed in approximately equal steps (≈ 5 $\mu\mu$f). Before and after a

[14] H. Tongue, *The Design and Construction of High Pressure Plant* (Chapman and Hall, Ltd., London, 1934).
[15] D. M. Newitt, *High Pressure Plant and Fluids at High Pressures* (Oxford University, New York, 1940).
[16] P. Cohen Henriquez, Physica **2**, 429 (1935).
[17] Lu, Newitt, and Ruhemann, Proc. Roy. Soc. (London) **A178**, 506 (1941).
[18] R. J. W. Le Fèvre, *Dipole Moments* (Methuen and Company, Ltd., London, 1938).
[19] L. Hartshorn and D. A. Oliver, Proc. Roy. Soc. (London) **A123**, 664 (1929).

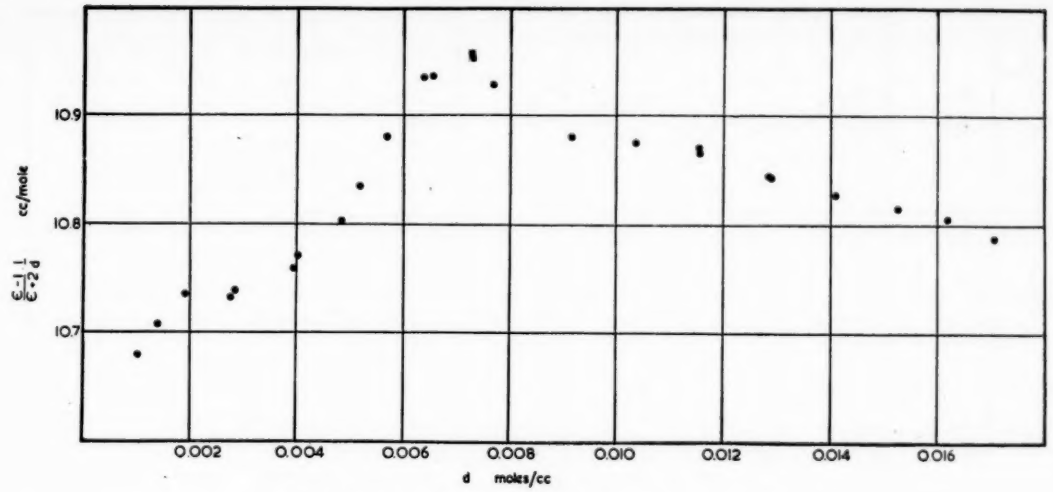

FIG. 1. Clausius-Mosotti function for ethylene at 25°C.

series of observations the gas condenser was evacuated and its capacity in this state checked. Throughout the measurements this value did not vary by more than ± 0.03 $\mu\mu$f.

The change in the condenser dimensions with pressure was shown by calculation to cause negligible error in the capacity measurements even at the highest pressures.

RESULTS

In order to determine densities from measured pressures the $P-V-T$ data of Michels and Geldermans[20] for ethylene were used. To convert the values of Amagat density so obtained to densities in moles/liter the normal volume is required. This was calculated from the relationship,

$$V_n = 22.414/(1+\lambda) \text{ liters}, \quad (1)$$

using the value of λ found by Cawood and Patterson.[21] The figure obtained was 22.251 liters.

The values of the Clausius-Mosotti function are shown in Tables I and II and in Figs. 1 and 2 for the temperatures 25°C and 50°C. For convenience in extrapolation an attempt was made to fit the low density values by a least squares analysis to an expression of the form,

$$(\epsilon-1)/(\epsilon+2)d = A+Bd+Cd^2, \quad (2)$$

d being the density and A, B, and C constants for a given temperature. A reasonable fit was impossible for the 25°C values but was achieved at 50°C with the constants:

$$A = 10.69 \pm 0.01 \text{ cm}^3 \text{ mole}^{-1}$$
$$B = 25 \pm 7 \text{ cm}^6 \text{ mole}^{-2}$$
$$C = 540 \pm 820 \text{ cm}^9 \text{ mole}^{-3}.$$

The curve corresponding to these values is shown in Fig. 2.

It will be noticed that the experimental points do not strictly lie on a smooth curve, but rather on a periodic curve superimposed on a smooth curve. For example, in our results there is a positive "peak" at density 0.002 mole/cc and a negative "peak" at density 0.004 moles/cc on each curve. This phenomenon is noticeable in the results of other workers, e.g., Michels and Kleerekoper[3] for CO_2 and Keyes *et al*[2] for CH_4, N_2, CO_2, and NH_3.

The evident agreement between the zero-density values of the Clausius-Mosotti function at the two temperatures (see Figs. 1 and 2) is in accord with the known absence of dipole moment in ethylene. The value (10.69) deduced from these measurements agrees well

TABLE I. Clausius-Mosotti function for ethylene at 25.00°C.

Pressure (int. atmos)	Density (moles/liter)	Dielectric constant	Clausius-Mosotti function (cc/mole)
21.696	1.0262	1.0332	10.680
28.221	1.4121	1.0461	10.708
35.593	1.9187	1.0631	10.737
45.530	2.7894	1.0926	10.733
46.209	2.8621	1.0951	10.740
54.615	3.9657	1.1337	10.760
55.083	4.0438	1.1366	10.772
59.263	4.8685	1.1666	10.804
60.606	5.1959	1.1790	10.836
62.426	5.7033	1.1985	10.881
64.491	6.3823	1.2251	10.937
64.924	6.5386	1.2311	10.938
66.888	7.2822	1.2602	10.960
66.908	7.2899	1.2603	10.954
67.930	7.6769	1.2748	10.930
72.839	9.146	1.3316	10.881
80.368	10.359	1.3809	10.876
94.287	11.524	1.4297	10.872
94.564	11.541	1.4303	10.868
125.62	12.851	1.4859	10.846
125.89	12.860	1.4862	10.845
181.59	14.092	1.5402	10.829
272.12	15.247	1.5925	10.816
385.54	16.193	1.6364	10.807
534.27	17.082	1.6778	10.789

[20] A. Michels and M. Geldermans, Physica **9**, 967 (1942).
[21] W. Cawood and H. S. Patterson, J. Chem. Soc. 619 (1933).

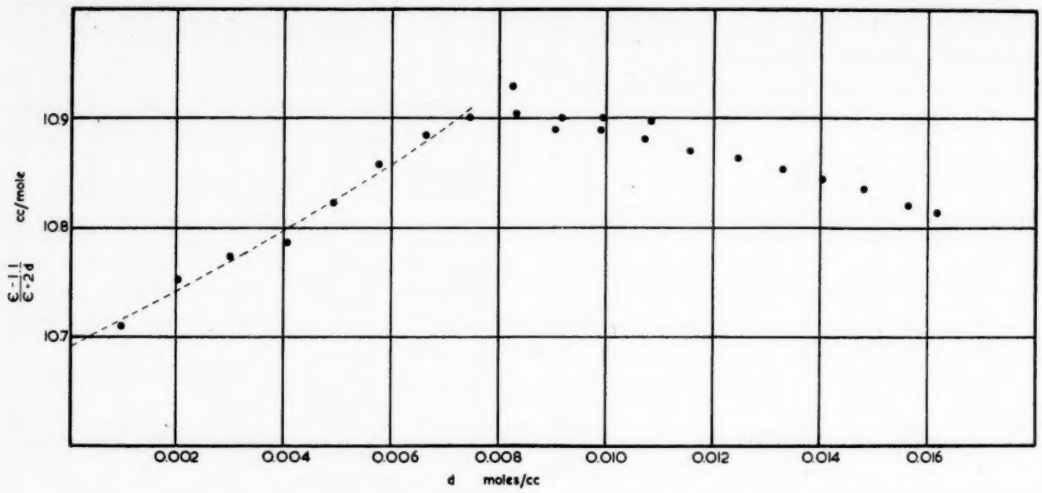

FIG. 2. Clausius-Mosotti function for ethylene at 50°C.

with the existing data[22] for 25°C, *viz.*:

Boltzmann	(1874)	9.74 cc/mole
Klemencic	(1885)	10.81 cc/mole
Smyth and Zahn	(1925)	10.72 cc/mole
Watson, Rao, and Ramaswamy	(1934)	10.74 cc/mole

DISCUSSION

The C-M relationship may be written in the form,

$$(\epsilon-1)/(\epsilon+2)d=4\pi\alpha N/3, \tag{3}$$

where ϵ is the dielectric constant of a substance, d is its density in molar units, α is its molecular polarizibility and N is Avogadro's number. If α is assumed to be constant the C-M function, $(\epsilon-1)/(\epsilon+2)d$, should also be constant. It has been found experimentally, however, that the function is to some extent dependent on density. Explanations of this effect have been based upon two considerations: (a) that α may vary with density,[6] (b) that the Lorentz molecular model is not applicable at high densities and the equality (3) does not necessarily hold.[4,5,7,8] No quantitative information has yet been provided by the first approach and we shall consider our results in the light of the theory which Kirkwood developed to replace the Lorentz derivation of Eq. 3.

TABLE II. Clausius-Mosotti function for ethylene at 50.00°C.

Pressure (int. atmos)	Density (moles/liter)	Dielectric constant	Clausius-Mosotti function (cc/mole)
23.527	0.9980	1.0324	10.711
42.234	2.0181	1.0665	10.753
56.186	3.0007	1.1002	10.774
67.851	4.0529	1.1372	10.787
75.783	4.9229	1.1688	10.823
82.733	5.7899	1.2013	10.859
89.241	6.6510	1.2342	10.886
95.683	7.4839	1.2665	10.902
102.42	8.2699	1.2981	10.931
102.87	8.3177	1.2993	10.906
110.32	9.045	1.3278	10.891
112.05	9.194	1.3342	10.902
121.50	9.900	1.3626	10.891
121.97	9.931	1.3643	10.902
135.96	10.721	1.3962	10.882
138.62	10.846	1.4021	10.899
157.39	11.593	1.4327	10.872
188.48	12.480	1.4706	10.865
229.19	13.304	1.5064	10.855
277.71	14.029	1.5384	10.846
347.23	14.808	1.5735	10.837
448.26	15.653	1.6118	10.821
529.43	16.186	1.6366	10.815

Kirkwood[4] determined statistically the effect of translational fluctuations on the average local electric field in a molecule and obtained an expression of the form:

$$(\epsilon-1)/(\epsilon+2)d=P_0(1+\gamma P_0 d+\delta P_0^2 d^2+\cdots) \tag{4}$$

where d is the density of the gas and P_0 is its molar polarization at zero density. He showed that the coefficient γ is given by

$$\gamma=(P_0/b)[1+(A/3bRT)] \tag{5}$$

in the special case of a gas consisting of hard spherical molecules with mutual attractive potentials, $V(r)$, which vary inversely as the sixth power of the intermolecular distance, r. A and b are the constants of the van der Waals equation of state.

There is some uncertainty as to the values that should be used for A and b in Eq. (4) and the adequacy of the van der Waals type of intermolecular field is, in any case, rather doubtful.[2] For these reasons we have calculated γ from equations based upon the more accurate representation of intermolecular forces which is given by the Lennard-Jones[23] expression:

$$V(\rho)=4E^*(\rho^{-12}-\rho^{-6}) \tag{6}$$
$$\rho=r/r_0.$$

[22] Summarized by Watson, Rao, and Ramaswamy, Proc. Roy. Soc. (London) **A143**, 558 (1934).

[23] J. E. Lennard-Jones, Proc. Roy. Soc. (London) **A106**, 463 (1924).

In Eq. (6) $-E^*$ is the minimum potential energy between two molecules and r_0 is their separation when $V(\rho)=0$. Putting (6) into the limiting expression for low densities:

$$\gamma=\frac{3P_0}{b_0}\int_0^\infty \rho^{-4}e^{-\beta V(\rho)}d\rho \qquad (7)$$

(where $\beta=1/kT$, $b_0=2\pi Nr_0^3/3$) and using the parameters $b_0=115.5$ cc/mole, $E^*/k=199.2$°K calculated by Bird, Spotz, and Hirschfelder[24] from the second virial coefficient data for C_2H_4, we find: $\gamma=+0.143$ at 50°C. This figure is somewhat lower than the value $\gamma=+0.22\pm0.06$ given by the least squares quadratic fit of our low density experimental data. In this respect our results are qualitatively similar to those of Keyes and Oncley[2] for CO_2 and C_3H_8. For these gases γ_{obs} is about twice γ_{calc}.

It is hardly profitable to speculate on these differences since the C-M/d curves are apparently of quite complex form even at the lowest densities,* and the extrapolated values of γ may be subject to very large errors. There is an obvious need for more accurate C-M measurements in the density range 0–0.002 moles/cc. These were not possible with our apparatus.

A point of interest is that the densities at which the slopes of the C-M/d plots abruptly change sign correspond quite closely with the critical densities of the gases. This is shown in Table III.

It may also be significant that above this density the C-M function decreases with increasing density, an effect which is generally found in liquid systems.

TABLE III.

Temp.	CO_2 50°C	CO_2 100°C	C_2H_4 25°C	C_2H_4 50°C	
d (for max. C-M)	0.0123[a]	0.0135[a]	0.0070	0.0083	mole/cc
d (critical)	0.0104[b]		0.0079[b]		mole/cc

[a] The data for CO_2 are taken from A. Michels and L. Kleerekoper, Physica 6, 586 (1939).
[b] Values from International Critical Tables 3, 248 (1928).

ACKNOWLEDGMENTS

The authors wish to express their thanks to Mr. D. R. Zeidler for his interest and for help in obtaining equipment, and to Mr. S. J. Lake for valuable assistance in the construction of apparatus.

[24] Bird, Spotz, and Hirschfelder, J. Chem. Phys. 18, 1395 (1950).
* The steps in these curves which are found in nearly all the recorded data suggest that there may be relatively sharp changes in the molecular distribution functions with density.

THE JOURNAL OF CHEMICAL PHYSICS VOLUME 19, NUMBER 12 DECEMBER, 1951

Semilocalized Orbitals. I. The Hydrogen Molecule

CHARLES R. MUELLER*
Department of Chemistry, Purdue University, Lafayette, Indiana

AND

HENRY EYRING
Department of Chemistry, University of Utah, Salt Lake City, Utah

(Received July 3, 1951)

Semilocalized orbitals are defined and applied to the hydrogen molecule. The basic criteria for the analytic form of this kind of orbital is that it shall assume either molecular or atomic orbital form for certain special values of the variational parameters. A binding energy of 4.20 ev is found in comparison with 3.60 and 3.76 ev obtained from the best molecular and atomic orbital calculations. The physical interpretation of the results is briefly discussed.

MOST of the quantum-mechanical calculations of molecular properties are either based on the molecular orbital or atomic orbital methods. We will introduce a third method utilizing semilocalized orbitals.

The basic criteria for the analytic form of the semilocalized orbital is that it will assume either L.C.A.O. molecular or atomic orbital form for special values of the variational parameters. In general the semilocalized orbital will have neither form. We will give an analytic definition in the next section.

We shall then employ a special form of semilocalized orbital to calculate the binding energy of the hydrogen molecule, and discuss very briefly the physical significance of the results.

* Formerly University of Utah Research Fellow.

I. SEMILOCALIZED ORBITALS

In order for semilocalized orbitals to satisfy the basic criteria for analytic form we will adopt the following definition:

(1) In the method of semilocalized orbitals the molecular eigenfunction will consist of the antisymmetrized product of individual one-electron orbitals.

$$\Psi=\sum_{P=1}^{n!}\lambda_P P\psi_1(1)\psi_2(2)\cdots\psi_n(n). \qquad (1)$$

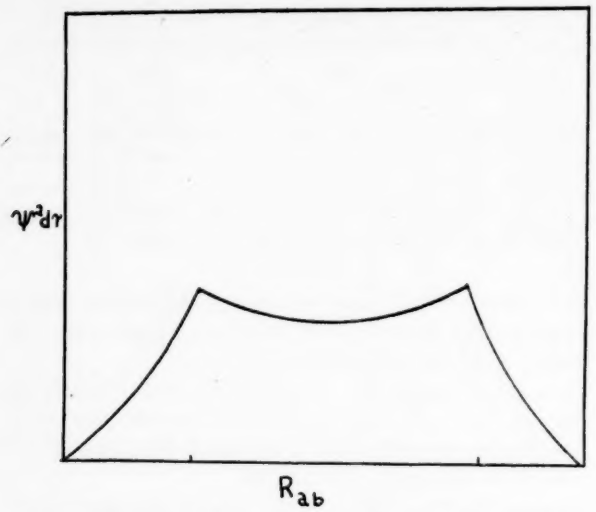

FIG. 1. Shape of the charge distribution for the one-electron eigenfunctions in a molecular orbital treatment of the hydrogen molecule.

P is one of the $n!$ permutations of n things and operates on the eigenfunction. λ_P assumes the value -1 or $+1$ according to the parity of the permutation P.

(2) The individual one-electron eigenfunctions shall be composed of linear combinations of atomic orbitals or of linear combinations of "distorted" atomic orbitals. The "distortion" of the atomic orbitals can be accomplished by the introduction of a scale factor,[1] displacement of the center of electronic charge from the individual nuclei,[2] or in any manner in which the "distorted" atomic orbitals assume the simpler atomic orbital form for special values of the variational parameters.

(3) The individual one-electron eigenfunctions shall consist of a linear combination of at least two atomic or "distorted" atomic orbitals and shall not contain more than one such orbital for each atom of the molecule

$$\psi_i = \varphi_1 + \lambda_1\varphi_2 + \cdots \lambda_j\varphi_j. \tag{2}$$

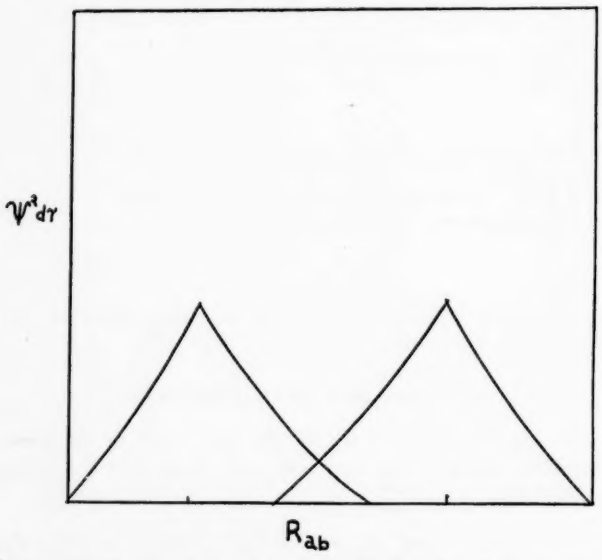

FIG. 2. Shape of the charge distribution for the two one-electron eigenfunctions in an atomic orbital treatment of the hydrogen molecule.

[1] J. Hirschfelder and J. Kincaid, Phys. Rev. **52**, 658 (1937).
[2] E. Gurnee and J. Magee, J. Chem. Phys. **18**, 142 (1950).

We shall illustrate the preceding definition using the hydrogen molecule as an example. The antisymmetrized product of the individual one electron eigenfunctions is the linear combination of two Slater determinants

$$\Psi = (1/N)\left|\begin{vmatrix}\psi_1(1)\alpha(1)\psi_1(2)\alpha(2)\\ \psi_2(1)\beta(1)\psi_2(2)\beta(2)\end{vmatrix}\right| + \begin{vmatrix}\psi_1(1)\beta(1)\psi_1(2)\beta(2)\\ \psi_2(1)\alpha(1)\psi_2(2)\alpha(2)\end{vmatrix}. \tag{3}$$

Expanding the determinants we get

$$\Psi = \{\psi_1(1)\psi_2(2)+\psi_1(2)\psi_2(1)\} \times\{\alpha(1)\beta(2)-\alpha(2)\beta(1)\}, \tag{4}$$

$$\psi_1 = \varphi_a + \lambda\varphi_b, \tag{5}$$

$$\psi_2 = \lambda\varphi_a + \varphi_b, \tag{6}$$

where φ_a and φ_b are the atomic orbitals or "distorted" atomic orbitals assigned to nuclei A and B.

When λ is unity, the orbitals assume molecular orbital form. When λ is zero, the same orbitals assume atomic orbital form, if φ_a and φ_b are atomic orbitals.

TABLE I.

Method	Binding energy In ev	Binding energy In percent	Total energy In ev	Total energy In percent
Best atomic orbital[a]	3.76	79.66	30.965	96.91
Best molecular orbital[b]	3.603	76.27	30.808	96.79
Semilocalized orbital	4.20	88.98	31.405	98.38

[a] S. Wang, Phys. Rev. **31**, 579 (1928).
[b] C. Coulson, Proc. Cambridge Phil. Soc. **34**, 204 (1938).

The orbitals of Eqs. (5) and (6), when φ_a and φ_b are atomic orbitals distorted by the introduction of a scale factor, are those used by Coulson and Fisher.[3]

Expansion of the eigenfunction of Coulson and Fisher shows that it is a rewritten form of the "Heitler-London plus ionic terms" eigenfunction in Weinbaum's[4] treatment of the hydrogen molecule.

There is however a possible difference in physical interpretation and this will be discussed in the last section of this paper. In any case, it should be remarked that this reformulation is very important, since it enables one to use directly either the formalism of the Slater method or the Dirac vector method in the treatment of complex molecules. We shall also retain the language of these methods. We refer to the integral, $\int\psi_i(k)\psi_j(l)H\times\psi_i(l)\psi_j(k)d\tau_1 d\tau_2$ as an exchange integral and $\int\psi_i(k)\psi_j(l)H\times\psi_i(k)\psi_j(l)d\tau_1 d\tau_2$ as a coulombic integral.

To digress for a moment from the hydrogen molecule, for heteropolar molecules the valence electrons are

[3] C. Coulson and I. Fisher, Phil. Mag. **40**, 393 (1949).
[4] S. Weinbaum, J. Chem. Phys. **1**, 593 (1933).

assigned to the orbitals,

$$\psi_1 = \varphi_a + \lambda_1 \varphi_b \tag{7}$$

and

$$\psi_2 = \lambda_2 \varphi_a + \varphi_b. \tag{8}$$

Substitution of (7) and (8) into the molecular eigenfunction and subsequent expansion will not give a "Heitler-London plus ionic terms" eigenfunction, but an eigenfunction with an extra parameter. Greater differences will arise with increasing molecular complexity, but these will be discussed in the course of actual computation.

II. CALCULATION FOR THE HYDROGEN MOLECULE

For the calculations which follow we have utilized the transformation from spherical to elliptic coordinates. The $1-s$ hydrogen atomic orbitals transform in the following manner

$$\varphi_a' = (Z^{\frac{3}{2}}/\pi^{\frac{1}{2}})e^{-Zr_a} = (Z^{\frac{3}{2}}/\pi^{\frac{1}{2}})e^{-(ZR/2)(\mu+\gamma)}$$

$$\varphi_b' = (Z^{\frac{3}{2}}/\pi^{\frac{1}{2}})e^{-Zr_b} = (Z^{\frac{3}{2}}/\pi^{\frac{1}{2}})e^{-(ZR/2)(\mu-\gamma)}$$

where $\mu = (r_a + r_b)/R$ and $\gamma = (r_a - r_b)/R$.

Apart from sign, the coefficients of μ and γ in the exponents are equal.

Destroying this equality we have

$$\varphi_a = (1/N)e^{-(\alpha\mu+\beta\gamma)} \tag{9}$$

$$\varphi_b = (1/N)e^{-(\alpha\mu-\beta\gamma)}, \tag{10}$$

thus introducing the parameters α and β instead of the single parameter Z. Increasing α increases the electronic charge distribution along the line joining the hydrogen nuclei.

Increasing β tends to concentrate the charge around the two nuclei. Equations (9), (10), (3), (5), and (6) then define the molecular eigenfunction.

The values of α, β, and λ were determined by the use of the integrated Fock-Hartree equation for the hydrogen molecule with nonorthogonality correction using successive variations to achieve a minimization of the energy. The value of α was 0.835, β was 0.775, and λ was 0.137.

Using these values and the complete hamiltonians the binding energy of the hydrogen molecule was found to be 4.20 ev. Since the James and Coolidge[5] eigenfunction without r_{12} terms gives a calculated binding energy of 4.27 ev, we may assume that we are within 0.07 ev of the greatest accuracy to be obtained from any one-electron eigenfunctional approximation.

The best atomic orbital and molecular orbital calculations are compared with the semilocalized orbital method in Table I.

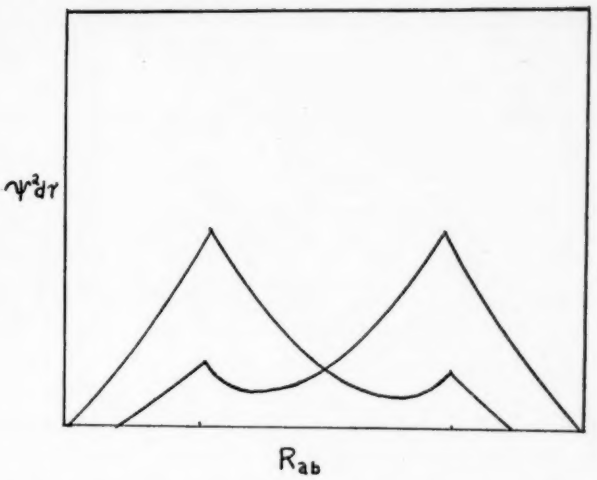

FIG. 3. Shape of the charge distribution for the two one-electron eigenfunctions in a semi-localized orbital treatment of the hydrogen molecule.

III. PHYSICAL INTERPRETATION

We shall conclude with a few remarks concerning the physical interpretation of the results. Omitting exchange terms from the variational calculation, and using the eigenfunction of Coulson and Fisher, the semilocalized orbitals assume atomic orbital form. We can conclude that the deviation from atomic orbital form is the result of exchange forces.

The approximate shapes of the charge distributions of the one-electron eigenfunctions for atomic, molecular, and semilocalized orbital methods are given in Figs. 1–3. Both atomic and semilocalized orbitals can be interpreted as postulating two resonance states. In the first resonance state, the state of electron one is represented by the one-electron eigenfunction on the left and the state of electron two is represented by the one-electron eigenfunction on the right. In the second resonance state, the positions of the electrons are reversed.

On the other the "Heitler-London plus ionic terms" eigenfunction has been interpreted as implying resonance between covalent and ionic states. Using the hydrogen $1-s$ atomic orbitals ($Z=1$), the calculated energy difference between the covalent state $(\varphi_a(1)\varphi_b(2))$ and the ionic state. $(\varphi_a(1)\varphi_a(2))$ is 67.28 kcal.

Using the Maxwell-Boltzmann distribution law, the ratio of the number of ionic systems to the number of covalent systems is $e^{-112.13}$ or approximately 10^{-49}.

While physical interpretations involving resonance states of equal energy may be naive, those involving resonance between states of widely different energies are likely to be ridiculous.

[5] H. James and A. Coolidge, J. Chem. Phys. **1**, 825 (1933).

Semilocalized Orbitals. II. A Comparison of Atomic, Molecular, and Semilocalized Orbital Method for Diatomic Hydrogen Fluoride

CHARLES R. MUELLER
Department of Chemistry, Purdue University, Lafayette, Indiana
(Received September 25, 1951)

In a previous paper the method of semilocalized orbitals was developed and applied to the hydrogen molecule. This method is applied to diatomic hydrogen fluoride simultaneously with atomic and molecular orbital calculation. In contrast to the results with the hydrogen molecule, the semilocalized orbitals are closer to molecular than atomic orbital form. The semilocalized orbitals give a much better binding energy than molecular orbitals and the improvement in dipole moment calculations is especially heartening. The results with the atomic orbital method are very discouraging.

IN a previous paper by Mueller and Eyring the method of semilocalized orbitals was developed and applied to the hydrogen molecule. We shall now proceed to apply this method, in conjunction with atomic and molecular orbital methods, to diatomic hydrogen fluoride, using the same integrals, the same hamiltonian, and the same atomic orbitals as constituent parts of the molecular eigenfunction.

I. EIGENFUNCTIONS

The atomic orbitals which are formed into molecular eigenfunctions are the Slater[1] $1s$, $2s$, $2p\pi$, and $2p\sigma$ atomic orbitals.

Letting

$$(\delta^5/\pi)^{\frac{1}{2}}e^{-\delta\gamma_a}\gamma_a=\kappa \tag{1}$$

$$\begin{aligned} a_1&=(Z^{\frac{3}{2}}/\pi^{\frac{1}{2}})e^{-Z\gamma_a} & a_4&=\kappa\sin\theta_a\cos\varphi_a\\ a_2&=(1/3)^{\frac{1}{2}}\kappa & a_5&=\kappa\cos\theta_a\\ a_3&=\kappa\sin\theta_a\sin\varphi_a & b&=(1/\pi)^{\frac{1}{2}}e^{-\gamma_b}, \end{aligned} \tag{2}$$

where $\delta=2.60$ and $Z=8.688$. The latter is obtained from a variational treatment of the fluorine atom. The eight nonvalence electrons of the fluorine atom are assigned to a_1, a_2, a_3, and a_4 in pairs. The valence electrons in the atomic orbital method are assigned to a_4 and b. In the molecular orbital method the valence electrons are assigned to (λa_4+b) in a pair, and in the semilocalized orbital method to $(a_4+\lambda_1 b)$ and $(\lambda_2 a_4+b)$. We shall refer to the eigenfunctions of the valence electrons as a_{v1} and a_{v2} to avoid repetition. The molecular eigenfunction is the linear combination of two Slater determinants (which are identical in the molecular orbital treatment). It should be noted that hybridization of the binding electrons is not discussed. While there are no *a priori* grounds for rejecting the occurrence of such a phenomenon, hybridization is usually associated with the promotion of an s-electron to a p-state and with multiple valence.

II. BINDING ENERGY CALCULATION

To calculate the binding energy, we have first calculated the self-consistent field energy of the valence electron in the fluorine atom. The reported binding energy is given by the formula

$$\epsilon=\epsilon_v+\epsilon_c+\epsilon_R-\epsilon_a-\epsilon_b. \tag{3}$$

ϵ_v is the self-consistent field energy of the valence electrons in the molecule. ϵ_c is the coulombic interaction of the nonvalence electrons and the hydrogen nucleus. ϵ_R is the energy of nuclear repulsion. ϵ_a and ϵ_b are, respectively, the self-consistent field energy of the fluorine and hydrogen valence electrons when the atoms are separated. The total energy of the system can be found by application of the Dirac[2] vector model.

With non-orthogonality correction, the total molecular energy is, neglecting multiple exchanges,

$$\begin{aligned} E=(C-\sum_{i>j}K(i,j)-\sum_{i=1}^{4}K(v_1,i)-\sum_{i=1}^{4}K(v_2,i)\\ +K(v_1,v_2))\div(c+k(v_1,v_2)-\sum_{i>j}k(i,j)\\ -\sum_{i=1}^{4}k(v_1,i)-\sum_{i=1}^{4}k(v_2,i)). \end{aligned} \tag{4}$$

C is the coulombic integral, $K(j,K)$ indicates the exchange integral $\int a_j(i)a_K(l)Ha_j(l)a_K(i)d\tau_1 d\tau_2$, and $k(j,K)$ indicates the corresponding integral without the hamiltonian. H is the complete hamiltonian including the effect of the K-shell electrons. The self-consistent field energy of the valence electrons is found by deleting the part of coulombic energy due to nonvalence electrons, except where this energy arises from interaction with valence electrons, and the term $\sum_{i>j}K(i,j)$.

The various parameters in the eigenfunction, as well as the binding energy, are found by minimization of the self-consistent field energy of the valence electrons.

The values of the necessary integrals are found in the tables of Kotani and Amemiya[3] or were evaluated by the author.

[1] J. Slater, Phys. Rev. **36**, 57 (1930).

[2] E. Corson, *Perturbation Methods in the Quantum Mechanics of n-Electron Systems* (Hafner Publishing Company, Inc., New York, 1951), Chapter 10.

[3] M. Kotani and A. Amemiya, Proc. Phys.-Math. Soc. Japan **22**, Ex. No. (1940).

III. DISCUSSION OF THE RESULTS

The results of the computation are summarized in Table I.

The most significant result is the great improvement of the calculated dipole moment.

Distortion of nonvalence electrons was not considered in the calculation. The small value of λ_1 seems to justify this approximation. The distortion of the fluorine valence electron is small, even with assistance of large exchange forces. It is these exchange forces which caused the valence electrons to lose their atomic orbital character in the semilocalized orbital calculation for the hydrogen molecule. We reason, then, that the distortion of the nonvalence electrons is smaller still because this deformation is opposed by small exchange forces.

The results for the hydrogen molecule showed that the second approximational semilocalized orbitals were closer to atomic than molecular orbitals. In the case of hydrogen fluoride, when the binding has a strong ionic character, the reverse is true. It appears, then, that the maximum utility of the semilocalized orbital method may be in the intermediate region of covalent binding in heteropolar molecules, particularly in organic compounds.

TABLE I.

Method	Parameter	Binding energy in A.U.*	Molecular dipole moment
Atomic orbital		−0.9688	$0.86H^-F^+$
Molecular orbital	$\lambda=1.75$	0.1352	$0.67H^+F^-$
Semilocalized orbital	$\lambda_1=0.14$ $\lambda_2=1.04$	0.1648	$1.56H^+F^-$
Observed		0.2440[a]	$1.91H^+F^-$[b]

* 1 A.U. = 27.205 electron-volts.
[a] Corrected for zero point energy. All calculations at internuclear distance of 0.92A.
[b] N. Hannay and C. Smyth, J. Am. Chem. Soc. **68**, 171 (1946).

THE JOURNAL OF CHEMICAL PHYSICS VOLUME 19, NUMBER 12 DECEMBER, 1951

A Comparative Study of Unpolarizable and Polarizable Metal-Solution Systems

D. MACGILLAVRY*
Department of Chemistry, Clark University, Worcester, Massachusetts
(Received April 16, 1951)

The properties of the metal-solution potentials of nickel in nickel free hydroxide and phosphate solutions are compared with the properties of unpolarizable electrodes and with the properties of polarizable metal-solution systems. The electrochemical equilibria of unpolarizable systems are analyzed in terms of transfer mechanisms between the phases present. In the absence of any electrochemical equilibria, the metal-solution potentials are interpreted as *adsorption potentials*. Chemisorption in the inner Helmholtz layer is discussed in connection with "reversibility" and polarizability of the system.

IN a recent publication[1] potential measurements for nickel in hydroxide and in phosphate buffer solutions under carefully controlled conditions were reported. The nickel samples were thoroughly freed from oxygen and oxides. Oxygen was eliminated from the solutions before making contact with the nickel. In short, oxygen was rigorously excluded at all times. Purified nitrogen or argon was used as a gas atmosphere. The potentials were measured with a potentiometer and an electrometer with capacitive input coupling as null point indicator.

In this way it was possible to obtain stationary and reproducible potentials† for nickel in solutions which remained free from nickel ions, as far as could be ascertained, even in acid phosphate solutions. The steady potentials observed in phosphate buffers and in potassium hydroxide solutions in the absence of air are represented in Fig. 1. The scale of potentials is referred to the standard hydrogen electrode. The properties of these nickel-solution potentials showed several characteristics of interest.

It was noted that in both sets of solutions the potentials of nickel showed a strong dependence on the activity of the hydroxyl ions. The plot of the potentials *versus* the *p*H for the hydroxide solutions showed an

* Present address: Department of Chemical Engineering, Columbia University, New York, New York.

[1] MacGillavry, Singer, Jr., and Rosenbaum, J. Chem. Phys. **19**, 1195 (1951).

† The phase boundary potentials of the nickel-foreign ion cells were measured with respect to a reference electrode, as with ordinary electrochemical cells. The electric states of the two metal electrodes were compared by compensation with a potentiometer. Thus, the terminology "measuring the potential difference" is retained. Since the potentiometer reading at balance is taken to give the numerical value of an electric property of the complete cell, regardless of the contact potential differences along each connecting lead, it is evident that this property is not the difference of the Volta potentials of the two electrodes. The potential in question is the difference of the total chemical potentials of the electrons of the two electrode metals. The total chemical potential of the electrons is constant along each lead to the potentiometer; when at balance these leads carry no current. The difference between these two total chemical potentials is measured by the electrostatic potential drop along the potentiometer wire, as read on the instrument, since the material of the wire is uniform. Reference may be made to the well-known analysis by E. A. Guggenheim, J. Phys. Chem. **33**, 842 (1929), especially p. 849.

apparently linear dependence over the range measured. The analogous plot for the phosphate buffer solutions over a much wider *p*H range showed a more complicated dependence. On the acid side the dependence appears linear with a slope of 44 mv/*p*H. This is followed by a less well-defined portion for the slightly alkaline solutions. The dependence on the high alkaline side is again apparently linear with a slope of about 43 mv/*p*H. It was noted furthermore, that besides the hydroxyl ions other types of ions seemed to influence the potentials.

Attempts to interpret the observed potentials in terms of a Ni^{++}/Ni electrode, or of a hydrogen electrode, or of other types of unpolarizable electrodes obeying the Nernst theory, led to serious contradictions or to great difficulties. This was demonstrated by comparing the measured potentials with potentials calculated for the unpolarizable electrodes which *a priori* might have been established in our half-cells.

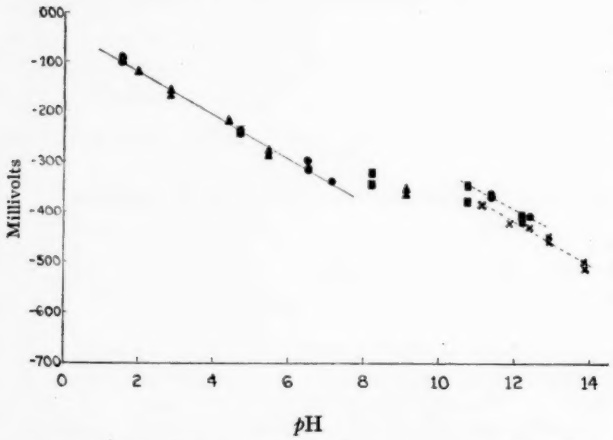

FIG. 1. Stationary potentials of nickel in potassium hydroxide and in 0.100 M phosphate solutions as a function of *p*H.
● Run XI
▲ Run XII } with 0.100 M phosphate solution.
■ Run XIV
× Run 4 and 5 with KOH solutions.

Instead of comparing numerical values, it may be of interest to compare the observed trends of the potentials with the properties of Nernst half-cells. It will be seen that the two sets of properties are at variance with respect to each other. To facilitate the comparison, a brief account follows of the distinctive properties of Nernst or unpolarizable half-cells.

UNPOLARIZABLE METAL-SOLUTION SYSTEMS

The theory of Nernst[2] ascribes to a metal or a metal amalgam a characteristic solution pressure. Such an active metal would develop a stationary potential when in contact with a common ion solution. Stationary equilibrium would be attained when the solution pressure, or the tendency of the metal ions in the electrode to go into solution, would balance the osmotic pressure, or the tendency of the common ions to escape from the solution and to redeposit on the electrode. The postulation of such a dynamic equilibrium in terms of the common metal ions provided a satisfactory interpretation of a number of metal-solution systems.

A comprehensive account of the older literature is presented by Kremann and Mueller.[3] Amalgam electrodes have been studied by numerous investigators and often conform well to the theory. Erdey-Gruz[4] and coworkers in more recent years made a painstaking investigation of a number of amalgam electrodes. The theory of amalgam potentials forms the basis of polarographic theory.[5]

Applying thermodynamic theory to this type of heterogeneous equilibrium, Nernst derived his well-known formula:

$$E = E^0 - \frac{RT}{nF} \ln \frac{a(Me^{+n} \text{ electrode})}{a(Me^{+n} \text{ solution})}.$$

The points pertinent here are the following. The formula shows that the observed potential difference can be expressed in terms of the "common" or so-called "potential determining" ions. Other components, if present, do not appear explicitly in the equation and influence the potential only in so far as they influence the activity of the common metal ions. An important quantity in a Nernst formula is the coefficient RT/nF, which is restricted to a few definite values, since by Faraday's law n must be integer.

A special property of a half-cell, where the common metal ions can transfer freely between the metal and the solution, is that such a cell is unpolarizable electrically. When it is attempted to accumulate electric charges on the metal by means of an externally applied potential difference, then at once transfers of common ions in the one direction will be accelerated while they will be slowed down in the other direction. Instead of electric polarization a net continuous current will result. The electric current is accompanied, of course, by a degree of concentration polarization increasing with current density.

If a particular metal is inert and possesses no measurable solution pressure, it often happens that a hydrogen electrode or an oxygen electrode may be established. Other gas electrodes have been investigated. The components taking part in the heterogeneous equilibria of a gas electrode are the electrons of the metal, the active molecules in the gas phase, and the corresponding ions in solution. All species of charged and neutral components transferring between the phases present will appear explicitly in the Nernst

[2] W. Nernst, Z. physik. Chem. 4, 129 (1889); S. Glasstone, *The Electrochemistry of Solutions* (Methuen and Company, Ltd., London, 1937), p. 293 ff.

[3] *Handbuch der allgemeinen Chemie*, edited by W. Ostwald and K. Drucker, Vol. 8, Part I, by R. Kremann and R. Mueller, on "Elektromotorische Kraefte" (Akademische Verlagsgesellschaft m.b.H., Leipzig, 1920).

[4] T. Erdey-Gruz, and A. Vazsanyi-Zilahy, Z. physik. Chem. **177A**, 292 (1936); T. Erdey-Gruz and L. Erdey, *ibid.* **183A**, 401 (1939).

[5] I. M. Kolthoff and J. J. Lingane, *Polarography* (Interscience Publishers, New York, 1946).

equation for a gas electrode as the potential determining components.

Metal-solution systems obeying the Nernst theory are usually referred to as "reversible" half-cells. The term "reversible" in this connection has a restricted meaning as it refers specifically to the heterogeneous equilibrium or the electrochemical equilibrium between the phases present. It should be understood that in the absence of electrochemical equilibria, an inert metal-solution system may be in stable equilibrium[5] in all other respects. Each phase individually would be in equilibrium, and also all adsorption equilibria would still be established in the metal-solution double layer.

For analogous reasons as before, it is evident that all systems in electrochemical equilibrium will approximate to unpolarizable electrodes. An applied potential difference causes an electric current to flow in the corresponding direction by shifting the equilibrium. This characteristic property has considerable practical importance. When measuring the potential of a "reversible" half-cell by the Poggendorff compensation method, it is possible to use a galvanometer as null point indicator. If the cell potential is not correctly balanced, then the unbalance will cause a current to flow which can be indicated by a galvanometer. No deflection of the galvanometer means that correct compensation has been obtained.

LIMITATIONS OF THE NERNST THEORY

It is clear that the perfectly unpolarizable half-cell is a theoretical conception. Although many metal-solution systems apparently are unpolarizable and reversible with respect to electric currents, it is not certain *a priori* that this is true for any arbitrary metal-solution cell. Actual systems may tend to show deviations and may appear poorly reversible electrochemically, when the natural rates of dissolution or of redeposition are relatively slow. The natural rate of dissolution will be less the more inert the metal in a given metal-solution combination happens to be. As pointed out by Haber,[7] the rate of redeposition will become insufficient if the concentration of common ions is excessively small. Haber's views would apply even more to electrolytic processes. When an alkaline solution is electrolyzed, by far the greater percentage of hydrogen generated at the cathode, especially at higher current densities, would be formed by the disruption of water molecules, rather than by the dissociation of water molecules giving hydrogen ions as an intermediate step. The latter mechanism could not account for a measurable rate of hydrogen evolution from alkaline solutions. Retardations of the rate of amalgam formation have been investigated at the dropping mercury electrode.[8]

Possible limitations of the Nernst theory in case of a cadmium electrode were subjected to an investigation by Mueller and Duerichen.[9] Their techniques were very exacting. It was concluded that the potentials vary according to the Nernst theory down to the lowest concentrations used. The results do not seem entirely definite, since it is not quite clear that the potentials for the lowest concentrations did reach stationary values. Thus, it is possible that actually the lower limit of agreement with the Nernst theory was reached and perhaps exceeded.

ELECTROSTATIC THEORY OF THE DOUBLE LAYER

Besides the considerations briefly summarized, the nature of metal-solution potentials may be interpreted from the point of view of electrostatic theory. Nernst himself indicated that his postulate of a dynamic equilibrium because of two opposing pressures across the interphase leads to the formation of an electric double layer. This is in accordance with the views expressed by Helmholtz.[10] Starting directly from general electrostatic principles, Helmholtz concluded that when two conductors make contact an electric double layer will be established. When this double layer has been built up, a steady potential field is generated by the spatial distribution of electricity in the interphase.

Gurney[11] described this field for the idealized fixed double layer or equivalent condenser and for the double layer made up of ions and molecules. When the individual charges are smoothed out into continuous charge densities, the equipotential surfaces run parallel with the double layer. When the actual ionic and molecular structure of the double layer is considered, then the equipotential surfaces show a degree of periodicity along the double layer. In the direction of the normal across the interphase, the electric potential varies from point to point attaining a steady value in the interior of each phase. Generally, there will be a net potential difference between the two phases. It is caused by the preferential adsorption of ions and the orientation of dipole molecules. In other words, all components present in the double layer contribute to the metal-solution potential.

It is important to stress here that according to electrostatic theory the potential field is determined by the spatial distribution of charges regardless of the mechanism by which the double layer is formed. In this sense the theoretical considerations of Helmholtz and Gurney are of a quite general nature. The Nernst theory is based on the existence of an electrochemical equilibrium between the phases present in the half-cell. In such a case, the Nernst type of equation for the half-cell potential can be derived. Only the potential determining components appear in this equation. In the absence of any electrochemical equilibrium, it is not possible to derive such a thermodynamic equation for the electrode

[6] D. C. Grahame, Chem. Revs. **41**, 441 (1947).
[7] F. Haber, Z. Elektrochem. **10**, 433, 773 (1904).
[8] M. Kalousek, Collection Czechoslav. Chem. Communs. **13**, 105 (1948).
[9] F. Mueller, and W. Duerichen, Z. physik. Chem. **182A**, 233 (1938).
[10] H. Helmholtz, Wied. Ann. Phys. **7**, 337 (1879).
[11] R. W. Gurney, *Ions in Solution* (University Press, Cambridge, 1936), p. 38.

potential. However, it now must be possible to represent the metal-solution potential as a function of all components present in the interphase. Hence, this other type of metal-solution potentials may be interpreted as *adsorption potentials*.

Here, an analogy may be drawn with the distinction between gas pressure and vapor pressure. The pressure of a pure gas by itself depends on two variables, the volume and the temperature. In case the gas phase is in equilibrium with a liquid phase, then the vapor pressure is explicitly dependent on only one variable, the temperature, but no more on the volume. From the kinetic point of view, the pressure is always caused by the molecular collisions against the wall.

The concept of "adsorption potentials" apparently was first mentioned by Baur.[12] He merely states the concept, but it is probable that he had in mind the electrostatic picture as explained.

The concept of adsorption potentials was developed further for the interpretation of other phase boundary potentials, the water-oil and the water-air potentials. Ehrensvard and Sillen[13] investigated the potentials at water-oil boundaries. They stated that a satisfactory interpretation as adsorption potentials would imply that no thermodynamic equilibrium exists between components of both phases and that only adsorption equilibria may exist on each side of the phase boundary. They mention especially the postulate that the interphase is impermeable to ions. Naturally, it has to be decided experimentally just when a water-oil system will conform to these postulates in its actual behavior. Adsorption potentials at water-air boundaries have been investigated by Schulman and Rideal[14] and others.[15] The increase of the surface potential due to a surface film is interpreted in terms of the apparent dipole moment.

Thus, one is led to inquire if under suitable conditions combinations of a metal and a solution can be found where no transfers occur across the interphase. It was realized that this appears to be possible in the case of mercury. Koenig[16] based the theory explaining the electrocapillarity of mercury on this postulate that no charged particles cross the interphase. The conditions under which transfers are inhibited were discussed by Craxford.[17] If then a mercury half-cell is polarized electrically, no continuous current can result theoretically but instead the double layer is distorted and consequently the surface tension is varied.

At this point, short comment on the hydrogen electrode may be added. The factors of the electrochemical equilibrium are the protons, which move back and forth between the solution and the gas phase forming molecules by combining with electrons, and the electrons which transfer between the gas phase and the metal. Although no charged particles transfer *directly* between the metal and the solution,[16] still an electric current can cross the interphase by virtue of the influencing of the electrochemical equilibrium.

In short, there are two alternative possibilities which are *mutually exclusive*. A metal-solution system tends to become unpolarizable as soon as at least one electrochemical equilibrium becomes operative, which implies that certain charged components exchange between the metal and the solution. Hydrogen electrodes are special in this respect as explained. In the absence of any electrochemical equilibrium, a metal-solution system becomes polarizable. A half-cell may approximate to either extreme depending upon its nature and on the conditions. Each extreme type must have certain characteristic properties. Those of unpolarizable Nernst systems have been investigated extensively. As to the properties of the other type, mercury has been investigated.[18] Other inert metals seem to have been investigated much less in this respect. It will be seen that the metal-solution potentials of nickel measured by us are an indication that under proper conditions nickel behaves like an inert metal.

When metal-solution half-cells are polarizable, they have a natural resistance against the passage of an electric current through the interphase. Excessive polarization might force a current through by forcing charged particles across the interphase. Then the passage of current is entirely because of forced mechanisms, but not caused by the influencing one way or the other of a naturally occurring reversible mechanism. For this reason, the compensation method with a galvanometer as null instrument would not be workable for measuring the potentials. To obtain a sensitive and reliable test for unbalance, an electrometer would have to be used. As will be explained in another article, the use of an electrometer with capacitive input coupling appears soundest on theoretical grounds.

COMPARISON OF PROPERTIES OF UNPOLARIZABLE AND POLARIZABLE SYSTEMS

In conclusion of the analysis presented, the main properties of the two idealized types of metal-solution systems will be summarized and contrasted.

Polarizable Systems

If no electrochemical equilibrium involving both the metal and the solution is operative, then the half-cell is polarizable by the application of an external potential difference; no continuous direct current can be made to pass through the half-cell; consequently, the metal-solution potential cannot be measured correctly with a galvanometer as null point indicator, but a suitable

[12] E. Baur, Z. Elektrochem. **19**, 590 (1913).
[13] G. C. H. Ehrensvard, and L. G. Sillen, Nature **141**, 789 (1938); Z. Elektrochem. **45**, 440 (1939).
[14] J. H. Schulman, and E. K. Rideal, Proc. Roy. Soc. (London) **A130**, 259 (1931).
[15] N. K. Adam, *The Physics and Chemistry of Surfaces* (Clarendon Press, Oxford, 1938), second edition, p. 33.
[16] O. Koenig, J. Phys. Chem. **38**, 111, 339 (1934).
[17] S. R. Craxford, Trans. Faraday Soc. **36**, 85 (1940).
[18] T. Erdey-Gruz, and P. Szarvas, Z. physik. Chem. **177A**, 277 (1936). S. E. S. ElWakkad, and T. M. Salem, J. Phys. and Coll. Chem. **54**, 1371 (1950).

electrometer may be used instead; its potential is determined by all the ions and all the oriented dipoles preferentially adsorbed in the interphase; and no equation for the potential involving special "potential determining" components is derivable.

Unpolarizable Systems

In case an electrochemical equilibrium involving the metal and the solution is operative, then the system approximates to an unpolarizable half-cell; application of an external potential difference causes a continuous direct current to flow through; the metal-solution potential may be measured with a galvanometer as null instrument but may be measured as well with an electrometer; a special equation for the electrode potential may be developed in terms of the "potential determining" components; the slope characteristic for this dependence is restricted to the values RT/nF with n integer; however, it is also true according to electrostatic theory, that all charged components in the double layer contribute to the metal-solution potential difference. This last point of view is not of much use until more will be known about the adsorption of individual components in the double layer.

It is stressed again that all metal-solution potentials may be measured with a suitable electrometric scheme. A galvanometer will be usable as well, the better a metal-solution combination approximates to a perfectly unpolarizable electrode.

FOREIGN ION NICKEL-SOLUTION POTENTIALS

The phenomena observed for nickel in foreign ion solutions may give information about the nature of the half-cells studied and the structure of the double layer. The potentials of nickel in hydroxide solutions showed a strong dependence on the *p*H. However, the potentials could not be interpreted as nickel hydroxide potentials, since the measured potentials would indicate a concentration of nickel ions greater than possible at the alkalinity of the solutions, while as a matter of fact, no nickel ions at all could be found in solution. The hydroxyl ions could not be considered to be potential determining by virtue of an oxygen electrode, since oxygen was excluded at all times. Then, the slope of the dependence is not in agreement with the slope for a reversible half-cell and other anions seem to have an influence as well. The potentials of nickel in other alkaline solutions gave evidence for this effect.

An interpretation as polarizable half-cells is entirely possible, since then there are no theoretical restrictions on the dependence of the potentials on the composition of the solutions. The behavior appears to indicate a strong adsorption of hydroxyl ions in the double layer. This is in agreement with observations made for mercury by Erdey-Gruz and Szarvas.[18] They concluded that in many electrolyte solutions the anions are preferentially adsorbed by mercury.

The graph of the nickel potentials in phosphate solutions looks very much similar on the highly alkaline side. Again there is a strong dependence on the *p*H, but the difference between the corresponding potentials in hydroxide and in phosphate solutions at the same *p*H seems to be greater than the experimental error in this region. On account of the slope an explanation in terms of polarizable half-cells is indicated. In the earlier publication it was suggested that again adsorption of the hydroxyl ions plays a dominant part in this region, while the other components in the double layer have some influence also. In terms of an unpolarizable half-cell this would be hard to explain, since the *p*H measures the activity of the hydroxyl ions. Again, a polarizable half-cell might very well show this behavior.

More information will be required for further interpretation of the observed potentials. It may be stated that none of the other properties is in apparent agreement with properties of unpolarizable electrodes. The nature of polarizable half-cells would impose no restrictions.

CHEMISORPTION IN THE DOUBLE LAYER AND POLARIZABILITY

It was suggested in the earlier article that the magnitude of the shifts of the nickel potentials in alkaline solutions might indicate that the anions are chemisorbed by the metal. Grahame[6] in his further development of the Koenig[16] double-layer theory estimated the charge densities in the inner and outer Helmholtz layers. He concluded that chemisorption of anions at the inner Helmholtz layer on mercury probably is an important factor. Since the chemisorbed ions apparently can leave the solution while on the other hand no new phase in bulk is formed, the question arises as to the reversibility and the polarizability of a system where chemisorption occurs.

To bring out the essential aspects, let it be assumed that a certain *p*H range has been found where hydroxyl ions actually are chemisorbed on nickel by the formation of covalent bonds. The electron of a hydroxyl ion when it is chemisorbed would pair with an electron from the metal. If the chemisorption is reversible, the hydroxyl ion could break away from the metal and return to the solution. Since the two bond electrons are equivalent, the electron originally on the ion has an equal chance to go into the metal. The electrons then do exchange between the metal interior and the interior of the solution exactly as the electrons of a halogen electrode. However, a further reaction beyond the chemisorbed state to a nickel-oxygen electrode or a nickel-oxide electrode is not probable, since the nickel cells were kept free from oxygen and oxides, and oxygen entering a nickel-foreign ion cell at once shifted the potential to very much more positive values. The experimental evidence is against further reaction. In case further reaction did occur, the system would be unpolarizable in principle, since the oxygen atoms would also exchange between two phases. This leaves the assumption that the hydroxyl ions transfer only between

the inner Helmholtz layer and the solution. This deficiency in transfer mechanism would make the system polarizable in principle, even if the degree of polarizability might remain small.

The reasons for this may be put as follows. An external potential difference tending to make the nickel more positive, would bring additional hydroxyl ions into the inner Helmholtz layer besides the hydroxyl ions present already. A finite variation of potential would cause a finite variation of the ratio of covered area to free area and this would cause the intensive properties to vary. The metal-solution potential determined by the double layer structure would vary until the double layer potential balances the applied potential. Liberation of more oxygen at an oxygen electrode would increase the volume of the gas phase, but would not cause variations of the intensive variables of the system.

The argument may be translated in thermodynamic terms. Let it be considered first that the OH^- ion is chemisorbed as a unit:

$$OH^- \text{ (solution)} \rightleftharpoons OH^- \text{ (helmholtz)},$$

hence, the total chemical potential $\bar{\mu}$ must be the same everywhere:

$$\bar{\mu}_s(OH^-) = \bar{\mu}_h(OH^-),$$

or

$$\mu_s(OH^-) - F\psi_s = \mu_h(OH^-) - F\psi_h,$$

and therefore

$$\psi_h - \psi_s = 1/F\{\mu_h(OH^-) - \mu_s(OH^-)\}.$$

It is seen that the potential of the inner Helmholtz layer occurs in this equation instead of the potential of the metal.

The equilibrium may be interpreted also as follows:

$$OH^- \text{ (solution)} \rightleftharpoons OH \text{ (helmholtz)} + e \text{ (metal)},$$

hence the equality

$$\bar{\mu}_s(OH^-) = \mu_h(OH) + \bar{\mu}_m(e)$$

or

$$\mu_s(OH^-) - F\psi_s = \mu_h(OH) + \mu_m(e) - F\psi_m$$

and therefore

$$\psi_m - \psi_s = 1/F\{\mu_h(OH) + \mu_m(e) - \mu_s(OH^-)\}.$$

Now it is possible to vary the metal-solution potential $\psi_m - \psi_s$, without varying the state of the metal and of the solution; since the hydroxyl groups can accumulate in the inner Helmholtz layer but cannot go beyond this, the term $\mu_h(OH)$ can vary with $\psi_m - \psi_s$. This amounts to electric polarization of the double layer.

THE JOURNAL OF CHEMICAL PHYSICS VOLUME 19, NUMBER 12 DECEMBER, 1951

Diffusion in CO_2 up to 150-Atmospheres Pressure*

W. L. Robb and H. G. Drickamer
Department of Chemistry, University of Illinois, Urbana, Illinois
(Received August 17, 1951)

Diffusion coefficients have been obtained for the system CO_2—$C^{14}O_2$ up to 150 atmospheres pressure and from 0°–45°C. The coefficients are consistent with theory up to a density of 0.067 g/cc. In the range from 0.067–0.70 g/cc the coefficients are higher than predicted by theory. This may be attributed to a reduced collision diameter due to orientation of the nonspherical molecules. At higher densities the experimental coefficients are lower than the theoretical ones. This is expected as the theory breaks down at these high densities. At densities above 0.65 g/cc no measurable temperature coefficient of D was obtained. This may be explained by increased orientation at lower temperatures and in the liquid state.

DIFFUSION coefficients, measured for gases at atmospheric pressure and below, have shown remarkable agreement with the diffusion theory of Enskog and Chapman, as calculated for the interaction potential of the Lennard-Jones molecular model. The extension of this work into the dense gas and liquid region is an important step in the understanding of the transport properties of compressed systems.

Essentially, self-diffusion coefficients of $C^{12}O_2$ were obtained by measuring the rate of diffusion of $C^{14}O_2$ in CO_2. A correction of one percent was made to account for the greater mass of the radioactive molecule, but all other properties were assumed to be alike for the tagged and untagged molecules.

* This work was supported in part by the AEC.

The diffusion took place in two porous packed cells, with analysis being made at the end of the one cell. A scintillation crystal and counting circuit enabled continuous analysis to be made without sampling.

Diffusion coefficients were measured from 9.7 to 150 atmospheres pressure and from 0 to 45°C. A density range from 0.0147 to 1.00 gram per milliliter was covered, extending the work of Timmerhaus and Drickamer,[1] who measured D's for the same system to a density of 0.059 g/ml.

The theory of Enskog and Chapman[2] using the

[1] K. D. Timmerhaus and H. G. Drickamer, J. Chem. Phys. 19, 1242 (1951).

[2] S. Chapman and T. G. Cowling, *Mathematical Theory of Non-Uniform Gases* (Cambridge University Press, London, 1939), pp. 134–167.

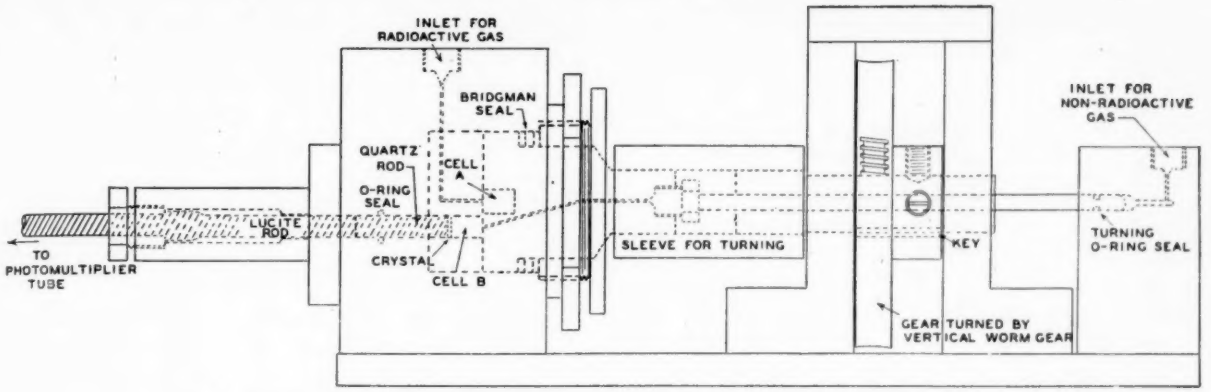

FIG. 1. Schematic drawing of diffusion apparatus for measuring diffusion coefficients.

Lennard-Jones model with the dense gas correction of Enskog[3] and the nomenclature of Hirschfelder, *et al.*[4] gives for the self-diffusion coefficient

$$D_{11}=\frac{16(kT)^{\frac{1}{2}}}{3(2\pi\mu)^{\frac{1}{2}}r_0^2 n W_1^{(1)}{}_{(1)}\chi}, \tag{1}$$

where

$$\chi=1+(5/12)\pi n\sigma^3+0.1275(\pi n\sigma^3)^2+\cdots. \tag{1'}$$

This equation is somewhat inconsistent in that the dense gas correction is developed only for the case of solid elastic spheres, but it is the best available to date. It is assumed here that r_0 and σ, the solid elastic sphere diameter, are identical.

Phenomenologically the experimental system described below was similar to that used by Timmerhaus and Drickamer.[1] In their paper it was shown that, for the latter part of a run, the following equation applies

$$I_f-I=\frac{4}{\pi}\exp\left(-\frac{\pi^2}{l^2}Dt\right) \tag{2}$$

so a plot of ln (I_f-I) *versus* t should give a slope of $S=-(\pi^2/l^2)D$. Where I_f could not be obtained, as on a very long run, an entity

$$\delta=(I_{t_1}-I_{t_2})/(I_{t_3}-I_{t_4}). \tag{3}$$

was introduced. Curves of δ *versus* S for many combinations of t_1, t_2, t_3, and t_4 were prepared and were used as discussed in the following material.

TABLE I. Comparison of packings.

Run no.	Type of packing	Actual length both cells	Effective length	R
Timmerhaus and Drickamer	'F' Fritted metal	29.4 cm	60.05 cm	2.04
1–23	'F' Fritted metal	4.97 cm	10.51 cm	2.11
24–36	'F' Fritted metal	3.33 cm	6.80 cm	2.04
42–50	'H' Fritted metal	0.32 cm	5.17 cm	2.04 (assumed)
	200 mesh screening	2.93 cm		1.54
68–78	'M' Fritted glass	3.11 cm	6.10 cm	1.96
79–104	'M' Fritted glass	1.41 cm	2.76 cm	1.96

Average pore size	
'F' Porosity fritted metal	20 microns
'H' Porosity fritted metal	5 microns
'M' Porosity fritted glass	14 microns

The apparatus for the measurement of diffusion coefficients of dense gases and liquids at high pressure is shown schematically in Fig. 1. Essentially it consisted of (1) a diffusion bomb and turning mechanism, by means of which two cells, containing different gases, were brought into contact with each other; (2) a scintillation counter, which measured the amount of radioactive gas diffused through one of the cells; and (3) auxiliary equipment for filling the cells, and generating and measuring the pressures. The diffusion bomb consisted of four main pieces: (1) a steel block with a large hole in the top, (2) a flat metal disk which was pinned to the bottom of the above hole, (3) a cylinder which fitted into the hole and rotated on the inserted disk, and (4) a nut to hold the cylinder tightly against the insert.

There were two diffusion cells, one in the cylinder (Cell A) and one in the insert (Cell B). In the filling position they were 135° apart. The insert and cylinder

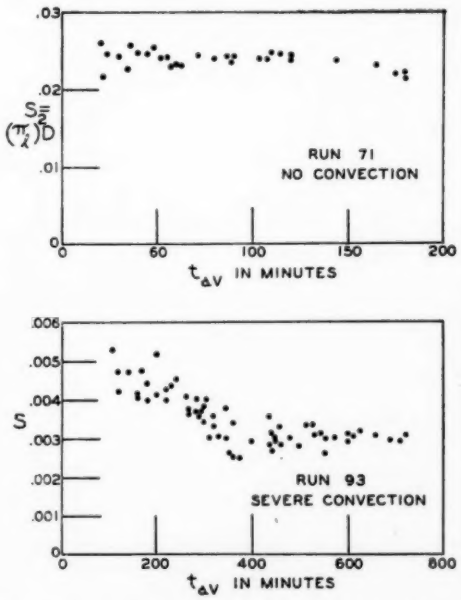

FIG. 2. Plots of π^2D/l^2 *versus* average time as obtained from Eq. (3).

[3] Reference 2, pp. 273–294.
[4] Hirschfelder, Bird, and Spotz, J. Chem. Phys. **16**, 968 (1948).

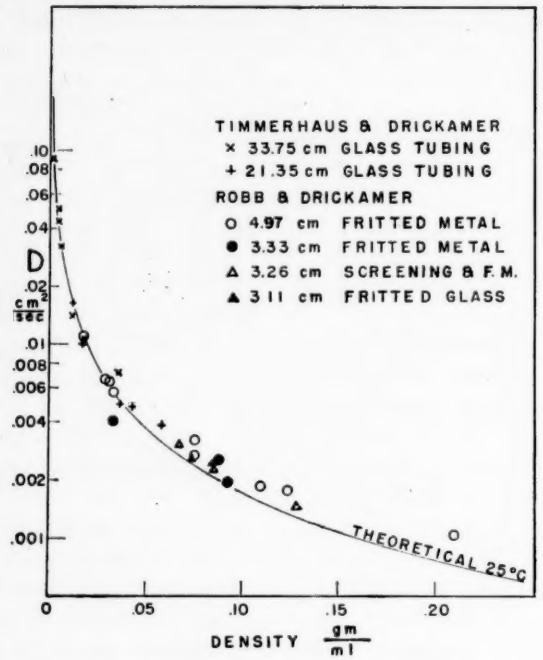

FIG. 3. Diffusion coefficients at low densities at 25°C.

face were surface ground to maintain a seal between the cells in this position. The cells were filled by simultaneously opening valves from two storage bombs both of which were pressurized from the same source (pressure was applied to oil by an injector and transmitted to the gas by mercury). The cells were then rotated by the gear mechanism and diffusion was measured. The cells were filled with various media to prevent convection. The

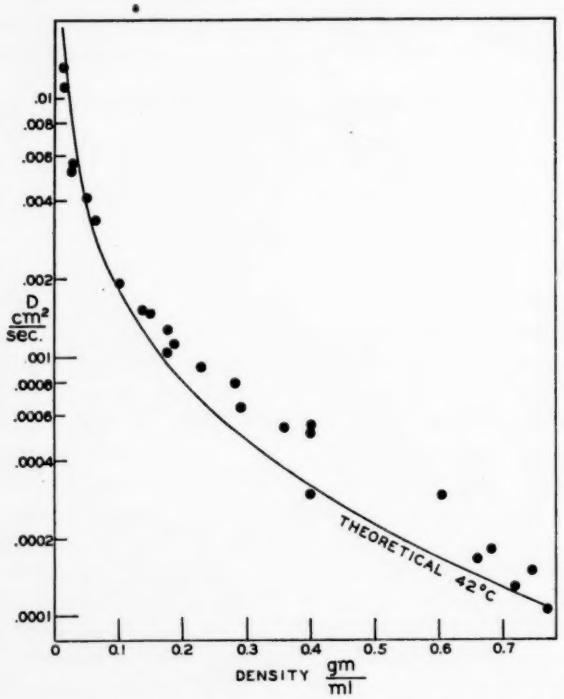

FIG. 4. Diffusion coefficients at 42°C.

TABLE II.

Run no.	Packing	l_{actual}	T °C	P atm	ρ gm/ml	D cm²/sec
2	*F* Fritted metal	4.97 cm	23	16.05	0.0313	0.0065
3			23	16.05	0.0313	0.0065
6			44.7	9.70	0.0160	0.0111
8			44.6	9.20	0.0157	0.0131
10			24.9	9.50	0.0174	0.0110
11			24.9	16.70	0.0346	0.00577
12			44.8	16.30	0.0295	0.00529
13			45.2	16.30	0.0291	0.00519
14			44.8	27.20	0.0522	0.00415
15			25.3	34.20	0.0756	0.00325
16			45.3	34.30	0.0680	0.00340
17			25.2	34.30	0.0757	0.00271
18			25.1	47.60	0.1235	0.00179
19			0.3	34.30	0.0956	0.00131
20			0.4	34.30	0.0955	0.00183
22			13.6	47.80	0.147	0.00119
24	*F* Fritted metal	3.33 cm	21.0	36.40	0.088	0.00260
25			22.0	38.40	0.092	0.00197
26			30.2	47.20	0.1155	0.00166
27			44.7	47.70	0.1045	0.00197
28			30.2	47.70	0.118	0.00158
29			23.8	16.70	0.0328	0.00410
31			0.75	34.30	0.095	0.00130
32			13.4	47.50	0.145	0.00114
33			43.8	61.20	0.152	0.00149
34			44.6	68.10	0.180	0.00105
35			44.5	68.10	0.180	0.00130
36			25.0	61.20	0.210	0.00106
42	Screening and fritted metal	2.94 cm +0.32 cm	22.8	36.40	0.0855	0.00228
43			22.5	36.40	0.0858	0.00250
44			22.4	30.60	0.0675	0.00306
45			23.3	47.70	0.128	0.00150
46			30.2	59.50	0.173	0.00126
47			30.3	61.20	0.1835	0.00105
48			30.3	65.50	0.217	0.000822
50			40.4	80.80	0.292	0.000638
69	*M* Fritted glass	3.14 cm	23.8	70.60	0.058	0.00269
70			30.8	45.60	0.1093	0.00192
71			40.6	57.60	0.1415	0.00154
72			40.6	68.00	0.189	0.00113
73			41.5	75.00	0.230	0.000924
74			40.5	79.50	0.275	0.000804
75			40.4	85.60	0.3602	0.00053
76			32.06	74.30	0.3898	0.000563
77			32.06	74.65	0.4535	0.000538
78			40.25	86.05	0.400	0.000507
80	*M* Fritted glass	1.41 cm	40.25	86.05	0.400	0.000550
81			40.08	96.30	0.608	0.000293
82			25.3	124.90	0.852	0.000105
83			32.06	73.60	0.3335	0.000345
85			40.26	86.05	0.40	0.000300
86			40.26	108.50	0.680	0.000182
87			40.26	129.90	0.745	0.000149
88			25.1	65.10	0.722	0.000216
89			25.1	90.20	0.802	0.000104
90			25.1	90.20	0.802	0.0000822
91			0.2	71.07	0.960	0.0000456
92			0.3	38.40	0.922	0.0000599
93			0.2	137.90	0.998	0.0000404
96			40.21	144.90	0.774	0.000104
99			25.1	89.05	0.800	0.000103
100			25.2	149.90	0.878	0.0000702
101			25.2	65.10	0.72	0.000133
102			40.1	107.90	0.68	0.000166
103			40.2	119.80	0.72	0.000130
104			25.4	65.10	0.716	0.000111

effective path length in each medium was obtained as described by Timmerhaus and Drickamer[1] by overlapping runs at lower density where the diffusion coefficient had previously been determined. The ratios between the effective and actual path length for the various media are shown in Table I. The diffusion coefficients for the various media varied with density in exactly the same way, so the results cannot be attributed to any property of the media.

The radiation was counted continuously by a scintillation crystal at the back of Cell *B*. This provides a considerable advantage over any sampling method.

Pressures were measured, after filling, with a dead weight gauge. The entire ensemble was submerged in an oil bath maintained to ±0.01°C.

As discussed above, the diffusion coefficient could be evaluated either from a plot of Eq. (2) or by use of Eq. (3). This latter method was especially effective where convection was present at the beginning of a run. Figure 2 shows plots of δ *versus* t_{Av} for a run with no convection and for one with considerable convection. Even in this latter case a good value for D is obtained. Convection was especially severe near the critical point where ρ/η goes through a maximum.

The results are shown in Table II and Figs. 3–6. The coefficients have been corrected for the difference in mass between $C^{14}O_2$ and CO_2. The major points of interest are as follows:

(1) At low densities (below about $\rho=0.067$ g/cc) the diffusion coefficients are consistent with the theory of Eq. (1). This is in agreement with the work of Timmerhaus and Drickamer.

(2) At densities higher than 0.067 g/cc and up to about 0.70 g/cc the diffusion coefficients are greater than theory predicts (see Figs. 4 and 5). The effect is as if the collision diameter r_0 were reduced with increasing density The effective values of r_0 are given in Table III. With a nonspherical molecule such as CO_2 it is possible that orientation effects tend to reduce r_0 at high density. Hirschfelder, *et al.*[5] have shown that r_0 calculated for CO_2 from the third virial coefficient is about 11 percent less than that calculated from the second virial coefficient This is in good agreement with our results.

(3) At high densities the diffusion coefficients are lower than theory predicts (see Fig. 6). Since higher terms in χ are significant above a density of 0.70 g/cc, it is not surprising that the predicted values are high. In any case the theory probably breaks down at densities greater than 1.5 times the critical density.

It should be noted that at these high densities no measureable temperature coefficient was obtained This is possible because of greater orientation and smaller r_0 at lower temperatures and in the liquid state.

The results indicate that no simple theory is adequate to explain diffusion for nonsymmetrical molecules at elevated densities.

TABLE III. Calculations for molecular diameters for CO_2.

Temp. °C	Density gm/ml	D_{exp} cm²/sec	D_{theo} cm²/sec	r_0 calc angstroms
42	0.05	0.00400	0.00387	3.95
	0.08	0.00259	0.00233	3.82
	0.12	0.00175	0.001481	3.73
	0.18	0.00120	0.00092	3.62
	0.30	0.000684	0.000476	3.53
	0.40	0.000488	0.000317	3.50
	0.50	0.000370	0.000225	3.47
	0.60	0.000287	0.000168	3.47
25	0.05	0.00400	0.003683	3.86
	0.08	0.00260	0.00222	3.75
	0.12	0.00169	0.00141	3.71
	0.18	0.00116	0.000875	3.57

[5] Hirschfelder, Curtis, Bird, and Spotz, *Properties of Gases* (John Wiley and Sons Inc., New York, to be published).

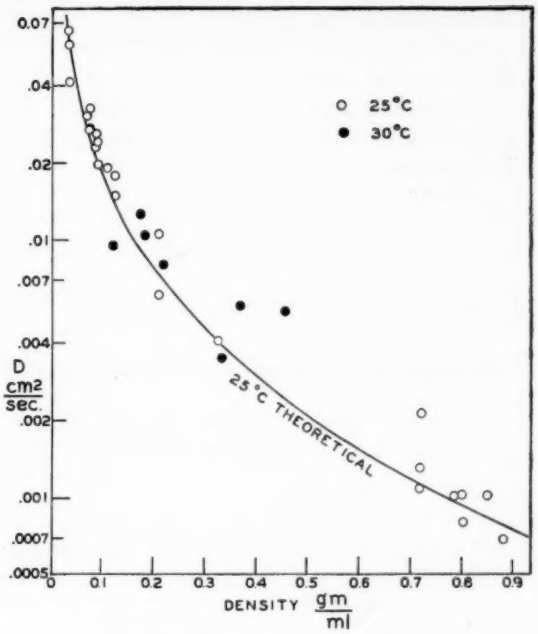

FIG. 5. Diffusion coefficients at 25°C.

W. L. Robb would like to acknowledge the assistance of the Pan American Refining Corporation and the General Electric Educational Fund for fellowship support.

NOMENCLATURE

D_{11} = diffusion coefficient;
I_f = counts per minute at end of run;
I_t = counts per minute at time t;

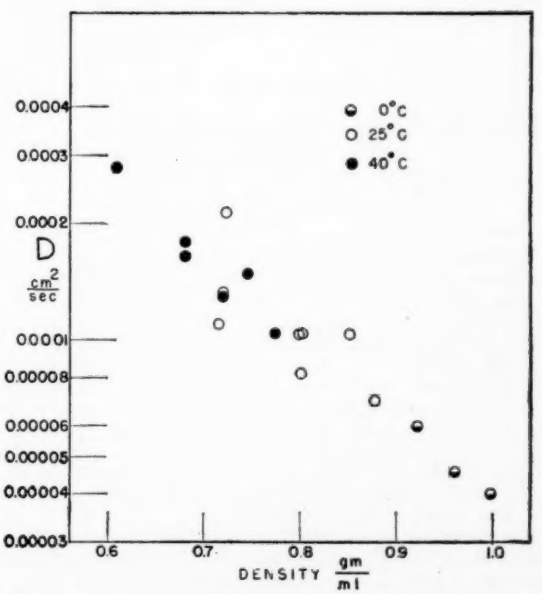

FIG. 6. Diffusion coefficients at high density.

k = Boltzmann's constant;
l = total length of diffusion cell;
m = molecular mass;
n = number of molecules per unit volume;
r_0 = collision diameter for the Lennard-Jones model;
T = absolute temperature;
t = time;
$W_{(1)}^{(1)}$ = integral depending on ϵ and T only;
ϵ = interaction energy at point of greatest attraction for the Lennard-Jones model;
η = viscosity;
μ = reduced mass = $m/2$ for self-diffusion;
ρ = density; and
σ = collision diameter for solid elastic spheres.

THE JOURNAL OF CHEMICAL PHYSICS VOLUME 19, NUMBER 12 DECEMBER, 1951

Statistical Theory of Rubber-Like Elasticity. IV. (Two-Dimensional Stretching)

AKIRA ISIHARA, NATSUKI HASHITSUME, AND MASAO TATIBANA
Department of Physics, Faculty of Science, University of Tokyo, Tokyo, Japan
(Received July 17, 1951)

The failure, revealed by the experiment of Treloar, of statistical theories of the rubber-like elasticity is removed. It comes from the neglection of the nongaussian character and of the nonlinear connectivity of the network structure. The theoretical formula derived here includes the semi-empirical formula given by Treloar.

INTRODUCTION

THE dynamic properties of a well-vulcanized rubber have been treated theoretically by several investigators with considerable success.[1] However, one of the present authors has shown that these theories differ in a few important respects.[2] First, they are classified in two groups according to whether the molecular weight of a chain M_c or that of a kinetic unit m of a chain enters into the expression of elastic modulus. These alternative expressions have different meanings from the viewpoint of the gas kinetic theory.[2] Second, most of the theoretical equations do not reproduce the *S-shape* of the stress-strain curve, which characterizes the simple elongation. As was pointed out in the previous papers,[2] the main reason for these two departures comes from the nongaussian character of the configurational entropy.

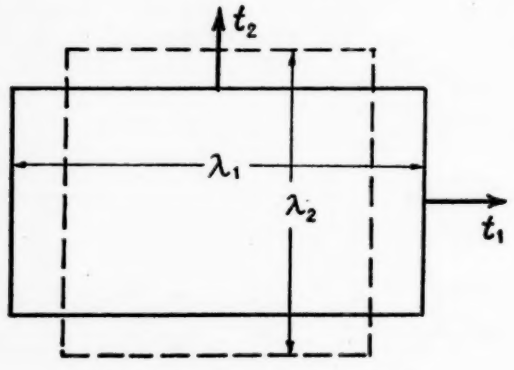

FIG. 1. Two-dimensional stretching.

Now another deviation of the statistical theories has been revealed by Treloar,[3] and it appears fundamental. His experiment is concerned with the two-dimensional stretching of the sample. Let the principal extension ratios be λ_1, λ_2, and λ_3 and the corresponding stresses be t_1, t_2, and $t_3=0$ (Fig. 1). He found that, in the plot t_1 against $\lambda_1^2-\lambda_3^2$, the experimental points did not fall on a single line:

$$t_1=C_1(\lambda_1^2-\lambda_3^2), \tag{1}$$

which was predicted theoretically, but on a series of discrete linear arrays, where in any one of these arrays $\sigma_1=t_1/\lambda_1$ was constant. Taking the strain invariants of Mooney[4] into consideration, he has obtained the semi-empirical formula which must replace Eq. (1):

$$t_1=(C_1+C_2\lambda_2^2)(\lambda_1^2-\lambda_3^2). \tag{2}$$

This formula reproduces the experiments well, and thus it becomes the next problem to deduce it from the molecular theories. The very object of this paper exists in this point. As will be shown in the next section, the failure of the prediction (1) comes from the neglect of the nongaussian character of the network structure. On this point, it belongs to the same category as the two departures mentioned in the earlier part of this section.

[1] W. Kuhn, Kolloid-Z. **76**, 258 (1936); Naturwiss. **24**, 346 (1936). (His recent investigations are not yet available to us.) F. T. Wall, J. Chem. Phys. **10**, 132, 485 (1942); **11**, 527 (1943). H. M. James and E. Guth, J. Chem. Phys. **11**, 455 (1943); J. Appl. Phys. **15**, 294 (1944); J. Chem. Phys. **15**, 669 (1947); J. Polymer Sci. **4**, 153 (1949). P. J. Flory and J. Rehner, J. Chem. Phys. **11**, 512 (1943). L. R. G. Treloar, Trans. Faraday Soc. **39**, 36, 241 (1943); **40**, 59 (1944); *The Physics of Rubber Elasticity* (Oxford University Press, Oxford, 1949). T. Sakai, Proc. Phys.-Math. Soc. Japan **17**, 226 (1943). J. J. Hermans, J. Colloid Sci. **1**, 235 (1946); Trans. Faraday Soc. **43**, 591 (1947). P. J. Flory, J. Chem. Phys. **15**, 397 (1947). H. M. James, J. Chem. Phys. **15**, 651 (1947). R. Kubo, J. Phys. Soc. Japan **2**, 47, 51, 84 (1947).

[2] For convenience, we shall number the present article IV, whereas the preceding articles are: I. T. Sakai and A. Isihara, J. Phys. Soc. Japan **3**, 171 (1948); II. A. Isihara, J. Phys. Soc. Japan **3**, 289 (1948); III. T. Sakai and A. Isihara, J. Colloid Sci. **4**, 71 (1949).

[3] L. R. G. Treloar, Proc. Phys. Soc. (London) **60**, 135 (1948).

[4] M. Mooney, J. Appl. Phys. **11**, 582 (1940).

THE NETWORK THEORY

As usual, we shall have to do with the ideal network, in which one assumes no steric hindrance or interaction, no free chains, no plasticity, and the coherent character discussed by James.[5] Some of the junctions which may be considered to be located on the surface of the sample are distinguished as "fixed junctions" from the other "free junctions." The fixed junctions play the role of external parameters determining the shape and the volume of the network. The Greek letters α, β, γ, $\cdots$ are used for these functions, whereas the Roman i, j, k, $\cdots$ for the free junctions, and a, b, c, $\cdots$ for the two kinds of junctions.

Now, we consider two neighboring junctions a and b, the coordinates of which are $\mathbf{r}_a$ and $\mathbf{r}_b$, respectively. The number of elements of a chain connecting these junctions is designated by N_{ab}. Taking the direction of $(\mathbf{r}_a-\mathbf{r}_b)$ as the polar axis, let $n_{ab}(\omega)d\omega$ be the number of the elements (kinetic units) of the chain oriented in the solid angle $d\omega$ of a direction ω. Then, the assumption of chains with no correlation leads to the following free energy expression:

$$F=kT\sum\int n_{ab}(\omega)\log n_{ab}(\omega)d\omega+U(\lambda_1\lambda_2\lambda_3), \quad (3)$$

where the summation is extended over all the chains of the network, and the internal energy U is assumed to be a function of the "volume" $\lambda_1\lambda_2\lambda_3$ only. In the thermodynamical equilibrium, F must be minimum with respect to the variation of $n_{ab}(\omega)$ satisfying the following auxiliary conditions:

$$\int n_{ab}(\omega)d\omega=N_{ab}, \quad (4)$$

$$\int n_{ab}(\omega)\cos\theta_{ab}d\omega=|\mathbf{r}_a-\mathbf{r}_b|/l. \quad (5)$$

Thus, $n_{ab}(\omega)$ is determined as a function of polar angle θ_{ab} as follows:

$$\lambda_{ab}n_{ab}(\omega)=\exp(\mu_{ab}\cos\theta_{ab}). \quad (6)$$

In these equations l is the length of an element, and λ_{ab} and μ_{ab} are Lagrange's undetermined multipliers, which in turn must satisfy the following equations:

$$\lambda_{ab}N_{ab}=4\pi\sinh(\mu_{ab})/\mu_{ab}, \quad (7)$$

$$|\mathbf{r}_a-\mathbf{r}_b|/(N_{ab}l)=L(\mu_{ab}), \quad (8)$$

where $L(\mu_{ab})$ denotes Langevin's function. Therefore, the free energy expression is rewritten:

$$F=kT\sum\{\mu_{ab}|\mathbf{r}_a-\mathbf{r}_b|/l-N_{ab}\log\lambda_{ab}\}+U(\lambda_1\lambda_2\lambda_3), \quad (9)$$

which must be minimum over again with respect to the variation of the coordinates of free junctions. From this condition these coordinates are given as functions of those of the fixed junctions. When $N_{ab}l\gg|\mathbf{r}_a-\mathbf{r}_b|$, the typical equation determining them becomes:

$$\sum_{b(\neq i)}\frac{x_i-x_b}{N_{ib}l}\left\{1+\tfrac{3}{5}\frac{|\mathbf{r}_i-\mathbf{r}_b|^2}{N_{ib}{}^2l^2}+\cdots\right\}=0, \quad (10)$$

which is nonlinear as has already been noted.[2]

To solve such equations, it is convenient to introduce the notation of James:[5]

$$\gamma_{aa}=\sum_{b(\neq a)}1/(N_{ab}l),$$
$$\gamma_{ab}=\gamma_{ba}=-1/(N_{ab}l)\quad(a\neq b). \quad (11)$$

If we confine ourselves within the approximation of the linearization of Eq. (10):

$$\textstyle\sum_j\gamma_{ij}x_j=-\sum_\alpha\gamma_{i\alpha}x_\alpha, \quad (12)$$

then the free junctions shift linearly with fixed junctions, so that we can put for example

$$x_i=x_i{}^0\lambda_1,\quad y_i=y_i{}^0\lambda_2,\quad z_i=z_i{}^0\lambda_3, \quad (13)$$

and we arrive at the following equation of the stress-strain relation for the simple elongation (assuming $\lambda_1\lambda_2\lambda_3=1$):

$$\sigma_1=C_1\left(\lambda_1-\frac{1}{\lambda_1{}^2}\right)+C_2\left(\lambda_1{}^3+\tfrac{1}{3}-\frac{4}{3\lambda_1{}^3}\right), \quad (14)$$

which is characterized by the following two elastic constants:

$$C_1=kT\sum\frac{|\mathbf{r}_i{}^0-\mathbf{r}_j{}^0|^2}{N_{ij}l^2};\quad C_2=\frac{9}{25}kT\sum\frac{|\mathbf{r}_i{}^0-\mathbf{r}_j{}^0|^4}{N_{ij}{}^3l^4}. \quad (15)$$

In these equations, the stress σ_1 is refered to the original cross section, and the summations of Eqs. (15) are extended over all the chains in unit cube of the sample (see references I, II).

Now, we shall go a further step by solving Eq. (10) in the second approximation. In this case the x-coordinate of the i-th free junction is determined as follows:

$$x_i=\lambda_1(D_x{}^i+D_{xx}{}^i\lambda_1{}^2+D_{xy}{}^i\lambda_2{}^2+D_{xz}{}^i\lambda_3{}^2); \quad (16)$$

$$D_x{}^i=-\frac{1}{\Gamma}\sum_\alpha x_\alpha{}^0\sum_j\gamma_{j\alpha}\Gamma_{ji},$$

$$D_{xx}{}^i=-\tfrac{3}{5}\sum_i\sum_{b(\neq j)}\left(\frac{x_j{}^0-x_b{}^0}{N_{jb}l}\right)^3\frac{\Gamma_{ij}}{\Gamma}, \quad (17)$$

$$D_{xy}{}^i=-\tfrac{3}{5}\sum_i\sum_{b(\neq j)}\frac{x_j{}^0-x_b{}^0}{N_{jb}l}\left(\frac{y_j{}^0-y_b{}^0}{N_{jb}l}\right)^2\frac{\Gamma_{ji}}{\Gamma},$$

where Γ is the determinant composed of γ_{ij}, Γ_{ij} is the cofactor of γ_{ij}, and the suffix zero means the equilibrium position before stretching. Thus, if we introduce the

[5] H. M. James, J. Chem. Phys. **15**, 651 (1947).

following notations:

$$A_x=\frac{3}{2}\left\{\sum_{i\neq j}N_{ij}\left(\sum_\alpha\frac{x_\alpha{}^0}{N_{ij}l}\sum_k\gamma_{k\alpha}\frac{\Gamma_{kj}-\Gamma_{ki}}{\Gamma}\right)^2+\sum_{i,\alpha}N_{i\alpha}\left(\frac{x_i{}^0-x_\alpha{}^0}{N_{i\alpha}l}\right)^2+\sum_{\alpha\neq\beta}N_{\alpha\beta}\left(\frac{x_\alpha{}^0-x_\beta{}^0}{N_{\alpha\beta}l}\right)^2\right\},$$

$$B_x=\frac{9}{20}\Bigg[\sum_{i\neq j}N_{ij}\left\{\left(\sum_\alpha\frac{x_\alpha{}^0}{N_{ij}l}\sum_k\frac{\Gamma_{kj}-\Gamma_{ki}}{\Gamma}\right)^4-4\sum_{k,m,\alpha}\gamma_{k\alpha}\frac{\Gamma_{kj}-\Gamma_{ki}}{\Gamma}\gamma_{ij}\frac{\Gamma_{mj}-\Gamma_{mi}}{\Gamma}\sum_{b(\neq m)}\frac{x_\alpha{}^0}{N_{ij}l}\left(\frac{x_m{}^0-x_b{}^0}{N_{mb}l}\right)^3\right\}$$
$$+\sum_{i,\alpha}N_{i\alpha}\left\{\left(\frac{x_i{}^0-x_\alpha{}^0}{N_{i\alpha}l}\right)^4-4\left(\frac{x_\alpha{}^0-x_i{}^0}{N_{i\alpha}l}\right)\sum_j\gamma_{i\alpha}\frac{\Gamma_{ji}}{\Gamma}\sum_{b(\neq j)}\left(\frac{x_j{}^0-x_b{}^0}{N_{jb}l}\right)^3\right\}+\sum_{\alpha\neq\beta}N_{\alpha\beta}\left(\frac{x_\alpha{}^0-x_\beta{}^0}{N_{\alpha\beta}l}\right)^4\Bigg],$$

$$C_{xy}=C_{yx}=\frac{9}{10}\Bigg[\sum_{i\neq j}N_{ij}\Bigg\{\left(\sum_\alpha\frac{x_\alpha{}^0}{N_{ij}l}\sum_k\gamma_{k\alpha}\frac{\Gamma_{kj}-\Gamma_{ki}}{\Gamma}\right)^2\left(\sum_\beta\frac{y_\beta{}^0}{N_{ij}l}\sum_m\gamma_{m\alpha}\frac{\Gamma_{mj}-\Gamma_{mi}}{\Gamma}\right)^2$$
$$-2\sum_{k,m,\alpha}\gamma_{k\alpha}\frac{\Gamma_{kj}-\Gamma_{ki}}{\Gamma}\gamma_{ij}\frac{\Gamma_{mj}-\Gamma_{mi}}{\Gamma}\sum_{b(\neq m)}\left(\frac{x_\alpha{}^0}{N_{ij}l}\left[\frac{x_m{}^0-x_b{}^0}{N_{mb}l}\right]\left[\frac{y_m{}^0-y_b{}^0}{N_{mb}l}\right]^2\right.$$
$$\left.+\frac{y_\alpha{}^0}{N_{ij}l}\left[\frac{x_m{}^0-x_b{}^0}{N_{mb}l}\right]^2\left[\frac{y_m{}^0-y_b{}^0}{N_{mb}l}\right]\right)\Bigg\}+\sum_{i,\alpha}N_{i\alpha}\left\{\left[\frac{x_i{}^0-x_\alpha{}^0}{N_{i\alpha}l}\right]^2\left[\frac{y_i{}^0-y_\alpha{}^0}{N_{i\alpha}l}\right]^2\right.$$
$$\left.-2\sum_j\gamma_{i\alpha}\frac{\Gamma_{ji}}{\Gamma}\sum_{b(\neq j)}\left(\frac{x_\alpha{}^0-x_i{}^0}{N_{i\alpha}l}\cdot\frac{x_j{}^0-x_b{}^0}{N_{jb}l}\left[\frac{y_j{}^0-y_b{}^0}{N_{jb}l}\right]^2+\left[\frac{x_j{}^0-x_b{}^0}{N_{jb}l}\right]^2\frac{y_\alpha{}^0-y_i{}^0}{N_{i\alpha}l}\cdot\frac{y_j{}^0-y_b{}^0}{N_{jb}l}\right)\right\}$$
$$+\sum_{\alpha\neq\beta}N_{\alpha\beta}\left(\frac{x_\alpha{}^0-x_\beta{}^0}{N_{\alpha\beta}l}\right)^2\left(\frac{y_\alpha{}^0-y_\beta{}^0}{N_{\alpha\beta}l}\right)^2\Bigg];$$

$$x_i{}^0=-\sum_\beta x_\beta{}^0\sum_j\gamma_{j\beta}\frac{\Gamma_{ji}}{\Gamma},\ \text{etc.,} \tag{18}$$

the free energy of Eq. (3) becomes

$$F=U(\lambda_1\lambda_2\lambda_3)-TS, \tag{19}$$

$$S=-k(A_x\lambda_1{}^2+A_y\lambda_2{}^2+A_z\lambda_3{}^2+B_x\lambda_1{}^4+B_y\lambda_2{}^4+B_z\lambda_3{}^4+C_{xy}\lambda_1{}^2\lambda_2{}^2+C_{yz}\lambda_2{}^2\lambda_3{}^2+C_{zx}\lambda_3{}^2\lambda_1{}^2). \tag{20}$$

Therefore, we obtain the following general expression of stresses for the original cross section:

$$\begin{aligned}\sigma_1&=-\lambda_2\lambda_3\varphi+2kT\lambda_1(A_x+2B_x\lambda_1{}^2+C_{xy}\lambda_2{}^2+C_{xz}\lambda_3{}^2),\\ \sigma_2&=-\lambda_3\lambda_1\varphi+2kT\lambda_2(A_y+C_{yz}\lambda_1{}^2+2B_y\lambda_2{}^2+C_{yz}\lambda_3{}^2),\\ \sigma_3&=-\lambda_1\lambda_2\varphi+2kT\lambda_3(A_z+C_{zx}\lambda_1{}^2+C_{zy}\lambda_2{}^2+2B_z\lambda_3{}^2),\end{aligned} \tag{21}$$

where $-\varphi$ is the internal pressure:

$$-\varphi=dU/d(\lambda_1\lambda_2\lambda_3). \tag{22}$$

In the case of two-dimensional stretching in the xy-plane, we can put $\sigma_3=0$. Thus, φ assumes the form:

$$\varphi=2kT\frac{\lambda_3}{\lambda_1\lambda_2}(A_z+C_{zx}\lambda_1{}^2+C_{zy}\lambda_2{}^2+2B_z\lambda_3{}^2). \tag{23}$$

For initially isotropic material, we can put

$$\begin{aligned}A_x&=A_y=A_z=A,\\ B_x&=B_y=B_z=B,\\ C_{xy}&=C_{yz}=C_{zx}=C.\end{aligned} \tag{24}$$

Then, the entropy (20) becomes

$$S=-k\{A(\lambda_1{}^2+\lambda_2{}^2+\lambda_3{}^2)+B(\lambda_1{}^4+\lambda_2{}^4+\lambda_3{}^4)+C(\lambda_1{}^2\lambda_2{}^2+\lambda_2{}^2\lambda_3{}^2+\lambda_3{}^2\lambda_1{}^2)\}. \tag{25}$$

Introducing the notations

$$2kTA=C_1,\quad 4kTB=C_3,\quad 2kTC=C_2, \tag{26}$$

the following stress equations for the two-dimensional stretching are derived:

$$\begin{aligned}t_1&=\lambda_1\sigma_1=\{C_1+C_2\lambda_2{}^2+C_3(\lambda_1{}^2+\lambda_3{}^2)\}(\lambda_1{}^2-\lambda_3{}^2),\\ t_2&=\lambda_2\sigma_2=\{C_1+C_2\lambda_1{}^2+C_3(\lambda_2{}^2+\lambda_3{}^2)\}(\lambda_2{}^2-\lambda_3{}^2).\end{aligned} \tag{27}$$

Here t's are the stresses for the actual cross section.

DISCUSSION OF THE RESULTS

The equations just obtained coincide with the semi-empirical formula of Treloar, but are characterized by three elastic constants C_1, C_2, and C_3. Thus our theoretical formula is more general than his result. As has been shown, our theoretical equations are originated in the nonlinear character of the network structures (Eq. (16)).

In the case of a simple elongation, these equations are reduced to:

$$\sigma_1=C_1\left(\lambda_1-\frac{1}{\lambda_1{}^2}\right)+C_3\left\{\lambda_1{}^3+\frac{C_2}{C_3}-\left(1+\frac{C_2}{C_3}\right)\frac{1}{\lambda_1{}^3}\right\} \tag{28}$$

in comparison with Eq. (14). Because of the complexity of the forms of the constants C's we cannot compare the magnitude of C_2 with that of C_3. However, if we take only the first terms of Eqs. (18) the ratio C_2/C_3 is approximately $\frac{1}{3}$ and Eq. (28) is reduced to Eq. (14).

Returning to the case of two-dimensional stretching, we shall now analyze the experiment of Treloar. As has already been explained in the introduction, the unexpected situation arises when we plot t_1 as a function of $\lambda_1^2-\lambda_3^2$ at constant σ_1. One value of σ_1 corresponds to one linear array, on which the value of σ_2 varies from point to point. Technically, this plot is somewhat difficult because t_1 and σ_2 in Eq. (27) are connected non-linearly with each other, and that the values of the constants C_1, C_2, and C_3 are unknown.

These values may be determined, for instance, by comparing Eq. (28) with the corresponding experiment. Unfortunately such a plot is determined almost by the value C_1, and the determination of C_2 or C_3 has to do with small quantities which are nearly of the order of magnitude of the experimental error. This difficulty is increased if we are forced to read experimental values from curves.

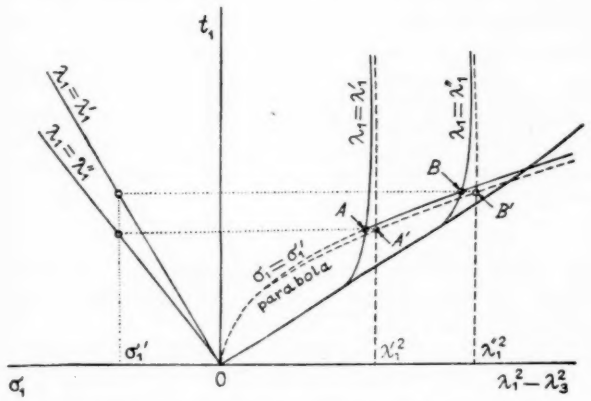

FIG. 2. Schematic representation of the plot t_1 *vs* $\lambda_1^2-\lambda_3^2$ at a constant value of σ_1.

Fortunately, however, we can see that the position of such linear arrays does not depend on the values of C_2 or C_3 seriously. We shall explain this fact schematically by Fig. 2. In the left half part of this figure the straight lines $t_1=\lambda_1\sigma_1$ with various values of λ_1, e.g. λ_1' and λ_1'', are shown. The curves $\lambda_1=\lambda_1'$ and $\lambda_1=\lambda_1''$ in the right half part of the figure represent the relation between t_1 and $\lambda_1^2-\lambda_3^2$ under the condition of λ_1 constant. These curves become infinite at the positions $\lambda_1^2-\lambda_3^2=\lambda_1'^2$ and $\lambda_1^2-\lambda_3^2=\lambda_1''^2$, where λ_3 vanishes and λ_2 becomes infinite because of $\lambda_1\lambda_2\lambda_3=1$. The curve of t_1 against $\lambda_1^2-\lambda_3^2$ with a constant value of σ_1, say σ_1', may be obtained by connecting the points such as A and B in this figure. As we can see from the figure, these points fall in the vicinity of such points as A' and B', which lie on the asymptotes $\lambda_1^2-\lambda_3^2=\lambda_1'^2$ and $\lambda_1^2-\lambda_3^2=\lambda_1''^2$, respectively. Therefore, the curve connecting A and B nearly coincides with that connecting A' and B'. The latter curve (parabola) does not depend on the special values of C_1, C_2, and C_3.

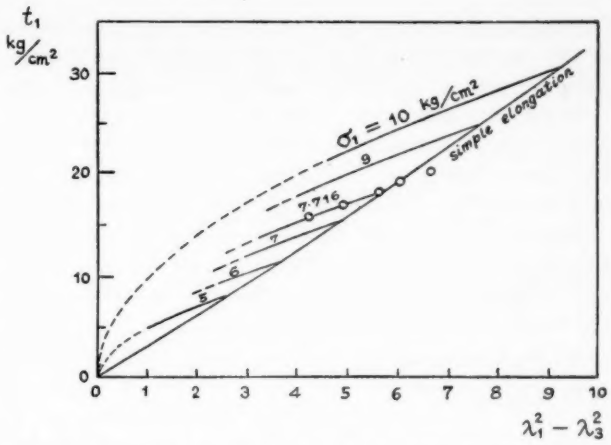

FIG. 3. Theoretical curves for t_1 *vs* $\lambda_1^2-\lambda_3^2$ at constant values of σ_1 in kg/cm². Circles represent the experiment of Treloar. Curve with $\sigma_1=7.716$ kg/cm² is the corresponding theoretical one.

We determined the value of C_1 so that it gives the right order of magnitude of the elastic constant of rubber-like substances, which is about 10 kg/cm², and took the value 3000 g/cm². C_2 was determined by virtue of the fact that, from Eq. (18), the ratio C_2/C_1 is approximately of the order of magnitude $(|x_i^0-x_j^0|/N_{ij}l)^2 \sim 1/100$, and the value 10 g/cm² was selected for the convenience of calculation, although this value seems to be rather small. Three times the value of C_2 was adopted for C_3 from the preceding consideration. Figure 3 represents the curves corresponding to such values of constants.

In this figure, the circles represent one set of the experimental values of Treloar.[3] The linear array with $\sigma_1=7.716$ kg/cm² represents the corresponding theoretical value. The coincidence is good, but this comes from the particular situation explained in this section and is somewhat accidental. The other experimental values also fall in the vicinity of the theoretical curves. As we have not determined the values of constants C_1,

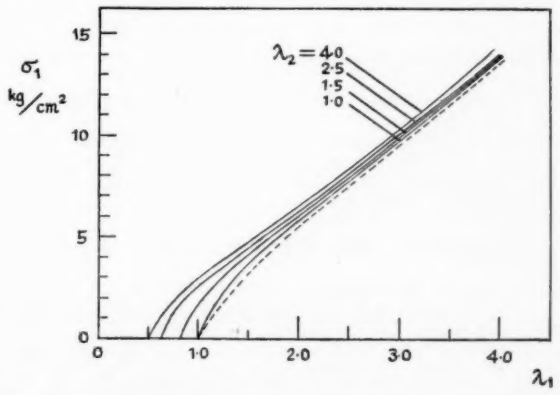

FIG. 4. Theoretical curve of stress σ_1 on original cross section as functions of extension ratio λ_1 at various values of λ_2. The dotted curve corresponds to the case of simple elongation.

C_2, and C_3 so as to reproduce the simple elongation curve of the experiment faithfully, some of the experimental circles lie beyond the theoretical simple elongation curve.

In passing, we want to add that we have obtained another set of constants $C_1=4400$ g/cm², $C_2=118$ g/cm² and $C_3=-218$ g/cm² which reproduce the experiment of Treloar (Fig. 5 of his article) more completely.

Again, it should be noted that Treloar's formula, Eq. (2), does not contain the term of C_3. The difference with ours comes from the fact that he has not adopted the strain invariant

$$\lambda_1^4+\lambda_2^4+\lambda_3^4=(\lambda_1^2+\lambda_2^2+\lambda_3^2)^2-2(\lambda_1^2\lambda_2^2+\lambda_2^2\lambda_3^2+\lambda_3^2\lambda_1^2)$$

in his theory.

Recently, another interesting datum of two dimensional stretching has been given by Boonstra.[6] We have not tried to fit our formula with his results because we must select another system of elastic constants C_1, C_2, and C_3. However, in Fig. 4 we have plotted σ_1 as a function of λ_1 at various values of λ_2 using the same values of C's as used in Fig. 3; the plot may be compared with Fig. 2 of Boonstra.

In conclusion, we hope that the values of the three elastic constants, especially those of C_2 and C_3, can be determined by experiments.

[6] B. B. S. T. Boonstra, J. Appl. Phys. **21**, 1098 (1950).

THE JOURNAL OF CHEMICAL PHYSICS VOLUME 19, NUMBER 12 DECEMBER, 1951

Photochemical Studies. XLVI. Photosensitization by Benzene and Pyridine Vapors*

JEAN T. DUBOIS† AND W. ALBERT NOYES, JR.
Department of Chemistry, University of Rochester, Rochester, New York

(Received August 13, 1951)

Attempts to sensitize the dissociations of the following molecules by means of benzene vapor have been made: hydrogen, oxygen, hydrogen chloride, nitrous oxide, methyl chloride, methyl bromide, methyl iodide. Positive results were obtained only with methyl iodide. The decompositions of methyl chloride and methyl bromine sensitized by pyridine vapor were also studied with negative results. The reasons for the results are discussed briefly.

THE transfer of energy between polyatomic molecules and other molecules on collision has been studied very little from a quantitative standpoint. This problem is basic to many problems of reaction kinetics and of photochemistry. A few results of a semiquantitative nature are available from studies of fluorescence, and energy chains have often been postulated during photochemical reactions. Nevertheless, in few, if any, of these cases involving polyatomic molecules are the results susceptible of definite interpretation.

Benzene and pyridine vapors offer, at first glance, good possibilities for studies of this type since their spectra are known and have been analyzed.[1,2] Moreover, neither of these molecules decomposes when exposed to radiation of wavelength 2537A.[3,4] Benzene does not show mercury sensitized decomposition at 2537A unless the temperature is raised considerably.[5] It also shows some at 1849A.

EXPERIMENTAL

The benzene was a Merck, cp, thiophene-free product. It was degassed in high vacuum at $-77°$ and further purified by bulb to bulb distillation, the middle third being retained. The vapor of the benzene thus prepared showed a small evolution of gas uncondensed by liquid nitrogen when exposed to a General Electric Company AH-6 arc, whether or not short wavelengths were removed by interposition of a one percent solution of acetic acid. At a benzene pressure of 1.1 cm the gas evolution amounted to about 9×10^{-4} mm/hr, but the evolution ceased after 20 to 25 hours. Fresh benzene could be added and the effect observed again so that the cessation was not due to a deposit on the windows which absorbed the radiation. It was proved by addition of hydrogen that a steady state was not being attained. No reduction in hydrogen pressure resulted. It was concluded that a trace of impurity, present in too small amount to be detected chemically, was responsible for this small gas evolution. Thiophene might behave in this manner.[6] All benzene vapor used in these experiments was exposed to radiation until gas evolution

* This work was supported in part by Contract N6onr-241, Task I, with the ONR.

† Holder of a Shawinigan Chemicals, Ltd. Fellowship during 1947–48 and 1948–49. Present address: Chemistry Group, Flight Research Laboratory, Research Division, Hq., Wright Air Development Center, Wright-Patterson Air Force Base, Dayton, Ohio.

[1] Sponer, Nordheim, Sklar, and Teller, J. Chem. Phys. **7**, 207 (1939).

[2] H. Sponer and H. Stucklen, J. Chem. Phys. **14**, 101 (1946).

[3] (a) G. I. Krassina, Acta Physicochim. U.R.S.S. **10**, 189 (1939); (b) N. A. Prilezhaeva, Acta Physicochim. **10**, 193 (1939); (c) J. E. Wilson and W. A. Noyes, Jr., J. Am. Chem. Soc. **63**, 3025 (1941); (d) G. S. Forbes and J. E. Cline, J. Am. Chem. Soc. **63**, 1713 (1941); (e) J. R. Bates and H. S. Taylor, J. Am. Chem. Soc. **49**, 2438 (1927).

[4] R. H. Linnell and W. A. Noyes, Jr., J. Am. Chem. Soc. (to be published).

[5] J. Y. Scott and E. W. R. Steacie, Can. J. Chem. **29**, 233 (1951).

[6] E. Sernagiotto, Atti accad. nazl. Lincei **23**, 70 (1914).

ceased, and the gases uncondensed at −77° were removed.

The purification of the pyridine has already been described.[4]

Oxygen was prepared by heating solid potassium permanganate to about 250° and was passed through a trap immersed in liquid nitrogen to remove condensable impurities. Tank hydrogen was purified by diffusion through a heated palladium thimble. Tank nitrous oxide was bubbled through concentrated potassium hydroxide, dried over phosphorus pentoxide, and fractionated by bulb-to-bulb distillation with liquid nitrogen. The middle third was retained. Hydrogen chloride gas was obtained from cp concentrated hydrogen chloride solution, dried by calcium chloride, calcium sulfate, and by passage through a trap immersed in dry ice and acetone. It was purified finally by bulb-to-bulb distillation with liquid nitrogen.

Methyl iodide was Eastman Kodak Company white label, purified by fractionation in a Todd[7] column with a reflux ratio of 20:1. Its purity was verified by its infrared spectrum. Methyl chloride was obtained from the Mathieson Alkali Works and was purified by bulb-to-bulb distillation. Methyl bromide was obtained from the Eastman Kodak Company and was purified by bulb-to-bulb distillation at −77°.

Some difficulty was experienced in obtaining reproducible results with methyl iodide. This was particularly true as regards the rate of photochemical decomposition of the pure material and as regards the percentage of radiation absorbed at relatively low pressures. In the present experiments it was necessary to have mercury vapor present to remove the iodine. Since methyl iodide is known to react with mercury, the possibility of interference by methyl mercury iodide had to be explored. At different times the methyl iodide was stored as follows: (1) in a bulb separated from the rest of the apparatus by an ordinary mercury cutoff; (2) in a bulb separated from the rest of the apparatus by a stopcock lubricated with fluorolube; (3) in a bulb painted black on the outside, containing gold foil to remove mercury vapor and separated from the rest of the apparatus by glass float valves actuated by mercury. Methyl iodide from all three sources was photochemically decomposed at constant incident intensity at a series of pressures. The results obtained by supplies (1) and (3) gave similar rates of ethane formation at various pressure, and all three supplies gave the same results at sufficiently high pressures. However, the material stored behind the stopcock lubricated with fluorolube attained the high pressure rate at a lower pressure than did the other two. It proved impossible to ascertain completely the reason for this phenomenon, but it was concluded that the stopcock grease introduced some impurity which affected the rate. There was a visible change in the appearance of the fluorolube

[7] F. Todd, Ind. Eng. Chem. 17, 175 (1945).

TABLE I. Results of exposure of mixtures of benzene vapor and other gases. (Radiation sources: (a) Low pressure dc Hg arc; (b) Hanovia type S-100 medium pressure Hg arc; (c) General Electric Company AH-6 high pressure Hg arc. The 1849A line was removed in all cases by a 1 percent aqueous solution of acetic acid. $T\sim25°$.)

Benzene pressure mm	Other gases and pressures in mm	Light sources	Remarks
3	H_2 (0.1)	a, c	No reduction in H_2 pressure, no evidence for H atoms by MoO_3.
3	O_2 (0.1)	a, c	No change in O_2 pressure.
2.5	H_2 (0.1–0.5) O_2 (0.1–0.5)	c	No change in pressure of gas uncondensed by liq. N_2.
23	H_2 (10^{-3}–2×10^{-4}) O_2 ($\sim10^{-3}$)	c	No change in pressure of gas uncondensed by liq. N_2.
2.5–92	N_2O (6–80)	c	No products formed uncondensed by liq. N_2.
2–3.5	HCl (0.1–100)	c	No H_2, no decrease in HCl when measurable.
8.5	CH_3Cl (12)	b	25 percent acetic acid and 5 cm Cl_2 at 1 atmos interposed. No CH_4 or C_2H_6 formed.
40	CH_3Cl (10)	b	No CH_4 or C_2H_6 formed.
74.5–110	CH_3Br (10–22)	b	No CH_4 or C_2H_6 formed.

during exposure to methyl iodide. Supplies (1) and (3) gave quantum yields of ethane formation independent of methyl iodide pressure in general agreement with results obtained by other workers.[8] It was concluded from these experiments that the slow formation of methyl mercury iodide at room temperature did not alter the course of the photochemical decomposition of methyl iodide.

During the experiments pressures of gases either uncondensed by liquid nitrogen or by pentane mush (about −160°) were measured. The former would be oxygen, hydrogen, nitrogen, methane, and nitric oxide (if the pressure is lower than 0.1 mm) together with traces of ethane. The latter would be ethane after

TABLE II. Results of exposure of mixtures of pyridine vapor and other gases. (Radiation source b. $T\sim25°$.)

Pyridine pressure mm	Alkyl halide and pressure mm	Remarks
4–14	CH_3Cl (25)	No CH_4, C_2H_6, or C_2H_4 formed. Short wavelengths removed by 25 percent acetic acid and longer wavelengths by Cl_2. No decrease of total pressure (to within 0.5 mm).
2–18	CH_3Br (9)	No CH_4, C_2H_6, or C_2H_4 formed. No decrease of total pressure (to within 0.5 mm).

[8] See R. D. Schultz and H. A. Taylor, J. Chem. Phys. 18, 194 (1950).

removal of the more nonpersistent gases. During some of the experiments with methyl iodide the methane was determined by removal at a temperature of about −210° at which ethane cannot be removed by a Toepler pump.

The presence of hydrogen atoms was detected by molybdenum trioxide in some instances. The sensitivity of the molybdenum trioxide was verified by exposure to hydrogen atoms produced by the mercury sensitized dissociation of hydrogen.

Three light sources were used at one time or another: (a) Low pressure dc mercury arc; (b) Hanovia Type S-100 medium pressure mercury arc (Alpine burner); (c) General Electric Company high pressure AH-6 arc.

RESULTS

The results for all gases except methyl iodide mixed with benzene are summarized in Table I, those for methyl chloride and methyl bromide mixed with pyridine are shown in Table II, and those for mixtures of methyl iodide and benzene are given in Table III. It will be noted that negative results were obtained in all cases except as regards mixtures of benzene vapor and methyl iodide. Actual quantum yields were not determined, but a yield as low as 10^{-4} could have been detected.

TABLE III. Results of exposure of mixtures of benzene vapor and methyl iodide. ($T\sim25°$. Light source C.)

Methyl iodide pressure mm	Benzene pressure mm	Rate of C_2H_6 formation mm $\times10^3$/hr	Cell length cm
2.2	0	0.79	5[a]
2.2	47	0.93	5[b]
0.87	47	1.93	30
0.87	0	1.1	30
9	27	7.8	30
9	50	8.2	30
9	118	9.8	30
9	0	6.8	30[c]
8	26	7.0	30
8	60	8.1	30
8	82	8.7	30
8	118	11.1	30
8	0	6.5	30[c]

[a] Average of 2 runs.
[b] Average of three runs.
[c] Mean of all blank runs at a given pressure.

Ethane was the main product formed either during the direct or benzene sensitized decomposition of methyl iodide. Traces of methane were also formed, but the amounts were always so small as to make the determination of the absolute amount subject to great uncertainties.

Methyl iodide is the only substance studied which absorbs appreciably at 2537A, the main wavelength used in these experiments. Thus it is necessary to obtain an estimate of the fractions of the radiation absorbed by the two molecular species. Since the radiation was not strictly monochromatic, this could only be done approximately. By use of a photocell the fraction of the incident radiation absorbed by each substance alone was determined as a function of pressure. These data would have been sufficient for monochromatic radiation and would permit a calculation of the fraction absorbed by each species. The fraction of the radiation absorbed at constant methyl iodide pressure as benzene is added was also determined.

The quantum yield of ethane formation in mixtures of benzene and methyl iodide relative to those in methyl iodide alone may be determined from the data in Table III and a knowledge of the relative amounts of light absorbed. The latter was measured by a photoelectric cell on the assumption that the response was independent of wavelength over the relatively small range of wavelengths absorbed. Thus with a pressure of 8 mm of methyl iodide and an assumed quantum yield of unity for its dissociation in the presence of mercury vapor,[9] one finds 0.8 with benzene present, and no significant trend with benzene pressure. At 9 mm pressure of methyl iodide the figure is also 0.8, but at 0.87 mm pressure of methyl iodide the figure is only 0.3. The latter figure is very uncertain.

It is impossible to calculate the quantum yield of the pure benzene sensitized reaction since it is impossible to calculate the fraction of the light absorbed by each component. Such a calculation is impossible in a mixture for which either one or both components shows a fine structure in its absorption spectrum unless the width of the incident line is small compared to single lines in the fine structure so that single absorption coefficients independent of pressure can be used. This condition is not met in the present experiments and indeed would be practically impossible of fulfillment with a molecule such as benzene which exhibits a fine structure practically impossible to resolve.[1] Methyl iodide almost certainly shows continuous absorption in the region in question[10] and hence would be less troublesome.

Certain conclusions are possible with regard to the benzene sensitized reaction, however. Thus at a methyl iodide pressure of 8 mm and a benzene pressure of 82 mm, the light absorbed is about 1.9 times that absorbed in the same cell by the methyl iodide alone. A minimum of 45 to 50 percent of the light must be absorbed by the benzene. The rate of ethane formation is 1.3 to 1.4 times as great as in the absence of benzene. Hence the quantum yield of the benzene sensitized reaction must be at least 0.4, relative to pure methyl iodide as unity, and is probably higher.

DISCUSSION

The conditions for simple photosensitization by collision represented by the equations

$$S+h\nu=S^*, \quad (1)$$

$$S^*+M=S+\text{dissociation products}, \quad (2)$$

[9] R. D. Schultz and H. A. Taylor, J. Chem. Phys. 18, 194 (1950).
[10] H. Sponer, *Molekülspektren* (Julius Springer, Berlin, 1935), p. 108. See also W. West and L. Schlessinger, J. Am. Chem. Soc. 60, 961 (1938).

may be stated as follows: (1) the energy which S^* may supply must be sufficient to dissociate M from the energy level in which it lies at the time of collision; (2) If the dissociation of M results from its transfer to a truly repulsive upper state, the Franck-Condon principle leads to the conclusion that the probability of energy transfer will be small unless the upper state is reached from the ground state with small change in configuration and in internuclear distances. The energy to be supplied may, under some conditions, exceed greatly the minimum energy required for dissociation; (3) Certain conditions concerning multiplicity, symmetry, etc., must be met. These conditions will often be difficult to specify unless detailed assumptions are made concerning the nature of the process.

Negative results are indicated for all cases listed in Table I. Condition (1) is fulfilled for all molecules except oxygen if the benzene molecule is assumed to retain the 4.88 ev energy acquired by absorption of the 2537 A line. The same would be true if the upper electronic state were to lose all vibrational energy prior to collision with M.[1] Condition (2) would require that more energy be supplied than is available for H_2, HCl, and probably for CH_3Cl, CH_3Br, and N_2O. The detailed application of condition (3) cannot be made, but the conservation of spin would make energy transfer improbable with H_2, O_2, and perhaps N_2O, since the upper electronic repulsive states would have different multiplicities from the ground state. The case of N_2O may not be excluded definitely because of condition (3), since upper repulsive states may exist which would dissociate into singlet states for the products.[11]

Thus methyl iodide is the only molecule studied for which positive results would be expected if the sensitization process may be expressed by the simple reactions (1) and (2). However the process might be described schematically by the formation of an intermediate complex as in the case of sensitization by mercury and other atoms in $^3P_1$ states. Equation (1) would then be followed by

$$S^*+MX=SX+M, \tag{3}$$

$$SX=S+X. \tag{4}$$

The detailed rules for this type of process may not be given, but (1) sufficient energy must be supplied, and (2) probably the rule regarding conservation of spin would apply. This mechanism might make dissociation of CH_3Cl and CH_3Br possible provided intermediates of the type C_6H_6Cl and C_6H_6Br are sufficiently stable. There are indications that such might be the case for bromine and iodine atoms,[12] but the situation for chlorine atoms is less certain.[13] The negative results obtained with CH_3Cl, CH_3Br, and HCl would indicate that the intermediate complex is either insufficiently stable or is formed with too low a probability to permit sensitization by reactions (3) and (4).

The positive results with methyl iodide are susceptible of more than one interpretation. West and his co-workers have already shown[14] that certain aromatic hydrocarbons may sensitize the decomposition of alkyl iodides in hexane solution. They state that more aromatic molecules are potential sensitizers than are potentially capable of fluorescence. Thus certain molecules may not fluoresce because the energy is degraded by internal conversion[15] but are nevertheless competent sensitizers if suitable foreign molecules are present. The fluorescence efficiency of benzene is low, and yet benzene does not quench its own fluorescence effectively.[16]

The results on benzene sensitized dissociation of methyl iodide are susceptible of only a semiquantitative interpretation. The fact that the quantum yield shows no conclusive trend with benzene pressure is evidence for the lack of self-quenching by benzene. The quantum yield is dependent, as would be expected, on the pressure of methyl iodide, even though exact calculations of the quantum yield of the sensitized reaction are impossible. If one neglects self-quenching, assumes the lifetime of excited benzene to be 10^{-7} sec, and that process (2) competes with internal conversion and fluorescence, one may derive the equation

$$\Phi_D=(M)/((M)+k_5/k_2), \tag{5}$$

where k_5 would have the value of 10^7 sec^{-1}, Φ_D is the quantum yield of dissociation, (M) is the concentration of the dissociative molecules, and k_2 is the constant for reaction (2). Thus k_5/k_2 may be given the limits of 6×10^{16} and 4×10^{17} molecules/cc and $k_2=0.2$ to 2×10^{-10} (molecules$\times$sec)$^{-1}$ cc. This would indicate that with an uncertainty of a factor of about ten, every collision between excited benzene and methyl iodide is effective in producing dissociation. This is in essential agreement with the conclusions of West and his co-workers in the liquid phase.[14] The uncertainties in treating the data do not warrant a more detailed treatment. If a long-lived state of benzene (possibly a triplet state) were formed which could dissociate methyl iodide by collision, these conclusions would be invalid. There is no evidence that this is the case although further work should be done on this point.

---

[11] W. A. Noyes, Jr., J. Chem. Phys. **5**, 807 (1937); Henriques, Jr., Duncan, and Noyes, Jr., J. Chem. Phys. **6**, 518 (1938).

[12] E. Rabinowitch and W. C. Wood, J. Chem. Phys. **4**, 497 (1936); Trans. Faraday Soc. **32**, 907 (1936).

[13] W. A. Noyes, Jr. and P. A. Leighton, *The Photochemistry of Gases* (Reinhold Publishing Corporation, New York, 1941), p. 294.

[14] W. West and W. E. Miller, J. Chem. Phys. **8**, 849 (1940).

[15] P. Pringsheim, *Fluorescence and Phosphorescence* (Interscience Publishers, Inc., New York, 1949), p. 245.

[16] Reference 12, p. 265.

THE JOURNAL OF CHEMICAL PHYSICS VOLUME 19, NUMBER 12 DECEMBER, 1951

The Concentration of Molecules on Internal Surfaces in Ice

E. J. MURPHY
Bell Telephone Laboratories, Murray Hill, New Jersey
(Received September 24, 1951)

In this paper the experimental expression for the "local conductivity" of ice is given. This expression has two terms, one of which has already been discussed and brought into close relation with the structure of ice, that is, with its heat of sublimation and its lattice constant. This paper brings out another relation, deriving it from the second term of the experimental expression. It is concluded from an analysis outlined here that the second term of the local conductivity gives the concentration of molecules in "internal surfaces." For the specimen of ice to which this method was applied the concentration of molecules on internal surfaces comes out as 1.03×10^{17} molecules/cc.

This is proposed as a new method of studying imperfections (internal surfaces) in dielectric crystals, and one which seems to be well suited to this purpose. It gains its advantages from the fact that it is not dependent upon the regularity of the imperfections, as in x-ray diffraction methods, or upon the connectivity of the system of internal surfaces, as in direct current conduction.

IN investigating conduction in dielectrics the writer has found it convenient and useful to define a quantity which is related to the motions required to form the dielectric polarization as the ordinary dc conductivity is related to ionic migration. This quantity is described as the polarization conductivity or local conductivity. It is a property of dielectrics which exhibit anomalous dispersion, and it can be measured as the limit approached by the alternating current conductivity as the frequency increases, the direct current conductivity having been subtracted.

The significance of this quantity and the relations into which it enters will be described more fully in other connections, for the present discussion is confined to describing an application which contributes to the study of the "secondary structure" of ice and which should be capable of extension to other solids of suitable type.

THE "LOCAL CONDUCTIVITY" OF ICE

By means of a simple theory, similar to that for ordinary ionic conduction, the local conductivity of ice for the temperature interval 0°C to −35°C has been shown to be essentially determined by two fundamental constants of the crystal, its heat of sublimation and a suitable lattice constant.[1] However, when the measurements are extended to still lower temperatures it becomes evident that the local conductivity of ice is an expression with two terms: the full expression is

$$\sigma_p=631e^{-11500/RT}+1.06\times10^{-3}e^{-5170/RT}\ (\text{ohm cm})^{-1}. \quad (1)$$

The lowest temperature at which accurate measurements were made was −139°C (at −190°C the local conductivity was barely detectable). The conclusions already derived about the polarization in ice[1] were obtained from the first term in the above experimental expression.* We now show that the second term yields independent information about the structure; namely, the concentration of molecules in *internal surfaces*.

The expression for the local conductivity σ_p is in the form

$$\sigma_p=\sigma_{01}e^{-W_1/kT}+\sigma_{02}e^{-W_2/kT}\cdots, \quad (2)$$

where k is Boltzmann's constant, W_1 and W_2 are energies, and T the absolute temperature. Because this is a local conductivity and thus associated with a dielectric polarization rather than with dissociation into ions, the energy $W_i(i=1, 2)$ in the Boltzmann factor may be interpreted immediately as an activation energy.†

The activation energy in the first term is 11.5 kcal/M (or 0.5 ev). This activation energy agrees essentially with the heat of sublimation which in turn has been attributed to the breaking of two hydrogen bonds per molecule. (Each H_2O molecule in ice is held in place by four hydrogen bonds, but as each bond is counted twice the heat of sublimation represents the breaking of only two bonds *per molecule*.)

The experimental activation energy for local conduction in the second term (W_2) is 5.17 kcal/M. This is somewhat less than one-half of the activation energy in the first term (W_1), that is, $W_2/W_1=0.45$. If then W_1 represents the breaking of two hydrogen bonds in the act of forming the polarization, W_2 may be taken to represent a polarization depending upon the breaking of one hydrogen bond per molecule, if a basis can be found for this interpretation. In the following discussion it is assumed that W_2 is an activation energy representing the breaking of one hydrogen bond but that its value is 5.17 kcal/M, rather than precisely $0.5W_1$.§

TWO-TERM CONDUCTION IN GENERAL

When there are two terms in an experimental conduction expression, as illustrated by Eqs. (1) and (2), a

[1] E. J. Murphy, Phys. Rev. **79**, 396 (1950).

* Equation (1) is an experimentally determined relation expressing data obtained by the writer and published in part in E. J. Murphy, Trans. Am. Electrochem. Soc. **65**, 133 (1934), and E. J. Murphy and S. O. Morgan, Bell System Tech. J. **18**, 502 (1939), and in particular in Fig. 5 of the latter.

† The meaning of this statement will be discussed more fully in another connection where its use can be brought out more fully.

§ W_2 is a less accurately measured experimental constant than W_1, and it may be that its true value is more accurately given by $0.5W_1$, rather than the directly observed value.

certain general restriction applies to the possible interpretations. For an expression of this kind can only be observed experimentally when σ_{02} is much smaller than σ_{01}, if W_2 is appreciably smaller than W_1; otherwise, the term with the smaller activation energy completely submerges the other term, which then is unobservable by this method. Consequently, whatever the explanation adopted for the term of smaller activation energy, it must yield a small value for the coefficient σ_{02}. We now consider various ways of achieving this, by returning to the theoretical expression for σ_p derived in reference 1. This expression, based upon a simple model, is

$$\sigma_p=(9\times10^{11}h)^{-1}ne^2d^2\exp(-W/kT)\ (\text{ohm cm})^{-1} \quad (3)$$

or

$$\sigma_{02}=ne^2d^2/9\times10^{11}h, \quad (4)$$

where e and h are universal constants, n is the number of protons per cc contributing to the second term in the local conductivity, and d is the distance moved by a proton in making its contribution to the polarization.

Four possible ways of making σ_{02} small as compared with σ_{01} appear in Eq. (4): (1) Making d much smaller than the value (0.39A) which served to give agreement between theory and experiment for the first term. But we know of no lattice constant of suitable length to give such a factor. (2) The possibility exists, in general, that neighboring molecules occasionally find themselves in especially favorable configurations for forming the polarization by preserving the activation energy among a set of neighboring molecules. In effect this amounts to local conduction by a comparatively small number of units, each consisting of a considerable number of unit cells and with a negative entropy of activation. This would introduce a further fractional factor in Eq. (4); but many neighboring unit cells would have to cooperate to produce as small a factor as is observed experimentally. Moreover there is no independent evidence for the occurrence of such structures. Therefore this possibility, like the first-mentioned one, is set aside. (3) The explanation of the second term, which ordinarily would be the first considered, is the presence of impurities. But the ice was prepared from good conductivity water and its impurity content is as small as could be achieved without disproportionate elaboration of the purification aspect of the experiments. For our purpose it is sufficient that there are no known impurities present which could account for the second term; we therefore set this possibility aside. (4) We are left then, with the remaining possibility that the second term represents the contribution of molecules in internal surfaces.

To summarize: both (3) and (4) single out from the totality of molecules in the crystal a comparatively small set which are in a different environment from the bulk of molecules. We have chosen to make σ_{02} small by making n small, and to do this by identifying n (for the second term) with the concentration of molecules on internal surfaces. This choice will be shown in the later discussion to lead to interesting results.

INTERNAL SURFACES

In the homogeneous interior of a specimen of ice each H_2O molecule is held in place by four hydrogen bonds. On an external surface each H_2O molecule is held in position by only two hydrogen bonds. For our purposes then we define an internal surface similarly. Definition: a molecule is in an internal surface if it is held in position only by about half the maximum number of bonds, that is, by two instead of by four hydrogen bonds in the case of ice. In order for this condition to prevail there must also be in the internal surface some space not occupied by H_2O molecules in crystal arrangement. This definition says nothing about how large a set of molecules is required to form an internal surface, about the shape of the surface, or about how it is produced. Nothing is implied except what is stated in the definition; namely, that there are molecules held in position by less than the maximum number of bonds, specifically by about one-half that number. The smallest internal surface would be one produced by the removal of a single molecule, or by some equivalent process which produced one molecule which is held in position by only two bonds.

On the basis of the hypothesis adopted here, the ratio of the coefficients of the two terms of the conduction formula (Eq. (2)) is the ratio of the number of molecules in internal surfaces to the total number of molecules in the crystal; its value is 1.67×10^{-6}. Multiplying the total number of molecules per cc by this fraction gives 1.03×10^{17}, as the number of molecules on internal surfaces per cubic centimeter of ice. (The second term had a somewhat different value for different specimens of ice, as would be expected on this interpretation of its origin. Therefore the concentration given above refers to a particular specimen, and other specimens may have somewhat different concentrations.) The concentration can also be obtained by substituting the value $\sigma_0=1.06\times10^{-3}$ (ohm cm)$^{-1}$ in the theoretical expression for the conductivity and solving for n, the concentration of molecules contributing to this term in the conduction. The two calculations of concentration are not independent, but the second method is mentioned because it brings out the fact that the theoretical expression may be applied to the second term as well as to the first.

The above calculation gives the concentration of a certain kind of structural defect in the crystal lattice by giving the number of molecules contained in such defects. It is evident that this is not a complete specification of the defect, for the shape of the internal surface is not given.

COMPARISON WITH FREE-ION CONDUCTION

The interpretation of the second term which we have used here recalls the proposal made by Smekal[2] in 1927

[2] A. Smekal, Z. tech. Physik 8, 561 (1927).

that the second term so often observed in the dc conductivity of crystals is due to "Lockerstellen," that is, to distortions of structure equivalent to what we mean by internal surfaces. When applied to dc conductivity this explanation of the term of lower activation energy suffers from the handicap that the "connectivity" of the system of internal surfaces should determine the dc conductivity quite as much as the number of molecules contained in them; for example, an isolated internal surface would not affect the dc conductivity. On this account it has not been possible to draw quantitative conclusions about the concentrations of ions on internal surfaces merely by taking the ratio of the two terms of the dc conduction formula. But the local conductivity is essentially independent of the connectivity of the system of internal surfaces; for example it receives contributions from isolated internal surfaces. The total number of molecules in isolated internal surfaces would ordinarily be expected to be greater than the number in connected internal surfaces; for the probability of multiple intersections of randomly distributed internal surfaces is small. (How small would depend on the size of the internal surfaces and how they were created; and the possibility would exist of comparing dc and ac conductivity so as to get a rough measure of the degree of connectivity and the size of the connected internal surfaces.)

In dealing with dc conduction on internal surfaces the degree of ionization of the molecules present there is a variable. But in dealing with the local conductivity the degree of ionization is not a variable, for we are mainly concerned with molecules rather than ions. It is however a fact that a third factor enters in this connection; namely, the contribution to apparent polarization coming from space charges in internal surfaces. This is a comparatively small effect, because the degree of dissociation is small in most cases. In any case it can, in principle, be separated from the main effect by means of its relaxation time.

DISCUSSION

The second term in the local conductivity of a dielectric exhibiting sufficiently simple anomalous dispersion can then be used as a measure of the concentration of molecules on internal surfaces. On the other hand, a second term in the direct-current conductivity (the conductivity due to free ions) could not be so used because the complicated connectivity of the system of internal surfaces is a practically complete barrier between the measured conductivity values and any molecular interpretation of them. (However, the second term in the dc conductivity has been used by the writer to obtain the concentration of *impurities* in a crystal. This will be discussed more fully elsewhere.)

The study of imperfections in a crystal is made difficult by the very nature of imperfections: they are ordinarily present in small concentration and irregular in size and shape. The lack of regularity handicaps analysis by x-ray diffraction, which only shows a feature of structure when it is repeated regularly a sufficient number of times, while the low concentration handicaps almost any method of analysis. It is suggested that the local conductivity method illustrated in the present data for ice may be of use in the analysis of aspects of structure such as internal surfaces not easily accessible to other methods.

The advantages claimed for this method depend upon three features: (1) the fact that a definition of internal surface is used which gives molecules in it a characteristic activation energy by which they can be recognized and differentiated from other molecules, (2) the fact that the local conductivity does not depend on the "connectivity" of the system of internal surfaces nor on their shape or the degree of order in them, and (3) the fact that the local conductivity does not depend significantly on the degree of dissociation into ions in the internal surfaces within the limits likely to be practically important.

Lattice Theories of the Liquid State*

J. S. ROWLINSON† AND C. F. CURTISS
The Naval Research Laboratory, Department of Chemistry, University of Wisconsin, Madison 6, Wisconsin
(Received August 14, 1951)

The assumptions underlying the lattice theory of liquids of Lennard-Jones and Devonshire are examined. Four modifications of this theory have been proposed which avoid some of these assumptions. These modifications are (a) by Cernuschi and Eyring, (b) by Ono, (c) by Peek and Hill, and (d) one suggested in this paper. It is shown that they may all be deduced as special cases of one mathematical treatment. They are intuitively more attractive than the original theory and avoid any mention of the so-called "communal entropy." They give reasonable values of the second virial coefficient. None of them, though, shows much improvement over the original theory in calculating the critical constants and vapor pressure curves.

NOTATION

r_0, ϵ	The distance and energy characteristic of the intermolecular potential. $E(r_0)=0$, and $-\epsilon$ is the minimum of the curve.
$a, E(0)$	The distance between two neighboring lattice sites and the energy of two molecules on such sites.
τ	The reduced temperature $=kT/\epsilon$.
v_0	$=r_0^3$.
b_0	$=\frac{2}{3}\cdot\pi\cdot N r_0^3$.
q	The reduced cell-size $=a^3/r_0^3\sqrt{2}$.
z	The coordination number of the lattice $=12$.
v	Volume per molecule.
V	Volume per mole.
x	$=\rho q$.
g, g_l, g_m	Integrals related to the free-volume and its derivatives. Eqs. (9), (14), (15). When primed the same functions at a temperature of $\tau/(1-\bar{\omega})$.
ξ	$=2g_l/g$. Eq. (13).
η	$=2g_m/g$. Eq. (13).
α	$1-\exp\{-2\zeta/zkT\}$, Eqs. (32), (40), (57), (70).
ζ	Equation (28).
β	$\beta^2=1-4x(1-x)\alpha$.
ω	The proportions of vacant sites around any one lattice site.
$\bar{\omega}$	The mean value of $\omega=2(1-x)/(\beta+1)$, Eq. (33).
$j(\omega)$	The generalized free-volume corresponding to ωz vacant sites around one lattice site. Eq. (25).
j_0, j_1	The values of $j(0)$ and $j(1)$ in the particular approximation being used. Eq. (26).
$J(x, \alpha)$	Equation (43).

I. INTRODUCTION

An exact theory of the liquid state is being developed by the methods of Kirkwood and Born and Green. Until this reaches the state at which numerical results can be obtained, it seems useful to discuss a less rigorous, though so far, more fruitful, approach. Liquids have been considered both as disordered solids and as very dense gases for the purpose of constructing approximate theories. Probably the first view has been more useful, as it is easier to extend these theories to include gases than it is to extend theories of dense gases to include liquids. It is these lattice, or "solid-like," theories of the liquid state which will be discussed here. The principal characteristic of all such theories is that they consider each molecule to be confined to the neighborhood of one of the lattice sites by the surrounding molecules. It is usual to consider only the effect of nearest neighbors on the motion of the molecule within its "cell."

Between the years 1936 and 1941, Eyring and those who worked with him,[1–7] made much progress in correlating the various properties of liquids by means of theories which assumed a regular lattice structure. These papers introduced the important idea that some of the lattice sites might be vacant. It was postulated that these vacant sites, or "holes," played a particularly important role in determining the behavior of a liquid near its critical point. However, this approach was, on the whole, empirical. No attempt was made to calculate the macroscopic properties directly from the intermolecular forces, but rather, theoretical considerations were used to relate different macroscopic properties to each other. In 1937 Lennard-Jones and Devonshire[8] placed the lattice theory on a more quantitative basis by introducing certain assumptions about the geometry of the distribution of lattice sites, the size of the cell surrounding each site and to which each molecule is confined, and about the motion of each molecule within its cell. These assumptions allowed them to obtain explicit relations between the thermodynamic properties and the intermolecular forces. All later refinements have been based on this model. Kirkwood[9] has shown re-

* This work was carried out under Contract NOrd 9938 with the Navy Bureau of Ordnance.
† Present address: University of Manchester, Manchester, England.

[1] H. Eyring, J. Chem. Phys. **4**, 283 (1936).
[2] H. Eyring and J. Hirschfelder, J. Chem. Phys. **41**, 249 (1937).
[3] Hirschfelder, Stevenson, and Eyring, J. Chem. Phys. **5**, 896 (1937).
[4] J. F. Kincaid and H. Eyring, J. Chem. Phys. **5**, 587 (1937).
[5] J. F. Kincaid and H. Eyring, J. Chem. Phys. **6**, 620 (1938).
[6] F. Cernuschi and H. Eyring, J. Chem. Phys. **7**, 547 (1939).
[7] J. Walter and H. Eyring, J. Chem. Phys. **9**, 393 (1941).
[8] J. E. Lennard-Jones, Proc. Roy. Soc. (London) **A106**, 463 (1934).
[9] J. G. Kirkwood, J. Chem. Phys. **18**, 380 (1950).

cently that the partition function derived from this model is a first approximation to the exact partition function, under certain well-defined approximations. However, both the original theory of Lennard-Jones and Devonshire and later improvements have been developed intuitively rather than as a well-defined series of successive approximations.

The theory of Lennard-Jones and Devonshire is discussed briefly. Some objections are mentioned including the uncertainty about what Eyring called the "communal entropy." The main part of the article is given to a discussion of four modifications of this theory which have been proposed since 1939. These all attempt to improve the theory by introducing into it Eyring's idea of "holes." One of their main virtues is that by using this idea they avoid any direct reference to the communal entropy. It is shown that there is one standard mathematical development which allows these four modifications to be obtained quite simply as four special cases. The form of the equation of state given by each is discussed and a comparison is made of the numerical results which they predict.

Classical statistical mechanics is used. Quantum corrections are important when considering the solid state, but except for helium, hydrogen, and probably neon, may be ignored in considering the liquid and gaseous states. One form of the intermolecular potential, due to Lennard-Jones, is used throughout. The energy of interaction of two spherical molecules at distance apart r is given by

$$E(r)=4\epsilon\{(r_0/r)^{12}-(r_0/r)^6\}. \quad (1)$$

Here r_0 and ϵ are the distance and energy characteristics of the potential. From Eq. (1), $E(r_0)=0$ and $E(r_0 2^{1/6})=-\epsilon$, the minimum value of $E(r)$. This potential has been very successful in interpreting both the equilibrium and transport properties of gases at low densities. As the potential has only two adjustable parameters, any equation of state based upon it conforms to the law of corresponding states.

It is assumed that the internal energy of each molecule is independent of its environment. Such energies are therefore ignored in writing down the partition functions.

II. THE THEORY OF LENNARD-JONES AND DEVONSHIRE

The assumptions of this theory are:

(1) Each molecule is considered to be confined to a cell by its nearest neighbors. Exchange of molecules between cells is ignored. The partition function of the whole assembly is, therefore, the product of the N individual partition functions. The fact that the whole volume is not available to each molecule is probably of little importance at high densities. In the limit of low densities it means that the partition function is too low by a factor of $N!/N^N \approx e^{-N}$. The free energy is high by RT. This may be formally accounted for by inserting an extra factor of e^N in the partition function. The extra term in the free energy is not a function of volume and so will not affect the equation of state. However, this is not very satisfactory. The factor of e^N is needed in the perfect gas limit, but not in the perfect crystal. Somewhere between these limits, it must become effective. Hirschfelder, Stevenson, and Eyring[3] took the view that it appears discontinuously at the melting point, where it contributed an extra amount of entropy R to the liquid. They called this term the "communal entropy." Rice[10] criticized this view and maintained the factor appeared more gradually. This would make it a function of volume as well as temperature and so would cause it to contribute to the equation of state.

(2) Each cell is occupied. Its volume is $v=V/N$. The exact shape of the cell should be fixed by defining it as that part of space which lies nearer to the cental molecule than to any other, but for practical purposes each cell is taken to be a sphere. If the lattice sites form a face-centered cubic structure the volume of this sphere is $a^3/\sqrt{2}$, where a is the distance between lattice sites. The number of nearest neighbors, z, to each lattice site is twelve for such a structure. This value is used in all calculations.

(3) The potential energy inside each sphere is assumed to be spherically symmetrical. It is found by averaging over all angles the potential due to 12 molecules at distance a. There are two approximations involved here: first, the assumption of symmetry, and secondly, the assumption that all neighbors are at distance a. Peek and Hill[11] think that the first is the greater source of error, particularly when the theory is modified to allow for some of the sites being vacant. The second assumption is similar to the Hartree approximation in quantum mechanics.

The mean energy of a molecule at a distance r from the center of its cell, due to one neighbor at distance a from this center is given by

$$\overline{E(r)}=\tfrac{1}{2}\int_0^\pi E([r^2+a^2-2ar\cdot\cos\theta]^{\frac{1}{2}})\cdot\sin\theta\cdot d\theta. \quad (2)$$

If z molecules surround each lattice site, then the mean energy of the central molecule is given by

$$z(\overline{E(r)}-E(0))=z\epsilon\{q^{-4}\cdot l(y)-2q^{-2}\cdot n(y)\}. \quad (3)$$

Here $zE(0)$ is the energy at the center of the cell. On the right-hand side, q is the reduced volume of the cell given by (for $z=12$),

$$q=a^3/r_0^3\sqrt{2}=v/r_0^3=v/v_0 \quad (4)$$

where,

$$y=r^2/a^2, \quad (5)$$

[10] O. K. Rice, J. Chem. Phys. **6**, 476 (1938).
[11] H. M. Peek and T. L. Hill, J. Chem. Phys. **18**, 1252 (1950).

and

$$l(y)=(1+12y+25.2y^2+12y^3+y^4)(1-y)^{-10}-1, \quad (6)$$

$$n(y)=(1+y)(1-y)^{-4}-1. \quad (7)$$

A "free volume" $j(0)$ may be defined by

$$j(0)=2\pi a^3\cdot g=\int_{\text{cell}} \exp\{-z[\overline{E(r)}-E(0)]/kT\}\cdot dr, \quad (8)$$

or

$$g=\int_0^s y^{\frac{1}{2}}\cdot\exp\left\{\frac{-z}{\tau}[q^{-4}\cdot l(y)-2q^{-2}\cdot n(y)]\right\}\cdot dy, \quad (9)$$

where, for a face-centered cubic lattice,

$$s=(3/4\pi\sqrt{2})^{\frac{1}{3}}=0.30544. \quad (10)$$

At infinite temperature $j(0)$ is $a^3/\sqrt{2}$, the volume of the cell. At finite temperature $j(0)$ is smaller than this, as each part of the cell is weighted with the approximate Boltzmann factor.

The partition function of a single molecule is given by

$$f=(2\pi mkT/h^2)^{\frac{3}{2}}\cdot 2\pi a^3\cdot g\cdot\exp\{-z\cdot E(0)/2kT\}. \quad (11)$$

The free energy and other thermodynamic properties may be expressed in terms of the partition function of the whole assembly, $Z=e^N\cdot f^N$. Here the communal entropy is arbitrarily included. The equation of state is given by (for $z=12$),

$$pV/RT=1+(24/\tau)[q^{-4}\cdot(1+\xi)-q^{-2}\cdot(1+\eta)]. \quad (12)$$

The symbols ξ and η are defined by

$$\xi=2g_l/g, \quad \eta=2g_m/g. \quad (13)$$

The integrals g_l and g_m are related to the derivative of g with respect to volume or temperature. They are defined by

$$g_l=\int_0^s y^{\frac{1}{2}}\cdot l(y)\times\exp\left\{\frac{-z}{\tau}[q^{-4}\cdot l(y)-2q^{-2}\cdot n(y)]\right\}\cdot dy, \quad (14)$$

$$g_n=\int_0^s y^{\frac{1}{2}}\cdot n(y)\times\exp\left\{\frac{-z}{\tau}[q^{-4}\cdot l(y)-2q^{-2}\cdot n(y)]\right\}\cdot dy. \quad (15)$$

The density enters into the right-hand side of Eq. (12) through the reduced cell-size (Eq. 4). (pV/RT) approaches the perfect gas limit of unity, if τ or q become large, that is, at high temperatures or low densities. Equation (12) shows a critical point, below which the isotherms are sigmoid.

Values of the integrals g, g_l, and g_m have been worked out by Lennard-Jones and Devonshire,[8] by Prigogine and Raulier;[12] by Prigogine and Garikian;[13] by Hill;[14] and by Wentorf, Buehler, Hirschfelder, and Curtiss.[15] These are in satisfactory agreement. Prigogine and Garikian also used other intermolecular potentials and showed that the thermodynamic properties were not sensitive to the shape of the potential.

This theory may be modified slightly to include the effect of the "shells" of molecules outside the nearest twelve. The coefficients of q^{-4} and q^{-2} in Eq. (12) become $1.0110(1+\xi)$ and $1.2045(1+\eta)$, respectively. This step was taken by Lennard-Jones and Devonshire. Wentorf, Buehler, Hirschfelder, and Curtiss included this effect when they computed the integrals g, g_l, and g_m. They replaced $l(y)$ and $m(y)$ by

$$L(y)=l(y)+(1/128)\cdot l(y/2)+(2/729)\cdot l(y/3), \quad (16)$$

and

$$M(y)=n(y)+(1/16)\cdot n(y/2)+(2/27)\cdot n(y/3). \quad (17)$$

These refinements make little difference to the results obtained.

III. FOUR MODIFICATIONS OF THE THEORY OF LENNARD-JONES AND DEVONSHIRE

These newer theories improve two of the assumptions made by Lennard-Jones and Devonshire. The communal entropy does not appear, and vacant cells are permitted. The third assumption, concerning the motion of the molecule within the cell, is retained. The general theory underlying all four modifications is presented first. The four special cases may then be deduced quite simply. The treatment of the general case follows most closely that of Ono.[16]

Consider the volume V, occupied by N molecules, to be divided into L cells, where $L\geqslant N$. The cell size, V/L, must be large enough for interactions between molecules which are not in adjacent cells to be ignored, but small enough for the chance of finding more than one molecule in a cell to be ignored. The number of cells, L, may change with both temperature and density. All cells are occupied in the theory of Lennard-Jones and Devonshire, and so the cell size increases as the density diminishes. If unoccupied cells are allowed, then it is possible to keep the cell size constant as the density diminishes and increase the number of holes. This is done in the first two approximations below. Alternatively, both the cell size and the number of holes may change with density. This is done in the third and fourth approximation. These differences may seem to be purely formal, as the cells are only imaginary, but they make considerable differences in the numerical predictions of the theories, particularly at low densities.

[12] I. Prigogine and S. Raulier, Physica **9**, 396 (1942).
[13] I. Prigogine and G. Garikian, J. Chim. Phys. **45**, 273 (1948).
[14] T. L. Hill, J. Phys. Colloid Chem. **51**, 1219 (1947).
[15] Wentorf, Buehler, Hirschfelder, and Curtiss, J. Chem. Phys. **18**, 1484 (1950).
[16] S. Ono, "Memoirs of the Faculty of Engineering," Kyushu University, Japan **10**, 190, No. 4 (1947).

The configuration partition function, Z_q is related to the total partition function of the whole assembly by

$$Z=[(2\pi m\cdot kT)/(h^2)]^{3N/2}\cdot Z_q. \tag{18}$$

There Z_q is given by the following sum of integrals over each cell,

$$Z_q=\sum\int dr_1\cdots\int dr_N\cdot e^{-E/kT}. \tag{19}$$

The sum is over all arrangements of N molecules in L cells which differ by more than a simple permutation of the molecules, and in which there is no more than one molecule per cell. The total potential energy of the system with respect to molecules at infinite separation is E.

Let $E(0)$ again be the energy of interaction between two molecules on neighboring sites. Then if $z\omega_i$ cells are vacant and $z(1-\omega_i)$ are occupied around the ith molecule, the potential energy at the center of the cell is

$$z(1-\omega_i)E(0) \tag{20}$$

and the potential energy of the whole assembly is

$$E=(z/2)\cdot(N-X)\cdot E(0), \tag{21}$$

where

$$X=\sum_i\omega_i. \tag{22}$$

The quantity X is characteristic of a particular configuration and is not defined completely by the number of holes. Then

$$E=(z/2)(N-X)\cdot E(0)+\sum_i(1-\omega_i)\cdot u_i, \tag{23}$$

where u_i is the instantaneous value of the energy of the ith molecule above the center of its cell, if that cell had z nearest neighbors. The third assumption in the theory of Lennard-Jones and Devonshire has been used in writing down the last term of Eq. (23). It has been assumed that the energy in a cell with ωz vacant neighbors is $(1-\omega)$ times that of one with none. The energy does not have such a simple dependence on ω, and depends on the arrangement of the vacant sites as well as on their number.

Equations (19) and (23) give

$$Z_q=\sum\exp\left\{\frac{-z(N-X)\cdot E(0)}{2kT}\right\}\cdot\prod_i j(\omega_i), \tag{24}$$

where

$$j(\omega_i)=\int_{\text{cell}}\exp\{-(1-\omega_i)u_i/kT\}\cdot dr_i. \tag{25}$$

If all the cells around the ith molecule are occupied then $\omega_i=0$ and $j(\omega_i)$ is identical with $j(0)$ of Eq. (8). If all the surrounding cells are empty, the $\omega_i=1$, and $j(1)$ becomes the volume of the cell. Thus $j(\omega)$ is a generalization of the concept of a "free volume." Equation (25) shows that $j(\omega)$ does not depend on ω in any simple way. However, it is necessary to assume some simple dependence in order to be able to sum Eq. (24). The logarithm of $j(\omega)$ is taken to be a linear function of ω. This line may be fixed at any given temperature and cell size, by its intercept at $\omega=0$ and $\omega=1$, which are denoted j_0 and j_1, respectively. That is,

$$\ln j(\omega)=\omega\cdot\ln j_1+(1-\omega)\cdot\ln j_0. \tag{26}$$

The values of j_0 and j_1 need not be specified yet, but it should be noted that they are not necessarily equal to $j(0)$ and $j(1)$. The four approximations described below correspond to four different choices of j_0 and j_1. Equation (26) simplifies the expression for Z_q as each term in the sum now depends only on $X=\sum\omega_i$, rather than on the complete details of the configuration.

$$Z_q=j_0{}^N\cdot\exp\left\{\frac{-N\cdot z\cdot E(0)}{2kT}\right\}\times\sum_X G(N,L,X)\cdot\exp\left\{\frac{X\zeta}{kT}\right\}, \tag{27}$$

where

$$\zeta=(z/2)\cdot E(0)+kT\cdot\ln(j_1/j_0), \tag{28}$$

and $G(N, L, X)$ denotes the number of ways of arranging N molecules on L sites to give X pairs of "holes" and molecules on adjacent sites. The function G cannot be evaluated explicitly. It may be estimated by means of the "quasi-chemical approximation" worked out in different forms by Guggenheim and by Bethe. (See Fowler and Guggenheim[17] pages 246–51, 361–64, 437–43.) The result is

$$Z_q=\binom{L}{N}\cdot j_0{}^N\cdot\exp\left\{\frac{-Nz\cdot E(0)}{2kT}\right\}\times\left[\frac{x(\beta+1-2x)}{(1-x)(\beta-1+2x)}\right]^{Nz/2}\times\left[\frac{(1-x)(\beta+1)}{(\beta+1-2x)}\right]^{Lz/2}, \tag{29}$$

where

$$x=N/L=v_0q/v \tag{30}$$

$$\beta^2=1-4x(1-x)\alpha \tag{31}$$

and

$$\alpha=1-\exp\{-2\zeta/zkT\}. \tag{32}$$

x is related to the average number of holes around any one molecule, $z\tilde{\omega}$, by

$$\tilde{\omega}=2(1-x)/(\beta+1). \tag{33}$$

At high densities, $x\to1$, $L\to N$, and $\tilde{\omega}\to0$. At low densities $x\to0$, $L\gg N$, and $\tilde{\omega}\to1$, while the cell size, q, and α both remain finite. The limiting forms of Eq. (29) at high and low densities are:

(High density)

$$Z_q=j_0{}^N\cdot\exp\left\{\frac{-Nz\cdot E(0)}{2kT}\right\}; \tag{34}$$

[17] R. H. Fowler and E. A. Guggenheim, *Statistical Thermodynamics* (Cambridge University Press, London, 1939).

(Low density)

$$Z_q=\binom{L}{N}\cdot q^N\approx e^N\cdot\left(\frac{V}{N}\right)^N. \tag{35}$$

If j_0 is the same as $j(0)$, then Eq. (34) is the Einstein approximation to the partition function of a crystal. The presence of the factor of e^N in Eq. (35) shows that the partition function for a perfect gas is given correctly. Thus, Eq. (29) avoids all mention of the doubtful "communal entropy" and goes smoothly from the highest to the lowest density.

The free energy per mole corresponding to Eq. (29) is given by

$$\left(\frac{A}{RT}\right)=\frac{z}{2}\cdot\frac{E(0)}{kT}-\frac{3N}{2}\cdot\ln\left(\frac{2\pi mkT}{h^2}\right)$$

$$-\ln j_0+\frac{1}{x}\{x\ln x+(1-x)\ln(1-x)\}$$

$$+\frac{z}{2x}\left\{x\ln\frac{\beta-1+2x}{x(\beta+1)}+(1-x)\ln\frac{\beta+1-2x}{(1-x)(\beta+1)}\right\}. \tag{37}$$

The pressure may be found by differentiating A with respect to volume at constant temperature and cell size. This cannot be done until it is known what approximation to use for j_0 and j_1. When these have been chosen, Eq. (37) gives the free-energy as a function of density, temperature and cell size. The latter must be eliminated before numerical calculations can be made. This may be done either by putting it equal to some arbitrary constant, independent of the density and temperature, or else by choosing it to make the free energy a minimum at each density and temperature. The latter course is to be preferred on theoretical grounds. The former, though, has the advantage that it sometimes allows explicit expressions to be written down for the critical constants.

The Approximations for the Generalized Free-Volume $j(\omega)$

The four different approximations for $j(\omega)$ as a function of ω must now be considered. Equation (25) shows that $j(\omega)$ at a temperature of T is the same as $j(0)$ at a temperature of $T/(1-\omega)$ and at the same cell size. It is thus theoretically possible to find the dependence of $j(\omega)$ on ω from tables of g as a function of temperature, using:

$$j(\omega,\tau)=2\pi a^3\cdot g\left(0,\frac{\tau}{1-\omega}\right). \tag{38}$$

Figure 1 shows a typical curve for $j(\omega)$. The value of $j(1)$ is always $a^3/\sqrt{2}$, when $z=12$. The value of $j(0)$ depends on q and τ; the smaller the cell size or the lower the temperature, then the larger, in general, the ratio of $j(1)/j(0)$. It has been assumed in the derivation of Eq. (37) that $\ln j(\omega)$ is a linear function of ω. Figure 1 shows that this is not a good approximation. However, the four choices which have been made are shown as the four dashed lines (a)–(d). At any temperature and density, it is reasonable to suppose that the best approximation will be that which best reproduces the features of the curve near $\bar{\omega}$, the average value of ω. Therefore, the chronological order, which is followed, should go from the worst to the best approximation.

(a) *The Approximation of Cernuschi and Eyring*

Cernuschi and Eyring[6] determined the distribution of molecules among cells by the method which Bethe used to treat order-disorder transitions in alloys. It has been shown that this method, although very different in appearance, is the same as the quasi-chemical approximation (see Fowler and Guggenheim,[17] pages 589–598). However, as Kirkwood[18] pointed out, they did not consider the effect of the vacant cells on the partition function of the individual molecule within its cell. That is, they put

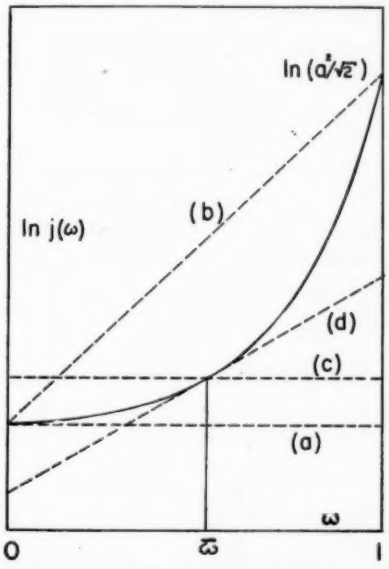

FIG. 1. The dependence of $j(\omega)$ on ω. The four approximations are shown by dotted lines (a) Cernuschi and Eyring (see reference 6) (1939), (b) Ono (see references 16 and 25) (1947), (c) Peek and Hill (see reference 11) (1950), and (d) This paper. $\bar{\omega}$ is the average value of ω at the temperature, density and cell size for which the curve was drawn.

$$j_0=j_1=j(0)=2\pi a^3\cdot g=2\pi\sqrt{2}\cdot r_0^3\cdot q\cdot g. \tag{39}$$

This gives for α, Eq. (28), (32),

$$\alpha=1-\exp\{-(1/\tau)(q^{-4}-2q^{-2})\}, \tag{40}$$

since

$$E(0)/kT=(1/\tau)(q^{-4}-2q^{-2}) \tag{41}$$

from Eqs. (1) and (4). The equation for the free-energy may be found by putting these expressions for j_0 and j_1

[18] J. G. Kirkwood, J. Chem. Phys. 7, 908 (1939).

and α into Eq. (37). The equation of state is given by

$$(pV/RT)=-V(\partial/\partial V)_{\tau,q}(A/RT) \tag{42}$$

$$=-\frac{1}{x}\left\{\ln(1-x)+(z/2)\ln\frac{(\beta+1-2x)}{(1-x)(\beta+1)}\right\}. \tag{43}$$

The right-hand side of Eq. (43) is a function of x and α only. It is denoted by $J(x, \alpha)$ as it occurs frequently in equations yet to be deduced. A similar expression occurs whenever the quasi-chemical approximation is applied. See, for example, Fowler and Guggenheim,[17] regular solutions, Eq. (819, 10), or adsorbed molecules, Eq. (1012, 15).

At low densities $x\rightarrow 0$, $\tilde{\omega}\rightarrow 1$, $\beta\rightarrow 1$. Here $J(x, \alpha)$ may be expanded as a power series in x, if the cell size remains finite. The second virial coefficient may be found by comparison with the virial expansion,

$$pV/RT=1+B/V+C/V^2+\cdots; \tag{44}$$

this gives

$$B=\tfrac{1}{2}Nv_0q(1+z\alpha). \tag{45}$$

Equation (43) shows a critical point. The isotherms are sigmoid for temperatures below the critical. The conditions for equilibrium of the vapor and liquid at a given temperature are the equality of the pressure and partial mole free-energy in each phase. The conditions are, respectively,

$$\left(\frac{\partial A_l}{\partial v_l}\right)_{N_l}=\left(\frac{\partial A_g}{\partial v_g}\right)_{N_g} \tag{46}$$

$$\left(\frac{\partial A_l}{\partial N_l}\right)_{v_l}=\left(\frac{\partial A_g}{\partial N_g}\right)_{v_g}, \tag{47}$$

when the subscripts denote liquid and gas. These conditions yield nothing simple unless it is assumed that the cell size is a constant, so that $(\partial\alpha/\partial v)_\tau=0$. Equations (46) and (47) then give

$$x_l+x_g=1, \quad \text{and so} \quad \beta_l=\beta_g, \tag{48}$$

and

$$\ln\left(\frac{1-x_l}{x_l}\right)=\frac{z}{z-2}\ln\left(\frac{\beta+1-2x_l}{\beta-1+2x_l}\right). \tag{49}$$

The gas and liquid phase become identical at the critical point and so Eq. (48) gives

$$x_c=\tfrac{1}{2}. \tag{50}$$

The other critical constants may be found by using two relations which hold at the critical point,

$$V\cdot(\partial/\partial V)_T(pV/RT)=(pV/RT); \tag{51}$$

$$V^2\cdot(\partial^2/\partial V^2)_T(pV/RT)=0. \tag{52}$$

Either of these, together with $x_c=\frac{1}{2}$ gives

$$\beta_c=z/(z-2) \quad \text{and} \quad \tilde{\omega}_c=(z-2)/2(z-1). \tag{53}$$

If z has its usual value of 12, then $\tilde{\omega}_c=5/11$. Thus the proportion of vacant cells around any one molecule, is on the average, nearly half at the critical point. These values of x_c and β_c give, for $z=12$,

$$(pV/RT)_c=2\ln 2+11\ln 11-12\ln 12=0.342, \tag{54}$$

and

$$\frac{-E(0)}{RT_c}=2\ln\frac{z}{z-2} \quad \text{or} \quad \frac{RT_c}{-E(0)}=2.742. \tag{55}$$

These numbers are discussed later. Equation (55) is interesting. First, it shows that there is no critical point if $E(0)$ is not negative. That is, two molecules on adjacent sites must attract each other for a fluid to pass from the gas to the liquid state. Secondly, it shows that there is no critical point in a hypothetical one-dimensional gas, where $z=2$. The equation of state of such a gas may be obtained rigorously and does, indeed, show no two-phase region.

(b) *The Approximation of Ono*

Ono[16] allows for the dependence of $j(\omega)$ on ω by putting

$$\begin{aligned} j_0&=j(0)=2\pi a^3\cdot g=2\pi\sqrt{2}\cdot r_0^3\cdot q\cdot g,\\ j_1&=j(1)=a^3/\sqrt{2}=r_0^3\cdot q. \end{aligned} \tag{56}$$

This approximation has the correct value at the extremes of high and low densities, but need not be very good in between. The equation of state is still formally given by Eq. (43) though α is now defined by

$$\alpha=1-\exp\{-(1/\tau)(q^{-4}-q^{-2})+(2/z)\ln 2\pi\sqrt{2}g\}. \tag{57}$$

The second virial coefficient is given by Eq. (45). If the cell size is a constant then the critical point may be found as before. Equations (48), (49), (50), (53), and (54) still apply. Equation (55) becomes

$$-E(0)/RT_c=2\ln\frac{z}{z-2}+(2/z)\ln(j_1/j_0). \tag{58}$$

Equation (58) cannot be solved without knowing the ratio j_1/j_0 as a function of temperature. Its solution is considered later.

Instead of taking the cell size constant, as Ono did, it is possible to minimize the free energy with respect to it. The free energy is found from Eq. (37) by inserting the appropriate values of j_0, Eq. (56) and α, Eq. (57). Differentiation with respect to V at constant q gives the equation of state and differentiation with respect to q and constant V gives the cell size. The two equations may be combined to give, for $z=12$.

$$(pV/RT)=J(x, \alpha)$$

$$=1+\frac{24(1-\tilde{\omega})}{\tau}[q^{-4}(1+\xi)-q^{-2}(1+\eta)]. \tag{59}$$

The first part of this equation is the same as Eq. (43).

The second part is very similar to Eq. (12), the equation of state given by the straightforward treatment of Lennard-Jones and Devonshire. The only formal difference is the appearance of the factor $(1-\bar{\omega})$ in the last term. The two equations behave differently, though, in the limit of low densities. In the treatment of Lennard-Jones and Devonshire, the cell size q is proportioned to the molar volume and so the last term on the right of Eq. (12) becomes small as q becomes large. In Eq. (59) the cell size generally increases as the density diminishes but always remains finite. The perfect gas behavior is reached as $\bar{\omega}=1$, that is, as the proportion of holes increases to unity.

Equation (59) may be used to give the second virial coefficient. From the first half of the equation B is given by Eq. (45). The cell size is no longer arbitrary, but is given by the low density limit of the second half. For $z=12$ this is

$$\{1+(4/\tau)[q^{-4}(1+\xi)-q^{-2}(1+\eta)]\}\times\exp[-(1/\tau)(q^{-4}-2q^{-2})+\tfrac{1}{6}\ln 2\pi\sqrt{2}\cdot g]=13/12. \quad (60)$$

No simple expression for the critical constants may be deduced from Eq. (59). If the cell size is a function of density then $(\partial\alpha/\partial v)_\tau\neq 0$, and Eqs. (48)–(50) do not hold.

(c) *The Approximation of Peek and Hill*

The average value of ω for any density and temperature is given in terms of x and α by Eqs. (31) and (33). Peek and Hill[11] assumed that deviations from this mean could be neglected and so put

$$j_0=j_1=j(\bar{\omega})=2\pi a^3 g'=2\pi\sqrt{2}\cdot r_0^3 q\cdot g'. \quad (61)$$

Here g' denotes g at a fictitious temperature of $\tau/(1-\bar{\omega})$. Compare Eq. (38). The same notation is used for ξ' and η'.

They did not consider the case with q constant but went straight to the more complicated case of finding q by minimizing the free energy. Algebraically this is the most complicated of the four approximations. Their expression for $j(\omega)$ is parallel to that of Cernuschi and Eyring (see Fig. 1), and so their expression for α is the same Eq. (40). The combined equation of state and equation for q is, for $z=12$.

$$\left(\frac{pV}{RT}\right)=J(x,\alpha)+\frac{12x}{\tau(\beta+1)}\left(1+\frac{\bar{\omega}\alpha(2x-1)}{\beta}\right)(q^{-4}\xi'-2q^{-2}\eta')=1+\frac{24(1-\bar{\omega})}{\tau}[q^{-4}(1+\xi')-q^{-2}(1+\eta')]-\frac{12\bar{\omega}}{\tau^2}\left(\frac{1-\beta}{\beta}\right)\left(\frac{1-\alpha}{\alpha}\right)(q^{-4}-q^{-2})\times(q^{-4}\xi'-2q^{-2}\eta'). \quad (62)$$

The second virial coefficient follows from the limiting form of Eq. (62) at low densities.

$$B=\tfrac{1}{2}Nv_0 q\left[(1+12\alpha)+\frac{12(1-\alpha)}{\tau}(q^{-4}\xi^\infty-2q^{-2}\eta^\infty)\right]. \quad (63)$$

The equation for cell size becomes

$$\left\{1+\frac{4}{\tau}[q^{-4}(1+\xi^\infty)-q^{-2}(1+\eta^\infty)]-\frac{1}{\tau}\left[1+\frac{4}{\tau}(q^{-4}-q^{-2})\right][q^{-4}\xi^\infty-2q^{-2}\eta^\infty]\right\}\times\exp\left[-\frac{1}{\tau}(q^{-4}-2q^{-2})\right]=13/12. \quad (64)$$

Here ξ^∞ and η^∞ are the values of these ratios, as $\tau'\to\infty$. They are pure numbers, see Appendix, Eqs. (83) and (84). Equations (62) and (64) are similar to Eqs. (59), (45), and (60), though they are much more complicated. Alternatively, Eq. (64) may be derived by considering the limiting form of the free energy at low densities and differentiating it. This needs the limiting form of g' as $\bar{\omega}\to 1$, see Appendix, Eq. (85).

Equation (62) gives no simple equations for the critical constants.

(d) *A Fourth Approximation*

The approximation of Peek and Hill is intuitively the most attractive of the three already presented, for it is the only one which attempts to reproduce $j(\omega)$ best in the region near its mean value, where it is most important. Now a straight line has two disposable parameters, and so it should be possible to improve this approximation by choosing the line so that both $j(\omega)$ and its first derivative are correctly given at $\omega=\bar{\omega}$. This may be done by writing the Taylor expansion

$$\ln j(\omega)=\ln j(\bar{\omega})+(\omega-\bar{\omega})(\partial/\partial\omega)_{\omega=\bar{\omega}}(\ln j(\omega)). \quad (65)$$

Comparison with Eq. (26) gives

$$j_0=j(\bar{\omega})\cdot\exp\left\{-\bar{\omega}\left(\frac{\partial}{\partial\omega}\right)_{\omega=\bar{\omega}}(\ln j(\omega))\right\},$$

$$j_1=j(\bar{\omega})\cdot\exp\left\{(1-\bar{\omega})\left(\frac{\partial}{\partial\omega}\right)_{\omega=\bar{\omega}}(\ln j(\omega))\right\}. \quad (66)$$

Now from Eq. (38)

$$\left(\frac{\partial}{\partial\omega}\right)_{\omega=\bar{\omega}}(\ln j(\omega))=\frac{\tau}{(1-\bar{\omega})^2}\cdot\frac{1}{g'}\cdot\left(\frac{\partial g'}{\partial\tau'}\right)_q, \quad (67)$$

and from Eqs. (9), (13), (14), and (15), putting $z=12$,

$$\left(\frac{\partial q'}{\partial\tau'}\right)_q=\frac{6g'(1-\bar{\omega})^2}{\tau^2}[q^{-4}\xi'-2q^{-2}\eta']; \quad (68)$$

this gives

$$j_0=j(\tilde{\omega})\cdot\exp\left\{-\tilde{\omega}\cdot\frac{6}{\tau}[q^{-4}\xi'-2q^{-2}\eta']\right\}$$
$$j_1=j(\tilde{\omega})\cdot\exp\left\{(1-\tilde{\omega})\cdot\frac{6}{\tau}[q^{-4}\xi'-2q^{-2}\eta']\right\} \quad (69)$$

and

$$\alpha=1-\exp\left\{\frac{-1}{\tau}[q^{-4}(1+\xi')-2q^{-2}(1+\eta')]\right\}. \quad (70)$$

The combined equation of state and equation of cell size becomes

$$\left(\frac{pV}{RT}\right)=J(x,\alpha)$$
$$=1+\frac{24(1-\tilde{\omega})}{\tau}[q^{-4}(1+\xi')-q^{-2}(1+\eta')]. \quad (71)$$

It is seen that although the expressions for j_0 and j_1 are complicated, the equation of state has recovered all the simplicity of the refinement of Ono's theory, Eq. (59). The only differences between Eqs. (59) and (71) is in the primes on ξ and η and in the definition of α.

At low densities, Eq. (71) gives the same second virial coefficient as in Eq. (45) and the following equation for the cell size,

$$\left\{1+\frac{4}{\tau}[q^{-4}(1+\xi^{\infty})-q^{-2}(1+\eta^{\infty})]\right\}$$
$$\times\exp\left\{\frac{-1}{\tau}[q^{-4}(1+\xi^{\infty})-2q^{-2}(1+\eta^{\infty})]\right\}=13/12. \quad (72)$$

Equation (71) gives no simple expressions for the critical constants.

IV. NUMERICAL RESULTS

The merits of these four approximations may be assessed by comparing the numerical results which they predict. Some of these results are taken directly from the original papers. Others, particularly in the case of the approximation of Cernuschi and Eyring, are calculated from the equations of the previous section. Values of the integrals g, g_l, and g_m are taken from the tables of Wentorf, Buehler, Hirschfelder, and Curtiss, as these are the most extensive. These values are not quite consistent with the postulates of the preceding section, as they are modified to include the effect of the second and third coordination shells. The difference is usually small and may be partially corrected for by inserting coefficients of 1.0110 and 1.2045 before q^{-4} and q^{-2} of Eqs. (59), (60), (62), and (71). Equations (64) and (72) do not need modifying, as ξ^{∞} and η^{∞} are the true "one-shell" values. Some calculations which lie outside the range of any tables of g, g_l, and g_m have been left undone.

The cell size, q, appears as an arbitrary constant in some of the approximations. Here it is taken to be unity. This is the value it would have in the perfect crystal, at zero temperature and pressure, for molecules which interact with their nearest neighbors only. Sato and Ono[19] chose $q=1.174$, by comparing r_0^3 from second virial coefficient measurements with the density of liquid argon below the boiling point. A fixed cell size puts an upper limit on the density. If $q=1$, then this limit is twice the critical density. The density of liquid argon at its melting point is 2.68 times the critical density.

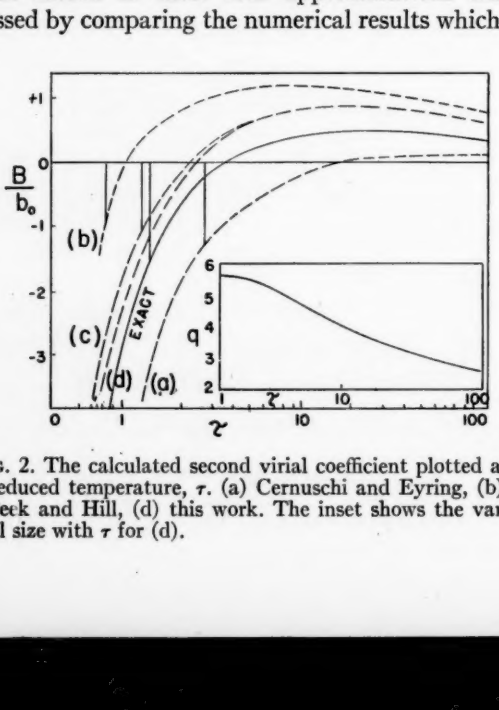

FIG. 2. The calculated second virial coefficient plotted against the reduced temperature, τ. (a) Cernuschi and Eyring, (b) Ono, (c) Peck and Hill, (d) this work. The inset shows the variation of cell size with τ for (d).

(a) The Low Density Limit

These theories are primarily designed to give the equation of state of liquids. It is a severe test to expect them to give good values of the second virial coefficient. On the other hand, there is reason to believe that any model which does not give a reasonable value for the second virial coefficient will not give a good value for the critical ratio $(pV/RT)_c$.

The treatment of Lennard-Jones and Devonshire gives zero for the second virial coefficient. Equation (12) shows that the first correction term is proportional to q^{-2}, or the square of the density. The second virial coefficient is given by Eq. (45) for approximations (a), (b), and (d), and by Eq. (63) for approximation (c). The cell size is put equal to unity for approximation (a) and (b) and is given by Eq. (64) for (c) and by Eq. (72) for (d). These equations have two solutions. The one corresponding to the *minimum* in the free energy must be chosen. ξ^{∞} and η^{∞} are given in the Appendix, Eqs. (83) and (84). Figure 2 shows a plot of these virial coefficients against the logarithm of the reduced temperature τ. The units of B are $b_0=\frac{2}{3}\pi\cdot Nr_0^3$. These calculated values are compared with the exact values computed for the intermolecular potential of Eq. (1) by the method of Lennard-Jones.[20] The figure also shows the variation of the cell size q with tempera-

[19] T. Sato and S. Ono, Japan. J. Phys. **4**, 103 (1949).

[20] J. E. Lennard-Jones, Proc. Roy. Soc. (London) **A106**, 463 (1924).

ture for approximation (d). Approximation (c) gives a similar cell size. It will be seen that q is finite in the limit of low densities.

(a) The theory of Cernuschi and Eyring gives a virial coefficent which is everywhere too low. The Boyle point occurs at $\tau=12.49$, instead of its true value of 3.42.

(b) The theory of Ono gives a virial coefficient which is everywhere too high. The Boyle point is at $\tau=0.96$.

(c) The approximation of Peek and Hill is much better. The virial coefficient is too high but the Boyle point has improved to $\tau=2.2$.

(d) This approximation is identical with Peek and Hill for $\tau>4$. Below that temperature it shows a slight improvement.

If Ono's theory is modified to eliminate the arbitrary cell constant, Eq. (60), then it gives a virial coefficient which is indistinguishable from that of approximations (c) and (d) for $\tau>7$. Calculations could not be made for lower temperatures as the cell size was too large for ξ and η to be found.

The behavior of B at very high temperatures is interesting. Equations (60), (64), and (72) become identical in the limit $\tau\rightarrow\infty$. They give

$$3q^{-4}(1+\xi^{\infty})-2q^{-2}(1+\eta^{\infty})=\tau/12. \tag{73}$$

This gives for the value of B at high temperatures

$$B=\frac{Nv_0}{2}\left[\frac{36(1+\xi^{\infty})}{\tau}\right]^{\frac{1}{4}}. \tag{74}$$

The exact value is

$$B=Nv_0\cdot\frac{2^{\frac{1}{2}}\pi}{3\tau^{\frac{1}{4}}}\cdot\Gamma(\tfrac{3}{4}). \tag{75}$$

Equation (74) shows the correct dependence on τ. The coefficient of $\tau^{\frac{1}{4}}$ is surprisingly accurate, being $(4.181\ Nv_0)$ instead of $(3.630\cdot Nv_0)$. The treatment of Cernuschi and Eyring, (a), and the unmodified treatment of Ono, (b), incorrectly gives the high temperature limit of B as a constant, $(\frac{1}{2}Nv_0)$.

This success with the second virial coefficient made it seem likely that the calculations of the equation of state of a gas at high temperature and pressure might give good results. These hopes were not borne out. Figure 3 shows a plot of (pV/RT) against the Amagat density for hydrogen at 0°C, taken from the measurements of Michels and Goudeket.[21] The force constants for the intermolecular potential were $r_0=2.968$A and $\epsilon/k=33.3$°K. Theoretical curves were calculated for the treatment of Lennard-Jones and Devonshire and for the approximation (d). It is seen that the two curves approach each other at high densities, where $\tilde{\omega}\rightarrow 0$, but that neither is an adequate representation of the experimental results.

(b) The Critical Point

The test most often applied to theories of this kind is to compare the value which they predict for the critical

[21] A. Michels and M. Goudeket, Physica **8**, 347 (1941).

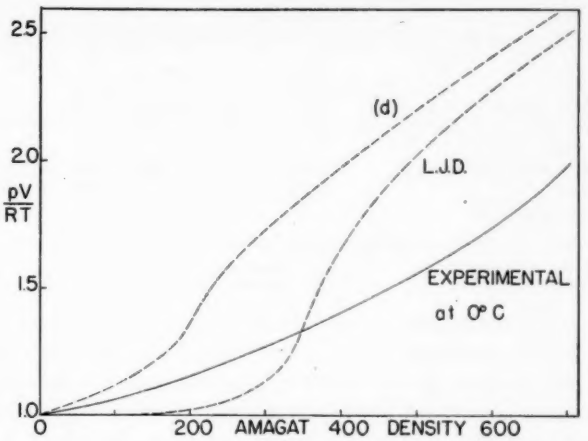

FIG. 3. The equation of state of hydrogen according to the theory of Lennard-Jones and Devonshire and according to the fourth approximation (d). The experimental curve is from Michels and Goudeket (see reference 21).

ratio, $(pV/RT)_c$, with the experimental one. The mean value for neon, argon, and nitrogen is 0.293. Lattice theories generally give a ratio somewhat larger than this. The theory of Lennard-Jones and Devonshire, in its most accurate form,[15] gives 0.591. The theories of Cernuschi and Eyring and of Ono are constrained by the form of the equation to give 0.342. This appears to be a great improvement. However, too much regard should not be paid to this ratio alone, unless the theories also give good values for the individual critical constants. Thus a simple equation of state containing only second and third virial coefficients is constrained to give a critical ratio of $\frac{1}{3}$, an even better value, subject only to the restriction that the second virial coefficient is negative and the third positive.[22] This, though, does not mean that such an equation would give an adequate representation of the properties of liquids. The approximation of Peek and Hill, (c), gives a critical ratio of 0.72, which is rather worse than that of the treatment of Lennard-Jones and Devonshire. This is rather surprising as the second virial coefficient is given quite well. Unfortunately no value can be given here for the fourth approximation, (d), as the critical point appears to lie at a cell size of about 5, which is outside the range of the tables of g, g_l, and g_m. This in itself is a weakness of the theory, for one of the conditions to which the cell size should conform is that it should be small enough for the chance of a cell containing more than one molecule to be neglected.

Table I shows a more detailed comparison of the critical constants. It is seen that although (a) and (b) give good values for the critical ratio, they are badly in error on the critical temperature.§ It is interesting to note that (a), (b), and (c) all give $B_c/b_0=-1.0$ to -1.2, (Fig. 1). The correct value is -1.63. If this criterion held for (d), then its critical temperature would be at

[22] J. S. Rowlinson, J. Chem. Phys. **19**, 831 (1951).

§ Sato and Ono[19] have $\tau_c=1.13$, but their calculations are wrong on this point. (Private communication from Dr. Ono.)

TABLE I.

	Ratio	τ_c	$p_c v_0/\epsilon$	v_c/v_0	$\bar{\omega}_c$
Mean value for Ne, A, N_2	0.293	1.28	0.121	3.09	...
Lennard-Jones and Devonshire[a]	0.591	1.30	0.434	1.77	0.000
Cernuschi and Eyring[b]	0.342	2.74	0.469	2.00	0.455
Ono[c]	0.342	0.75	0.128	2.00	0.455
Peek and Hill[d]	0.719	1.18	0.261	3.25	0.175

[a] See reference 15. [b] See reference 6. [c] See references 16 and 19. [d] See reference 11.

$\tau_c=1.3$, the correct value. It is impossible to say, though, without performing the calculation, how good values it would give for the other cirtical constants. The last column of Table I shows the average value of ω at the critical point, which one would expect to be about $\frac{1}{2}$. The value of Peek and Hill is very low.

(c) The Liquid-Vapor Equilibrium

The vapor pressure curves will be presented for two of the approximations, Lennard-Jones and Devonshire and Ono (b). The last two approximations need values of g, g_l, and g_m, at higher values of q than are available, to treat the vapor phase. The figures of Lennard-Jones and Devonshire[23] for the vapor pressure curve will be quoted directly. Equations (48) and (49) will be used to make the calculations for the theory of Ono. Here the critical point occurs at $\tau_c=0.75$. The available tables do not go below $\tau=0.70$ and so it is necessary to find some formula for extrapolating g to low temperatures. It is shown in the Appendix that g varies as $\tau^{\frac{1}{2}}$ at low temperatures. For $z=12$ and $q=1$, the first approximation to g is

$$(2\pi\sqrt{2}\cdot g)=(1/219.44)\cdot\tau^{\frac{1}{2}}.$$

The coefficient on the right-hand side was changed to 1/249.9 so that this approximation agreed with the tables of Wentorf and others for $\tau=0.70$ and, by interpolation, $q=1.0000$. The equation for α, Eq. (57) then becomes

$$\alpha=1-\exp\left\{\frac{1}{\tau}+\frac{1}{4}\ln\tau-\frac{1}{6}\ln 249.9\right\}. \qquad (76)$$

Equations (48), (49), and (76) give the vapor pressure and the densities of the two phases as a function of τ. The result is shown together with the experimental curve and that of Lennard-Jones and Devonshire in Figure 4. Both calculated curves have the correct shape, that is, $\ln p^*$ varies linearly with $1/\tau$, when p^* is the vapor pressure. The lines may be represented.

(Experimental)

$$\ln(p^* v_0/\epsilon)=2.97-6.53/\tau. \qquad (77)$$

(L. J. D.)

$$\ln(p^* v_0/\epsilon)=4.41-8.14/\tau. \qquad (78)$$

(Ono)

$$\ln(p^* v_0/\epsilon)=5.91-5.99/\tau. \qquad (79)$$

[23] J. E. Lennard-Jones and A. F. Devonshire, Proc. Roy. Soc. (London) **A163**, 63 (1937).

The equation of Lennard-Jones and Devonshire does not hold near the critical point.

The boiling point of a liquid at one atmosphere is not a quantity which can be calculated from equations of the "corresponding states" kind. However, if it is assumed that most critical pressures are about 40 atmospheres, then the boiling point may be taken as that temperature at which $p^*/p_c=1/40$. The experimental value of τ_b is about 0.77. The theory of Lennard-Jones and Devonshire gives about 0.80 and that of Ono about 0.51. However, the ratios of τ_b to τ_c are remarkably constant.

(Experimental) $\tau_b/\tau_c=0.60$

(L. J. D.) $\tau_b/\tau_c=0.62$

(Ono) $\tau_b/\tau_c=0.68$.

An old empirical rule due to Guldberg and Guye says that this ratio is about $\frac{2}{3}$.

Finally, the entropies of evaporation at the boiling point may be calculated. The experimental value of these is about 16.8 cal/mole for the rare gases, though this increases to about 21 cal/mole for higher boiling nonpolar compounds. The theory of Lennard-Jones and Devonshire gives 20.3 cal/mole and that of Ono, 23.2 cal/mole.

None of the models discussed in this article will show a second transition, to the solid state. For a model to do this, it must provide, by means of alternative sites for the molecules, for two phases of about the same density, one of which has, and one of which has not, long-range order. Such models have been devised by Lennard-Jones and Devonshire[24–26] and by Walter and Eyring.[7] The liquids discussed here show perfect order, when $\bar{\omega}\to 0$, at infinite pressure or zero temperature.

CONCLUSIONS

It is disappointing that none of these modifications shows much improvement over the original theory of Lennard-Jones and Devonshire. Some give good critical temperatures, some good pressures, and some good volumes, but none is altogether satisfactory. It is doubtful if much more progress can be made without removing some of the other approximations of these theories. For example, Kirkwood[9] has shown, in theory, how the potential within the cell could be improved by dropping the restriction that all neighbors are at the centers of their cells. The labor needed to carry this out might be considerable and would probably not be worthwhile. More direct and more accurate methods of calculating the distribution function of molecules in liquids are now being worked out both by Kirkwood and Born and Green.

[24] J. E. Lennard-Jones and A. F. Devonshire, Proc. Roy. Soc. (London) **A169**, 317 (1939).
[25] J. E. Lennard-Jones and A. F. Devonshire, Proc. Roy. Soc. (London) **A170**, 464 (1939).
[26] J. E. Lennard-Jones, Proc. Phys. Soc. (London) **52**, 38 (1940).

APPENDIX: SOME PROPERTIES OF THE INTEGRALS g, g_l, AND g_m

These integrals are defined by Eqs. (9), (10), (14), and (15). The series $l(y)$ and $n(y)$ are defined by Eqs. (6) and (7). The number of nearest neighbors will be put equal to twelve. In general, these integrals must be computed numerically. However, the limiting values at high and low temperatures have several useful properties. For g', g_l', and g_m', the expression "high temperatures" must be taken to include low densities, for $\tau'(=\tau/(1-\tilde{\omega}))$ can become large either by $\tau\to\infty$ or $\tilde{\omega}\to 1$.

High Temperatures

As

$$\tau\to\infty$$

$$g\to\int_0^s y^{\frac{1}{2}}\cdot dy=\frac{1}{2\pi\sqrt{2}}, \tag{80}$$

$$g_l\to\int_0^s y^{\frac{1}{2}}\cdot l(y)\cdot dy=7.586, \tag{81}$$

$$g_n\to\int_0^s y^{\frac{1}{2}}\cdot n(y)\cdot dy=0.2233, \tag{82}$$

where

$$s=(3/4\pi\sqrt{2})^{\frac{2}{3}}=0.30544.$$

The integrals of Eqs. (81) and (82) were evaluated by Gregory's method of numerical integration. Values of y at intervals of 0.01 were chosen, and differences up to the fourth were used. These numbers were later checked by expanding $l(y)$ and $n(y)$ by the binomial theorem, up to the twelfth power of y, and integrating term by term. From Eqs. (80) and (82)

$$\xi^\infty=2g_l^\infty/g^\infty=134.8, \tag{83}$$

$$\eta^\infty=2g_n^\infty/g^\infty=\quad 3.969. \tag{84}$$

At moderately high temperatures the exponential in the integrand of g may be expanded to give this useful expression

$$g=\frac{1}{2\pi\sqrt{2}}\left\{1+\frac{6}{\tau}[q^{-4}\xi^\infty-2q^{-2}\eta^\infty]+\cdots\right\}. \tag{85}$$

Low Temperatures

The exponent in the integrand of g, g_l, and g_m becomes large and negative at low temperatures and small cell size. The only effective part of the integral is then that close to $y=0$.

It is now useful to expand $l(y)$ and $n(y)$ as a power series in y.

$$l(y)=22y+200.2y^2+1144y^3+\cdots, \tag{86}$$

$$n(y)=5y+14y^2+30y^3+\cdots. \tag{87}$$

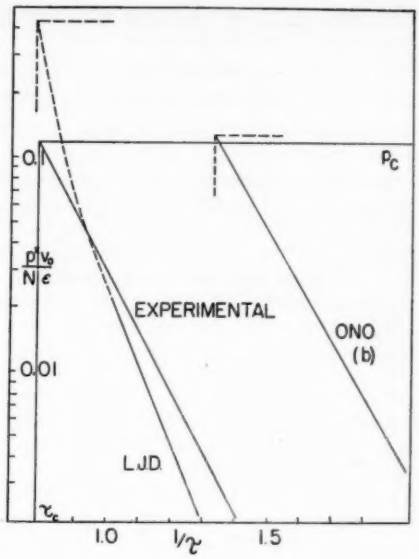

FIG. 4. The vapor pressure curves for the approximations of Lennard-Jones and Devonshire and of Ono. The curve L.J.D. is not linear up to the critical point.

The exponential may now be written

$$\exp\{-(12/\tau)[q^{-4}l(y)-2q^{-2}\cdot n(y)]\}$$
$$=\exp(-ay)\cdot\exp(-by^2-cy^3\cdots), \tag{88}$$

where

$$a=(12/\tau)(22q^{-4}-10q^{-2})$$
$$b=(12/\tau)(200.2q^{-4}-28q^{-2}),\text{ etc.} \tag{89}$$

The second exponent on the right-hand side of Eq. (88) may be expanded and the integration performed to give a series of Γ functions. The integration is very similar to that by which Lennard-Jones integrated the expression for the second virial coefficient for an inverse power potential (11). To be exact the Γ functions should be incomplete, as the limit of the integral is not infinity. The functions needed are $\Gamma_{sa}[(2n+1)/2]$, but these differ insignificantly from the complete function in the region where the series converges reasonably rapidly. This method cannot be used to calculate the integrals at any but the lowest temperatures. The series of Γ-functions oscillates, and converges slowly only at higher temperatures. However, the first terms are useful for extrapolation to low temperatures. They are

$$g=\quad a^{-3/2}\cdot\Gamma(3/2), \tag{90}$$

$$g_l=22a^{-5/2}\cdot\Gamma(5/2), \tag{91}$$

$$g_n=\ 5a^{-5/2}\cdot\Gamma(5/2), \tag{92}$$

where a is given by Eq. (89). These equations show that g varies as $\tau^{3/2}$ and g_l, and g_n, as $\tau^{5/2}$. If $q=1$, then

$$(2\pi\sqrt{2}g)=(1/219.44)\tau^{3/2}, \tag{93}$$

and

$$\xi=(11/24)\tau,\quad \eta=(5/48)\tau. \tag{94}$$

THE JOURNAL OF CHEMICAL PHYSICS VOLUME 19, NUMBER 12 DECEMBER, 1951

Heat Generation by Electric Sparks and Rate of Heat Loss to the Spark Electrodes*

WALTER ROTH, P. G. GUEST, GUENTHER VON ELBE, AND BERNARD LEWIS
Explosives and Physical Sciences Division; Bureau of Mines, Pittsburgh, Pennsylvania
(Received August 13, 1951)

In a capacitance spark the gas between the electrodes is heated almost instantaneously; subsequently, the spark-generated heat flows from the gas to the material of the electrodes. In the present experiments sparks of 0.1 to 2 millijoules were passed between Pt electrodes in a bulb containing helium or argon or xenon, and either the pressure change, Δp, at constant volume v or the volume change, Δv, at constant pressure p was recorded, the former by means of a sensitive diaphragm and the latter by the movement of a droplet in a capillary tube attached to the bulb. The spark-generated heat H residing in the gas at any instant was computed from the equations $H=1.5v\Delta p$ and $H=2.5p\Delta v$, which apply to constant volume and pressure, respectively, and are derived from the gas law and the energy equation, using the heat capacity of monoatomic gases. From the values of H and the discharge energy corresponding to the measured capacitance and breakdown voltage, the percentage of spark-generated heat residing in the gas was obtained. Immediately after discharge the percentage was found to exceed 95. The rate at which the percentage decreases with time was found to be independent of total energy and vessel diameter above a critical value of the latter. It was found to become smaller with decreasing heat conductivity of the gas, decreasing diameter of the spherical electrodes, and increasing gap length, as expected on the basis of heat loss from the gas to the electrodes. With electrode diameters of 1 mm, the heat loss after about 30 milliseconds ranged from a few percent for xenon and 10 mm gap length to 75 percent for helium and 1 mm gap length. An increase of the electrode diameter to 3 and 4.6 mm caused a substantial increase of the rate of heat loss; for example, for xenon and 10 mm gap length the heat loss after about 30 milliseconds was 28 percent and 35 percent, respectively. It was found that for constant electrode diameter the data for the several gases and gap lengths could be combined in a plot of percentage heat loss against a dimensionless parameter, ϑ, representing the product of thermal diffusivity and time elapsed since discharge, divided by the square of the gap length. By means of the latter parameter, one may estimate an upper bound of the heat loss during the formation of a combustion wave from a spark in an explosive gas, i.e., during the process of spark ignition, on the basis that the combustion wave is formed in a time interval smaller than the time required for the wave to travel a distance equal to its width. It is found that the loss of spark energy during the ignition process is always rather small.

THE theory of ignition of explosives predicts that for an instantaneous point source of heat the energy required for ignition attains a minimum value.[1] The measurement of this minimum ignition energy is evidently of considerable theoretical and practical interest. For explosive gases, at least, electric capacitance sparks seem to approximate the requirements of an instantaneous point source reasonably well, but it must be determined whether the discharge energy $0.5CV^2$, computed from the capacitance C and the gap voltage V, is a true measure of the heat imparted to the gas between the electrodes, and whether it is justified to assume that in the time interval between gap breakdown and establishment of a self-propagating combustion wave the heat loss to the electrodes is negligibly small.

In order to measure the small and rapidly disappearing amount of heat that is generated by a spark, the electrodes are mounted in a small vessel containing a monoatomic gas such as argon, and a record is taken either of the pressure change at constant volume or of the volume change at constant pressure. From such records, the spark-generated heat H that resides in the gas at any instant is determined as follows: The heat is initially confined to the spark channel. From there it spreads gradually over the volume of gas enclosed in the calorimeter vessel. In this process heat is lost to the electrodes and the vessel wall. If the total volume remains constant, one may write the equation

$$H=\int_0^n c_v(T-T_i)dn, \tag{1}$$

where n is the total number of moles in the vessel, T is the temperature in a volume element containing dn moles, T_i is the initial temperature, and c_v is the molar specific heat at constant volume. For constant pressure, c_p is substituted for c_v. From the gas law it follows that for constant volume,

$$v\Delta p=R\int_0^n (T-T_i)dn, \tag{2}$$

and for constant pressure,

$$p\Delta v=R\int_0^n (T-T_i)dn, \tag{3}$$

where Δp or Δv denotes the measured increase of pressure p or volume v and R is the gas constant. If c_v and c_p are constant, one may eliminate the integral in Eq. (1) by substituting Eq. (2) or (3), respectively. This applies to the monoatomic gases helium, argon, and xenon, which have been used in these experiments. For these gases, c_v is $1.5R$ and c_p is $2.5R$, so that one obtains for the case of constant volume

$$H=1.5v\Delta p, \tag{4}$$

and for the case of constant pressure

$$H=2.5p\Delta v. \tag{5}$$

* This research is a part of the work being done at the Bureau of Mines on Contract NA onr 25-47, NR 090 117, (33-038) 51-4151, supported by the ONR and the Department of the Air Force.

[1] B. Lewis and G. von Elbe, *Combustion, Flames, and Explosions of Gases* (Academic Press, Inc., New York, 1951).

APPARATUS

Both helium and argon were taken from tanks (helium, 99.9 percent purity; argon, 99.6 percent purity). Xenon was obtained in a 1-liter glass bulb at 1 atmosphere pressure and was at least 99.7 percent pure, krypton accounting for most of the impurity.

For argon and xenon experiments a bank of vacuum capacitors was charged through a high feed resistance by a high voltage DC power supply (Fig. 1). A static voltmeter and the spark gap were in parallel with the capacitance. The electrodes were platinum wires about 0.5 mm diameter tipped with platinum spheres of varying diameters. With closed gap, the entire spark circuit had a resistance of 0.04 ohm. The capacitance could be varied in several steps from 28 to 194 micromicrofarads by adding one or more vacuum capacitors. The capacitance of the circuit, including voltmeter, wiring, and gap, was measured with a General Radio Company R. F. capacitance meter, Type 1612-A, having an accuracy of ± 4–6 percent, depending upon the range. The interval between sparks was controlled by the feed resistance and was made long enough to permit undisturbed registration of the record from a single spark. In helium the discharge potential was very low, and much higher capacitances than those available with the vacuum capacitors were necessary to obtain comparable energies. In this case, therefore, a Leeds & Northrup type 1187 variable standard air capacitor having a range of 50 to 1300 micromicrofarads was used. The breakdown voltage indicated by the meter was read and was used to calculate the energy, $0.5CV^2$, stored just prior to discharge. As is well known, a spark discharge usually leaves a small residual charge on the condenser. For gap lengths up to 5 mm the residual potential was found to be approximately 100 volts, substantially independent of breakdown voltage and capacitance. This represented an unreleased energy of less than 1 percent and was therefore negligibly small. With larger gap lengths, the character of the discharge changed to the corona type, as is usual for small ratios of electrode diameter to gap length. A slow rise of pressure in the calorimeter, indicative of a low rate of energy dissipation, and a large residual charge were observed in such cases. However, by placing a weak ionizing source in the vessel (a small piece of radioactive foil) it was possible to obtain occasionally a normal spark discharge, permitting measurements with gaps of 10 mm length.

In the constant-volume calorimeter (Fig. 1) the sparks were generated in a spherical cavity at the center of a hard-rubber block. A silver tube of $\frac{3}{8}$-in. inside diameter communicating with this chamber was sealed at the end with a silver diaphragm approximately 3×10^{-4} in. thick. The diaphragm was prepared by filling the end of the tube with a plug of zinc $\frac{1}{32}$-in. thick, electroplating silver onto the zinc plug and silver tube, and finally dissolving the zinc with HCl. The platinum spark electrodes entered the calorimeter horizontally and intersected the axis of the silver tube at right angles. The gap was adjustable. The calorimeter was flushed and filled with gas through a hollow needle entering at the rear and extending almost to the diaphragm. The scavenging gas escaped through the top of the calorimeter. The gas entry and exit were sealed when this process was completed. For helium and argon experiments, the calorimeter was flushed at a rate of 10 cc/sec for 5 minutes. For xenon experiments, the calorimeter was first filled with argon, and then four 25-cc portions of xenon were forced through the apparatus by a column of mercury. The resulting mixture contained about 85 percent xenon, and the remainder was argon.

A spark occurring in the gap caused a thermal pressure rise within the calorimeter, bulging the diaphragm slightly. The deflection of such a diaphragm can be

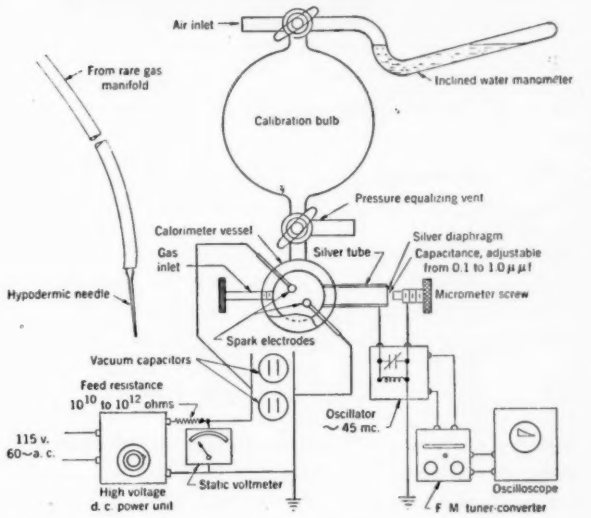

FIG. 1. Constant-volume calorimeter for measuring spark energies.

calculated from the equation[2]

$$\frac{a_1}{h}+0.488\left(\frac{a_1}{h}\right)^3=\frac{3}{16}\frac{p}{E}\left(\frac{a}{h}\right)^4(1-\sigma^2), \qquad (6)$$

where a_1 is the deflection at the center, p is the pressure on the diaphragm, σ and E are Poisson's ratio and Young's modulus for the diaphragm, respectively, and h and a are the diaphragm thickness and radius, respectively. Using $\sigma=0.38$ and $E=11.3\times10^6$ psi$=7.8\times10^{11}$ d/cm^2 for silver, and 4 mm $H_2O\simeq4\times10^2$ d/cm^2 for the maximum pressure developed during these experiments, the largest deflection is found to be about 8.3×10^{-4} in.

The deflection of the diaphragm changed its capacitance with respect to the plane end of a small micrometer screw. This capacitance change was proportional

[2] S. Timoshenko, *Theory of Plates and Shells* (McGraw-Hill Book Company, Inc., New York, 1940), p. 335, Eq. (196), and substituting $Eh^3/12(1-\sigma^2)$ for the flexural rigidity D.

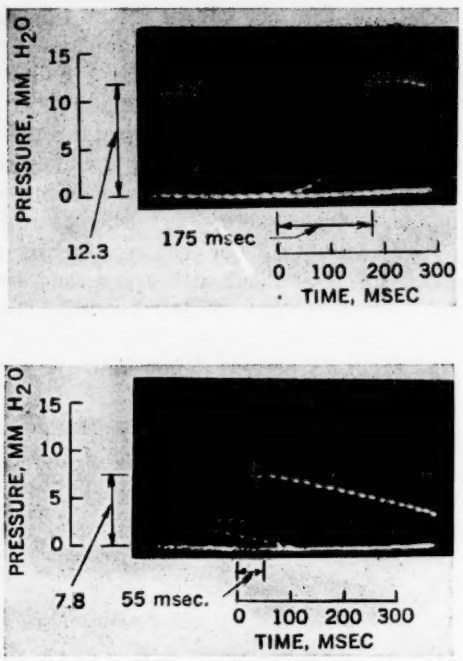

FIG. 2. Oscilloscope traces of calibration (above) and spark discharge (below).

within small limits to the pressure increase and was made to modulate proportionately the frequency of a 45 mc Clapp oscillator. The lowest natural frequency of the diaphragm in cps was calculated from the equation[3]

$$f=0.469l/r_0^2(E/\rho(1-\nu^2))^{\frac{1}{2}} \qquad (7)$$

where ρ is the density of the diaphragm material. The frequency was calculated to be about 500 cps, which was low enough to avoid interference with the oscillator frequency. By coupling an FM converter to the oscillator, any frequency change was converted into a proportional voltage pulse, which was recorded on a Dumont, Type 208, oscilloscope and photographed. To obviate the necessity for a synchroscope, a Type *P*-2 long-persistence screen was installed in the oscilloscope, and the phosphorescent trace was photographed. Similar instruments designed for the measurement of higher pressures are described in the literature.[4]

A wide-bore three-way stopcock on top of the calorimeter permitted rapid connection to be made with a large glass bulb. The apparatus was calibrated by allowing air in the bulb at known pressures to expand suddenly against the diaphragm and measuring the heights of the resulting voltage-time curves. A static calibration was not feasible because grid leak in the ac amplifiers of the oscilloscope caused the voltage to decay; however, with dynamic calibration the leakage from the amplifier was slow enough to be negligible during the period of pressure rise. The sensitivity of the instrument could be increased by decreasing the diaphragm capacitor space. Calibration curves were plotted for several sensitivities, and experiments were run in the range of linearity only. Air pressures were measured with a U-type water manometer, except for the higher sensitivities where an inclined manometer was used.

Observations of undamped oscilloscope traces showed that the pressure peak was obtained within about a millisecond in good agreement with the calculated half-period of the natural frequency of the diaphragm; this was followed by irregular violent oscillations ("hash"), which were presumably composed of spark-induced gas vibrations and the inertia oscillations of the diaphragm and which decayed to a smooth cooling curve within 10 to 50 milliseconds. These observations were made visually in a completely darkened room because photography of the trace in the region of rapid oscillations was made impossible by the low intensity corresponding to the high writing rate. Readable records were obtained by inserting a capacitor of about 0.2 microfarad across the input terminals of the oscilloscope; this filter capacitor eliminated the "hash" except for some ac pickup, and smooth traces were obtained whose maxima occurred about 25 to 70 milliseconds after the discharge. An example of such a trace and also a calibration trace obtained as described above are shown in Fig. 2.

A few experiments were also made with a constant-pressure calorimeter. In this apparatus a glass capillary tube of carefully measured bore was substituted for the silver tube and diaphragm. The capillary bore contained a tiny droplet of water with an added wetting agent for control of the viscosity and surface tension. Thermal expansion of the gas in the calorimeter by a spark caused movement of the droplet, again disturbed by superimposed oscillations, which could be damped by suitable adjustment of the viscosity. The movement was photographed, through a microscope, with a rotating-drum camera. A volume-time curve was thus obtained. Results for the constant-pressure calorimeter were found to be consistent with the results for the constant-volume calorimeter.

DATA AND DISCUSSION

In the constant-volume calorimeter, the pressure evidently attains a maximum immediately following the spark discharge and decreases thereafter owing to heat loss from the gas. The damping of the oscilloscope beam by a filter capacitor introduced considerable lag in the recording system, so that the early part of an experimental record did not represent the true pressure curve. Analogous considerations apply to the constant-pressure calorimeter. The true pressure or volume was recorded only after the experimental trace had passed through the peak. We introduce the symbol H_s to denote the

[3] S. Timoshenko, *Vibration Problems in Engineering* (D. Van Nostrand Company, Inc., New York, 1937), second edition, pp. 423–30.

[4] P. A. Bricout and M. Boisvert, Rev. Sci. Instr. **21**, 98 (1950); N. J. Thompson and E. W. Cousins, Electronics **20**, 90 (Nov. 1947).

values of H corresponding to the peaks of the experimental records. The corresponding fraction of the spark energy residing in the gas is $2H_s/CV^2$, the symbols having been explained previously. The dependence of this ratio on several parameters was investigated. In one series of runs the diameter of the spherical electrode chamber was varied, retaining argon as the gas in the chamber and keeping the gap length constant at 2 mm. For a diameter of 1.8 cm, the ratio $2H_s/CV^2$ decreased from 65 percent to 28 percent as the spark energy was increased from 0.08 millijoule to 1.18 millijoules. On increasing the diameter to 2.8 cm, the ratio $2H_s/CV^2$ became independent of the spark energy. The average value was found to be 65.6 percent±about 3 percent. Further increase of the diameter to 3.5 cm gave the same result within the limits of error. From these observations it appears that the larger sparks in the 1.8-cm vessel lost a considerable percentage of their heat to the wall before the pressure records attained their peaks, but that in the larger vessels the heat loss to the wall was insignificant. A vessel diameter of 3.5 cm was therefore chosen for all subsequent experiments, and the ratio $2H_s/CV^2$ was always found to be independent of spark energy over the range of the experimental conditions.

The diameter of the spherical electrode tips, the gap length, and the nature of the gas in the chamber were varied. The results are summarized in Table I. It is seen that, other conditions being constant, the ratio $2H_s/CV^2$ increases (1) with increasing gap length, (2) with decreasing heat conductivity of the gas (in the order helium-argon-xenon), and (3) with decreasing diameter of the electrode tips. The data thus confirm that during the time t_s between the instant of electric discharge and the attainment of the peak on the experimental record, a part of the spark-generated heat is lost to the material of the electrodes. The lengths of the time intervals, t_s, have been approximately determined from the records; these values are listed in the last column of Table I. In principle, other pressure-time or volume-time points on the experimental records might also have been listed in order to obtain additional data on the rate of cooling, but the records did not conform to simple exponential cooling curves at larger time intervals. It is probable that convection induced by buoyancy increased the cooling rate by contact of the hot gas with the wall. In addition, the pressure-time records were believed to be unreliable at larger time intervals because of the grid leakage in the oscilloscope. Qualitatively, the slopes of the cooling curves were found to be consistent with the heat losses in the time intervals t_s. However, extrapolation of the cooling curves back to the origin proved to be uncertain and arbitrary.

A measure of the heat imparted to the gas at the instant of spark discharge was obtained by plotting the ratios $2H_s/CV^2$ from comparable runs against (1) the reciprocal of the electrode distance, (2) the thermal diffusivity of the gas, and (3) the electrode diameter, and extrapolating the data back to the origin. Such curves are shown in Fig. 3. It is seen that immediately after the spark discharge more than 95 percent of the spark energy is found in the gas in the form of heat. The result shows that other forms of energy dissipation, in particular the radiation of Hertzian waves, were insignificant in these experiments. To minimize electromagnetic radiation, the circuit leads had been made as short as practicable. However, an experiment in which a large antenna served as a capacitor failed to show any significant contribution of electromagnetic radiation to the energy balance.

Earlier estimates,[5] which seemed to indicate that only a small fraction of the spark energy is imparted to the gas between the electrodes, are thus shown to be in error. These estimates did not allow for heat absorption by the electrodes. They were based on experiments with spherical electrodes of about 1-cm diameter and recording systems of very slow response, so that after the time interval t_s only a small fraction of the spark-generated heat remained in the gas.

The values of thermal diffusivities used in Fig. 3 are 1.59, 0.179, and 0.070 cm^2 sec^{-1} for helium, argon, and

TABLE I. Summary of data.

Electrode diameter, mm	Gap length, mm	Gas	Energy range, millijoules	$2H_s/CV^2$, average	t_s, average, millisec
Constant-volume calorimeter. Volume=24.4 cc, pressure≃740 mm Hg					
1	1	He	0.3–0.8	(25)[a]	
1	2	He	0.5–1.3	36.7	40
1	5	He	0.8–1.3	64.7	24
1	1	A	0.4–0.8	51.0	52
1	1.5	A	0.3–0.7	54.3	52
1	2	A	0.5–1.2	56.0	52
1	5	A	0.5–0.9	76.3	33
1	10	A	0.6–0.9	82.3	50
1	1	Xe	0.5–1.5	57.5	66
1	2	Xe	0.7–2.0	62.8	73
1	5	Xe	0.7–2.1	81.7	53
1	10	Xe	1.2–2.0	84.7	45
3	1	A	0.1–0.2	28.8	27
3	2	A	0.2–0.5	40.8	40
3	5	A	0.5–1.1	60.5	30
3	10	A	0.8–0.9	66.2	45
3	1	Xe	0.6–1.0	39.5	30
3	2	Xe	1.2–2.6	44.2	60
3	5	Xe	1.5–2.4	62.5	40
3	10	Xe	1.0–1.7	71.6	22
4.6	2	A	0.3–0.4	30.8	30
4.6	5	A	0.7–1.4	39.3	30
4.6	10	A	1.7–2.9	61.1	28
4.6	2	Xe	0.9–1.3	26.8	23
4.6	5	Xe	1.8–3.0	50.0	20
4.6	10	Xe	1.9–3.0	65.5	22
Constant-pressure calorimeter. Pressure=740 mm Hg, volume≃24 cc.					
1	1	A	0.2–0.4	36.9	50
1	1.5	A	0.2–0.5	48.0	80
1	2	A	0.3–0.8	52.3	70

[a] Value in parentheses estimated from measurements made at the limit of sensitivity of the instrument.

[5] W. Kaufmann, Ann. Physik **60**, 653 (1897). F. Broihan, Z. Angew. Chemie **B20**. 169 (1948).

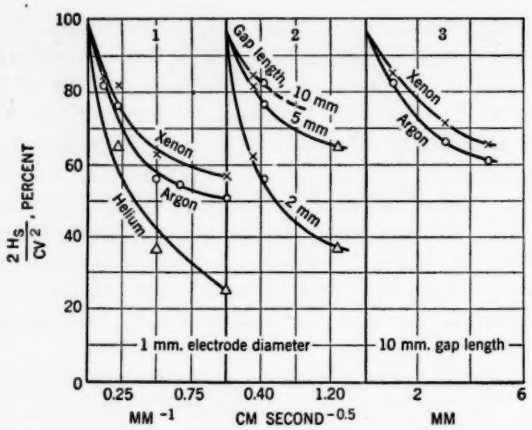

FIG. 3. Plot of $2H_s/CV^2$ *vs* (1) reciprocal of gap length, (2) square root of thermal diffusivity, and (3) electrode diameter. ×Xenon. ○Argon. △Helium.

xenon, respectively. They were obtained by dividing the values of heat conductivities (35.2×10^{-5}, 3.97×10^{-5}, and 1.24×10^{-5} cal cm^{-1} sec^{-1}°C^{-1}, at 0°C for helium, argon, and xenon, respectively[6]) by the molar specific heat at constant volume, which for monoatomic gases is 1.33×10^{-4} cal cm^{-3}°C^{-1}. The values have been arbitrarily adjusted to a temperature of 110°C, taking the diffusivity to be proportional to the $\frac{3}{2}$ power of the absolute temperature. As for xenon experiments, the calorimeter contained only 85 percent xenon with the remainder argon, the thermal diffusivity of the mixture was calculated from the equation†

$$K_{\text{mixture}}=\frac{K_1}{1+\frac{p_2}{p_1}\left\{\frac{1}{2}\left[1+\left(\frac{M_1^{\frac{1}{3}}K_1}{M_2^{\frac{1}{3}}K_2}\right)^{\frac{1}{2}}\right]\right\}^2}+\frac{K_2}{1+\frac{p_1}{p_2}\left\{\frac{1}{2}\left[1+\left(\frac{M_2^{\frac{1}{3}}K_2}{M_1^{\frac{1}{3}}K_1}\right)^{\frac{1}{2}}\right]\right\}^2} \quad (8)$$

where K is thermal diffusivity, p is the partial pressure, and M is the atomic weight.

In problems of heat flow where heat is transported from a source along one space coordinate only, one may always determine a dimensionless parameter, ϑ, which is the product of thermal diffusivity, K, and time, t, divided by the square of a characteristic length. The percentage changes of temperature and heat content anywhere in the system are functions of ϑ only. A spark discharge poses the problem of heat flow to the ambient atmosphere as well as to the two heat sinks represented by the electrodes. At present we know of no theoretical treatment of this problem. However, one may attempt to correlate the experimental values of $2H_s/CV^2$ in a plot against the parameter, ϑ. The time is t_s and the characteristic length is taken as the gap length. Such plots of the data are shown in Fig. 4. It is seen that for constant electrode diameter the points for the various gases and electrode distances are grouped reasonably well around common curves. The curves again extrapolate to a value of approximately 95 percent.

On the basis of 95 percent heat release in the gas at the instant of spark discharge, it is noted that for $\vartheta^{\frac{1}{2}}=0.1$, about 10 percent heat loss occurs with the small electrodes; for larger electrodes the heat loss may become as large as 50 percent. These values change when the thermal diffusivities are computed for temperatures other than 110°C. In principle, the values of K should be determined by averaging over the temperature gradients. This is not possible here, but it also does not seem to be very important. In the first place, the average temperature can hardly be very high, as the temperature in the spark channel rapidly decreases, owing to heat flow not only to the electrodes but also to the surrounding gas; and, furthermore, the heat loss is rather insensitive to the choice of temperature for computing K. For example, if the temperature is taken to be 1400°C, which corresponds to $\vartheta^{\frac{1}{2}}=0.3$, the heat losses for the smallest and largest electrodes become about 25 percent and 70 percent, respectively, as compared with the previous values of 10 and 50 percent for 110°C. It appears, therefore, that the curves in Fig. 4 provide a fairly reliable scale of the cooling process.

With regard to the problem of measuring minimum ignition energies, it is seen that the discharge energy $0.5CV^2$ is indeed a substantially correct measure of the heat imparted to the gas. The question remains whether any substantial fraction of the spark-generated heat leaks back into the electrodes before combustion-wave propagation has become independent of source energy. In the ideal case of an instantaneous point source a

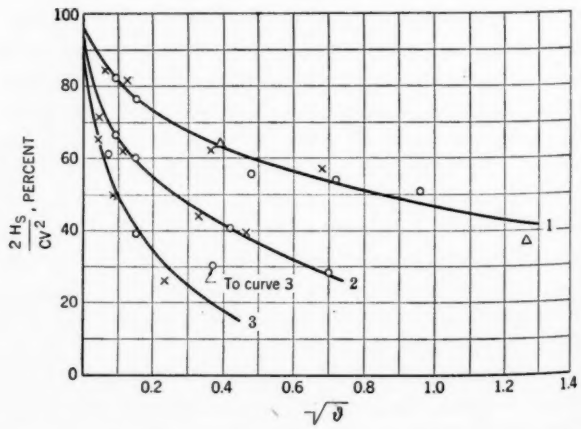

FIG. 4. Plot of $2H_s/CV^2$ *vs* $\vartheta^{\frac{1}{2}}$. Diameter of electrodes: Curve 1, 1 mm; curve 2, 3 mm; curve 3, 4.6 mm. ×Xenon. ○Argon. △Helium.

[6] S. Chapman and T. G. Cowling, *The Mathematical Theory of Nonuniform Gases* (Cambridge University Press, Cambridge, England, 1939), p. 241.

† Derived for a binary mixture of monoatomic gases by Dr. J. M. Richardson, Explosives and Physical Sciences Division, Bureau of Mines.

spherical flame develops. At the instant at which the heat flow from the source ceases, and in the case that the energy supply does not exceed the theoretical minimum, the flame core consists of completely burned gas at a temperature somewhat below the adiabatic combustion temperature,[1] and the surrounding shell that is occupied by the combustion wave contains an enthalpy excess equal to the source energy.[1] The wave is now self-propagating, provided that the explosive gas is not enclosed by cooling surfaces of proximity equal to or smaller than the quenching distance. The time required for establishment of this state—the "build-up" time of the combustion wave—is estimated to be shorter, and probably much shorter, than the time within which the wave travels a distance equal to its own width.[1] The latter time can be estimated from experimental data. For a given gap length it is thus possible to determine from the data of Fig. 4 an upper bound of the heat loss during the build-up time. Taking the gap length as equal to the quenching distance and using values of thermal diffusivities for temperatures of 100° to 200°C, ϑ^1 is always found to be about 0.1.[1] The heat loss during the build-up time is therefore smaller and probably much smaller than ~50 percent for an electrode diameter of 4.6 mm. This is sufficiently small, as the theoretical minimum ignition energy can be only approximately calculated, and comparison between theory and experiment is therefore valid only with respect to trend and order of magnitude.

In confirmation of the estimate that heat loss during the build-up time is small, one generally observes that at gap lengths beyond the quenching distance the minimum ignition energy of electric sparks is independent of the size and shape of the electrodes and remains constant over a considerable range of gap lengths.[1] Finally, it has been found[1] that the minimum ignition energies determined in this manner indeed agree in trend and order of magnitude with theoretical values that have been computed by taking the flame diameter equal to the quenching distance and introducing the expression of excess enthalpy per unit area from the theory of combustion waves. There is thus sufficient interlinking of experiment and theory to warrant the conclusion that the minimum ignition energy of electric sparks closely approximates the theoretical minimum ignition energy if the gap length is moderately larger than the quenching distance, a corollary conclusion being that for such sparks ignition is dependent primarily on the spark energy, other variables contributing only second-order effects.

Infrared Studies of Mixed Crystals: Naphthalene in Anthracene

GEORGE C. PIMENTEL
Department of Chemistry and Chemical Engineering, University of California, Berkeley, California
(Received July 20, 1951)

Polarized infrared studies have been made using single crystals of dilute solid solutions of naphthalene in anthracene in the spectral region 755 to 830 cm^{-1}. The ab plane at normal incidence was studied with the plane of polarization either parallel or perpendicular to the *b* axis. The mole fraction of naphthalene was varied from 0.009 to 0.029. The contour of the naphthalene band at 787 cm^{-1} shows a dependence upon concentration, approaching the contour observed in pure naphthalene. There is an increasing dichroic splitting of the band which is attributed to space group coupling as the number of nearest identical neighbors increases. It is likely that the magnitude of this splitting in naphthalene is only about 5–10 cm^{-1} and that the crystal forces in naphthalene as well as in the mixed crystals of naphthalene in anthracene are sufficiently weak that the "oriented gas" model is applicable. Using this model, the 787 cm^{-1} band of naphthalene is assigned as a single fundamental of either B_{1u} or B_{3u} class.

RECENTLY it has been noted that infrared studies of dilute solid solutions may offer valuable information in the interpretation of the infrared absorption spectra of solids.[1] It should be possible to determine the utility of the site group analysis and to verify the predictions of the factor group analysis.[2,3] Stated roughly, those features of the spectra which can be related to the coupling among molecules in the lattice should be identifiable and distinguishable from those features which can be attributed merely to orientation of the molecule within a perturbing field. Assuming weak coupling with the host lattice, the specific predictions for the spectra of mixed crystals by the model described in reference 1 are listed:

(a) multiplet splitting due to coupling should decrease as concentration decreases;
(b) dichroism should approach that of an "oriented gas", i.e., of molecules oriented in space by the host lattice;
(c) the selection rules should approach those appropriate to the site group of the host lattice.

Recent studies of the *ab* plane of single crystals of naphthalene using polarized infrared radiation[4] indicate an opportunity to test the statements in the first paragraph. These polarized spectra gave evidence that the coupling among the two types of molecules of the unit cell results in doublet splitting in the infrared of the order of a few wave numbers, a splitting difficult to resolve with conventional prism spectrometers. One of the strongest bands of naphthalene occurs at 787 cm^{-1}, a spectral region of relatively high resolution using NaCl optics. The dichroism of this band includes a frequency shift as well as an intensity change, suggesting either that there are two fundamental vibrations of different gas phase symmetry classes at this frequency or that the doublet splitting of a single fundamental vibration has been partially resolved. The gas phase spectrum indicates a contour which does not suggest the presence of two bands (see Fig. 1(a)). This band has the qualifications necessary for a mixed crystal study:

(a) the band is sufficiently intense to study in dilute solid solution;
(b) the band occurs in a transparent region of a suitable host lattice;
(c) multiplet splitting is (presumably) partially resolved.

Anthracene was selected as a suitable host lattice because of the similarity in the crystal structures of naphthalene and anthracene. Both crystals are monoclinic with two molecules per unit cell; the angle β has the value 122°55′ in naphthalene and 124°22′ in anthracene.[6,7] The precise calculations made by Robertson *et al.* of the molecular orientations aid in interpreting the dichroism.

TABLE I.

Solution	Mole ratio $C_{10}H_8/C_{14}H_{10}$ in solution	Mole fraction $C_{10}H_8$ in crystal	Probability nearest $C_{10}H_8$ neighbor
1	7.6	0.009	0.04
2	11.6	0.018	0.07
3	16.1	0.029	0.12
4	25.0	0.058	0.23

EXPERIMENTAL

The anthracene used in these experiments was purified by Dr. W. G. Dauben and showed the blue fluorescence characteristic of very pure samples. Baker's resublimed naphthalene and laboratory solvents were used without further purification.

Crystals were prepared by slow precipitation from solutions using a solvent of diethyl ether and absolute ethyl alcohol in the volume ratio 1:7. The solubility of anthracene in this solvent mixture is about 2 grams per liter while that of naphthalene exceeds 50 grams per liter. A volume of 75 ml of this solvent was saturated with anthracene and the desired amount of naphthalene

[1] H. J. Hrostowski and G. C. Pimentel, J. Chem. Phys. **19**, 661 (1951).
[2] D. F. Hornig, J. Chem. Phys. **16**, 1063 (1948).
[3] H. Winston and R. S. Halford, J. Chem. Phys. **17**, 607 (1949).
[4] G. C. Pimentel and A. L. McClellan, "The infrared spectra of naphthalene crystals, vapor and solutions" (to be published).
[6] Abrahams, Robertson, and White, Acta Cryst. **2**, 233 (1949).
[7] Mathieson, Robertson, and Sinclair, Acta Cryst. **3**, 245 (1950).

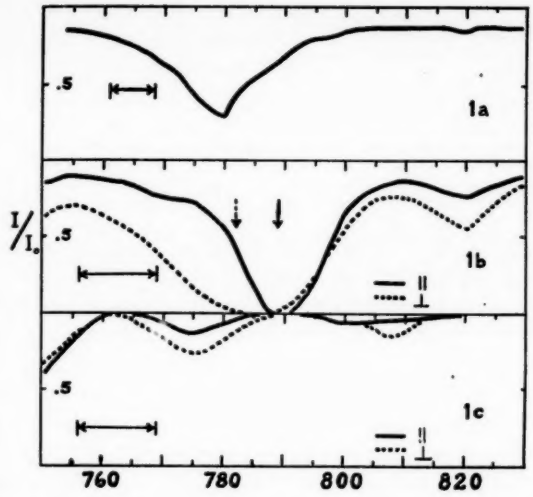

FIG. 1. Spectra of $C_{10}H_8$ and $C_{14}H_{10}$ near 787 cm^{-1}. 1(a). $C_{10}H_8$ (gas) $p=2$ mm, 10 cm cell. 1(b). $C_{10}H_8$ (*ab* plane, solid) polarized light. 1(c). $C_{14}H_{10}$ (*ab* plane, solid) polarized light.

and 20 mg additional anthracene were added. The solution was warmed to dissolve the anthracene, then cooled slowly to allow crystal growth. The precipitation thus occurred from a solution whose mole ratio of anthracene to naphthalene did not change by more than 15 percent, assuring reasonably homogeneous crystals. Single crystals were identified by completeness of extinction when observed in a petrographic microscope between crossed Nicol prisms. For infrared study, several crystals were arranged on a KBr plate so as to cover the beam as completely as possible. By use of the isogyre patterns, the *b* axes of all of the crystal fragments were located and oriented mutually parallel. In all polarized spectra the dichroism of the anthracene bands was observed to be the same as that observed for pure anthracene, thus ensuring properly oriented single crystals.

The spectra were taken on a Perkin-Elmer Model 12C spectrometer with NaCl optics. A conventional transmission polarizer with ten AgCl sheets was used. Slit widths are shown on the spectra. Frequencies in this region should be correct to within 3 cm^{-1} and the 667 cm^{-1} CO_2 band was used to recalibrate after every spectrum to avoid calibration shifts. Each of the spectra given here was taken several times.

The concentrations of naphthalene in the solid solutions were determined spectroscopically. Since only about 10–20 mg of solid was precipitated from each solution, it was necessary to work with small amounts. About 4 mg of mixed crystal was washed with absolute ethyl alcohol and weighed to ± 0.1 mg. This material was placed in a liquid cell holder of measured volume 0.18 ml and the cell filled with CS_2. The maximum percent absorption was measured at 780 cm^{-1} and compared to a reference curve obtained from standard solutions of naphthalene in CS_2 almost saturated with anthracene. Table I shows the mole fractions of $C_{10}H_8$ in the crystal for each of the precipitating solutions from which single crystals were obtained (solutions 1–3). Repeated attempts at slow crystallization of anthracene from solution 4 and also from a solution with mole ratio 18.8:1 failed to give single crystals large enough for polarized infrared study.

RESULTS

Figure 1 shows the spectrum of naphthalene in the region 755 to 830 cm^{-1}. Figure 1(a) shows the vapor phase spectrum while Fig. 1(b) shows the spectra of the solid at normal incidence to the *ab* plane using polarized light parallel or perpendicular to the *b* axis of the crystal. The apparent change in band contour of the solid phase spectra is conveniently expressed in terms of the center of the band at half-depth, i.e., where the percent absorption is half the maximum absorption. The centers calculated in this fashion are indicated in Fig. 1(b).

Figure 1(c) shows the polarized spectrum of a single crystal of anthracene in this spectral region. The spectrum of a thick crystal is given to show the location of the very weak band at 774 cm^{-1}. In mixed crystals with a mole fraction $C_{10}H_8=0.003$ the naphthalene absorption becomes as strong as this anthracene band. Since much higher naphthalene concentrations were of interest, this anthracene band did not interfere.

Figure 2 shows the spectra of the *ab* plane of mixed cyrstals of anthracene containing successively higher naphthalene concentrations. Table II lists the centers at half-depth for the spectra of Fig. 2.

DISCUSSION

The dichroism of the 787 cm^{-1} band in the mixed crystals verifies that the molecules of naphthalene are oriented with reference to the anthracene lattice. If it is assumed that the naphthalene molecules merely replace

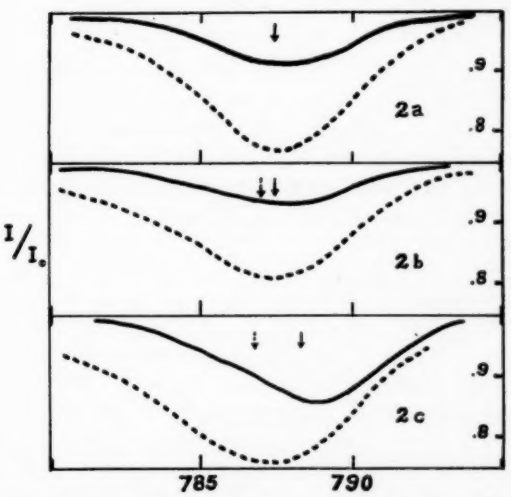

FIG. 2. Polarized spectra of mixed crystals, $C_{10}H_8$ in $C_{14}H_{10}$. ———*b* axis ‖ to plane of polarization. – – – –*b* axis ⊥ to plane of polarization. 2(a). Solid solution No. 1, mole fraction $C_{10}H_8=0.009$. 2(b). Solid solution No. 2, mole fraction $C_{10}H_8=0.018$. 2(c). Solid solution No. 3, mole fraction $C_{10}H_8=0.029$.

TABLE II.

Solution	Center at half-depth (cm^{-1}) ⊥	∥
1	787.5	787.7
2	787.0	787.4
3	786.8	788.3
pure $C_{10}H_8$	782	789

anthracene molecules in the lattice, it is possible to utilize the "oriented gas" model to calculate the dichroism for the three classes of infrared active vibrations.[4,8] The dichroic ratio is defined as the ratio of the absolute intensities $I_\perp/I_\parallel$.

$I_\parallel$ = integrated intensity when plane of polarization includes the *b* axis and at normal incidence to the *ab* plane.
$I_\perp$ = integrated intensity when plane of polarization is perpendicular to the *b* axis and at normal incidence to the *ab* plane.

The calculated dichroic ratios are shown in Table III for both naphthalene and anthracene. The accurate molecular orientations given by Robertson *et al* were used.[6,7] The dichroic ratio for pure naphthalene was not measured experimentally because the thinnest crystal which could be obtained gave almost complete absorption at the center of the band. Unfortunately the experimental dichroic ratios for the mixed crystals are not very accurate. The complete absorption or zero level was difficult to determine because the oriented crystals did not completely cover the beam. The strong band of anthracene at 730 cm^{-1} was usually sufficiently broad to guarantee complete absorption at the band center and was used to establish this zero level. A further problem in intensity measurement concerns determination of I_0. Since energy is lost by scattering and reflection, the percent transmission was determined using an assumed I_0 curve interpolated from the shoulders of the band. The experimental dichroic ratio was found to be about 3.

The spectra of Fig. 2 and the centers at half-depth in Table II show a trend approaching the characteristics of the spectra for pure solid naphthalene. The results are in accord with the interpretation that intermolecular coupling between naphthalene molecules alters the band contours as the concentration of naphthalene

[8] Ambrose, Elliott, and Temple, Proc. Roy. Soc. (London) **206**, 192–206 (1951).

TABLE III.

Class	Calc. dichroic ratio $C_{14}H_{10}$	$C_{10}H_8$
B_{1u}	3.5	2.8
B_{2u}	0.13	0.21
B_{3u}	16	4.1

increases. It is likely that the four nearest neighbors in the *ab* plane dominate the perturbation since the ease of cleavage along the *ab* plane suggests weak forces between adjacent planes. Assuming four nearest neighbors and that the positioning of naphthalene in the lattice is random, the probability of finding two naphthalenes as nearest neighbors can be calculated. The results, given in the last column of Table I, are also compatible with the conclusion that nearest identical neighbors are required to produce the band contour obtained for this band in pure solid naphthalene. This evidence seems to substantiate the conclusion that there is but one naphthalene band at 787 cm^{-1} and that the splitting due to coupling with the lattice has been resolved in the polarized spectra.

If the conclusion is established that space group coupling is a weak perturbation in the mixed crystals, then the dichroism may be interpreted using the "oriented gas" model. From the calculated and experimental dichroic ratios, it is possible to assign this fundamental to either the B_{1u} or the B_{3u} class. The dichroic ratio seems to favor the B_{1u} class but this conclusion assumes a quantitative applicability of the model which can be justified only after further experimental work.

CONCLUSION

The polarized spectra of mixed crystals of naphthalene in anthracene indicate that the band contour of the 787 cm^{-1} naphthalene band changes as the concentration increases, apparently approaching that of pure naphthalene. It is likely that the splitting due to intermolecular coupling is responsible. This indicates that this splitting is of the order of 5–10 cm^{-1} and that the forces of coupling are relatively weak. These conditions are suitable for applicability of the "oriented gas" model in interpreting the dichroism observed for these mixed crystals and also for solid naphthalene. With this model, the band at 787 cm^{-1} is assigned as a single fundamental of either B_{1u} or B_{3u} class.

The Diffusion of Copper in Cuprous Oxide

WALTER J. MOORE AND BERNARD SELIKSON
Department of Chemistry, The Catholic University of America, Washington, D. C.
(Received August 3, 1951)

Cuprous oxide strips were prepared by the oxidation of copper at 1000°C. The diffusion of radiocopper in this material at 800 to 1050° gave a self-diffusion coefficient, $D=0.0436\exp(-36100/RT)$. Virtually the same D is obtained from experiments in which radiocopper is plated on copper strips, and the distribution of activity measured in the cuprous oxide film formed on oxidation in air. The observed D values are in accord with a predicted relation $k/D=4$, where k is the parabolic rate constant for copper oxidation. It is suggested that parabolic rate constants with large negative entropies of activation and low heats of activation may be due to grain boundary diffusion.

THERE is good evidence[1] that the formation of protective reaction-product films on metals at high temperatures takes place by way of the diffusion through the film of metal ions from the underlying metal. Metal-oxide films are typical semiconductors; electrons from the metal traverse the film and, arriving at the oxide-oxygen interface, react with adsorbed oxygen atoms to form a layer of oxide ions. The cations that diffuse through the film occupy sites adjacent to these adsorbed oxide ions, and thus a new layer of metal oxide is formed.

On the basis of this picture, the parabolic rate constant for metal oxidation can be written[2] as

$$k=2D_i(f_1-f_2). \tag{1}$$

Here D_i is the diffusion coefficient of either interstitial ions or vacancies, and f_1 and f_2 are the fractions of defects at the metal-oxide and oxide-oxygen interfaces, respectively. Provided that all the diffusion is due to defects, the ordinary self-diffusion coefficient D of the cations in an oxide, as determined for example by radioactive tracer measurements, can be related to the diffusion coefficient for defects D_i by $D=D_i\bar{f}$ where $\bar{f}$ is the average defect fraction throughout the film. For a linear gradient of defects $\bar{f}=\frac{1}{2}(f_1+f_2)$, and Eq. (1) becomes

$$k=4D(f_1-f_2)/(f_1+f_2). \tag{2}$$

In case the defect concentration f_2 at one interface is virtually zero, e.g., concentration of interstitial ions at oxide-oxygen interface or of vacancies at metal-oxide interface, Eq. (2) reduces to

$$k=4D. \tag{3}$$

There should thus be a very simple relation between the parabolic rate constant and the self-diffusion coefficient.

The work described in this paper was undertaken to provide an experimental test of Eqs. (1) and (3), and to study the process of cationic diffusion in a typical p-type semi-conductor, cuprous oxide, in which the diffusion mechanism is the migration of positive vacancies. It was considered desirable also to repeat the diffusion experiments in which radioactive copper is plated onto copper strip, and the distribution of activity measured in the oxide film subsequently formed on the strip.[3] Comparison of diffusion coefficients calculated from these experiments with those in bulk cuprous oxide should indicate whether the ordinary bulk diffusion coefficient can be used in Eq. (3), and whether the outward flow of copper ions during oxidation has any effect on the inward diffusion of radioactive copper.

EXPERIMENTAL PROCEDURES

Materials

The cuprous oxide was prepared by the oxidation of strips of "spectroscopically pure" grade copper, supplied by the American Smelting and Refining Company. Pieces of copper $1\times\frac{3}{4}\times0.035$ in. were placed in an alumina boat lined with platinum foil. Oxidation proceeded at 1000°C in a 300 cc per min current of pure dry nitrogen (Seaforth) into which dried oxygen from an electrolytic cell was bled at a rate of 0.04 cc per min. Oxidation was complete in 24 hr, the cuprous oxide strip being clear, red, and translucent. The surfaces of the strips appeared dark by reflected light, and exhibited a well-defined grain boundary pattern with grains about 1 mm in average diameter. After the oxidation was complete, the cuprous oxide strips were annealed for 48 hr at 1000°C under the oxidation conditions. Little further grain growth occurred. The gain in weight on oxidation corresponded to completion of the reaction $2Cu+\frac{1}{2}O_2=Cu_2O$ to within ±0.1 percent. A typical x-ray powder pattern was given by the cuprous oxide preparations.

The radioactive copper was obtained from The Carnegie Institution of Washington. It was prepared by a (d, p) reaction on a copper cyclotron target, $Cu^{63}+{}_1H^2={}_{29}Cu^{64}+{}_1H^1$. Copper-64 has a half-life of 12.8 hr, and emits mainly β^- (0.57 Mev), β^+ (0.65 Mev), with a lesser amount of γ (1.34 Mev) and K-capture x-rays.

[1] C. Wagner, Z. physik. Chem. **B21**, 25 (1933).
[2] N. F. Mott and R. W. Gurney, *Electronic Processes in Ionic Crystals* (Oxford University Press, New York, 1948), second edition, p. 257, Eq. (13). The rate constant k is defined by the rate law $dy/dt=k/y$, where y is the film thickness.
[3] Bardeen, Brattain, and Shockley, J. Chem. Phys. **14**, 714 (1946); G. W. Castellan and W. J. Moore, J. Chem. Phys. **17**, 41 (1949).

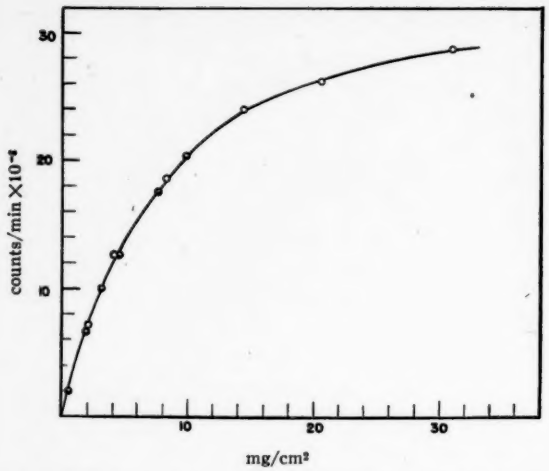

FIG. 1. Self-absorption of Cu^{64} radiation in electroplated copper. Counts per min *vs* mg per cm² of copper. Half-circles Exp. (a), open circles Exp. (b).

The principal long-lived contaminant of the target is the 250-day Zn^{65} formed by a $(d, 2n)$ reaction on Cu^{65}. The Zn^{65} emits principally 1.11-Mev γ-rays, and it must be completely removed from the copper used for tracer work.

The 1.3-in.-diameter target disk was placed in a beaker with its active face upward. Warm nitric acid was dropped onto the disk until about 0.5 g of copper were dissolved from the surface. The solution was transferred to another beaker, diluted, and 2 g of zinc sulfate added, together with sufficient sulfuric acid for the electroplating of copper. The copper was electroplated onto a platinum gauze cathode, washed thoroughly with distilled water, and then dissolved in nitric acid to yield the cupric nitrate solution used for the tracer experiments.

Procedure for Diffusion Runs with Cuprous Oxide

While one side and the edges of a cuprous oxide strip were protected by paraffin wax, a thin layer of radioactive copper with about 10^4 cpm was deposited on the uncoated side by dipping the specimen into the active cupric nitrate solution. Two similar specimens were used, with their active faces in light contact during the diffusion period so as to decrease evaporation losses to a negligible amount. The specimens were maintained at controlled temperature (±1°) in the oxidizing atmosphere used for preparation. The times ranged from 10 min at 1000° to 8 hrs at 800°. After rapid cooling, the back of the specimen was coated with Glyptal varnish, which also served to mount the specimen on a glass rod. Successive immersions in 50 percent nitric acid uniformly removed 50 to 100 mg of copper in each of 6 to 8 etches. This copper was electroplated onto polished weighed copper disks,[4] 1½ in. in diameter. The amount of cuprous oxide removed in each etch was calculated from the gain in weight of the disks.

The reaction by which solid cuprous oxide on immersion in acid cupric nitrate becomes coated with metallic copper is of intrinsic interest. The over-all reaction appears to be

$$2Cu^{+}(s)+{}^{*}Cu^{++}(l)={}^{*}Cu(s)+2Cu^{++}(l).$$

A possible mechanism would be:

$$Cu_2O(s)+2HNO_3=2Cu^{+}(l)+2NO_3^{-}+H_2O,$$
$$Cu^{+}(l)+{}^{*}Cu^{+2}(l)={}^{*}Cu^{+}(l)+Cu^{+2}(l),$$
$$2{}^{*}Cu(l)={}^{*}Cu(s)+{}^{*}Cu^{+2}.$$

This mechanism implies dilution of the radioactive copper in the course of its deposition, and the reaction should be further investigated by specific activity and kinetic measurements.

The copper disks were counted by means of a mica-window Geiger tube and associated scaler. Reproducible geometry was obtained with a special mount for the tube and holder for the disks. Background averaged 40 cpm, and the statistical error was generally 1 or 2 percent. Correction for self-absorption in the specimen was made from a measured self-absorption curve. Self-absorption was measured by two different methods. (a) Aliquot volumes of active cupric nitrate were diluted with increasing portions of inactive cupric nitrate, and a series of electroplated disks was prepared in which a constant amount of radioactive copper was distributed in various amounts of inactive copper. (b) Disks were

TABLE I. Diffusion runs with radiocopper in cuprous oxide.

Run No.	Temperature °C	Time min	Diffusion coefficient D-cm² sec⁻¹ ×10¹⁰
A 1	1000	15	350
A 3	1000	15	220
A 6	1000	15	380
A 2	900	40	55
A 4	900	40	62
S 7	1050	10	390
S 1	1000	15	350
S 4	1000	15	200
S 12	1000	10	180
S 9	950	15	80
S 10	950	15	210
S 13	950	15	130
S 6	900	60	90
S 8	900	50	90
S 2	850	180	40
S 11	850	90	70
S 14	850	50	73
S 3	800	665	9
S 5	800	700	29
K 2	1000	15	230
K 4	1000	15	325
K 3	900	50	52
K 5	900	40	46

[4] The disks were polished by immersion in Batelle Polishing Solution (Lea Manufacturing Company), washed in water, dried, and stored in a desiccator.

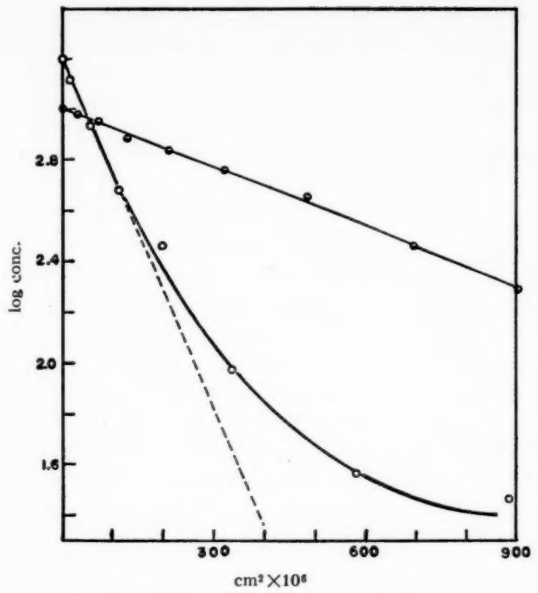

FIG. 2. Typical plots of distribution of radiocopper in cuprous oxide, according to Eq. (5). Open circles, Run *S*-7, showing reflexion effect. Half-circles, Run *S*-5.

electroplated with different amounts of copper from a stock solution of active cupric nitrate, the specific activity of the copper therefore being constant in plates of varying thickness. The results obtained from experiments (a) and (b) were in good agreement, as shown in Fig. 1.

Diffusion of Radiocopper During Oxidation

One side of a copper strip ($1\times\frac{3}{4}\times0.035$ in.) was plated with about 20,000 cpm of radiocopper, and the specimen was placed in the furnace at the required temperature. An atmosphere of air was used, but the specimen was cooled after oxidation in the nitrogen-0.013 percent ozygen mixture, in order to prevent oxidation of cuprous to cupric oxide. After oxidation, successive layers of oxide were removed by solution in nitric acid, about 30 to 50 mg of copper in each of 6 etches until the oxide layer was completely removed. The mass and activity of the copper were determined in the usual way.

Calculation of the Diffusion Coefficient

Solutions of radioactive tracers in solids are generally so dilute that it is possible to use the diffusion equation in terms of concentration, c, without any activity-coefficient corrections. The differential equation of diffusion in the x-direction normal to the face of a slab is

$$\frac{\partial c}{\partial t}=\frac{\partial}{\partial x}\left(D\frac{\partial c}{\partial x}\right). \tag{4}$$

The diffusion coefficient D may be a function of the concentration. It is most likely that diffusion in cuprous oxide occurs through the medium of cationic vacancies, associated with the stoichiometric excess of oxygen in the oxide under the usual conditions of preparation. Since the mobility of a cuprous ion depends therefore on the vacancy concentration, a dependence of D on vacancy concentration would be expected. This effect should not yield an inconstant D in a single experiment, but might lead to some variation of the D with sample preparation. The 48-hr anneal at 1000° was intended to obviate this possible source of variation. In the experiments on diffusion during oxidation, a variation of D with distance x in the specimen might have been expected[3] but was not in fact observed.

With the assumptions that D is constant, that the slab approximates a semi-infinite solid, and that the boundary conditions are $c=c_0$ at $x=0$, $t=0$; $c=0$ at $x>0$, $t=0$, Eq. (4) yields

$$c=c_0(\pi Dt)^{-\frac{1}{2}}\exp(-x^2/4Dt). \tag{5}$$

The concentration c is taken as the corrected count in a given etch divided by the thickness of cuprous oxide removed in the etch, and the distance x is calculated from the original surface of the slab to the midpoint of the etch. According to Eq. (5) a plot of $\log c$ against x^2 should yield a straight line, whose slope is $-1/(4Dt)$. The reported D's were calculated in this way. An alternate procedure is to integrate Eq. (5) to obtain the total activity up to a given point, and to evaluate D from the integrated equation.[3] The second method gave virtually the same results as the first, but was more tedious.

In the present experiments, there may be a barrier to diffusion at or beyond the midpoint of the slab. In the preparation of the cuprous oxide, the copper strip oxidizes from both sides and the copper ions diffuse outwards. As a result, there is a section through the middle of the slab (or often about two-thirds in from the exposed face, since the under face oxidizes more slowly) that becomes depleted of copper. If oxidation is stopped just after complete conversion of metal to oxide, the two distinct layers of oxide are readily de-

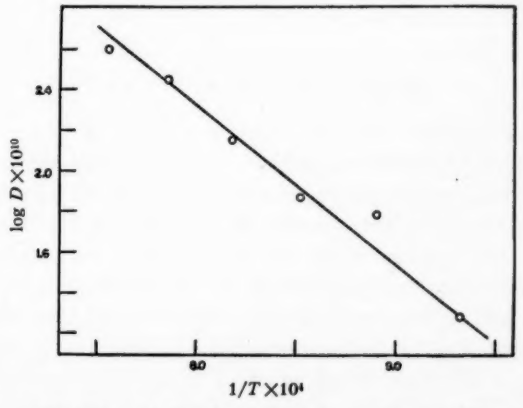

FIG. 3. Variation of D with temperature. Average D's at each temperature and the least squares straight line for all the runs.

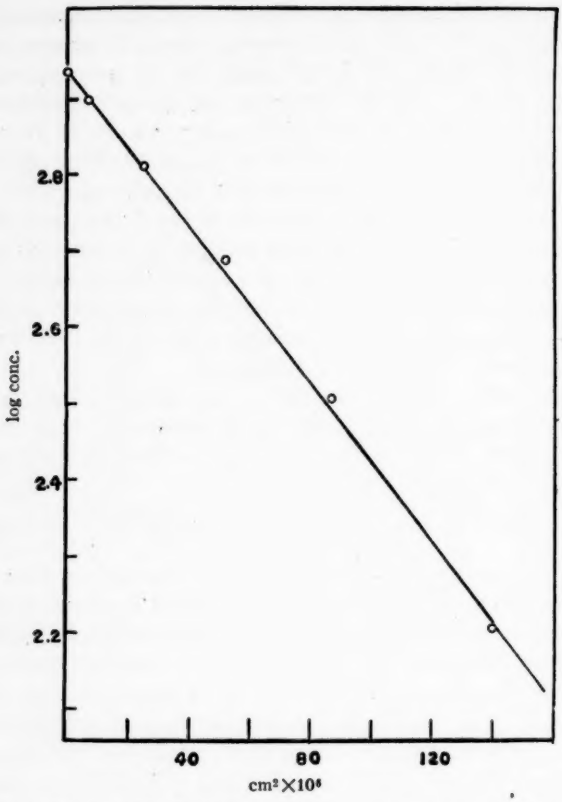

FIG. 4. Typical distribution of radiocopper in cuprous oxide after oxidation of copper strip, Run *K*-2.

tected, and in some cases can be separated with a razor blade. Even after 48-hr anneal at 1000° the boundary gap is detectable. In all the later runs, therefore, the effective slab thickness was considered to be one-half the total thickness, and the diffusion time was chosen so that etching could be carried to zero activity short of the midpoint. In some earlier runs a curvature of the later points of the log c against x^2 plot, convex to the x^2 axis, was observed, which is believed to be due to reflexion from the internal barrier. In such cases only the intial slopes of the curves were used to obtain values of D. The curves for diffusion during copper oxidation showed no curvature of the log c against x^2 plots.

RESULTS AND DISCUSSION

Typical log c against x^2 plots are shown in Fig. 2. In Table I are summarized the results of all the diffusion runs made after the procedure was definitely established. Runs in the *A*-series differ from the *S*-series in that there was no 48-hr anneal at 1000°, and a single specimen was used instead of two face-to-face. In some runs subsequent to *S*-10, the edges of the specimens were filed away before etching, to eliminate possible surface diffusion. None of these changes in procedure appeared to have any systematic effect on the results.

The average D-values at each temperature (excluding the *K*-series) are plotted in Fig. 3 as log D *vs* $1/T$, and the least squares straight line based on all the individual runs is also shown. This line corresponds to $D=0.0436 \times \exp(-36100/RT)$ cm² sec⁻¹. The probable error in the activation energy is ±2.5 kcal. If the data are fitted to the Eyring equation[5]

$$D=2kTh^{-1}d^2 \exp[(T\Delta S^*-\Delta H^*)/RT]$$

with the jump distance

$$d=3.05\times10^{-8}\text{ cm}, \quad \Delta S^*=-2.1\pm2.0\text{ cal deg}^{-1}\text{ mole}^{-1}$$

and $\Delta H^*=33.8\pm2.5$ kcal mole⁻¹.

It may be noted that the value of D at 1000° is in good agreement with the value calculated from the Einstein relation, $D=(kT\sigma\tau)/(e^2n)$, where σ is the conductivity, τ the transference number of Cu^+ ions, and n the number of Cu^+ ions in a cc of cuprous oxide. The experimental value of these quantities[1] are $\sigma=4.8$ ohm⁻¹ cm⁻¹, $\tau=4\times10^{-4}$, $n=5.05\times10^{22}$, yielding $D=2.6\times10^{-8}$ cm² sec⁻¹ compared to the average experimental value of 2.8×10^{-8} cm² sec⁻¹ at 1000°. The agreement provides a good experimental check of the validity of the Einstein relation in this semi-conducting solid. It also indicates that no appreciable fraction of the observed diffusion occurs through electrically neutral "trapped vacancies."

In Fig. 4 is shown a plot of the distribution of radiocopper in the cuprous oxide formed during oxidation of copper. The linear log c against x^2 plot is evidence for the validity of the assumption previously made by Castellan and Moore[3] that experiments of this kind measure the diffusion of the cation in the oxide. According to Eq. (3) the parabolic rate constant is about four times the diffusion coefficient, so that there should always be sufficient oxide into which diffusion can occur. In addition, there is an initial oxidation of the bare copper surface that is considerably more rapid than the parabolic oxidation of Eq. (3).

In Table II the parabolic rate constants for copper oxidation[6] are compared with the diffusion coefficients at different temperatures. The k values cited in the table were obtained in an independent investigation at an oxygen pressure of 0.5 cm. Under these conditions no cupric oxide is formed. The formation of a surface

TABLE II. Comparison of diffusion coefficients and parabolic rate constants.

Temperature °C	k cm² sec⁻¹	D cm² sec⁻¹	k/D ···
1000	10.0×10^{-8}	3.2×10^{-8}	3.2
950	6.5×10^{-8}	1.4×10^{-8}	4.6
900	2.2×10^{-8}	7.7×10^{-9}	3.5
850	1.45×10^{-8}	6.1×10^{-9}	4.2
800	3.6×10^{-9}	1.9×10^{-9}	1.9

[5] H. Eyring, J. Chem. Phys. 4, 283 (1936).
[6] J. K. Lee and W. J. Moore (unpublished data).

coating of cupric oxide has vitiated the results of many studies of the reaction kinetics of $2Cu+\frac{1}{2}O_2=Cu_2O$, for the cupric oxide film is often very protective. Considering the inevitable experimental uncertainties in the study of surface reactions of this kind, the close approach of the k/D ratio to the predicted value of 4 lends considerable support to the theoretical model underlying Eq. (3).

The question that naturally arises is how general is the relation $k/D=4$. A recent tabulation of oxidation rate constants,[7] as determined by various investigators showed that large negative entropies of activation ΔS^* often occur in the parabolic rate constants. As Zener[8] pointed out with reference to diffusion in metals, one would expect ΔS^* for diffusion always to be positive. It is significant that the large negative ΔS^* values occur for aluminum, iron, zirconium, and titanium. The oxidation of these metals was studied[9] at relatively low temperatures, always below 600°C, and the observed negative ΔS^*'s were coupled with unusually low ΔH^*'s. Thus grain boundary diffusion is strongly suggested as a mechanism for oxidation in these metals. In the case of copper oxidation at 800° to 1000°C the volume diffusion through cuprous oxide by a vacancy mechanism probably greatly exceeds the transport along grain boundaries. This conclusion is supported by the relatively high vacancy concentration in the oxide, the large grain size, the linear log c *vs* x^2 plots,[10] and the fact that the ΔS^* is practically zero.

This work was done under Contract NOrd 10260. A Frederick Gardiner Cottrell Grant from the Research Corporation provided much of the experimental equipment, and we wish to thank Mr. Dean Cowie of the Carnegie Institution of Washington for his generous assistance in arranging the supply of radiocopper.

[7] W. J. Moore, J. Chem. Phys. **18**, 231 (1950). The interpretation of the correlation between ΔH^* and ΔS^* given in this note was based on the erroneous assumption that D_i could be replaced by D, and it is superseded by the present suggestion.

[8] C. Zener, J. Appl. Phys. **22**, 372 (1951).

[9] E. A. Gulbransen and W. S. Wysong, J. Phys. Colloid Chem. **51**, 1087 (1947); E. A. Gulbransen and K. F. Andrew, Metals Trans. **185**, 515, 741 (1949).

[10] J. Fisher, J. Appl. Phys. **22**, 74 (1951).

THE JOURNAL OF CHEMICAL PHYSICS VOLUME 19, NUMBER 12 DECEMBER, 1951

The Vibration Spectrum of Rutile*

FRANK MATOSSI
Naval Ordnance Laboratory, White Oak, Silver Spring, Maryland

(Received August 20, 1951)

Raman effect data for rutile are evaluated for the force constants. It is shown that quasi-molecules TiO_2 are formed with strong Ti—O bonds although every Ti atom is surrounded by 6 O atoms in about equal distances. The main force constants are (in 10^5 dynes/cm) 1.7 for the Ti—O bond of the quasi-molecules, 0.06 for the other Ti—O bonds, 0.2 for O—O bonds. The spectrum can be interpreted as that of coupled modified TiO_2 molecules whose effective bond strength is a combination of the actual bond strengths.

INTRODUCTION

THE lattice of rutile, TiO_2, has been said[1] to belong to a transition type between ionic and molecular types. Whatever the evidence for such a statement may be (chemical or thermal behavior), the geometrical structure of the lattice would not necessarily have suggested it. It is true that the lattice admits a description in terms of TiO_2 molecules arranged in the manner indicated by Fig. 1. But the Ti atoms actually are centers of octahedra of 6 oxygen atoms with about equal Ti—O distances. The distances from Ti to the two O atoms assigned to the TiO_2 molecule are even somewhat greater than the distances to the four other O atoms. These near equal distances would suggest equal forces, and this would destroy the possibility of discerning separate TiO_2 molecules. It is the question whether the statement about the transition character of the rutile lattice can be supported quantitatively from a dynamical standpoint.

We may state the general problem involved by discerning a "local symmetry" of an atomic group, defined by the symmetry of the immediate environ of an atom[2] (here, the TiO_6-group of symmetry D_{4h}) and the overall symmetry of the crystal (for rutile, also D_{4h}, but with different orientations of the C_4-axes). Then the question is whether the vibrations are determined predominantly by local or by crystal symmetry, and whether the particle distances necessarily determine the dynamics of the lattice, i.e., the forces between the atoms, or not.

In order to determine the binding forces, we have to interpret the vibrational spectrum of rutile.

* Paper presented at the Symposium on Molecular Structure and Spectroscopy at Ohio State University, June 11–15, 1951.

[1] For instance in F. Seitz, *The Modern Theory of Solids* (McGraw-Hill Book Company, Inc., New York, 1940), p. 50.

[2] "Local symmetry" is not to be confused with the notion of "site symmetry" defined by the symmetry elements passing through a certain particle or site. Site symmetry describes the view of the lattice seen from the particular site. Local symmetry describes the symmetry of an environ of finite extension.

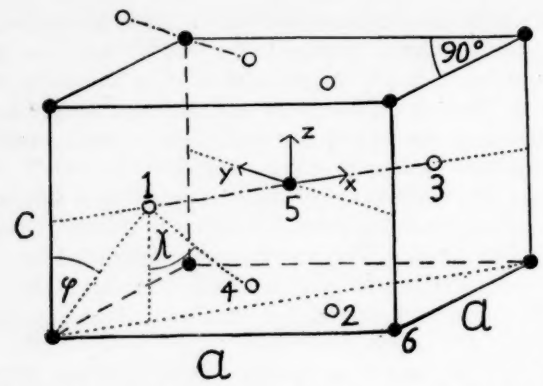

FIG. 1. Rutile unit cell. ●=Ti, ○=O. ·—·—· indicates TiO_2-"molecules." ..... auxiliary lines. $a=4.58$A, $c=2.95$A, $\cos\varphi=0.77$, $\cos\chi=0.53$.

VIBRATION SPECTRUM OF RUTILE

The Raman spectrum of rutile has recently been observed by Narayanan[3] who found three strong lines at 236, 440, and 589 cm^{-1}, several weak ones at 150, 515, and 650 cm^{-1}, and a very broad weak band between 350 and 420 cm^{-1}. The infrared data are much older. Broad reflection maxima at about 256 and 625 cm^{-1} for the ordinary ray, and at 330 cm^{-1} for the extraordinary ray had been observed.[4] Fortunately, there is no need to use these not too well-defined values for establishing the main result of our analysis, because the Raman effect gives sufficient information.

By standard group theoretical methods, we obtain the frequency formulas for the different species.[5] There is one vibrational mode each for the species A_{1g}, A_{2g}, A_{2u}, B_{1g}, B_{2g}, and E_g, two for B_{2u}, and three for E_u. A_{2u} and E_u are active in the infrared spectrum only, A_{2g} and B_{2u} are inactive in both Raman and infrared spectra. All others are Raman active species.

The (harmonic) force system used considers bond-stretching forces between: (Fig. 1)

Ti and O ("horizontal," e.g., 5—1 and equivalent bonds), force constant k_1;
Ti and O ("oblique," e.g., 5—2), force constant k_2;
O and O (horizontal, e.g., 4—2), force constant k';
O and O (oblique, e.g., 4—1), force constant k'';

bond-bending forces at:

Ti (e.g., angle 1—5—3 in horizontal plane), force constant d_1;
Ti (e.g., angle 1—5—3 in vertical plane), force constant d_2;
O (e.g., angle 5—4—5′), force constant d_3.

Only the fundamental frequencies of the first-order spectrum, i.e., the frequencies for infinite wavelength, have been considered. In these, all homologous particles vibrate exactly in phase. This restriction needs some justification. Indeed, we must be aware of the possibility of combinations not only among the first-order fundamentals ("first-order combination spectrum") but among virtually the entire set of frequencies contained in the different branches of the spectrum ("second-order spectrum"). This may lead to apparent violations of the selection rules. For instance, at the place of an inactive first-order frequency, a certain set of combination frequencies (particularly with the low frequencies of the acoustic branches) may appear as an apparently active band. Actually, we shall use one of these possibilities in the interpretation of the observations. However, in general, interference by branch combinations can be expected to be of minor importance, and, in any case, the determination of the first-order spectrum must be the basis of any interpretation at all.

In view of the extreme difficulty to obtain a complete account of the frequency distribution of the branches for a complicated lattice, the consideration of the second-order spectrum can be of a qualitative nature only. If, therefore, we select the first-order fundamentals for infinite wavelength as a well-defined working basis, we do not expect serious disadvantage from following this common practice.

Of course, it has to be considered that we deal with a crystal, and that, therefore, the atoms of the unit cell are not isolated but are part of a lattice. We must take into account, in the energy function, not only the forces between the particles of the unit cell itself but also those between these particles and certain of their nearest neighbors in adjacent cells.

Standard procedure then gives the following frequency formulas in which M and m are the masses of Ti and O, respectively; $\cos\psi=\tan\varphi/\tan\chi$, φ and χ being defined by Fig. 1 (ψ is the projection of the angle 1—4—5 in a horizontal plane).

A_{1g}:

$$\omega_1^2=[k_1+2k_2\sin^2\varphi+2k'+4k''(\cos\psi-\sin\psi)^2+4d_3\cos^2\varphi]/m;$$

A_{2g}:

$$\omega_2^2=[4k''(\cos\psi+\sin\psi)^2]/m;$$

B_{1g}:

$$\omega_3^2=[4k''(\cos\psi-\sin\psi)^2]/m;$$

B_{2g}:

$$\omega_4^2=[k_1+2k_2\sin^2\varphi+2k'+4k''(\cos\psi+\sin\psi)^2+4d_3\cos^2\varphi]/m;$$

[3] P. S. Narayanan, Proc. Indian Acad. Sci. (A) **32**, 279 (1950).
[4] T. Liebisch and H. Rubens, Berl. Ber. (1921), p. 211. D. N. Kendall, *Symposium on Molecular Spectroscopy* (Ohio State University, June 14, 1951) reports some weak absorption bands between 970 and 1200 cm^{-1} which may be interpreted as combination bands.
[5] Frequency formulas have also been given by B. Dayal, Proc. Indian Acad. Sci. (A) **32**, 304 (1950). Because Dayal uses a somewhat different force system and gives his results only with numerical coefficients for the particular TiO_2-lattice, I give the general system of frequency equations for any rutile type lattice. Besides, some of Dayal's terms seem to be erroneous.

E_g:

$$\omega_5^2=[2k_2\cos^2\varphi+8k''\cos^2\chi+4d_3\sin^2\varphi]/m;$$

A_{2u}:

$$\omega_6^2=[k_2\cos^2\varphi+d_1+2d_3\sin^2\varphi][2/m+4/M],$$
$$\omega_7^2=0\ \text{(translation)};$$

B_{2u}:

$$\omega_8^2+\omega_9^2=[16k''\cos^2\chi+2k_2\cos^2\varphi+2d_1]/m+[4k_2\cos^2\varphi+4d_1]/M,$$
$$\omega_8^2\omega_9^2=[64k''(k_2\cos^2\varphi+d_1)\cos^2\chi+32k_2d_1\cos^2\varphi]/Mm;$$

E_u:

$$\omega_{10}^2+\omega_{11}^2+\omega_{12}^2=[k_1+2k_2\sin^2\varphi+2d_2+4d_3\cos^2\varphi]\times[1/m+2/M]+8k''/m,$$
$$\omega_{10}^2\omega_{11}^2+\omega_{11}^2\omega_{12}^2+\omega_{12}^2\omega_{10}^2=[k_1k_2\sin^2\varphi+k_1d_2+2k_1d_3\cos^2\varphi][8/Mm+8/M^2]+2k_1d_2/m^2+[k_1k''+2k_2k''\sin^2\varphi+k_2d_2\sin^2\varphi+2k''d_2+4k''d_3\cos^2\varphi+2d_2d_3\cos^2\varphi][4/m^2+16/Mm],$$
$$\omega_{10}^2\omega_{11}^2\omega_{12}^2=[2k_1k_2k''\sin^2\varphi+k_1k_2d_2\sin^2\varphi+2k_1k''d_2+4k_1k''d_3\cos^2\varphi+2k_1d_2d_3\cos^2\varphi]\times[16/Mm^2+32/M^2m];$$
$$\omega_{13}^2=0\ \text{(translation)}.$$

The modes are characterized by the following relations between Cartesian point coordinates whose x-axes and y-axes are parallel to 1−3 and 2−4, respectively. For the E-modes, any combination of the orthogonal components given may occur. Except for B_{2u} and E_u, the relations represent normal coordinates.

A_{1g}: $x_1=-y_2=-x_3=y_4$;

A_{2g}: $y_1=x_2=-y_3=-x_4$;

B_{1g}: $-y_1=x_2=y_3=-x_4$;

B_{2g}: $x_1=y_2=-x_3=-y_4$;

E_g: $z_1=z_2=-z_3=-z_4$ or $z_1=-z_2=-z_3=z_4$;

A_{2u}: $z_1=z_2=z_3=z_4$, $z_5=z_6$ with $Mz_5+2mz_1=0$;

B_{2u}: $z_1=-z_2=z_3=-z_4$, $z_5=-z_6$;

E_u: $x_1=y_2=x_3=y_4$, $y_1=x_2=y_3=x_4$, $x_5=y_6$, $y_5=x_6$ or $x_1=-y_2=x_3=-y_4$, $y_1=-x_2=y_3=-x_4$, $x_5=-y_6$, $y_5=-x_6$, with $2m(x_1+x_2)+M(x_5+x_6)=0$.

NUMERICAL EVALUATION

The numerical values of the force constants depend, of course, on a correct assignment of the observed Raman frequencies to the several species. Although polarization measurements are missing, it is possible to find an unambiguous assignment. There is only one that leads to reasonable force constants at all. The force constant k'' can readily be found from $\omega_1^2-\omega_4^2$. Then ω_2, the inactive band, can be calculated. Its position coincides with the broad but weak band near 400 cm^{-1} which thus may be interpreted as being activated by combinations with frequencies of one of the acoustical branches whose frequency range, however, is unknown but may easily cover the extension of that band.

The values of k_1 and k_2 would depend on the values of k' and d_3 which cannot be determined unambiguously. However, the order of magnitude of the constants k_1 and k_2 is not affected by any reasonable choice of the other force constants. We assumed $k'=d_3=0$. The values of k_1 and k_2 are, therefore, obtained as upper limits. d_1 and d_2 are adjusted to give a reasonable account of the infrared bands, which, however, are not observed with a degree of accuracy comparable to that of the Raman spectrum.

The result of the numerical evaluation is given in Table I together with Dayal's results.[5]

DISCUSSION

The agreement between observed and calculated frequencies is as good as can be expected. Only two very weak Raman frequencies are not explained, and the difference for ω_3 is not serious. Any neglect of forces (as such between more distant neighbors) and of second-order effects would affect low frequency vibrations more than the other bands.

The principal result of our interpretation is the great difference between k_1 and k_2, which is certainly not due to any of the above-mentioned simplifications. This can be understood as indicating the molecular character of the rutile lattice. Only two O atoms are strongly bound to Ti, forming TiO_2-molecules. The spectrum, however, has not the aspect of that of isolated TiO_2-molecules, not even of coupled ones. Although the formulas for ω_1 and ω_4 suggest the interpretation that the difference between these frequencies is because of a splitting effect caused by coupling, the forces k_2 and k''

TABLE I. Interpretation of rutile spectrum.

	ω_{obs}	Int.	Interpret.	ω_{calc}	ω_{calc} (Dayal)	Remarks
RE	650	*vw*	···	···	···	···
	589	*st*	ω_4	588	590	···
	515	*vw*	···	···	···	···
	440	*st*	ω_1	440	441	···
	380	*w*	ω_2	400	388	very broad
	236	*st*	ω_5	236	249	···
	150	*vw*	ω_3	97	101	···
IR	330		ω_8	325	256	extra ordinary ray
	625		ω_{10}	620	400	ordinary ray
	256		ω_{11}	316	333	ordinary ray
	···		ω_{12}	130	94	beyond observed range
	···		ω_7	415	455	inactive
	···		ω_9	173	345	inactive

Force constants (10^5 dynes/cm):

$k_1=1.7$		0.65	Ti-O horizontal
$k_2=0.06$		0.65	Ti-O oblique
$k'=0$		0.3	···
$k''=0.2$		0.3	···
$d_1=0.26$		···	bending at Ti, horizontal
$d_2=0.06$		···	bending at Ti, vertical
$d_3=0$		···	bending at O
$k_5=\cdots$		0.31	Ti-Ti
$k_4=\cdots$		−0.24	see text

are, although small, still influential enough to shift the hypothetical frequency of free TiO_2-molecules (with k_1 only) appreciably and to give rise to the many other frequencies. If it is wanted to describe the spectrum in terms of TiO_2 frequencies at all, it must be said that the spectrum may be considered as one of modified coupled TiO_2-molecules.

Of course, the vibrational analysis can reveal only the facts but not the reasons why the Ti—O forces are as different as we have found them to be.

From the foregoing we may say that the rutile lattice is (1) geometrically a coordination lattice, (2) dynamically a molecular lattice, and (3) spectroscopically a transition type if there is no other possible explanation of the data.

In fact, Dayal[5] has offered another interpretation. His force system is different from ours mainly in the respect that he presupposes k_1 to be equal to k_2. Some other differences or slight errors (e.g., incorrect frequency for ω_5) are of minor quantitative importance. His assignment of the Raman frequencies is identical with that given here. But the infrared bands are interpreted differently.[6] Because of the assumption $k_1=k_2$, Dayal is compelled to admit a negative value for one of his other force constants. This constant refers to a term $(1/2)k_4\sum_{i=1}^{4} z_i^2$ of Dayal's energy function. A negative force constant[7] means that the corresponding force has a destabilizing effect on the point system. It is true that in our case the natural motions of the particles in the vibrational modes of the lattice are always such that the destabilizing term is overcompensated by the contributions of other internal forces. But it is possible to imagine suitable external forces which, in connection with some natural vibration, would tend to disintegrate the lattice. For instance, the vibration E_g would be unstable if, by periodic compressions of the lattice with an appropriate frequency, the atomic distances would be kept constant. Although this is certainly not a practical way of performing a disintegration, it shows the principle involved. Negative force constants should be permitted only if every possible deformation leads to a positive value of the energy function. Therefore, I do not think that Dayal's evaluation of the vibration spectrum of rutile is sufficient to invalidate the results derived here.

An experimental decision between the two interpretations discussed here may be possible by a re-examination of the infrared spectrum. There, the differences are largest. So far, the infrared data slightly favor our interpretation, but not decisively so.

[6] For the infrared bands, Dayal considers also the species B_{1u} which, for the first-order spectrum, is inactive.

[7] Negative force constants have already been used for quartz by B. D. Saksena, Proc. Indian Acad. Sci. **A19**, 357 (1944).

REMARKS ABOUT ANALOGOUS CASES

There are other cases in which the dynamical behavior is not uniquely related to the geometry of the lattice at all or at least not to the local symmetry of some atomic group. They may be pointed out briefly:

(a) In BeO, as crystallizing in the wurtzite lattice, every Be is surrounded by a nearly regular O_4 tetrahedron and vice versa. The local symmetry is that of the group T, but the BeO forces may be different in different BeO directions because of the C_{6v} symmetry of the lattice. This problem may be solved if the infrared data[8] would permit to decide whether there are one or two independent active infrared bands. Their frequencies are given by

$$\omega_1^2=(k+k'/3)/\mu \quad \text{and} \quad \omega_2^2=(4/3)k'/\mu,$$

where μ is the reduced BeO mass, and k and k' are the Be—O force constants. k refers to the direction of the C_6 axis, k' refers to the other directions. No definite conclusion is possible yet. If there is a difference between k and k' at all, it is not great, the upper limit of k/k' being about equal to 2 if the data of Tolksdorf are interpreted as revealing two separate bands at about 750 and 950 cm^{-1}. Therefore, any possible tendency of forming BeO molecules is negligible.

(b) The crystals of Li_2WO_4 and Be_2SiO_4 are isomorphous but have entirely different infrared spectra,[9] because the lattices have different dynamical character. Li_2WO_4 is an ionic lattice of Li and WO_4 ions. The silicate has the typical silicate coordination lattice of BeO_4 and SiO_4 groups whose O atoms are shared by one SiO_4 and two BeO_4 groups. Accordingly, the wolframate spectrum shows the typical internal vibrations of a WO_4 group. In the silicate spectrum, however, BeO and SiO vibrations may be identified.

(c) Also the familiar case of the internal vibrations of carbonates and similar crystals can be considered from the viewpoint discussed here. Indeed, it is not so much the geometrical lattice structure which leads to the conclusion of the existence of nearly isolated CO_3 groups than the spectral characteristics. The CO distances in these groups are not so much different from the MeO distances as to justify an *a priori* expectation of the particular spectroscopic properties of the carbonates. It is the spectrum and, of course, chemical evidence which give information about the dynamics of lattices.

[8] S. Tolksdorf, Z. physik. Chem. **132**, 161 (1928).

[9] F. Matossi and H. Krueger, Z. Physik **99**, 1 (1936).

Fourier Analysis of the X-Ray Scattering from Soap Solutions*

G. W. BRADY†
George Herbert Jones Chemical Laboratory, University of Chicago, Chicago 37, Illinois
(Received August 3, 1951)

A Fourier analysis of the x-ray diffraction of sodium dodecyl sulfate has been made on the basis that the micelles formed by aggregation of the long-chain molecules are spherical. The radial distribution of the micelles has been determined at two concentrations; the distribution functions show definite peaks indicating a preferred distance for neighboring micelles. It is concluded that the spherical micelle is compatible with the x-ray evidence. The deficiencies of the lamellar micelle are discussed.

INTRODUCTION

THE structure of the soap micelles found in solutions of long-chain electrolytes has been the subject of study for many years.[1] In general, two types of aggregates with very different properties have been proposed. The first of these is the lamellar[1–3] or "sandwich" structure, advocated by McBain and others, which consists of plates of long-chain molecules doubly oriented with the polar end of the molecule toward the external phase and with the hydrocarbon tails lined up end to end in the interior of the micelle. The strongest argument for the lamellar model is based on the x-ray diffraction of these solutions.[2] The essential features of the diffraction patterns are (1) a short spacing which varies only slightly from a Bragg value of 4.7A for most long-chain electrolytes (this spacing has been interpreted as a measure of the distance between hydrocarbon chains in the micelle); (2) a long-spacing (I-band) which has been assumed to measure the distance between lamellae. This spacing varies with the length of the long-chain ion, and increases with dilution. It has been assumed to arise from the diffraction of the x-rays by the planes of long-chain ions of the lamellae which are regularly separated by layers of water;[1] the latter increase with dilution and thus lead to a greater separation of the diffracting planes.

In addition, Harkins, Stearns, and Mattoon[4] found that a third band (M-band) was present in all solutions whose concentration exceeded the critical concentration for micelle formation. The spacing calculated from the peak of this band appears to be independent of the concentration and has been interpreted as a measure of the micelle thickness.

In opposition to this model, Hartley has proposed the spherical micelle.[1,5,6] This model has the great advantage that it leads to an optimum size for the micelle and, as Hartley has shown,[1] is much more reasonable on free energy grounds. The lamellar model is assumed to have an indefinite lateral dimension and the terminal hydrocarbon chains must be in contact with water unless the end of the micelle is rounded off in some manner. Calculations on the solubilizing properties of these solutions show that the lamellar model does not account for either the amount of oil capable of being solubilized[7] or the amount of water bound in layers between the micelles.[1] Also, in the x-ray diffraction patterns taken so far, the long spacing I-band has not been resolved from the M-band, and thus some doubt is introduced into the validity of the change of spacing as being due to a simple dilution effect. The I-band appears to be superimposed as a shoulder on the broader M-band, and since the intensities of both bands increase with concentration of electrolyte, any shift in spacing of one band must be distorted somewhat by the presence of the other band.

It seems hard to accept the lamellar model, particularly when the spherical micelle can satisfactorily explain all other phenomena observed with colloidal electrolytes. So far the analysis of the x-ray scattering has been done on the basis of a periodic structure which could be characterized by spacings calculated from the Bragg equation. The validity of this procedure is questionable because it assumes a quasi-crystalline arrangement of the micelles and offers no real basis for assigning a structure to the aggregates, or for interpreting their distribution in the solution. Corrin,[8] by assuming a simplified radial distribution of spherical micelles showed that the observed x-ray spectrum could result from such a distribution. Accordingly, it appeared worthwhile to attempt an analysis of the x-ray pattern by assuming a spherical form for the aggregates to determine their distribution. The present paper gives an analysis of the x-ray diffraction pattern of sodium dodecyl sulfate solutions using the Fourier transform method.

* This investigation was carried out under the sponsorship of the Reconstruction Finance Corporation, Office of Rubber Reserve, in connection with the Government's synthetic rubber program.

† Present address: Department of Chemistry, Harvard University, Cambridge, Massachusetts.

[1] See G. S. Hartley, *Ann. Reports on the Progress of Chemistry* **45**, 33 (1948). A comprehensive bibliography is included in this review.

[2] J. W. McBain, *Advances in Colloid Science* (Interscience Publishers, New York, 1942).

[3] P. Krishnamurti, Indian J. Phys. **3**, 307 (1929).

[4] Mattoon, Stearns, and Harkins, J. Chem. Phys. **16**, 644 (1948).

[5] G. S. Hartley and D. F. Runnicles, Proc. Roy. Soc. (London) **A168**, 420 (1938).

[6] G. S. Hartley, *Aqueous Solutions of Paraffin Chain Salts* (Hermann et Cie, Paris, 1936).

[7] Harkins, Mattoon, and Corrin, J. Colloid Sci. **1**, 105 (1946).

[8] M. L. Corrin, J. Chem. Phys. **16**, 844 (1948).

EXPERIMENTAL

The diffraction patterns were obtained with a GE XRD-3 unit fitted with parallel beam slits, having a maximum divergence of 0.4°. Zirconium filtered molybdenum radiation at 39 kv was used; the use of molybdenum radiation was dictated by the low intensities obtained with copper when operated at twice the ionization potential to insure radiation with as little white radiation as possible. Strictly monochromatic radiation although desirable was not obtainable with our present experimental arrangement.‡ Intensities were recorded with a Geiger-Mueller counter by scaling at intervals of 0.02° from 0.35° to 2.4°. Scaling times were so chosen that each point was counted for at least five minutes to compensate for background fluctuations; the probable counting error was $\frac{3}{4}$ percent. The cell used to contain the solution was made from a polystyrene block 5 mm thick by drilling a rectangular hole larger than the x-ray beam through the center. Polystyrene sheets 0.001 inch thick were cemented in tightly for the windows. The absorption of the windows was found to be negligible. Inlet and outlet holes were drilled horizontally at the top and bottom of the cell and the cell was filled by gently aspirating the solution through the lower hole until it reached the level of the top hole. The thin windows used made it necessary to fill the cell slowly because any appreciable pressure would rupture them.

Procter and Gamble reagent grade sodium dodecyl sulfate was extracted with ether to remove non-ionic material and unconverted acids, and was recrystallized twice from absolute ethanol before use. Solutions were made up by weight.

The scattering pattern of the soap solution was corrected for background by subtracting the intensity pattern of the solution at its critical concentration. In this way the contribution of the solvent and the nonmicellar soap was eliminated from the pattern, leaving only the small angle scattering due to the micelles. The concentration of ions in equilibrium with the micelles is not quite constant, but it is assumed that the error introduced by this assumption is not serious.

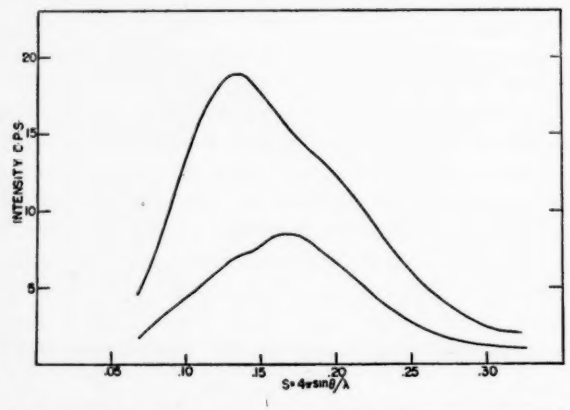

FIG. 1. The diffraction patterns of 29.42 percent and 14.71 percent sodium dodecyl sulfate. The upper curve is the more concentrated solution.

‡ Our unit is at present being modified to take care of this difficulty.

Analysis of the Intensity Pattern

The intensity of scattering of x-rays by N particles is given by the formula[9]

$$I=Nf^2\sum_n\sum_m\frac{\sin sr_{nm}}{sr_{nm}}. \tag{1}$$

In this expression r_{nm} is the distance between two scattering centers, m and n; f is the structure factor for the particles and $s=4\pi\sin\theta/\lambda$ where λ is the wavelength and θ is one-half the scattering angle. The value of f depends on the particle shape and for a particle of radius R and uniform electron density is[10,11] $n\phi(sR)$, where

$$\phi(sR)=\frac{3}{(sR)^3}(\sin sR-sR\cos sR), \tag{2}$$

and n is the number of electrons in the particle. The intensity is then

$$I=Nn^2\phi^2\sum_n\sum_m\frac{\sin sr_{nm}}{sr_{nm}}. \tag{3}$$

The array of particles may be characterized by a radial distribution function $\rho(r)$ such that $4\pi r^2\rho(r)dr$ gives the average number of particles between r and $r+dr$ from any one particle. Then for a large sample of average uniform density $\rho_0(3)$ may be written as

$$I=Nn^2\phi^2\left[1+\int_0^\infty 4\pi r^2(\rho-\rho_0)\frac{\sin sr}{sr}dr\right]. \tag{4}$$

By introducing the function $si(s)=s[(I/Nn^2\phi^2)-1]$, (4) is transformed by the Fourier integral theorem to give

$$4\pi r^2\rho(r)=4\pi r^2\rho_0+\frac{2r}{\pi}\int_0^\infty si(s)\sin rs\,ds, \tag{5}$$

and

$$q_r=2r/\pi\int_0^\infty si(s)\sin rs\,ds.$$

Yudowich[10] has pointed out the errors arising from collimation effects in small angle scattering. These errors depend upon the slit geometry and the wavelength. To compensate for them the scattering factor was averaged over the minimum and maximum scattering angles. The integral

$$\int_{\epsilon_1}^{\epsilon_2}\frac{\phi^2(sR)}{\Delta\epsilon}d\epsilon$$

[9] N. S. Gingrich, Revs. Modern Phys. **15**, 90 (1943).
[10] K. L. Yudowich, J. Appl. Phys. **20**, 174 (1949).
[11] L. H. Lund and G. H. Vineyard, J. Appl. Phys. **20**, 593 (1949).

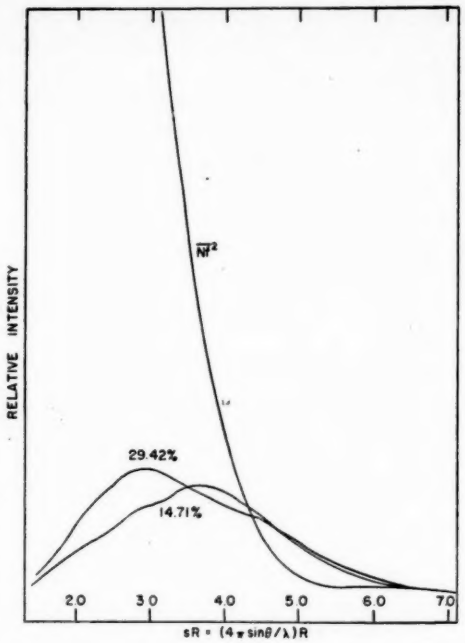

FIG. 2. Intensity *vs* sR. The ordinates have been adjusted to make the three curves coincide at $sR=7.0$.

was evaluated graphically from a plot of $\phi^2(sR)$ and used for f^2 in the transform expression (Eq. 5).

The radius of the micelles as measured from the x-ray diffraction patterns was 22A. This value is obtained from the diffraction patterns of solutions at low concentrations[4] where interference is small and agrees with the value obtained by Harkins, *et al.* and by Hartley and Runnicles[5] from diffusion measurements. It is also in good agreement with the value calculated from atomic constants.

The diffraction curves were fitted in the usual manner described by Warren and Gingrich,[12] by assuming independent scattering at $s=0.309$. This procedure allows the observed intensity and $N\bar{f}^2$ to be expressed in the same units. The integral of Eq. (5) was evaluated graphically from a plot of the product of $si(s)$ and $\sin rs$ against s, for various values of r. The calculations were not extended below the distance of minimum approach of the micelles. Corrections for incoherent scattering were neglected because of the small values of the scattering angles. The assumption of independent scattering at $s=0.309$ appears justified, for beyond this value of s no interference peaks are observed.

DISCUSSION

The measured diffraction patterns for two concentrations of sodium dodecyl sulfate are shown in Fig. 1, and in Fig. 2 the intensities are plotted together with the independent scattering function $N\bar{f}^2$, and the ordinates have been adjusted to make the three curves coincide at $kR=7.0$. The curves in Fig. 1 are similar to those observed previously in this laboratory.[4,7] The curves have been corrected for background as described. The higher concentration shows a relatively sharp maximum at $s=0.1335$. This appears to be superimposed on a broader band whose maximum is ill-defined. The lower concentration exhibits a maximum at $s=0.166$ (the M-band).

The values of q_r are shown in Fig. 3. At the higher concentration a sharp peak occurs at about 58A, while the lower concentration shows a slight shift to about 60–61A and a decrease in area of the peak. The function q_r gives the excess concentration of scattering matter over the average and the peaks give the position of nearest neighbors from any micelle. It is seen that there is a definite probable distance at which the neighboring micelles are to be found, and this is the only organization of the scattering centers necessary to give rise to the x-ray diffraction. The q_r values calculated from the areas under the peaks are 2.3 and 1.9 micelles, respectively, for the two concentrations.

The estimation of ρ for a micellar solution is complicated by the fact that the number of molecules which aggregate to form a micelle is not really known. ρ_0 may be roughly estimated by assuming that the minimum observed just before the maximum of the radial distribution function corresponds to a value of zero for ρ_0. This minimum occurs at about 44A, a distance which is twice the radius of the spheres and therefore the minimum distance of approach of the scattering centers. If ρ is calculated on this assumption the curve of Fig. 4 results, giving the values of $4\pi r^2\rho$ as a function of r. The number of nearest neighbors calculated on this basis is about 12 for the higher concentration, indicating that the micelles tend to assume a close-packed hexagonal arrangement of spheres. The fact that the shift of the peak in the distribution function with concentration is small indicates that the strong repulsion of the highly charged micelles acting with the cohesive forces produces a definite potential well near each micelle, leading

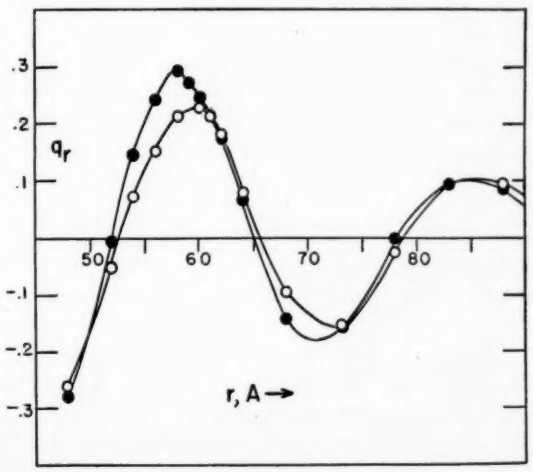

FIG. 3. q_r *vs* r. q_r gives the excess over the average density and the figure shows the peaks in the two curves at 58A and 60A for the two concentrations.

[12] B. E. Warren and N. S. Gingrich, Phys. Rev. 46, 368 (1934).

to a preferred distance which does not vary greatly with concentration. This is substantiated by the high viscosity of the solutions, particularly at the higher concentration, 29.42 percent, which lies close to the maximum solubility of the detergent, and by the gel-forming properties of soap solutions in general. These strong forces impart a rather rigid organization to the solutions, and attempts to explain the change in the Bragg long spacing as a dilution effect have not been successful; there does not appear to be any explicit relation between concentration and the I-band shift. The repulsion of the many-charged aggregates would in fact tend to prevent

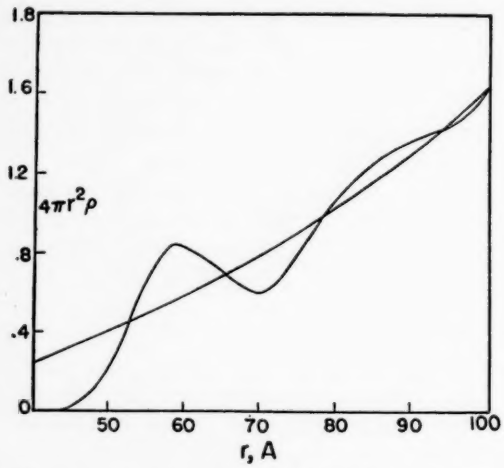

FIG. 4. The radial distribution $4\pi r^2\rho$ as a function of r. The area under the peak gives the number of micelles at that distance.

a decrease in spacing with increased concentration. A decrease in concentration would lead to a relaxation of the repulsive forces of the micelles with a consequent flattening of the distribution peak and a decrease in its area. At lower concentrations the peak presumably disappears indicating random organization. The experimental error involved in measuring these low intensities did not make their determination worthwhile however.

The spherical model for the micelle does not appear incompatible with the x-ray properties of soap solutions but rather eliminates many of the obvious difficulties inherent in the picture of an assemblage of lamellar diffracting planes sufficiently organized to give rise to the observed intensity of the diffraction pattern. The radial distribution picture shows an average concentration of nearest neighbors which would give rise to x-ray scattering in the same manner as in any liquid. The assumption of a periodic structure to which Bragg spacings may be applied is extreme and not at all necessary, and at best gives only a qualitative picture of the system. It may be remarked that application of the Debye-Ehrenfest equation,

$$\lambda = 0.814r \sin\theta,$$

gives a value of 57.5A for r, in good agreement with the peak at 58A in the distribution function.[13]

The distribution function for liquids is similar to a smoothed-out crystalline arrangement of scattering centers; particularly the right-hand side of the maximum does not go down to the axis. From Fig. 4 it appears that this is so for the liquid-like system of micelles. The second peak at 95A may or may not have significance; in any case the peak is smeared out and indicates only that one should expect scattering matter in this region. Beyond this distance the distribution is essentially random.

The assumption of a constant electron density in the micelles is of course extreme, but the actual electron distribution cannot be calculated because the degree of dissociation of the micelle is not known. Actual calculation of the scattering factor of a sphere of an assumed non-uniform electron density shows that the error resulting from the neglect of the non-uniformity of electron density is not too great. In any case the accuracy of the data does not justify the approximations and lengthy calculations necessary to correct for this effect.

ACKNOWLEDGMENTS

This work was done under the direction of the late Professor W. D. Harkins. I wish to thank Dr. M. L. Corrin, who suggested this problem, for his encouragement, and Dr. George Vineyard, University of Missouri, for a very helpful discussion of small-angle scattering.

[13] B. E. Warren, Phys. Rev. 44, 969 (1933).

The Effect of Ultrasonic Radiation on the Electrolytic Separation of Deuterium

DONALD F. MASON, ROYCE E. BIDDICK, AND CHARLES A. BOYD
Naval Research Laboratory, Department of Chemistry, University of Wisconsin, Madison, Wisconsin
(Received August 13, 1951)

The application of ultrasonic radiation to the polished platinum cathode of an electrolysis cell increases the coefficient for the electrolytic separation of deuterium. The radiation also decreases the temperature dependence of the separation coefficient. This is thought to be due to the rapid removal of the discharged gases by the ultrasonic radiation. This prevents the surface-catalyzed exchange reaction between the discharged gases and the electrolyte.

INTRODUCTION

ONE of the more interesting effects of ultrasonic radiation occurs in the field of electrochemistry. It has been shown[1,2] that the ultrasonic irradiation of a metal electrode at which gaseous products are being discharged results in marked lowering of the overvoltage characteristics of the process. In fact, one patent[3] claims an ultrasonic process which can lower the hydrogen overvoltage to such an extent that aluminum and magnesium can be separated from water solutions. However, as Bergmann[4] has pointed out, no practical successful demonstration of this particular effect has yet been made.

Schmidt and Ehret[1] have suggested that the ultrasonic induced reduction in overvoltage is due to cavitation at the electrode-electrolyte interface. These cavities in turn tend to remove the newly formed hydrogen gas from the electrode essentially by suction, resulting in a decrease of the overvoltage. One of the facts which they use to support this interpretation is that the cathode potential decrease occurs simultaneously with the start of the hissing noise which is characteristic of cavitation in ultrasonic fields.

It was felt that this effect might be of importance in the electrolytic separation of deuterium. It has been proposed that one of the processes which tends to lower the separation coefficient is the reaction between the discharged gases and the electrolyte according to the over-all reaction,

$$H_{2(g)}+HDO_{(l)}\rightleftarrows HD_{(g)}+H_2O_{(l)}, \qquad (1)$$

since any process which tends to increase the number of deuterium atoms in the evolved gases will lower the observed separation coefficient. If this reaction were allowed to go to equilibrium, one would expect to obtain a separation coefficient equal to the equilibrium constant for the reaction (written in the reverse direction). At room temperature this would have a value of approximately 3.

Reaction (1) is catalyzed by the electrode surface, where the newly formed gases tend to accumulate. Consequently, if the ultrasonic effect is to promote the rapid removal of the gases from the electrode, then one might expect to decrease the contact time between the gas and the electrolyte at the electrode surface and thus reduce the amount of exchange occurring. This in turn would be manifested as an increase in the separation coefficient.

Experimentally, this was found to be the case. In the electrolysis of a normal solution of Na_2SO_4 using polished platinum electrodes at room temperature, the separation coefficient was approximately 5, whereas with the application of ultrasonic radiation it increased to a value of 6.35.

EXPERIMENTAL APPARATUS AND PROCEDURE

The ultrasonic equipment used in these experiments consisted of an oscillator having a power output of approximately 200 watts. This was coupled to a quartz crystal transducer through a matching network in the regular fashion. A curved crystal was used which had a radius of curvature of three inches and a resonant frequency of approximately 400 kc/sec. The crystal was mounted in an oil bath with the focused beam pointing vertically upward. The oil in the bath was circulated through an external cooling coil so as to prevent excessive heating.

The electrolysis cell was mounted above the crystal transducer with the cathode chamber in the focused beam, the plane surface of the electrode being parallel to the direction of propagation of the ultrasonic waves. Before an experiment, the distance between the crystal and the cell was varied until a maximum in the output current was obtained. This insured maximum coupling between the cell and the crystal.

The acoustic power output of the crystal was about 50 watts, but calorimetric measurements indicated that the power absorbed in the electrolysis cell was about 20 watts.

Polished platinum electrodes were used in the cell, since previous investigations had shown that deuterium separation coefficients obtained with this type of electrode are relatively insensitive to concentration and current density variations.

The complete electrolysis cell is illustrated schematically in Fig. 1. Alcohol which had been previously

[1] G. Schmidt and L. Ehret, Z. Electrochem. **43**, 597 (1937).
[2] R. Piontelli, Atti accad. nazl. Lincei, Classe sci. fis. mat. e nat. **27**, 581 (1938).
[3] E. E. Dutt, French patent No. 749007 (1938).
[4] L. Bergmann, *Der Ultraschall* (S. Hirzel, Zurich, 1949), fifth edition.

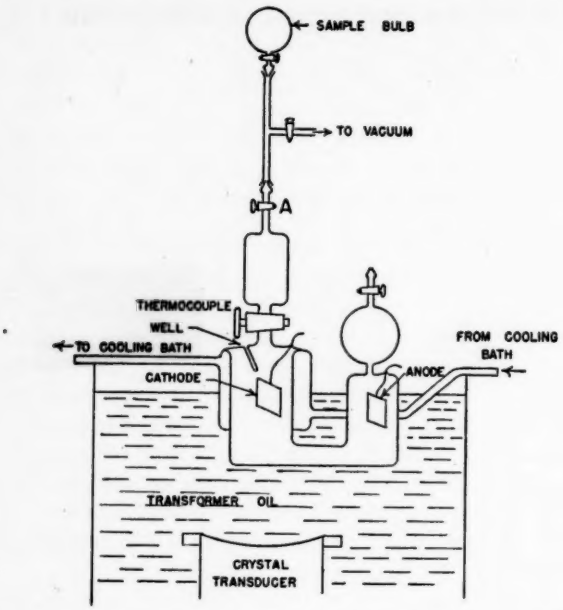

FIG. 1. Experimental electrolytic separation cell mounted over the ultrasonic transducer.

cooled by passage through a cell immersed in a dry ice-acetone mixture was circulated at a controlled rate through the cooling jacket around the cathode chamber. This was necessary in order to maintain constant temperatures within the cell. The cooling action was made more efficient by having fingers protrude into the electrolyte from the inner wall of the cooling jacket. The temperature in the cell was measured with a copper-constantan thermocouple junction located in a well close to the cathode.

The electrolyte used in these experiments consisted of a normal solution of Na_2SO_4 in water containing an atom ratio of deuterium/hydrogen equal to 0.09. During all runs the current density was held at a constant value of 0.0125 amp/cm^2.

Before starting an electrolysis run, the solution was forced into the reservoir above the cathode chamber and stopcock *A* was closed. As the cathode gas was formed during the electrolysis it collected in this reservoir, forcing the electrolyte into the reservoir above the anode chamber. Upon completion of the run, the gas sample was withdrawn from the reservoir into an evacuated bulb. This bulb was then immersed in liquid air to remove any water vapor, and the remaining gas sample was transferred to a second evacuated bulb for analysis.

Care was taken to insure that all gas in each sample was collected under the same conditions. In all cases the apparatus was operated until the desired conditions of temperature, ultrasonics, and current density had been maintained for ten to fifteen minutes. Stopcock A was then opened, the electrolyte was again forced into the reservoir above the cathode chamber and electrolysis was resumed.

Analyses of the hydrogen-deuterium ratios in the gas samples were made on a mass spectrometer. This was standardized according to the method of Alfin-Slater, Rock, and Swislocki.[5] It may be mentioned that foreign gases (i.e., air, oxygen, etc.) were present in the solution only in extremely small amounts. This was checked by noting the pressure required by the mass spectrometer to give a hydrogen peak of eighteen (18) volts. If the pressure was too high the sample was discarded, but even in these cases the foreign gases probably were due to a leaky stopcock in the sample bulb and not from the electrolyte itself.

Calculation of the separation coefficient, α, was made according to the equation,

$$\alpha=(H_g/D_g)/(H_s/D_s), \tag{2}$$

where H_g and D_g are the atomic concentrations of hydrogen and deuterium in the gas, and H_s and D_s are the corresponding values for the solution. Since only a negligible quantity of solution was electrolyzed in order to get a gas sample for analysis, the concentration of the electrolyte could be assumed to remain constant.

TABLE I. Separation coefficient without ultrasonic irradiation.

Electrolyte temperature	Separation coefficient
4.7	6.60
10.2	5.81
15.7	5.25
21.2	4.95
26.1	4.61
30.7	4.41
36.0	4.14
41.2	3.95
51.7	4.02
51.7	3.62

This assumption was also borne out by check determinations of the hydrogen-deuterium ratio of the electrolyte during the course of the experiments.

EXPERIMENTAL RESULTS AND DISCUSSION

Experimental determination of the electrolytic separation coefficient was made with and without ultrasonic irradiation over a temperature range from 5 to 50°C. The data are given in Tables I and II and summarized in Fig. 2. It is seen that for all temperatures the separation coefficients with ultrasonic irradiation are higher than the corresponding values without irradiation. It is also apparent that ultrasonic irradiation tends to lessen the temperature dependence of the separation process.

Visual observation of the cathode chamber during the runs showed that a marked change in the character of the process occurred when the ultrasonic generator was turned on. When electrolysis took place without ultrasonic irradiation, the gaseous products appeared in the form of minute bubbles completely covering the elec-

[5] Alfin-Slater, Rock, and Swislocki, Anal. Chemi. **22**, 421 (1950).

trode and clouding up the electrolyte in the immediate vicinity. However, when the ultrasonic generator was turned on the electrode surface was immediately cleaned, and the small bubbles rapidly coalesced into large bubbles which then rose into the sample reservoir.

It is immediately apparent that the results obtained in these experiments cannot be due to secondary heating of the system by ultrasonic radiation. This follows from consideration of Fig. 2, which shows that an increase in temperature tends to lower the separation coefficient. This is the inverse of the effect observed when the ultrasonic radiation is applied to the cathode of the separation cell.

In considering the effect of ultrasonic radiation upon the electrolytic separation of deuterium, several modes of action can be proposed as possibilities. First the ultrasonic radiation may increase the rate of formation of H_2 over that of HD and of D_2, thus increasing the measured separation coefficient. Since the detailed mechanisms for these processes are not yet fully understood, it is difficult to assess the reasonableness of this proposal. However, if such were the case, one might

TABLE II. Separation coefficient with ultrasonic irradiation.

Electrolyte temperature	Separation coefficient
5.0	7.20
5.0	6.96
11.5	6.76
18.5	6.31
24.0	6.17
30.0	5.97
35.5	5.50
40.0	5.90
45.0	5.50
50.0	5.42

expect it to be due to a resonant condition wherein a particular type of bond would be affected for one isotope and not for the other. Since a bond energy of 1 cal/mole corresponds to a frequency of 10^{10} sec^{-1}, it is apparent that any bond which would be in resonance with an ultrasonic frequency of the order of 10^5 sec^{-1} would be extremely weak. There are other types of resonant phenomena occurring in ultrasonic fields which involve the excitation of the molecular rotations. However, it is not immediately apparent how these resonances could affect the discharge process.

Another mode of action of ultrasonic radiation might be an efficient stirring of the electrolyte in the immediate vicinity of the electrode, and a subsequent alteration of the electrode layers. Again, this does not lead directly to an explanation of the increased separation coefficient.

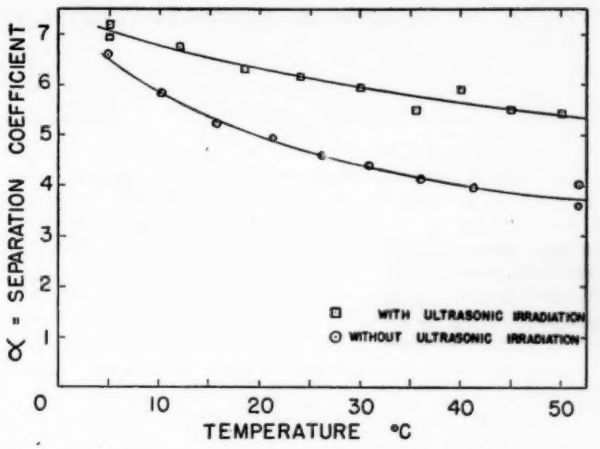

FIG. 2. Hydrogen-deuterium separation coefficient as a function of temperature with and without ultrasonic irradiation.

It seems that the most apparent interpretation of the observed results lies in the experimental fact that the discharged gases are removed from the electrode surface more rapidly with ultrasonic radiation than without it. Under these conditions the electrode-catalyzed exchange reaction between the discharged gas and the electrolyte does not have time to proceed as far as it does in the unirradiated electrolysis. Consequently, the experimentally observed separation coefficient more closely approaches the value that would be obtained if there were not exchange with the electrolyte.

In this connection, it is interesting to note that Glasstone, Laidler, and Eyring[6] have suggested that the decrease in the separation coefficient, obtained with platinum electrodes as the temperature is raised, is due to the increase in the rate of attaining the equilibrium between the discharged gas and the electrolyte. If the contact time between the discharged gas and the electrolyte on the electrode surface is decreased with ultrasonic radiation, one would expect a lower temperature dependence according to this interpretation. This was verified experimentally as shown by Fig. 2.

SUMMARY

It was found that ultrasonic radiation applied to the cathode of an electrolytic separation cell increases the coefficient for deuterium separation. This is interpreted as being due to the rapid removal of the discharged gases from the electrode surface, which at least partially prevents the exchange between these gases and the electrolyte.

[6] Glasstone, Laidler, and Eyring, *The Theory of Rate Processes* (McGraw-Hill Book Company, Inc., New York, 1941), first edition.

THE JOURNAL OF CHEMICAL PHYSICS VOLUME 19, NUMBER 12 DECEMBER, 1951

Vibrational Intensities. III. Carbon Dioxide and Nitrous Oxide*

DAVID F. EGGERS, JR.,† AND BRYCE L. CRAWFORD, JR.
School of Chemistry, University of Minnesota, Minneapolis, Minnesota

(Received August 13, 1951)

Experimental intensity measurements can be combined with known harmonic and anharmonic potential constants of molecules to determine the variation of dipole moment with displacement. We have used a finite Taylor's series for both potential energy and dipole moment. The effect on intensity of frequency variation over the band is included explicitly for both parallel and perpendicular bands as is Fermi resonance between several bands. Intensities of two fundamental and four combination bands in carbon dioxide were measured. A complete second-order perturbation treatment of intensities was carried out for several bands, and the possible relation of the results to resonance structures is mentioned. The relative importance of electrical and mechanical anharmonicity is indicated.

Two cubic potential constants were determined for nitrous oxide from measured intensities, known rotational convergence, normal coordinates, and bond distances. Using these constants a first-order intensity treatment was carried out for several combination bands. The intensities of three fundamental and three combination bands were measured. Discrepancies in measured rotational convergences are mentioned, and possible lines are suggested for further work on nitrous oxide.

INTRODUCTION

PREVIOUS work[1] relating the absolute absorption intensity of vibrational infrared bands to electrical properties of polyatomic molecules has largely been done on the basis of a zeroth-order treatment which assigns to each type of bond a dipole moment and a derivative of this moment with respect to bond length. The variation of these moments in the same molecule for different vibrational modes suggests that there may be large departures from this simple model. Mecke and co-workers[2] have done some interesting work on overtone intensities of C—H and O—H bonds; however, this treatment is limited to vibrations which interact only slightly with other vibrations in the molecule.

Work on diatomic molecules[3] suggested the lines along which the present work was done: intensity measurements on fundamentals plus certain overtone and combination bands are made; a perturbation treatment is carried out relating measured intensities to harmonic and anharmonic potential constants and a Taylor's series expansion of the dipole moment in normal coordinates; with sufficiently high symmetry, values of the higher order terms in the Taylor's series for the dipole moment are obtained. We shall refer to the anharmonic potential constants and their contribution to the intensity as mechanical anharmonicity; the higher-order terms in the Taylor's series for the dipole moment and their contribution to the intensity will be denoted electrical anharmonicity. Two linear triatomic molecules, carbon dioxide and nitrous oxide, were investigated.

BASIC THEORY

We shall employ the usual Born-Oppenheimer molecular model, with the nuclei regarded as point masses moving in the potential energy field produced by the averaged motion of the electrons. We shall also use the well-established relation[3] between the absorption coefficient, α_ν, and the line-strength, $S_A{}^B$

$$\alpha_\nu=(8\pi^3\nu_A{}^B/3hc)(N_A/g_A)[1-\exp(-h\nu_A{}^B/kT)]S_A{}^B \quad (1)$$

$\nu_A{}^B$ is the frequency of the line, N_A is the population of the energy-level A, g_A is its statistical weight. $S_A{}^B$ is defined:

$$S_A{}^B=\sum_{a,b}|(b|p|a)|^2 \quad (2)$$

p is the dipole moment. The experimentally observed intensity, A, is related to α_ν by

$$A=\int_{\text{band}}\alpha_\nu d\nu. \quad (3)$$

The usual procedure in summing α_ν over a vibrational band was to replace $\nu_A{}^B$ by the band-center frequency. Crawford and Dinsmore[3] investigated the summation for diatomic molecules including the frequency variation over the band and found the sum, neglecting vibrational dependence of B_e, to be

$$A_v{}^{v'}=[8\pi^3N(v)/3hc](\omega_v{}^{v'}+2B_e)\times S_v{}^{v'}[1-\exp(-hc\omega_v{}^{v'}/kT)] \quad (4)$$

$\omega_v{}^{v'}$ is the band-center frequency, B_e is the rotational constant, and the separation of rotational and vibrational problems permits expressing $S_A{}^B$ as a product of rotational and vibrational line-strengths:

$$S_A{}^B=S_j{}^{j'}S_v{}^{v'};\quad S_v{}^{v'}=|(v|p|v')|^2. \quad (5)$$

This sum is also independent of the presence of orbital electronic angular momentum about the internuclear

* This paper is based on a thesis submitted to the Graduate Faculty of the University of Minnesota by D. F. E. in partial fulfilment of the requirements for the Ph.D. degree.

† Present address: Department of Chemistry and Chemical Engineering, University of Washington, Seattle, Washington.

[1] E. B. Wilson, Jr., and A. J. Wells, J. Chem. Phys. **14**, 578 (1946); Thorndike, Wells, and Wilson, J. Chem. Phys. **15**, 157 (1947); A. M. Thorndike, J. Chem. Phys. **15**, 868 (1947); Bell, Vago, and Thompson, Proc. Roy. Soc. (London) **A192**, 498 (1948); A. R. H. Cole and H. W. Thompson, Trans. Faraday Soc. **46**, 103 (1950); E. R. Nixon and P. C. Cross, J. Chem. Phys. **18**, 1316 (1950).

[2] R. Mecke, Z. physik. Chem. **B33**, 156 (1936); R. Mecke, Z. Electrochem. **54**, 38 (1950). The latter contains references to his other intensity work.

[3] B. L. Crawford, Jr., and H. L. Dinsmore, J. Chem. Phys. **18**, 983, 1682 (1950).

axis as long as it does not change during the transition. The sum for parallel bands of linear polyatomic molecules, in which there is, of course, no change in the vibrational angular momentum, is computed in identical fashion with the electronic orbital angular momentum replaced by the vibrational angular momentum, giving Eq. (4).

We shall also need the similar sum for the perpendicular bands of a linear triatomic molecule; we start with the line-strengths given by Rademacher and Reiche,[4]

$$\begin{aligned} S_j{}^{j-1}{}_l{}^{l+1}&=(j-l)(j-l-1)/4j \\ S_j{}^{j}{}_l{}^{l+1}&=(j-l)(j+l+1)(2j+1)/4j(j+1) \\ S_j{}^{j+1}{}_l{}^{l+1}&=(j+l+2)(j+l+1)/4(j+1). \end{aligned} \tag{6}$$

Here l is the quantum number of vibrational angular momentum and takes on the values $n_2, n_2-2, \cdots, -n_2$; n_2 is the quantum number of the perpendicular vibration. Combining these with the expression for the frequency of the vibration-rotation components and summing gives

$$\begin{aligned} A_v{}^{v'}{}_l{}^{l+1}=&[8\pi^3N(v)/3hc]\textstyle\sum_j \frac{1}{2}(2j+1)(\omega_v{}^{v'}+B_e) \\ &\times\exp(-E_j/kT)[1-\exp(-h\omega_v{}^{v'}/kT)]S_v{}^{v'}/Z \end{aligned} \tag{7}$$

$$Z=\textstyle\sum_j g_j\exp(-E_j/kT) \tag{8}$$

the sum over j in Eq. (7) then cancels the Z in the denominator to give

$$\begin{aligned} A_v{}^{v'}{}_l{}^{l+1}=&[8\pi^3N(v)/3hc](\omega_v{}^{v'}+B_e)\tfrac{1}{2}|(v|p|v')|^2 \\ &\times[1-\exp(-h\omega_v{}^{v'}/kT)]. \end{aligned} \tag{9}$$

The transition $l\rightarrow l-1$ gives exactly the same expression. In the case $l\neq 0$ these two transitions will give rise to two different vibration-rotation bands. If $l=0$, both transitions will coincide, and we have

$$\begin{aligned} A_v{}^{v'}{}_{l=0}{}^{|l|=1}=&[8\pi^3N(v)/3hc](\omega_v{}^{v'}+B_e)|(v|p|v')|^2 \\ &\times[1-\exp(-h\omega_v{}^{v'}/kT)]. \end{aligned} \tag{10}$$

We are left, then, with the purely vibrational problem in axes fixed in the molecule.

We shall make use of a Taylor's-series expansion in two connections: the potential energy and the dipole moment of the molecule will each be expressed as a Taylor's series about the equilibrium position. The validity of this approach is amply justified in the mechanical problem since all the observed energy levels can be predicted to within a very few wave numbers in our two molecules. However, its applicability to the dipole moment has not been justified, though the higher order coefficients do turn out smaller than the zeroth-order.

Crawford and Dinsmore[3] have shown how the various orders in the matrix of the dipole moment in the perturbed problem, $\mathbf{p}$, can be expressed as matrix products of the dipole moment matrices in the zeroth-order problem, $\mathbf{p}_0$, and the unitary matrix which diagonalizes the Hamiltonian, $\mathbf{C}$.

$$\begin{aligned} \mathbf{p}^0&=\mathbf{p}_0{}^0 \\ \mathbf{p}'&=\mathbf{C}^{+\prime}\mathbf{p}_0{}^0+\mathbf{p}_0{}^0\mathbf{C}'+\mathbf{p}_0{}' \\ \mathbf{p}''&=\mathbf{C}^{+\prime\prime}\mathbf{p}_0{}^0+\mathbf{p}_0{}^0\mathbf{C}''+\mathbf{C}^{+\prime}\mathbf{p}_0{}'+\mathbf{p}_0{}'\mathbf{C}' \\ &\qquad +\mathbf{C}^{+\prime}\mathbf{p}_0{}^0\mathbf{C}'+\mathbf{p}_0{}'' \end{aligned} \tag{11}$$

$$\begin{aligned} \mathbf{p}_0&=\mathbf{p}_0{}^0+\gamma\mathbf{p}_0{}'+\gamma^2\mathbf{p}_0{}''+\cdots \\ \mathbf{C}&=\mathbf{C}^0+\gamma\mathbf{C}'+\gamma^2\mathbf{C}''+\cdots \\ \mathbf{p}&=\mathbf{p}^0+\gamma\mathbf{p}'+\gamma^2\mathbf{p}''+\cdots \end{aligned} \tag{12}$$

$\mathbf{C}^+$ denotes the hermitian conjugate of the matrix $\mathbf{C}$, and $\mathbf{C}^0$ is the unit matrix. The power of γ indicates the order of the term in which it occurs; it is the usual "parameter of smallness" and is set equal to unity for computations. We shall find it convenient to employ dimensionless coordinates, μ_i, for the displacements; these are related to the normal coordinates, q_i, by

$$\mu_i=2\pi(c\omega_i/h)^{\frac{1}{2}}q_i \tag{13}$$

$i=1$, 2, and 3 for triatomic molecules, and ω_i is the ith zeroth-order normal frequency. We shall assume that terms of the potential energy which are quadratic in the μ_i are zeroth order, cubic in the μ_i first order and quartic in the μ_i second order. For the dipole moment we shall take terms linear in the dimensionless coordinates as zeroth order, quadratic as first order, and cubic as second order.

The elements of $\mathbf{C}$ which connect Fermi-resonant levels are omitted from the perturbation calculation and Fermi resonance is introduced explicitly after the perturbation calculation. Let ψ_G be the (vibrational) wave function of the ground state and ψ_{+0} and ψ_{-0} the perturbed wave functions of the upper and lower states of a Fermi-resonant pair before the introduction of Fermi resonance; then

$$\begin{aligned} \psi_+&=s\psi_{+0}-t\psi_{-0} \\ \psi_-&=t\psi_{+0}+s\psi_{-0} \\ s^2+t^2&=1 \end{aligned} \tag{14}$$

ψ_+ and ψ_- are the perturbed wave functions including Fermi resonance. Let A_{+0}, A_{-0}, A_+, and A_- be the band intensities of transitions from the ground state to the corresponding states. Then from Eqs. (4) and (10),

$$\begin{aligned} A_{+0}&=k\nu_{+0}\left|\int\cdots\int\psi_G{}^*p\psi_{+0}d\tau\right|^2=k\nu_{+0}|p_{+0}|^2 \\ A_{-0}&=k\nu_{-0}\left|\int\cdots\int\psi_G{}^*p\psi_{-0}d\tau\right|^2=k\nu_{-0}|p_{-0}|^2 \end{aligned} \tag{15}$$

$$\begin{aligned} A_+&=k\nu_+\left|\int\cdots\int\psi_G{}^*p\psi_+d\tau\right|^2 \\ &=k\nu_+\left|\int\cdots\int\psi_G{}^*p(s\psi_{+0}-t\psi_{-0})d\tau\right|^2 \\ A_-&=k\nu_-\left|\int\cdots\int\psi_G{}^*p(t\psi_{+0}+s\psi_{-0})d\tau\right|^2 \end{aligned} \tag{16}$$

[4] H. Rademacher and F. Reiche, Z. Physik **41**, 453 (1927).

$\nu_i = \omega_i' + B_e$ for perpendicular bands and

$\nu_i = \omega_i' + 2B_e$ for parallel bands; ω_i' is the band center.

$k = [8\pi^3 N(v)/3hc][1-\exp(-h\nu/kT)]$.

Finally, we have

$$\begin{aligned} A_+ &= k\nu_+ |sp_{+0} - tp_{-0}|^2 \\ A_- &= k\nu_- |tp_{+0} + sp_{-0}|^2. \end{aligned} \tag{17}$$

Even if $s \cong t$, we can distinguish three cases of interest:

1. $|p_{+0}| \gg |p_{-0}|$ or $|p_{-0}| \gg |p_{+0}|$
2. $p_{+0} \cong p_{-0}$
3. $p_{+0} \cong -p_{-0}$.

Case 1 is the usual one, and we find that $A_+ \cong A_-$. However, in case 2, $A_- \gg A_+$, and in case 3, $A_+ \gg A_-$. Thus we see that even if the two bands are in complete Fermi resonance, they need not have the same intensity. The pair at 1932 and 2076 cm^{-1} in CO_2 corresponds to case 3: A_+ is an order of magnitude larger than A_-, even though s^2 and t^2 are 0.60 and 0.40, respectively.

As an aid in reducing the number of elements in $\mathbf{C}^{+\prime}\mathbf{p}_0^0 + \mathbf{p}_0^0\mathbf{C}'$ to be computed, we note that $\mathbf{C}'$ is skew hermitian by its definition,[5]

$$C_{ln}' = H_{ln}'/(G_n^0 - G_l^0) \tag{18}$$

if $\mathbf{H}'$, the matrix of the first-order hamiltonian, is hermitian. G_i^0 is the energy of the state i. $\mathbf{H}'$ is hermitian in N_2O and CO_2 since it contains only coordinates (from V'). We may, then, replace $\mathbf{C}^{+\prime}$ by $-\mathbf{C}'$, and get

$$\mathbf{C}^{+\prime}\mathbf{p}_0^0 + \mathbf{p}_0^0\mathbf{C}' = \mathbf{p}_0^0\mathbf{C}' - \mathbf{C}'\mathbf{p}_0^0, \tag{19}$$

which is the commutator of $\mathbf{C}'$ and $\mathbf{p}_0^0$. If, then, $\mathbf{C}'$ and $\mathbf{p}_0^0$ should commute, Eq. (19) will vanish. Now in both CO_2 and N_2O we can express any arbitrary displacement of the molecule about its center of mass in terms of the four dimensionless coordinates μ_1, μ_{2x}, μ_{2y} and μ_3. Or, we can change to the coordinates ρ and ϕ instead of μ_{2x} and μ_{2y} where $\rho^2 = \mu_{2x}^2 + \mu_{2y}^2$ and $\phi = \tan^{-1}(\mu_{2x}/\mu_{2y})$. We shall denote the quantum numbers corresponding to the coordinates μ_1, ρ, ϕ, and μ_3 by n_1, n_2, l, and n_3. If we have an operator which can be factored into four factors, one depending only on μ_1, another only on ρ, another only on ϕ, and a last only on μ_3; i.e.,

$$\alpha = \alpha_1(\mu_1)\alpha_2(\rho)\alpha_\phi(\phi)\alpha_3(\mu_3),$$

then the matrix of this operator can be written as the direct product of four ordinary, or "two-dimensional" matrices:

$$\begin{aligned} (n_1 n_2^l n_3|\alpha|n_1' n_2'^{l'} n_3') = (n_1|\alpha_1|n_1') \times (n_2|\alpha_2|n_2') \\ \times (l|\alpha_\phi|l') \times (n_3|\alpha_3|n_3'). \end{aligned} \tag{20}$$

In forming the direct product we can write the factors in any order we choose; i.e., the factors commute among themselves; therefore, in checking for commutation between two direct products of different operators each of which satisfies our factoring condition, we need only look at the components in the direct products.

As an example, consider the commutation of the matrices of μ_3 and μ_1^3. By the orthogonality of the wave functions the μ_3 matrix is the direct product of unit matrices in n_1, n_2, and l, and a non-unit matrix in n_3. The μ_1^3 matrix is the direct product of a non-unit matrix in n_1 and unit matrices in n_2, l, and n_3. By recalling that a unit matrix commutes with every matrix and applying this in turn to each of the four simple matrix products, we see that the μ_1^3 and the μ_3 matrices commute.

Experimental intensity measurements give us the perturbed dipole moment matrix elements, the $(v|p|v')$ of Eqs. (4) and (10); by writing a Taylor's series in the dipole moment with undetermined coefficients and using the known harmonic and anharmonic potential constants, which determine $\mathbf{C}$, we can relate the coefficients in the dipole moment series to the observed intensity and determine the unknown coefficients.

TABLE I. Observed intensities.

Band, cm^{-1}	Intensity, cps cm at S.T.P. This research	Dispersion[a,b]	Wilson *et al.*[b]
A CO_2			
667	$48_4 \times 10^{10}$	538×10^{10}	560×10^{10}
2349	8080	7680	8600
1932	0.01_4		
2076	0.43 (*P* and *Q*)		
2076	0.15_7 (*Q* only)		
3614	$81._9$		
3716	$117._2$		
B N_2O			
589	$62._6 \times 10^{10}$	108×10^{10}	120×10^{10}
1285	73_4	802	1150
2224	4950	4584	5600
1167	25.5	28	
1868	1.22		
2798	7.2_3		

[a] See references 19 and 1.
[b] See reference 1.

[5] J. H. Van Vleck, *Electric and Magnetic Susceptibilities* (Oxford University Press, New York, 1932).

EXPERIMENTAL

The spectra were obtained with the aid of a Perkin-Elmer monochromator using LiF, NaCl, and KBr prisms. The radiation from either the Globar or Nernst glower was chopped at 5 cps, dispersed by the monochromator, detected by an evacuated thermocouple, amplified by a tuned ac amplifier, and recorded on a strip-chart potentiometer. The source unit was designed for greater flexibility of sample mounting and completely enclosed. This latter feature permitted flushing with dry tank nitrogen which eliminated all trace of atmospheric CO_2 absorption at 2350 cm^{-1} even with the LiF prism.

The stronger bands were run using a 10-cm Perkin-Elmer gas cell; gas pressures were measured by a mercury manometer and barometric readings; pressures were corrected to mercury at 0°C. For the lower partial pressures, samples were made up by successive dilution and expansion with dry tank nitrogen in such a way as to assure thorough mixing of gases at all times.

Gases were, with the exception noted below, taken directly from commercial steel cylinders without further purification; analysis by the mass spectrometer showed only insignificant amounts of impurities were present. The only case of interference was by CO in the 2076 cm^{-1} band of CO_2; the trace of CO was oxidized to CO_2 by traces of oxygen in the gas in the presence of a catalyst.

A White cell was constructed for measurement of weak bands and used on the 1932 and 2076 cm^{-1} bands in CO_2. The mirrors were standard ones used in the Perkin-Elmer one-meter gas cell with the large one cut in half. Paths of 275 cm were used in this research, but paths up to six or seven meters were attainable with this cell. The mirrors and associated mountings were bolted to a half-inch steel plate eleven inches in diameter which also contained the entrance and exit windows. The housing was a piece of six-inch steel pipe with a cap welded on one end; the other end bolted on the eleven-inch plate so as to enclose the mirrors. Sealing on the plate was effected by an asbestos gasket, and mirror motion was possible by a shaft sealed with an O-ring. In this manner pressures up to several hundred pounds per square inch could be attained, though only sixty were used in this work.

A point of caution in the design of a White cell with large aperture is that both movable mirrors must be pivoted about the same axis, the center of curvature of the fixed mirror, for minimum aberrations.

The methods justified by Wilson and Wells[1] for experimentally obtaining the true integrated absorption coefficient, A in Eq. (3), were used. Briefly, one employs a non-absorbing gas in each sample to broaden the rotational fine structure of the absorbing gas, and one extrapolates the apparent (integrated) absorption coefficient B, to zero partial pressure to obtain the true absorption coefficient A.

All observed bands were replotted as $\ln T$ *vs* frequency, where T, the transmittance, is the ratio of transmitted to incident energy. The area between a band envelope and the $T=1$ line is, then, apparent absorption in frequency units. Reduction of this to the value it would have for atmospheric pressure and one centimeter thickness gives the apparent absorption coefficient, B.

Finally, the apparent absorption coefficients of a band at a series of partial pressures were plotted as a function of partial pressure and extrapolated to zero partial pressure to give A for the band in question. This procedure is illustrated in Figs. 2–4.

All CO_2 samples in the 10-cm cell were run at a total pressure of approximately two atmospheres. A check of the pressure effect in CO_2 showed that this pressure was adequate at the low partial pressures. The CO_2 samples run in the White cell were at a total pressure of five atmospheres; this broadened the rotational structure amply even at higher partial pressures. Earlier work on N_2O[1] indicated that even one atmosphere was sufficient; therefore, one atmosphere of air was used for it.

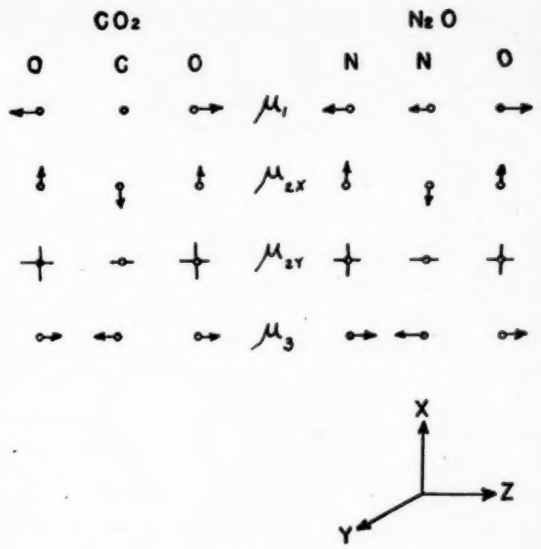

FIG. 1. Coordinates.

Our absorption coefficients for all bands measured are given in Table I together with values of other workers. We have, somewhat arbitrarily, assigned errors of ± 10 percent to our absorption coefficients because of better present-day instruments, except for the 1932 and 2076 cm^{-1} bands in CO_2, which were given ± 50 and ± 20 percent respectively because of greater measuring difficulties. Replotting of the bands introduces considerable personal judgment, as does also extrapolation of the apparent absorption coefficient. Operation of the polar planimeter in measuring areas was found to introduce only negligible error; each area was measured at least four times, twice in the clockwise and twice in the counterclockwise sense and the average of the results used. A tangent at the origin of a plot: apparent absorption *vs* partial pressure was also tried to determine the absorption coefficient, but since more personal judgment is involved, the method was discarded. Finally, the experimental value for the matrix element of the dipole moment is computed using our absorption coefficient in the square root of Eq. (4) or (10) for parallel or perpendicular bands with DuMond and Cohen's fundamental constants.[6]

CARBON DIOXIDE

The positive senses of the dimensionless coordinates are indicated in Fig. 1. The hamiltonian used is that of

[6] J. W. M. DuMond and E. R. Cohen, Revs. Modern Phys. 20, 82 (1948).

TABLE II. Dipole moment coefficients of CO_2 in debyes.

Upper state	Band (cm^{-1})	Coefficient	This research		Remarks
01^10	667	$d_2 = +0.150 \pm 0.007$			
00^01	2349	$d_3 = +0.45 \pm 0.02$			
			d_{13}	d_{223}	
10^01 }	3614–3716		$+0.122 \pm 0.003$	-0.013 ± 0.010	++
02^01 }			$+0.050 \pm 0.003$	$+0.044 \pm 0.017$	+−
			$+0.029 \pm 0.003$	-0.068 ± 0.011	−+
			-0.039 ± 0.003	-0.011 ± 0.006	−−
03^10 }	2076	$d_{12} = +0.058 \pm 0.009$			+, P & Q
11^10 }		-0.034 ± 0.009			−, P & Q
03^10 }		$+0.040 \pm 0.006$			+, Q only
11^10 }		-0.016 ± 0.006			−, Q only
	1932	$d_{12} = +0.021 \pm 0.005$			+
		$+0.001 \pm 0.005$			−

Potential constants used: (in cm^{-1})

k_{111}	-35 ± 5	k_{2222}	-1.6 ± 2.1
k_{122}	$+71.3 \pm 0.4$	ω_1	1351.2
k_{133}	$+250 \pm 7$	ω_2	672.2
k_{2233}	-25.7 ± 0.6	ω_3	2396.4

Dennison;[7] the vibrational part is, in ergs,

$$H=(2\pi^2c/h)[\omega_1 p_1^2+\omega_2(p_{2x}^2+p_{2y}^2)+\omega_3 p_3^2] +[1/2I(1+\gamma_1\mu_1)^2]\{[-(\omega_3/\omega_2)^{\frac{1}{2}}\mu_{2y}p_3 +(\omega_2/\omega_3)^{\frac{1}{2}}\mu_3 p_{2y}]^2+[-(\omega_2/\omega_3)^{\frac{1}{2}}\mu_3 p_{2x} +(\omega_3/\omega_2)^{\frac{1}{2}}\mu_{2x}p_3]^2\}+V \quad (21)$$

$$\gamma_1=(2B_e/\omega_1)^{\frac{1}{2}}. \quad (22)$$

p_i is the momentum conjugate to μ_i.

$$V=\tfrac{1}{2}hc[\omega_1\mu_1^2+\omega_2\rho^2+\omega_3\mu_3^2] +\gamma hc[k_{111}\mu_1^3+k_{122}\mu_1\rho^2+k_{133}\mu_1\mu_3^2] +\gamma^2hc[k_{1111}\mu_1^4+k_{2222}\rho^4+k_{3333}\mu_3^4 +k_{1122}\mu_1^2\rho^2+k_{1133}\mu_1^2\mu_3^2+k_{2233}\rho^2\mu_3^2]. \quad (23)$$

The first set of terms in H is the usual zeroth-order kinetic energy, the second set is the (second-order) kinetic energy of vibrational angular momentum, while the last term is the potential energy. The separation of V into zeroth-, first-, and second-order terms is indicated by the corresponding power of γ in the coefficient.

By carrying out the perturbation treatment described earlier, all first- and second-order terms in the matrix **p** for the transitions (00^00) to (11^10), (03^10), (10^01), and (02^01) were computed; $(n_1n_2^ln_3)$ is the usual symbol for the state with the indicated quantum numbers. The

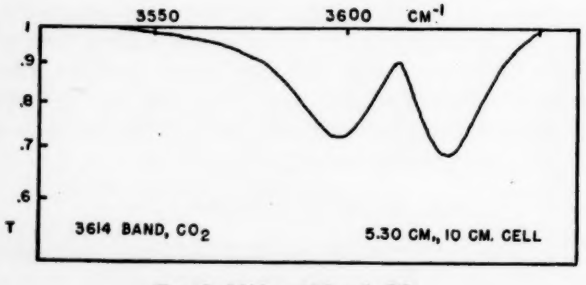

FIG. 2. 3614 cm^{-1} band, CO_2.

[7] D. M. Dennison, Revs. Modern Phys. **12**, 175 (1940).

form of the Taylor's series assumed for the dipole moment was

$$p=d_2\rho+d_3\mu_3+\gamma(d_{12}\mu_1\rho+d_{13}\mu_1\mu_3) +\gamma^2(d_{223}\rho^2\mu_3+\cdots)+\cdots. \quad (24)$$

The results of this straightforward but rather lengthy calculation are the following:

$$(00^00|\,p'\,|11^10)=-2^{\frac{1}{2}}k_{122}d_2(\omega_1+\omega_2)/[\omega_1(\omega_1+2\omega_2)]-2^{-\frac{1}{2}}d_{12}$$

$$(00^00|\,p''\,|03^10)=2^{\frac{1}{2}}d_2[-3k_{2222}/2\omega_2-(k_{122}/4\omega_2) \times\{-[(\tfrac{3}{2}k_{111}+4k_{122}+\tfrac{1}{2}k_{133})/\omega_1] \times[1-2\omega_2/(\omega_1+2\omega_2)] +(\tfrac{3}{2}k_{111}+3k_{122}+\tfrac{1}{2}k_{133})/(\omega_1+2\omega_2)\} +k_{122}d_{12}/2d_2(\omega_1+2\omega_2)]$$

$$(00^00|\,p'\,|10^01)=k_{133}d_3[\omega_2/\omega_1(\omega_1+2\omega_2)]+d_{13}/2 \quad (25)$$

$$(00^00|\,p''\,|02^01)=2^{-\frac{1}{2}}d_3[k_{2233}[(1/\omega_2)-1/(\omega_2+\omega_3)] +(k_{122}/4\omega_2)\{[(\tfrac{3}{2}k_{111}+3k_{122}+\tfrac{1}{2}k_{133})/(\omega_1+2\omega_2)]-[(\tfrac{3}{2}k_{111}+3k_{122}+\tfrac{3}{2}k_{133})/\omega_1] \times[1-2\omega_2/(\omega_1+2\omega_2)]\} +k_{122}k_{133}/4(\omega_2+\omega_3)(\omega_1+2\omega_2) +B_e(\omega_2+\omega_3)/2\omega_2^2 -k_{122}d_{13}/2d_3(\omega_1+2\omega_2)]-2^{-\frac{1}{2}}d_{223}$$

$$(00^00|\,p^0\,|01^10)=-d_2$$

$$(00^00|\,p^0\,|00^01)=2^{-\frac{1}{2}}d_3$$

$(00^00|\,p''\,|11^10)$, $(00^00|\,p'\,|03^10)$, $(00^00|\,p''\,|10^01)$, and $(00^00|\,p'\,|02^01)$ all vanish as do the first-order corrections to the fundamentals; we have neglected the second-order corrections to the fundamentals.

Placing the observed intensities and known potential constants in these relations enables us to calculate the d's. We also use Eq. (17) to include the effect of Fermi resonance. The s and t for Fermi resonance come from the potential constant k_{122}.

The square root necessary in using Eqs. (4) and (10) introduces an ambiguity in the signs of the d's. Electronegativities suggest that a slight excess negative charge resides on the oxygen atoms and an excess positive charge on the carbon atom; this fixes the signs of d_2 and d_3. The positive sense of the dipole moment is taken from the positive to the negative charge.

The precision of the data on the 3614 and 3716 cm^{-1} bands was thought to warrant the second-order coefficient d_{223}; therefore, appropriate p's were put in Eqs. (17), and the two equations solved simultaneously for d_{13} and d_{223}. All four possibilities introduced by sign ambiguity are given in Table II; the plus and minus signs under "remarks" indicate the choice for the square root. The precision of the data on the 1932 and 2076 cm^{-1} bands was not thought to warrant a second-order term. Table II also contains the potential constants used in the calculation and the errors assumed in them. Values of the potential constants are those of Dennison[7] except for k_{111}; the average of Dennison's

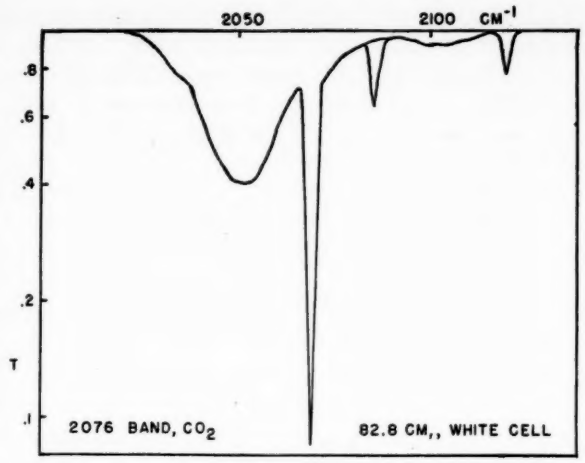

FIG. 3. 2076 cm^{-1} band, CO_2.

value and that computed from the Lake Angelus work[8] on CO_2 solar is used for k_{111}. An independent value of the Fermi resonance coefficients for the 3614–3716 cm^{-1} pair was had from Jones and Bell;[9] this was useful in estimating errors. Measured intensity errors are those previously given. All independent errors were combined in random phase to give the probable errors in the final results.

None of the four sets of possible pairs of d_{13} and d_{223} values is sufficiently unreasonable to be discarded. The greater number of solutions seems to favor a positive value for d_{13}; this would mean that stretching of both bonds gives rise to a greater change in dipole moment for the antisymmetric vibration and is just the opposite of the situation with the force constants, where $k_{133}<0$. It might be argued that this is in agreement with the five principal resonance structures for CO_2;

$$O=\underset{1}{C}=O \quad \overset{+}{O}\equiv\underset{2}{C}-\bar{O} \quad \bar{O}-\underset{3}{C}\equiv\overset{+}{O}$$

$$\bar{O}-\overset{+}{\underset{4}{C}}=O \quad O=\overset{+}{\underset{5}{C}}-\bar{O},$$

where simultaneous stretching of both bonds, one more than the other, would favor structures 4 and 5 and give rise to a positive value of d_{13}. In any event, the electrical anharmonicity seems definitely the predominant factor accounting for the observed intensity of the 3614 and 3716 cm^{-1} bands.

The situation in the 1932 and 2076 cm^{-1} bands is much less satisfactory; we can only say that mechanical anharmonicity appears to be relatively more important than in the 3614 and 3716 cm^{-1} bands.

The envelope of the 2076 cm^{-1} band is very odd: Fig. 3 shows a P branch and a Q branch but no R branch. This is consistent with the low dispersion traces of Martin and Barker,[10] of Barker and Wu,[11] and the high dispersion solar work of Shaw *et al.*[12] However, since all our traces on the 1932 cm^{-1} band have only a Q branch, we have calculated the d's involved with both total band intensity and Q branch intensity only for the 2076 cm^{-1} band.

[8] Goldberg, Mohler, McMath, and Pierce, Phys. Rev. **76**, 1848 (1949).
[9] R. Jones and E. E. Bell, Phys. Rev. **79**, 1004 (1950).

NITROUS OXIDE

The coordinate system used for N_2O and the positive senses for the various normal coordinates are indicated in Fig. 1; the numbering of the vibrations is that of Herzberg.[13] In terms of the dimensionless coordinates the vibrational hamiltonian to first orders is, in cm^{-1}:

$$\begin{aligned}H=(2\pi^2/h^2)[&\omega_1 p_1^2+\omega_2(p_{2x}^2+p_{2y}^2)+\omega_3 p_3^2]\\&+\tfrac{1}{2}[\omega_1\mu_1^2+\omega_2\rho^2+\omega_3\mu_3^2]\\&+\gamma[k_{111}\mu_1^3+k_{113}\mu_1^2\mu_3+k_{122}\mu_1\rho^2\\&\quad+k_{133}\mu_1\mu_3^2+k_{223}\rho^2\mu_3+k_{333}\mu_3^3]. \quad (26)\end{aligned}$$

There are also nine second-order potential constants, making a total of eighteen zeroth-, first-, and second-order potential constants to be determined. The experimental band centers give us only ten relations among these constants; therefore, even with the addition of the three rotational convergences recently determined by G. and L. Herzberg,[14] we still have insufficient data to determine all potential constants through second orders.

However, a vibration-rotation perturbation calculation[15] shows that α_1 is related only to k_{111} and k_{113}, α_2 is related only to k_{223} and k_{122}, and α_3 is related only to k_{133}

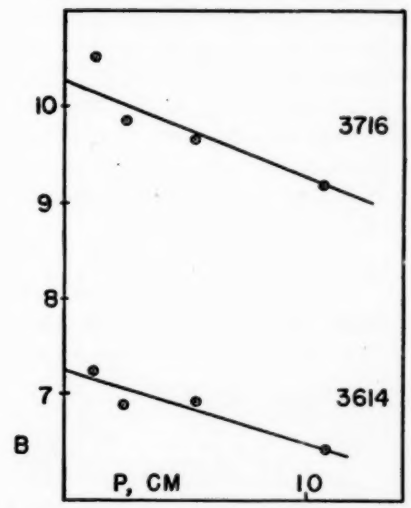

FIG. 4. Extrapolation of B, 3716 and 3614 cm^{-1} bands, CO_2.

[10] P. E. Martin and E. F. Barker, Phys. Rev. **41**, 291 (1932).
[11] E. F. Barker and T. Y. Wu, Phys. Rev. **45**, 1 (1934).
[12] Shaw, Chapman, Howard, and Oxholm, Astrophys. J. **113**, 268 (1951).
[13] G. Herzberg, *Infrared and Raman Spectra of Polyatomic Molecules* (D. Van Nostrand Company, Inc., New York, 1945).
[14] G. Herzberg and L. Herzberg, J. Chem. Phys. **18**, 1551 (1950).
[15] A. H. Nielsen, J. Chem. Phys. **11**, 160 (1943).

TABLE III. Dipole moment coefficients of N_2O in debyes.

Upper state	Band (cm^{-1})	Coefficient	This research	Using dispersion[a] d_2	Remarks
10^00	1285	d_1	$+0.185\pm.0009$		
01^10	589	d_2	$+0.058$ (?)	$+0.074\pm0.004$	
00^01	2224	d_3	$+0.364\pm0.02$		
11^10	1868	d_{12}	$\pm0.0041\pm0.0007$	$\pm0.0035\pm0.0007$	
		d_{12}	$\pm0.0084\pm0.0007$	$\pm0.0090\pm0.0007$	
01^10	2798	d_{23}	$+0.010\pm0.002$	$+0.010\pm0.002$	small k_{223}
		d_{23}	-0.014 ± 0.002	-0.015 ± 0.002	
		d_{23}	-0.007 ± 0.002	-0.012 ± 0.002	large k_{223}
		d_{23}	-0.032 ± 0.002	-0.037 ± 0.002	

Potential constants used, in cm^{-1}:
k_{122} $\pm31.4\pm3$; k_{223} -66.8 or -684 ± 43; ω_1 1288.2; ω_2 588.0; ω_3 2237.2

[a] See reference 19.

and k_{333}. Thus, if some means were available for determining one of these first-order potential constants, another could be obtained from the observed rotational convergence.

Fortunately, k_{122} is accessible by the Fermi resonance between (10^00) and (02^00). We had hoped that Plyler and Barker's work[16] on N_2O would give this, but their observed convergences, $+0.0017$ cm^{-1} for the 1285 cm^{-1} band and -0.0009 cm^{-1} for the 1167 cm^{-1} band give either no Fermi resonance or "less than none" when combined with Herzberg's[14] $\alpha_1=+0.0017_0$ cm^{-1} and $\alpha_2=-0.0002_2$ cm^{-1}. Perhaps those with access to grating instruments might examine these bands again to check the convergences. Instead of using rotational convergence to determine k_{122} we measured the intensities of both bands; and assuming all the intensity of the 1167 cm^{-1} band to be due to Fermi resonance, we found s and t by Eqs. (17). Then $k_{122}=\pm31.4$ cm^{-1}, since[7] $k_{122}=\Delta st/2^{\frac{1}{2}}$; Δ is the difference, in cm^{-1}, between the observed upper and lower states.

Nielsen's expressions[15] for the α_i were checked, and the only discrepancies found were that the sign of the term in α_1 involving k_{113} should be negative and not positive, and a square root was omitted in printing of $\sin\gamma$; the correct relation is

$$\sin\gamma=(\tfrac{1}{2})^{\frac{1}{2}}\{1+[(k_1'-k_3')^2/(4k_4'^2+(k_1'-k_3')^2)]^{\frac{1}{2}}\}^{\frac{1}{2}}. \quad (27)$$

Professor Nielsen has confirmed these changes. The relation which we shall use to compute k_{223} is

$$\alpha_2=B_e\{8^{\frac{1}{2}}B_e^{\frac{1}{2}}(\xi_{2231}k_{122}/\omega_1^{\frac{1}{2}}-\xi_{2211}k_{223}/\omega_3^{\frac{1}{2}}) -(B_e/\omega_2)[(3\omega_2^2+\omega_1^2)\xi_{2211}^2/(\omega_2^2-\omega_1^2) +(3\omega_2^2+\omega_3^2)\xi_{2231}^2/(\omega_2^2-\omega_3^2)]\} \quad (28)$$

$B_e=h/8\pi^2Ic$; I is the equilibrium moment of inertia. Nielsen gives expressions for the ξ_{ijkl}; these involve the atomic masses, equilibrium bond distances, and the coefficients $\sin\gamma$ and $\cos\gamma$ in the transformation from his coordinates q_1' and q_3' to the normal coordinates q_1 and q_3. It should be noted in comparing this expression for α_2 with Nielsen's that our potential constants are defined in terms of dimensionless coordinates and his are defined in terms of normal coordinates.

Coles, Elyash, and Gorman[17] have determined the ground-state bond distances from microwave work; these were used as equilibrium distances. Richardson and Wilson[18] have determined the zeroth-order interaction constant, and the normal coordinates were computed from their work. In terms of cartesian displacements of the atoms, Δz_i (see Fig. 1), they are

$$q_1=-0.5939m_1^{\frac{1}{2}}\Delta z_1-0.2300m_2^{\frac{1}{2}}\Delta z_2+0.7709m_3^{\frac{1}{2}}\Delta z_3$$
$$q_3=+0.5736m_1^{\frac{1}{2}}\Delta z_1-0.7930m_2^{\frac{1}{2}}\Delta z_2+0.2053m_3^{\frac{1}{2}}\Delta z_3. \quad (29)$$

We have, then,

$$\xi_{2211}=-0.2269$$

and

$$\xi_{2231}=-0.9739.$$

Herzberg's $\alpha_2=-0.0002_2$ cm^{-1} and $k_{122}=\pm31.4$ cm^{-1} give $k_{223}=-66.8$ or -684 cm^{-1}.

The probable errors in the potential constants determined in this way are quite large. k_{122} may be in error by more than the precision of intensity measurements indicates, if the 1167 cm^{-1} band has intensity "of its own" in addition to that from Fermi resonance. We have assigned a ten percent error to k_{122}. α_2 was given an error of ±0.00005 cm^{-1}, and errors in the normal coordinates were computed from Richardson and Wilson's error estimates on their force constants. All independent errors were combined in random phase to give the probable error of ±43 cm^{-1} to k_{223}. The smaller value, -66.8 cm^{-1} for k_{223} seems much more reasonable; it arises from the positive sign on k_{122}, and in CO_2, k_{122} is positive.

The assumed form of the Taylor's series for the dipole moment is

$$p=d_1\mu_1+d_2\rho+d_3\mu_3+d_{12}\mu_1\rho+d_{23}\rho\mu_3+\cdots. \quad (30)$$

Application of our criterion for the vanishing of the commutator of $\mathbf{p}^0$ and $\mathbf{C}'$ shows that only k_{122} can give a first-order mechanical correction to the $(00^00)\rightarrow(11^10)$ band intensity, and only k_{223} can give a first-order mechanical correction to the $(00^00)\rightarrow(01^11)$ band intensity. Therefore, a first-order treatment could be done on both of these bands. The form of the equation for the $(00^00)\rightarrow(11^10)$ band is identical with the corresponding equation for CO_2; the equation for the other band, $(00^00)\rightarrow(01^11)$, is of the same form except that 1 anywhere in a subscript is replaced by 3. The signs of d_1, d_2, and d_3 were determined by resonance structures which suggest that the central atom should be positive and the end atoms negative. Because of the large difference in the measured intensity of the 589 cm^{-1} band between our work and the work of others, we

[16] E. K. Plyler and E. F. Barker, Phys. Rev. **38**, 1827 (1931).

[17] Coles, Elyash, and Gorman, Phys. Rev. **72**, 973 (1947).

[18] W. S. Richardson and E. B. Wilson, Jr., J. Chem. Phys. **18**, 694 (1950).

have made the calculations using both our d_2 and the dispersion value. We have also computed d_{23} using both values for k_{223}, though the large value is probably not correct. The results are given in Table III; estimated errors are only those which can be computed, and do not include errors due to poor representation by a Taylor's series, etc.

We should like to suggest that a measurement of higher vibrational levels on isotopic N_2O, preferably N_2O^{18}, should give a set of different α_i from which one could get a rough estimate of all the cubic potential constants of N_2O and also equilibrium bond distances.

There is not enough certainty in the results to warrant detailed conclusions; however, we may note that even though electrical anharmonicity could account for the greater part of the observed intensity in most cases, the d_{12} and d_{23} coefficients are still quite small. This may indicate that bending vibrations are more nearly harmonic in both the electrical and the mechanical sense.

ACKNOWLEDGMENTS

We wish to express our gratitude to Dr. G. Herzberg and Dr. L. Herzberg for communicating the results of their work before publication. This research forms part of a program which receives support from the ONR through contract N5ori-147, T.O. II. One of us (D.F.E.) wishes to acknowledge support received as DuPont Postgraduate Fellow in chemistry at Minnesota, 1949–1950.

THE JOURNAL OF CHEMICAL PHYSICS VOLUME 19, NUMBER 12 DECEMBER, 1951

Substituted Methanes. VII.* Vibrational Spectra, Force Constants, and Calculated Thermodynamic Properties for CH_3I and CD_3I†

PAUL F. FENLON,‡ *Physics Department, Armour Research Foundation, Chicago 16, Illinois*

AND

FORREST F. CLEVELAND AND ARNOLD G. MEISTER
Spectroscopy Laboratory, Department of Physics, Illinois Institute of Technology, Chicago 16, Illinois

(Received August 16, 1951)

Raman displacements for the liquid, and infrared absorption wave numbers for both liquid and gas, have been obtained for CH_3I, together with quantitative depolarization factors for the Raman lines and semi-quantitative relative intensities for both the Raman and infrared bands. The present and previous data were critically compared, and probable values of the wave numbers corresponding to the fundamental vibrational frequencies were determined for both liquid and gaseous states. Force constants in a modified valence force potential function, containing all possible quadratic interaction constants, were calculated; these then were used to calculate the fundamentals of CD_3I. Finally, the heat content, free energy, entropy, and heat capacity for both CH_3I and CD_3I were calculated for 11 temperatures from 200° to 1000°K, for the ideal gaseous state at 1 atmos pressure.

RAMAN displacements and visual estimates of the relative intensities of the Raman lines for CH_3I have been obtained in 6 investigations,[1–6] but depolarization factors (for some of the lines) have been reported only twice.[7,8] Infrared spectral data for the gas, in the region 400–4000 cm^{-1}, have been reported in 5 investigations,[9–13] but no data for the liquid seem to have been reported.

EXPERIMENTAL

The sample of CH_3I was obtained from the Eastman Kodak Company, Rochester, New York, and was purified by distillation at atmospheric pressure. The compound decomposed slowly upon exposure to the Hg arcs; consequently, the sample had to be renewed after about 20 hrs of exposure.

The Raman spectra were obtained at 30°C with previously described instruments and methods.[14] East-

* For previous papers of this series, see J. Chem. Phys. **18**, 346, 1073, 1076, 1081 (1950); **19**, 119, 784 (1951).

† Presented in part at the Chicago meeting of the American Physical Society, November, 1950; abstract in Phys. Rev. **81**, 301 (1951).

‡ Based upon investigations carried out in partial fulfillment of the requirements for the degree of Master of Science.

[1] G. N. Ball, Z. Physik **66**, 257 (1930).
[2] A. Dadieu and K. W. F. Kohlrausch, Sitzber. Akad. Wiss., Wien, Math. naturw. Klasse IIa, **139**, 717 (1930); Monatsh. Chem. **57**, 488 (1931).
[3] C. E. Cleeton and R. T. Dufford, Phys. Rev. **37**, 362 (1931).
[4] N. G. Pai, Indian J. Phys. **7**, 285 (1932).
[5] J. Wagner, Z. physik. Chem. **B40**, 36 (1938).
[6] T. Doehaerd and M. de Hemptinne, Bull. acad. roy. méd. Belg. **30**, 783 (1943).
[7] J. Cabannes and A. Rousset, Ann. phys. **19**, 229 (1933).
[8] S. Venkateswaran, Phil. Mag. **15**, 263 (1933).
[9] W. H. Bennett and C. F. Meyer, Phys. Rev. **32**, 888 (1928).
[10] W. W. Sleator, Phys. Rev. **38**, 147 (1931).
[11] E. F. Barker and E. K. Plyler, J. Chem. Phys. **3**, 367 (1935).
[12] R. T. Lagemann and H. H. Nielsen, J. Chem. Phys. **10**, 668 (1942).
[13] C. Courtoy, Ann. bull. soc. roy. sci. méd. nat. Bruxelles Ser. I, **60**, 122 (1946).
[14] F. F. Cleveland, J. Chem. Phys. **11**, 1, 227 (1943); **13**, 101 (1945).

TABLE I. Vibrational data, calculated wave numbers, and assignments for iodomethane (methyl iodide, CH_3I).[a]

Raman									Infrared							Theoretical		
		$\Delta\nu$		I		ρ		PS	ν_l	I_l	ν_g				I_g	ν_c	Assignment	Type
PR	N	PV	AD	PR	V	CR	PR		PR	PR	PR	N	PV	AD	PR			
523	5	523	0.6	1000	0.6	0.25	0.21	P	522	vs	532	3	**533**	0.3	m	**532**	ν_3	A_1
	1	701		w												*718*	$\nu_2-\nu_3$	A_1
890	3	892	2.3	1			0.87	D	887	vs	883	4	**882**	1.3	vs	**882**	ν_6	E
	1	1028		w								1	1053		w	*1066*	$2\nu_3$	A_1
1242	5	1241	0.8	20		P	0.16	P	1242	vs	1250	4	**1252**	1.0	vs	**1252**	ν_2	A_1
1429	3	1430	2.3	1		D	0.85	D	1429	vs	1441	4	**1440**	4.5	vs	**1440**	ν_5	E
1762	3	1761	1.0	1								1	1770		w	*1785*	$\nu_2+\nu_3$	A_1
	1	2050		w												*2092*	$4\nu_3$	A_1
									2118	w		1	2137		w	*2134*	$\nu_2+\nu_6$	E
	1	2461		w					2475	w	2481	2	2463	18.0	m	*2504*	$2\nu_2$	A_1
2841	3	2843	4.3	1					2841	w	2849	3	2851	3.7	m	*2880*	$2\nu_5$	A_1+E
2948	5	2948	0.6	90	0.4	0.05	0.08	P	2950	s	2967	4	**2975**	5.0	s	**2975**	ν_1	A_1
3047	4	3048	1.8	10		~6/7	0.86	D	3050	w	3058	4	**3061**	4.3	m	**3061**	ν_4	E

[a] $\Delta\nu$ = Raman displacement in cm^{-1}; I = relative intensity; ρ = depolarization factor; PS = the deduced polarization state (P = polarized, D = depolarized); ν_l and ν_g = wave numbers in cm^{-1} for liquid and gas, respectively, and I_l and I_g are the corresponding estimated intensities (s = strong, m = medium, w = weak v = very); PR = present results; N = number of apparently reliable, independent determinations; PV = probable value; AD = average deviation; V = Venkateswaran, reference 8; CR = Cabannes and Rousset, reference 7; and ν_c = calculated wave number in cm^{-1}.

man 103-J plates were used and excitation was by Hg 4358A. The relative intensities are only semi-quantitative since no correction was made for the variation of plate sensitivity with wavelength. The depolarization factors, however, are quantitative, having been obtained by the well-tested single-exposure method.[14] Exposures up to 150 hr were required to obtain the depolarization factors of the weakest Raman lines, 2 of which were exceedingly weak. Use was made of a Leeds and Northrup microphotometer in determining the depolarization factors of the weak lines.

The infrared absorption spectra were obtained at 30°C, for both gas and liquid, with a Beckman IR-2 spectrophotometer (KBr optics) and with a Perkin-Elmer 12-C spectrometer (NaCl optics). The liquid cell lengths were 0.11 mm for the Beckman records and 0.10 and 0.025 mm for the Perkin-Elmer. The cell lengths for the gas measurements were 10 cm in each case, and the vapor pressure in the cell was 20-cm Hg.

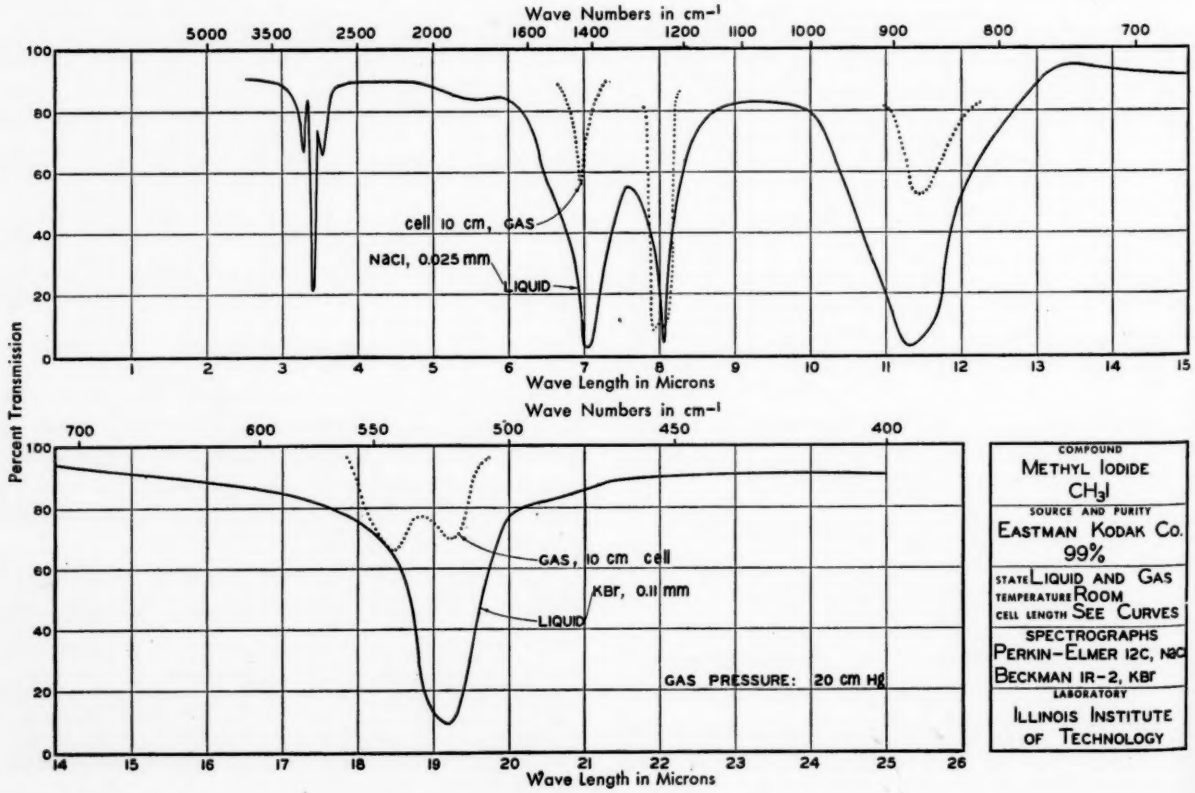

FIG. 1. Infrared absorption bands for iodomethane.

SPECTRAL DATA FOR CH_3I

The Raman spectral data for CH_3I are summarized in Table I. The $\Delta\nu$ values of Ball[1] and of Cleeton and Dufford[3] were excluded, in determining the probable values, since their results differ from those of others by more than the usual experimental error. Also excluded, for the same reason, were the values 1416 and 2889 of Dadieu and Kohlrausch[2] and the value 1410 cm^{-1} of Wagner.[5] No simple assignment could be found for the 2557 line, reported only by Pai,[4] so it, too, was omitted from the table.

The present depolarization factors are in excellent agreement with the results given by Cabannes and Rousset[7] for the 2 lines for which they give quantitative values. However, the results of Venkateswaran[8] for these lines are greatly different, perhaps due to the use by him of a double-exposure method, with relative times of exposure for the vertical and horizontal components adjusted to compensate for the polarization produced by the spectrograph. Despite long exposures, it was impossible to obtain polarization data for the weak 1762 and 2841 lines, but quantitative values were obtained for all the fundamentals.

The infrared spectral data also are summarized in Table I, and the percent transmission curves are shown in Fig. 1. Bands observed at 3640, 3845, 4150, 4350, and 5350 cm^{-1} for the liquid were not included in the table because of the low dispersion and low resolution of the prisms in this region. For the gas, the wave numbers 882, 1252, 1440, 2975, and 3061 of Lagemann and Nielsen[12] were taken as the probable values, since they used a grating spectrograph with high resolution. For other bands, both infrared and Raman, the probable value is the mean of the N reliable determinations. No simple assignments could be found for the 1167, 1182, and 1307 bands observed by Courtoy[13] alone, so they were omitted from the table. Also omitted are all data for the region beyond 3061 cm^{-1}, the position of the highest fundamental.

SPECTRAL DATA FOR CD_3I

The related CD_3I molecule could not be investigated for lack of a sample. In previous work, Raman displacements and estimated relative intensities seem to have been obtained for the liquid in only one investigation,[6] and the infrared spectrum of the gas likewise in only one investigation.[13] The 2 sets of data are given in Table II. The infrared spectrum was not investigated below 665 cm^{-1}, so ν_3 has not been observed for the gas. It seems that the infrared bands 2092 and 2151 must correspond to the Raman doublets 2062, 2135 and 2176, 2285, respectively. The failure to resolve these doublets in the infrared is probably due to the low dispersion of the NaCl prism in this region.

ASSIGNMENTS

For CH_3I, the assignments shown at the right in Table I were made, taking account of the selection rules (Paper I, p. 350), and of the observed depolarization factors and infrared band types. The assignment for the weak 2050 cm^{-1} Raman line may be questioned, for it seems unlikely that $4\nu_3$ would appear when $3\nu_3$ was not observed. However, no satisfactory ternary combination could be found for it. Since the line has been reported only once, it is possible that it does not belong in the CH_3I spectrum. Likewise, the existence of the 701 cm^{-1} Raman line, reported only by Wagner, seems doubtful, for, if it is the difference band $\nu_2-\nu_3$, the agreement of the observed and calculated values should be more exact.

Aside from these 2 weak bands, only binary combinations and 1st overtones have been used, and the as-

TABLE II. Vibrational data, calculated wave numbers, and assignments for iodotrideuteromethane (CD_3I).[a]

Raman (liquid)		Infrared (gas, NaCl prism)		Theoretical		
$\Delta\nu$	I_e	ν_0	I_e	ν_c	Assignment	Type
493	12			**483**	ν_3	A_1
644	0	[b]665	s	**659**	ν_6	E
		~736	w		?	
753	1	764	w	*770*	$(\nu_2+\nu_3)-\nu_6$	E
938	8	941 955	s s	**964**	ν_2	A_1
981 1007	0 0	1008 1017	m m	*986*	$2\nu_3$	A_1
1046	0	1070	m	**1046**	ν_5	E
1160	0	1159 1174	m m	*1158*	$\nu_3+\nu_6$	E
		1274 1307	m m	*1330*	$2\nu_6$	A_1+E
		1387	w	*1405*	$2\nu_2-\nu_3$	A_1
		1422 1449	m m	*1441*	$\nu_2+\nu_3$	A_1
		1527	m	*1563*	$\nu_3+\nu_5$	E
		1613	w	*1613*	$\nu_2+\nu_6$	E
		1709	w	*1735*	$\nu_5+\nu_6$	A_1+A_2+E
		1898	m	*1896*	$2\nu_2$	A_1
2062	1	2092	vs	*2092*	$2\nu_5$	A_1+E
2135	8			**2154**	ν_1	A_1
2176	1			*2183*	$\nu_3+\nu_5+\nu_6$	A_1+A_2+E
2285	3	2151	s	**2254**	ν_4	E
		2604	w	*2628*	$\nu_1+\nu_3$	A_1
		3021	w	*3083*	$\nu_1+\nu_2$	A_1
		3322	w	*3355*	$\nu_4+\nu_5$	A_1+A_2+E

[a] I_e=estimated relative intensity; other symbols have the same meaning as in Table I.
[b] The infrared spectrum was not investigated below 665 cm^{-1}.

TABLE III. Wave numbers and degeneracies for the fundamentals of CH_3I and CD_3I.

Designation	Degeneracy	Wave number CH_3I	Wave number CD_3I
ν_1	1	2975	2135[a]
ν_2	1	1252	948
ν_3	1	533	493[a]
ν_4	2	3061	2285[a]
ν_5	2	1440	1070
ν_6	2	882	665

[a] Liquid state.

signment appears satisfactory. No attempt was made to assign the observed infrared bands beyond 3061 cm^{-1} because of the uncertainties arising from the greater effects of the anharmonicity in this region.

For CD_3I, the present assignments are given at the right in Table II. No assignment could be found for the weak band at ~736 cm^{-1}, and its existence as a part of the spectrum of CD_3I seems questionable. All the assignments are binary combinations and 1st overtones, except for the weak 764, 1387, and 2176 bands, for which ternary combinations had to be used. The Raman doublets 2062, 2135 and 2176, 2285 presumably arise from Fermi resonance interaction between ν_1 and $2\nu_5$, and ν_4 and $\nu_3+\nu_5+\nu_6$. As for CH_3I, no assignments were attempted in the overtone and combination region beyond 3322 cm^{-1}, despite the fact that Courtoy[13] also obtained bands in this region by use of a quartz prism.

After a critical study of the present and previous spectral data, summarized in Tables I and II, the wave number values given in Table III were selected as the most probable ones for the fundamentals of CH_3I and CD_3I.

FORCE CONSTANTS FOR CH_3I

As a check on the assignments, as well as to obtain reliable values of the force constants, a normal coordinate treatment (Wilson FG matrix method) was carried out, using the most general quadratic potential function (Paper I, p. 352). For the present work, D is the C−I bond distance, d is the C−H bond distance, α is the H−C−H angle, and β is the H−C−I angle. Tetrahedral angles were assumed for the equilibrium configuration.

In previous calculations, simplified potential functions were used: Wagner[5] used a 4-constant function with square terms only; Slawsky and Dennison,[15] and Doehaerd and de Hemptinne,[6] used 4 diagonal terms plus an interaction constant corresponding to $f_{D\beta}$; Linnett[16] used square terms and a constant corresponding to $f_{D\alpha}$; and Crawford and Brinkley[17] used diagonal terms plus terms corresponding to $f_{D\gamma}$ and $f_{\alpha\beta}$. Of these investigations, 2 were based on liquid frequencies,[5,6] while the other 3, as well as the present work, were based on gaseous frequencies.[15–17]

The present force constants are compared with those obtained by previous workers in Table IV. The constants are not reliable to more than 3 significant figures, but the ones shown were used in obtaining the calculated wave numbers given in Table I. Approximate values of the F matrix elements containing f_d and f_{dd} were obtained by the "splitting out" technique, after which the diagonal elements were modified to obtain the best agreement with the observed wave numbers. The constants f_α (slightly modified), $f_{\alpha\beta}$, $f_{d\alpha}$, and $f_{d\alpha}'$ were transferred from H_3C-CCl_3,[18] since these are the ones determined principally by the methyl group.

The force constants obtained for CH_3I (Table IV) were then used to calculate the wave numbers for the fundamentals of CD_3I. The results, listed under ν_c in Table II, are within 2.2 percent (mean 1.3 percent) of the observed values. Exact agreement is not to be expected because of the differing effects of anharmonicity in the 2 molecules. This may account for the fact that the calculated value of ν_3 is lower than the value observed for the liquid by 10 cm^{-1}, whereas, from the behavior of the other fundamentals in this region, one would have expected the calculated value for the gaseous state to be about 10 cm^{-1} higher than the liquid value, at about 500 cm^{-1} rather than 483 cm^{-1}. Unfortunately no observed value is available for settling this uncertainty.

TABLE IV. Force constants for CH_3I.[a]

Type	Present	Wagner[d]	Doehaerd, Hemptinne[e]	Linnett[f]	Slawsky, Dennison[g]	Crawford, Brinkley[h]
f_D	2.24_{67}	2.26	2.28	2.32	3.292	2.648
f_d	5.05_{41}	4.94	4.96	5.00	4.878	4.790
f_{dd}	−0.0254	...	...	...	...	...
f_{dD}	0.0635_{09}	...	...	...	...	...
$f_{d\alpha}$	[b]0.205_{86}	...	...	...	...	...
$f_{d\alpha}'$	[b]-0.0878_4	...	...	...	...	...
$f_{d\beta}$	0.367_{80}	...	...	...	...	...
$f_{d\beta}'$	0.167_{80}	...	...	...	...	...
f_α	[b]0.442_{17}	0.233	0.429	0.432	0.443	0.46
$f_{\alpha\alpha}$	-0.0144_{77}	...	...	...	...	...
$f_{\alpha\beta}$	[b]0.0128_{48}	...	...	...	...	0.01
$f_{\alpha\beta}'$	0.0000	...	...	...	...	...
f_β	0.463_{44}	0.414	0.462	0.460	0.463	0.45
$f_{\beta\beta}$	-0.00101_4	...	...	...	...	...
$f_{D\alpha}$	[c]...	...	...	-0.146_5	...	...
$f_{D\beta}$	[c]...	...	0.301	...	0.652	...
$f_{D\gamma}$	[c]-0.110_{40}	...	...	...	...	−0.456

[a] The numbers in the headings are reference numbers; D=C−I, d=C−H, α=H−C−H, and β=H−C−I; in $f_{d\alpha}'$ and $f_{d\beta}'$, d is not one of the sides of α or β (as it is for $f_{d\alpha}$ and $f_{d\beta}$), and in $f_{\alpha\beta}'$ neither side of α is a side of β (as is the case for $f_{\alpha\beta}$). The units are md/A.
[b] Transferred from H_3C-CCl_3, reference 18. (f_α was modified slightly.)
[c] The constants $f_{D\alpha}$ and $f_{D\beta}$ could be obtained only as the combination $f_{D\gamma}=(f_{D\alpha}-f_{D\beta})$.
[d] See reference 5.
[e] See reference 6.
[f] See reference 16.
[g] See reference 15.
[h] See reference 17.

[15] Z. I. Slawsky and D. M. Dennison, J. Chem. Phys. 7, 522 (1939).
[16] J. W. Linnett, J. Chem. Phys. 8, 91 (1940).
[17] B. L. Crawford, Jr., and S. R. Brinkley, Jr., J. Chem. Phys. 9, 69 (1941).
[18] El-Sabban, Meister, and Cleveland, J. Chem. Phys. 19, 855 (1951).

THERMODYNAMIC PROPERTIES OF CH_3I AND CD_3I

The heat content, free energy, entropy, and heat capacity were calculated for 11 temperatures from 200 to 1000°K, using the wave numbers and degeneracies given in Table III. A rigid rotator, harmonic oscillator model was assumed and the values were calculated for the ideal gaseous state at 1 atmos pressure. The moments of inertia used were those obtained from microwave studies by Gordy, Simmons, and Smith[19] for CH_3I and by Simmons[20] for CD_3I; the values were, for CH_3I,

$$I_{zz}=3.31 \text{ awu } A^2(5.50\times10^{-40} \text{ g cm}^2)$$

and

$$I_{xx}=I_{yy}=67.34 \text{ awu } A^2(111.8\times10^{-40} \text{ g cm}^2);$$

TABLE V. Heat content, free energy, entropy, and heat capacity of CH_3I for the ideal gaseous state at 1 atmos pressure.[a]

T	$(H^0-H_0^0)/T$	$-(F^0-H_0^0)/T$	S^0	C_p^0
200	8.16	48.64	56.81	8.93
210	8.20	49.04	57.25	9.07
298.16	8.67	51.99	60.66	10.54
300	8.68	52.04	60.72	10.57
400	9.38	54.63	64.01	12.33
500	10.13	56.81	66.93	13.91
600	10.87	58.72	69.59	15.26
700	11.59	60.45	72.03	16.43
800	12.26	62.04	74.30	17.45
900	12.89	63.52	76.41	18.35
1000	13.47	64.91	78.38	19.14

[a] Here, and in Table VI, T is in °K and the other quantities are in cal deg^{-1} mole^{-1}.

and for CD_3I,

$$I_{zz}=6.62 \text{ awu } A^2(10.99\times10^{-40} \text{ g cm}^2)$$

and

$$I_{xx}=I_{yy}=83.65 \text{ awu } A^2(138.9\times10^{-40} \text{ g cm}^2).$$

The symmetry number is 3 for both molecules. Birge's[21] values of the physical constants were used throughout.

The values obtained for CH_3I and CD_3I are given in Tables V and VI, respectively. The heat capacity of CH_3I for several of the temperatures included here, as well as the entropy at 298.1°K have been calculated by Edgell and Glockler,[22] using the moments of inertia given by Dennison[23] and the fundamentals of Bennett and Meyer.[9] Agreement between their values of C_p and those of the present work is very close. However, their value for the entropy at 298.1°K differs from the present value at 298.16°K by 0.3 percent, due to a difference of 13 percent in the value they used for the product $I_{xx}I_{yy}I_{zz}$.

TABLE VI. Heat content, free energy, entropy, and heat capacity of CD_3I for the ideal gaseous state at 1 atmos pressure.

T	$(H^0-H_0^0)/T$	$-(F^0-H_0^0)/T$	S^0	C_p^0
200	8.34	49.87	58.21	9.69
210	8.41	50.28	58.69	9.93
298.16	9.17	53.35	62.52	12.07
300	9.20	53.41	62.61	12.12
400	10.21	56.19	66.40	14.26
500	11.19	58.57	69.76	15.99
600	12.12	60.70	72.82	17.43
700	12.97	62.63	75.60	18.63
800	13.74	64.41	78.15	19.64
900	14.44	66.07	80.51	20.49
1000	15.08	67.63	82.71	21.19

ACKNOWLEDGMENTS

The Hilger E518 spectrograph used for the depolarization spectrograms was obtained in part with a grant from the American Academy of Arts and Sciences (with further aid from a 2nd recent grant), and the optical parts of the 2-prism spectrograph used for the Raman displacement spectrograms were secured with a grant from the Society of the Sigma Xi. The diagram used as Fig. 1 was prepared by Mr. Alfons Weber. The authors are grateful for this assistance. Thanks also are due to Mrs. Lorna Patterson of the Armour Research Foundation for obtaining the excellent infrared spectrograms with the NaCl optics. Finally, one of us (P. F. F.) wishes to express his gratitude to the Armour Research Foundation for the Industrial Research Fellowship which made it possible for him to carry out his part of this research.

[19] Gordy, Simmons, and Smith, Phys. Rev. **74**, 243 (1948).
[20] J. W. Simmons, Phys. Rev. **76**, 686 (1949).
[21] R. T. Birge, Revs. Modern Phys. **13**, 233 (1941).
[22] W. F. Edgell and G. Glockler, J. Chem. Phys. **9**, 484 (1941).
[23] D. M. Dennison, Revs. Modern Phys. **12**, 175 (1940).

Ultrasonic Propagation in Binary Liquid Systems near Their Critical Solution Temperature

A. G. CHYNOWETH* AND W. G. SCHNEIDER
National Research Laboratories, Ottawa, Canada

(Received August 3, 1951)

An investigation has been made on the propagation of ultrasonic waves (at 600 kc) through the critical solution temperature of two binary liquid systems; (1) aniline and *n*-hexane and (2) triethylamine and water. Results are given for the variation of the velocity with temperature. The behavior of the sound attenuation through the critical point is also shown. In both systems studied the attenuation exhibited a marked maximum at the critical solution temperature. A possible explanation of this effect is that the sound wave gives rise to configurational relaxation processes of greatly increased magnitude on account of the molecular clustering in the liquid system near its critical solution temperature.

A LARGE anomalous absorption of sound energy in the neighborhood of the liquid-vapor critical point of sulfur hexafluoride has been previously reported.[1] It was anticipated that a similar phenomenon might also occur near the critical solution temperature of binary liquid systems. This paper describes experiments that have been made to determine the behavior of the sound velocity and absorption near the critical solution temperature for two different binary liquid systems. The systems chosen were (1) aniline-hexane, which has an upper critical solution temperature, and (2) triethylamine-water, which has a lower critical solution temperature.

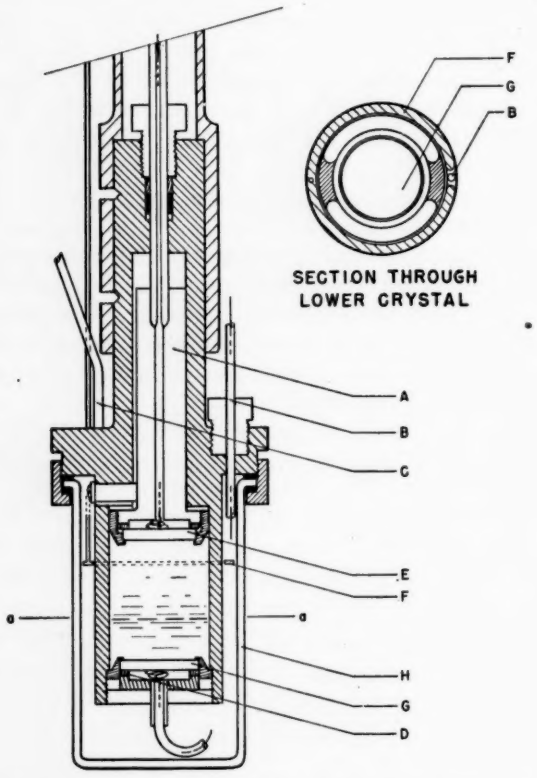

FIG. 1. Section through the double crystal interferometer.

EXPERIMENTAL TECHNIQUE

As previously, the investigations were made with a double crystal interferometer, somewhat similar to the one used in the earlier work. The lower part of the interferometer, including the acoustic chamber, is shown in Fig. 1. The lower crystal *G* was fixed and held in a stirrup that was attached to the body of the interferometer. The upper crystal was movable, it being mounted on a keyed piston *A* which could be caused to move slowly up or down by a synchronous motor drive acting on an accurately turned metric thread. The driving signal was fed to the lower crystal by means of a wire passing down the tube *B*. The crystals were each clamped against metal retaining rings so that the faces adjacent to the liquid were connected directly to ground. Sufficient pressure to keep the crystals in position was applied to the inner faces of the crystals using the teflon washers *D* for electrical insulation. The signal leads made spring contact with the surfaces of the crystals. The acoustic chamber itself was formed by a glass container *H* surrounding the crystal assembly, thus enabling the liquid to be observed. It made an air-tight joint with the body of the interferometer by means of rubber gaskets. To enable thermal equilibrium to be attained quickly a manual stirrer *F* was fitted into the chamber.

The methods of determining the values of the sound velocity and the absorption were exactly as described previously. The reaction curve obtained from the upper crystal was automatically traced out on an Esterline-Angus paper recorder. All measurements were made at a frequency of about 600 kc.

Before assembling, the various components of the interferometer were thoroughly cleaned, after which it was placed in an oil-bath thermostatically controlled to within ±0.001°C. The interferometer was connected to a vacuum system, though because of the large number of gland nuts, joints, etc., no vacuum better than one mm could be obtained. However, the vacuum system was kept pumping for several hours in order to remove all traces of the volatile substances used during the cleaning process. In filling the interferometer the more dense component was first added being followed immediately by the lighter phase. The liquid system was then thoroughly stirred and allowed to reach thermal

* National Research Laboratories Postdoctorate Fellow.
[1] W. G. Schneider, Can. J. Chem. **29**, 243 (1951).

equilibrium. Bubbles that were observed to collect on the under face of the upper crystal were easily removed by gentle manipulation of the stirrer.

Between readings at different temperatures, a time of three to four hours was allowed in order that the system could reach thermal equilibrium.

THE ANILINE-HEXANE SYSTEM

The interferometer was thermostated at a temperature several degrees below the critical mixing temperature and was then filled in the manner described above. Commercially pure aniline was further purified by first neutralizing it with dilute hydrochloric acid. The solution was steam distilled and made alkaline with sodium hydroxide, the aniline then being recovered by steam distillation, separated, and dried over potassium hydroxide pellets and finally distilled in vacuum. Phillips Research grade *n*-hexane was used. The volume of the aniline was 52 cc and that of the hexane was 73 cc, i.e., 47.6 percent by weight of hexane. Such values allowed the interface between the two liquids (the line aa in Fig. 1) to lie about one cm above the upper face of the lower crystal.

Runs were commenced with the crystals within two or three mm of each other and as the upper crystal moved upwards, a curve showing the resonance peaks peculiar to stationary waves in the lower liquid was obtained. After passing through the interface, resonance peaks corresponding to stationary waves in the upper liquid were produced. In this way the sound velocity and absorption could be measured in both of the liquid phases during the one run.

The coexistence curve for the aniline-hexane system has been given by Keyes and Hildebrand[2] and from their results, the above mixture is seen to give rise to approximately the maximum critical solution temperature which the above authors give as 59.5°C. It will be noticed that in the work being described, the critical temperature appeared to lie around 68.3°C, even when a separate sample of the mixture was slowly warmed with constant agitation. The discrepancy in these two figures was most probably due to the presence of impurities.

The results of the measurements of the velocity over the temperature range of 55°C to 75°C are shown in Fig. 2. It is seen that, as would be expected, the velocities in the two phases approach each other in value as the compositions of the two phases become identical. Thereafter, in the single phase system, there is a small steady increase in velocity with temperature. Experimental error does not allow of any detailed interpretation of the behaviour of the sound velocity in the immediate vicinity of the critical temperature though the tentative conclusion may be made that the velocity does not exhibit any anomalous behaviour.

To determine the absorption coefficient per wavelength Fry[3] has shown theoretically that the upper and lower envelopes bounding the trace obtained from the interferometer may be written as

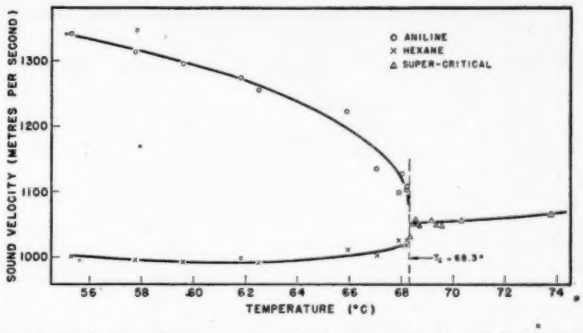

FIG. 2. Variation of the sound velocity through the critical region of the aniline-hexane system.

$$u=C/\sinh\{(\mu L/\lambda)+b\} \tag{1}$$

and

$$l=C/\cosh\{(\mu L/\lambda)+b\}, \tag{2}$$

respectively, where u, l are the amplitudes of the upper and lower envelopes, C is a constant, μ is the coefficient of absorption per wavelength, L is the separation between the crystals, λ is the wavelength of the sound wave, and b is another constant. In the experiments described here there was some doubt as to where the base line occurred in the traces. Consequently, the following approach was made: One can easily show that

$$\left\{\left(\frac{du}{dL}\right)\Big/\left(\frac{dl}{dL}\right)\right\}^{\frac{1}{2}}_{L=L_0}=\coth\left\{\frac{\mu L_0}{\lambda}+b\right\}$$

$$=\psi_{L_0} \quad \text{(Say)}.$$

Similarly,

$$\psi_{L_0+n\lambda}=\coth\left\{\frac{\mu(L_0+n\lambda)}{\lambda}+b\right\}.$$

Hence,

$$\mu=1/n\{\coth^{-1}\psi_{L_0+n\lambda}-\coth^{-1}\psi_{L_0}\}. \tag{3}$$

Equation (3) shows that in order to obtain μ, it is only necessary to determine the quotients of the gradients of the two envelopes at two points on the trace. In practice, however, most of the traces showed a lower envelope of slope, very nearly zero throughout, and consequently, it was impossible to make accurate determinations of the absorption in this way. The absorption was therefore measured in a somewhat arbitrary manner in order to give at least a qualitative account of its behavior through the critical region; the method that was used has been described previously in connection with the experiments in the critical region of sulfur hexafluoride where it gave satisfactorily consistent and reproducible results. The absorption curve so obtained is shown in Fig. 3 and it is immedi-

[2] D. B. Keyes and J. H. Hildebrand, J. Am. Chem. Soc. **39**, 2126 (1917).

[3] W. J. Fry, J. Acoust. Soc. Am. **21**, 17 (1949).

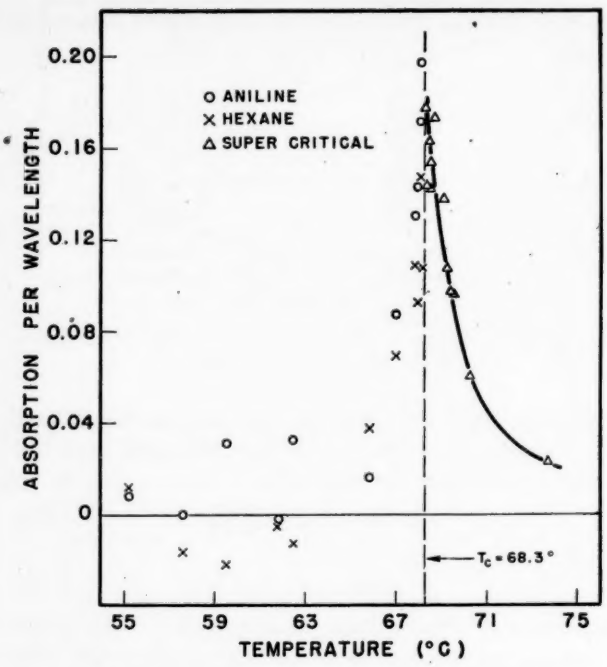

FIG. 3. Behavior of the sound attenuation for the aniline-hexane system.

ately apparent that there is a large attenuation of the sound over a temperature range extending for a few degrees on either side of the critical temperature. In the single phase, the experimental points are seen to lie satisfactorily on a smooth curve, and, in fact, it was always found that measurements in the single phase gave the more reliable and reproducible results. In the two phase system the measurements at low absorption show a rather large scatter and this was no doubt because of the difficulties in measuring low absorption coefficients from the traces produced by a double crystal interferometer in liquids.

TRIETHYLAMINE-WATER SYSTEM

The system triethylamine-water has been investigated by Roberts and Mayer[4] in an attempt to find evidence for an anomalous first-order transition in the region of critical solution. They found a minimum critical solution temperature of a little over 18°C for a mixture 25 percent by weight of triethylamine. The mixture used in the present investigations was composed of 66 cc of amine and 59 cc of water, i.e., 44.6 percent by weight of amine. The latter was commercially pure though it was redistilled before being used in the interferometer. Conductivity water was used as the other component.

The results for the velocity measurements given in Fig. 4 show a behaviour analagous to that of the previous system. In the single phase a smooth curve is obtained except for one point very near the critical temperature. The absence of experimental points for the lower phase immediately above the critical temperature is because of the fact that the interface (aa in Fig. 1) was only slightly above the upper surface of the lower crystal over this range. However, it may be reasonably assumed that the velocity will behave in a manner analagous to that exhibited by the aniline-hexane system.

The curves showing the absorption are given in Fig. 5, and it is again noticeable that there is a large attenuation in the critical region.

DISCUSSION OF RESULTS

The most interesting fact that has resulted from these measurements is the large sound attenuation in the critical region. It is probable that the processes causing the large attenuation are (1) scattering of the sound wave and (2) configurational relaxations.

The opalescence and light scattering near the critical solution temperature have been intensively studied and are attributed to "critical fluctuations" or cluster formation. From such studies Krishnan[5] has concluded that the diameter of the clusters is of the order of the wavelength of visible light. It would seem that scattering centers of such small dimensions could not give rise to appreciable sound attenuation. Furthermore, the clusters cannot be regarded as rigid but will undoubtedly partake in the motion of the sound field. Hence, it is difficult to conceive of a scattering in the ordinary sense to any large extent.

Assuming, in view of the foregoing paragraph, that scattering is not of major importance in causing the attenuation of the sound wave, we ascribe this attenuation mainly to configurational relaxation processes. In the critical region, accompanying the large degree of association, i.e., clustering, there is an increase in the free volume per molecule (as evidenced by the relatively

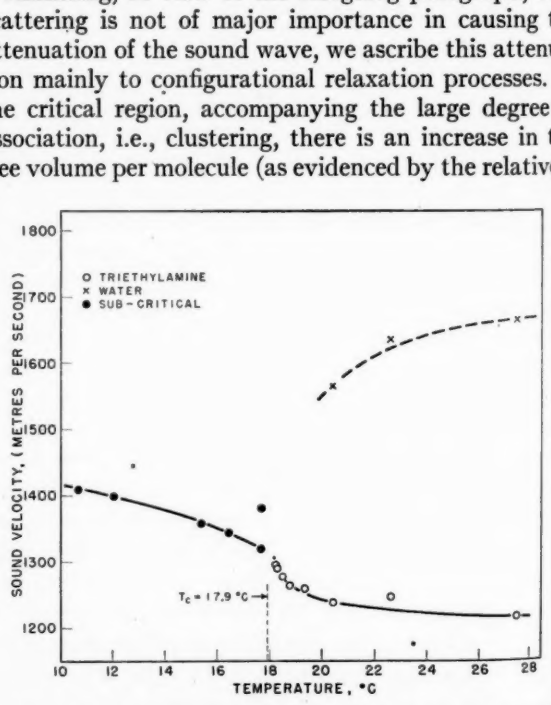

FIG. 4. Variation of the sound velocity through the critical region of the triethylamine-water system.

[4] L. D. Roberts and J. E. Mayer, J. Chem. Phys. **9**, 852 (1941).

[5] R. L. Krishnan, Proc. Indian Acad. Sci. **1A**, 211, 915 (1935); **2A**, 221 (1935); **5A**, 577 (1937); **9A**, 303 (1939).

large expansion in the critical region). It is, therefore, quite conceivable that the sound wave will affect changes in both (1) the relative positions of the molecules in the clusters themselves, and (2) the distribution of the clusters throughout the medium. To bring about these various changes, certain potential barriers have to be overcome, corresponding to which there will be various relaxation times. In liquids in the normal state it appears that the relaxation time accompanying a change in the molecular configuration is much smaller than 10^{-8} sec.[6] In the critical region, however, owing to the clustering, the relaxation time is expected to be much longer, particularly for changes in the cluster distribution. Evidence for this effect is given by the fact that the shear viscosity shows a marked maximum in the region of the critical solution temperature.[7] A similar increase in the volume viscosity can also be expected and because of the time dependence of these two viscosities[8] it is possible that the "mean" relaxation time will come much closer to the frequency at which the experiments were performed, i.e., 600 kc. In this case, the sound attenuation will be expected to show a maximum.

In conclusion, it appears reasonable to ascribe most of the observed attenuation near the critical solution temperature to visco-elastic behavior accompanying the configurational changes caused by the sound wave. However, the actual mechanism on the molecular scale remains to be determined. Further experiments over a range of frequencies would, no doubt, help further the understanding of the problem.

Note added in proof: Values of the sound velocity given in the above communication should be divided by two and the absorption coefficients per wavelength (as defined previously) divided by two. These corrections also apply to a later paper (W. G. Schneider, Can. J. Chem. **29**, 243 (1951)).

The corrections are necessitated by a recent observation that on the recording of the resonance peaks of the double crystal acoustic interferometer every other peak was missing. This behavior can be accounted for by the presence of a superimposed emf having the same frequency as the resonant frequencies of the quartz crystals. At temperatures well below the critical temperature, where the sound attenuation is small, all the resonance peaks can be recorded with but a slight alternation of amplitude. As the critical temperature is approached this alternation becomes very marked, alternate peaks appearing as small satellites. Very close to the critical temperature, where the sound absorption is very high, these "satellites" are completely obscured. This interpretation and the correct sound velocity were verified by employing a pulsing technique and measuring the transit time of a sound pulse between the two crystals at a known distance apart.

I am indebted to G. J. Thiessen, E. A. Shaw, and R. R. Aggarival for assistance in analyzing the resonance behavior of the double crystal ultrasonic interferometer, a more detailed account of which is to be given in a forthcoming publication.

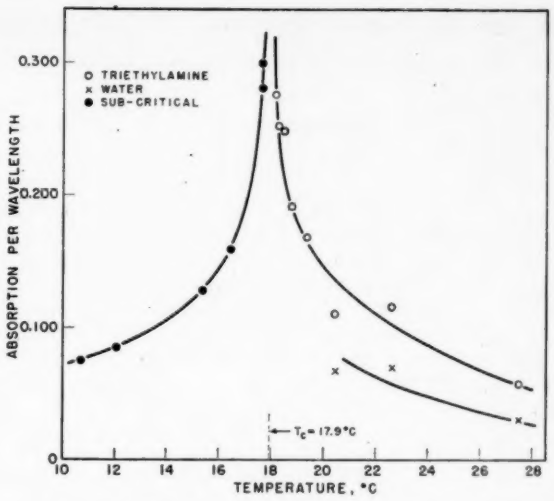

FIG. 5. Behavior of the sound attenuation for the triethylamine-water system.

ACKNOWLEDGMENT

The authors wish to express their thanks to Mr. A. Dubois and Mr. W. A. Stevenson for the construction of the interferometer and other apparatus used in the present work.

[6] J. Frenkel [*Kinetic Theory of Liquids* (Oxford University Press, London, 1946), pp. 234–235] points out that, owing to the absence of a velocity dispersion for frequencies of up to 10^8 per second, the relaxation time must be shorter than 10^{-8} sec. Also, L. Hall [Phys. Rev. **73**, 775 (1948)], by using a structural relaxation model for sound absorption in water, has estimated that the relaxation time is of the order of 10^{-12} sec.

[7] Wo. Ostwald, Trans. Faraday Soc. **29**, 1002 (1933), and **9**, 34 (1913).

[8] J. Frenkel, *Kinetic Theory of Liquids* (Oxford University Press, London, 1946).

THE JOURNAL OF CHEMICAL PHYSICS VOLUME 19, NUMBER 12 DECEMBER, 1951

On the Quantum-Mechanical Calculation of the Cohesive Energy of Molecules and Crystals. Part I. A General Energy Formula for the Ground State

PER-OLOV LÖWDIN
Institute of Mechanics and Mathematical Physics, University of Uppsala, Uppsala, Sweden
(Received August 13, 1951)

A simple expression for the energy of the ground state of a molecule or a crystal is derived by starting from a total wave function, which is a Slater determinant of molecular spin orbitals or Bloch spin orbitals, formed by linear combinations of atomic orbitals. By the introduction of the new idea of "combined atomic orbitals," the energy is expressed only in terms of two-center integrals of atomic orbitals, but the formula still includes the bonding and the overlapping between neighbors of all orders, and further, all the three-center and four-center integrals occurring in previous formulas. A simplified expression of the cohesive energy is given for the case the given atomic orbitals belong to the self-consistent field with exchange of the free atoms.

1. INTRODUCTION

THE theory of molecules and the theory of crystals are very closely connected, since a crystal always can be considered as a molecule of an immense size. In the one-electron approximation there are two fundamental methods for investigating the properties of these systems, namely the *valence bond method* developed by Heitler and London, Slater, Pauling, and others, and the *molecular orbital method* developed by Lennard-Jones, Hund, Mulliken, and others. It is a well-known fact that the valence bond method including ionized states and the molecular orbital method including interaction between configurations give identical results, but it is also known that in the common naive approximations these methods often lead to different conclusions.

In the valence bond method the starting point is the atomic orbitals associated with the atoms constituting the system under consideration. In the molecular orbital method, the fundamental one-electron wave functions are, instead, of a "molecular" type; they may be found by solving the Schrödinger equation of the one-electron system (as in the cellular method in the theory of crystals) or by linear combinations of the given atomic orbitals (LCAO). The MO-LCAO method has been extensively developed for the molecules, but, for crystals, this method has essentially been used only for qualitative purpose, since the quantitative agreement with experience until now has failed.

The valence bond method, as well as the molecular orbital method, has hitherto mostly been used in its simplified or naive form only. These simplified forms give the same results for systems having completely filled shells, but, in all other cases, one has to choose the method which seems to be the best for describing the physical properties under discussion. For the ground state of a system having simple geometrical symmetry properties, the naive MO-method based on a wave function consisting of a determinant of molecular spin-orbitals (MSO) formed by LCAO seems to be the most convenient choice. However, even in this simple approach the evaluation of the energy is associated with considerable mathematical difficulties, depending on the effect of the bonding and overlapping between atomic neighbors of the first, second, and higher orders and on the occurrence of an immense number of atomic three-center and four-center integrals.

The purpose of this paper is not to introduce any new physical ideas but to investigate this energy expression more closely in order to overcome these mathematical difficulties. By introducing the new idea of "combined atomic orbitals" (CAO), we will show that, without neglecting the effects mentioned above, it is possible to express the energy only in terms of *two-center* integrals of atomic orbitals, which may be computed by numerical integration. In a second part of this paper, we will numerically apply this formula to the calculation of the cohesive energy of metallic sodium.

2. THE TOTAL ENERGY OF THE GROUND STATE OF A MOLECULE OR A CRYSTAL

Let us consider a molecule or a crystal containing N electrons. For the sake of simplicity we will assume that the atomic nuclei of the system have fixed positions, which means that we confine ourselves to the case of absolute zero of temperature and that we further neglect the zero-point vibrations.* Let Z_g be the atomic number of the nucleus situated at the point g. The fundamental hamiltonian operator for the system has then the form,

$$H_{op}=W+\sum_i H_i+\sum_{ik}{}' G_{ik}. \tag{1}$$

Here W represents the coulomb interaction between the nuclei, H_i is the kinetic energy of the electron i plus its potential energy in the field of the nuclei, and G_{ik} is half the coulomb interaction between the electrons i and k:

$$W=(e^2/2)\sum_{g_1g_2}{}'(Z_{g1}\cdot Z_{g2}/r_{g_1g_2});$$
$$H_i=\frac{1}{2m}\mathbf{p}_i^2-e^2\sum_g\frac{Z_g}{r_{ig}};\quad G_{ik}=\frac{e^2}{2r_{ik}}. \tag{2}$$

* Our model is therefore not directly applicable to systems, where the energy of the zero-point vibrations constitutes a large part of the total energy, e.g., solid helium.

The energy spectrum of the system is now given by the eigenvalues $\mathcal{E}$ of the Schrödinger equation,

$$H_{op}\Psi=\mathcal{E}\Psi, \tag{3}$$

for antisymmetric eigenfunctions,

$$\Psi=\Psi(\mathbf{x}_1', \mathbf{x}_2', \mathbf{x}_3', \cdots \mathbf{x}_N'),$$

where $\mathbf{x}_i'$ denotes the space and spin coordinates of the electron i, $\mathbf{x}_i'=(\mathbf{x}_i, \zeta_i)$. In general the sign $'$ on a quantity will indicate that spin is included.

According to a well-known theorem, the energy $\mathcal{E}_0$ of the ground state is the lower bound of the integral

$$E=\frac{\int \Psi^* H_{op}\Psi d\tau_1' d\tau_2' \cdots d\tau_N'}{\int \Psi^*\Psi d\tau_1' d\tau_2' \cdots d\tau_N'}, \tag{4}$$

for arbitrary antisymmetric wave functions Ψ. We note that, in Eq. (4), the elements $d\tau_i'$ imply also summations over all spin variables:

$$\int d\tau_i'=\sum_{\zeta_i}\int d\tau_i.$$

The eigenfunction Ψ_n for any excited state $\mathcal{E}_n$ satisfies the variational principle

$$\delta E=0 \tag{5}$$

with the supplementary condition that Ψ_n has to be orthogonal against all the lower functions Ψ_0, $\Psi_1, \cdots \Psi_{n-1}$.

Even if in the hamiltonian (1) zero-point vibrations, relativistic effects, spin-spin interactions, and other effects are neglected, it is generally assumed that one would obtain a very accurate quantum chemistry of the system under consideration if one could solve the eigenvalue problem (3) exactly. However, since the solution of the many-body problem (3) is extremely complicated, one is still far from this goal, and we have therefore to be satisfied even with rather rough approximations. The best approximate method used hitherto in the general theory is the one-electron approximation, of which we have mentioned two different types in the introduction. Here we will base our theory on a molecular wave function consisting of a *single* Slater determinant of molecular spin orbitals, which means that we will neglect the "interaction between configurations." The latter process, which is necessary in order to obtain higher accuracy for the ground state and in treating the excited states, can be taken into account by considering a linear superposition of a number of Slater determinants, each representing a "configuration" of the electrons over the available MSO, and by using the variational principle (5). The method outlined in this paper can be applied even to this more general case, but the results will be confined for later publication.

In treating the *ground state* of the system, we will therefore now consider the molecular wave function,

$$\Psi=1/(N!)^{\frac{1}{2}}\det\{\psi_{j'}(\mathbf{x}_i')\}, \tag{6}$$

where the one-electron wave functions $\psi_{j'}(\mathbf{x}_i')$ are molecular spin-orbitals (MSO) formed by LCASO. The quantum number j' consists of an orbital quantum number j and a spin quantum number s, $j'=(j, s)$, and each MSO is a product of a MO and a spin function

$$\psi_{j'}(\mathbf{x}_i')=\psi_j(\mathbf{x}_i)\begin{cases}\alpha(\zeta_i)\\ \beta(\zeta_i)\end{cases} \tag{7}$$

where α and β are the spin functions belonging to plus and minus spin, respectively.

It was early pointed out by Wheland[1] that the substitution of (6) into (4) would lead to a rather difficult problem of computation, since the expression for E, in addition to a number of two-center integrals, would contain also a very large number of three-center and four-center integrals. These many-center integrals were at first neglected or only roughly estimated,[2] then treated by approximate formulas,[3] and finally investigated by an exact method.[4] However, here we will entirely avoid this many-center integral problem by another approach.

Since we will construct our molecular orbitals by LCAO, the given atomic orbitals form the essential basis of our theory, and we will therefore consider them in greater detail. Let us assume that in the system under discussion there are M atomic orbitals ϕ_μ ($\mu=1, 2, \cdots M$) at our disposal and that $2M\geq N$. These functions may be real or complex, and we assume that they are always normalized, so that $\int \phi_\mu^* \phi_\mu d\tau=1$, where $d\tau$ is the volume element and the integration has to be carried out over the whole space. The "overlap integrals" are, as usual, defined by

$$S_{\mu\nu}=\int \phi_\mu^* \phi_\nu d\tau-\delta_{\mu\nu}, \tag{8}$$

with $S_{\mu\mu}=0$. The problem of taking the overlap integrals into account have been treated by various authors,[5] and here we will follow the simple method previously developed by the present author.[6] Let $\mathbf{S}$ be the self-adjoint matrix formed by the elements $S_{\mu\nu}$. Let further $\boldsymbol{\phi}$ be the row matrix formed by the elements ϕ_μ.

[1] G. H. Wheland, J. Chem. Phys. **2**, 474 (1934).

[2] See, for instance, M. Goeppert-Mayer and A. L. Sklar, J. Chem. Phys. **6**, 645 (1938); A. L. Sklar and R. H. Lyddane, J. Chem. Phys. **7**, 374 (1939).

[3] A. L. Sklar, J. Chem. Phys. **7**, 984 (1939); A. London, J. Chem. Phys. **13**, 396 (1945); R. S. Mulliken, J. chim. phys. **46**, 497, 675 (1949), and others.

[4] S. O. Lundqvist and P. O. Löwdin, Arkiv Fysik **3**, 147 (1951). *Note added in proof:* Another, related method has recently been developed by K. Rüdenberg, J. Chem. Phys. **19**, 1433 (1951).

[5] R. Landshoff, Z. Physik **102**, 201 (1936); G. H. Wannier, Phys. Rev. **52**, 191 (1937); B. H. Chirgwin and C. A. Coulson, Proc. Roy. Soc. (London) **A201**, 196 (1950).

[6] P. O. Löwdin, J. Chem. Phys. **18**, 365 (1950).

Now we will introduce another row matrix φ formed by the elements φ_μ by the relation,

$$\varphi=\phi(1+S)^{-\frac{1}{2}}, \tag{9}$$

or

$$\varphi_\mu=\sum_\alpha \phi_\alpha(1+S)^{-\frac{1}{2}}_{\alpha\mu}. \tag{10}$$

It is easily proved that the functions φ_μ are normalized and orthogonalized:

$$\int \varphi_\mu^* \varphi_\nu d\tau=\delta_{\mu\nu}. \tag{11}$$

In the following we may consider the functions φ_μ as the *real* atomic orbitals involved in the problem, since this assumption does not cause any additional complications in the molecular orbital theory. In the valence bond theory one must be more careful about this assumption, as has recently been pointed out by Slater,[7] since an uncritical use of the functions φ_μ here can lead to erroneous results. However, we note that it is always possible to use the orthonormalized functions φ_μ even in the valence bond theory if one follows the simple scheme recommended in reference 6 and first constructs the ordinary valence bond wave function, expressed in the given AO ϕ_μ, and then introduces the functions φ_μ by the substitution $\phi=\varphi(1+S)^{\frac{1}{2}}$.

The MO ψ_j $(j=1, 2, \cdots M)$ may be formed by linear combinations from the given AO ϕ_μ, but according to (10) they may then also be found by linear combinations of the orthonormalized AO φ_μ:

$$\psi_j=\sum_{\mu=1}^{M} \varphi_\mu C_{\mu j}. \tag{12}$$

Since even the set ψ_j $(j=1, 2, \cdots M)$ has to be orthonormalized, the matrix $\mathbf{C}$ of the coefficients $C_{\mu j}$ has to be unitary:

$$\mathbf{C}^\dagger\mathbf{C}=\mathbf{C}\mathbf{C}^\dagger=\mathbf{1}. \tag{13}$$

In this paper we will assume that the coefficients $C_{\mu j}$ are given from the very beginning, for instance by group theoretical considerations of the geometrical symmetry of the system. Even in the case of a general system, the coefficients $C_{\mu j}$ can be determined by using the variational principle (5), but this calculation of a "self-consistent solution" is a rather complicated non-linear problem involving solving of a series of secular equations in a process of successive approximations. This problem has recently been taken up to treatment by the Chicago group.[7a]

According to a well-known theorem in the one-electron scheme, we obtain by putting (6) into (4) the Hartree-Fock energy,

$$E=W+\sum_{j'}^{\text{occ.}} \{j'|H|j'\} + \sum_{j'k'}^{\text{occ.}} \{j'k'|G|j'k'\}-\sum_{j'k'}^{\text{occ.}} \{j'k'|G|k'j'\}, \tag{14}$$

where we have used the notations,

$$\{j'|H|j'\}=\int \psi_{j'}^*(\mathbf{x}_1')H_1\psi_{j'}(\mathbf{x}_1')d\tau_1',$$

$$\{j'k'|G|l'm'\}=\int \psi_{j'}^*(\mathbf{x}_1')\psi_{k'}^*(\mathbf{x}_2') \times G_{12}\psi_{l'}(\mathbf{x}_1')\psi_{m'}(\mathbf{x}_2')d\tau_1'd\tau_2', \tag{15}$$

and the summations are to be carried out over all *occupied* MSO. We note that the last term in (14) gives contributions only when the states j' and k' have parallel spins.

In order to calculate the approximate value of the energy given by (14), we will now introduce some new notations. At first we will let the symbols plus and minus over a summation sign indicate that the summation is to be carried out over the molecular orbitals j which are occupied with electrons having plus spin and minus spin, respectively. We will then introduce the *bonding matrix* $\mathbf{Q}$, originally defined by Coulson and Longuet-Higgins[8] for the case of overlap neglected $(\mathbf{S}=0)$ and later generalized even to the general case:[9]

$$q_{\mu\nu}^{(+)}=\sum_j^{+} C_{\mu j}C_{j\nu}^\dagger, \quad q_{\mu\nu}^{(-)}=\sum_j^{-} C_{\mu j}C_{j\nu}^\dagger, \qquad Q_{\mu\nu}=q_{\mu\nu}^{(+)}+q_{\mu\nu}^{(-)}. \tag{16}$$

Here $\mathbf{q}^{(+)}$ and $\mathbf{q}^{(-)}$ refer to electrons with plus spin and minus spin, respectively, and $\mathbf{Q}$ is the total matrix with the interpretation that $\mathbf{Q}_{\mu\mu}$ is the *charge density* at the atom μ and $\mathbf{Q}_{\mu\nu}$ is the *bond order* of the atomic bond $\mu-\nu$. We note that, in case all orbitals are occupied by two electrons, the unitary property (13) of $\mathbf{C}$ gives $Q_{\mu\nu}=2\delta_{\mu\nu}$, which corresponds to the case of *non-bonding* between filled shells.[10] Further, we will introduce a new matrix $\mathbf{R}$:

$$\mathbf{R}=(1+S)^{-\frac{1}{2}}\mathbf{Q}(1+S)^{-\frac{1}{2}}, \tag{17}$$

which we will call the *bonding-overlapping matrix*. With the notation $\mathbf{T}=(1+\mathbf{S})^{-1}$, we can also write the definition

$$\mathbf{T}=(1+\mathbf{S})^{-1}, \quad \mathbf{R}=\mathbf{T}^{\frac{1}{2}}\mathbf{Q}\mathbf{T}^{\frac{1}{2}}. \tag{18}$$

We note that $\mathbf{R}$ is self-adjoint. In addition to the given atomic orbitals, ϕ_μ, we will in the following also consider

[7] J. C. Slater, Phys. Rev. **81**, 385 (1951).

[7a] *Note added in proof:* C. C. J. Roothaan, Ph.D. thesis (University of Chicago), 1948–49 ONR report, has now been published in part in Revs. Modern Phys. **23**, 69 (1951). See also R. S. Mulliken, J. Chim. Phys. **46**, 675 (1949); R. G. Parr and R. S. Mulliken, J. Chem. Phys. **18**, 1338 (1950).

[8] C. A. Coulson and H. C. Longuet-Higgins, Proc. Roy. Soc. (London) **A191**, 39 (1947); compare also reference 5, Chirgwin and Coulson.

[9] See reference 6, p. 369.

[10] See also C. A. Coulson and H. C. Longuet-Higgins, Phil. Mag. (7) **40**, 1172 (1949).

the *combined atomic orbitals* (CAO), $\phi_\mu{}^C$, defined by

$$\phi_\mu{}^C=\sum_\alpha \phi_\alpha R_{\alpha\mu}, \quad \phi_\mu{}^{C*}=\sum_\alpha R_{\mu\alpha}\phi_\alpha{}^* \tag{19}$$

and characterized by a symbol with the superscript C (=Combined AO). They are many-orbital functions, and their properties will be discussed in greater detail in the next section.

In treating matrix elements, we will in the following let brackets of different types refer to different types of one-electron functions: $\{\ \}$ will refer to the MSO $\psi_{j'}$, $\{\ \}$ to the MO ψ, $[.]$ to the orthonormalized AO φ_μ, and $(\ )$ to the given AO ϕ_μ. Finally, elements with respect to the CAO $\phi_\mu{}^C$ will be indicated by the symbol μ^C. This means, for instance, that we have

$$\begin{aligned}
\{j'|H|k'\}&=\int \psi_{j'}{}^*(1')H_1\psi_{k'}(1')d\tau_1',\\
\{j|H|k\}&=\int \psi_j{}^*(1)H_1\psi_k(1)d\tau_1,\\
[\mu|H|\nu]&=\int \varphi_\mu{}^*(1)H_1\varphi_\nu(1)d\tau_1,\\
(\mu|H|\nu)&=\int \phi_\mu{}^*(1)H_1\phi_\nu(1)d\tau_1,\\
(\mu^C|H|\nu)&=\int \phi_\mu{}^{C*}(1)H_1\phi_\nu(1)d\tau_1,
\end{aligned} \tag{20}$$

where 1′ indicates the variable $\mathbf{x}_1'$ and 1 the variable $\mathbf{x}_1$.

The relations (9), (12), and (19) may be written in matrix form

$$\boldsymbol{\psi}=\boldsymbol{\varphi}\mathbf{C}, \quad \boldsymbol{\varphi}=\boldsymbol{\phi}\mathbf{T}^{-\frac{1}{2}}, \quad \boldsymbol{\phi}^C=\boldsymbol{\phi}\mathbf{R}. \tag{21}$$

By using (21) and the bracket notations, we obtain

$$\begin{aligned}
\{j|H|j\}&=\sum_{\mu\nu} C_{j\mu}{}^\dagger[\mu|H|\nu]C_{\nu j},\\
[\mu|H|\nu]&=\sum_{\alpha\beta} T^{-\frac{1}{2}}{}_{\mu\alpha}(\alpha|H|\beta)T^{-\frac{1}{2}}{}_{\beta\nu}.
\end{aligned} \tag{22}$$

Summing over all occupied MSO, eliminating the spin, and using (16) and (19), we then get for the second term in the expression (14):

$$\begin{aligned}
\sum_{j'}^{\text{occ.}}\{j'|H|j'\}&=\sum_j^{+}\{j|H|j\}+\sum_j^{-}\{j|H|j\}\\
&=\sum_{\mu\nu} q_{\nu\mu}{}^{(+)}[\mu|H|\nu]+\sum_{\mu\nu} q_{\nu\mu}{}^{(-)}[\mu|H|\nu]\\
&=\sum_{\mu\nu} Q_{\nu\mu}[\mu|H|\nu]=\sum_{\mu\nu}\sum_{\alpha\beta} Q_{\nu\mu}T^{-\frac{1}{2}}{}_{\mu\alpha}(\alpha|H|\beta)T^{-\frac{1}{2}}{}_{\beta\nu}\\
&=\sum_{\alpha\beta}\Big(\sum_{\mu\nu} T^{-\frac{1}{2}}{}_{\beta\nu}Q_{\nu\mu}T^{-\frac{1}{2}}{}_{\mu\alpha}\Big)(\alpha|H|\beta)=\sum_{\alpha\beta} R_{\beta\alpha}(\alpha|H|\beta)\\
&=\sum_\beta(\beta^C|H|\beta)=\sum_\mu(\mu^C|H|\mu).
\end{aligned} \tag{23}$$

For the matrix elements of G we find, by using (21),

$$\begin{aligned}
\{jk|G|jk\}&=\sum_{\mu\nu\kappa\lambda} C_{j\mu}{}^\dagger C_{k\nu}{}^\dagger[\mu\nu|G|\kappa\lambda]C_{\kappa j}C_{\lambda k}.\\
[\mu\nu|G|\kappa\lambda]&=\sum_{\alpha\beta\gamma\delta} T^{-\frac{1}{2}}{}_{\mu\alpha}T^{-\frac{1}{2}}{}_{\nu\beta}(\alpha\beta|G|\gamma\delta)T^{-\frac{1}{2}}{}_{\gamma\kappa}T^{-\frac{1}{2}}{}_{\delta\lambda}.
\end{aligned} \tag{24}$$

By using (16) and (19), this gives for the third term in (14):

$$\begin{aligned}
&\sum_{j'k'}^{\text{occ.}}\{j'k'|G|j'k'\}\\
&=\Big(\sum_j^{+}\sum_k^{+}+\sum_j^{+}\sum_k^{-}+\sum_j^{-}\sum_k^{+}+\sum_j^{-}\sum_k^{-}\Big)\{jk|G|jk\}\\
&=\sum_{\mu\nu\kappa\lambda}\big(q_{\kappa\mu}{}^{(+)}q_{\lambda\nu}{}^{(+)}+q_{\kappa\mu}{}^{(+)}q_{\lambda\nu}{}^{(-)}+q_{\kappa\mu}{}^{(-)}q_{\lambda\nu}{}^{(+)}\\
&\quad+q_{\kappa\mu}{}^{(-)}q_{\lambda\nu}{}^{(-)}\big)[\mu\nu|G|\kappa\lambda]\\
&=\sum_{\mu\nu\kappa\lambda} Q_{\kappa\mu}Q_{\lambda\nu}[\mu\nu|G|\kappa\lambda]\\
&=\sum_{\mu\nu\kappa\lambda}\sum_{\alpha\beta\gamma\delta} Q_{\kappa\mu}Q_{\lambda\nu}T^{-\frac{1}{2}}{}_{\mu\alpha}T^{-\frac{1}{2}}{}_{\nu\beta}(\alpha\beta|G|\gamma\delta)T^{-\frac{1}{2}}{}_{\gamma\kappa}T^{-\frac{1}{2}}{}_{\delta\lambda}\\
&=\sum_{\alpha\beta\gamma\delta}\Big(\sum_{\kappa\mu} T^{-\frac{1}{2}}{}_{\gamma\kappa}Q_{\kappa\mu}T^{-\frac{1}{2}}{}_{\mu\alpha}\Big)\Big(\sum_{\lambda\nu} T^{-\frac{1}{2}}{}_{\delta\lambda}Q_{\lambda\nu}T^{-\frac{1}{2}}{}_{\nu\beta}\Big)(\alpha\beta|G|\gamma\delta)\\
&=\sum_{\alpha\beta\gamma\delta} R_{\gamma\alpha}R_{\delta\beta}(\alpha\beta|G|\gamma\delta)=\sum_{\gamma\delta}(\gamma^C\delta^C|G|\gamma\delta).
\end{aligned} \tag{25}$$

or

$$\sum_{j'k'}^{\text{occ.}}\{j'k'|G|j'k'\}=\sum_{\mu\nu}(\mu^C\nu^C|G|\mu\nu). \tag{26}$$

The last term in (14) is slightly more complicated, and, in order to treat it, we will introduce the matrices $\mathbf{R}^+$ and $\mathbf{R}^-$, which are connected with $\mathbf{q}^+$ and $\mathbf{q}^-$ in the same way as $\mathbf{R}$ is connected with $\mathbf{Q}$, see Eq. (17). The corresponding CAO will be denoted by $\phi_\mu{}^{C+}$ and $\phi_\mu{}^{C-}$, respectively, and associated matrix elements will be indicated by μ^{C+} and μ^{C-}:

$$\begin{aligned}
&\mathbf{R}^+=\mathbf{T}^{-\frac{1}{2}}\mathbf{q}^{(+)}\mathbf{T}^{-\frac{1}{2}}, \quad \mathbf{R}^-=\mathbf{T}^{-\frac{1}{2}}\mathbf{q}^{(-)}\mathbf{T}^{-\frac{1}{2}}, \quad \mathbf{R}=\mathbf{R}^{(+)}+\mathbf{R}^{(-)}.\\
&\boldsymbol{\phi}^{C+}=\boldsymbol{\phi}\mathbf{R}^+, \quad \boldsymbol{\phi}^{C-}=\boldsymbol{\phi}\mathbf{R}^-, \quad \boldsymbol{\phi}^C=\boldsymbol{\phi}^{C+}+\boldsymbol{\phi}^{C-}.
\end{aligned} \tag{27}$$

Using (21), we get for the matrix elements of G

$$\begin{aligned}
\{jk|G|kj\}&=\sum_{\mu\nu\kappa\lambda} C_{j\mu}{}^\dagger C_{k\nu}{}^\dagger[\mu\nu|G|\lambda\kappa]C_{\lambda k}C_{\kappa j}.\\
[\mu\nu|G|\lambda\kappa]&=\sum_{\alpha\beta\gamma\delta} T^{-\frac{1}{2}}{}_{\mu\alpha}T^{-\frac{1}{2}}{}_{\nu\beta}(\alpha\beta|G|\delta\gamma)T^{-\frac{1}{2}}{}_{\delta\lambda}T^{-\frac{1}{2}}{}_{\gamma\kappa}.
\end{aligned} \tag{28}$$

Summing over all occupied MSO, noting that we get contributions only for parallel spins, and using (16)

and (27), we obtain for the last term in (14):

$$\sum_{j'k'}^{\text{occ.}} \{j'k'|G|k'j'\}$$

$$=(\sum_{j}^{+}\sum_{k}^{+}+\sum_{j}^{-}\sum_{k}^{-})\{jk|G|kj\}$$

$$=\sum_{\mu\nu\kappa\lambda}(q_{\kappa\mu}{}^{(+)}q_{\lambda\nu}{}^{(+)}+q_{\kappa\mu}{}^{(-)}q_{\lambda\nu}{}^{(-)})[\mu\nu|G|\lambda\kappa]$$

$$=\sum_{\alpha\beta\gamma\delta}\sum_{\mu\nu\kappa\lambda}(q_{\kappa\mu}{}^{(+)}q_{\lambda\nu}{}^{(+)}+q_{\kappa\mu}{}^{(-)}q_{\lambda\nu}{}^{(-)})T^{\frac{1}{2}}{}_{\mu\alpha}T^{\frac{1}{2}}{}_{\nu\beta}$$

$$\times(\alpha\beta|G|\delta\gamma)T^{\frac{1}{2}}{}_{\delta\lambda}T^{\frac{1}{2}}{}_{\gamma\kappa}$$

$$=\sum_{\alpha\beta\gamma\delta}(R_{\gamma\alpha}{}^{+}R_{\delta\beta}{}^{+}+R_{\gamma\alpha}{}^{-}R_{\delta\beta}{}^{-})(\alpha\beta|G|\delta\gamma)$$

$$=\sum_{\gamma\delta}\{(\gamma^{C+}\delta^{C+}|G|\delta\gamma)+(\gamma^{C-}\delta^{C-}|G|\delta\gamma)\}, \quad (29)$$

or

$$\sum_{j'k'}^{\text{occ.}}\{j'k'|G|k'j'\}$$

$$=\sum_{\mu\nu}\{(\mu^{C+}\nu^{C+}|G|\nu\mu)+(\mu^{C-}\nu^{C-}|G|\nu\mu)\}. \quad (30)$$

In the case of a general distribution of the spins we have to use this formula. However, in the following we will mainly confine ourselves to considering only *singlet ground states*, where each molecular orbital j is occupied with two electrons having opposite spins. According to (16) and (27), we then have

$$\mathbf{q}^{(+)}=\mathbf{q}^{(-)}=\tfrac{1}{2}\mathbf{Q}, \quad \mathbf{R}^{+}=\mathbf{R}^{-}=\tfrac{1}{2}\mathbf{R}. \quad (31)$$

which gives the simplified formula

$$\sum_{j'k'}^{\text{occ.}}\{j'k'|G|k'j'\}=\tfrac{1}{2}\sum_{\mu\nu}(\mu^{C}\nu^{C}|G|\nu\mu). \quad (32)$$

For the *total energy* (14) of the ground state of the molecule or crystal under consideration, we obtain therefore the final expression

$$E=W+\sum_{\mu}(\mu^{C}|H|\mu)$$

$$+\sum_{\mu\nu}(\mu^{C}\nu^{C}|G|\mu\nu)-\tfrac{1}{2}\sum_{\mu\nu}(\mu^{C}\nu^{C}|G|\nu\mu)$$

$$=W+\sum_{\mu}\int\phi_{\mu}{}^{C*}(1)H_1\phi_{\mu}(1)d\tau_1$$

$$+\frac{e^2}{2}\sum_{\mu\nu}\int\int\frac{\phi_{\mu}{}^{C*}(1)\phi_{\nu}{}^{C*}(2)\phi_{\mu}(1)\phi_{\nu}(2)}{r_{12}}d\tau_1d\tau_2$$

$$-\frac{e^2}{4}\sum_{\mu\nu}\int\int\frac{\phi_{\mu}{}^{C*}(1)\phi_{\nu}{}^{C*}(2)\phi_{\nu}(1)\phi_{\mu}(2)}{r_{12}}d\tau_1d\tau_2. \quad (33)$$

As we will see in the next section, the CAO $\phi_{\mu}{}^{C}$ have essentially the character of atomic orbitals, and hence all integrals in (33) are *two-center* integrals of atomic orbitals, which may be evaluated. Because of the occurrence of the matrix $\mathbf{R}$ in the CAO, this formula contains the bonding and the overlapping between neighbors of all orders. We note that the formula has an *asymmetric* form, being expressed in $\phi_{\mu}{}^{C}$ as well as in ϕ_{μ}. A completely symmetric form can also be constructed, but the form (33) seems to be more suitable for the numerical calculations. The energy formula (14) has a simple physical meaning, but we will not try to give any interpretation of the form (33), since this expression has been constructed essentially to overcome the mathematical difficulties mentioned in the introduction. However, a possible interpretation of (33) can be given in terms of a special *density matrix*, but this discussion will be confined for a later publication.

3. TREATMENT OF THE COMBINED ATOMIC ORBITALS

In the previous section we have shown that the whole problem of taking the bonding, the overlapping, and the many-center integrals into account can be concentrated in the calculation of the combined atomic orbitals

$$\phi_{\mu}{}^{C}=\sum_{\alpha}\phi_{\alpha}R_{\alpha\mu}, \quad (34)$$

where $\mathbf{R}$ is the bonding-overlapping matrix defined by (17). In order to investigate the properties of these functions, we will now introduce a system of spherical coordinates (r, ϑ, φ) with its origin in the nucleus g_{μ} associated with the given AO ϕ_{μ}. If $Y_{lm}(\vartheta, \varphi)$ denotes the normalized spherical harmonics

$$Y_{lm}(\vartheta,\varphi)=\left(\frac{2l+1}{4\pi}\cdot\frac{(l-m)!}{(l+m)!}\right)^{\frac{1}{2}}P_l{}^{m}(\cos\vartheta)e^{im\varphi}, \quad (35)$$

we can derive the expansion

$$\phi_{\mu}{}^{C}(r,\vartheta,\varphi)=\sum_{l=0}^{\infty}\sum_{m=-l}^{+l}\phi_{\mu,lm}{}^{C}(r)Y_{lm}(\vartheta,\varphi) \quad (36)$$

with the radial coefficients

$$\phi_{\mu,lm}{}^{C}(r)=\sum_{\alpha}\phi_{\alpha,lm}(r)R_{\alpha\mu}, \quad (37)$$

$$\phi_{\alpha,lm}(r)=\int_0^{2\pi}d\varphi\int_0^{\pi}\phi_{\alpha}Y_{lm}{}^{*}(\vartheta,\varphi)\sin\vartheta d\vartheta. \quad (38)$$

The quantities $\phi_{\alpha,lm}(r)$ can be computed according to methods previously developed.[11] The formula (36) means that we have expressed the CAO $\phi_{\mu}{}^{C}$ essentially in terms of s-, p-, d-, $\cdots$ functions around the point g_{μ}. Hence $\phi_{\mu}{}^{C}$ can be considered as a sum of ordinary atomic orbitals, even if the radial parts may have a somewhat larger extension and more nodes.

[11] See P. O. Löwdin, *A Theoretical Investigation into Some Properties of Ionic Crystals*, thesis (Almquist and Wicksell, Uppsala, 1948), pp. 18–22. See also Part II of this paper.

In the case of high geometrical *symmetry* of the system, the summation in (37) may sometimes render considerable simplifications. As an example, we will consider a crystal with cubic symmetry where all given AO have s-character. According to Bethe,[12] the first spherical harmonics which are consistent with the cubic symmetry are $l=0$ and $l=4, \cdots$, i.e., s- and g-functions. This means that, in the summation (37), the contributions from $l=1, 2$, and 3 vanish identically, and that $\phi_\mu{}^C$ is essentially an *s-function* with a small contribution of g-type, etc. A similar idea of summing the contributions from the whole crystal in order to utilize the symmetry has previously been used in the "cellular method" due to Wigner and Seitz for other purposes. Later we will use this simplification in the application to metallic sodium (Part II).

In (36) we have developed the CAO $\phi_\mu{}^C$ in spherical harmonics, but we note that we may develop $\phi_\mu{}^C$ also in other complete systems if this seems to be more convenient with respect to the geometrical symmetry.

Finally, we will investigate the overlap integral between a CAO and an ordinary AO. By using matrix multiplication and (19), (8), and (18), we obtain

$$\int \phi_\mu{}^{C*}\phi_\nu d\tau=(\mathbf{T}^{\frac{1}{2}}\mathbf{Q}\mathbf{T}^{-\frac{1}{2}})_{\mu\nu}. \tag{39}$$

The matrix $T^{\frac{1}{2}}QT^{-\frac{1}{2}}$ is non-hermitean and has therefore no direct physical interpretation. In connection with (16) we remarked that $Q_{\mu\mu}$ is interpreted as the charge density in the atomic orbital ϕ_μ. However, for the numerical work it is convenient to use also the "asymmetric" charge $n_\mu{}^C$, defined by

$$n_\mu{}^C=(\mathbf{T}^{\frac{1}{2}}\mathbf{Q}\mathbf{T}^{-\frac{1}{2}})_{\mu\mu} \tag{40}$$

which satisfies the relation

$$\sum_\mu n_\mu{}^C=\sum_\mu Q_{\mu\mu}. \tag{41}$$

We note that the asymmetry is again caused by the simultaneous use of the CAO $\phi_\mu{}^C$ and the ordinary AO ϕ_μ.

4. THE COHESIVE ENERGY OF A MOLECULE OR A CRYSTAL

The cohesive energy of a system is defined as the difference between its total energy and the energy of its natural dissociation products. Here we will derive an expression for the cohesive energy in the case the given AO ϕ_μ are represented by the *self-consistent fields with exchange for the free atoms*.

In the following we will use a notation which seems to have been introduced by Landshoff.[5] For a certain index μ, it may sometimes be convenient to divide the summation $\sum_\nu$ from 1 to M into two parts: a summation over all indices (μ) associated with the same atom or ion as μ, and a summation over all other indices (μ_1), i.e.,

$$\sum_{\nu=1}^{M}=\sum_{\nu}{}^{(\mu)}+\sum_{\nu}{}^{(\mu_1)}. \tag{42}$$

We will also use the symbols

$$H_i=H_i{}^{(\mu)}+H_i{}^{(\mu_1)},$$

$$H_i{}^{(\mu)}=\frac{1}{2m}\mathbf{p}_i{}^2-e^2\frac{Z_{g_\mu}}{r_{ig_\mu}}, \quad H_i{}^{(\mu_1)}=-e^2\sum_g{}^{(\mu_1)}\frac{Z_g}{r_{ig}}. \tag{43}$$

If μ' and ν' are atomic spin-orbitals (ASO) with $\mu'=(\mu, s)$ etc., and we assume that the basic wave functions can again be approximated by *single* Slater determinants, we have for the energy of the free constituents of the dissociation products

$$E_{\text{free}}=\sum_{\mu'}(\mu'|H^{(\mu)}|\mu')$$
$$+\sum_{\mu'}\sum_{\nu'}{}^{(\mu)}\{(\mu'\nu'|G|\mu'\nu')-(\mu'\nu'|G|\nu'\mu')\}, \tag{44}$$

where the summations have to be carried out over all occupied ASO. We will now divide the AO of the free constituents into two classes, I and II: such as are occupied by a single electron (I), and such as are occupied by two electrons with opposite spin (II). Further, we will introduce a quantity $\kappa_{\mu\nu}$ having the properties

$$\kappa_{\mu\nu}=\begin{cases}1, & \text{if } \mu \text{ and } \nu \text{ both belong to } I,\\ \frac{1}{2}, & \text{if at least one of } \mu \text{ and } \nu \text{ belongs to } II,\end{cases} \tag{45}$$

and satisfying the symmetry relation $\kappa_{\nu\mu}=\kappa_{\mu\nu}$. If n_μ denotes the *number of electrons* in ϕ_μ in the *free* constituent, we can then eliminate the spin in (44) and obtain

$$E_{\text{free}}=\sum_\mu n_\mu(\mu|H^{(\mu)}|\mu)$$
$$+\sum_\mu\sum_\nu{}^{(\mu)}n_\mu n_\nu\{(\mu\nu|G|\mu\nu)-\kappa_{\mu\nu}(\mu\nu|G|\nu\mu)\}. \tag{46}$$

The cohesive energy of the system can now simply be obtained by subtracting the expression (46) from the expression (33). Up till this point the AO have been considered as being of a quite arbitrary type: hydrogen like wave functions, Slater orbitals, etc.

The rest of this section we will devote to a discussion of the cohesive energy in case the given AO are Hartree-Fock functions associated with the self-consistent field with exchange of the free constituents. These functions are certainly not the best AO, which can be used in investigating the molecule or crystal under discussion, for better AO can always be found by applying the variational principle (5) to the expression (33) for the total energy. However, we note that the cohesive energy is always a relatively *small* quantity, being the difference between two *large* quantities, namely the total energy of the composed system and the total energy of the free constituents. This means that, if we are mainly interested in the cohesive energy, it is very convenient to use the *same* AO in treating the composed system and the free constituents, for, in forming the difference between (33) and (46), all the really large terms will then cancel, as we will show here.

[12] H. Bethe, Ann. Physik (5) **3**, 133 (1929).

We note that our basic functions ϕ_μ satisfy the differential equations,

$$H_1^{(\mu)}\phi_\mu(1)+e^2\sum_\nu{}^{(\mu)}\, n_\nu\Big\{\int\frac{\phi_\nu^*(2)\phi_\nu(2)}{r_{12}}d\tau_2\cdot\phi_\mu(1) - \kappa_{\mu\nu}\int\frac{\phi_\nu^*(2)\phi_\mu(2)}{r_{12}}d\tau_2\cdot\phi_\nu(1)\Big\}=\epsilon_\mu\phi_\mu(1), \quad (47)$$

which easily may be derived from (46) by using the variational principle (5). Here the eigenvalues ϵ_μ are the *orbital energies* (one-electron energies) associated with the free constituents. By multiplying (47) with $\phi_\mu^*(1)$ and $\phi_\mu{}^{C*}(1)$, respectively, and by integrating over the variable $\mathbf{x}_1$, we get the two relations,

$$(\mu|H^{(\mu)}|\mu)+2\sum_\nu{}^{(\mu)}\, n_\nu \times\{(\mu\nu|G|\mu\nu)-\kappa_{\mu\nu}(\mu\nu|G|\nu\mu)\}=\epsilon_\mu, \quad (48)$$

$$(\mu^C|H^{(\mu)}|\mu)+2\sum_\nu{}^{(\mu)}\, n_\nu \times\{(\mu^C\nu|G|\mu\nu)-\kappa_{\mu\nu}(\mu^C\nu|G|\nu\mu)\}=\epsilon_\mu n_\mu{}^C,$$

where $n_\mu{}^C$ is given by (40), and, by combination of them,

$$\begin{aligned}\sum_\mu(\mu^C|H^{(\mu)}|\mu)-\sum_\mu n_\mu(\mu|H^{(\mu)}|\mu)&=\sum_\mu\epsilon_\mu(n_\mu{}^C-n_\mu)\\ -2\sum_\mu\sum_\nu{}^{(\mu)}\, n_\nu\{(\mu^C\nu|G|\mu\nu)-n_\mu(\mu\nu|G|\mu\nu)\}&\\ +2\sum_\mu\sum_\nu{}^{(\mu)}\, n_\nu\kappa_{\mu\nu}\{(\mu^C\nu|G|\nu\mu)-n_\mu(\mu\nu|G|\nu\mu)\}.&\quad(49)\end{aligned}$$

Forming the difference between the expressions (33) and (46), and using the identity (49), we now obtain for the *cohesive energy* of the molecule or crystal under consideration

$$\begin{aligned}E_{\text{coh}}&=E_{\text{tot}}-E_{\text{free}}\\ &=W+\sum_\mu(\mu^C|H^{(\mu_1)}|\mu)+\sum_\mu\sum_\nu{}^{(\mu_1)}(\mu^C\nu^C|G|\mu\nu)\\ &-\tfrac{1}{2}\sum_\mu\sum_\nu{}^{(\mu_1)}(\mu^C\nu^C|G|\nu\mu)+\sum_\mu\epsilon_\mu(n_\mu{}^C-n_\mu)\\ &+\sum_\mu\sum_\nu{}^{(\mu)}\{(\mu^C\nu^C|G|\mu\nu)-2n_\nu(\mu^C\nu|G|\mu\nu)\\ &+n_\mu n_\nu(\mu\nu|G|\mu\nu)\}-\tfrac{1}{2}\sum_\mu\sum_\nu{}^{(\mu)}\{(\mu^C\nu^C|G|\nu\mu)\\ &-4n_\mu\kappa_{\mu\nu}(\mu^C\nu|G|\nu\mu)+2n_\mu n_\nu\kappa_{\mu\nu}(\mu\nu|G|\nu\mu)\}. \quad (50)\end{aligned}$$

We will finally put this result in the form,

$$\left\{\begin{aligned}E_{\text{coh}}&=E_{\text{elstat}}+E_{\text{exch}}+E_{\text{rearr}},\\ E_{\text{elstat}}&=W+\sum_\mu(\mu^C|H^{(\mu_1)}|\mu)\\ &\quad+\sum_\mu\sum_\nu{}^{(\mu_1)}(\mu^C\nu^C|G|\mu\nu),\\ E_{\text{exch}}&=-\tfrac{1}{2}\sum_\mu\sum_\nu{}^{(\mu_1)}(\mu^C\nu^C|G|\nu\mu),\\ E_{\text{rearr}}&=\sum_\mu\epsilon_\mu(n_\mu{}^C-n_\mu)\\ &\quad+\sum_\mu\sum_\nu{}^{(\mu)}\{(\mu^C-n_\mu\mu,\,\nu^C-n_\nu\nu|G|\mu\nu)\\ &\quad-\kappa_{\mu\nu}(\mu^C-n_\mu\mu,\,\nu^C-n_\nu\nu|G|\nu\mu)\}\\ &\quad+\sum_\mu\sum_\nu{}^{(\mu)}(\kappa_{\mu\nu}-\tfrac{1}{2})(\mu^C\nu^C|G|\nu\mu),\end{aligned}\right. \quad (51)$$

where, in the last energy term, the indices $\mu^C-n_\mu\mu$ and $\nu^C-n_\nu\nu$ refer to the atomic orbitals $\phi_\mu{}^C-n_\mu\phi_\mu$ and $\phi_\nu{}^C-n_\nu\phi_\nu$, respectively. The value of $\kappa_{\mu\nu}$ is given by (45).

The three terms in (51) have here been called the electrostatic (elstat) energy, the exchange (exch) energy, and the rearrangement (rearr) energy of the system under consideration, but we note that these notations refer more to the *mathematical* form of the different terms than to real physical interpretations. The terms in the energy expression (14) have, at least conventionally, a simple physical meaning which is also preserved by the terms in (33), but this meaning is partly lost in carrying out the subtraction process (50) due to the use of the identity (49). However, it has been remarked by several authors that the so-called exchange energy in (14) is nothing but an ordinary electrostatic energy for a particular charge distribution. In fact, the fundamental hamiltonian (1) contains only two kinds of energy, kinetic energy and coulomb interaction energy, and every physical interpretation going beyond these two concepts must therefore be without real significance. If we remember this limitation, the names introduced in (51) may still be convenient and useful.

We note that, in (51), the electrostatic energy and the exchange energy have really cohesive properties, i.e., that they correspond to interactions between *different* atoms (or ions) in the composed system. The last term in (51), the *rearrangement energy*, is of a new type, and it depends on interactions within the *same* atom. Its name is derived from the fact that it counts for the energy change due to the rearrangement of the electronic distribution over the atomic orbitals when the system goes over from the free constituents to the composed form, i.e., due to the change in charge number from n_μ to $n_\mu{}^C$ and associated bonding, overlapping, and repulsion effects. The first term in E_{rearr} is simply the change in *orbital energy* due to the formation of a composed system.

The author[13] has previously given an energy formula for the ground state of a system having completely filled shells with particular reference to ionic crystals, but we note that the new formula (51) has a much more condensed form, taking account of the overlapping between neighbors of *all* orders in a simple way. Formula (51) has also a much more general applicability, since we have removed the previous limitation as to completely filled shells, and it may therefore be applied to all molecules and crystals (metals, ionic crystals, solid states of the rare gases, etc.) which satisfy our basic assumption (compare first footnote).

5. CALCULATION OF THE DIFFERENT ENERGY TERMS

Let us now investigate the various energy terms in (51) in greater detail. In fact, except for the first term in the rearrangement energy, they are all electrostatic

[13] P. O. Löwdin, Arkiv Mat., Astron. Fysik **35A**, No. 9 (1947); see also reference 11, p. 15.

potentials associated with different quantum mechanical charge distributions, and they are therefore all of the type

$$e^2\int\int \frac{\Omega_I(\mathbf{x}_1)\Omega_{II}(\mathbf{x}_2)}{r_{12}}d\tau_1 d\tau_2, \tag{52}$$

where each of the densities Ω_I and Ω_{II} is a product of two atomic orbitals. In order to evaluate[14] the integral (52), we will introduce a system of polar coordinates (r, ϑ, φ) having a fixed origin. By developing $1/r_{12}$ in Legendre polynomials and using the addition theorem for the spherical harmonics (35), we obtain

$$\frac{1}{r_{12}}=\sum_{l=0}^{\infty}\sum_{m=-l}^{+l}\frac{4\pi}{2l+1}\frac{r_i^{\,l}}{r_k^{\,l+1}}Y_{lm}(\vartheta_1,\varphi_1)Y_{lm}^*(\vartheta_2,\varphi_2), \tag{53}$$

where r_i and r_k denote the smallest and the largest of the quantities $r_1=|\mathbf{x}_1|$ and $r_2=|\mathbf{x}_2|$, respectively. Putting the expansion (53) into (52) and using the notation,

$$\Omega_{N,\,l}^{\,m}(r)=\int_0^{2\pi}d\varphi\int_0^{\pi}\Omega_N(r,\vartheta,\varphi)\times Y_{lm}(\vartheta,\varphi)\sin\vartheta\cdot d\vartheta,\quad N=I,\,II, \tag{54}$$

we obtain the general potential formula,

$$\begin{aligned}
&\int\int\frac{\Omega_I(1)\Omega_{II}(2)}{r_{12}}d\tau_1 d\tau_2\\
&=\sum_{l=0}^{\infty}\sum_{m=-l}^{+l}\frac{4\pi}{2l+1}\Big\{\int_0^{\infty}\Omega_{I,\,l}^{\,m}(r_1)r_1^{-l+1}dr_1\\
&\times\int_0^{r_1}\Omega_{II,\,l}^{\,-m}(r_2)r_2^{\,l+2}dr_2+\int_0^{\infty}\Omega_{I,\,l}^{\,m}(r_1)r_1^{\,l+2}dr_1\\
&\times\int_{r_1}^{\infty}\Omega_{II,\,l}^{\,-m}(r_2)r_2^{-l+1}dr_2\Big\}\\
&=\sum_{l=0}^{\infty}\sum_{m=-l}^{+l}\frac{4\pi}{2l+1}\Big\{\int_0^{\infty}\Omega_{I,\,l}^{\,m}(r_1)r_1^{-l+1}dr_1\\
&\times\int_0^{r_1}\Omega_{II,\,l}^{\,-m}(r_2)r_2^{\,l+2}dr_2+\int_0^{\infty}\Omega_{II,\,l}^{\,-m}(r_1)r_1^{-l+1}dr_1\\
&\times\int_0^{r_1}\Omega_{I,\,l}^{\,m}(r_2)r_2^{\,l+2}dr_2\Big\},
\end{aligned}\tag{55}$$

where the last term in the second expression has been transformed by using Dirichlet's formula for double integrals. Formula (55) may be used for evaluating atomic integrals of two-center, three-center, and four-center type.[14] However, since it will here be applied only for the two-center case, the calculations will be essentially simplified.

In treating the term E_{elstat} in (51), some caution is necessary in the crystal theory, since the different terms are in reality *divergent* for a crystal, whose volume tends to infinity. However, since the crystal energy per unit volume is a finite quantity, this divergency is only of a formal character and can be removed by a special transformation of the terms, which we now will carry out.

Let us introduce the notations,

$$\Omega_g(\mathbf{x})=\textstyle\sum_\mu{}^g\,\phi_\mu{}^C{}^*(\mathbf{x})\phi_\mu(\mathbf{x}), \tag{56}$$

$$Z_g{}^C=\int\Omega_g(\mathbf{x})d\tau=\textstyle\sum_\mu{}^g\,n_\mu{}^C=Z_g-\mathcal{E}_g, \tag{57}$$

where $\Omega_g(\mathbf{x})$, $Z_g{}^C$, and $\mathcal{E}_g$ may be interpreted as the asymmetric quantities corresponding to the total *charge density*, the total *charge number* (in units of e), and the actual *valency* (including sign) of the atom or ion g in the composed system. The word "asymmetric" refers here to the simultaneous use of the CAO $\phi_\mu{}^C$ and the ordinary AO ϕ_μ; see Eqs. (39) and (40). In addition we will also use the "radial" charge density U_g defined by

$$U_g(\mathbf{x})=4\pi r^2\Omega_g(\mathbf{x}), \tag{58}$$

and we note that, in general, this quantity is not necessarily spherically symmetrical around the point g. Using the expansion (53), putting the origin of the spherical coordinate system in the point g, introducing the expansion coefficient

$$U_{g,\,lm}(r)=\int_0^{2\pi}d\varphi\int_0^{\pi}U_g(r,\vartheta,\varphi)\times Y_{lm}(\vartheta,\varphi)\sin\vartheta d\vartheta, \tag{59}$$

and treating the term for $l=0$ separately according to (57), we obtain for the potential associated with the charge distribution Ω_g:

$$\int\frac{\Omega_g(2)}{r_{12}}d\tau_2=\frac{Z_g{}^C}{r_{1g}}-\omega_g(1). \tag{60}$$

$$\begin{aligned}
\omega_g(1)=&\frac{1}{(4\pi)^{\frac{1}{2}}}\Big(\frac{1}{r_{1g}}\int_{r_{1g}}^{\infty}U_{g,\,00}(r_2)dr_2\\
&-\int_{r_{1g}}^{\infty}\frac{U_{g,\,00}(r_2)}{r_2}dr_2\Big)-\sum_{l=1}^{\infty}\sum_{m=-l}^{+l}\frac{1}{2l+1}Y_{lm}{}^*(1)\\
&\times\Big\{\frac{1}{r_{1g}{}^{l+1}}\int_0^{r_{1g}}U_{g,\,lm}(r_2)r_2{}^l dr_2\\
&+r_{1g}{}^l\int_{r_{1g}}^{\infty}\frac{U_{g,\,lm}(r_2)}{r_2{}^{l+1}}dr_2\Big\}.
\end{aligned}\tag{61}$$

Here the function $\omega_g(1)$ is a *deformation potential*, giving the difference between the potential from a point charge of the strength $Z_g{}^C$ in the point g and the actual poten-

[14] See reference 4.

tial. We note that this function tends to zero much more rapidly than $1/r_{1g}$ for $r_{1g}\to\infty$. In the special case when the density U_g is spherically symmetrical around the nucleus g, the double sum in the expression for $\omega_g(1)$ will vanish identically.

Using (51), (56), (57), and (60), and denoting the positions of the nuclei by g and h, we now obtain the following transformation of the expression for the electrostatic energy:

$$E_{\text{elstat}}=W+\sum_\mu(\mu^C|H^{(\mu_1)}|\mu)$$
$$+\sum_\mu\sum_\nu{}^{(\mu_1)}(\mu^C\nu^C|G|\mu\nu)=\frac{e^2}{2}\sum_{gh}{}'\frac{Z_gZ_h}{r_{gh}}$$
$$-e^2\sum_\mu\sum_g{}^{(\mu_1)}Z_g\int\frac{\phi_\mu{}^{C*}(1)\phi_\mu(1)}{r_{1g}}d\tau_1$$
$$+\frac{e^2}{2}\sum_\mu\sum_\nu{}^{(\mu_1)}\int\int\frac{\phi_\mu{}^{C*}(1)\phi_\nu{}^{C*}(2)\phi_\mu(1)\phi_\nu(2)}{r_{12}}d\tau_1d\tau_2$$
$$=\frac{e^2}{2}\sum_{gh}{}'\left\{\frac{Z_gZ_h}{r_{gh}}-2Z_g\int\frac{\Omega_h(1)}{r_{1g}}d\tau_1\right.$$
$$\left.+\int\int\frac{\Omega_g(1)\Omega_h(2)}{r_{12}}d\tau_1d\tau_2\right\}$$
$$=\frac{e^2}{2}\sum_{gh}{}'\frac{\mathcal{E}_g\mathcal{E}_h}{r_{gh}}+\frac{e^2}{2}\sum_{gh}{}'\left\{(Z_g+\mathcal{E}_g)\omega_h(g)\right.$$
$$\left.-\int\Omega_g(1)\omega_h(1)d\tau_1\right\},\quad(62)$$

This is the desired *convergent* expression for the electrostatic energy, and we note that it is very convenient for numerical evaluation in crystals as well as in molecules, since all really large terms have been eliminated. The first term is the coulomb interaction between the atoms or ions of the system, being considered as point charges situated at their respective nuclei, and the second term gives the correction depending on the actual extension of these constituents. For a crystal with $\mathcal{E}_g\neq0$, the first sum is nothing but the well-known Madelung energy, which may be computed by means of the special methods developed in the theory of ionic crystals by Madelung, Ewald, and others. The second sum may be evaluated by using numerical integration according to the methods described, for instance, in reference 11.

In case of high symmetry, it may sometimes be suitable to introduce the function,

$$\Gamma_g(\mathbf{x})=\sum_{h\neq g}\omega_h(\mathbf{x}),\quad(63)$$

i.e., the sum of all deformation potentials of the system except the term associated with the nucleus g, and (62) takes then the form,

$$E_{\text{elstat}}=\frac{e^2}{2}\sum_{gh}{}'\frac{\mathcal{E}_g\mathcal{E}_h}{r_{gh}}$$
$$+\frac{e^2}{2}\sum_g\left\{(Z_g+\mathcal{E}_g)\Gamma_g(g)-\int\Omega_g(1)\Gamma_g(1)d\tau_1\right\}.\quad(64)$$

If we introduce the expansion of Γ_g in spherical harmonics with the coefficients

$$\Gamma_{g,\,lm}(r)=\int_0^{2\pi}d\varphi\int_0^{\pi}\Gamma_g(r,\vartheta,\varphi)Y_{lm}(\vartheta,\varphi)\sin\vartheta d\vartheta,\quad(65)$$

the last term in (64) can be computed from the relation,

$$\int\Omega_g(1)\Gamma_g(1)d\tau_1$$
$$=\frac{1}{4\pi}\sum_{l=0}^{\infty}\sum_{m=-l}^{+l}\int_0^{\infty}U_{g,\,lm}(r_1)\Gamma_{g,\,lm}{}^*(r_1)dr_1.\quad(66)$$

In case U_g has spherical symmetry, all these calculations will be essentially simplified, and (66) reduces to the first term.

The remaining terms in (51), the exchange energy and the rearrangement energy, do not show any such complications as were involved in the electrostatic energy, and they may therefore be evaluated in a straightforward way by using the general formula (55). Since here our basic AO are chosen to be Hartree-Fock functions belonging to the self-consistent fields with exchange for the free constituents, they are originally given only in numerical form, and numerical methods will therefore be of special importance. A detailed description of the methods of computing coefficients in expansions in spherical harmonics and of carrying out numerical integrations may be found in reference 11, and particularly method *I* described there will be recommended for the general case. Numerical methods of this type may be considered somewhat tedious and laborious, but we note that, in all events, it is possible to evaluate all the terms in (51) for a molecule or a crystal by the aid of only ordinary desk machines.

The general theory developed here has been applied to the calculation of the cohesive energy and the lattice parameter of metallic sodium, and the results will be published in Part II of this series of papers.

THE JOURNAL OF CHEMICAL PHYSICS VOLUME 19, NUMBER 12 DECEMBER, 1951

On the Quantum-Mechanical Calculation of the Cohesive Energy of Molecules and Crystals. Part II. Treatment of the Alkali Metals with Numerical Applications to Sodium*

PER-OLOV LÖWDIN
Institute of Mechanics and Mathematical Physics, University of Uppsala, Uppsala, Sweden
(Received August 13, 1951)

In Part I, an expression for the cohesive energy of a crystal was derived in the case the wave function for the ground state is approximated by a single Slater determinant of Bloch spin orbitals, formed by linear combination of the atomic spin orbital associated with the self-consistent fields with exchange for the free constitutents. By using the new idea of "combined atomic orbitals," all energy terms were reduced to only atomic two-center integrals, which could be evaluated by numerical integration. This method is here applied to the calculation of the cohesive energy of the alkali metals, where, due to the crystal symmetry, the combined atomic orbitals for the valence electrons are almost pure *s*-functions. It is shown that the conventional method, taking only the interaction between nearest neighbors into account, is entirely insufficient and that it is necessary to consider even bonding, overlapping, and electronic repulsion effects between neighbors of a rather high order.

Numerical applications, including interactions between neighbors up to the order nine, are carried out for metallic sodium, giving the cohesive energy 24.7 kcal/mol and the interatomic distance 3.69A, in good agreement with the experimental values 26 kcal/mol and 3.67A, respectively. Except for the values of the fundamental constants $e, m, h, \cdots$, no empirical data are used.

1. INTRODUCTION

IN the one-electron approximation of quantum mechanics, there are two fundamental methods for investigating the properties of crystals, namely the *valence bond method* and the *crystal orbital method*, which are closely associated with the corresponding methods in the theory of molecules.[1] Here we will give a short survey of how these two methods have been used in investigating the cohesive properties of metals.

The electron theory of metals, developed by Sommerfeld,[2] was essentially based on the idea of free electrons in a box, and it may therefore be classified as a crystal orbital (CO) treatment. The first attempt to find better one-electron wave functions was made by Bloch,[3] who constructed real crystal orbitals by linear combination of the atomic orbitals associated with the constituents, a process which will here be denoted by CO-LCAO. Numerical applications[4] of Bloch's theory to the calculation of energy bands gave, however, rather bad quantative agreement with experience, and from this fact one has usually drawn the conclusion that the whole LCAO-approach is too rough an approximation for metals.

Using the naive valence bond method, Slater[5] has investigated the cohesive forces in monovalent metals, and later even the inclusion of ionized states has been discussed.[6] In another resonance treatment, Pauling,[7] using highly hybridized AO, has investigated the transition metals and related intermetallic compounds. Most of the results obtained by using the valence bond method have mainly been of a qualitative character, and only a few quantitative results have been presented.

A very successful attempt of treating the cohesive properties of metals was made by Wigner and Seitz.[8] They used the crystal orbital method, but, instead of using LCAO, they computed more accurate wave functions by solving the Hartree-Fock equation for the system, utilizing the high symmetry of the crystal. Even the error in the one-electron approximation, the correlation energy, has been investigated by Wigner.[9] This "cellular method" has often given an excellent agreement with experimental experience, but a test, given by Shockley,[10] shows also that it fails in describing the one-electron wave functions having higher orbital energies.

After this survey, let us now return to the CO-LCAO-method originally introduced by Bloch.[3] It seems rather surprising that the LCAO-approach can give such good results for molecules, where the atoms are often bound still more tightly together, and fails so entirely in

* Part I appears on p. 1570 of this issue and will in the following be referred to as I.

[1] See also the introduction to Part I.

[2] A. Sommerfeld, Z. Physik **47**, 1 (1928); A. Sommerfeld and N. H. Frank, Revs. Modern Phys. **3**, 1 (1931).

[3] F. Bloch, Z. Physik **52**, 555 (1929).

[4] See, for instance, A. Sommerfeld and H. Bethe, *Handbuch der Physik* (Julius Springer, Berlin, 1933), XXIV: 2, p. 405. N. F. Mott and H. Jones, *The Theory of Properties of Metals and Alloys* (Oxford University Press, London, 1936).

[5] J. C. Slater, Phys. Rev. **35**, 509 (1930); see also Revs. Modern Phys. **6**, 209 (1934).

[6] S. Schubin and S. Wonsowsky, Proc. Roy. Soc. (London) **A145**, 159 (1934); Physik. Z. Sowjetunion **7**, 292 (1935); **10**, 348 (1936).

[7] L. Pauling, Phys. Rev. **54**, 899 (1938), Nature **161**, 1019 (1948), Proc. Roy. Soc. (London) **196**, 343 (1949). L. Pauling and F. J. Ewing, Revs. Modern Phys. **20**, 112 (1948).

[8] E. Wigner and F. Seitz, Phys. Rev. **43**, 804 (1933); **46**, 509 (1934). J. C. Slater, Revs. Modern Phys. **6**, 209 (1934); F. Seitz, Phys. Rev. **47**, 400 (1935); G. E. Kimball, J. Chem. Phys. **3**, 560 (1935); E. Wigner and H. B. Huntington, J. Chem. Phys. **3**, 764 (1935); H. Fröhlich, *Elektronentheorie der Metalle* (Struktur der Materie, Berlin, 1936); Proc. Roy. Soc. (London) **A158**, 97 (1937); J. Bardeen, J. Chem. Phys. **6**, 367 (1938); S. Raimes, Phil. Mag. **41**, 568 (1950); T. S. Kuhn and J. H. van Vleck, Phys. Rev. **79**, 382 (1950); T. S. Kuhn, Phys. Rev. **79**, 515 (1950).

[9] E. Wigner, Phys. Rev. **46**, 1002 (1934); Trans. Faraday Soc. **34**, 678 (1938).

[10] W. Shockley, Phys. Rev. **51**, 129 (1937).

metals.[4] A closer investigation of Bloch's assumptions shows now that he considered only interaction between nearest atomic neighbors and that he completely neglected all overlap effects. On this point we wish to make a remark.

In investigating the ionic crystals, the present author[11] found that the overlap integrals were very small ($S\approx 0.04$) but that they were nevertheless theoretically responsible for all the repulsive forces giving the equilibrium state of the crystal. In a metal like sodium, the overlap integrals are not small at all ($S\approx 0.5$), and they must therefore certainly be of importance in any theory of metals. In addition, due to this very large overlapping, it is no longer justified to neglect the electronic interaction between atomic neighbors of the second, third, and higher orders. Consequently, there are good reasons for the quantitative breakdown of the earlier applications[4] of Bloch's theory, and it would therefore be of some interest to reexamine the whole CO-LCAO-method for metals, taking the overlap effects into full account and considering even interactions between atomic neighbors of a rather high order.

In Part I we derived an expression for the cohesive energy of a molecule or a crystal in case the wave function for the ground state was approximated by a single Slater determinant of molecular or crystal spin orbitals, formed by LCAO from the Hartree-Fock functions associated with the self-consistent fields with exchange for the free constituents. By using the new idea of "combined atomic orbitals," all energy terms were reduced to atomic two-center integrals which could be evaluated by numerical integration. We will now apply formula (I, 51) to the calculation of the cohesive energy and the lattice parameter of an alkali metal, with numerical applications, including interactions between neighbors up to the ninth order, to sodium. The purpose of the paper is not to introduce any new physical ideas but to show that it is possible to overcome the mathematical difficulties involved in such a problem. The good agreement between the results and experimental experience indicates that the simple Bloch orbitals may be more useful in the theory of metals than it has earlier been supposed.

2. THE ALKALI METAL CRYSTAL. THE BODY-CENTERED STRUCTURE

Let us consider a metal crystal, where the atomic nuclei have fixed positions[12] forming a perfect and infinite lattice. This means that, if the basic vectors in the space lattice are $\mathbf{a}_1$, $\mathbf{a}_2$, $\mathbf{a}_3$, the nuclei are situated in the points $\mathbf{g}=g_1\mathbf{a}_1+g_2\mathbf{a}_2+g_3\mathbf{a}_3$, where g_1, g_2, g_3 are all integers between $-\infty$ and $+\infty$. When treating such a crystal, we will consider a cyclic domain, the microcrystal, denoted by (G), defined by a Born-von Kármàn boundary condition. Every crystal orbital $\psi(\mathbf{x})$ must therefore satisfy a periodicity condition of the form,

$$\psi(\mathbf{x}+G\mathbf{a}_\kappa)=\psi(\mathbf{x}), \quad \kappa=1, 2, 3, \tag{1}$$

where G is a very large integer. At the same time we will also introduce the ordinary $\mathbf{k}$-vectors,

$$\mathbf{k}=(k_1\mathbf{b}_1+k_2\mathbf{b}_2+k_3\mathbf{b}_3)/G, \tag{2}$$

where $\mathbf{b}_1$, $\mathbf{b}_2$, $\mathbf{b}_3$ are the basic vectors of the reciprocal lattice ($\mathbf{a}_k\cdot\mathbf{b}_l=\delta_{kl}$), and k_1, k_2, k_3 are integers. In summations over the lattice points $\mathbf{g}$ and $\mathbf{k}$ in the ordinary space and the $\mathbf{k}$-space, respectively, we let an index (∞) denote a summation over *all* lattice points and an index (G) a summation only over the *ground points*, i.e., the G^3 lattice points of each type, satisfying the condition,

$$-G/2\leq g_\kappa<+G/2, \quad -G/2\leq k_\kappa<+G/2. \tag{3}$$

The crystal orbitals $\psi_k(\mathbf{x})$ must always be constructed so that they will be orthonormalized with respect to the ground domain:

$$\int_{(G)}\psi_k(\mathbf{x})\psi_l(\mathbf{x})d\tau=\delta_{kl}. \tag{4}$$

Each lattice point $\mathbf{g}$ in the ordinary space is associated with the elementary volume $V_g=\mathbf{a}_1\cdot(\mathbf{a}_2\times\mathbf{a}_3)$, and each lattice point $\mathbf{k}$ in the $\mathbf{k}$-space with the volume,

$$V_k=\mathbf{b}_1\cdot(\mathbf{b}_2\times\mathbf{b}_3)/G^3=1/G^3V_g=1/V, \tag{5}$$

where V is the total volume of the microcrystal. The density ρ_k of lattice points in the $\mathbf{k}$-space is therefore extremely large, $\rho_k=1/V_k=V$, and each sum over a certain domain in the $\mathbf{k}$-space can consequently be easily transformed into an integral:

$$G^{-3}\sum_k F(\mathbf{k})=G^{-3}\int F(\mathbf{k})\rho_k(dk)=V_g\int F(\mathbf{k})(dk). \tag{6}$$

Basic Assumptions

The notations and symbols introduced in Part I will be used also throughout this paper. We will assume that the crystal orbitals (CO) ψ_k may be found by LCAO from the given AO ϕ_μ or from the orthonormalized AO φ_μ:

$$\psi_k=\sum_\mu \varphi_\mu C_{\mu k}, \tag{7}$$

according to (I, 12). In treating the cohesive properties of the monovalent metals, we will further make the additional assumptions:

(1) The treatment of the valence electrons can be separated from the treatment of the ion cores.

(2) The distribution of occupied valence electron orbitals in the k-space is spherically symmetrical around the origin.

The first assumption is essentially made in order to simplify the numerical work. We note that there are no principal difficulties in taking the interaction between all orbitals into account,[13] and that the "nightmare of

[11] P. O. Löwdin, *A Theoretical Investigation into Some Properties of Ionic Crystals*, thesis (Almquist and Wicksell, Uppsala, 1948); see also J. Chem. Phys. **18**, 365 (1950).

[12] Compare Part I, first footnote.

[13] See reference 11; in treating ionic crystals we have taken even the inner AO into full account, when it was necessary. For instance, in NaCl, we have treated the interaction between the $1s$, $2s$, and $2p$ orbitals of Na^+ and the $3p$ and $3s$ orbitals of Cl^-.

the inner shells"[14] can be eliminated by a certain amount of labor. However, since we are mainly interested in the bonding and overlapping effects of the valence electrons, this simplification may be justified in a first approximation. At first we will assume that there is no hybridization between the ion core (=IC) AO and the valence electron (=VE) AO in the formation of the CO, which means that the matrix $\mathbf{C}$ of the coefficients in (7) has the form,

$$\mathbf{C}=\begin{pmatrix}\mathbf{C}_{\mathrm{IC}} & 0\\ 0 & \mathbf{C}_{\mathrm{VE}}\end{pmatrix}. \tag{8}$$

Hence, the interaction between the IC energy bands and the VE energy bands will be neglected. From the point of view of the valence bond theory,[5,6] Eq. (8) means that, in addition to neutral atoms (A), we will consider singly ionized states of the type $(A)^+$ and $(A)^-$ but neglect ionized states of the type $(A)^{++}$, $(A)^{+++}$, etc., where at least one electron has been removed from the ion core.

As in Part I, the letters μ and ν will indicate arbitrary AO. However, when it is desirable to distinguish between different types of AO, we will let α and β indicate IC AO and g the VE AO associated with the nucleus at the point g:

$$\mu=\begin{cases}\alpha & \text{IC AO (class } II)\\ g & \text{VE AO (class } I);\end{cases} \tag{9}$$

compare (I, 45). Even when neglecting the hybridization mentioned above, we will find that, in the energy expressions (33) and (51), there are terms corresponding to interactions between IC AO and VE AO, and it is therefore necessary to complete our assumption (1) with some additional statements.

The screening effect of all ion cores will, of course, be taken into full account. Further, we will consider the exchange effect between a VE AO and the IC AO belonging to the *same* atom, since the corresponding integrals will be strictly eliminated by the subtraction process (I, 50) in forming the cohesive energy. On the other hand,

> we will neglect all exchange integrals and all overlap integrals associated with a VE AO or an IC AO of one atom and an IC AO of one of its neighbors. (10)

Even if these integrals are really not extremely small, the neglection may be justified in a first approximation. The overlap matrix $\mathbf{S}$, defined by (I, 8), takes now the simple form,

$$\mathbf{S}=\begin{pmatrix}0 & 0\\ 0 & \mathbf{S}_{\mathrm{VE}}\end{pmatrix}. \tag{11}$$

Combining (8) and (11), we find for the bonding-overlapping matrix $\mathbf{R}$, defined by (I, 16) and (I, 17):

$$\mathbf{R}=\begin{pmatrix}\mathbf{R}_{\mathrm{IC}} & 0\\ 0 & \mathbf{R}_{\mathrm{VE}}\end{pmatrix}. \tag{12}$$

Since the ion core orbitals are all completely filled with two electrons having opposite spins, we get at once $Q_{\alpha\beta}=2\delta_{\alpha\beta}$ from (I, 16), independent of the special form of the unitary matrix C_{IC} and of possible mutual hybridization between the IC AO, and further

$$R_{\alpha\beta}=2\delta_{\alpha\beta},\quad \phi_\alpha{}^C-n_\alpha\phi_\alpha\equiv 0. \tag{13}$$

Using (I, 45), thus we find that the whole first double sum of E_{rearr} in (I, 51) will vanish identically. In an alkali metal we have further $n_\mu{}^C=n_\mu$, and for the cohesive energy (I, 51) we then obtain the simplified expression:

$$\begin{cases} E_{\mathrm{coh}}=E_{\mathrm{elstat}}+E_{\mathrm{exch}}+E_{\mathrm{rearr}},\\ E_{\mathrm{elstat}}=W+\sum_\mu(\mu^C|H^{(\mu_1)}|\mu)\\ \qquad\qquad +\sum_\mu\sum_\nu{}^{(\mu_1)}(\mu^C\nu^C|G|\mu\nu),\\ E_{\mathrm{exch}}=-\tfrac{1}{2}\sum_{gh}{}'(g^Ch^C|G|hg),\\ E_{\mathrm{rearr}}=\tfrac{1}{2}\sum_g(g^Cg^C|G|gg), \end{cases} \tag{14}$$

where we have to take the ion core AO explicitly into account only in the electrostatic part. The main problem is now the calculation of the CAO g^C, and we will therefore first treat the bonding and overlapping matrices in greater detail.

The Bonding Matrix

Since we have already found the bonding matrix for the IC AO, we can here confine ourselves to considering only the valence electrons. According to Bloch,[3] we have for the matrix C:

$$C_{gk}=G^{-\frac{1}{2}}\exp(2\pi i\mathbf{g}\cdot\mathbf{k}), \tag{15}$$

where the indices $g, h, k, \cdots$ correspond to the vectors $\mathbf{g}, \mathbf{h}, \mathbf{k}, \cdots$, and this gives the *crystal orbitals*[15]

$$\psi_k(\mathbf{x})=G^{-\frac{1}{2}}\sum_g{}^{(\infty)}\varphi_g(\mathbf{x})\exp(2\pi i\mathbf{g}\cdot\mathbf{k}). \tag{16}$$

Here φ_g are the orthonormalized AO. We note that the matrix $\mathbf{C}$ is unitary with respect to the ground domain (3), and that the CO (16) are orthonormalized with respect to the microcrystal.

Now we will use our second assumption that the CO corresponding to the valence electrons are in the $\mathbf{k}$-space occupied with *spherical symmetry* within the domain $|\mathbf{k}|\leq k_F$ and that each of these orbitals contains two electrons having opposite spins. Since our vector $\mathbf{k}$ corre-

[14] J. H. van Vleck and A. Sherman, Revs. Modern Phys. **7**, 167 (1935).

[15] See also, P. O. Löwdin, J. Chem. Phys. **18**, 365 (1950); compare G. H. Wannier, Phys. Rev. **52**, 191 (1937); J. C. Slater, Phys. Rev. **81**, 385 (1951).

TABLE I. Some properties of the neighbors of an arbitrary lattice point in a body-centered cubic lattice. k=order of neighborhood, a_k=distance, N_k=numbers of neighbors of this order, Q_k=elements of the bonding matrix.

k	a_k	N_k	Q_k
0	0	1	1.000 00
1	a	8	0.237 19
2	1.1547 a	6	0.108 11
3	1.6330 a	12	−0.083 42
4	1.9149 a	24	−0.068 38
5	$2a$	8	−0.054 02
6	2.3094 a	6	0.003 78
7	2.5166 a	24	0.028 96
8	2.5820 a	24	0.033 04
9	2.8284 a	24	0.032 12
10	$3a$	32	0.020 24
11	3.2660 a	12	−0.001 27

sponds to the momentum vector in the free electron theory, our second assumption can be said to imply the existence of the Fermi energy.

However, we note that a still better quantum mechanical treatment would be obtained by considering different distributions of occupied orbitals in the **k**-space, and by taking into account the "interaction between configurations." This can be done by constructing the total wave function as a linear superposition of Slater determinants over the various configurations, and by minimizing the energy by using the variational principle (I, 5). This is necessary in order to obtain higher accuracy for the cohesive energy and for the elastic constants, and particularly in investigating the excited states.

Here we will go on considering only a single Slater determinant. We will now calculate the bonding matrix **Q**, defined by (I, 16). According to (15) and (6), we obtain

$$Q_{gh}=2G^{-3}\sum_{k}^{|\mathbf{k}|\leq k_F}\exp[2\pi i\mathbf{k}\cdot(\mathbf{g}-\mathbf{h})]$$
$$=2V_g\int^{|\mathbf{k}|\leq k_F}\exp[2\pi i\mathbf{k}\cdot(\mathbf{g}-\mathbf{h})](dk). \quad (17)$$

In the alkali metal crystal, too, we have *one* valence electron per atom ($\frac{1}{2}$ electron with + spin and $\frac{1}{2}$ electron with − spin), and the condition $Q_{gg}=1$ gives then

$$k_F=(3/8\pi V_g)^{\frac{1}{3}}. \quad (18)$$

The integration in (17) can now easily be carried out by introducing polar coordinates (the polar axis along the line gh), and, by elementary integrations, we get finally

$$Q_{gh}=3(\sin\xi-\xi\cos\xi)/\xi^3, \quad \xi=2\pi k_F|\mathbf{g}-\mathbf{h}|. \quad (19)$$

The function Q, obtained here, is also well-known from the "cellular method,"[8] where $1-\frac{1}{2}Q^2$ describes the "Fermi hole" in the charge distribution, and from Slater's[15] simplified treatment of the general exchange forces. Here the function enters in a somewhat different way with another interpretation, describing the *bonding* in the crystal. The elements of the matrix **Q** are given for the body-centered structure in Table I.

Crystal Matrices

Here we will investigate the matrix elements with respect to the VE AO in greater detail. We have based our calculation of the total energy (I, 33) on the matrix transformations (I, 22)–(I, 32). In this connection we observe that, if F_{op} is any operator having the periodicity (G) of the microcrystal, we have the identities,

$$\begin{cases}\displaystyle\int_{(G)}\psi_k^*F_{op}\psi_l d\tau=\sum_{gh}^{(G)}C_{kg}^\dagger\bar{F}_{gh}C_{hl}.\\ \displaystyle\bar{F}_{gh}=\sum_{\lambda}^{\infty}F_{g,h+\lambda G}=\sum_{\lambda}^{\infty}\int_{(\infty)}\varphi_g^*F_{op}\varphi_{h+\lambda G}d\tau.\end{cases} \quad (20)$$

Here F_{gh} are the usual matrix elements with respect to the functions φ_g, and $\bar{F}_{gh}$ is the result of a summation, in which generally only *one* term is of practical importance, due to the large magnitude of G. We note that $\bar{F}_{gh}$ is a cyclic matrix, which depends only on the difference $(\mathbf{h}-\mathbf{g})$ between its indices. In the following we will call an arbitrary matrix **A** having the properties,

$$A_{gh}=A_{0,h-g}, \quad A_{g+\lambda G,h}=A_{g,h+\lambda G}=A_{g,h}, \quad (21)$$

a "crystal matrix." In treating a crystal, we note that we have to replace the matrix elements in (I, 22)–(I, 32) by their crystal equivalents.

In considering a crystal matrix A_{gh}, we will always refer its indices to the ground domain (G) given by (3). By using the definition (21), it is easily shown that two arbitrary crystal matrices **A** and **B** always *commute*, i.e., **AB**=**BA**. Further, they are all transformed into diagonal form by the unitary matrix **C**, given by (15), with the diagonal elements,

$$(\mathbf{C}^\dagger\mathbf{A}\mathbf{C})_{kk}=\sum_{\kappa}^{(G)}A_{0,\kappa}\exp(2\pi i\mathbf{k}\cdot\boldsymbol{\kappa}). \quad (22)$$

Since, in our special problem, the matrix elements A_{gh} depend only on the absolute magnitude of the difference $(\mathbf{h}-\mathbf{g})$, the elements A_{gh} are the same for all neighbors **g** and **h**, having the same order k of their neighborhood (**g**, **h**). In the following we will frequently use the order $k=(\mathbf{g},\mathbf{h})$, and we will let a_k denote the distance between two neighbors of order k, and N_k the number of neighbors of order k to an arbitrary atom in the crystal. The numbers a_k and N_k are listed for the body-centered structure in Table I. Instead of the square matrix A_{gh} we can therefore use the equivalent row matrix A_k, given by the correspondence

$$A_{\mathbf{gh}}\leftrightarrow A_k, \quad k=(\mathbf{g},\mathbf{h}). \quad (23)$$

We note that the letter k, indicating order of neighborhood, must not be confused with the momentum vector **k** or with the index **k**, representing this vector. For a matrix product we have, according to the ordinary

multiplication law,

$$(\mathbf{A}\cdot\mathbf{B})_{gh}=\sum_{\alpha}^{(G)} A_{g\alpha}B_{\alpha h}, \tag{24}$$

which for the associate row matrices gives

$$(\mathbf{A}\cdot\mathbf{B})_k=\sum_{pq} A_p\cdot n_k{}^{pq}B_q. \tag{25}$$

Here $n_k{}^{pq}$ is an integer, giving the number of lattice points of the neighborhood p to $\mathbf{g}$ and of the neighborhood q to $\mathbf{h}$, when $(\mathbf{g},\mathbf{h})=k$. The numbers $n_k{}^{pq}$ are conveniently arranged as matrices $\mathbf{n}_k$ ($k=0, 1, 2, \cdots$), having the symmetry relation $n_k{}^{pq}=n_k{}^{qp}$. These matrices can be systematically evaluated by considering the formulas for the mutual distances between the lattice points. A few of these matrices, for the body-centered structure, are given in Table II.

Using formula (20) in the transformations (I, 22)–(I, 32), we obtain matrices with crystal properties (21). Since $\mathbf{S}$ and $\mathbf{Q}$ are both crystal matrices, they commute, and the bonding-overlapping matrix $\mathbf{R}$, given by (I, 17), will simplify to the form,

$$\mathbf{R}=(\mathbf{1}+\mathbf{S})^{-1}\mathbf{Q}=\mathbf{TQ}. \tag{26}$$

We obtain for the corresponding row matrix,

$$R_k=\sum_{pq} T_p n_k{}^{pq}Q_q, \tag{27}$$

and for the combined wave function,

$$\phi_0{}^c(\mathbf{x})=R_0\phi_0(\mathbf{x})+\sum_{k=1}^{\infty} N_kR_k\phi_k(\mathbf{x}). \tag{28}$$

Now it remains to consider the overlapping.

Calculation of the Matrices S and $(1+S)^{-1}$

We will now investigate the overlap integrals S_k for the valence electrons. Special formulas for overlap integrals were given by Bethe[16] and by Landshoff,[17] and a more general formula was presented by us.[18] Later the same problem has been treated with numerous applications by Mulliken[19] and his group. In the case of s-functions, given by

$$\phi_g(\mathbf{x}_1)=\frac{1}{(4\pi)^{\frac{1}{2}}}\frac{f(r_{1g})}{r_{1g}}, \tag{29}$$

we have, according to reference 18, for the overlap integrals between neighbors of order k:

$$S_k=\frac{1}{2a_k}\int_0^{\infty} f(r)dr\int_{|a_k-r|}^{a_k+r}\mathbf{f}(\xi)d\xi, \tag{30}$$

which quantity is easily determined by numerical or analytical integration.

The calculation of the matrices $(\mathbf{1}+\mathbf{S})^{-\frac{1}{2}}$ and $\mathbf{T}=(\mathbf{1}+\mathbf{S})^{-1}$ is slightly more complicated. In our previous treatments of the overlapping problem, we have used expansions in power series in $\mathbf{S}$, but, in the case of the alkali metals, this is impossible, since these power series appear to be strongly *divergent*, due to the large magnitude of the elements S_k and the immense numbers of neighbors. In order to examine this problem in greater detail, we note that the sum,

$$\sum_h |S_{gh}|=\sum_{k=1}^{\infty} N_kS_k=M, \tag{31}$$

is convergent. Let us now introduce a complex parameter λ. According to a well-known theorem,[20] the series

$$\begin{aligned}(\mathbf{1}+\lambda\mathbf{S})^{-\frac{1}{2}}&=\mathbf{1}-\tfrac{1}{2}\lambda\mathbf{S}+\tfrac{3}{8}\lambda^2\mathbf{S}^2-+\cdots,\\ (\mathbf{1}+\lambda\mathbf{S})^{-1}&=\mathbf{1}-\lambda\mathbf{S}+\lambda^2\mathbf{S}^2-+\cdots,\end{aligned} \tag{32}$$

are convergent at least within the circle $|\lambda|\leq 1/M$ in the complex λ-plane. In order to fix the square root, we split up this plane from the point $\lambda=-1$ along the negative real axis, and the matrices $(\mathbf{1}+\mathbf{S})^{-\frac{1}{2}}$ and $(\mathbf{1}+\mathbf{S})^{-1}$ can then be found by analytical continuation of the series (32) up to the point $\lambda=1$. The value of these matrices in $\lambda=1$ can sometimes be found by summing the divergent series (32) for $\lambda=1$ by a summation procedure corresponding to the analytical continuation.

However, there are also other methods of finding the matrices $(\mathbf{1}+\mathbf{S})^{-\frac{1}{2}}$ and $(\mathbf{1}+\mathbf{S})^{-1}$. A simple method is based on the fact that every crystal matrix (and hence even $\mathbf{S}$) is transformed into diagonal form by the unitary transformation $\mathbf{C}$ given by (15). An arbitrary function $F(\mathbf{S})$ of the matrix $\mathbf{S}$ can therefore be determined by

TABLE II. The matrices n_k for $k=0, 1, 2$. If g and h are two neighbors of the order k, then $n_k{}^{pq}$ gives the number of lattice points which are neighbors of the orders p and q with respect to the lattice points g and h, respectively.

$$n_0=\begin{pmatrix}1&\cdot&\cdot&\cdot&\cdot&\cdot&\cdot&\cdot\\ \cdot&8&\cdot&\cdot&\cdot&\cdot&\cdot&\cdot\\ \cdot&\cdot&6&\cdot&\cdot&\cdot&\cdot&\cdot\\ \cdot&\cdot&\cdot&12&\cdot&\cdot&\cdot&\cdot\\ \cdot&\cdot&\cdot&\cdot&24&\cdot&\cdot&\cdot\\ \cdot&\cdot&\cdot&\cdot&\cdot&8&\cdot&\cdot\\ \cdot&\cdot&\cdot&\cdot&\cdot&\cdot&6&\cdot\\ \cdot&\cdot&\cdot&\cdot&\cdot&\cdot&\cdot&24\end{pmatrix},\quad n_1=\begin{pmatrix}\cdot&1&\cdot&\cdot&\cdot&\cdot&\cdot&\cdot\\ 1&\cdot&3&3&\cdot&1&\cdot&\cdot\\ \cdot&3&\cdot&\cdot&3&\cdot&\cdot&\cdot\\ \cdot&3&\cdot&\cdot&6&\cdot&\cdot&3\\ \cdot&\cdot&3&6&\cdot&3&3&\cdot\\ \cdot&1&\cdot&\cdot&3&\cdot&\cdot&\cdot\\ \cdot&\cdot&\cdot&\cdot&3&\cdot&\cdot&\cdot\\ \cdot&\cdot&\cdot&3&\cdot&3&\cdot&\cdot\end{pmatrix},$$

$$n_2=\begin{pmatrix}\cdot&\cdot&1&\cdot&\cdot&\cdot&\cdot&\cdot&\cdot\\ \cdot&4&\cdot&\cdot&4&\cdot&\cdot&\cdot&\cdot\\ 1&\cdot&\cdot&4&\cdot&\cdot&1&\cdot&\cdot\\ \cdot&\cdot&4&\cdot&\cdot&4&\cdot&\cdot&4\\ \cdot&4&\cdot&\cdot&8&\cdot&\cdot&8&\cdot\\ \cdot&\cdot&\cdot&4&\cdot&\cdot&\cdot&\cdot&4\\ \cdot&\cdot&1&\cdot&\cdot&\cdot&\cdot&4&\cdot\\ \cdot&\cdot&\cdot&\cdot&8&\cdot&\cdot&4&\cdot\\ \cdot&\cdot&\cdot&4&\cdot&\cdot&4&\cdot&8\end{pmatrix},\text{ etc.}$$

[16] H. A. Bethe, *Handbuch der Physik* (Julius Springer, Berlin, 1933), XXIV: 1, p. 524.
[17] R. Landshoff, Z. Physik **102**, 201 (1936).
[18] See reference 11, p. 40.
[19] Mulliken, Rieke, Orloff, and Orloff, J. Chem. Phys. **17**, 1248 (1949). R. S. Mulliken, J. Am. Chem. Soc. **72**, 4493 (1950).
[20] See, for instance, Courant-Hilbert, *Methoden der Mathematischen Physik* (Julius Springer, Berlin, 1931), I, p. 16.

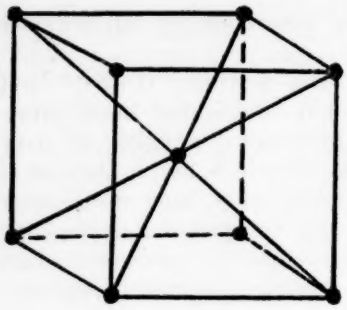

FIG. 1. The arrangement of the atomic nuclei in the body-centered cubic lattice structure.

the formulas,

$$\begin{cases} \mathbf{F}=F(\mathbf{S})=\mathbf{C}F(\mathbf{s})\mathbf{C}^{\dagger}, \\ \mathbf{s}=\mathbf{C}^{\dagger}\mathbf{S}\mathbf{C}=\text{diagonal matrix} \\ s_{kk}=\sum_{\kappa} S_{0,\kappa}\exp(2\pi i\mathbf{k}\cdot\boldsymbol{\kappa}). \end{cases} \tag{33}$$

In calculating the diagonal elements s_{kk}, considerable simplifications can often be obtained by expanding the exponential function into spherical harmonics and by utilizing the symmetry of the lattice. The method described by (33) is closely associated with Wannier's[21] way of constructing orthonormalized atomic orbitals.

According to (26), we need in our treatment of the energy only the matrix $\mathbf{T}=(\mathbf{1}+\mathbf{S})^{-1}$, which can be determined by still more elementary methods.[22] According to the definition of $\mathbf{T}$, we have $\mathbf{T}(\mathbf{1}+\mathbf{S})=\mathbf{1}$, or, for the corresponding row matrices,

$$\sum_{pq} T_p n_k^{pq}(\delta_{0q}+S_q)=\delta_{0k}. \tag{34}$$

Here we first calculate the coefficients,

$$d_{pk}=\delta_{pk}+\sum_{q} n_k^{pq}S_q, \tag{35}$$

and then we obtain a system of linear equations for the calculation of T:

$$\sum_{p=0}^{p=l} T_p d_{pk}=\delta_{0k}. \tag{36}$$

This system is formally infinite, and, in order to be able to solve it by ordinary elementary methods, one has to introduce a "cut-off," which in our applications was put at $l=8$, 9, 10, and 11.

The Body-Centered Structure

In addition to the description of the body-centered structure (see Fig. 1), which may be found in many textbooks on crystals, we will here say a few words about data which are of importance in our calculation of the cohesive properties. As lattice parameter a we will use the distance between nearest neighbors, $a=a_1$. As before, a_k denotes the distance between neighbors of order k and N_k is the number of such neighbors. For the elementary volume of a lattice point, we have $V_0=\frac{1}{2}(2a/\sqrt{3})^3$, and, according to (18) and (19), we then obtain for the bonding matrix,

$$\begin{aligned} Q_k&=3(\sin\xi_k-\xi_k\cos\xi_k)/\xi_k^3. \\ \xi_k&=(9\pi^2\sqrt{3}/4)^{\frac{1}{3}}a_k/a=3.379a_k/a. \end{aligned} \tag{37}$$

The numbers a_k, N_k, and Q_k for $k=0, 1, 2, \cdots 11$ are given in Table I.

Table I shows that, by including neighbors up to the order $k=9$, we will take the 136 first neighbors of each atom into account. The values of Q_k are alternatively positive and negative, showing that the bond orders for the bonds between an atom and its first-order and second-order neighbors are really *bonding*, but that those for bonds with respect to neighbors of the third, fourth, and fifth orders are *anti-bonding*, etc.

TABLE III. Overlap integrals for metallic sodium. Na 3*s*/Na 3*s*.

k \ a	6.5	7	7.5	8	12
0	0.	0.	0.	0.	0.
1	0.45567	0.40630	0.35939	0.31551	0.08970
2	0.35884	0.30854	0.26281	0.22187	0.04336
3	0.14363	0.10903	0.08182	0.06087	0.00513
4	0.07619	0.05369	0.03748	0.02602	0.00163
5	0.06232	0.04297	0.02940	0.02003	0.00121
6	0.02928	0.01879	0.01206	0.00778	0.00053
7	0.01746	0.01077	0.00670	0.00423	0.00041
8	0.01482	0.00905	0.00559	0.00351	
9	0.00805	0.00477	0.00289	0.00182	

Of particular importance in the computations are the matrices n_k used in the formation of matrix products (see Eq. (25)). The matrices up to $k=10$ have been evaluated, and, in Table II, we have given a few examples of them.

3. CALCULATION OF THE COMBINED ATOMIC ORBITALS FOR METALLIC SODIUM

In order to treat metallic sodium, we have used, as basic AO, the wave functions associated with the self-consistent field with exchange for the free Na-atoms numerically given by Hartree and Hartree.[23] This field seems to be somewhat smoother than the field originally presented by Fock and Petrashen.[24] The calculations will be carried out in atomic units,[25] i.e., with e, m, and $\hbar=h/2\pi$ as standard units. Using the values of the fundamental constants recommended by Birge, we find for the units of length and energy:

$$\begin{aligned} 1\ L_H&=\hbar^2/me^2=(0.529\ 19_4\pm 0.000\ 8)\times 10^{-8}\ \text{cm}, \\ 1\ E_H&=me^4/\hbar^2=(4.358\ 3_4\pm 0.008_5)\times 10^{-11}\ \text{erg}, \end{aligned} \tag{38}$$

and the conversion formula,

$$\begin{aligned} 1\ E_H/\text{atom}&=(L/J_{15})\cdot 4.3583_4\times 10^{-21}\ \text{kcal}_{15}/\text{mol} \\ &=627.15\ \text{kcal}_{15}/\text{mol}. \end{aligned}$$

[21] G. H. Wannier, Phys. Rev. **52**, 191 (1937).
[22] Compare P. O. Fröman and S. O. Lundqvist, Arkiv för Fysik **2**, 431 (1951).
[23] D. R. Hartree and W. Hartree, Proc. Roy. Soc. (London) **A193**, 299 (1948).
[24] V. Fock and M. Petrashen, Physik. Z. Sowjetunion **6**, 368 (1934).
[25] D. R. Hartree, Proc. Cambridge **24**, 89 (1928).

We have computed the cohesive energy for metallic sodium for four values of the lattice parameter: $a=6.5$, 7, 7.5, and 8. In addition, the bonding-overlapping matrix $\mathbf{R}$ is formed for $a=12$. The valence electron AO are given by the relation,

$$\phi_g(\mathbf{x}_1)=[1/(4\pi)^{\frac{1}{2}}][f_{3s}(r_{1g})/r_{1g}], \quad (39)$$

where the function $f_{3s}(r)$ is numerically tabulated.[23] All calculations have therefore to be carried out in numerical form, using numerical integration by means of Simpson's rule (or the trapezoidal rule) with central difference correction.

At first the overlap integrals were found according to (30). The calculations were performed for a number of equidistant values of the distance between the atoms g and h, and the actual values, given in Table III, were determined (with an accuracy of 0.1 percent) by logarithmic interpolation. We note that the overlap integrals are very large, and that they therefore never can be neglected in the case of metallic sodium, not even in the case $a=12$. In fact, they must play a very important role in a theory based on the use of atomic orbitals.

We have also investigated the overlapping between the VE AO and the IC AO, and, as an example, we will mention the value $S_{2s/3s}=-0.041385$ for $a=7$ and $k=1$. This means that the overlapping here is considerably smaller but certainly not negligible. However, we have neglected this interaction in a first approximation, since it is probable that the contribution to the cohesive energy is small in the same proportion. These terms must be taken into account in treating the elastic properties.

TABLE IV. The elements of the matrix $\mathbf{T}=(\mathbf{1}+\mathbf{S})^{-1}$.

k \ a	6.5	7	7.5	8	12
0	4.1924	3.1439	2.4502	1.9940	1.0629
1	−1.0944	−0.8104	−0.5911	−0.4386	−0.0820
2	−0.0547	0.0077	0.0011	−0.0123	−0.0184
3	0.5035	0.3564	0.2450	0.1679	0.0103
4	0.0129	−0.0042	−0.0033	0.0017	0.0021
5	0.1647	0.1115	0.0838	0.0627	0.0053
6	0.0414	−0.0016	0.0002	−0.0021	−0.0001
7	−0.1469	−0.0821	−0.0565	−0.0413	−0.0014
8	−0.0298	−0.0173	−0.0106	−0.0067	
9	0.0472	0.0170	0.0106	0.0071	

By combining the results in Tables II and III, the coefficients d_{pk} in (35) can easily be determined, and then the matrix $\mathbf{T}=(\mathbf{1}+\mathbf{S})^{-1}$ is found by solving the system (36). The results are given in Table IV.

Combining the results in Tables I, II, and IV, and using formula (27), we then obtain the results for the bonding-overlapping matrix $\mathbf{R}$, given in Table V.

The combined atomic orbitals $\phi_g{}^C$ can now be calculated by using Table V, formula (28), and the expansion in spherical harmonics described by (I, 36)–(I, 38). Here we will utilize the high symmetry of the body-centered lattice, and, according to Bethe,[26] we will then in the sum (I, 36) have contributions only for $l=0$ and $l=4$, and higher. This means that the CAO is a sum of a s-function, a g-function, etc., and, if we neglect the small contribution from the g-function and the higher functions, we obtain simply

$$\phi_g{}^C(\mathbf{x}_1)=\frac{1}{(4\pi)^{\frac{1}{2}}}\frac{f_{3s}{}^C(r_{1g})}{r_{1g}},$$
$$f_{3s}{}^C(r)=R_0 f_{3s}(r)+\sum_{k=1}^{\infty}\frac{N_k R_k}{2a_k}\int_{|r-ak|}^{r+ak} f_{3s}(\xi)d\xi, \quad (40)$$

where the radial part $f_{3s}{}^C(r)$ can be evaluated and tabulated. We note that there are no principal difficulties in calculating the g-part, etc., but that, in the approximation under consideration, they give negligible contributions. The functions $f_{3s}{}^C(r)$ are illustrated in Fig. 2. They are "many-body-functions," which are different for different values of the lattice parameter a. They are continuous but have weak peaks at the points $r=a_k$ ($k=1, 2, 3, \cdots$) due to the dependence on the magnitude $|r-a_k|$ in (40).

The bonding-overlapping effects give the result that the combined functions $f_{3s}{}^C(r)$ have a certain *oscillatory* character in comparison to the ordinary function $f_{3s}(r)$. In order to find out how the bonding and the overlapping together are responsible for the cohesive properties of the metal, we have to find out how this oscillatory character influences the various energy terms, causing a minimum of E_{coh} for a certain value of a.

4. CALCULATION OF THE VARIOUS ENERGY TERMS. THE COHESIVE ENERGY OF METALLIC SODIUM

The cohesive energy for a sodium crystal is, in our approximation, given by the expression (14), and it consists of three terms: the electrostatic energy, the exchange energy, and the rearrangement energy. In the following we will consider a mol of the crystal, and we let L denote Avogadro's number. According to (I, 64), we obtain for the electrostatic energy per mol:

$$E_{\text{elstat}}=(e^2/2)L\left\{11\Gamma(0)-\int_0^{\infty}U(r)\Gamma(r)dr\right\}. \quad (41)$$

Since, in our approximation, we consider only the s-part

TABLE V. The elements of the bonding-overlapping matrix $\mathbf{R}=\mathbf{TQ}=(\mathbf{1}+\mathbf{S})^{-1}\mathbf{Q}$.

k \ a	6.5	7	7.5	8	12
0	1.3750	1.1549	1.0138	0.9272	0.8784
1	0.0741	0.0857	0.0913	0.0974	0.1640
2	−0.0873	−0.0665	−0.0417	−0.0236	0.0518
3	−0.2263	−0.1805	−0.1555	−0.1396	−0.1020
4	−0.0780	−0.0767	−0.0717	−0.0687	−0.0688
5	−0.0697	−0.0480	−0.0465	−0.0458	−0.0559
6	0.1126	0.0621	0.0518	0.0423	0.0140
7	0.1237	0.0953	0.0765	0.0628	0.0359
8	0.1265	0.0999	0.0805	0.0674	
9	0.0707	0.0646	0.0547	0.0486	

[26] H. A. Bethe, Ann. Phys. (5) 3, 133 (1929).

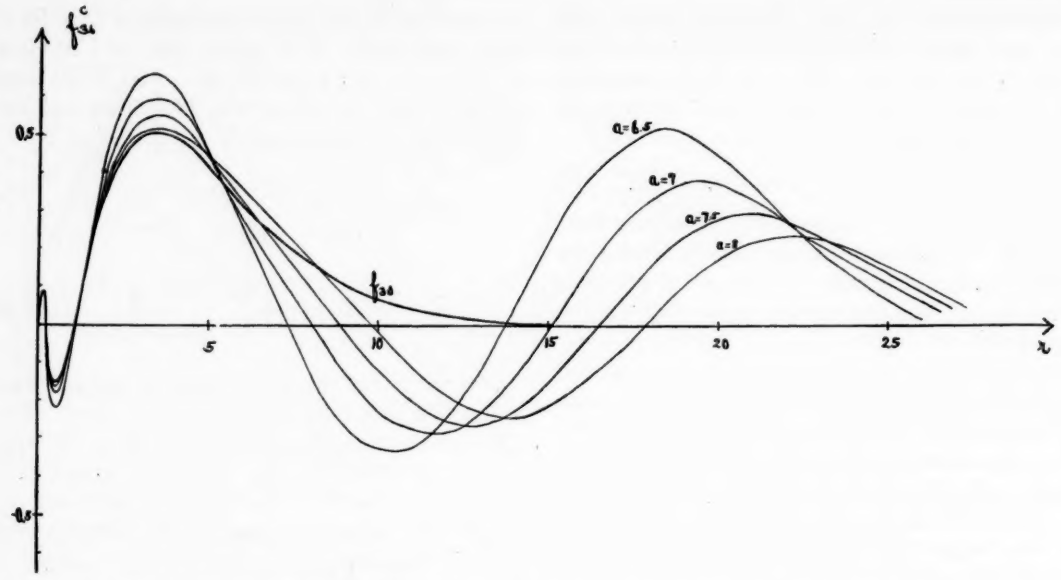

FIG. 2. The combined atomic orbitals $f_{3s}{}^{C}(r)$ for different a-values and the ordinary orbitals $f_{3s}(r)$; r in L_H.

of the CAO, the radial density U_g is spherically symmetrical around the lattice point g, which will essentially simplify Eqs. (I, 56)–(I, 66). The calculations can now be carried out according to the equations,

$$\begin{cases} U(r)=2f_{1s}{}^{2}(r)+2f_{2s}{}^{2}(r)+6f_{2p}{}^{2}(r)+f_{3s}{}^{C}(r)f_{3s}(r), \\ \omega(r)=\dfrac{1}{r}\displaystyle\int_r^\infty U(\xi)d\xi-\int_r^\infty \frac{U(\xi)}{\xi}d\xi, \\ \Gamma(r)=\displaystyle\sum_{k=1}^{\infty}\frac{N_k}{2ra_k}\int_{|r-a_k|}^{r+a_k}\omega(\xi)\xi d\xi, \\ \Gamma(0)=\displaystyle\sum_{k=1}^{\infty}N_k\omega(a_k), \end{cases} \tag{42}$$

by means of numerical integrations.

We will now investigate how the bonding-overlapping effects influence the various energy terms, particularly the simple term $11\Gamma(0)$. As is seen at once from the second of Eqs. (42), also the function $\omega(r)$ is oscillatory, and, in Fig. 3, the functions $r\omega(r)$ are given for $a=6.5$, 7, 7.5, and 8. The curves have the same general shape, but there are also some characteristic differences, since the four curves all cross each other in the region between $r=8$ and $r=10$. The phenomenon is perhaps best illustrated by the Table VI, where, according to the last Eq. (42), the contributions $11N_k\omega(a_k)$ to $11\Gamma(0)$ are tabulated. When considering these contributions for $k=3$ and different a-values, we note that they are negative for higher a-values, but that they change sign in going over to the point $a=6.5$. This corresponds to a rather rapid decrease in the attractive forces, and we shall see that this phenomenon is largely responsible for the existence of a minimum, i.e., of an equilibrium state of the crystal. Of course, the oscillatory character of $f_{3s}{}^{C}(r)$ influences all energy terms, but the effect on the contribution to $11\Gamma(0)$ from neighbors of the third order ($k=3$) is the most obvious.

The electrostatic energy is easily computed according to (41) and (42), and a survey of the results for different a-values may be found in Table VII.

According to (14), the rearrangement energy has the simple form,

$$E_{\text{rearr}}=\tfrac{1}{2}\sum_{g}(g^{C}g^{C}|G|gg), \tag{43}$$

which is essentially the self-potential of the $3s$-electrons on each atom ($\frac{1}{2}$ electron with $+$ spin and $\frac{1}{2}$ electron with $-$ spin), including some bonding-overlapping effects. By using the general formula (I, 55) this term can be evaluated from the relations,

$$\begin{cases} U_{3s}(r)=f_{3s}{}^{C}(r)\cdot f_{3s}(r), \\ \omega_{3s}(r)=\dfrac{1}{r}\displaystyle\int_r^\infty U_{3s}(\xi)d\xi-\int_r^\infty\frac{U_{3s}(\xi)}{\xi}d\xi, \\ E_{\text{rearr}}=\dfrac{e^2}{4}L\left\{\displaystyle\int_0^\infty\frac{U_{3s}(r)}{r}dr-\int_0^\infty\omega_{3s}(r)U_{3s}(r)dr\right\}. \end{cases} \tag{44}$$

It is characteristic for the rearrangement energy (43) that, in our approximation, it does not tend to zero for $a\to\infty$. In fact, we have

$$\lim_{a\to\infty}f_{3s}{}^{C}(r)=f_{3s}(r),\quad \lim_{a\to\infty}E_{\text{rearr}}=\frac{e^2}{2}L\cdot 0.107\,506. \tag{45}$$

This means also that the cohesive energy as a whole does not tend to zero for $a\to\infty$, but to a limit given by (45), which is certainly a wrong prediction of the theory. This effect of giving a too strong ionization is characteristic for the naive CO-LCAO method, and the phenomenon

is well-known also from the theory of molecules.[14] This disadvantage, which will influence the shape of the energy curve and then the elastic properties, can be removed only by considering the "interaction between configurations," mentioned previously in connection with our basic assumption (2).

By using (44), the rearrangement energy can be evaluated by means of numerical integration, and the results may be found in Table VII.

Finally, the exchange energy in (14) is given by the formulas,

$$\left\{\begin{aligned} &E_{\text{exch}}=-\tfrac{1}{2}\sum_{gh}{}'\,(g^C h^C|G|hg)=-\frac{e^2}{4}L\sum_{k=1}^{\infty}N_k I_k,\\ &I_k=\int\!\!\int\frac{\phi_g{}^{C*}(1)\phi_h{}^{C*}(2)\phi_h(1)\phi_g(2)}{r_{12}}d\tau_1 d\tau_2,\\ &\qquad\qquad k=(\mathbf{g},\mathbf{h}), \end{aligned}\right. \tag{46}$$

where, in the last integral, g and h are two lattice points of the order k of neighborhood. By using the general formula (I, 55), we obtain after some calculations:

$$\begin{aligned} I_k=\sum_{l=0}^{\infty}\frac{1}{(2l+1)^2}\Big\{&\int_0^{\infty} f_{3s}{}^C(r_1)\alpha_l{}^C(a_k|r_1)r_1{}^{-l+1}dr_1\\ &\times\int_0^{r_1} f_{3s}(r_2)\alpha_l(a_k|r_2)r_2{}^{l+2}dr_2\\ &+\int_0^{\infty} f_{3s}{}^C(r_1)\alpha_l{}^C(a_k|r_1)r_1{}^{l+2}dr_1\\ &\times\int_{r_1}^{\infty} f_{3s}(r_2)\alpha_l(a_k|r_2)r_2{}^{-l+1}dr_2\Big\}. \end{aligned} \tag{47}$$

This formula is a generalization of a relation originally given by Landshoff.[27] Here the radial functions α_l may be considered as the coefficients in the expansion of ϕ_g in spherical harmonics. The general form of these coefficients may be found in reference 11. For s-functions, we have in particular

$$\alpha_l(a_k|r)=\frac{2l+1}{2ra_k}\int_{|r-a_k|}^{r+a_k} f_{3s}(R)P_l\left(\frac{r^2+a_k{}^2-R^2}{2ra_k}\right)dR, \tag{48}$$

or explicitly

$$\left\{\begin{aligned} &\alpha_0(a_k|r)=\frac{1}{2ra_k}\int_{|r-a_k|}^{r+a_k} f_{3s}(R)dR,\\ &\alpha_1(a_k|r)=\frac{3}{4r^2a_k{}^2}\left\{(r^2+a_k{}^2)\int_{|r-a_k|}^{r+a_k} f_{3s}(R)dR-\int_{|r-a_k|}^{r+a_k} f_{3s}(R)R^2dR\right\},\\ &\quad\cdots\cdots\cdots\cdots\cdots\cdots\cdots\cdots\cdots \end{aligned}\right. \tag{49}$$

Hence, the functions α_l can be evaluated by means of numerical integration. For the corresponding "combined" quantities, we have

$$\alpha_l{}^C(a_k|r)=\frac{2l+1}{2ra_k}\int_{|r-a_k|}^{r+a_k} f_{3s}{}^C(R)\times P_l\left(\frac{r^2+a_k{}^2-R^2}{2ra_k}\right)dR, \tag{50}$$

etc. All terms in the infinite series in (46) can therefore be computed by using numerical integration, but we note that, in our approximation, it is necessary to consider only the first few terms. The results are given in Table VII, and the exchange energy appears to be only slowly decreasing in the interval between $a=6.5$ and $a=8$, which is probably due to the oscillatory character of $f_{3s}{}^C$.

The results of the numerical computations of all energy contributions are collected in Table VII, which shows that E_{coh} has a minimum in the vicinity of the point $a=7$. In order to find the position of this minimum, we must determine the values of the energy terms even in the intermediate points, and, for this purpose, we have used logarithmic subtabulation to the interval 0.1, utilizing all four points. However, we wish to emphasize that this interpolation is, in reality, a rather delicate problem, due to the hidden oscillatory effect in each contribution. Here we have only four points at our disposal, but it would certainly be desirable to carry out the actual computations in a few more points; the point $a=12$ is too far away from the interval under discussion

TABLE VI. Contributions to $11\Gamma(0)$ from neighbors of different orders. The quantity $11N_k\omega(a_k)$ in units of $\frac{1}{2}E_H$/atom.

k \ a	6.5	7	7.5	8
1	−0.335 753	−0.212 124	−0.122 804	−0.068 057
2	−0.145 079	−0.095 260	−0.058 432	−0.037 345
3	+0.005 390	−0.025 564	−0.002 871	−0.005 291
4	0.033 231	0.008 602	0.006 127	0.000 000
5	0.009 031	0.004 169	0.002 739	0.000 286
6	0.002 343	0.001 441	0.003 047	0.000 352
7	0.003 223	0.003 300	0.006 523	0.001 617
8	0.002 618	0.003 795	0.004 994	0.002 134
9	0.000 957	0.001 419	0.000 418	0.000 968
10	0.001 199			
11	0.000 209			
Sum =	−0.422 631	−0.310 222	−0.160 259	−0.105 336 = $11\Gamma(0)$

TABLE VII. Survey of the various contributions to the cohesive energy in metallic sodium, according to formula (14). Unit = $\frac{1}{2}E_H$/atom.

a	E_{rearr}	E_{elstat}		E_{exch}	E_{coh}
6.5	0.135 559	−0.422 631	0.373 985	−0.101 708	−0.014 795
7	0.120 122	−0.310 222	0.213 741	−0.102 075	−0.078 434
7.5	0.116 450	−0.160 259	0.101 400	−0.094 387	−0.036 796
8	0.109 022	−0.105 336	0.064 370	−0.087 845	−0.019 789

[27] See reference 17; compare also S. O. Lunqvist and P. O. Löwdin, Arkiv för Fysik **3**, 147 (1951).

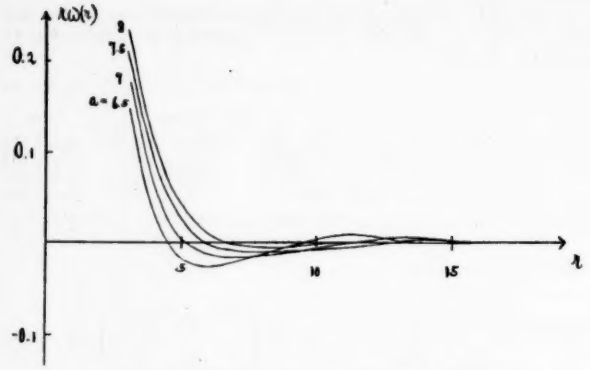

FIG. 3. The function $r\omega^{(r)}$ given by (42) for different values of the lattice parameter a.

to be of real use. The result of the subtabulation is illustrated by Fig. 4. The table with the interval 0.1 shows that there is a minimum for the cohesive energy:

$$E_{\text{coh, min}} = -24.66 \text{ kcal/mole for } a = 6.97 \; L_H = 3.69\text{A}, \quad (51)$$

in comparison with the corresponding experimental data—26 kcal/mol and 3.67A, respectively. A survey of the various energy contributions in kcal/mol in the vicinity of the minimum point is given in Table VIII. However, even if the excellent agreement with experimental experience obtained here may be somewhat fortuitous, the existence of the minimum itself is remarkable. It goes back to the change of the oscillatory character of the CAO $f_{3s}{}^C$ for different a-values, which is again the result of the bonding-overlapping effect. Hence, the existence of an equilibrium state of the crystal seems to depend theoretically on the simultaneous influence of the bonding and the overlapping.

We note that, in our present treatment, we have not taken the "correlation energy" into consideration, i.e., the error due to the use of the one-electron approximation. Our calculation, using the same basic AO in treating the crystal and its free constituents, is essentially based on the assumption that, in forming the cohesive energy by the subtraction process (I, 50), the correlation energy of the crystal and the correlation energy of the free constituents will cancel each other.[28] It would be highly desirable to take up this problem in a more detailed investigation by using, for instance, Wigner's[9] idea or the method due to Möller and Plesset.[29] However, the problem is certainly difficult, since one has not yet obtained any accurate solution for many-electron atoms, and the case of molecules and crystals seems to be still more complicated.

The close agreement between theory and experimental experience for metallic sodium is, in the approximation treated here, confined to the cohesive energy and to the lattice parameter. When treating the elastic properties, we will find that the minimum on our energy curve is too sharp to give a good value of the compressibility, which is partly depending on the effect mentioned in connection with Eq. (45). This means that we obtain a good result for the energy in (14) and its first derivative, but not for the higher derivatives.

In conclusion, we will give a survey of the various approximations introduced in our theory. Principally, we have neglected the interaction between configurations and the correlation energy. Practically, we have neglected the exchange and overlap integrals between a VE AO or a IC AO of one atom and an IC AO of one of its neighbors. In treating the CAO we have further omitted the contributions from g-functions and higher functions. In treating other properties of the crystal, it may be necessary to include one or more of these effects.

5. JUSTIFICATION OF THE CO-LCAO-APPROXIMATION

In treating the energy of metallic sodium, we have started from the AO ϕ_μ associated with the self-consistent field with exchange for the *free* atoms, and the crystal orbitals have then been found by LCAO. The question is now whether better crystal orbitals could be found by a change of the AO forming the starting point. In order to examine this problem, we will use the variational principle (I, 5). By starting from the energy expression (I, 33),

$$E = W + \sum_\mu (\mu^C|H|\mu) + \sum_{\mu\nu} (\mu^C\nu^C|G|\mu\nu) - \tfrac{1}{2}\sum_{\mu\nu} (\mu^C\nu^C|G|\nu\mu), \quad (52)$$

with the supplementary condition (I, 39), simplified by using the fact that T and Q here commute,

$$\int \phi_\mu{}^{C*}\phi_\nu d\tau = Q_{\mu\nu}, \quad (53)$$

and by varying $\phi_\mu{}^C$ and ϕ_μ independently of each other,

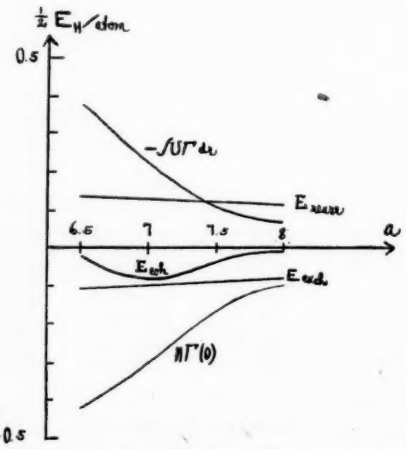

FIG. 4. The different contributions to the cohesive energy of metallic sodium as functions of the lattice parameter a. Energy unit $= \frac{1}{2}E_H$/atom.

[28] See, for instance, the discussion of this problem given by Seitz in F. Seitz, *Modern Theory of Solids* (McGraw-Hill Book Company, Inc., New York, 1940), p. 348.

[29] C. Möller and M. S. Plesset, Phys. Rev. 46, 618 (1934).

the extremum condition $\delta E=0$ gives the two relations,

$$H_1\phi_\mu(1)+e^2\sum_\nu\int\frac{\phi_\nu^{C*}(2)\phi_\nu(2)}{r_{12}}d\tau_2\cdot\phi_\mu(1)$$
$$-\frac{e^2}{2}\sum_\nu\int\frac{\phi_\nu^{C*}(2)\phi_\mu(2)}{r_{12}}d\tau_s\cdot\phi_\nu(1)=\sum_\nu\phi_\nu(1)\lambda_{\nu\mu}, \quad (54)$$

and

$$H_1\phi_\mu^C(1)+e^2\sum_\nu\int\frac{\phi_\nu^{C*}(2)\phi_\nu(2)}{r_{12}}d\tau_2\cdot\phi_\mu^C(1)$$
$$-\frac{e^2}{2}\sum_\nu\int\frac{\phi_\nu^{C*}(2)\phi_\mu^C(2)}{r_{12}}\cdot\phi_\nu(1)=\sum_\nu\phi_\nu^C(1)\lambda_{\nu\mu}. \quad (55)$$

We note that these two equations are *consistent*, for, if $\boldsymbol{\lambda}$ is chosen as a crystal matrix, we have $\boldsymbol{\lambda}\mathbf{R}=\mathbf{R}\boldsymbol{\lambda}$, and (55) can then be derived from (54) by multiplying Eq. (54) with $R_{\mu\kappa}$ and summing over μ.

Let us now investigate in which respects Eq. (54) is different from Eq. (I, 47) for the free atoms. Here we are mainly interested in the valence electron AO g, and for $\mu=g$ (I, 47) takes the form,

$$H_1^{(\mu)}\phi_\mu(1)+e^2\sum_{\nu\neq\mu}^{(\mu)}n_\nu\left\{\int\frac{\phi_\nu^*(2)\phi_\nu(2)}{r_{12}}d\tau_2\cdot\phi_\mu(1)\right.$$
$$\left.-\frac{1}{2}\int\frac{\phi_\nu^*(2)\phi_\mu(2)}{r_{12}}d\tau_2\cdot\phi_\nu(1)\right\}=\epsilon_\mu\phi_\mu(1). \quad (56)$$

Considering the same approximation as used in this paper, i.e., neglecting all exchange and overlap integrals between a VE AO or an IC AO of one atom and an IC AO of one of its neighbors, we will find that Eq. (54) contains a perturbation potential of the form,

$$H_{\text{pert}}(1)=H_1^{(\mu_1)}+e^2\sum_\nu^{(\mu_1)}\int\frac{\phi_\nu^{C*}(2)\phi_\nu(2)}{r_{12}}d\tau_2$$
$$+\frac{e^2}{2}\int\frac{\phi_g^{C*}(2)\phi_g(2)}{r_{12}}d\tau_2=-e^2\Gamma_g(1)$$
$$+\frac{e^2}{2}\left\{\frac{1}{r_{1g}}-\omega_{3s}(r_{1g})\right\}, \quad (57)$$

where Γ and ω_{3s} are given by (42) and (44), respectively. This perturbation potential is therefore almost purely spherically symmetrical, and, for sodium and $a=6.5$, it is illustrated by Fig. 5. It is seen that H_{pert} is almost constant around the nucleus under consideration, and that it then has small peaks at the neighboring lattice points. It is possible that our crystal orbitals could be slightly improved by a perturbation calculation, but the general shape of H_{pert} shows also that our approximation of these orbitals is perhaps more satisfactory than one could expect without a closer investigation.

TABLE VIII. Survey of the various contributions to the cohesive energy of metallic sodium, according to formula (14), in the vicinity of the minimum point. Unit = kcal/mol.

a	E_{rearr}	E_{elstat}		E_{exch}	E_{coh}
6.9	38.19	−106.43	76.09	−32.20	−24.36
7.0	37.67	−97.28	67.02	−32.01	−24.60

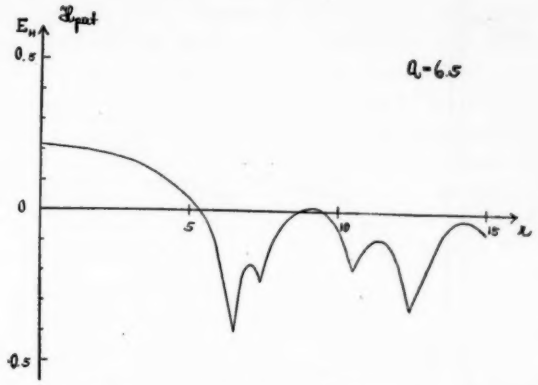

FIG. 5. The perturbation potential H_{pert} given by (57) for $a=6.5$ as a function of r. This potential is constant around the nucleus, but then has peaks for the r-values associated with the neighboring lattice points.

6. COMPARISON WITH THE CELLULAR METHOD

In the cellular method,[8] developed by Wigner, Seitz, Slater, and others, the crystal orbitals for $\mathbf{k}=\mathbf{0}$ are determined by numerical integration of the one-electron Schrödinger equation by using the "cellular idea." In order to carry out a comparison with this method, we will now investigate the shape of our CO ψ_k in the s-cell. Since the overlapping matrix $\mathbf{S}$ is transformed into a diagonal matrix $\mathbf{s}$ by the unitary transformation $\mathbf{C}$, given by (15), we have

$$\boldsymbol{\psi}=\boldsymbol{\varphi}\mathbf{C}=\boldsymbol{\phi}(\mathbf{1}+\mathbf{S})^{-\frac{1}{2}}\mathbf{C}=\boldsymbol{\phi}\mathbf{C}\cdot(\mathbf{1}+\mathbf{s})^{-\frac{1}{2}}, \quad (58)$$

or

$$\psi_k(\mathbf{x})=\frac{G^{-\frac{1}{2}}}{(1+s_{kk})^{\frac{1}{2}}}\sum_g\phi_g(\mathbf{x})\exp(2\pi i\mathbf{k}\cdot\mathbf{g}); \quad (59)$$

compare Wannier.[21] Here the diagonal elements of $\mathbf{s}$ are given by (33). In the case of $\mathbf{k}=\mathbf{0}$, we simply obtain

$$\begin{cases} s_{00}=\sum_{k=1}^{\infty}N_kS_k, \\ \psi_0(\mathbf{x})=\dfrac{G^{-\frac{1}{2}}}{(1+s_{00})^{\frac{1}{2}}}\sum_g\phi_g(\mathbf{x})=\dfrac{G^{-\frac{1}{2}}}{(1+s_{00})^{\frac{1}{2}}}\dfrac{1}{r\sqrt{4\pi}} \\ \qquad\times\left\{f_{3s}(r)+\sum_{k=1}^{\infty}\dfrac{N_k}{2a_k}\int_{|r-a_k|}^{r+a_k}f_{3s}(\xi)d\xi\right\}, \end{cases} \quad (60)$$

where in the last expansion we have neglected the g-part and higher functions. The function $\psi_0(\mathbf{x})$ is, of course, periodical in the lattice, but we are here considering only

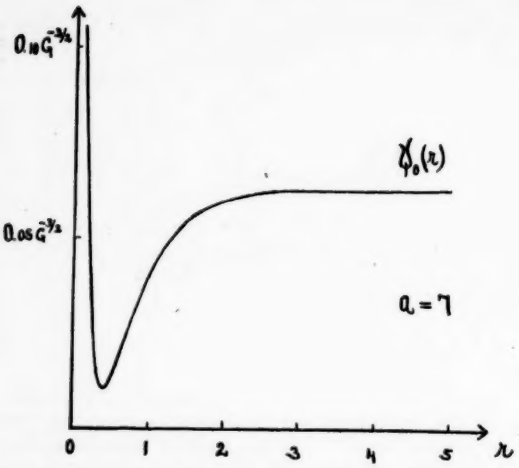

FIG. 6. The one-electron wave function $\psi_k(x)$ given by (16) for $\mathbf{k}=0$ and $a=7$. We note that this function is almost perfectly constant over the main part of the cell, and that it thus has the same basic property as the corresponding function in the cellular method.

its s-part in the fundamental s-cell. The shape of $\psi_0(\mathbf{x})$ is illustrated by Fig. 6, and we note that this function is almost perfectly constant over the main part of the cell. Hence, the lowest wave function in our theory has the same characteristic property as the basic wave function in the cellular method.

We wish to emphasize that the overlap integrals S_k are extremely important in forming $\psi_0(\mathbf{x})$ according to (60). The normalization factors $(1+s_{00})^{\frac{1}{2}}$ for the different a-values are given in Table IX, and they are very large in comparison to the value 1, obtained when overlap is neglected. Table X gives the contributions to s_{00} from neighbors of different orders for $a=7$, and we note how important even the higher neighbors are.

We observe that the wave functions $\psi_k(\mathbf{x})$ for $\mathbf{k}\neq 0$ are constructed according to different principles in our treatment and in the cellular method. The crystal orbitals must always fulfil the Bloch condition,

$$\psi_k(\mathbf{x}+\mathbf{a}_\kappa)=\psi_k(\mathbf{x})\exp(2\pi i\mathbf{a}_\kappa\cdot\mathbf{k}), \quad \kappa=1, 2, 3, \quad (61)$$

and this relation is automatically satisfied by the Bloch orbitals (16) used here. On the other hand, there are some difficulties in the cellular method having the condition (61) fulfilled even on the boundaries of the cell; compare also reference 10.

It would perhaps also been of some interest to compare our treatment with the valence bond method,[5,6,7] developed by Slater, Pauling, and others. This can be done by expanding the fundamental wave function (I, 6) in determinants of the given AO ϕ_μ by using (I, 12) and (I, 10) and elementary theorem concerning determinants of products of rectangular matrices, but the mathematical details will be confined for a later publication. The valence bond wave function for N valence electrons ($N/2$ with plus spin and $N/2$ with minus spin) distributed over N atoms, obtained in this way, implies a resonance phenomenon between bond structures containing atoms which are neutral or singly ionized, and the result shows therefore a close resemblance with Pauling's model for the alkali metals.

TABLE IX. Normalization factors according to (60) for different values of the lattice parameter.

a	$(1+s_{00})^{\frac{1}{2}}$
6.5	3.492
7	3.141
7.5	2.842
8	2.587
12	1.568

TABLE X. Contributions to s_{00} from neighbors of different orders for $a=7$.

k	N_kS_k	k	N_kS_k
1	3.250 40	7	0.258 48
2	1.851 24	8	0.217 25
3	1.308 36	9	0.114 41
4	1.288 56	10	0.099 65
5	0.343 76	11	0.020 28
6	0.112 74		
			$s_{00}=8.865\ 13$

7. CONCLUDING REMARKS

This calculation of the cohesive properties of metallic sodium has partly been carried out in order to reexamine the possibility of utilizing the simple Bloch orbitals, constructed by LCAO, as crystal orbitals. It has been shown that the overlap integrals, instead of being negligible, are of fundamental importance for the whole theory and its applications. It has further been shown that it is possible to overcome the mathematical difficulties which were previously associated with the LCAO-approach, namely, the problem of the many-center integrals and the problem of including bonding and overlapping effects between neighbors of sufficiently high orders. In fact, we have here considered each atom in two-body interaction with its 136 first nearest neighbors, which implies many-body interaction with a still larger number.

Our main result is that, even if the excellent agreement between theory and experimental experience obtained for sodium may be somewhat fortuitous, our method can be used for quantitative purposes. The numerical calculations may be rather tedious and laborious, but they can be carried out in a straightforward way by using purely numerical methods, particularly numerical integration. In reality we have used only ordinary desk machines of the type "Facit ESA" (Åtvidaberg, Sweden).

8. ACKNOWLEDGMENT

The author would like to express his gratitude to Professor Ivar Waller for the favor of discussing this

theory at the seminars at the Institute of Mechanics and Mathematical Physics, University of Uppsala, and for the opportunity of using the computational equipment of the Institute. I am further indebted to *Fil.kand.* A. Sjölander, and Messrs. K. Appel, S. Gronowitz, S. Lidin, Z. Nordahl, and B. Åberg for their valuable and kind assistance in the numerical work. I wish also to express my sincere gratitude to the Swedish State Council for Scientific Research ("Staten Naturvetenskapliga Forskningsråd") for a grant, which made possible the numerical applications to sodium.

This work was concluded during a stay at the Department of Physics, Duke University, Durham, North Carolina, and finally I should like to thank Professor Hertha Sponer and Professor Walter M. Nielsen for their great hospitality.

THE JOURNAL OF CHEMICAL PHYSICS VOLUME 19, NUMBER 12 DECEMBER, 1951

The Spherical Interface. I. Thermodynamics*

FRANK P. BUFF
Chemistry Department, University of Rochester, Rochester, New York
(Received September 6, 1951)

An extension of the Gibbs thermodynamic theory of spherical interfaces leads to generalized forms for the Kelvin relation and the Gibbs adsorption equation. Quantities of physical interest are calculated in terms of the particular dividing surface making the superficial density of matter vanish, frequently more convenient than the surface of tension. An expression is proposed for the work required to form a droplet which is not in equilibrium with the surrounding vapor.

I

IN a recent note[1] on the surface tension of small droplets the convenience of extending the Gibbs[2] thermodynamic theory of spherical interfaces to general dividing surfaces was discussed. It is the purpose of this paper to examine the thermodynamic functions of practical importance from this more general standpoint and incidentally to include the derivation of useful expressions which had been anticipated in our earlier note. Some of the thermodynamic results to be obtained presently will also be of value in the statistical mechanical theory of the plane and spherical interface which will be discussed in the succeeding paper in this series.

We consider a two phase region consisting of a liquid phase α and a vapor phase β with a curved transition zone separating the two bulk phases. Following Gibbs an imaginary dividing surface is placed in the transition zone so that the total volume is divided into a volume V_α containing the liquid phase and a volume V_β containing the vapor phase. The exact location of the dividing surface is still arbitrary at this point of the development, although it should be emphasized that all expressions of physical significance must be invariant in the sense that their numerical value must be independent of the location of the imaginary surface, even though the explicit formulas will, in general, be different. The use of these dividing surfaces is not only possible but indispensable in the treatment of curved interfaces, since precise meaning is given to the concept of area and curvature. In the case of the plane interface the concept of a dividing surface is still useful but not necessary, and valid alternative expositions exist,[3] the ultimate justification for which is to be found in the fact that in the absence of external fields the component of the stress tensor perpendicular to the plane interface is uniform throughout.

The starting point of the theory is provided by variations in the state of the system originally in a condition of equilibrium. By restricting our discussion to a one component system in the absence of external fields, the Gibbs phenomenological theory leads to the following fundamental equation for the variation in state of a small segment of the two phase system characterized by the area s and principal curvatures c_1 and c_2 of the dividing surface,

$$\begin{aligned}&\delta E-T\delta S-\mu\delta N+p_\alpha\delta V_\alpha+p_\beta\delta V_\beta\\&\quad=\gamma\delta s+C_1\delta c_1+C_2\delta c_2\\&\quad=\gamma\delta s+C\delta((c_1+c_2)/2)+(C_1-C_2)\delta[(c_1-c_2)/2];\quad(1)\\&C=C_1+C_2,\end{aligned}$$

where E, S, and N are, respectively, the energy, entropy, and number of moles of the system, and where we have already utilized Gibbs' demonstration of the uniformity of the temperature T and chemical potential μ, i.e.,

$$\mu=\mu_\alpha(T, p_\alpha)=\mu_\beta(T, p_\beta),\qquad(2)$$

a relation which determines the pressure p_α of the bulk phase α in terms of the pressure p_β of the bulk phase β

---

* Presented at the Pittsburgh meeting of the American Physical Society, March 8–10, 1951.

[1] F. P. Buff and J. G. Kirkwood, J. Chem. Phys. **18**, 991 (1950).

[2] J. W. Gibbs, *Collected Works* (Yale University Press, New Haven, Connecticut, 1948), Vol. I, pp. 55–353.

[3] E. A. Guggenheim, *Thermodynamics* (North-Holland Publishing Company, Amsterdam, 1949), pp. 35–39.

and which thus provides operational significance to p_α and p_β in Eq. (1). γ is the generalized surface tension, and C_1 and C_2 are the curvature terms† which Gibbs had the great foresight to include in his theory, all referred to the dividing surface selected. It will be shown subsequently, Eq. (16), that the elusive term C permits of a simple interpretation for a convenient dividing surface of the spherical interface.

At this point in his theory, Gibbs selected a particular dividing surface, the surface of tension, chosen so as to make C vanish. It was then assumed by him that this selection would simultaneously make C_1-C_2 vanish, which although valid for the plane, cylindrical and spherical interfaces, is an approximation in the general case, the assessment of which is a task for molecular theory. We shall see, however, that new results may be obtained if the selection of the dividing surface is delayed. Thus with use of the Gibbs criteria for equilibrium

$$p_\alpha\delta V_\alpha+p_\beta\delta V_\beta=\gamma\delta s+C\delta\left(\frac{c_1+c_2}{2}\right)+(C_1-C_2)\delta\left(\frac{c_1-c_2}{2}\right), \quad (3)$$

$$\delta V_\alpha=-\delta V_\beta,$$

a generalized Gibbs-Kelvin relation may be deduced

$$p_\alpha-p_\beta=\gamma(c_1+c_2)-\frac{C}{2s}(c_1^2+c_2^2)-\left(\frac{C_1-C_2}{2s}\right)(c_1^2-c_2^2), \quad (4)$$

from the familiar relations,

$$\begin{aligned}&\delta V_\alpha=s\delta N; \qquad \delta s=(c_1+c_2)s\delta N;\\ &\delta c_1=-c_1^2\delta N; \quad \delta c_2=-c_2^2\delta N;\end{aligned} \quad (5)$$

where δN is the uniform normal distance through which all parts of the dividing surface move.

Although the subsequent analysis may still be pursued for an interface with arbitrary curvatures, we shall restrict ourselves from now on to the spherical drop since this is the case of main interest, so that Eq. (4) reduces to

$$p_\alpha-p_\beta=2\gamma c-(c^2C/s). \quad (6)$$

Additional consequences of the theory may be obtained by utilizing the form of Eq. (1) corresponding to a reversible change from the original equilibrium state,

$$dE=TdS-p_\alpha dV_\alpha-p_\beta dV_\beta+\mu dN+\gamma ds+Cdc. \quad (7)$$

Subtracting the corresponding equations for the bulk phases α and β, taken to hold in amount up to the dividing surface,

$$\begin{aligned}dE_\alpha&=TdS_\alpha-p_\alpha dV_\alpha+\mu dN_\alpha\\ dE_\beta&=TdS_\beta-p_\beta dV_\beta+\mu dN_\beta,\end{aligned} \quad (8)$$

we obtain

$$\begin{aligned}dE^s&=TdS^s+\mu dN^s+\gamma ds+Cdc,\\ E^s&=E-E_\alpha-E_\beta; \quad S^s=S-S_\alpha-S_\beta;\\ N^s&=N-N_\alpha-N_\beta.\end{aligned} \quad (9)$$

Thus N^s is the actual excess in moles over the amount computed under the assumption that the respective bulk properties hold up to the dividing surface. Integration of Eq. (9) at constant curvature, keeping uniform properties throughout the extent of the surface, leads to

$$\begin{aligned}E^s&=TS^s+\mu N^s+\gamma s,\\ E&=TS+\mu N-p_\alpha V_\alpha-p_\beta V_\beta+\gamma s.\end{aligned} \quad (10)$$

Equating the result of differentiation of Eq. (10) to Eq. (9) yields a generalized Gibbs adsorption equation,

$$\begin{aligned}&S_s dT+\Gamma d\mu+d\gamma=(C/s)dc\\ &S_s=(S^s)/(s); \quad \Gamma=(N^s)/(s).\end{aligned} \quad (11)$$

With use of Eq. (2) and the power series expansion,

$$\mu_\alpha(T,p_\alpha)=\mu_\alpha(T,p_\infty)+\bar{V}_\alpha(p_\alpha-p_\infty)-\mathrm{K}\bar{V}_\alpha/2(p_\alpha-p_\infty)^2+\cdots, \quad (12)$$

where $\bar{V}_\alpha$ and K are the partial molar volume and isothermal compressibility coefficient of the liquid at the pressure p_∞ at which the two phases meet at a plane interface, the Gibbs-Thomson formula for the vapor pressure of the drop is immediately obtained,

$$RT\log p/p_\infty=\bar{V}_\alpha[(p_\alpha-p_\beta)-\mathrm{K}/2(p_\alpha-p_\beta)^2+\cdots]+\cdots, \quad (13)$$

where p/p_∞ is the supersaturation ratio.

The Gibbs formula for the work of formation W of a droplet from a large amount of vapor is derived by subtracting Eq. (10) from the corresponding expression for the original vapor under the condition of constant entropy, volume, and composition

$$E_{or}=T_{or}S+N\mu_{or}-p_{or}(V_\alpha+V_\beta), \quad (14)$$

with the result

$$W=\gamma s-(p_\alpha-p_\beta)V_\alpha, \quad (15)$$

where terms involving differences of temperature, chemical potential, and pressure have been neglected. It will be noted that the formula for W, Eq. (15), is also equal to the change in Helmholtz free energy, ΔA, for the process considered.

II

We shall now express the invariant quantities Eqs. (6), (13), and (15) in terms of the two dividing surfaces of major importance. The first is the classical surface

† It may be readily shown from the statistical mechanical derivation of the generalized Gibbs-Kelvin relation, Eq. (6), on the basis of the virial theorem, that C is an external force similar to p_α, p_β, and γ.

of tension of radius r, chosen so as to make C vanish. The other is the dividing surface of radius R, chosen so as to make the superficial density of matter Γ vanish. It is the latter dividing surface, which we shall distinguish by a prime, which has been intuitively employed in applications, although the formulas commonly utilized incorrectly correspond to the surface of tension. From the first form of Eq. (10) it is worth noting that only $\gamma's'$ may be properly labelled a surface free energy. The curvature dependence of γ' is determined by Eq. (11)

$$(\partial\gamma'/\partial c')_T = C'/s', \tag{16}$$

which is to be contrasted with the analogous Gibbs[4]-Tolman[5]-Koenig[6] formula pertaining to the surface of tension

$$\left(\frac{\partial\gamma}{\partial c}\right)_T = \frac{-2\delta\gamma[1+\delta c+(\delta c)^2/3]}{1+2\delta c[1+\delta c+(\delta c)^2/3]}, \tag{17}$$
$$\delta = R-r.$$

The formulas for the temperature dependence of γ and γ' may be readily deduced

$$\left(\frac{\partial\gamma'/T}{\partial 1/T}\right)_{c'} = E_s',$$

$$\left(\frac{\partial\gamma/T}{\partial 1/T}\right)_c = \frac{E_s+\delta[1+\delta c+(\delta c)^2/3][(E_\beta/\bar V_\beta)-(E_\alpha/\bar V_\alpha)]}{1+2\delta c[1+\delta c+(\delta c)^2/3]}, \tag{18}$$

which in conjunction with Eqs. (16) and (17) prove of value in connection with discussions[1,7] concerning the temperature dependence of an "effective surface tension" defined in terms of the Becker-Döring theory of nucleation.

With use of Eq. (16) the Gibbs-Kelvin expression‡ may be exhibited in the two forms,

$$p_\alpha - p_\beta = 2\gamma/r = 2\gamma'/R + (\partial\gamma'/\partial R)_T. \tag{19}$$

Substitution of Eq. (19) into Eq. (15) leads to the following expression for the work of formation of a drop

$$W = \Delta A = \frac{4\pi r^2\gamma}{3} = \frac{4\pi R^2\gamma'}{3}\left[1-\left(\frac{\partial\log\gamma'}{\partial\log R}\right)_T\right], \tag{20}$$

while the Gibbs-Thomson formula for an incompressible fluid is given by

$$RT\log p/p_\infty = \frac{2\bar V_\alpha\gamma(T,r)}{r} = \bar V_\alpha\left[\frac{2\gamma'}{R}+\left(\frac{\partial\gamma'}{\partial R}\right)_T\right]. \tag{21}$$

It is of interest to remark that in applications of Eq. (21) to small droplets the mass of the droplet in moles is properly given by $(4\pi R^3/3\bar V_\alpha)=[4\pi(r+\delta)^3/3\bar V_\alpha]$.

III

Although the application of macroscopic thermodynamic concepts to the kinetics of nucleation of supersaturated vapors is to be considered approximate,[1] it has led to extraordinarily useful qualitative conclusions. In this connection we shall indicate that by violating the condition (2), while retaining all other thermodynamic relations, a plausible expression may be obtained for the work of formation of a droplet which is not in equilibrium with a large mass of surrounding dilute vapor. This formula, which describes the one dimensional Eyring surface employed in current nucleation theories, will also give us additional insight into the nature of the unstable equilibrium for the one component system.

The droplet will be characterized by the statement that N_α' moles of the liquid phase are contained within the $\Gamma=0$ dividing surface of radius R. In accordance with the preceding discussion the following expression is assumed

$$E^+ = TS - p_\alpha V_\alpha - p_\beta V_\beta + \gamma s + N_\alpha'\mu_\alpha(T,p_\alpha) + (N-N_\alpha')\mu_\beta(T,p_\beta). \tag{22}$$

The desired expression for the work of formation W^+ is then immediately obtained

$$W^+(N_\alpha') = \Delta A^+ = N_\alpha'(\mu_\alpha-\mu_\beta)+W(N_\alpha'), \tag{23}$$

where W is the work required to form a droplet of radius R in equilibrium with the surrounding vapor. With use of the alternative relations,

$$\left(\frac{\partial\gamma s/3}{\partial r}\right)_T = -V_\alpha'\left(\frac{\partial[p_\alpha-p_\beta]}{\partial r}\right)_T;$$
$$p_\alpha - p_\beta = \left(\frac{\partial\gamma's'}{\partial V_\alpha'}\right)_T; \tag{24}$$

it may be shown that

$$\left(\frac{dW^+}{dN_\alpha'}\right)_{\mu_\alpha=\mu_\beta}=0; \quad \left(\frac{d^2W^+}{dN_\alpha'^2}\right)_{\mu_\alpha=\mu_\beta}<0; \tag{25}$$

i.e., W^+ has a maximum for the droplet which is of such a size so as to be in equilibrium with the vapor phase and where the formula for W^+ is rigorous. For an incompressible liquid the approximations

$$\mu_\beta=\mu_\alpha(T,p_\alpha^{\text{crit}}); \quad p_\beta=p_\beta^{\text{crit}}, \tag{26}$$

---

[4] Reference 2, p. 232.
[5] R. C. Tolman, J. Chem. Phys. **17**, 333 (1949).
[6] F. O. Koenig, J. Chem. Phys. **18**, 449 (1950).
[7] G. M. Pound and V. K. LaMer, J. Chem. Phys. **19**, 506 (1951).

‡ G. Bakker's [*Handbuch der Experimentalphysik* (Akad. Verlags., Leipzig, 1928)], Vol. VI, early work on Eq. (19), based on his alternative thermodynamic approach and his quasi-thermodynamic definition of surface tension, unfortunately led to the erroneous conclusion that surface tension is curvature independent.

where p_α^{crit} and p_β^{crit} are the pressures in the respective bulk phases when the droplet is in equilibrium, lead to

$$W^+ \approx \gamma' s' - (p_\alpha^{\text{crit}} - p_\beta^{\text{crit}}) V_\alpha', \tag{27}$$

which may also be derived on the basis of the kinetic considerations employed by Becker and Döring.[8]

IV

Additional information concerning the curvature dependence of surface tension and the validity of Gibbs' phenomenological assumption Eq. (1) may be obtained from statistical mechanics. In the case of the plane interface the virial theorem as well as the thermodynamic definition of surface tension used in conjunction with a device introduced by H. S. Green,[9] lead to results in complete agreement with the mechanical definition of surface tension employed by Kirkwood and Buff.[10] For the spherical interface the virial theorem yields our generalized Gibbs-Kelvin relation, Eq. (6), while the mechanical and thermodynamic definitions lead to identical results for drops large compared to the range of intermolecular force, the only ones to which thermodynamic concepts are applicable. The expressions for γ and C surmised by Tolman[11] on the basis of his quasi-thermodynamics can be confirmed by molecular theory

$$\begin{aligned} \gamma &= \int (\sigma_T(z) - \sigma_{\alpha\beta})(1+cz)^2 dz, \\ C/s &= 2\int (\sigma_T(z) - \sigma_{\alpha\beta}) z(1+cz) dz, \\ \sigma_{\alpha\beta} &= -p_\alpha[1 - A(z)] - p_\beta A(z), \\ A(z) &= 0, \quad z<0; \quad A(z) = 1, \quad z \gtrsim 0, \end{aligned} \tag{28}$$

where z is a coordinate directed outward from the arbitrary dividing surface of curvature c, $A(z)$ is the unit step function and σ_T is the tangential component of the point function stress tensor, recognized to be determined by molecular theory. With use of Eqs. (16), (17), and (28) the curvature dependence of γ and γ' is given by

$$\begin{aligned} \gamma/\gamma_\infty &= 1 - (2\delta_\infty/r) + \cdots, \\ \gamma'/\gamma_\infty &= 1 - (2\delta_\infty/R) + \cdots, \end{aligned} \tag{29}$$

where δ_∞ is the distance δ corresponding to the plane interface. δ_∞ has been previously calculated[10] for representative systems and found to be positive and of the order of magnitude of a molecular diameter.

APPENDIX

We shall now show that the curvature dependence of surface tension may also be included in Frenkel's[12] approximate surface thermodynamics for a one component system which utilizes a dividing surface corresponding roughly to the $\Gamma=0$ dividing surface on the exact Gibbs formulation. The starting point for a spherical interface is provided by the equation,

$$\begin{aligned} &\delta E = T\delta S + \mu_\alpha(T, p_\beta)\delta N_\alpha + \mu_\beta(T, p_\beta)\delta N_\beta - p\delta V + \gamma\delta s + C\delta c, \\ &V = V_\alpha + V_\beta; \quad V_\alpha = N_\alpha \bar{V}_\alpha(T, p_\beta); \quad V_\beta = N_\beta \bar{V}_\beta(T, p_\beta), \end{aligned} \tag{A1}$$

where μ_α and $\bar{V}_\alpha$ are the chemical potential and partial molar volume, respectively, of the liquid phase α, both taken at the pressure p_β of the vapor phase β. The remaining symbols have their usual significance. With use of the criteria for equilibrium Eq. (A1) immediately leads to

$$\mu_\alpha - \mu_\beta = -\bar{V}_\alpha(2\gamma c - (c^2 C/s)). \tag{A2}$$

Upon integration of Eq. (A1) at constant curvature and subsequent differentiation, we obtain

$$\begin{aligned} E &= TS + N_\alpha\mu_\alpha + N_\beta\mu_\beta - p_\beta V + \gamma s, \\ (\partial\gamma/\partial c)_T &= C/s, \end{aligned} \tag{A3}$$

so that

$$\mu_\alpha - \mu_\beta = -\bar{V}_\alpha(\partial\gamma s/\partial V_\alpha)_T, \tag{A4}$$

and

$$W = \gamma s + \frac{(\mu_\alpha - \mu_\beta)V_\alpha}{\bar{V}_\alpha} = \left(\frac{\partial(\gamma s/V_\alpha)}{\partial(1/V_\alpha)}\right)_T.$$

It should be noted, however, that although these equations bear a formal resemblance to the results of the Gibbs formulation, the latter should always be used in applications.

[8] R. Becker and W. Döring, Z. Physik **24**, 719 (1935).
[9] M. Born and H. S. Green, *A General Kinetic Theory of Liquids* (Cambridge University Press, London, 1949), p. 23.
[10] J. G. Kirkwood and F. P. Buff, J. Chem. Phys. **17**, 338 (1949).
[11] R. C. Tolman, J. Chem. Phys. **16**, 758 (1948).
[12] J. Frenkel, *Kinetic Theory of Liquids* (The Clarendon Press, Oxford, 1946).

The Infrared Dispersion of Acetylene and the Dipole Moment of the C−H Bond

R. L. KELLY,* R. ROLLEFSON, AND B. S. SCHURIN
University of Wisconsin, Madison, Wisconsin

(Received July 6, 1951)

The index of refraction of acetylene has been measured at 55 wavelengths in the infrared between 1 and 20 microns. The contributions of the molecular vibrations to the index of refraction have been determined and interpreted in terms of effective charges on the constituent atoms. According to the analysis, during the infrared-active bending vibration the hydrogen atoms have an effective charge of 0.991×10^{-10} esu. The product of this effective charge by the separation of the carbon and hydrogen atoms is interpreted as giving an estimate of the C−H bond moment, the value obtained being $(1.05\pm0.01)\times10^{-18}$ esu cm. For the active stretching vibration, the computed effective charge was 0.515×10^{-10} esu, which is the rate of change of bond moment with internuclear distance. A comparison of these results with previous work indicates a possible regularity in the C−H bond moment in going from methane to ethylene to acetylene, although the regularity may be only apparent.

INTRODUCTION

FOR simple molecules whose absorption is strong enough, measurements of infrared dispersion provide a sensitive and accurate method for determining the intensities of infrared bands. From the intensities, the effect of the molecular vibrations on the dielectric constant can be calculated, as well as the electric bond moment or the rate of change of bond moment with internuclear distance. The reasons for measuring refractive index rather than intensity of absorption have been pointed out by Van Vleck[1] and explained in a previous paper.[2] The results of previous dispersion work of methane[3] and ethylene[4] made it desirable to determine the magnitude of the C−H bond in acetylene, since there appeared to be a possibility of a regular change in the C−H moment associated with changing carbon-carbon bonding.

EXPERIMENTAL

The apparatus used and the method of obtaining data have been described previously.[3] The major change since the measurements on methane was the use of a KBr hollow prism, placed at a position about midway between the NaCl hollow prism and the thermopile, and used interchangeably with the NaCl prism. This addition, with a KBr monochromator prism, provides a means for obtaining data at wavelengths longer than are possible with NaCl, and increases the aperture and therefore the intensity at the thermopile. It suffers the disadvantage that, since the optical lever arm (and hence the thermopile displacement) is smaller, minor experimental variations in the measurement of thermopile displacement correspond to relatively large variations in the calculated refractive index of the gas. For this reason, the precision of the data is not as high when using the KBr components as with the NaCl. However, the contribution of the lowest frequency vibration to the index was large enough in the KBr region (15 to 20 microns) so that the lack of precision was not a serious problem.

The monochromator was of the Wadsworth type and the KBr calibration was calculated by the method of Cross[5] from the data of Gundelach.[6] Discrepancies in the wavelengths of known absorption bands indicated that the published index of refraction data for KBr was not satisfactory. The wavelengths in this research in the KBr region were taken from an empirical correction curve and may be in error by as much as 1 percent. However, in view of the good agreement between the calculated and experimental data at the shorter wavelengths, the dispersion equation for acetylene cannot be greatly in error.

The gas used was Matheson's 99.5 percent pure tank acetylene, dissolved in acetone for shipping. The acetone was removed by bubbling the gas through a water trap, and the acetylene was purified by several fractional distillations between liquid air traps. In many runs, attempts were made to detect the presence of acetone in the gas by measuring the infrared absorption in the 5.8 micron region, where the acetone bands are not overlapped by those of acetylene. The absorption measured was negligible and therefore the acetone present was at most about 1 part in 1000. Because of the possibility of explosions in working with pure acetylene at higher pressures, all data were taken at pressures of about 1 atmosphere absolute with the gas in a system of small glass tubing with a total volume of 1 liter.

All data were taken at 25°C. The values of the refractive index obtained were reduced to 0°C and 760-mm pressure by means of the coefficient of expansion and *pv* data given in the International Critical Tables. Since most data were taken at about 760 mm, the *pv* correction was usually negligible, being at most 0.03 percent.

* Now at Stanford Research Institute, Stanford, California.

[1] J. H. Van Vleck, *The Theory of Electric and Magnetic Susceptibilities* (Oxford University Press, London, 1932).

[2] R. Rollefson and A. H. Rollefson, Phys. Rev. **48**, 779 (1935).

[3] R. Rollefson and R. Havens, Phys. Rev. **57**, 710 (1940).

[4] C. F. Hammer, thesis, *Infrared Dispersion of HCl, DCl, N_2O and C_2H_4* (University of Wisconsin, 1948).

[5] P. C. Cross, Rev. Sci. Instr. **4**, 197 (1933).

[6] E. Gundelach, Z. Physik **66**, 775 (1930).

TABLE I. Intensities of absorption bands in C_2H_2.

Assignment	ν_i	A_i
ν_5'	710 cm^{-1}	803.6×10^{10} cm^{-1} sec^{-1}
ν_5''	733	803.6
ν_5'''	760	803.6
ν_5	733	2410.8±2%
ν_{45}'	1306	151
ν_{45}'''	1350	151
$\nu_{45}(\nu_4+\nu_5)$	1328	302±5%
ν_3	3285.5	325
$\nu_{345}(\nu_2+\nu_4+\nu_5)$	3296.5	651
$\nu_{3;245}$	3293	976±5%

RESULTS

The index of refraction n of a gas can be represented by an equation of the form,

$$n-1=\sum(c_i)/(\nu_i^2-\nu^2),$$

where the ν_i are characteristic frequencies of the molecule. If the equation representing the index in the visible region be extrapolated into the infrared, the observed index will differ from this "extrapolated" index by an amount given by the contributions of the infrared rotation and vibration-rotation bands, since these contributions are not detected by observations in the visible.

For acetylene, Watson and Ramaswamy[7] have made the most complete measurements in the visible region and give a dispersion equation which fits their data. It should be noted that these authors made their measurements at 25°C, and the results were reduced to those which would have been obtained had the gas been ideal. Removing this correction increases their tabulated values by 0.84 percent, and reduction to 0°C gives the equation,

$$n_0-1=5453\times10^8/(9403\times10^6-\nu^2), \quad (1)$$

where ν is the frequency in cm^{-1}.

In order to make the averaged experimental data agree at 1 micron with the values of the index obtained from the extrapolation formula (1), the observed index and the extrapolated index had to be shifted with respect to each other by 0.29 percent. It was assumed that index of refraction data, either in the visible or infrared, gives the slope of the dispersion curve more accurately than it gives absolute value. Shifting the extrapolation formula amounts to a calibration of Watson and Ramaswamy's apparatus in terms of the dispersion of nitrogen as obtained by Bennett,[8] since nitrogen was used for calibration in this research. Increasing Eq. (1) by 0.29 percent gives the final extrapolation equation,

$$(n_0-1)_{ext}=5468.6\times10^8/(9403\times10^6-\nu^2). \quad (2)$$

[7] H. E. Watson and K. L. Ramaswamy, Proc. Roy. Soc. (London) **156A**, 144 (1936).
[8] C. E. Bennett, Phys. Rev. **45**, 200 (1934).

TABLE II. The index of refraction n of C_2H_2 in the infrared at 0°C and 760-mm pressure. Here $(n_0-1)_{exp}$ is the average experimental value of n_0-1; $(n_0-1)_{ext}$ is the value obtained by extrapolating the equation (2) of Watson and Ramaswamy; and $(n_0-1)_{calc}$ is calculated by the dispersion formula (3) in the text.

λ	$(n_0-1)_{ext}\times10^8$	$(n_0-1)_{calc}\times10^8$	$(n_0-1)_{exp}\times10^8$
1.015 microns	587.56	586.89	586.82
1.078	86.87	86.11	86.16
1.165	86.10	85.21	85.37
1.257	85.46	84.40	84.31
1.382	84.72	83.44	83.48
1.745	83.58	81.40	81.33
1.872	83.32	80.74	80.66
2.003	83.09	80.03	79.91
2.628	82.45	74.59	74.41
2.670	82.43	73.80	73.10
2.712	82.40	72.85	72.41
2.756	82.37	71.58	71.04
2.797	82.35	70.03	68.77
3.214	82.16	91.22	91.02
3.293	82.13	86.94	86.61
3.458	82.08	82.75	82.46
3.535	82.06	81.59	81.30
4.061	81.94	76.83	76.20
4.700	81.85	72.41	72.56
4.824	81.84	71.51	71.57
5.060	81.81	69.70	69.73
5.292	81.80	67.82	67.87
5.522	81.78	65.74	65.69
5.745	81.77	63.42	62.97
5.958	81.76	61.06	61.22
6.155	81.74	58.54	58.34
6.344	81.73	55.64	56.00
6.52	81.72	52.48	52.57
6.61	81.72	50.56	50.59
6.69	81.71	48.63	47.82
8.15	81.66	62.14	61.60
8.23	81.66	58.51	57.61
8.30	81.66	55.81	54.40
8.44	81.66	50.97	50.20
8.58	81.65	46.61	45.50
8.72	81.65	42.15	41.43
8.86	81.65	38.33	37.38
8.99	81.64	34.67	34.00
9.13	81.64	30.80	30.19
9.26	81.64	26.93	26.80
9.38	81.64	23.08	23.10
9.63	81.64	14.81	15.02
9.87	81.63	6.02	6.30
10.10	81.63	496.95	497.20
10.33	81.62	486.42	486.66
10.55	81.62	474.86	475.46
10.77	81.62	461.48	462.39
10.98	81.62	446.56	447.38
11.20	81.62	428.15	429.30
16.70	81.59	818.09	819.18
16.90	81.59	807.21	806.73
17.28	81.59	790.04	789.25
17.75	81.59	773.39	774.23
18.19	81.59	761.04	760.81
19.04	81.59	743.01	740.70
∞	81.57	661.71	...

The index of refraction of acetylene has been measured at 55 points between 1 micron and 20 microns. The data can be fitted by an equation of the form,

$$(n_0-1)_{\text{calc}}=(n_0-1)_{\text{ext}}+\sum A_i/2\pi^2c(\nu_i^2-\nu^2), \quad (3)$$

where the A_i are integrated absorption coefficients. The values of A_i and ν_i are given in Table I. The ν_i are taken from the absorption curves of Bell and Nielsen,[9] where ν_5', ν_5'', ν_5''' are the centers of the P, Q, and R branches of the ν_5 band. It is, of course, not strictly correct to give equal intensities to the three branches, but since only the total absorption coefficient $A_5=A_5'+A_5''+A_5'''$ could be measured by this method, small changes among A_5', A_5'', A_5''', keeping A_5 constant, would hardly be significant in the calculations. What is called here ν_{45} is the combination band $\nu_4+\nu_5$. The ν_3 and ν_{245} values are those given by Bell and Nielsen for the overlapping bands at 3.04 microns, and A_3 and A_{245} are adjusted to fit their estimate of relative intensity. Except very near this band, there is little error in the calculated contribution to the index by using $A_{3;245}$ and $\nu_{3;245}$, where $A_{3;245}$ is the sum A_3+A_{245} and $\nu_{3;245}$ is the weighted average of ν_3 and ν_{245}. At wavelengths shorter than 5 microns, it is sufficiently accurate for most computations to use the combined terms A_5 and ν_5, A_{45} and ν_{45}.

Table II and Fig. 1 show the complete final results, where $(n_0-1)_{\text{exp}}$ is the average value of several measurements, $(n_0-1)_{\text{ext}}$ is the extrapolated value from Eq. (2), and $(n_0-1)_{\text{calc}}$ is the value calculated by means of Eq. (3) and the coefficients in Table I.

Because it was not possible in one run to take data over the complete wavelength range, it was necessary to shift the individual runs into agreement at overlapping points, to eliminate kinks in the experimental curve which would have no physical significance. That is, the absolute value of the index curve measured in any one run might differ from that of any other run by a small amount, the largest difference observed being about 1×10^{-6} or 0.16 percent.

The relative values of $(n_0-1)_{\text{exp}}$ are considered accurate to better than 0.2 percent, although the absolute values may be in error by as much as 0.65 percent. The estimates of the accuracy of the A_i were obtained by calculating the refractive index, using values of A_i which were so small or so large that the calculated curve obviously did not match the experimental points.

INTERPRETATION

In order to obtain the value of the dipole moment of the C−H bond from measurements of the contributions of the infrared bands, it is necessary to calculate the effective charges existing on the atoms in the molecule in order to give the observed index of refraction. Acetylene is known to be a linear, symmetric molecule and the analysis can be carried out in two parts, neglecting the interaction of parallel and perpendicular vibrations. Following Colby,[10] the potential energy V_0 for the linear vibrations can be expressed

$$2V_0=k_1(Q_{12}^2+Q_{34}^2)+k_2Q_{23}^2+2k_3Q_{23}(Q_{12}+Q_{34}), \quad (4)$$

where $Q_{12}=x_2-x_1$, etc., and x_i is the Cartesian displacement coordinate of the ith atom along the axis of the molecule, numbering from one end of the molecule to the other. The kinetic energy T, after the necessary substitutions, becomes

$$2ST=m(m+2M)(\dot{Q}_{12}^2+\dot{Q}_{34}^2)+\tfrac{1}{4}S^2\dot{Q}_{23}^2 +mS\dot{Q}_{23}(\dot{Q}_{12}+\dot{Q}_{34})+2m^2\dot{Q}_{12}\dot{Q}_{34}, \quad (5)$$

where m and M are the masses of the hydrogen and carbon atoms respectively, and $S=2(m+M)$. The solution for the normal frequencies $\nu_i=\lambda_i^{\frac{1}{2}}/2\pi c$ is straightforward and gives

$$\begin{aligned}\lambda_1+\lambda_2&=(k_1/2\mu)-2(2k_3-k_2)/M,\\ \lambda_1\lambda_2&=2(k_1k_2-2k_3^2)/mM,\\ \lambda_3&=2k_1/\mu,\end{aligned} \quad (6)$$

if $1/\mu=(1/2m)+(1/2M)$. Only the ν_3 vibration is infrared-active, using the notation of Herzberg.[11]

If a periodic electric field E be applied parallel to the axis of the molecule, there will be an additional potential energy $qE(-x_1+x_2+x_3-x_4)$, if q is the effective charge on each hydrogen atom. Now the potential energy V_E in the presence of the field becomes

$$V_E=V_0+qE(Q_{12}-Q_{34}), \quad (7)$$

and the kinetic energy is given by (5). The solution now shows that $Q_{23}=0$, $Q_{12}+Q_{34}=0$. Letting $\lambda=(2\pi\omega)^2$, where ω is the frequency of the incident electric field,

$$Q_{12}=q_3E/(k_1-\tfrac{1}{2}\mu\lambda), \quad (8)$$

where q_3 is the effective charge for the ν_3 vibration. The

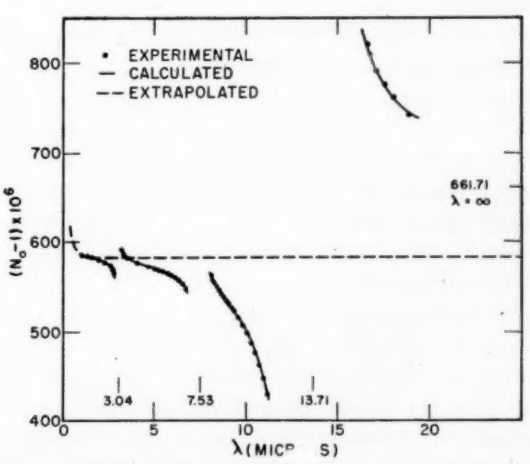

FIG. 1. The refractive index of acetylene in the infrared.

[9] E. E. Bell and H. H. Nielsen, J. Chem. Phys. **18**, 1382 (1950).

[10] W. F. Colby, Phys. Rev. **47**, 388 (1935).

[11] G. Herzberg, *Infrared and Raman Spectra of Polyatomic Molecules* (D. Van Nostrand Company, Inc., New York, 1945).

TABLE III. Values of constants used in computations.

c	2.99776×10^{10} cm/sec
e	4.8021×10^{-10} esu
m	1.67324×10^{-24} g
M	19.9235×10^{-24} g
μ	3.0872×10^{-24} g
N	2.7128×10^{19} molecules/cm^3
a	1.06×10^{-8} cm
b	1.20×10^{-8} cm
α	0.003738/C°
β	1.12×10^{-5}/mm

polarization per molecule $p=q_3(-x_1+x_2+x_3-x_4)$ or

$$p=4Eq_3^2/\mu(\lambda_3-\lambda), \tag{9}$$

using the results in (6). The contribution to the square of the index of refraction is given by the well-known expression,

$$\Delta(n^2-1)=4\pi P/E, \tag{10}$$

where P is the polarization per cm^3. If N is the number of molecules per cm^3, $P=Np/3$ after averaging over all orientations of the molecules. Since $n\approx1$, $\Delta(n-1)=\frac{1}{2}\Delta(n^2-1)$, so that

$$\Delta_3(n-1)=2Nq_3^2/3\pi\mu c^2(\nu_3^2-\nu^2), \tag{11}$$

if $\lambda_3=(2\pi c\nu_3)^2$ and ν is the frequency in cm^{-1}. The contribution of the ν_3 band may also be expressed

$$\Delta_3(n-1)=A_3/2\pi^2c(\nu_3^2-\nu^2). \tag{12}$$

From Table I, $A_3=325\times10^{10}$ cm^{-1} sec^{-1}. Equating (11) and (12), and using the values of the constants shown in Table III, leads to the result $q_3=0.515\times10^{-10}$ esu or $q_3=0.107e$, if e is the charge on the electron. It must be remembered that the value of A_3 shown in Table I is based on the assignment and estimate of relative intensities given by Bell and Nielsen. If the assignment be reversed, as they suggest might be necessary, the values of A_3 and A_{245} must be reversed and hence $q_3=0.73\times10^{-10}$ esu.

For the perpendicular vibrations, the kinetic and potential energies may be written

$$2T=m\dot{y}_1^2+M\dot{y}_2^2+M\dot{y}_3^2+m\dot{y}_4^2, \tag{13}$$

$$2V_0=k_4(\delta_1^2+\delta_2^2)+2k_5\delta_1\delta_2. \tag{14}$$

Here y_i is the displacement of the ith atom in a direction perpendicular to the axis of the molecule, and δ_1 and δ_2 are angular displacements from the equilibrium configuration defined by

$$\begin{aligned}\delta_1&=(y_2-y_1)/a+(y_2-y_3)/b,\\ \delta_2&=(y_3-y_2)/b+(y_3-y_4)/a,\end{aligned} \tag{15}$$

where a is the C–H separation and b is the C–C separation at equilibrium. The conditions that the center of mass remain at rest and that the internal angular momentum vanish are given by

$$\begin{aligned}my_1+My_2+My_3+my_4&=0,\\ May_2+M(a+b)y_3+m(2a+b)y_4&=0.\end{aligned} \tag{16}$$

The Eqs. (15) and (16) may be used to change (13) to the form,

$$2ZT(4/a^2\mu)=(Z+db^2)(\dot{\delta}_1^2+\dot{\delta}_2^2)+2(Z-db^2)\dot{\delta}_1\dot{\delta}_2, \tag{17}$$

where $Z=(2a+b)^2+Mb^2/m$ and $d=1+(M/m)$. The frequencies for the normal vibrations obtained from (14) and (17) are

$$\begin{aligned}\lambda_4&=(k_4-k_5)Z/Ma^2b^2,\\ \lambda_5&=2(k_4+k_5)/a^2\mu,\end{aligned} \tag{18}$$

where as before $\lambda_i=(2\pi c\nu_i)^2$. Only the ν_5 vibration is infrared-active.

A periodic electric field E parallel to the y axis gives an additional potential energy, and expression (14) becomes

$$V_E=V_0-qEa(\delta_1+\delta_2), \tag{19}$$

since $\delta_1+\delta_2=(-y_1+y_2+y_3-y_4)/a$. The solution now shows that $\delta_1=\delta_2$ or that only the ν_5 vibration contributes in the presence of the electric field. The polarization per molecule is

$$p=q_5(-y_1+y_2+y_3-y_4)=aq_5(\delta_1+\delta_2),$$

from which

$$p=2Eq_5^2/a\mu(\lambda_5-\lambda). \tag{20}$$

Averaging over all orientations of the molecules for this doubly-degenerate vibration gives the result $P=2Np/3$. Thus, from (10),

$$\Delta_5(n-1)=4Nq_5^2/3\mu\pi c^2(\nu_5^2-\nu^2), \tag{21}$$

where ν is again the frequency in cm^{-1}. Equating (21) to the expression,

$$\Delta_5(n-1)=A_5/2\pi^2c(\nu_5^2-\nu^2), \tag{22}$$

where $A_5=2410.8\times10^{10}$ cm^{-1} sec^{-1}, we obtain $q_5=0.991\times10^{-10}$ esu or $q_5=0.206e$.

It is interesting, in order to have a physical picture of the molecule during the vibrations, to calculate the magnitude of the displacements of each atom from equilibrium. By setting $T+V=hc\nu$, it can be shown that the maximum displacements during the ν_3 vibration are $0.096A$ for the hydrogen atoms and $0.008A$ for the carbon atoms. Since $a=1.06A$, the change in bond length is only 0.1 the bond length itself, and q_3 can be interpreted as the rate of change of C–H bond moment with bond length.

In the perpendicular vibration ν_5, each angle δ has a maximum value of 0.207 radians or 11.8° on each side of equilibrium, and the separation of the carbon and hydrogen atoms changes by at most $0.025A$. Since the bond length is essentially constant in this vibration, the product of effective charge by internuclear distance can be interpreted as an effective dipole moment. The value of this moment in acetylene is $\mu_{CH}=0.991\times10^{-10}\times1.06\times10^{-8}=(1.05\pm0.01)D$, where $1D=10^{-18}$ esu cm.

We cannot, however, determine the polarity of the moment, about which there is some controversy.

Coulson,[12] on the basis of theoretical studies, has shown that the carbon atom is the positive end of the dipole. On the other hand, Cole and Thompson[13] have used measurements on the extinction coefficients of benzene derivatives in solution to prove that the hydrogen is the positive atom. Gent,[14] in a survey on the polarity of the C−H bond, points out that there is very possibly a reversal of polarity from methane to acetylene, and that the carbon end of the bond is likely to be negative in acetylene but positive in methane.

From dispersion measurements on methane, Rollefson and Havens[3] found the C−H bond moment to be $0.307D$. For the out-of-plane bending in ethylene, Hammer[4] calculated a moment of $0.629D$. (For other vibrations, values of 0.72 and $0.315D$ were obtained.) The effective charge for the stretching vibrations was approximately 0.5×10^{-10} esu for each of the three hydrocarbons. It appears from this research that the magnitude of the C−H bond shows some regularity, being almost in the ratio 1:2:3 as the carbon-carbon link goes from zero to double to triple bonding, although this regularity may be entirely accidental, since the signs may not be the same.

An additional item of interest is the extrapolation of the refractive index to infinite wavelength, where $\epsilon=n^2$. Watson, Rao, and Ramaswamy[15] have measured essentially the static dielectric constant, obtaining the value $\epsilon-1=1330\times10^{-6}$ after reduction to 0°C. From Eq. (3), $(n_0-1)_\infty=661.71\times10^{-6}$ or $(n_0^2-1)_\infty=1323.9\times10^{-6}$. The difference between n^2 and ϵ is only 6×10^{-6}, which is within the limits of experimental error. The contributions of the infrared bands thus completely account for the difference between the dielectric constant and the square of the refractive index extrapolated to zero frequency from the visible.

[12] C. A. Coulson, Trans. Faraday Soc. **38**, 433 (1942).
[13] A. R. H. Cole and H. W. Thompson, Trans. Faraday Soc. **46**, 103 (1950).
[14] W. L. G. Gent, Quart. Rev. **2**, 383 (1948).
[15] Watson, Rao, and Ramaswamy, Proc. Roy. Soc. (London) **143A**, 558 (1934).

THE JOURNAL OF CHEMICAL PHYSICS VOLUME 19, NUMBER 12 DECEMBER, 1951

The Infrared Spectrum and the Structure of Gaseous Nitrous Acid*

LLEWELLYN H. JONES, RICHARD M. BADGER, AND GORDON E. MOORE
Gates and Crellin Laboratories of Chemistry, California Institute of Technology, Pasadena, California

(Received September 5, 1951)

An investigation of the infrared spectrum of nitrous acid has shown that in the gaseous state this substance exists in two tautomeric species which are believed to be *trans*- and *cis*-forms. The *cis*-form is of higher energy by about 506 calories mole^{-1}. A complete vibrational analysis is given and the OH in plane bending frequencies are found to be 1260 cm^{-1} and ~1292 cm^{-1}, and the out of plane frequencies 543 cm^{-1} and 637 cm^{-1} for the *trans*- and *cis*-molecules, respectively. From the rotational constants the O−N−O angle is estimated to be 118° for the *trans*-form and 114° for the *cis*-form, from which conclusions are drawn regarding the electronic structure of the molecule. The standard entropy of nitrous acid at 25° is calculated.

INTRODUCTION

To the best of our knowledge the only previous observation on the infrared spectrum of nitrous acid was made by E. J. Jones[1] who observed what appeared to be a double band in the 1.4μ region. This he explained as due to the presence of two isomeric forms of the acid. Strangely enough an investigation recently completed in this laboratory has shown that this belief of Jones is indeed correct though it was not at all justified by his observations. He had observed merely the P and R branches of a single A type band, of which the central Q branch was not evident, probably because of the lack of resolving power of his spectrometer. Our investigation has encountered some unusual problems, but has been very rewarding as the experimental results finally all appear to fit into a very plausible pattern.

EXPERIMENTAL PROCEDURES

Since the equilibrium between nitrous acid, NO, NO_2, and water vapor is very rapidly established it was not possible to study the first substance in the pure state and it was necessary to investigate an equilibrium mixture. Such a mixture may contain a considerable number of species which have strong absorption bands and may produce considerable interference. It was consequently necessary to identify all bands due to contaminants and to choose conditions such that interference from this source was at a minimum. A typical mixture employed contained NO and NO_2 at partial pressures of 570 mm and 15 mm, respectively, and the vapor of water, or of heavy water, at the saturation pressure at 25°C. With the use of existing thermodynamic data[2] this mixture was estimated to contain

* Contribution No. 1630.
[1] E. J. Jones, J. Am. Chem. Soc. **65**, 2274 (1943).
[2] For references see L. G. Wayne and D. M. Yost, J. Chem. Phys. **19**, 41 (1951).

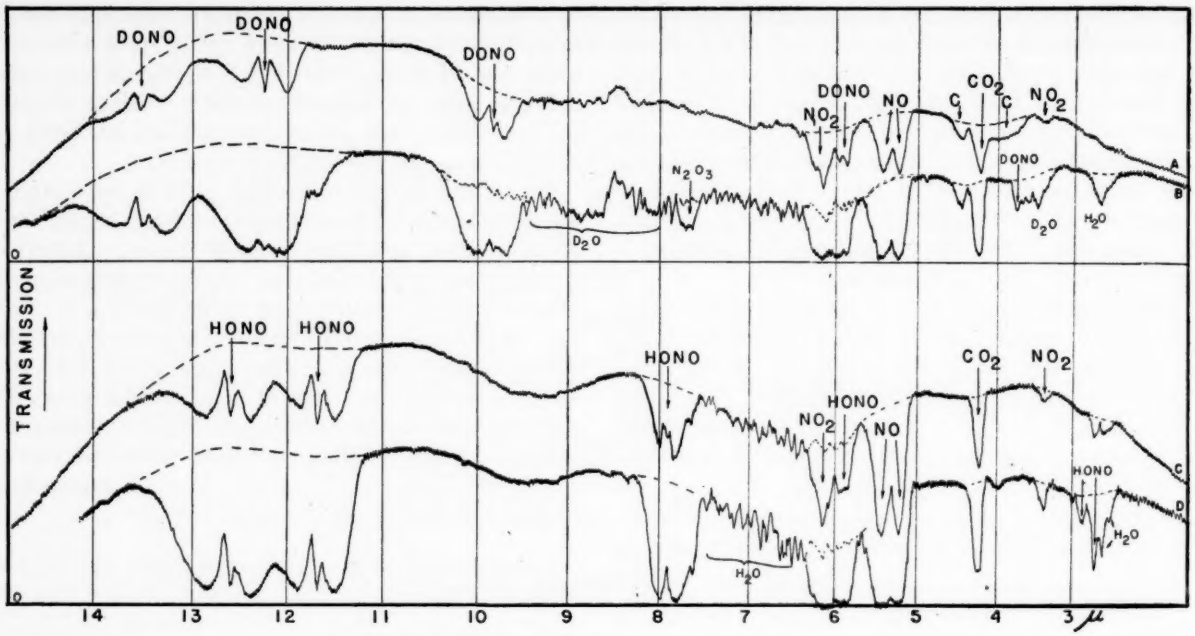

FIG. 1. Prismatic spectrum of heavy and light nitrous acid in the NaCl region. The absorptions indicated by *C* are definitely due to contaminants. Nitrous acid pressure was 2–3 mm throughout, path length was 5 cm in curves *A* and *C* and 50 cm in curves *B* and *D*.

nitrous acid at a pressure of about 18 mm, together with traces of N_2O_3 and nitric acid.

The spectra were mapped under low dispersion from 2–15μ with a Beckmann IR-2 spectrometer equipped for recording, and provided with a simple automatic slit control which keeps the background intensity reasonably constant through this region. In the region 14–25μ a vacuum spectrometer[3] with potassium bromide optics was employed. The fine structure investigation of the O—H fundamentals, overtones and combination bands out to 3.2μ was made with a vacuum grating spectrometer previously described.[4] A selected lead sulfide photoconductive cell cooled with solid CO_2 was employed as detector. The water vapor lines, recently measured with high accuracy by R. C. Nelson[5] were used for wavelength calibration.

EXPERIMENTAL RESULTS

The prismatic spectra of nitrous acid and of deutero nitrous acid are shown in Figs. 1 and 2. Portions of the region investigated with high dispersion are represented in Figs. 3–5. In Table I are given the frequencies of band origins, together with a description of the bands and assignments.

INTERPRETATION

The spectrum of nitrous acid exhibits several unusual features of which the most striking is the duplication of many of the more intense bands which one appears obliged to attribute to the presence of two tautomeric forms. This is most immediately evident in the region of the O—H stretching frequencies and their overtones.

In both fundamental and overtone regions two rather intense bands appear in the spectra of both light and heavy nitrous acid. The more intense of these is in each case an *A* type band, while the other has hybrid structure but is predominately of *B* type. The frequency difference between the two bands in the overtone region is approximately twice that in the fundamental region, and the isotope shift of all four bands is well within the range to be expected for hydrogen valence frequencies. These facts appear to exclude the possibility that any of the bands could be assigned to a combination tone, and indicate that there are indeed two O—H stretching fundamentals.

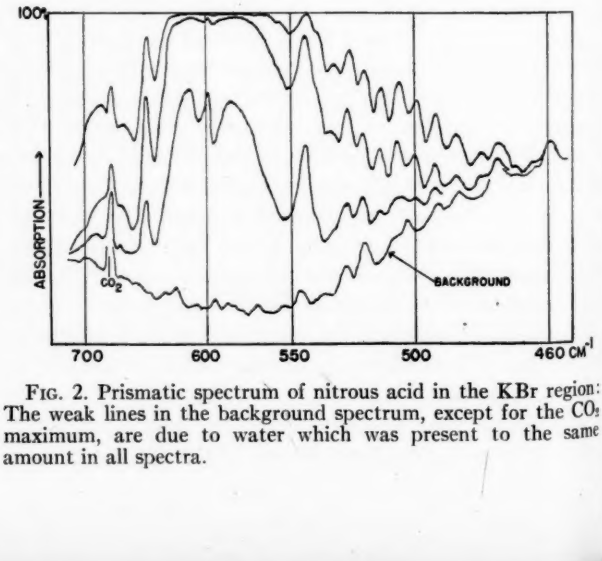

FIG. 2. Prismatic spectrum of nitrous acid in the KBr region: The weak lines in the background spectrum, except for the CO_2 maximum, are due to water which was present to the same amount in all spectra.

[3] A recent gift from the Shell Development Company. For description see R. R. Brattain, Phys. Rev. **60**, 164 (1941).

[4] Badger, Zumwalt, and Giguère, Rev. Sci. Instr. **19**, 861 (1948).

[5] R. C. Nelson, Summary Report No. IV, Contract NObs 28373, Dept. Physics, Northwestern University.

We attribute the fundamental of lower frequency to a *cis*-form of nitrous acid and that of higher frequency to a *trans*-form (see Figs. 6(a) and (b)). This assignment was first suggested by the band types and is strongly supported by the rotational constants. The possibility that a nitro form (Fig. 6(c)) may occur has been considered, but for several reasons it seems evident that such a form does not contribute to the spectrum. A nitro form would almost certainly be planar and its N−H fundamental band would consequently be of pure *B* type. Although one of the observed fundamental bands is predominantly of *B* type it is actually a hybrid as it quite definitely has a weak central *Q* branch. Furthermore, the change of rotational constant with deuterium substitution seems quite impossible to account for with a nitro model although it is perfectly compatible with the *cis*-structure.

TEMPERATURE EFFECT

It is immediately evident that the spectrum of nitrous acid in the region 5–25μ contains too many bands to

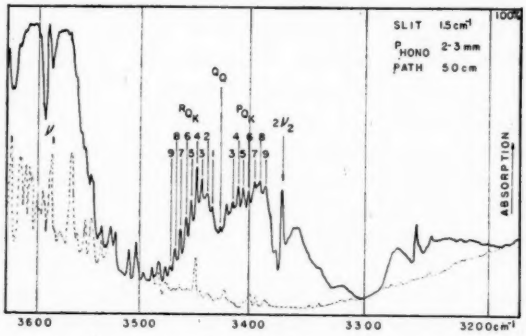

FIG. 3. Bands of *cis*- and *trans*-nitrous acid in the 3μ region.

be ascribed to one molecule but in the beginning it was by no means obvious how they were to be apportioned to two molecular species. It is now clear that this can be done for the most part on the basis of intensity. As will be shown later, the *trans*-tautomer is about three times as prevalent as the *cis*-form and its bands are correspondingly more intense and more numerous. There is, however, one important exception to this generalization, namely the pair of similar bands near 12μ, which led us into great difficulty. This was not resolved until an investigation was made of the effect of temperature on the relative intensities of certain bands.

The temperature range in which it is practical to investigate nitrous acid is unfortunately not very great and in most cases the situation is rather unfavorable for observing small changes in the relative intensities of analogous bands. In the O−H overtones no effect could be detected with certainty in the range 10–65°C. Since the band envelopes are quite different and the rather high intensity ratio of corresponding bands is unfavorable, we could only conclude that the difference

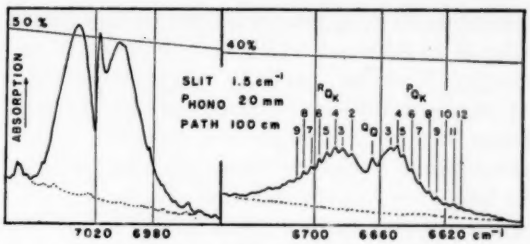

FIG. 4. First overtone of the O−H stretching vibration in *trans*- and *cis*-HONO.

in energy of the *trans*- and *cis*-tautomers is not large, probably not much greater than 350 cal mole^{-1}.

Fortunately the pair of bands at 12μ present a very favorable case owing to their practically identical envelopes and intensities. As shown in Fig. 7 a definite although small temperature effect was observed. The integrated intensity of 856 cm^{-1} was found to increase relative to that of 794 cm^{-1} by about 19 percent when the temperature was raised from 0° to 70°C. A similar effect was noticed with respect to the bands at 637 cm^{-1} and 543 cm^{-1}, whose intensity ratio was estimated to increase about 22 percent in the same temperature interval.

These estimates, although in reasonable agreement, may be considerably in error since there is considerable overlapping of bands, the band envelopes change somewhat with temperature, and the presence of overlapping contaminant bands could lead to error. We believe the last effect is absent and are convinced that the temperature effect is definitely real. The bands at 794 cm^{-1} and 543 cm^{-1} are consequently attributed to the tautomer of lower energy which will later be identified as the *trans*-form. From the temperature effect the difference in energy of *cis*- and *trans*-forms is estimated to be 506±250 cal mole^{-1}.

ASSIGNMENT OF BANDS IN THE REGION 5–25μ

The assignment of 1696 cm^{-1} and 1690 cm^{-1} in light and heavy nitrous acid, respectively, to a double bond N=O valence vibration, ν_2, seems straightforward. We believe that this is a *trans*-band and that the *cis*-fundamental of lower frequency and intensity is obscured by NO_2, although its first overtone does appear. Because of the isotope shift we assign 1260 cm^{-1} and 1018 cm^{-1} to the hydrogen and deuterium bending vibrations in the plane of the molecule, ν_3. The former

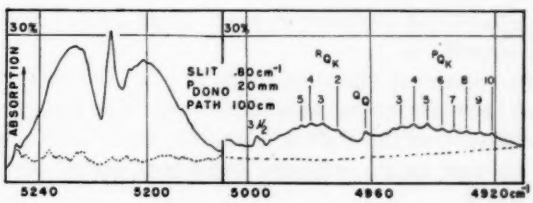

FIG. 5. First overtone of the O−D stretching vibration in *trans*- and *cis*-DONO.

band exhibits an extra maximum on the high frequency shoulder of its R branch which we believe represents the R branch of a weaker, partially overlapping band with center at about 1292 cm^{-1}. Since the out of the plane hydrogen torsional frequency is found to be higher for the *cis*-tautomer it is plausible to attribute the (weaker) higher frequency in plane bending also to the *cis*-form. The corresponding band is not resolved in the DONO spectrum.

The bands at 794 cm^{-1} and 856 cm^{-1} are believed to represent the N—O single bond valence vibrations, ν_4, of *trans*- and *cis*-tautomers, respectively, which are shifted to 739 cm^{-1} and 816 cm^{-1} in heavy nitrous acid. The above assignment to *cis*- and *trans*-forms is required by the temperature effect which shows that 794 cm^{-1} originates in the same molecular species as 543 cm^{-1}, which is definitely a *trans*-band. It is furthermore supported by the Teller-Redlich rule of isotope

TABLE I. Band centers and assignments in the spectrum of nitrous acid.

HONO ν (cm^{-1})	HONO I	DONO ν (cm^{-1})	DONO I	Band type	Assignment *cis*	Assignment *trans*	Description
543	80	416	60	C		ν_6	H out of plane
598	120	591	120	A	(ν_5)?	ν_5	O—N—O bend
637	50	508	40	C	ν_6		H out of plane
794	100	739	40	A		ν_4	O—N stretch
856	100	816	100	A	ν_4		O—N stretch
1260	50	1018	60	A		ν_3	O—H bend
~1292	~10?			A	ν_3		O—H bend
1696	20	1690	20	?		ν_2	O=N stretch
2505	2	···		?		$2\nu_3$	
3257	1	3196	0.5	A	$2\nu_2$[a]		
3372	1.5	3361	1.5	A		$2\nu_2$	
3426	1.5	2530	1	$B(A)$[b]	ν_1		O—H stretch
3590	5	2650	3	A		ν_1	O—H stretch
4124	0.0005			A		$\nu_2+2\nu_3$	
4378	0.001			A		$\nu_1+\nu_4$	
4830	0.02			A		$\nu_1+\nu_3$	
5038	0.002	4999		$B(A)$[c]		$3\nu_2$	
6050	0.001			A		$\nu_1+2\nu_3$	
6664.8	0.03	4963		$B(A)$[b]	$2\nu_1$		
7015	0.10	5212		A		$2\nu_1$	

[a] Assigned on the basis of intensity, frequency, and isotope shift. Fundamental estimated to be around 1640 in HONO and 1610 in DONO, obscured by NO_2.
[b] Hybrid, predominantly B type.
[c] DONO band is hybrid.

shift, which is poorly satisfied by an alternative assignment.

The band at 543 cm^{-1} clearly has C type structure though one branch of the band is obscured. The structure and large isotope shift identify it as the OH torsional or out of the plane vibration. It is attributed to the *trans*-tautomer since the rotational spacing is much greater than that of the OH valence fundamental of the *cis*-species. The rotational structure of the companion band of the *cis*-species at 637 cm^{-1} could not be resolved but the breadth of the band and its isotope shift identify it.

The remaining vibration is the O—N—O bending to which the most intense band in the spectrum is assigned. On deuteration the shift is from 598 cm^{-1} to 591 cm^{-1}. In this case again, only one band is observed for the two species.

The assignments of a number of combination bands are given in Table I.

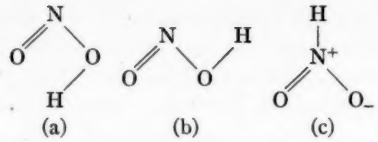

FIG. 6.

If the band origins are represented by the usual expression $\nu=\sum v_i\omega_i+\sum\sum v_iv_j\chi_{ij}$ the following approximate values of convergence and interaction constants are found for the *trans*-tautomer of nitrous acid:

$$\chi_{11}=-83,\quad \chi_{11}(\text{DONO})=-45,\quad \chi_{22}=-9,\quad \chi_{33}=-8,$$
$$\chi_{13}=-21,\quad \chi_{14}=-6,\quad \chi_{23}=-38.$$

Unless otherwise indicated these values refer to HONO.

ROTATIONAL STRUCTURE

Details of the bands showing a resolvable rotational structure are given in Tables II and III. Unfortunately only the low frequency branch of the band at 543 cm^{-1} was observable, which furthermore was contaminated with water lines, some of which practically coincide with HONO lines. The interference was not serious at high nitrous acid pressures and allowance was made for it in measuring the maxima. Because of the limits of KBr optics only the high frequency branch of the corresponding band for DONO was observed. In the latter case the central Q branch was observed but for some unexplained reason no rotational structure could be resolved, though strong continuous absorption was found from 460 cm^{-1} to the limit of the KBr optics. Consequently the rotational constant for the *trans*-molecule is known only roughly, and only for HONO.

For the ground state of the *trans*-molecule we take the most probable value of the rotational constant $A-(1/2)(B+C)$ to be 2.40 cm^{-1} for *cis*-HONO, 1.94 cm^{-1} for *cis*-DONO, and 3.2 cm^{-1} for *trans*-HONO. Probable values for the moments of inertia of the various molecular species have been calculated from these constants and from estimated parameters and are given in a subsequent table.

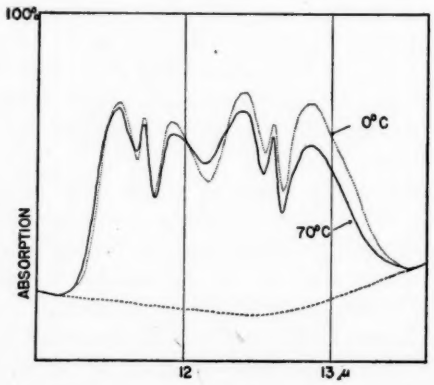

FIG. 7. The change of relative intensity with temperature of the 856 cm^{-1} and 794 cm^{-1} bands of *cis*- and *trans*-HONO.

TABLE II. Frequencies of the Q branches and combinations in the OH perpendicular bands of the *cis*-form of nitrous acid.

	HONO ν_1=3426.1 cm^{-1}				HONO $2\nu_1$=6664.8 cm^{-1}				DONO $2\nu_1$=4962.8 cm^{-1}			
K	^PQ	^RQ	(A_0-B_0)[a]	(A_1-B_1)	^PQ	^RQ	(A_0-B_0)	(A_2-B_2)	^PQ	^RQ	(A_0-B_0)	(A_2-B_2)
0	...	...	...	...	...	...	...	...	...	...	...	...
1	...	3432.04	...	...	...	...	...	...	...	...	...	...
2	...	37.11	1.99	...	6658.19	6675.46	...	...	...	4972.11	...	...
3	3414.09	42.71	2.30	2.39	...	80.84	2.28	...	4953.65	76.23	1.87	1.88
4	09.52	47.24	2.35	2.36	48.06	85.90	2.30	2.37	49.68	79.88	1.92	1.89
5	05.17	52.29	2.35	2.36	44.08	91.18	2.35	2.36	45.43	83.44	1.94	1.90
6	00.19	56.86	2.38	2.36	38.98	95.63	2.40	2.36	50.99		1.95	
7	3395.17	61.69	2.37	2.38	33.59	6700.51	2.40	2.39	36.65			
8	90.53	66.54	2.38	2.38	28.50	05.19	2.40	2.40	37.52			
9	85.56	70.86	2.38	2.37	23.64	09.98	2.40					
10	80.97		2.38	...	18.67		2.41					
11	75.70				13.70							

[a] A_i-B_i is the rotational constant of the ith vibrational level when $B_i=(1/2)(B_i+C_i)$.

A comparison of the separation of the P and R maxima of the A type bands of the spectrum with that predicted from the moments of inertia above has shown that these bands have in reality considerable hybrid character. The presence of weak central branches in the *cis*-O−H bands has likewise shown this to be true of these apparently B type bands. Nevertheless it is remarkable, considering the lack of molecular symmetry, that bands of as nearly pure type are observed. This is particularly true of the bending fundamental at 598 cm^{-1} which is unexpectedly of A type. An explanation of this fact may be found in the electronic structure of the molecule discussed below.

THE STRUCTURE OF NITROUS ACID

The two parameters of the nitrous acid molecule which it would be most difficult to predict from previous experience are the O−N−O angle and the long O−N distance. Fortunately the choice of these quantities is very much restricted by the known rotational constants, which are relatively insensitive to the remaining parameters. We have consequently chosen to estimate the latter parameters by the comparison of force constants and frequencies with those of other molecules of known structure and to use the rotational constants to solve for the angle and distance mentioned above. The rotational constants are accounted for by the parameters given in Table IV.

The following arguments support the foregoing choice. The O−H distance was estimated from the O−H frequencies with the assistance of Badger's rule.[6] It can scarcely be in error by 0.01A. The choice of the HON angle is rather arbitrary and could be in considerable error since it has little effect on the rotational constants. However the change of rotational constant with deuterium substitution seems to exclude the possibility that it is as small as 90°. The angle has been taken somewhat smaller in the *cis*-modification in line with the smaller O−N−O angle which we attribute to an interaction between hydrogen and remote oxygen.

The O−N−O angle is rather accurately determined since with any plausible set of the remaining parameters the rotational constants require values which do not differ by more than about 2° from those already given.

It is of interest to compare nitrous acid with two other substances which are isoelectronic with it and have nearly equal mass. These are formic acid and ONF. The former has an O−C−O angle of about 125°.[7] The latter presumably has an apex angle around 116°, considerably closer to that of nitrous acid. Unfortunately ONF has not been investigated by electron diffraction but a comparison of vibrational frequencies[8,9] shows that this molecule has a structure essentially identical with those of ONCl and ONBr. These molecules both have an apex angle of 116° [10] and have unusual internuclear distances which have been taken

TABLE III. Frequencies of maxima in the HONO band at 543.2 cm^{-1}.

K	^PQ	K	^PQ
1	(536.4)	6	505.4
2	530.8	7	498.9
3	523.5	8	492.4
4	517.7	9	486.0
5	(511.5)		

[6] R. M. Badger, J. Chem. Phys. **2**, 128 (1934).

TABLE IV. Probable values of the molecular parameters of HONO.

	cis	*trans*
r_{HO}	0.98A[a]	0.98A[a]
r_{ON}	1.46[b]	1.46[c]
r_{NO}	1.20[a]	1.20[a]
∠HON	(103°)	(105°)
∠NON	114°[b]	118°[b]

Estimated moments of inertia (g cm^2×10^{40})

	HONO	DONO	HONO	DONO
I_A	10.13	12.1	7.83	8.21
I_B	68.4	69.6	75.2	80.8

[a] Estimated with assistance of frequency and force constant comparison.
[b] Calculated from rotational constants with use of remaining parameters.
[c] Assumed to be same as in *cis*-form.

[7] Van Zandt Williams, J. Chem. Phys. **15**, 232 (1947).
[8] W. G. Burns and H. J. Bernstein, J. Chem. Phys. **18**, 1669 (1950).
[9] E. A. Jones and P. J. H. Woltz, J. Chem. Phys. **18**, 1516 (1950).
[10] J. A. Ketelaar and K. J. Palmer, J. Am. Chem. Soc. **59**, 2629 (1937).

to indicate the contribution of an ionic structure to the ground state.

The higher NO frequency of nitrous acid (1696 cm^{-1}) is, however, considerably lower than the corresponding frequency of ONF (1844 cm^{-1}) which suggests that the short NO distance is considerably longer than the 1.14A found in the nitrosyl compounds. A comparison of the force constant with those of N_2O and NO_2 leads to the conclusion that it is not greatly different from that found in those molecules, namely 1.20±0.01A, which is close to a double bond N−O distance.

The lower NO frequency of nitrous acid ($\nu_4(trans)$ = 794 cm^{-1}, $\nu_4(cis)$ = 856 cm^{-1}) lies between the NF valence frequency of ONF (767 cm^{-1}) and that of NF_3 (ν_1 = 908 cm^{-1}). The longer N−O distance in HONO is consequently bracketed by the 1.37A[11] found in NF_3, and the rather long N−F distance presumed to exist in ONF. It is fixed within rather close limits by the change of rotational constant with deuterium substitution which we believe shows that it is certainly not less and probably slightly greater than a normal N−O single bond distance.

From the foregoing it seems probable that the following three structures contribute significantly to the ground state of nitrous acid, though we are not in a position at present to estimate precisely their relative importance.

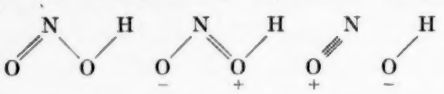

The last of these we presume to be responsible for the greater stability of the *trans*-isomer, which would be difficult to account for on the basis of the first two structures. From the O−N−O angle and the N−O frequency we conclude that the contribution of this structure is less than in the nitrosyl halides, although its effect is nevertheless extremely significant. The relative contributions of the second and third structures are presumably rather dependent on the O−N−O angle. As this angle changes in the bending vibration an unusually large change in charge distribution would consequently be expected. We suggest that this effect is responsible both for the "parallel" character of the 598 cm^{-1} fundamental and for its high intensity as compared with the very weak bending fundamental of NO_2.

Since the third structure stabilizes the *trans*-tautomer one might reasonably expect its contribution to be greater to this form. This is indeed supported by the fact that in the *trans*-tautomer the low NO frequency is slightly lower and the high frequency higher than in the *cis*-form. The smaller O−N−O angle of the *cis*-form is probably not in contradiction to this belief but presumably results from an interaction between hydrogen and extreme oxygen indicated by the lower O−H valence frequency of the *cis*-form.

As points of dissimilarity between nitrous and formic acid we mention that the latter substance does not exist in a *trans*-form under circumstances so far investigated and does associate at pressures at which no indication of nitrous acid dimers was found.

THERMODYNAMIC AND OTHER PROPERTIES OF NITROUS ACID

Although the energy of the *trans*-form of nitrous acid is lower than that of the *cis*-form by about 506 calories, the torsional frequency of the *trans*-form is considerably the lower. Consequently it is evident that if the torsional potential is represented by a sum of cosine terms, at least three terms are required to fit the facts. The data available probably do not warrant an attempt to evaluate this function exactly, but we estimate that it has maxima of the order of 12 kcal $mole^{-1}$ above the lower minimum, at approximately ±88° from the *trans*-position. This potential barrier is sufficiently large that one may question whether equilibrium was fully established in the studies of the rate of formation of nitrous acid by Wayne and Yost.[2] On the other hand, it is not so large that there can be much doubt that equilibrium was established in our measurements of the effect of temperature on relative intensities.

From the frequencies and moments of inertia given above we estimate for the standard molal entropies at 25°C: $\bar{S}$ (*trans*) = 54.9 e.u. and $\bar{S}$ (*cis*) = 54.8 e.u. From ΔS and ΔE we estimate for the equilibrium between the two forms: $K_{25°} = p\,trans/p\,cis = 2.5$. This corresponds roughly to the average ratio of intensities of *trans*- and *cis*-bands. The standard entropy of the equilibrium mixture of nitrous acid is consequently 56.0 eu per mole at 25°.

ACKNOWLEDGMENT

The authors are greatly indebted to Dr. Oliver R. Wulf who suggested this investigation and gave very helpful advice, and to Dr. Verner Schomaker for discussions regarding structural problems.

[11] V. Schomaker and C. S. Lu, J. Am. Chem. Soc. **72**, 1182 (1950).

The Microwave Spectrum of Methyl Stannane*

DAVID R. LIDE, JR.
Mallinckrodt Chemical Laboratory, Harvard University, Cambridge, Massachusetts
(Received August 13, 1951)

The microwave spectrum of methyl stannane between 25,500 and 29,000 mc is reported. All of the observed lines may be assigned to the $J=1\rightarrow2$ rotational transitions of the isotopic species representing the five most abundant tin isotopes. The dipole moment was found from the Stark splitting to be 0.68 ± 0.03 Debye unit. Insufficient information is available for a complete structure determination, but if tetrahedral angles and a C—H distance of 1.090A are assumed, the data can be fitted with a C—Sn distance of 2.143 ± 0.002A and a Sn—H distance of 1.700 ± 0.015A. The influence of hindered internal rotation on the spectrum is discussed.

INTRODUCTION

THERE have been several recent investigations of the influence of hindered internal rotation on microwave spectra; among the compounds which have been studied are methyl alcohol,[1] 1,1,1-trifluoroethane,[2] methyltrifluorosilane,[3] and methyl silane.[4] Another simple symmetric rotor whose microwave spectrum would be expected to yield information on internal rotation is methyl stannane, CH_3SnH_3. Furthermore, this molecule seemed of interest from the standpoint of structural parameters, since no spectra of tin compounds in the microwave region had previously been reported. The microwave spectrum of CH_3SnH_3 in the region between 25,500 mc and 29,000 mc is reported in this paper. The spectrum was observed on a Stark modulation spectrograph which employed zero-based 100 kc square-wave modulation.

PREPARATION

Methyl stannane was prepared by the reduction of CH_3SnCl_3 with lithium aluminum hydride.[5] The CH_3SnCl_3 was prepared by bubbling methyl chloride through fused anhydrous stannous chloride at 365°C.[6] Solutions of CH_3SnCl_3 and $LiAlH_4$ were made in thoroughly dried tetrahydrofuran, and the CH_3SnCl_3 solution was added very slowly to the $LiAlH_4$ solution in an evacuated system. The gaseous products were frozen out from time to time during the course of the addition. After three bulb-to-bulb distillations of this product from −78°C to −190°C, a sample was obtained whose infrared spectrum (taken with a Baird infrared spectrophotometer) showed no trace of tetrahydrofuran bands. The bands which did appear in this spectrum included the characteristic vibrations of the CH_3 group, plus a very intense band at 1870 cm^{-1}, which presumably is the Sn—H stretching frequency.

Although an impure sample gradually deposited a tin mirror on the glass sample bulb, samples of CH_3SnH_3 from which the tetrahydrofuran had been removed showed no noticeable decomposition after standing in a glass bulb for one month. There was rapid decomposition, however, when the sample was admitted to a copper wave guide. It was found that searching could be carried out and frequency measurements made by working rapidly after a sample was introduced into the guide, although both the sensitivity of the spectrograph and accuracy of frequency measurements were somewhat impaired.

MICROWAVE SPECTRUM

If covalent bond radii[7] are used to calculate bond distances, the $J=1\rightarrow2$ transition of CH_3SnH_3 is predicted to be in the neighborhood of 26,700 mc. A search from 25,500 mc to 29,000 mc yielded only the group of lines given in Table I. The observed relative intensities of the last five lines agree qualitatively with reported isotopic abundances of the five strongest tin isotopes.[8] As a further check the frequencies of all tin isotopes may be predicted (in the rigid symmetric-rotor approximation) from the observed frequencies of any two isotopic species, using no other data besides atomic masses.[9] If the lines at 27,560.69 mc and 27,641.99 mc are assigned

TABLE I. Observed spectrum of CH_3SnH_3.

Frequency	Approximate relative intensity (30°C)	Assignment
27,517.58 mc	2	Sn^{120} (excited torsional state)
27,558.79	1	Sn^{118} (excited torsional state)
27,560.69	4	Sn^{120}
27,580.52	1	Sn^{119}
27,600.80	3	Sn^{118}
27,621.20	1	Sn^{117}
27,641.99	2	Sn^{116}

* The research reported in this paper was made possible by support extended Harvard University by the ONR under ONR Contract N5ori-76, Task Order V.

[1] D. K. Coles, Phys. Rev. **74**, 1194 (1948); Hughes, Good, and Coles, "Microwave spectrum of methyl alcohol" (to be published).

[2] Dailey, Minden, and Shulman, Phys. Rev. **75**, 1319(A) (1949).

[3] Minden, Mays, and Dailey, Phys. Rev. **78**, 347(A) (1950); John Sheridan and Walter Gordy, J. Chem. Phys. **19**, 965 (1951).

[4] D. R. Lide and D. K. Coles, Phys. Rev. **80**, 911(L) (1950).

[5] A. E. Finholt, *et al.*, J. Am. Chem. Soc. **69**, 2692 (1947).

[6] Albert C. Smith, *Direct Synthesis of Organotin Halides*, Ph.D. thesis (Harvard University, 1951), p. 150.

[7] L. Pauling, *Nature of the Chemical Bond* (Cornell University Press, Ithaca, New York, 1945), second edition, p. 164.

[8] J. R. White and A. E. Cameron, Phys. Rev. **74**, 991 (1948).

[9] Masses were taken from Bethe, *Elementary Nuclear Theory* (John Wiley and Sons, Inc., New York, 1947).

TABLE II. Predicted and observed frequencies of tin isotopes.

Isotope	Predicted	Observed
Sn^{120}	...	27,560.69
Sn^{119}	27,580.52	27,580.52
Sn^{118}	27,600.71	27,600.80
Sn^{117}	27,621.21	27,621.20
Sn^{116}	...	27,641.99

to Sn^{120} and Sn^{116}, respectively, such a calculation gives the results in Table II. The agreement is seen to be satisfactory, especially in view of the fact that pressure broadening from the decomposition limited the accuracy of frequency measurements to about ± 0.10 mc. The still weaker tin isotopes whose frequencies were predicted in this way were below the sensitivity of the spectrograph.

The lines at 27,517.58 mc and 27,558.79 mc appeared noticeably stronger at room temperature than at dry ice temperature, indicating that they are due to molecules in excited vibrational states. In view of their intensities it is reasonable to assign them to the first excited torsional state of the Sn^{120} and Sn^{118} species, respectively. The corresponding satellite line from Sn^{116} was expected to be slightly above noise level, but it was obscured by the Stark components of the 27,600.80 mc line.

The observed Stark effect of the above lines was in agreement with that expected for the $J=1\rightarrow 2$ transition of a rigid symmetric rotor; *viz.*, one pair of first-order components, a strong second-order component moving to high frequency, and a weaker (one-third the intensity) second-order component moving to low frequency. The dipole moment calculated from the second-order Stark effect is 0.68 ± 0.03 Debye unit. The electrode spacing and voltmeter were calibrated from measurements on the OCS line at 24,325.92 mc.[10]

The absorption coefficient of the Sn^{120} line at 27,560.69 mc is calculated to be 2×10^{-6} cm^{-1}, if it is assumed that 50 percent of the molecules are in the ground vibrational state.

STRUCTURAL PARAMETERS

The fact that the lines of CH_3SnH_3 were found almost 1000 mc above the predicted frequency indicates some error in the parameters which were assumed. The assumed C—Sn and Sn—H distances were ultimately based on x-ray diffraction measurements of the Sn—Sn distance in crystals of grey tin, and thus involve a rather uncertain extrapolation. A complete determination of the structure of CH_3SnH_3 involves five parameters—three distances and two angles; however, only two independent equations may be obtained from the observed microwave frequencies, and the accuracy of these is reduced by the fact that the Sn atom is so close to the center of mass of the molecule. An unsuccessful search was made for the C^{13} lines in their natural abundance; these lines would have permitted an accurate calculation of at least the C—Sn distance. Since these lines could not be found, it appears that the available data can be handled best by treating the two most questionable parameters—the C—Sn and Sn—H distances—as unknowns, while using reasonable values for the other parameters. If we assume tetrahedral angles for both the CH_3 and SnH_3 groups and a C—H distance of 1.090A, then the best fit for the observed frequencies is obtained with a C—Sn distance of 2.143 ± 0.002A and a Sn—H distance of 1.700 ± 0.015A. These distances are consistent with a single bond radius for Sn of 1.37A, as compared with 1.40A given in the tables of Pauling.[7]

All stable tin isotopes are reported to have spins of either zero or one-half. The spectrum of CH_3SnH_3 offers no evidence to the contrary, since all lines can be explained without the assumption of a quadrupole hyperfine structure.

INTERNAL ROTATION

As mentioned above, the original interest in CH_3SnH_3 resulted from studies of hindered internal rotation. It was hoped that intensity measurements on the torsional satellite lines would give potential barrier information which could be compared with data already obtained on similar molecules. However, the instability of the compound made quantitative intensity measurements infeasible without fairly elaborate equipment, which does not seem to be justified at the present stage of intensity-measuring techniques.

The theory of internal rotation[11] predicts a splitting of each torsional energy level as a result of tunneling through the hindering potential barrier. This energy splitting should lead to corresponding changes in the moments of inertia, and hence to a splitting in the pure rotational lines. Such a splitting has been observed in the microwave spectra of CH_3SiH_3[4] and CH_3SiF_3.[3] The lines of CH_3SnH_3 showed no internal structure; however, it must be remembered that the resolution was far from optimum because of the unavoidably high pressures. In CH_3SiH_3 the ground-state line-structure could not be resolved, and the first excited torsional line showed a splitting of only 0.7 mc. Somewhat greater splittings might be expected in CH_3SnH_3, since the potential barrier is undoubtedly lower. It is thus likely that the use of an absorption cell in which CH_3SnH_3 is reasonably stable would make it possible to resolve this splitting, either in the lines already seen or in weaker lines of more highly excited torsional states.

ACKNOWLEDGMENTS

The author wishes to express his appreciation to Professor E. Bright Wilson, Jr. for continual help in this investigation, and to Mr. Rodger Humberger for assistance with the chemical preparations.

[10] R. G. Shulman and C. H. Townes, Phys. Rev. **77**, 500 (1950).

[11] J. S. Koehler and D. M. Dennison, Phys. Rev. **57**, 1006 (1940).

Letters to the Editor

THIS section will accept reports of new work, provided these are terse and contain few figures, and especially few half-tone cuts. The Editorial Board will not hold itself responsible for opinions expressed by the correspondents. Contributions to this section should not exceed 600 words in length and must reach the office of the Editor not later than the 15th of the second month preceding that of the issue in which the letter is to appear. No proof will be sent to the authors. A publication charge of $10.00 per Letter is made which, when honored, will entitle the Institution to 100 free reprints.

Thermodynamics of the Critical Point

W. G. SCHNEIDER AND A. CHYNOWETH
National Research Laboratories, Ottawa, Canada
(Received October 15, 1951)

IN a recent communication with the above title Curtiss, Boyd, and Palmer[1] have given a relation for the thermodynamic velocity of sound at the critical point, and it was suggested that this relation could be employed to derive C_V at the critical temperature. We have recently concerned ourselves with just this problem and have been led to the conclusion that the above procedure is difficult and is likely to lead to large errors unless the sound velocity measurements are made at very low frequencies. We have made use of the relation

$$c^2=(Tv^2/C_v)(\partial P/\partial T)_v^2-v^2(\partial P/\partial v)_T, \qquad (1)$$

where c is the velocity of sound and v is the specific volume. This relation is equivalent to Eq. (3) of the above article. The coefficients $(\partial P/\partial T)_v$ and $(\partial P/\partial v)_T$, when derived from equation of state data may be regarded as static quantities in the sense that they refer to equilibrium measurements at zero frequency. The abnormally high absorption of sound observed in the neighborhood of the critical point absorption of sound observed in the neighborhood of the critical point (2) can, according to present evidence, be interpreted on the basis of a configurational relaxation process. Hence $(\partial P/\partial v)_T$, (and possibly also $(\partial P/\partial T)_v$) will be time dependent, and its value for a high frequency periodic force will in general be greater than the static value. In particular, while $(\partial P/\partial v)_T$, as derived from Pv isotherm measurements (static measurements) is zero at the critical point, the "dynamic" value of $(\partial P/\partial v)_T$ will not be zero. In other words, while a system in the critical state is highly compressible with respect to infinitely slow pressure changes, it is relatively hard (incompressible) with respect to very rapid pressure variations.

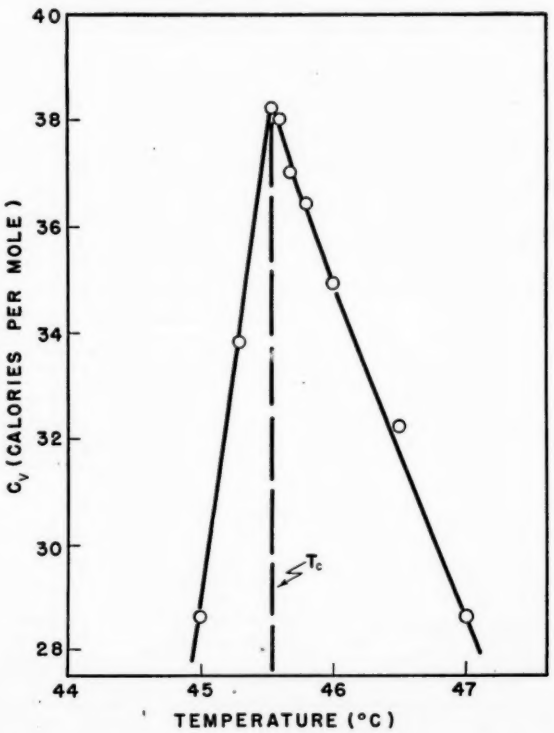

FIG. 1. Heat capacity near the critical point for sulfur hexafluoride.

Figure 1 shows a plot of C_v *vs* temperature for sulfur hexafluoride in the neighborhood of the critical point. The heat capacity values were derived from recent isotherm measurements[2] and sound velocity data.[3*] Unfortunately no calorimetric measurements of C_v for sulfur hexafluoride are available for comparison. There are, however, calorimetric measurements for carbon dioxide[4] and ethylene,[5] which can be compared with the heat capacity values derived from Eq. (1) with the aid of acoustic data. In Table I are shown the values at the critical point for carbon dioxide, which were previously given by Curtiss, Boyd, and Palmer, and also the corresponding data for ethylene. For both gases the calorimetric values are seen to be greater by roughly a factor of two. If the calorimetric measurements are regarded as static (zero frequency) measurements, this difference can be accounted for on the basis of the above interpretation.

TABLE I.

	C_v^0 (cal/mole)	C_v at the critical temp (cal/mole) From acoustic and isotherm data	Calorimetric
CO_2	6.82	17.5	~50
C_2H_4	8.12	19.6	~34
SF_6	22.20	38.3	
Xe	2.98	13.0	

The second column of the table shows for comparison, values of the heat capacity at zero pressure, C_v^0, for the several gases listed. Also included in the table is the value of C_v for xenon at the critical temperature which was derived from recent sound velocity measurements.

[1] Curtiss, Boyd, and Palmer, J. Chem. Phys. **19**, 801 (1951).
[2] K. E. MacCormack, and W. G. Schneider, Can. J. Chem. **29**, 699 (1951).
[3] W. G. Schneider, Can. J. Chem. **29**, 243 (1951).
* See also the above note immediately preceding the present communication.
[4] A. Michels and J. C. Strijland, Physica **16**, 813 (1950).
[5] Pall, Broughton, and Maass, Can. J. Res. **B16**, 230 (1938).

Infrared Spectra of Rapidly Solidified Vapors

F. E. MALHERBE AND H. J. BERNSTEIN
National Research Council, Ottawa
(Received October 11, 1951)

BROWN and Sheppard[1] recently described the formation of glassy solids during the rapid freezing of liquid hydrocarbons. We observed a similar phenomenon during an investigation of rotational isomerism in 1,2-dichloroethane, when condensing the vapor rapidly onto a rocksalt or KBr plate in a cell of the type that has been previously described.[2,3] When the vapor is condensed on the plate at 94°K,* which is the steady temperature attained by cooling with liquid nitrogen, a white solid is produced which shows an infrared spectrum similar to that of the liquid (i.e., there are bands resulting both from the *gauche-* and *trans-*isomers of dichloroethane). On allowing the solid to warm gently, a sharp temperature interval (123±2°K) is reached during which the *gauche-*bands disappear and the *trans-*bands increase in intensity. The exact temperature at which this change takes place is dependent on the conditions, especially the rate and

temperature (below 118°K) of the initial condensation. If the vapor is condensed on a plate above 123°K, the *gauche*-bands are not present in the solid spectrum.

During this transition, which corresponds apparently to the crystallization of the original glassy solid, there is a frequency shift in the maxima of the *trans*-bands which amounts to, roughly, the shift between the liquid and solid spectra. On further warming very little change occurs until a temperature of approximately 173°K is reached, where again a small frequency shift in the *trans*-bands is observed, a shift which is reversible with temperature around approximately 177°K. The two *trans*-bands which are sufficiently strong and narrow to permit of accurate measurement show the following shifts for rising temperature:

Band frequency	Shift in maximum
1229.8 cm^{-1}	$+2.3\pm0.7$ cm^{-1} } Average for 10
1455.6 cm^{-1}	-2.6 ± 0.8 cm^{-1} } different samples

Pitzer[4] has reported a peak in the heat capacity curve of dichloroethane at 177°K and proposes that the lattice for this substance is essentially the same above and below this transition point. The observed frequency shifts do, however, seem to indicate slight changes in the lattice constants.† For the case of dibromoethane it has not been possible to produce a solid showing *gauche*-bands. This is probably because of the fact that, owing to the lesser volatility, the effective rate of condensation is less than in the case of dichloroethane and allows the solid sufficient time to crystallize at 94°K.

It should be mentioned that under certain conditions of condensation (in particular the single deposition of a relatively thick layer, rather than its building up by succesive depositions of thinner layers), solids are obtained which show very markedly the Christiansen filter effect.[5,6] ‡ In such cases there are additional frequency shifts which are irreversible with temperature and difficult to measure accurately owing to the symmetry of the bands. In the case of dichloroethane, but particularly of dibromoethane, the general level of absorption increases as the the temperature rises above 210°K up to the melting points. It should be emphasized that the shifts measured around the 177°K transition in dichloroethane were on samples showing no scattering anomalies.

[1] J. K. Brown and N. Sheppard, J. Chem. Phys. **19**, 976 (1951).
[2] E. L. Wagner and D. F. Hornig, J. Chem. Phys. **18**, 296 (1950).
[3] A. Walsh and J. B. Willis, J. Chem. Phys. **18**, 552 (1950).
* All temperatures were measured with a copper-constantan thermocouple, the tip of which was in contact with the rocksalt plate.
[4] K. S. Pitzer, J. Am. Chem. Soc. **62**, 331 (1940).
† A similar conclusion was reached by S. Mizushima and Y. Morino (Proc. Indian Acad. Sci. **A8**, 315 (1938)) on the basis of the Raman spectra of solid 1,2-dichloroethane obtained at 230°K and 130°K, in which changes in lattice frequencies were observed.
[5] Christiansen, Wied. Ann. (1884).
[6] W. C. Price and K. S. Tetlow, J. Chem. Phys. **16**, 1157 (1948).
‡ We have observed a very pronounced Christiansen effect in the infrared spectrum of solid dimethyl ether produced by rapid condensation.

Temperature Dependent Magnetic Shielding in Ethyl Alcohol*

URNER LIDDEL, *Office of Naval Research, Washington, D. C.*
AND
NORMAN F. RAMSEY, *Harvard University, Cambridge, Massachusetts*
(Received September 24, 1951)

ARNOLD, Dharmatti, and Packard[1] have reported three distinct proton resonances in ethyl alcohol, whose intensities are approximately in the ratio of 3:2:1 and hence presumably associated with the CH_3, CH_2, and OH groups, respectively. The relative displacements of these lines are of magnitudes consistent with Ramsey's[2] theory of magnetic shielding in molecules. However, Packard and Arnold[3] find that the position of the weakest resonance, which presumably is associated with OH, is markedly temperature dependent, while the others are not, even though all of them at room temperature are shifted comparable amounts. The existence of a temperature dependence is consistent with the general formulation of Ramsey's[2] theory if there are alternative molecular states whose energy separation is of the order of kT, and it is of interest to note that suitable low-lying states should be expected in the case of ethyl alcohol.

One mechanism for the production of such states is the process of association of ethyl alcohol which has long been known to be an associated liquid.[4,5] Since this association is by a hydrogen bond involving the hydrogen in the OH group, this hydrogen should experience a different magnetic shielding in the associated and unassociated state. If the correlation time[6] for the lifetimes of the different states is sufficiently small (less than a millisecond), the hydrogen resonance will be observed at the frequency corresponding to the average shielding for the states. Since changes of temperature will alter the distribution between the associated and unassociated states, the resonance frequency should be temperature dependent.

Alternative mechanisms for the temperature dependence are effects of temperature on the hydrogen angle vibrations and hindered rotations. The frequency of the hydrogen angle vibrations is such[7] that appreciable change in the population occurs in the temperature range of the experiment, and the amplitude of the vibration is sufficiently large that the shielding could be noticeably different in the two lowest vibrational states.

Experimentally, it should be possible to distinguish between the two alternatives by dissolving the alcohol in a solvent such as CCl_4 which is known to alter the extent of association. Also, the effect of a hydrogen bond on the magnetic shielding could be studied by comparing the proton magnetic resonance frequencies in ortho-nitrophenol and para-nitrophenol or in similarly related compounds.

* This work was supported by the joint program of the ONR and AEC.
[1] Arnold, Dharmatti, and Packard, J. Chem. Phys. **19**, 507 (1951).
[2] N. F. Ramsey, Phys. Rev. **78**, 699 (1951).
[3] M. E. Packard and J. T. Arnold, Phys. Rev. **83**, 210 (1951).
[4] Hilbert, Wulf, Hendricks, and Liddel, J. Am. Chem. Soc. **58**, 2287 (1936), and unpublished results.
[5] W. C. Pierce and D. P. MacMillan, J. Am. Chem. Soc. **60**, 779 (1938).
[6] Bloembergen, Purcell, and Pound, Phys. Rev. **73**, 679 (1948).
[7] S. C. Schumann and J. G. Aston, J. Chem. Phys. **6**, 480 (1938).

Variations in Absolute Chemical Shift of Nuclear Induction Signals of Hydroxyl Groups of Methyl and Ethyl Alcohol*

J. T. ARNOLD AND M. E. PACKARD†
Stanford University, Stanford, California
(Received October 12, 1951)

IN connection with observations of chemical effects in proton nuclear induction signals,[1] it was reported[2] that the absolute chemical shift of signals because of the OH groups of methyl and ethyl alcohol shows a temperature dependence, while that of the CH_2 and CH_3 groups does not.

We have measured this effect, with particular attention to ethyl alcohol in the temperature range of 150° to 350°K. In Fig. 1 the

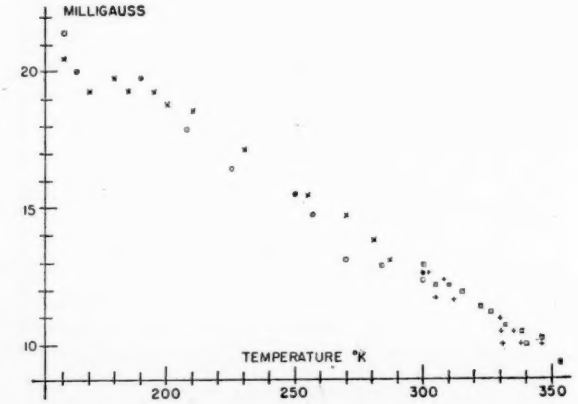

FIG. 1. Separation of OH and CH_2 signals in milligauss *versus* temperature. The different symbols represent results obtained in different runs.

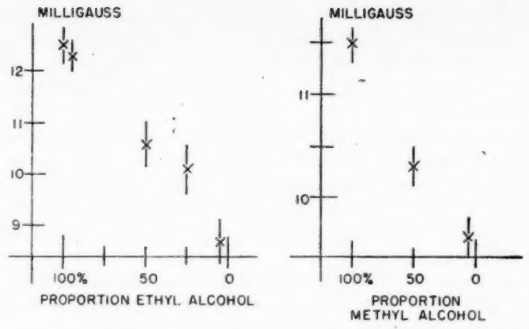

FIG. 2. Separation of nuclear induction signals of OH groups from the neighboring groups in ethyl and methyl alcohols dissolved in carbontetrachloride.

chemical shift between the OH and CH_2 groups of ethyl alcohol is plotted as a function of temperature.

More recently, we have observed that dilution of the alcohols has an effect similar to raising their temperature. A one-to-one solution of ethyl alcohol in chloroform at room temperature gives the aspect of pure alcohol at 350°K. In Fig. 2 we have plotted the effect of dissolution in carbon tetrachloride upon the chemical shift of the OH group. In the case of ethyl alcohol it is seen that the chemical shift between the OH and CH_2 groups at concentrations of about 10 percent is very nearly that of pure boiling alcohol.

The samples used in the determination of the temperature dependence were cylindrical of approximately 1-mm diameter by 5-mm length, contained in small unsilvered vacuum flasks. It was not feasible to measure temperatures by direct means in such small samples. The temperatures indicated in Fig. 1 are taken from a cooling curve which was deduced from signal amplitudes. The signal amplitudes over most of the temperature range are assumed to be inversely proportional to temperature in accordance with the Curie law. (Below about 200°K the signal amplitudes fall off because of viscosity effects and ultimate freezing out of the alcohol.) Data obtained at measured time intervals after initial heating or cooling to known temperatures indicate very closely an exponential time dependence of temperature in the interval 200° to 350°K.

In the slow passage observation of nuclear induction signals chemical shifts may be measured directly on the face of a persistent screen oscilloscope. The calibration of sweep fields in the present measurements was accomplished by observing signals because of a pure water sample (which gives a discrete sharp line) when the linear sweep field had superposed on it a low amplitude sinusoidal variation at a known frequency ν in the audio range. The resulting display is equivalent to excitation of nuclear induction signals with a radiofrequency field having side bands spaced at intervals from the center frequency.[3] This method permits accurate calibration of sweep fields.

We wish to thank Professor Felix Bloch for his continued interest in chemical effects in nuclear induction.

* Assisted by the joint program of the AEC and ONR.
† Now associated with Varian Associates, San Carlos, California.
[1] Arnold, Dharmatti, and Packard, J. Chem. Phys. **19**, 507 (1951).
[2] M. E. Packard and J. T. Arnold, Phys. Rev. **83**, 210(A) (1951).
[3] Robert Karplus, Phys. Rev. **73**, 1027 (1948).

The Microwave Spectrum of Furan*

M. H. SIRVETZ
Brookhaven National Laboratory, Upton, Long Island, New York
(Received October 12, 1951)

THE heterocyclic 5-membered ring compound furan has been found to give rise to over fifty strong absorptions in the microwave K-band. Of these 26 have been assigned to specific rotational transitions. The derived rotational constants correspond to a planar molecule of near oblate symmetry, with electric dipole moment oriented along the principal axis of least moment of inertia. The spectrometer, utilizing Stark effect modulation, has been described recently.[1] It is estimated that frequencies are accurate to better than 0.1 mc.

TABLE I. Observed and computed frequencies (Mc).

Transition	ν(obs)	ν(calc)
$8_{8,2}\rightarrow 8_{8,1}$	19011.46	19009.36
$12_{10,3}\rightarrow 12_{10,2}$	19767.98	19773.51
$9_{7,2}\rightarrow 9_{9,1}$	20624.34	20621.60
$11_{9,3}\rightarrow 11_{9,2}$	20637.71	20642.40
$10_{8,3}\rightarrow 10_{8,2}$	21377.91	21381.72
$9_{7,3}\rightarrow 9_{7,2}$	21984.30	21987.29
$8_{6,3}\rightarrow 8_{6,2}$	22455.99	22461.19
$10_{8,2}\rightarrow 10_{10,1}$	22540.27	22536.54
$7_{5,3}\rightarrow 7_{5,2}$	22810.92	22812.60
$6_{4,3}\rightarrow 6_{4,2}$	23055.80	23057.01
$5_{3,3}\rightarrow 5_{3,2}$	23213.45	23214.25
$1_{1,1}\rightarrow 2_{1,2}$[a]	23259.30	23259.29
$4_{2,3}\rightarrow 4_{2,2}$	23305.88	23305.81
$3_{1,3}\rightarrow 3_{1,2}$	23352.47	23352.23
$3_{0,3}\rightarrow 3_{2,2}$[a]	23384.46	23384.46
$4_{1,3}\rightarrow 4_{3,2}$	23402.53	23402.72
$5_{2,3}\rightarrow 5_{4,2}$	23440.06	23440.49
$1_{0,1}\rightarrow 2_{0,2}$[a]	23453.13	23453.13
$6_{3,3}\rightarrow 6_{5,2}$	23507.71	23508.45
$7_{4,3}\rightarrow 7_{6,2}$	23619.06	23620.11
$8_{5,3}\rightarrow 8_{7,2}$	23790.73	23792.15
$9_{6,3}\rightarrow 9_{8,2}$	24043.08	24044.78
$10_{7,3}\rightarrow 10_{9,2}$	24399.77	24401.97
$11_{9,2}\rightarrow 11_{11,1}$	24767.50	24763.31
$11_{8,3}\rightarrow 11_{10,2}$	24888.97	24891.49
$12_{9,3}\rightarrow 12_{11,2}$	25541.64	25544.58

[a] Parameters adjusted to give agreement at these points.

In Table I are listed, together with the transition assignments, the frequencies observed and those computed on the basis of standard rigid asymmetric rotor theory.[2] The average discrepancy is of the order of 1.7 mc. Centrifugal stretching effects are apparently unimportant up to rather high J, although the steady increase, with J discrepancy between observation and prediction, is undoubtedly to be attributed to this cause. All transitions through $J=12$ predicted to fall in the K-band were observed, with the exception of one which should appear in a small inaccessible region.

From the two $J=1$ to $J=2$ transitions, and the transition $3_{0,3}\rightarrow 3_{2,2}$ we obtained the rotational constants: $(A+C)/2=7058.94$, $(A-C)/2=2388.10$, and $\kappa=0.916142$. These correspond to moments of inertia 53.5067, 54.6656, and 108.2204 amu-A,[2] which may be compared with the values 56.44, 54.58, and 111.02, respectively, computed from the structure of furan proposed by Pauling and Schomaker[3] on the basis of electron diffraction work (together with reasonable assumptions about the C−H bonds). Though there is no great disagreement, it may be noted that the preliminary estimates indicated that the dipole moment lay along the axis of intermediate moment of inertia. It turns out that taking

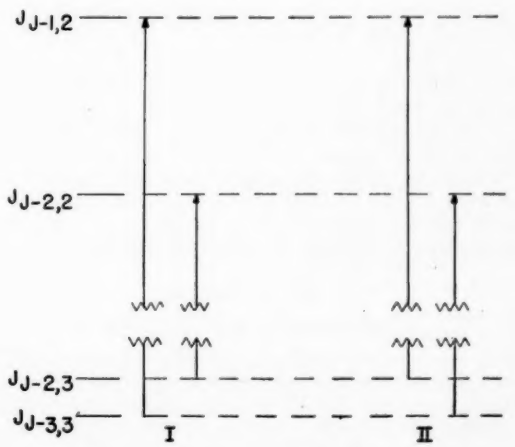

FIG. 1. Allowed transitions: I. for μ_a; II. for μ_b.

this as an assumption leads at first sight to no obvious inconsistency in the interpretation of the spectrum. The selection rules, though changed, still permit two $J=1$ to $J=2$ transitions as well as a doublet of the form $J_{K_1=3} \rightarrow J_{K_1=2}$ for every $J \geqq 3$. Even a large measure of quantitative agreement is possible, since only the splitting of the two levels of lower value of K_1 is involved, in first approximation, in producing the doublet splitting (see Fig. 1). The Stark effect of the $1 \rightarrow 2$ transitions, however, may be used to show unambiguously that the dipole moment in fact lies along the least axis of inertia. For the line at 23259 mc the ratio of the displacements of the $M=1$ and $M=0$ components is observed to be 5.64, in good agreement with the value 5.690 computed for the transition $1_{1,1} \rightarrow 2_{1,2}$ on the basis of the above given structure. If μ were oriented along the b-axis, the corresponding transition would be $1_{1,1} \rightarrow 2_{0,2}$ and the computed ratio would differ in sign as well as in magnitude from that observed. The value of the dipole moment is determined to be 0.661 ± 0.006 debye.

It may be noted that the effective moments of inertia here obtained show only a very slight effective aplanarity; i.e., I_c is very nearly equal to $I_a + I_b$. This is, of course, an essential condition for the possibility of equating effective moments of a molecule believed to be planar to equilibrium moments in determining structural parameters. It is thus hoped that the use of various deuterated furans may lead to a microwave structural determination.

The author would like to thank Dr. V. W. Cohen for much helpful advice during this research.

* Research carried out at Brookhaven National Laboratory, under the auspices of the AEC.
[1] Wentink, Koski, and Cohen, Phys. Rev. **81**, 948 (1951).
[2] King, Hainer, and Cross, J. Chem. Phys. **11**, 27 (1943). The notation developed by these authors is used in this report.
[3] L. Pauling and V. Schomaker, J. Am. Chem. Soc. **61**, 1769 (1939).

Infrared Spectrum of Some Complex Hexafluorides

A. DE LATTRE
Centre d'Analyse spectrale, Moléculaire de l'Université de Liége, Liége, Belgium
(Received September 14, 1951)

THE infrared (IR) spectra in the KBr region of 3 samples of synthetic cryolite have been investigated by the powder method. One of the samples was obtained by precipitation, the other by fusing together AlF_3+3NaF, and the third was a commercial product. All samples give maximum absorption at about 599 cm^{-1}, which can be safely considered as the highest of the two F_{1u} frequencies of AlF_6^{---} octahedra, the lowest one falling outside of the region of observation.

Using Wilson's formula for XY_6 and the Al-F distance from x-ray measurements on cryolite, we can calculate from the observed frequency the valence stretching constant k_{01} of the AlF bond as a function of the ratio of the deformation constant to the valence stretching constant. (See Table I.)

It is seen that within the range of reasonable values for ρ, k_{01} varies from 2.15 to 1.10 while in any case the lowest IR active vibration falls far outside our range of observation. Badger's rule would require $k_{01}=2.3\times10^5$. On the other hand, assuming a central force field with Coulombic forces and Born-type repulsion, we find $k_{01}=1.43\times10^5$ if Al^{+++} is supposed to have 3 elementary charges and F^- one. It is remarkable that the force constant predicted for a purely ionic molecule falls within the range of values permitted by experiment.

TABLE I. F_{1u} vibrations.

ρ	k_{01}	Highest: observed	Lowest: predicted
0.05	2.15×10^5	599	221
0.10	1.83	599	281
0.20	1.10	599	311
	dynes/cm	cm^{-1}	

A further study of the Raman and IR spectra of solids and solutions containing ions of the type XY_6 is in progress. Four samples of fluoferriates of sodium and ammonium studied by the powder method all give a diffuse band in the region 492-458 cm^{-1}, and a sample of KPF_6 gives strong well-defined peaks at 847 and 561 cm^{-1}.

Seifert[1] states that KPF_6 contains PF_4^+ tetrahedra rather than PF_6^- octahedra. Recently Bode and Voss[2] announced the forthcoming publication of the x-ray structure of KPF_6.

Our observed IR frequencies are shown in Table II.

TABLE II.

	Tetrahedron hypothesis	Octahedron hypothesis
k_{01}	3.18×10^5 dynes/cm	4.0×10^5 dynes/cm
k_{φ}	1.29×10^5 dynes/cm	0.84×10^5 dynes/cm

In PF_3 the valence and deformation constants are 4,6, and 1.07, respectively. From IR data alone, no decision can be taken as to the structure, since both models give reasonable force constants. If Seifert's conclusion is confirmed by Bode and Voss, $k_{01}=3.18$ can be adopted as a fairly safe value for the stretching constant of the P-F bond in PF_4^+.

[1] Seifert, Z. Krist. **76**, 455.
[2] Bode and Voss, Z. anorg. Chem. **264**, 144 (1951).

On the Theoretical Calculation of Transition Probabilities*

HARRISON SHULL AND FRANK O. ELLISON
Department of Chemistry and Institute for Atomic Research, Iowa State College, Ames, Iowa
(Received October 4, 1951)

THE theoretical computation of transition probabilities[1] for electric dipole transitions in electronic spectra of molecules requires the evaluation of the transition integral

$$\mathbf{Q}=\int \Psi_i \left(\sum_k^N \mathbf{r}_k \right) \Psi_f d\tau, \qquad (1)$$

where Ψ_i and Ψ_f are the antisymmetrized and normalized N-electron wave functions of the initial and final states, respectively, and $\mathbf{r}_k$ is the radius vector of the kth electron referred to a system of coordinate axes. The transition probability is proportional to the square of $\mathbf{Q}$. In most of the previous literature, integrals of the type (1) have been evaluated utilizing the center of the system as an origin for $\mathbf{r}_k$. Bayliss[2] has recently suggested that this choice of origin is not merely one of convenience, but of necessity. He states that "the value of $\mathbf{Q}$ *in general*, although not necessarily in particular cases, depends on the origin of x." One would suspect *a priori* that the transition integral is independent of the choice of origin, inasmuch as the quantity calculated is a function only of the electronic states of the system. If such a dependency did exist, previous theoretical treatments would be seriously questioned until the exact criteria for selecting a proper origin were determined. It does not seem immediately obvious why the center of the molecule would be the most natural choice.

It may be shown quite easily that the transition integral is independent of the choice of origin with but one restriction. If, in the integral (1), the origin of the vectors $\mathbf{r}_k$ is transformed, such that $\mathbf{r}_k' = \mathbf{r}_k + \mathbf{r}_0$, the integral becomes

$$Q' = \int \Psi_i \Big(\sum_k^N r_k' \Big) \Psi_f dv = \int \Psi_i \Big[\sum_k^N (r_k + r_0) \Big] \Psi_f dv$$
$$= Q + r_0 N S_{if}.$$

Therefore, if the wave functions of the initial and final states are orthogonal to each other (i.e., $S_{if}=0$), the transition integral is independent of the choice of origin of the dipole length operator. If the functions were not orthogonal, it would be implied that some of the initial state is mixed in with the final state.

In the actual calculation of transition probabilities, the electronic configurations of the lower and upper states are usually expanded in terms of atomic orbitals (AO's) either by the valence bond or molecular orbital approach. Therefore, the ultimate evaluation of (1) reduces to the computation of one-electron integrals of the form $\int \phi_1 r \phi_2 dv$ where ϕ_1 and ϕ_2 are typical AO's, generally of the Slater-type, directly involved in the transition. These one-electron integrals often depend upon the choice of origin, since ϕ_1 and ϕ_2 are not necessarily orthogonal. Therefore, when carrying out the integration (1), with orthogonal functions Ψ_i and Ψ_f, a unique origin should be chosen, but the final answer will be independent of this choice.

It should be pointed out that the calculations by Bayliss[3] of the transition probabilities for a one-dimensional electron gas in a field of uniform potential are correct, contrary to the statement in his recent paper.[2] This is a consequence of the orthogonality of the eigenfunctions concerned, making the transition integral independent of whether the origin of x be placed at the center or boundary of the system.

* Contribution No. 155 from the Institute for Atomic Research and Department of Chemistry, Iowa State College, Ames, Iowa. This work was supported in part by the Ames Laboratory of the AEC.

[1] For an extensive review of methods and references, see R. S. Mulliken and C. A. Rieke, Phys. Soc. Rep. Prog. Phys. **8**, 231 (1941).
[2] N. S. Bayliss, Australian J. Sci. Research **A3**, 109 (1950).
[3] N. S. Bayliss, J. Chem. Phys. **16**, 287 (1948).

The Spectra of Bromine Pentafluoride*

T. G. Burke and E. A. Jones†
K-25 Laboratories, Carbide and Carbon Chemicals Company, Oak Ridge, Tennessee
(Received October 3, 1951)

THE Raman spectrum of liquid bromine pentafluoride has been studied at room temperature using a Lane Wells spectrograph and 4358-Hg excitation. The Raman tubes were fabricated from the inert plastic Fluorothene,[1] a polymer of trifluorochloroethylene. Some infrared studies were made on gaseous bromine pentafluoride in the region from 400-cm^{-1} to 700-cm^{-1} using a Perkin-Elmer 12C spectrometer equipped with KBr optics. All infrared runs were made on the gas at low pressure because BrF_5 readily attacks the window material used in the KBr region.

Bromine pentafluoride was prepared by the direct combination of bromine and fluorine according to the method reported by Ruff and Menzel.[2] Purification was accomplished by condensing the reaction mixture and fractionally distilling it in an all-metal still.

The results through the region of the fundamentals are given in Table I. The nine Raman frequencies listed in Table I have been designated as the fundamentals of BrF_5. The lack of infrared data on the low frequency fundamentals and polarization of the Raman lines prevents a definite structural assignment from this study. However, for the two likely models, the tetragonal pyramid and the triagonal bypyramid, the data do favor the former, since for the C_{4v} structure one expects nine Raman frequencies and for the D_{3h} structure only six Raman frequencies.

Table I. Infrared and Raman frequencies in the spectrum of bromine pentafluoride.

Raman lines (liquid) cm^{-1}	Relative intensities*	Infrared bands (gas) cm^{-1}
684	V.S.	690
629	V.W.	645
569	V.S.	583
539	V.S.	...
480	V.W.	...
410	M.S.	418
365	S.	...
310	M.S.	...
241	W.	...

* V.S. = very strong; S. = strong; M.S. = medium strong; W. = weak, V.W. = very weak.

A normal coordinate treatment and investigation of the polarization of the Raman lines are in progress in the Physics Department at Vanderbilt University.

We wish to thank G. J. Vogel and R. W. Vogel of the K-25 Chemistry Department for the sample used in this investigation.

* This document is based on work performed for the AEC by Carbide and Carbon Chemicals Company at Oak Ridge, Tennessee.
† Now at the Department of Physics, Vanderbilt Univeristy, Nashville, Tennessee.
[1] J. S. Kirby-Smith and E. A. Jones, J. Opt. Soc. Am. **39**, 780 (1949).
[2] O. Ruff and W. Menzel, Z. anorg. u. Allgem. Chem. **202**, 49, (1931).

Density Measurements in Gaseous Detonation Waves*

G. B. Kistiakowsky
Gibbs Chemical Laboratory, Harvard University, Cambridge, Massachusetts
(Received October 17, 1951)

MEASUREMENTS of detonation velocities permit the deduction of the parameters of thermodynamic equilibrium behind the wave front,[1] in the so-called Chapman-Jouguet plane, but they provide virtually no information on the intervening deflagration zone. To obtain an independent experimental check of such thermodynamic calculations and to observe the deflagration zone, it is essential to measure some other wave parameter, e.g., pressure, temperature, or mass velocity. None of these measurements, however, are readily carried out in a time short enough to avoid the disturbing effects of the walls of the confining vessel. The literature, indeed, reveals no trustworthy data on any of these variables.

A time record of gas density in the wave provides as much information as that of the pressure, and it has the advantage that the ratio of densities of the shocked but unreacted gas and of the fully reacted gas is quite high, since according to v. Neumann[2] the pressure drops and the temperature rises in the intervening deflagration zone. Moderately soft x-rays, detected by a scintillation counter, provide a practical method, because their absorption coefficients are in the useful range, and yet they do not depend on the state of chemical binding. Moreover, an absorption measurement integrates the density over the entire path of the rays, parallel to the wave front, instead of measuring the events immediately at the wall, as is done by a pressure gauge; thus wall effects are minimized.

For the present experiments a G. E. X-Ray Corporation[3] copper tube type CA7 was used, operating on 20 kv dc potential at 30 m A current. It faced suitably reinforced 10 mil thick beryllium windows mounted oppositely in the walls of a 10 cm i.d. steel pipe. The width of the x-ray beam in the direction of wave travel varied from 2 to 4 mm. The beam was faced by a terphenyl crystal backed by a 1P21 photomultiplier. The output was fed through a cathode follower to a Du Mont CRO type 248. Time resolution was only slightly better than 1 μsec, since it was not desired to display individual pulses; on the contrary, the number of quanta reaching the counter was sufficient to produce a steady output with statistical fluctuations of the order of a few percent of the total.

The first trace in the figure is a time-density record of the detonation of a mixture of oxygen, acetylene and methyl bromide, sweep time being 300 microseconds. The second trace, of 140 μsec duration, shows the detonation of a mixture of methyl bromide and oxygen. The passage of the shock reflected from the end of the pipe is also seen in the first trace. The apparent steepness of the wave front in the second trace is 2 μsec, as would be expected

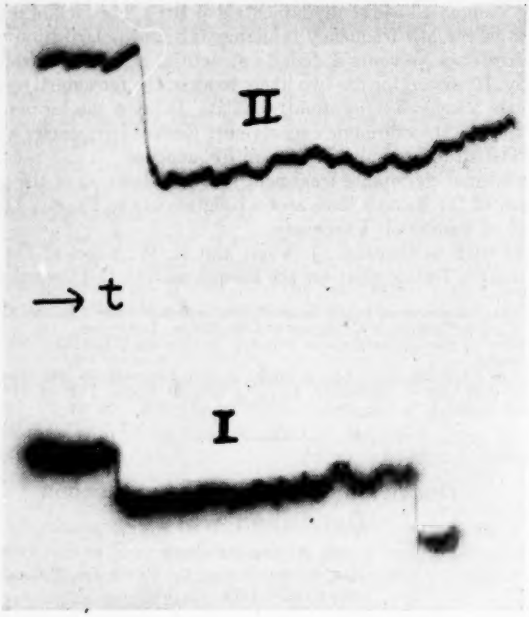

FIG. 1. Time-density records of two detonations.

from the time of passage by the x-ray beam of a square wave, plane and normal to the pipe axis.

The most interesting feature of these records is the absence of the high density region preceding the state of the fully reacted gas. The width of this region must be small compared to the width of the x-ray beam; thus the Chapman-Jouguet plane in these detonations follows the shock front less than a millimeter behind.

Further work with this equipment and its improvements are now underway and will be described later.

* This research was made possible by funds extended to Harvard University under the ONR Contract M5ori-76, T. O. XIX, NR-053-094.
[1] Kistiakowsky, Knight, and Malin, J. Am. Chem. Soc. **73**, 2972 (1951).
[2] J. v. Neumann, OSRD Report No. 549 (May, 1942).
[3] It is a pleasure to acknowledge my thanks to the G. E. X-Ray Corporation and particularly to Mr. H. W. Pickett for the loan of the tube and for useful suggestions.

Note on the Electron Affinity of Fluorine

RICHARD B. BERNSTEIN
Argonne National Laboratory and Illinois Institute of Technology, Chicago, Illinois
AND
MAX METLAY
School of Mines, Columbia University, New York, New York
(Received October 15, 1951)

IT seems advisable to reconsider the available facts regarding the electron affinity of the fluorine atom in the light of the recent definitive value for the heat of dissociation of fluorine, 37.7±0.4 kcal/mole, obtained by Doescher.[1] Evans, Warhurst, and Whittle[2] pointed out clearly that the electron affinity calculated by Mayer and Helmholtz,[3] using the Born-Haber cycle, was dependent on the particular choice of $D(F_2)$ employed.

The early value of 63.5 kcal/mole had been used to obtain the now "accepted" value of 95.3 kcal/mole for the electron affinity of fluorine, which is the average result based on calculations for each of the various alkali metal fluorides. Employing the new dissociation energy gives a corrected value of $95.3-\frac{1}{2}(63.5-37.7)=82.4$ kcal/mole for the affinity.

An experimental study to determine the electron affinity of fluorine has been reported by Metlay and Kimball.[4] The results were considered anomalous at the time for two reasons. First, the apparent electron affinity showed a trend with temperature over and above the random scatter in the data. Second, the numerical values obtained were considerably lower than the expected value of 95 kcal/mole.

The observed trend was attributed to incomplete dissociation of fluorine on the hot, fluoride-coated tungsten filament, i.e., an accomodation coefficient for dissociation of less than unity. This conclusion no longer appears tenable. It is possible that both the large scatter in the data and the apparent temperature effect may be due to the considerable experimental difficulties encountered with such measurements on fluorine.

The mean value of their results (27 observations) is 82.2 kcal/mole (a.d.=±3.9 kcal/mole). This is in good agreement with the calculated value of 82.4 kcal/mole as stated above. In the absence of a more reliable experimental determination this would appear to be the best available estimate for the electron affinity of fluorine.

Thanks are due Professor J. E. Mayer and Dr. J. J. Katz for valuable discussions.

[1] R. N. Doescher, J. Chem. Phys. **19**, 1070 (1951).
[2] Evans, Warhurst, and Whittle, J. Chem. Soc. 1524 (1950).
[3] J. E. Mayer and L. Helmholtz, Z. Physik **75**, 19 (1932).
[4] M. Metlay and G. E. Kimball, J. Chem. Phys. **16**, 779 (1948).

Irreducible Representations of Cubic Groups

FRANK MATOSSI
Naval Ordnance Laboratory, White Oak, Silver Spring, Maryland
(Received October 15, 1951)

THE determination of degenerate symmetry coordinates of molecular vibrations requires the knowledge of the actual matrix representations of the respective irreducible representations. These matrices should be orthogonal (or unitary). The matrix belonging to the product of two symmetry elements should be the product of the matrices of the factors. A certain power of the matrix must be equal to the unit matrix. The sum of the diagonal matrix elements must be equal to the respective group characters. It is not necessary that all matrices should be different.

A set of matrices satisfying these conditions for cubic groups[1] is given below for the *E*-species and *F*-species. Only the group T_d is considered explicitly. The matrices for the other cubic groups can easily be derived from the T_d-matrices. Because the matrices may be different for different orientations of the symmetry elements, these elements are described by the permutations of the corners 1, 2, 3, 4 of a regular tetrahedron. A few of the differences are indicated.

The *E*-matrices are,

for C_3, $\begin{vmatrix} -\frac{1}{2} & +\frac{\sqrt{3}}{2} \\ -\frac{\sqrt{3}}{2} & -\frac{1}{2} \end{vmatrix}$ in all directions;

for C_2, $\begin{vmatrix} 1 & 0 \\ 0 & -1 \end{vmatrix}$ in all directions;

for S_4 (1234), $\begin{vmatrix} -\frac{1}{2} & -\frac{\sqrt{3}}{2} \\ -\frac{\sqrt{3}}{2} & \frac{1}{2} \end{vmatrix}$; for S_4 (1324), $\begin{vmatrix} 1 & 0 \\ 0 & -1 \end{vmatrix}$;

for σ (12) (3) (4), $\begin{vmatrix} 1 & 0 \\ 0 & -1 \end{vmatrix}$; for σ (34) (1) (2), $\begin{vmatrix} -\frac{1}{2} & -\frac{\sqrt{3}}{2} \\ -\frac{\sqrt{3}}{2} & \frac{1}{2} \end{vmatrix}$.

The matrix for (1324), for instance, is the product of the matrices for (1234) and (123) (4).

For the species F_1 and F_2, we have (the upper sign corresponds to F_1; the lower, to F_2)

$$\text{for } C_3 \text{ (123) (4)}, \begin{vmatrix} 0 & 0 & -1 \\ 1 & 0 & 0 \\ 0 & -1 & 0 \end{vmatrix}; \text{ for } C_3 \text{ (143) (2)}, \begin{vmatrix} 0 & 1 & 0 \\ 0 & 0 & 1 \\ 1 & 0 & 0 \end{vmatrix};$$

$$\text{for } C_2 \text{ (12) (34)}, \begin{vmatrix} 1 & 0 & 0 \\ 0 & -1 & 0 \\ 0 & 0 & -1 \end{vmatrix};$$

$$\text{for } S_4 \text{ (1234)}, \begin{vmatrix} 0 & \pm 1 & 0 \\ \mp 1 & 0 & 0 \\ 0 & 0 & \pm 1 \end{vmatrix}; \text{for } S_4 \text{ (1324)}, \begin{vmatrix} \pm 1 & 0 & 0 \\ 0 & 0 & \pm 1 \\ 0 & \mp 1 & 0 \end{vmatrix};$$

$$\text{for } \sigma \text{ (12) (3) (4)}, \begin{vmatrix} \mp 1 & 0 & 0 \\ 0 & 0 & \mp 1 \\ 0 & \mp 1 & 0 \end{vmatrix};$$

$$\text{for } \sigma \text{ (34) (1) (2)}, \begin{vmatrix} 0 & \pm 1 & 0 \\ \pm 1 & 0 & 0 \\ 0 & 0 & \mp 1 \end{vmatrix}.$$

The F-matrices are obtained with the method indicated by Venkatarayudu, i.e., applying the symmetry operations to the symmetry coordinates of translations (F_2) and rotations (F_1), which can be written down immediately in any appropriate coordinate system. Of course, the signs in the matrices depend on the arbitary orientation of this coordinate system. The matrices given above are obtained if an orthogonal system is chosen with x, y, z axes going, respectively, from the center of side 34 to 12, from 13 to 24, from 14 to 23. The E-matrices may be obtained by starting from some reasonably obvious ones (C_3, C_2, some σ) to form the necessary products. The assignment of $\begin{vmatrix} 1 & 0 \\ 0 & -1 \end{vmatrix}$ to σ (21) (3) (4) is, of course, arbitrary. But nothing essential is changed with other possible assignments. The assignment of the matrices to the symmetry elements has been checked by determining the symmetry coordinates of a tetrahedral X_4-molecule in agreement with Born's data.[2]

[1] T. Venkatarayudu, Proc. Indian Acad. Sci. (A) **17**, 75 (1943) has given representations which do not agree with some of the requirements mentioned. For other than cubic groups, no problem is involved.
[2] M. Born, *Optik* (Verlag. Julius Springer, Berlin, Germany, 1933), p. 554 ff.

The Pure Quadrupole Spectrum of Solid Vinyl Chloride

J. H. Goldstein
Department of Chemistry, Emory University, Emory University, Georgia
AND
Ralph Livingston
Chemistry Division, Oak Ridge National Laboratory, Oak Ridge, Tennessee*
(Received October 3, 1951)

PURE quadrupole transitions for Cl^{35} in vinyl chloride have been observed at a frequency of 33.414 Mc at 77°K and 33.613 Mc at 20°K, using a technique that has been previously reported.[1] On the assumption of a cylindrically symmetrical field,[2] these frequencies lead to a value of about -67 Mc for the coupling constant, $eQ\phi_{zz}$.

It is of interest to compare the present result with that obtained from the hyperfine structure in the microwave spectrum of this molecule.[3] The theory employs two parameters, $\chi_{aa}=eQ\phi_{aa}$ and $\chi_{bb}=eQ\phi_{bb}$, where a and b are the in-plane principal inertial axes. Because of the asymmetrical structure of the molecule, the unique (a) axis does not coincide with the C-Cl bond axis. Since the χ-tensor is incompletely determined in the inertial system its transformation to any other axis system is impossible unless certain assumptions are introduced. In particular it has been found that by assuming the C-Cl bond to be a principal (z) axis of the field gradient tensor, a value of -67 ± 2 Mc is obtained for $eQ\phi_{zz}$, in good agreement with the present result.

The physical properties of vinyl chloride indicate that the intermolecular forces in the solid are of the van der Waals type. The electric field at the nucleus should therefore be determined almost solely by the C-Cl bond, which suggests the above comparison. Because of the agreement between the two values of $eQ\phi_{zz}$, it is felt that the assumption of the C-Cl bond as a principal axis of the field gradient tensor is a reasonable one.

Dehmelt and Krüger have reported the somewhat higher value of 70.8 Mc for the coupling constant in solid *trans*-dichloroethylene.[4] In this molecule a decrease in the double-bond character of the C-Cl bond, as compared with vinyl chloride, is not unreasonable, and a corresponding increase in $eQ\phi_{zz}$ should follow. Unfortunately, this molecule possesses no pure rotational spectrum so that comparison with microwave results is not possible.

It is also possible, using the microwave data for vinyl chloride, to estimate the effect of bond asymmetry on the calculated coupling constant in the solid. The Hamiltonian for a quadrupolar nucleus in an inhomogeneous electric field[4] may be written in the form

$$H=H_0+H_1=\frac{eQ\phi_{zz}}{2I(2I-1)}(\tfrac{3}{2}\mathbf{I}_z^2-\mathbf{I}^2)+\frac{eQ\epsilon}{4I(2I-1)}(\mathbf{I}_x^2-\mathbf{I}_y^2), \quad (1)$$

where $\epsilon=\phi_{xx}-\phi_{yy}-\phi_{yy}$. The first term in (1) is the Hamiltonian for the cylindrically symmetrical case. The second operator, which may be treated as a perturbation, has matrix elements completely defined by

$$(Im|\mathbf{I}_x^2-\mathbf{I}_y^2|Im+2) = \tfrac{1}{2}[(I+m+1)(I-m)(I+m+2)(I-m-1)]^{\frac{1}{2}}. \quad (2)$$

In the case of Cl, $I=\frac{3}{2}$, the eigenvalues of H_0 are $E_{\pm\frac{3}{2}}=\alpha/4$ and $E_{\pm\frac{1}{2}}=-\alpha/4$, where $\alpha=eQ\phi_{zz}$. The secular equation for the complete Hamiltonian, H, factors into two identical quadratic blocks with solutions

$$E=\pm\alpha/4[1+\beta^2/3\alpha^2]^{\frac{1}{2}} \quad (3)$$

where $\beta=eQ\epsilon$. From the microwave spectrum of vinyl chloride, β was found to be equal to -7 Mc (3) and with $\alpha=-67$ Mc, from Eq. (3) we obtain $E=\pm16.78$ Mc and $\nu=33.56$ Mc, which would lead to an apparent value of -67.1 Mc for α. Thus the effect of bond asymmetry is in this case quite negligible.

* The work at this Laboratory was performed for the AEC.
[1] R. Livingston, Phys. Rev. **82**, 289 (1951).
[2] H. G. Dehmelt and H. Krüger, Naturwiss. **37**, 111 (1950).
[3] J. H. Goldstein and J. K. Bragg, Phys. Rev. **75**, 1453 (1949).
[4] H. G. Dehmelt and H. Krüger, Z. Physik **129**, 401 (1951).

The Reaction Sites in a Field of Stationary Ultrasonic Waves

Olle Lindström
Division of Physical Chemistry, The Royal Institute of Technology, Stockholm 26, Sweden
(Received October 2, 1951)

THE oxidizing action of ultrasonic waves is most generally considered to be in some way connected with the phenomenon of cavitation. Recently it has been pointed out by several authors that there is an analogy between most of the chemical effects of ultrasonic waves and those of ionizing radiation.[1–4] It is assumed that water molecules are split into hydroxyl radicals and hydrogen atoms, and these reactive species are supposed to be responsible for the various chemical effects observed.

The production of reactive molecules may occur (i) at the moment of birth of the cavity, e.g., because of the violent rupture of the light;[5] (ii) during the lifetime of the cavity, e.g., by electrical discharges in the cavity's atmosphere;[6] and (iii) at the collapse, e.g., because of the ensuing high pressure and temperature.[7] Furthermore, there is the possibility that the cavity will be filled with gas and transformed into a small gas bubble. The gas bubble will move from its birthplace in a velocity node to an antinode,

FIG. 1. The starch paper is placed around the metal strip and the whole assembly inserted in the slit of the reflector.

and here active molecules may be generated (iv) by interaction between the surface-layer of the bubble and the oscillating liquid medium.[8] It is observed that in the first three alternatives the induced reactions will take place in the nodes, whereas reactions of type (iv) should be located in the antinodes.

In order to decide between the two main possibilities an experiment was performed, in which the sites of reaction in a field of stationary waves were determined. As a suitable reaction the production of iodine from an aqueous solution of potassium iodide and carbon tetrachloride was chosen.[9] The reaction centers were indicated in a most simple way by means of a potassium iodide starch paper arranged perpendicularly to the reflector (Fig. 1). The production of iodine was found to take place in distinct zones, and the distance between the zones amounted to half of the sound wavelength (Fig. 2). Since the first reaction zone appeared

FIG. 2. Reaction zones on the starch paper (reaction solution: 5 g KJ per 100 ml of water saturated with carbon tetrachloride; 700 kc/s; 2 W/cm^2; 30 s; and 25°C).

precisely in the plane of the reflector, it is evident that the reaction in question preferably takes place in the nodes. This result supports the concept that oxidation promoted by ultrasonic waves is intimately connected with the cavitation process itself and does not depend on any processes in which the gas bubbles produced by cavitation may take part.

The author wishes to thank Professor Ole Lamm for his kind interest and encouragement. Thanks are also due the Swedish State Council of Technical Research for financial support.

[1] P. Günther in G. Schmid, Naturwiss. **37**, 16 (1950).
[2] R. O. Prudhomme and P. Grabar, J. chim. phys. **46**, 323 (1949).
[3] N. Miller, Trans. Faraday Soc. **46**, 546 (1950).
[4] O. Lindström and O. Lamm, J. Phys. and Colloid Chem. 55, No. 7 (1951).
[5] W. A. Weyl and E. C. Marboe, Research **2**, 19 (1949).
[6] J. Frenkel, Acta Physicochim. URSS **12**, 317 (1940).
[7] Lord Rayleigh, Phil. Mag. (6) **34**, 94 (1917).
[8] H. Beuthe, Z. physik. Chem. **A163**, 161 (1933).
[9] Weissler, Cooper, and Snyder, J. Am. Chem. Soc. **72**, 1769 (1950).

The Dielectric Constant of Uranium Hexafluoride Vapor at 9400 mc/sec*†

DALE W. MAGNUSON
K-25 Laboratories, Carbide and Carbon Chemicals Company, Oak Ridge, Tennessee

(Received October 1, 1951)

PREVIOUS determinations of the dielectric constant of uranium hexfluoride have resulted in considerable discrepancies.[1,2] Although Smyth and Hannay[1] found no significant variation of the molar polarization, the results of the two investigators are in better agreement if a small dipole moment is postulated. The structure of the uranium hexafluoride molecule which best fits the electron diffraction data[3] is slightly asymmetrical and would probably have a permanent dipole moment. In addition, Burns, McKown, and Asbury[4] have made dielectric constant measurements on liquid uranium hexafluoride which are not in agreement with the measurements on the vapor. These previous investigations are summarized in Table I.

The dielectric constant of uranium hexafluoride vapor at 9400 mc/sec was determined at five temperatures by measuring the change in the resonant frequency of a cavity as it is filled with dielectric. These data are also given in Table I. The absence of any significant variation with temperature of the molar polarization confirms the results of Smyth and Hannay[1] that the dipole moment is probably zero. The minimum detectable dipole moment is less than 0.15 Debye unit. The mean value of and the average deviation of the molar polarization is (31.453±0.025) cc which is 14 percent higher than the results of Smyth and Hannay.[1]

TABLE I. Dielectric constant and molar polarization of uranium hexafluoride.

Temp. °C	$(\epsilon-1)\times10^6$	$(\epsilon-1)T/T_0\times10^6$	Molar polarization cc	Reference
		Previous investigations		
59.5			27.0±0.2	1
67.4			27.2±0.3	1
89.0			27.0±0.2	1
19.7			30.7±1.0	2
70.0			33.6	4
		This investigation		
83.1	3229.5±3.7	4211.8±4.8	31.468±0.036	
28.2	3815.4±5.7	4209.2±6.3	31.448±0.047	
40.0	3676.5±3.8	4214.8±4.4	31.490±0.033	
61.1	3441.5±4.5	4211.2±5.5	31.463±0.041	
83.1	3221.9±4.1	4201.9±5.3	31.394±0.040	
Mean		4209.8	31.453	
Average Dev. from Mean		±3.4	±0.025	

The cavity and gas handling manifold were previously exposed to uranium hexafluoride so that no appreciable reaction occurred during the runs. The uranium hexafluoride purity was better than 99.8, mole percent which was determined by experiments on the lowering of the freezing point. The most likely impurity is hydrogen fluoride which has a larger dielectric constant. It is estimated that 0.2, mole percent of hydrogen fluoride would change the dielectric constant by 10×10^{-6}. This is the largest source of error. The apparatus and possible errors of measurement are discussed in a previous report.[5]

* This document is based on work performed for the AEC by Carbide and Carbon Chemicals Company, Oak Ridge, Tennessee.
† The results of this investigation are also included in a doctoral thesis submitted to the University of Tennessee.

[1] C. P. Smyth and N. B. Hannay, *The Dipole Moment and Molecular Structure of Uranium Hexafluoride* (Princeton University Press, Princeton, New Jersey, 1944), MDDC-441.
[2] Amphlett, Mullinger, and Thomas, Trans. Faraday Soc. **44**, 928 (1948).
[3] S. H. Bauer, J. Chem. Phys. **18**, 27 (1950).
[4] Burns, McKown, and Asbury, "The electrical resistivity and dielectric constant of liquid uranium hexafluoride," (Carbide and Carbon Chemicals Company, K-25 Plant, August 10, 1949), *K*-482.
[5] D. W. Magnuson, J. Chem. Phys. (to be published).

Charge Densities in Conjugated Systems

R. MCWEENY
King's College, University of Durham, Newcastle-Upon-Tyne, England

(September 27, 1951)

IN simple MO theory (LCAO with neglect of overlap between AO*s*) the mobile "charge densities" ($q\mu$) give a useful picture of the division of mobile charge among the atoms of a conjugated system, while the "bond orders" ($p\mu\nu$) may be empirically related to properties of the bonds. Recently, the unrealistic assumption of nonoverlapping AO*s* has been removed;[1,2] in Löwdin's scheme the original definitions of the *q's* and *p's* may be retained, provided the MO*s* are written as LCAO*s*, AO*s* being certain orthogonal combinations of the AO*s* which they replace. But the *q's* and *p's* now have a many-orbital or molecular character which detracts from their immediate conceptual value: it is, for example, quite misleading to think of $q\mu$ as the charge *on* atom μ. The total mobile charge has, in fact, been divided out among the *orbitals* (AO*s*) rather than among the *atoms*. In many cases it seems preferrable to divide the "charge cloud" into localized regions; but although this type of division has been tacitly accepted in certain

cases (diatomic molecules), its generality and its implications do not appear to have been appreciated.

We rewrite the LCAO*s*, appearing from Löwdin's treatment of the secular equations, as LCAO*s*. Thus, with an obvious notation,

$$\psi_j=\Sigma_\mu\phi_\mu'C_{\mu j}(\text{LCAO})=\Sigma_\mu\phi_\mu C_{\mu j}'(\text{LCAO}),$$

and we define *local* charges

$$q_\mu'=\Sigma_j C_{\mu j}'^2 \text{ ("atom charge")},$$
$$q_{\mu\nu}'=2S_{\mu\nu}\Sigma_j C_{\mu j}'C_{\nu j}' \text{ ("bond charge")}$$

(terms arising from doubly filled orbitals being counted twice in the summations). Assuming the mobile system is described by a single antisymmetrized product of MO*s* (the usual assumption of one configuration) it follows easily that:

(1) The total mobile charge is divided out among the atoms *and the bonds* in amounts q_μ' and $q_{\mu\nu}'$, respectively, distributed with (normalized) densities $\rho_\mu=\phi_\mu^2$ and $\rho_{\mu\nu}=\phi_\mu\phi_\nu/S_{\mu\nu}$. These densities are localized in so far as they decay rapidly from well-defined maxima *on the atoms* and *in the bonds*. Thus $\Sigma_\mu q_\mu'+\Sigma_{\mu>\nu}q_{\mu\nu}'=N$, the total mobile charge, and $\Sigma_\mu q_\mu'\rho_\mu+\Sigma_{\mu>\nu}q_{\mu\nu}'\rho_{\mu\nu}=p$, the total charge density function.

(2) A portion of the charge density $p_\mu=q_\mu'\rho_\mu+\Sigma_\nu'\frac{1}{2}q_{\mu\nu}'\rho_{\mu\nu}$ may be formally associated with atom μ, the corresponding amount of charge being $q_\mu=q_\mu'+\Sigma_\nu'\frac{1}{2}q_{\mu\nu}'$. This latter quantity is then found to be identical with the formal charge (q_μ) introduced by Chirgwin and Coulson and, of course, $\Sigma_\mu q_\mu=N$.

(3) In contrast with the q's, the local charges provide an *analytical* picture of the charge distribution about an atom. For two atoms with equal formal charges may bear sensibly different local charges, q_μ', and the surrounding charge distributions may be quite differently distorted, as would be indicated by disparities among the various $q_{\mu\nu}'$. Figure 1 shows the charge distribution of the π-electrons in naphthalene.

(4) Equality of the q's (e.g., in alternant hydrocarbons) has usually been taken to imply (i) "self-consistency" of the customary assumption of equal Coulombic and resonance integrals, (ii) chemical equivalence towards attack by charged radicals, and (iii) complete absence of the charge shifts which would account for the small dipole moments of many conjugated hydrocarbons. From (3), the existence of overlap is seen to invalidate all these contentions.

(5) In terms of the charge allocation of (2), such quantities as the "effective dipole moment" the "effective scattering factor," etc. may be conveniently defined for atoms *in molecules* (i.e., with shared electrons). Thus a dipole moment $\mathbf{M}_\mu=\Sigma_\nu'\frac{1}{2}q_{\mu\nu}'\bar{\tau}_{\mu\nu}$ may be associated with atom μ, $\bar{\tau}_{\mu\nu}$ being the position vector relative to μ of the centroid of $\rho_{\mu\nu}$ (simply the midpoint of $\mu-\nu$ when atoms μ, ν are of one kind). This concept of localized dipoles might be useful in dealing with the interactions between large molecules. Summation of the individual vectors leads, except in cases of high symmetry, to a resultant molecular dipole moment even in pure hydrocarbons (e.g., phenanthrene). Effective scattering factors are being investigated elsewhere.[3]

(6) Many properties of the whole electron configuration (e.g., the usual approximation to the total energy) may be determined immediately once the local charges are known. For, with $A_{\mu\nu}=(1/S_{\mu\nu})\int\phi_\mu\hat{A}\phi_\mu d_\tau$ (quantities substantially independent of the particular molecule and overlap-problem), the mean or approximate value of A is

$$\bar{A}=\Sigma_\mu q_\mu'A_{\mu\mu}+\Sigma_{\mu,\nu}'\tfrac{1}{2}q_{\mu\nu}'A_{\mu\nu}.$$

In using q_μ, $p_{\mu\nu}$ for this purpose the conventional $A_{\mu\nu}$ must be replaced by "transformed" matrix elements, between AO*s*—involving an independent transformation for each particular A.

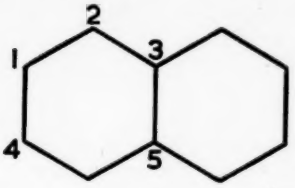

FIG. 1. Charge distribution in naphthalene. $q_1'=0.757$, $q_2'=0.767$, $q_3'=0.719$, $q_{12}'=0.273$, $q_{23}'=0.193$, $q_{14}'=0.213$, $q_{35}'=0.178$.

(7) Just as the q_μ may be misleading in discussing charge distributions, the nonlocal character of the $p_{\mu\nu}$ may introduce inconsistencies into bond length predictions. Thus, equality of $p_{\mu\nu}$ and $p_{\rho\sigma}$ does not imply a similarity between the wave functions in the regions $\mu-\nu$ and $\rho-\sigma$. On the other hand, on simple MO theory, the energy term associated with a bond corresponds roughly to electrostatic interaction between the nuclei and the bond charge; this would suggest a close connection between bond properties and the $q_{\mu\nu}'$. Unfortunately the whole technique of correlating bond properties with any measure of "bond order" is too uncertain to admit any fruitful comparison; but the $q_{\mu\nu}'$ are certainly no less satisfactory than the $p_{\mu\nu}$.

[1] B. H. Chirgwin and C. A. Coulson, Proc. Roy. Soc. (London) **A201**, 196 (1950).
[2] P. Löwdin, J. Chem. Phys. **18**, 365 (1950).
[3] R. McWeeny, Acta Cryst. (1951) (to be published).

Erratum: Errata: The Dielectric Constant of Water and the Saturation Effect

[J. Chem. Phys. **19**, 1327 (1951)]

F. BOOTH
Department of Theoretical Physics, King's College, London, England

THE publishers regret that the wrong figure was printed with the above Errata. The correct curve is printed herewith.

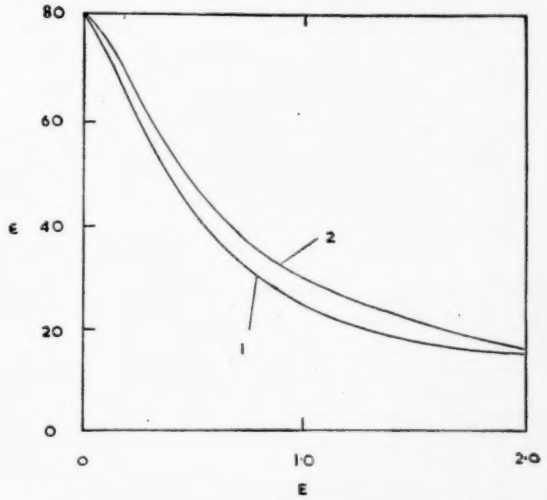

FIG. 1. The dielectric constant ϵ of water at 300°C, as a function of the field strength E (in 10^7 volts per cm). Curve 1, Eq. (3.15), paper I. Curve 2, from Eqs. (1) and (2).

Tables may be typewritten on sheets separate from the accompanying text. Each table must have a caption which will enable the data in the table intelligible without reference to the text. Avoid complicated column headings.

Wherever possible figures should be planned for the width of a column (3 in.). A convenient reduction ratio is about 2:1 or 3:1. Lettering should be large enough on the original that when reduced it shall not be less than about 1/16 in. (~1.5 mm). Line drawings must be in black ink on white paper or tracing cloth. Coordinate paper is not desirable but if used must be blue lined and the coordinate lines which are to show must be inked over. Photographs should have maximum black and white contrast. Identify each original drawing or photograph on the back with the author's name and the figure number. Figures should be numbered consecutively. Captions should be typed on a separate sheet of paper.

A limited number of alterations in proof are unavoidable, but the cost of making extensive alterations after the article has been set in type will be charged to the author.

Proof and all correspondence concerning papers for the purpose of publication should be addressed to the Publication Manager, American Institute of Physics, 57 East 55 Street, New York 22, New York.

Subscription Rates

	U.S. and Canada	Elsewhere
To members and associate members of the American Institute of Physics	$12.00	$13.00
To all others	$8.00	16.00

Back Numbers Bound

Yearly rate when complete year is available: $18.00

Single copies: $1.25 each.

Subscriptions, renewals, and orders for single copies should be addressed to the American Institute of Physics, 57 East 55 Street, New York 22, New York.

Changes of address should be sent to the American Institute of Physics.